

3rd International Conference
SCANNING PROBE MICROSCOPY

4th Russia-China
**WORKSHOP ON DIELECTRIC
AND FERROELECTRIC MATERIALS**

International Youth Conference
FUNCTIONAL IMAGING OF NANOMATERIALS

August 25 – 28, 2019

*Ural Center for Shared Use “Modern Nanotechnologies”
Insutute of Natural Sciences and Mathematics
Ural Federal University*

Abstract book



**Ural Federal
University**

named after the first President
of Russia B.N.Yeltsin



UrFU

**Institute
of Natural Sciences
and Mathematics**



УДК 538.9

ББК 22.37

C-423

Scanning Probe Microscopy. Russia-China Workshop on Dielectric and Ferroelectric Materials. Abstract Book of Joint International Conference
(Ekaterinburg, August 25-28, 2019) Ekaterinburg, Ural Federal University, 2019- 301 c.
ISBN 978-5-9500624-2-1

Organizers

School of Natural Sciences and Mathematics, Ural Federal University named after the first President of Russia B.N. Yeltsin (UrFU)

<http://www.urfu.ru>

Ural Center for Shared Use “Modern Nanotechnology” UrFU

<http://nanocenter.urfu.ru>

Labfer Ltd.

<http://www.labfer.com>

Ferroelectric Laboratory, INSM UrFU

<http://labfer.ins.urfu.ru>

Laboratory for Nanoscale Ferroelectric Materials, INSM UrFU

SPM General Chairs

Prof. Vladimir Shur
Prof. Victor Mironov

RCWDFM General Chairs

Prof. Alexander Sigov
Prof. Zhuo Xu

SPM International Program Committee

Prof. A.V. Ankudinov
Prof. A.A. Bukharaev
Prof. V.A. Bykov
Prof. S.A. Chizhik
Prof. A.L. Gruverman
Prof. A.L. Kholkin
Prof. O.V. Kolosov
Prof. A.V. Latyshev
Prof. V.L. Mironov
Prof. A.A. Saranin
Prof. V.Ya. Shur
Prof. V.V. Shvartsman
Prof. A.P. Volodin
Prof. I.V. Yaminsky

RCWDFM International Program Committee

Prof. I.N. Chugueva
Prof. H.S. Gu
Prof. A.L. Kholkin
Prof. L.N. Korotkov
Prof. H.X. Liu
Prof. W. Ren
Prof. I.V. Shnidshtein
Prof. V.Ya. Shur
Prof. T.R. Volk
Prof. S.B. Vakhrushev
Prof. X.Y. Wei
Prof. Z.G. Ye

Local organizing committee

| | |
|--------------------------|----------------------|
| Prof. Vladimir Shur | Ekaterinburg, Russia |
| Mrs. Elena Pelegova | Ekaterinburg, Russia |
| Dr. Dmitry Pelegov | Ekaterinburg, Russia |
| Mrs. Alevtina Shur | Ekaterinburg, Russia |
| Mrs. Ekaterina Shishkina | Ekaterinburg, Russia |
| Dr. Victoria Pryakhina | Ekaterinburg, Russia |
| Ms. Olga Dyachuk | Ekaterinburg, Russia |

ISBN 978-5-9500624-2-1



9 785950 062421

ББК 22.37

Ural Federal University
named after the first President
of Russia B.N. Yeltsin

SPM-2019-RCWDFM sponsors

Taylor and Francis Group
<http://www.taylorandfrancis.com>



Crystals
<https://www.mdpi.com/journal/crystals>



NT-MDT Spectrum Instruments
<http://www.ntmdt-si.com>



SPECS TII RUS
<https://www.specs-tii.ru/>



Ostec ArtTool
<http://www.arttool.ru>



INTERTECH Corporation
<http://www.intertech-corp.ru/>



OPTEC
<http://www.optecgroup.com/>



MTEON
<https://www.mteon.ru/>



IMC Group
<http://imc-systems.ru/>



Promenergolab
<http://www.czl.ru>



TUTORIAL LECTURES



Magnetic resonant force microscopy

V.L. Mironov

*Institute for physics of microstructures RAS, 603950, Nizhny Novgorod, Russia
mironov@ipmras.ru*

We present the methods for diagnostics of magnetic nanostructures based on magnetic force probe microscopy.

A magnetic force microscope (MFM) registers the force interaction of a magnetic probe with a non-uniform stray magnetic field of the sample. As a result, the spatial distributions of the MFM contrast correlate with the domain structure of the sample. The MFM method is especially effective in analyzing the magnetization distributions of patterned magnetic nanostructures, such as arrays of nanoparticles and nanowires [1]. On the other side, the MFM probe affects the sample magnetization causing effects of local magnetization reversal, which opens up great opportunities for selectively controlling the magnetic state of nano-dimensional objects [2].

In addition, the oscillations of magnetic probe leads to the formation of eddy currents in the conducting samples, which create magnetic fields damping the cantilever oscillations. This effect is used in microscopy of eddy currents when a change in the amplitude and quality factor of the resonant oscillations of the cantilever over areas with different conductivities is recorded as the data signal. The spatial resolution of this method reaches 20 nm [3].

In recent years, a new method for diagnosing resonant properties of ferromagnetic structures has been developed – magnetic resonance force microscopy based on the phenomenon of ferromagnetic resonance. In magnetic resonance force microscope (MRFM), a sample is placed in a microwave field modulated in amplitude at the frequency of the mechanical resonance of a cantilever. As a result, the oscillation amplitude of the cantilever becomes proportional to the amplitude of the ferromagnetic resonance in the sample. This method can detect the local spin-wave spectra in magnetic nanostructures and study the spatial distributions of the resonant oscillations of the magnetization in the samples [4].

This work is supported by contract #0035-2019-0022-C-01, Presidium RAS Program #0035-2018-0016 and Russian Foundation for Basic Researches (project #18-02-00247).

1. D. Rugar, H.J. Mamin, P. Guethner, et al., *Journal of Applied Physics*, **68**, 1169 (1990).
2. V.L. Mironov, A.A. Fraerman, B.A. Gribkov, et al., *The Physics of Metals and Metallography*, **110**(7), 708 (2010).
3. S. Hirsekorn, U. Rabe, A. Boub, W. Arnold, *Surface and Interface Analysis*, **27**, 474 (1999).
4. O. Klein, G. de Loubens, V. V. Naletov, et al., *Physical Review B*, **78**, 144410 (2008).

Visualization of polarization and electrical charges using Atomic Force Microscopy

S. Hong

*Department of Materials Science and Engineering, KAIST, Korea
seungbum@kaist.ac.kr*

In this tutorial, I will explain the basic principles of AFM (contact mode and ac-mode) starting from topography acquisition. Then, I will lay out the foundation of piezoresponse force microscopy (PFM), where we use the piezoelectric strain as the marker of polarization vector. This will lead to the discussion of various contributions to the strain induced by the voltage applied to the tip, such as electrostatic force (or capacitive force) induced indentation (or non-contact vibration of the cantilever), electrochemical strain, flexoelectric strain, electrostrictive strain, polarization switching induced strain, joule heating induced strain as well as Lorentz force induced deflection. In addition to all of these tip-sample interactions, one should not neglect the electrostatic force interaction between the cantilever and the sample. With all of the contributions sorted out, I will discuss about vertical and lateral PFM to build 3D vector polarization map using angle-resolved PFM. In addition, dual ac resonance tracking PFM, band excitation PFM, Switching Spectroscopy PFM will also be briefly introduced. Other markers such as screening charges are being used to map polarization vectors, which led to the invention of Charge Gradient Microscopy (CGM) as well as Scanning Resistive Probe Microscopy (SRPM). Furthermore, I will discuss electrochemical strain microscopy (ESM) and conducting AFM (C-AFM) as well as Kelvin Probe Force Microscopy (KPFM)/Electrostatic Force Microscopy (EFM), which will provide valuable information about the transport/diffusion properties of dielectric materials. All of these advanced AFM techniques will add insight into the multiscale electrical properties of dielectric materials, which will be part of our grand vision of Materials and Molecular Modelling, Imaging, Informatics and Integration (M3I3).

Study of ferroelectric domains by scanning probe microscopy

V.Ya. Shur

School of Natural Sciences and Mathematics, Ural Federal University, 620000, Ekaterinburg, Russia

Application of various methods of the scanning probe microscopy for investigation of the ferroelectric domain structure, domain imaging with high spatial resolution, local switching and creation of the micro- and nanodomain patterns will be presented systematically.

The brief review and comparison of various modern methods of domain imaging in ferroelectrics including optical microscopy, scanning electron microscopy and scanning probe microscopy (SPM) will be presented. The merits and demerits of SPM methods will be considered. The first successive domain imaging using atomic force microscopy (AFM) by measuring the ferroelectric surface relief revealed by selective etching will be demonstrated. The main advantages of the most popular Piezoresponse Force Microscopy (PFM) will be discussed.

The multiple examples of successive application of the SPM tip-induced ferroelectric domain local switching for study of the domain structure with high spatial resolution and obtaining important results will be presented: (1) new mechanism of the forward domain growth in polar direction based on results of local switching on nonpolar cuts of lithium niobate crystals; (2) interaction of the isolated domains leading to intermittency and formation of the quasiperiodic and chaotic structures on polar cut of lithium niobate; (3) decay of the poled state (spontaneous backswitching) and formation of the nanodomain structures during polarization reversal in uniform field in crystals of relaxor ferroelectric strontium-barium niobate (SBN); (4) role of the external screening on spontaneous backswitching after external field switch-off on nonpolar cut of lithium niobate crystals; (5) influence of the adsorbed surface layer and increased relative humidity on the domain growth during local switching; (6) domain structure and local switching in single grains of lead-free piezoceramics; (7) influence of the charged domain walls on dielectric relaxation in lead-free piezoceramics $(\text{K},\text{Na})\text{NbO}_3$; (8) ferroelectric domains in microtubes of diphenylalanine peptide; (9) as-grown domain structure and features of the domain growth in non-polar cut of glycine organic crystals.

Quantifying nanoscale electromechanical response with the AFM

R. Proksch

*Asylum Research, Santa Barbara, CA, USA
roger.proksch@oxinst.com*

The wide variety of electromechanical effects introduced earlier all depend on a sharp tip at the end of a flexible cantilever to localize the physical interactions. The tip radius can easily be less than 100 nm in diameter, allowing routine structural and functional measurements well below the diffraction limit of optical microscopes and competitive with high resolution electron microscopy techniques. This tip does not exist in isolation. It is connected to flexible cantilever which is in turn connected to the mechanical structure of the AFM itself. These connections are all required to use the cantilever in a practical microscope – to control the tip-sample distance and to raster the tip over the surface for example.

In this tutorial, we will dig into understanding the pitfalls and opportunities in quantifying the strain induced the electric field from a biased tip. A good understanding of these pitfalls and how to account for them in your measurements are critical for avoiding false results. Examples include:

- Cantilever dynamics – frequency dependence, instrumental sensitivity and long-range electrostatically driven motion;
- Tip-sample contact mechanics;
- Instrumental effects including crosstalk and noise floors – along with simple methods for characterizing the level of crosstalk in your AFM. I will include a couple case studies from different AFMs.

Finally, I will survey some current challenges and opportunities in electromechanical imaging, especially in the small-electromechanical response limit.

Infrared imaging: fundamentals and applications

S.A.M. Tofail^{1,2*}, C. O'Mahony^{1,2}, S. Markham^{1,2}, A. Mani^{1,2}, C. Silien^{1,2}, J. Bauer³,
E. Korsakova⁴, A. Korsakov⁴, L. Zhukova⁴

¹Department of Physics, University of Limerick, Limerick, V94 T9PX, Ireland
*tofail.syed@ul.ie

²Bernal Institute, University of Limerick, Limerick, V94 T9PX, Ireland

³Department of Bioengineering, Faculty of Fundamental Problems of Technology, Wroclaw University of Science and Technology, 50-370 Wroclaw, Poland

⁴Department of Physical Chemistry and Chemistry of Colloids, Ural Federal University named after the first President of Russia B.N. Yeltsin, 620002 Yekaterinburg, Russia

From astronomy to chemical imaging to melt-pool detection to night vision – Infrared imaging (IR) has been used in a number of applications where visible imaging provided limited information. This tutorial discusses the fundamental physics and instrumentation related to imaging using infrared, the portion of electromagnetic spectrum that lies beyond the visible and below the millimeter wave. It focuses on the translation of infrared imaging techniques in nondestructive testing (NDT) and medical imaging within the purview of metrological applications related to advanced manufacturing with a particular focus on real time, in situ imaging to obtain process information. Optical, X-ray, e-beam, ultrasound or scanning probes are widely used in nondestructive testing and medical imaging. The scope of IR imaging has so far been quite limited. The purpose of this tutorial is to make the attendee aware of the far wider capabilities of IR imaging than has normally been used so far. As such, we will discuss a few case studies from our ongoing activities in the applications of IR imaging [1-6]. We will also discuss practical instrumentation issues as well as steps needed to overcome bottleneck that currently restricts wider use of IR imaging to enable rapid, real time ambient measurements.

1. J. Bauer, C. O'Mahony, D. Chovan, J. Mulcahy, C. Silien, S.A.M. Tofail, *J. Therm. Biol.* **79**, 56 (2019).
2. R. Mouras, M.R. Noor, L. Pastorino et al., *ACS Omega* **3**, 6143 (2019).
3. S.A.M. Tofail, A. Mani, J. Bauer, C. Silien, *Adv. Eng. Mater.* **20**, 1800061 (2018).
4. M. Kumbham, R. Mouras, A. Mani et al., *Opt. Express* **25**, 13145 (2017).
5. C. Silien et al. Differential Infra-Red Nanoscopy System and Method, WO2014106657 (2014).
6. S.A.M. Tofail et al. A spectroscopic imaging device, EP15170819.5 (2015).

PLENARY LECTURES



Getting to zero - quantitative electromechanical atomic force microscopy

R. Proksch

Asylum Research and Oxford Instruments, Santa Barbara, California 93117, USA
Roger.Proksch@oxinst.com

Since the very early days of atomic force microscopy (AFM), voltage modulation (VM) of AFM has been used to try to quantify a host of electronic, electrochemical and electromechanical functionalities across nanometer length scales. The critical importance of such information has resulted in the development of a plethora of VM-AFM techniques for exploration of either long or short-range forces. Of relevance for ferroelectrics, piezoresponse force microscopy (PFM) imaging and associated spectroscopies have effectively opened the door to the exploration of nanoscale ferroelectric properties. The rise of PFM, however, has also brought about claims of ferroelectricity in materials which were subsequently thought to be not ferroelectric,[1] even unlikely materials such as soda-lime glass. Explanations for the origins of these unexpected nanoscale phenomena have not been in short supply, including new material properties, surface-mediated polarization changes and/or spatially resolved behavior that is not present in bulk measurements. At the same time, it is well known that VM-AFM measurements are susceptible to numerous forms of crosstalk and despite efforts within the AFM community, a global approach for quantitative, crosstalk-free techniques remains elusive. In an effort to understand the true origins of the measured VM-AFM signals we demonstrate the presence of hysteretic (“false ferroelectric”) long-range interactions between the sample and cantilever body and show that these are intrinsic to traditional VM-AFM detection methods. However, we show that with interferometric displacement sensor (IDS) [2] it is possible to separate the true tip motion from the cantilever dynamics. Using the IDS we have established a rapid and simple flagging routine of false piezo and ferroelectric responses and are able to demonstrate fully quantitative and repeatable nanoelectromechanical characterization. We attribute a lot of the observed unexpected hysteretic behavior to surface water, since it is ubiquitous in ambient conditions for even mildly hydrophilic surfaces and may explain the plethora of behaviors discussed above. Finally, we demonstrate that through using the interferometric approach allows for putting of quantitative limits on the electromechanical sensitivity. For example, we were able to show a $d_{eff} \leq 40$ fm/V for soda-lime glass using the IDS is much smaller than that implied by conventional VM-AFM measurements. These quantitative measurements are critical for a wide range of new devices ranging from mems actuators, memristor devices, energy storage and dynamic computer memory.

1. R.K. Vasudevan, et al., *Applied Physics Reviews* **4**, 021302 (2017).
2. A. Labuda and R. Proksch, *Applied Physics Letters* **106**, 253103 (2015).

Ultrafast ferroelectric switching: what are the limitations?

V.R. Bilyk, E.D. Mishina, A.S. Sigov

MIREA – Russian Technological University, 119454 Moscow, Russia
 assigov@yandex.ru

Manipulation of the atomic lattice using high power single-period THz pulses has been proven already directly by time-resolved X-Ray diffraction (XRD) techniques in different types of dielectrics [1-2]. Possibility to contactless displacement of polar ion is particularly important in ferroelectrics, where the frequency limitation arises due to the conventional circuit limitations for coupling electrical pulses through electrode structures on a sub-100-picosecond (ps) time scale. At the same time, the dynamics of electric polarization lies at the heart of ferroelectric-based ultrafast next-generation piezoelectric, electro-optic, and nonvolatile memory devices. Along with XRD, optical second harmonic generation (SHG) is widely used for justification ferroelectric switching under THz pulse [3-4].

In ferroelectrics, analogously to magnetic materials, short electromagnetic pulses may cause coherent collective excitations. In ferroelectric these are phonons, including the soft mode ones. Amplitude of such excitations is much larger than in case of thermal excitations. Excitations take place coherently over macroscopic area of illuminating spot (from tens to thousands of square microns). In this case, one can consider dynamical switching of ferroelectric polarization within the electromagnetic pulse duration following by relaxation. If the amplitude of coherent oscillations is high enough to transfer the process into highly nonlinear regime, than oscillating polar ion may relax to the different position of two-minima potential regarding to its initial position. In contrast to coherency of oscillation, these relaxations are stochastic. Thus, polarization switching, if takes place, is temporally limited: in dynamical range – to the reverse soft mode frequency; for polarization reversal – to the pulse duration.

In this presentation, we focused on theoretical justification on the conditions (parameters of ferroelectric crystal and electromagnetic pulse) providing both regimes of polarization switching within the Landay-Khalatnikov (LK) model. The model describes not only the ion displacements, but also the nonlinear-optical response of the materials. We took real parameters of the potential function of different crystals and considered LK equations with 1 ps THz pulse as external force. In this way, SrTiO₃, KTaO₃, BaTiO₃, (BaSr)TiO₃ were investigated. We make search for parameters and materials which can provide conditions for both types of switching. In description of the non-linear optical response we take into account the initial non-polarized multidomain state. Due to the nonidentical initial conditions for such a state, the solutions of the Landau–Khalatnikov equation are also nonidentical, and their interference gives a nonzero second harmonic field under THz electric field. We consider the temperature dependences of the second harmonic in the framework of such a model.

Experimentally, we performed a comparative study of THz field induced SHG in different ferroelectrics, incipient ferroelectric and multiferroic materials: SrTiO₃, KTaO₃, (BaSr)TiO₃, BiFeO₃, (BaSr)TiO₃/BiFeO₃. In these materials using time-domain spectroscopy (THz pump–optical probe), studies have been carried out of the temporal dependences of the intensity of the optical second harmonic. The highest switching efficiency was revealed in (BaSr)TiO₃ multidomain films near the phase transition where the soft mode is very wide and overlaps with the THz pulse in a frequency domain. In this material, we have proven the dynamic switching of the ferroelectric polarization with a THz pulse starting from a field of 300 MV/cm.

1. F. Chen, Y. Zhu, et al, *Phys. Rev. B* **94**, 180104(R) (2016).
2. C. Hauf, A.A.H. Salvador, et al, *Structural Dynamics* **5**, 024501 (2018)
3. E. Mishina, K. Grishunin, A. Sigov, et al, *Ferroelectrics* **532**, 199 (2018).
4. K. Grishunin, V. Bilyk, et al, *Scientific Reports* **9**, 697 (2019).

Structures and properties of novel antiferro-/ferroelectric materials with high energy-storage performance

Z.-G. Ye,^{1,2} P. Gao,^{2,1} Z. Liu,^{2,1} N. Zhang,^{2,1} H. Wu,^{3,1} W. Ren²

¹*Department of Chemistry and 4D LABS, Simon Fraser University, Burnaby, BC, V5A 1S6, Canada*

²*Electronic Materials Research Laboratory & Intl. Center for Dielectric Research, Xi'an Jiaotong University, Xi'an, 710049, China*
zye@sfu.ca

³*Department of Applied Physics, Donghua University, Songjiang District, 201620 Shanghai, China*

Energy resources are the driving force of social development and electrical energy-storage technology has received extensive attention. With their excellent positive DC bias feature, accompanied by high density, ultra-fast discharge and expansion of cell volume in the field-induced antiferroelectric (AFE) to ferroelectric (FE) phase transition process, antiferroelectrics have been considered as promising materials for high energy storage capacitors, large strain actuators, explosive transducers, electric-caloric refrigeration and microelectromechanical systems. To meet the increasing demands for high-performance energy storage capability, new AFE materials need to be developed.

In this paper, we present a novel concept for designing AFE materials based on the formation of solid solutions between two AFE systems of different anti-dipolar structures, namely between the conventional AFE PbZrO_3 or PbHfO_3 and the complex perovskite AFE $\text{Pb}(\text{Mg}_{1/2}\text{W}_{1/2})\text{O}_3$. A series of new AFE solid solutions of $(1-x)\text{PbZrO}_3 - x\text{Pb}(\text{Mg}_{1/2}\text{W}_{1/2})\text{O}_3$ (PZ-PMW) and $(1-x)\text{PbHfO}_3 - x\text{Pb}(\text{Mg}_{1/2}\text{W}_{1/2})\text{O}_3$ (PHf-PMW) have been synthesized, which has allowed us to reduce the critical field, and to realize the electric-induced AFE-FE phase transition at room temperature. In addition, the intermediate phase and structure-property relationship are studied in connection with the features of Pb^{2+} ion on the A-site and the evolution of chemically ordered structures on the B-site, leading to the establishment of comprehensive phase diagrams.

In particular, the crystal structure and energy storage properties of the PHf-PMW solid solution are systematically studied. The mismatch of B-site cations is believed to disrupt the long-range order of AFE dipoles. The competition between two different types of Pb ion displacement on A-site causes dipole frustration, reduces the critical field E_{cr} and increases the maximum polarization P_{max} , thus improving the recoverable energy density W_{rec} . With the PMW content of 10%, the best energy storage performance is obtained, which is superior to the so-far reported perovskite ceramics under similar electric field, and the W_{rec} is the highest in AFE-AFE system, making the PHf-PMW AFE solid solution ceramics a new class promising material for room-temperature energy storage applications.

These results indicate that the novel solid solutions form an interesting family of soft antiferroelectric materials, promising for high-density energy storage applications. The structural characterization and theoretical modeling shed light on the mechanisms underlying the AFE properties. This work not only gives the design method and synthesis strategy, but also provides ideas and guiding significance for developing other new AFE-AFE solid solution materials for high energy storage applications.

**INVITED
PRESENTATIONS**

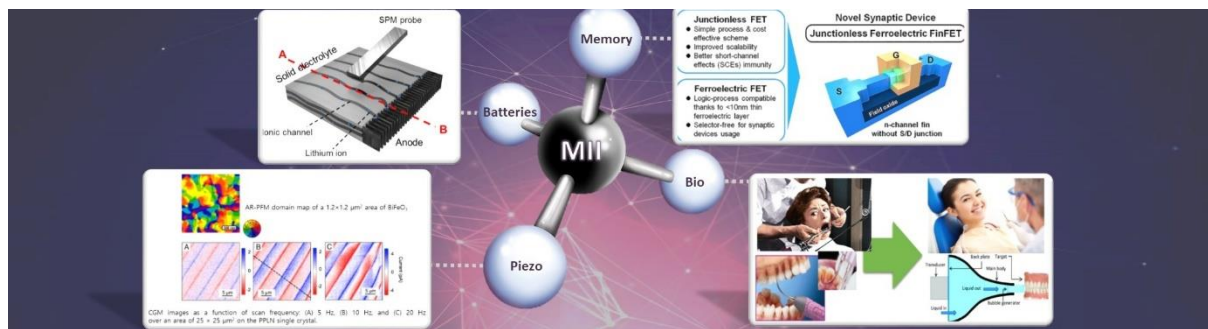


Materials Imaging and Integration (MII): new paradigm of nanoscale materials design and discovery

S. Hong, S. Cho, G. Park, H. Kim, P. Li, J. Ryu, C. Oh, H.J. Kim, J. Kim, S. Yun,
J. Oh, M. Glasser, J. Yeom, S. Eom, A. Jetybayeva, H.G. Kim, Y.J. Han

*Department of Materials Science and Engineering, KAIST, Daejeon, 34141, Republic of Korea
seungbum@kaist.ac.kr*

Renaissance established the scientific method, a system by which both observation and reason are employed in order to test the proposed mechanisms for planetary motion. Descartes promoted science by first questioning everything and then building up a theory based on sound observational evidence. Materials science is no exception in the sense that visualization of order parameters or materials properties provides the solid ground on which materials theory and design can flourish. Here I will present our current research thrusts to visualize polarization, electrical charges and ionic transport to understand the emerging phenomena on materials surfaces as well as interfaces and how they help design future memory and energy storage devices [1-4]. Last but not least, I will discuss the vision of materials imaging and integration, which will lead to a new paradigm of nanoscale materials design and discovery.



1. S. Hong *et al.*, *Proc. Natl. Acad. Sci. USA* **111**, 6566 (2014).
2. S. Hong *et al.*, *Rep. Prog. Phys.* **79**, 076501 (2016).
3. M. Owczarek *et al.*, *Nat. Comm.* **7**, 13108 (2016).
4. Y. Cho and S. Hong, *MRS Bulletin* **43**, 365 (2018).

Piezoresponse force microscopy and electron backscattering diffraction of 90° ferroelectric twins in BaTiO₃ positive temperature coefficient (PTC) thermistors

S.A.M. Tofail^{1,2}, M. Karimi-Jafari^{1,2}, A. Stapleton^{1,2}, Y. Guo², K. Kowal^{1,2}, D. Chovan^{1,2},
L. Kailas^{1,2}, A. Gandhi^{1,2}, K. O'Sullivan³, A. Maher³, C. Silien^{1,2}, E. Ul-Haq^{1,2}

¹Department of Physics, University of Limerick, Limerick, V94 T9PX, Ireland
tofail.syed@ul.ie

²Bernal Institute, University of Limerick, Limerick, V94 T9PX, Ireland

³BorgWarner Beru Systems, Monavalley Industrial Estate, Tralee, Co. Kerry, Ireland

Barium titanate (BaTiO₃) with positive temperature coefficient (PTC) of resistivity is widely used in surge protection devices, self-regulating heaters and temperature sensing applications. BaTiO₃ is a ferroelectric insulator at room temperature; however, the materials can become a ferroelectric semiconductor by suitable doping with ions La⁺³, Sm⁺³, Ho⁺³, or Nb⁺⁵. The resistivity of donor doped BaTiO₃ can increase by several orders of magnitude near the phase transition temperature ' T_C ' for the ferroelectric tetragonal to the paraelectric cubic phase transformation. It is believed that the huge resistivity change at T_C in donor doped barium titanate (BaTiO₃) is a grain boundary effect [1,2]. In this study, we combine two surface analysis tools, electron backscatter diffraction (EBSD) and piezoresponse force microscopy (PFM) to investigate the role of crystallographic orientation, topography and intergranular polarization in polycrystalline PTC BaTiO₃ ceramic that leads to PTC effect. EBSD of BaTiO₃ reveals individual grains of BaTiO₃ possess a preferred orientation. Ferroelectric domains and twinning is evident in both electron back scattered images and PFM images. In individual grains, the domains mostly appear in a single twin pair set rather than random pairs of all available phase variants. While the EBSD on these thermally etched samples showed 90° domains it could not discern the type between a - a and a - c domains. PFM on the other hand clearly distinguishes a - a and a - c type domains using vertical and lateral piezoresponse. The work reported here will contribute to grain boundary control of PTC effect in semiconducting ferroelectric barium titanate ceramics.

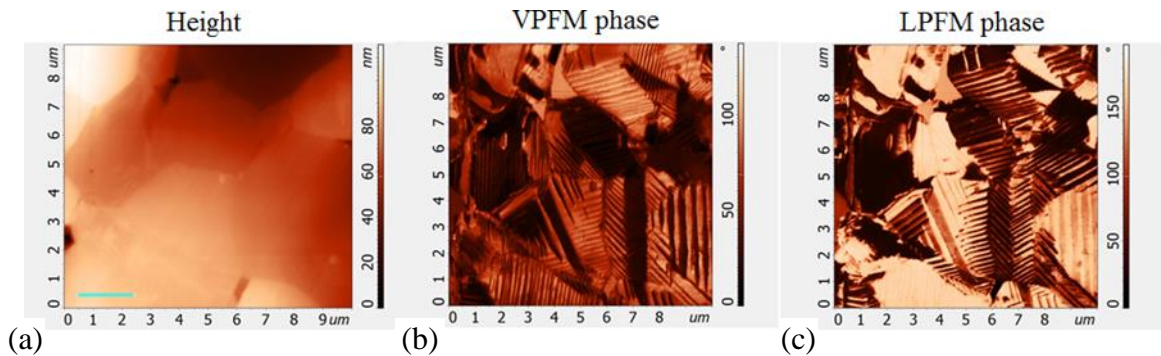


Figure 1. PFM images of BaTiO₃ showing (a) height, (b) vertical piezoresponse VPFM (phase) and (c) lateral piezoresponse LPFM (phase) of the same area. A clear herringbone pattern is evident on most of the grains (b, c), indicating that the domains are ferroelectric in nature. The scale bar indicated in (a) is 2 μm.

The authors acknowledge funding from the European Union's Horizon 2020 research and innovation program, OYSTER (Open characterisation and modelling environment to drive innovation in advanced nanoarchitected and bio-inspired hard/soft interfaces) under grant agreement No 760827, Enterprise Ireland, Innovation Partnership Programme (Project No: IP/2013/0281), Irish Research Council postgraduate scholarship and Higher Education Authority (HEA).

1. W. Heywang, *Journal of the American Ceramic Society* **47**, 484 (1964).
2. G.H. Jonker, *Solid-State Electronics* **7**, 895, (1964).

New possibility of scanning probe microscopy and spectroscopy

V. Bykov^{1,2}, Y. Bobrov¹, V. Polyakov¹, P. Veenar¹, A. Shelaev¹

¹*NT-MDT-Spectral Instruments, 124460, Russia, Moscow, Zelenograd*
www.ntmdt-si.com, spm@ntmdt-si.ru

²*Moscow Institute of Physics and Technology, 141701, Russia, Moscow6 Dolgoprudny*

The development of scanning probe microscopy (SPM) as itself and in a combination with optical and spectroscopic technic in a combination with micromechanics for different type of cantilevers and modern controllers based on the modern development in microelectronics and intellectual SW based on the algorithms of the fast self-optimization of scanning parameters can give a lot of information as for the physical properties of nanostructures right for the specialists of the materials science:

- Electron state density and work function distribution to use Scanning Tunneling microscopy and spectroscopy;
- The profile of surface structures and its dependence on the pressing pressure;
- Inhomogeneity of the frictional force in the probe-surface system;
- Heterogeneity of adhesion forces;
- Distribution of surface potential (Kelvin-mode);
- Distribution of electrical conductivity and capacity in the cantilever-surface contact;
- Distribution of thermal conductivity;
- Young's modulus distribution;
- Diagnostics of limits of elastic deformation;
- Distribution of undersurfaces magnetic forces;
- Distribution of piezoelectric characteristics of surface structures as for the hard and delicate materials such as peptides nanotubes;
- The distribution of the optical properties of the surface with a resolution significantly exceeding diffraction limits in aperture and cantilevers aperture less near-field optical microscopy with a number of AFM modes;
- Possibility of surface modification by tension, current or electric fields actions.

The application field was increased very wide – from one side micro- and nanoelectronics with extra high-level the metrology requirements and up to material science, biology, ecology and medical diagnostics with requirements to the side of simplification in operation procedures, possibility of the materials and molecules recognitions and types of problems with living cells.

New generation of AFM control electronics now allows a real-time cantilever deflection tracking and analyzing. Based on a fast force-distance measurement we developed a new group of non-resonant atomic force microscopy methods of scanning probe spectroscopy – called Hybrid mode. Hybrid mode is the most proposal AFM mode since it summarizes all advantages of amplitude modulation and contact modes allowing simultaneously: free of share force topography measurement with direct tip-sample interaction control, real-time quantitative nanomechanical measurements, conductivity, piezoresponse and electrostatic imaging, all with conventional scanning speed. Hybrid mode is also very helpful for liquid measurements because it utilizes the issue with cantilever eigenfrequency detection.

Progress in micromechanics manufacturing resulted in significant increase of the cantilever yield rate (to practically 100%) with repeatability of resonant characteristics at 10% level, thus preconditioning implementation of the concept of multi-probe cartridges for AFM.

One of the most demanding application of modern AFM is routine and repeatable atomic and molecular resolution. This requires extra-low tip-sample thermal drift assumed us lower than 1 Å/min. Development of thermally stabilized cabinet with 0.01 °C temperature control accuracy and drift-minimized mechanical design of AFM helped us to achieve mentioned drift level and repeatable atomic/molecular resolution imaging. But conventional cantilever exchange procedure

requires opening the cabinet and manipulating with AFM therefore destabilizing perfect temperature conditions. So the concept of automated multi-probe cartridge together with active thermal stabilization and drift-minimized mechanical design can be a perfect tool for routine high-resolution AFM imaging.

AFM is a candidate to solve some of “Metrology Difficult Challenges” proposed by The International Technology Roadmap for Semiconductors like: “Structural and elemental analysis at device dimensions and measurements for beyond CMOS”, “Nondestructive, production worthy wafer and mask-level microscopy for critical dimension measurement for 3D structures, overlay, defect detection, and analysis”. A rapid development of polymer and single-molecular electronics also requires AFM to measure and control the topography, nanomechanical, conductivity, temperature and other properties at the nanoscale.

To summarize, future electronics development and manufacturing can be a wide field for AFM application, especially for large-sample AFMs. But the biggest drawback of AFM technology to overcome is low throughput.

Throughput of AFM is limited by: system adjustment time before scanning (OBD system and lock-in adjustment, area of interest searching time etc.), scanning parameters adjustment time, scanning speed and amount of data gathered after one scanning session. So to develop the next-generation AFM all these limits should be overcome.

To minimize system adjustment and scanning parameters tuning time we develop and improve new software algorithms allowing fully automated topography imaging. New high-speed control electronics together with Hybrid mode allow more data points and different properties to be recorded per one scanning session. We also develop new AFM-scanner control algorithms to increase a topography imaging speed noticeably.

These developments implemented to the fully motorized large-sample AFM is a promising tool for nanotechnology industry.

To use AFM-cluster technology in the portable SPM, such as Solver-NANO (<https://www.ntmdt-si.ru/products/practical-afm/solver-nano>) can open the road for the using of this unit right on the Space Stations for material quality control in the Space and Space Station conditions.

Development of modes for scanning spectroscopy combined with SPM in the instruments NTEGRA-SPECTRA-II provides new options of confocal laser luminescence spectroscopy and Raman spectroscopy as well as higher reliability of detection for TERS and high-resolution scanning probe-optical microscopy and spectroscopy. Probes with diamond nanocrystals containing N-V defects are capable to detect magnetic states as microscopic as single spins and so they are promising for studies of surface catalytic activity and for detection of free radicals, including applications in biology and medicine.

Apertureless scanning nearfield optical microscope (ASNOM) probe induce light scattering give the possibility to investigate infrared as chemical nature of surface functional groups and to measure the doped impurity implantations in microelectronic structures that it impossible to observed in electron microscopy.

Accuracy of probe-sample contact stiffness measurements in an atomic force microscope

A.V. Ankudinov

Ioffe Institute, Saint Petersburg 194021, Russia
Alexander.ankudinov@mail.ioffe.ru

In atomic force microscopy (AFM), the local mechanical properties of a sample are studied using load-unloading dependences of the indentation force on the sample deformation (force curves). The force curves play a special role in the novel AFM techniques: Hybrid mode (NT-MDT SI), PeakForce QNM (Bruker), Fast force mapping mode (Asylum Research), – they are also used to determine the height of the relief and serve as the basis for electrical, piezoelectric, magnetic, and thermal measurements.

Friction at the AFM probe-sample contact can significantly change the shape of the measured force curve. If the cantilever probe slides the surface, the force applied to its tip acts normal to the sample and the console bends so that the bending angle monotonously increases along the console [1]. If the probe is clamped by the sample, a substantial lateral component of the friction force is added, due to which the console buckles (the deflection angle changes non-monotonously) [1, 2]. Most of the AFM use an optical beam deflection (OBD) technique. Therefore the profile of the angle of deflection of the console is not controlled, and instead just the value of the angle is detected at a single point – at the focus of the OBD laser on the console. Because of this, the AFM control system is not able to distinguish the buckling from bending [3, 4], which leads to errors of the measured amplitude and direction of the indentation force. In principle, the OBD may detect two parameters (bending and twisting angles of the console at the selected point), but the contact point displacement vector and the concentrated force have three spatial components. Only recently a commercially available scheme for monitoring cantilever deflections has appeared [5], combining the OBD with an interferometer that allows measuring the missing third parameter – the vertical displacement of the selected point on the console.

In AFM, the normal local stiffness of the probe-sample contact k_S is calculated from the force curves slopes, S at the point of interest on the sample and S_0 on the conditionally infinitely rigid and flat sample, and the console bending stiffness k_C [6]:

$$k_S = k_C S / (S_0 - S). \quad (1)$$

Expression (1) corresponds to the representation of the cantilever and the sample as a model of two series-connected springs. This view does not take into account: the probe is clamped or slides over the sample, the deformation of the probe itself, the local inclination of the sample and the possible anisotropy of its mechanical properties, design features and location of the cantilever above the sample. As a result, expression (1) determines not the k_S , but rather the apparent stiffness k_A .

The above has a negative effect on the accuracy and reliability of nanomechanical measurements in AFM and the subsequent theoretical analysis of AFM experiments. As a consequence, there is a need in accurate analytical calculations of the AFM cantilever deformations, taking into account: the contact friction effects, features of the console and probe design, sample anisotropic mechanical properties. In this lecture, such calculations are presented and discussed, and the results of these calculations are compared with AFM measurements.

1. D. Sarid, *Exploring Scanning Probe Microscopy with MATHEMATICA. Second edition. Weinheim: WILEY-VCH Verlag GmbH & Co. KGaA, 310 (2007).*
2. A.V. Ankudinov, M.M. Khalisov, V. Penniyaynen, et al., *Tech. Phys. Lett.* **44** (8), 671 (2018).
3. S. Fujisawa, M. Ohta, T. Konishi, Ya. Sugawara, S. et al., *Rev. Sci. Instr.* **65** (3), 644 (1994).
4. H. Kawakatsu, H. Bleuler, T. Saito, et al., *Jpn. J. Appl. Phys.* **34**, 3400 (1995).
5. *Asylum Research Quantifies the “Last Axis” in Atomic Force Microscopy* (09 February 2018) <https://www.oxinst.com/news/cypher-ids-option/>
6. H.-J. Butt, D. Cappella, M. Kappl, *Surf. Sci. Rep.* **59**, 1 (2005).

Nanomotion based antibiotic sensitivity test

S. Kasas^{1,2}

¹Laboratoire de Physique de la Matière Vivante, EPFL, CH-1015 Lausanne, Switzerland

²Unité Facultaire d'Anatomie et de Morphologie, CUMRL, Université de Lausanne, Switzerland
Sandor.kasas@epfl.ch

Several years ago we noticed that attaching living organisms onto an atomic force microscope (AFM) cantilever can be a very efficient way to detect life-death transitions in a label free manner [1]. The technique is based on the observation that all living organisms oscillate at a nanometric scale as long they are alive and stop these movements as soon the organism dies. Traditional AFM cantilevers and their associated deflection sensors can easily detect these tiny oscillations. Therefore, such an experiment can be carried on in any biologically oriented commercially available AFM. A typical experiment consists in attaching the organism of interest onto a cantilever and inserting it into the AFM. The oscillations of the lever are monitored for about 15 minutes and eventually a drug that modifies the organism's metabolism is injected into the analysis chamber. The modifications occurring in the oscillation pattern before and after the injection are used to assess the action of the drug. The technique was successfully tested on bacteria, yeast, vegetal and animal cells. The technique offers novel avenues to explore living organisms in a label free and chemistry independent manner.



Figure 1. Home-made nanomotion detector.

In our laboratory we are using this technique as an ultra-rapid antibiotic sensitivity test (AST). The method permits to assess the sensibility of a given bacteria to antibiotics in a timeframe of minutes instead of days or weeks as it is the case nowadays with the traditional ASTs. In order to reduce the costs and simplify the use of the instrument we develop our own dedicated nanomotion detectors. Several such prototypes are already implemented in research centers and university hospitals for validation proposes.

During the presentation, the working principle of the technique will be explained and numerous potential applications will be discussed.

1. Kasas S. et al., *PNAS*, 112, 378 (2015).

Flexible all-solid-state supercapacitors based on transition metal oxide nanocomposites

Sh. Wang, Zh. Xiong, P. Hu, Y. Hu, H. Gu

*Hubei Key Laboratory of Ferro- & Piezoelectric Materials and Devices,
Faculty of Physics and Electronic Science, Hubei University, Wuhan 430062, P. R. China
huym@hubu.edu.cn*

In recent years, flexible all-solid-state supercapacitors (FASCs), as one of the most promising emerging energy storage devices, have attracted great attention to use as the power sources of portable and wearable electronic devices due to their high flexibility, small size, better safety operation and environmental benignancy. A series kind of FASCs based on $\text{Co}_3\text{O}_4/\text{rGO}$ nanocomposite, MoS_2/rGO nanocomposite and $\text{Ni}(\text{OH})_2$ nanoflowers electrodes were fabricated using KOH or K_2SO_4 -PAAK gel as electrolyte. High specific capacitance were obtained for different materials, e.g., 190 F/g for $\text{Co}_3\text{O}_4/\text{rGO}$ nanocomposites, 185 F/g for MoS_2/rGO nanocomposite and 1916 F/g for $\text{Ni}(\text{OH})_2$ nanoflowers electrodes. Especially, the as-fabricated devices also showed good stability and excellent flexibility, an excellent cycling performance (capacitance retention of ~90%) after 10,000 cycles. The cyclic voltammeters of SCs are almost unchanged and can work normally when its bent from 0 to 180°, exhibiting good flexibilities and reliabilities. In addition, a light-emitting diode, electronic watch and electronic scale are successfully powered by the as-fabricated SCs and can work for several minutes. All the performances have shown that the transition oxide nanocomposites could have potential practical applications in flexible energy storage devices in the future.

Manifestation of local polar regions in spectroscopic investigations in ferroelectrics and relaxors

A.M. Pugachev, I.V. Zaytseva,

*Institute of Automation and Electrometry, Russian Academy of Sciences, Novosibirsk, 630090 Russia
apg@iae.nsk.su*

A number of unique properties of ferroelectrics with a diffuse phase transition are determined by noncentrosymmetric polar nanoregions which appear in the paraelectric phase. To study the role of polar nanoregions in ferroelectrics and relaxors, spectroscopic studies in the typical relaxor $\text{Pb}_3(\text{MgNb}_2)\text{O}_9$ (PMN), conventional ferroelectric crystal BaTiO_3 and $\text{Sr}_x\text{Ba}_{1-x}\text{Nb}_2\text{O}_6$ (SBN- x) are carried out. Transformation of a conventional ferroelectric to a relaxor within the same class of symmetry occurs in SBN- x : these crystals exhibit properties of both relaxors ($x > 0.6$) and conventional ferroelectrics ($x < 0.6$).

Brillouin spectra and generation of the second optical harmonic in a series of SBN- x crystals, PMN and BaTiO_3 are investigated in the 115-850 K temperature range. The second harmonic generation (SHG) is observed in paraelectric phase in all crystals under study, revealing the presence of polar regions in the paraelectric crystals. The spectral width of the SHG spectrum does not exceed 0.3 cm^{-1} and is temperature independent. Upper limit of the spectral width of the SHG spectrum provides lower limit of the lifetimes of polar regions, which are longer than 15 ps. It suggests that the doubled frequency signal in the paraelectric phase is generated in areas with lifetimes longer than 15 ps.

Elastic modulus C_{33} extracted from the Brillouin experiment revealed peculiarities of its temperature behavior near the phase transition temperature. Comparison of the SHG temperature dependences with ones of the elastic modules showed that the coupling of elastic modulus and polar state via electrostriction provides the description of the acoustic anomalies. The temperature dependences of the relaxation times of local polar regions are determined from the anomaly of width of the Brillouin peak in the vicinity of the phase transition.

The reported study was funded by RFBR according to the research project 18-02-00399 and State assignment No AAAA-A17-117052410033-9. Experiments were performed in the multiple-access center “High-Resolution Spectroscopy of Gases and Condensed Matter” in IA&E SBRAS (Novosibirsk, Russia).

Lead free KTN single crystals: from composition regulation, space charge field engineering to application

H. Tian, Ch. Hu

*School of Physics, Harbin Institute of Technology, 150001, Harbin, China
tianhao@hit.edu.cn*

Lead-free crystals, as a classic example of environmentally-friendly materials, have received the extensive concern and key development recently at the forefront of high-technology advanced materials. Among these lead-free candidates, $\text{KTa}_{1-x}\text{Nb}_x\text{O}_3$ (KTN) is the most potential systems due to their giant electro-optic, piezoelectric and electrocaloric properties. However, large-size and high quality KTN crystals are difficult to grow, which limits its development and application. In this work, we successfully grew a series of large-size and high quality pure and Fe doped KTN crystals by the top-seeded solution growth method. The as-grown KTN crystals exhibit good crystallinities and have large quadratic electro-optic coefficients ($s_{11} = 1.04 \times 10^{-14} \text{ m}^2\text{V}^{-2}$), indicating their quality and suitability for device application. We investigate the segregation of as-grown crystals which enables precise control of the individual components of crystals during growth, and propose effective energy models to explain the crystal morphology and guide the size uniformity crystal growth which ensures the quality of as-grown crystals. Component regulation and space charge field engineering are used to improve the optical and ferroelectric properties. We successfully utilize the composition gradient, light-induced space charge field and external electric field to achieve the micro-domains manipulations in KTN, which greatly enhance the crystal performances. Further, the variable gradient functional materials is proposed by the light induced space charge field engineering. Based on this variable gradient refractive index KTN, a MHz high-speed electro-deflector was produced. The controllable growth of high quality KTN crystals will be valuable for the lead-free crystal performance improvement and photonic and electronic device development, and provides a basis for exploring the origin of giant electro-optic, piezoelectric effects.

Processing of BiFeO₃ thin films to control their dielectric response

S.P. Reis^{1,2}, E.B. Araujo¹

¹*Department of Physics and Chemistry, São Paulo State University, 15385-000 Ilha Solteira, Brazil
eudes.borges@unesp.br*

²*Federal Institute of Education, Science and Technology of São Paulo, 15503-110 Votuporanga, Brazil*

Leakage current in the BiFeO₃ thin films is a problem that still limits their practical applications, despite the announced potential of this multiferroic for the next generation of microelectronic devices. The mechanisms behind the large leakage current observed in BiFeO₃ are often associated to the valence fluctuation of the Fe ions, formation of oxygen vacancies and inhomogeneities associated to the Bi volatilization during synthesis. The search for alternatives to control the leakage current in this system has stimulated the recent research in this field. In the present work, the impact of defects on the electrical properties of BiFeO₃ thin films is reported for a set of samples with different defects introduced during the synthesis. Secondary phases and oxygen vacancies were the most apparent defects during film synthesis compared to single-phase films. The electrical properties of the films were studied in terms of impedance and electric modulus spectroscopies, and electrical conductivity as a function of frequency (10²-10⁶ Hz), temperature (300-480 K) and *dc* bias field (0-60 kV.cm⁻¹). From thermally activated process, the activation energies of dielectric relaxation and conduction were very similar for films with secondary phases. The activation energies of conduction, 0.42 eV (grain) and 0.43 eV (grain boundary), were attributed to the first ionization level of oxygen vacancies in these films. On the other hand, the activation energy of conduction increases to 0.68 eV for single-phase film post annealed in oxygen, an indicative of effective reduction of defects in this film and that second ionization oxygen vacancies are responsible for conduction in this sample. DC bias influence on dielectric properties reveal an electrically excited relaxation process similar to the thermally activated. The Cole-Cole curves of complex impedance were greatly depressed by increasing dc bias, whereas the Cole-Cole curves of electric modulus were almost independent of bias. These results are discussed in terms of interfacial polarization in the low frequency range. The different scenarios demonstrated the importance of the synthesis to control the electrical conductivity and other related parameters of BiFeO₃ thin films.

Dielectric and magnetic responses in nanocrystalline BaTiO₃

L.N. Korotkov¹, M.A. Kashirin¹, T.N. Korotkova², V.S. Filatov¹,
F.M. Aljaafari¹, N.A. Emelianov³

¹Voronezh State Technical University, Voronezh, Russia;

²Voronezh Institute of the RF Ministry of Internal Affairs, Voronezh, Russia;

³Kursk State University, Kursk, Russia

l_korotkov@mail.ru

Barium titanate (BaTiO₃) is well known ferroelectrics, which is characterized by diamagnetic properties in the bulk state. However the ultrafine BaTiO₃ demonstrates the weak ferromagnetism, as well as a much other ultradispersive oxides. The nature of unusual ferromagnetism in BaTiO₃ is not clear up to now. However, it is supposed that ferromagnetism observed in nanostructured materials originated due to point defects, which are predominantly localized on the surface of nanoparticles. Ferroelectric properties of BaTiO₃ also depend on lattice defect concentration. Since concentration of lattice defects essentially depends on the thermal annealing regime then the purpose of present work was the study of an influence of sintering temperature and the thermal treatment in H₂ atmosphere on magnetic properties of nanostructured barium titanate.

The ultrafine barium titanate powders produced by Sigma-Aldrich were used for experiments. The initial nanopowders have an average particle size about 100 nm and the cubic perovskite lattice at room temperature. The disc-shaped samples 10 mm in diameter and 1 mm thick were pressed from the powder. These samples were sintered at following regimes. The sample N1 was annealed at 700 °C during 1.0 h; the sample N2 was annealed at 1000 °C for 5.0 h and the sample N3 was firstly annealed at 1000 °C for 5.0 h and then at 1200 °C for 0.5 h.

The temperature dependences of dielectric permittivity (ϵ) of prepared materials were studied using capacity bridge at a frequency of 10 kHz.

The magnetic measurements were carried out with using a vibrating sample magnetometer at a frequency of measuring magnetic field 10⁻⁴ Hz and amplitude H_A = 10000 Oe. The error of measured values of magnetization σ does not exceeded of 10%. For magnetic measurements the initial samples and the samples which were sequentially annealed in hydrogen at 250 °C (1.5 h) and 350 °C (1.5 h) were used.

The analysis of our experimental results can be summarized as follows:

1. Different defects in grains surfaces of the nanostructured BaTiO₃ are mainly responsible for electron states, which produce ferromagnetic and diamagnetic responses.
2. The annealing of nanostructured BaTiO₃ under experimental condition leads to increase in the both ferromagnetic and diamagnetic responses. Observed change of magnetic properties probably due to desorption of absorbed atoms from the surface of nanosizes grains as well as filling of electron states by the electrons that appeared owing to the emptying of the traps when the sample is heated.
3. Increasing the sintered temperature of BaTiO₃ nanostructured samples leads to rise of dielectric permittivity and to the decrease of both the ferromagnetic and the diamagnetic responses owing to decrease of lattice defects concentration.
4. Thermal annealing of BaTiO₃ nanoparticles with initially cubic perovskite crystalline lattice at temperature ≥ 1000 °C leads to an increase in the dielectric permittivity and to the occurrence of ferroelectric phase transition near $T_C \approx 393$ K.
5. An influence of thermal prehistory on magnetization of nanostructured BaTiO₃ should take in account at the analysis of its magnetic properties.

This work was supported by Russian Foundation for Basic Research (Research Project No.18-52-00039 Bel_a).

Pyroelectric and electrocaloric effects in PMN-based relaxors

E. Smirnova¹, G. Sotnikova¹, N. Zaitseva¹, G. Gavrilov¹, A. Sotnikov^{1,2}

¹*Ioffe Institute, 19402126, St Petersburg, Russian Federation
esmirnoffa@gmail.com*

²*Leibniz IFW Dresden, D-01069, Dresden, Germany*

Electrocaloric effect (ECE) is considered as physical background for promising cooling technology based on effects and phenomena in solid materials at present time. ECE occupies a special place among other caloric effects since its use allows to minimize the size of the cooling elements controlled by an electric field and to adapt them to micro- and nanoelectronic devices.

Relaxor ferroelectrics are considered as promising ECE materials. As compared to conventional ferroelectrics, their characteristic features are diffuseness of the phase transition (thus, wide working temperature range is expected) as well as a high sensitivity to external influences including electric field. The extraordinary physical properties underlying numerous applications of relaxors are determined by the existence of a natural nanostructure in such media (polar nanoregions in the paraelectric matrix).

ECE is inextricably linked with the pyroelectric effect that mainly determines ECE response. In turn, two contributions to the pyroelectric effect have to be distinguished, namely, the dielectric contribution (primary pyroelectric effect) which is determined by the change of the polarization with temperature for clamped samples and electromechanical contribution (the secondary pyroelectric effect) whose influence is important for free samples. The contribution of the secondary pyroelectric effect to the total pyroelectric one is governed by piezoelectric and elastic properties of the material, as well as by its thermal expansion [1].

Relaxors do not exhibit real piezoelectric properties due to the macroscopically isotropic state. However, they have so-called giant electrostriction characterized by high effective piezoelectric coefficient up to $1000 \cdot 10^{-12}$ m/V as a result of induced polarization under external DC electric field. Therefore, solid solutions based on classical relaxor – lead magnesium niobate with high induced polarization and, respectively, induced piezoelectric properties were selected as the model objects for the study.

The numerous published values of pyroelectric and electrocaloric coefficients for relaxors are contradictory and largely depend on measurement and calculation methods. In the present study, to clarify the situation and to improve results, pyroelectric and electrocaloric measurements were performed by two different methods. Pyroelectric properties were investigated by LMM (Laser Intensity Modulation Method) and MIR (Mid-Infrared Radiometry) methods for direct temperature measurements. Electrocaloric properties were studied by using quasi-adiabatic calorimeter and MIR method at actual heat exchange conditions between the sample under study and environment.

Specific features of pyroelectric and electrocaloric effects in relaxors as well as their correlation with other properties such as dielectric nonlinearity and electromechanical properties, including giant electrostriction and elasticity, have been studied and discussed.

The work was supported by the Russian Foundation of Basic Research under grant 18-02-00394.

1. J.F. Nye, *Physical Properties of Crystals* (Clarendon Press) 376 (1964).

Characterization of oxygen-vacancy-related relaxation by thermally stimulated depolarization current and impedance spectroscopy

Y. Zhang, X.W. Liang, Z.Y. Zhao

Beijing Key Laboratory of Fine Ceramics, State Key Laboratory of New Ceramics and Fine Processing, Institute of Nuclear and New Energy Technology, Tsinghua University, Beijing, 100084 P. R. China
yzhang@tsinghua.edu.cn

The correlation between dielectric relaxation processes and oxygen vacancy defects has been investigated by thermally stimulated depolarization current (TSDC) measurement and impedance spectroscopy (IS) analysis.

As a result of the variations of peak current intensity and peak temperature with different polarization temperatures in the TSDC curves of antiferroelectric ceramics, three successive relaxation peaks with different origins have been found to occur: a low-temperature defect dipoles peak, an intermediate-temperature in-grain oxygen vacancy migration peak, and a high-temperature transgranular oxygen vacancy migration peak. These results demonstrated that the improved resistance degradation process with the increase of barium substitution is related to the decrease in oxygen vacancy concentration.

The effect of thermal annealing atmosphere on the dielectric properties of barium strontium titanate ((Ba,Sr)TiO₃, BST) glass-ceramics was investigated by IS and TSDC methods. The thermal annealing atmosphere variation was shown to be sensitive to oxygen vacancy concentration. It is shown that the oxygen vacancy concentration of the N₂-sintered samples is much higher than that of air-annealed and O₂-annealed glass-ceramic samples.

1. X. Z. Song, T. Y. Zhang, Z. Y. Zhao, et al, *J. Am. Ceram. Soc.* **102**, 901 (2019).
2. X. Z. Song, T. Y. Zhang, Y. Zhang, et al, *Ceram. International* **44**, 5668 (2018).
3. Z. Li, X. Z. Song, Y. Zhang, et al, *J. Appl. Phys.* **121**, 204102 (2017).
4. Q. Zhang, Y. Zhang, X. L. Liu, et al, *J. Electr. Mater.* **45**, 4044 (2016).

Tristate ferroelectric memory effect in Fe, Nb co-doped $\text{Bi}_{1/2}(\text{Na}_{0.8}\text{K}_{0.2})_{1/2}\text{TiO}_3$ lead-free ceramics

H. Zhang, W. Jin, J. Zhou, J. Shen, T. Wang, W. Chen

*State Key Laboratory of Advanced Technology for Materials Synthesis and Processing, School of Materials Science and Engineering, Wuhan University of Technology, Wuhan 430070, P. R. China
chenw@whut.edu.cn*

Ferroelectric memory is currently regarded as one of the most promising candidate technologies for the future universal memories, due to its advantages including non-volatile, fast read/write speed, high endurance, low power consumption, etc. The high cost and the low data storage density are the main challenges in extensive applications of ferroelectric memories [1]. To develop ferroelectric memories with higher storage densities, multistate ferroelectric memory has attracted great research interests in recent years [2-4]. To date, most of the proposed concepts of multistate ferroelectric memory are involved with complex fabrication techniques. To meet with the low cost requirement, more facile ways to multistate ferroelectric memory are still remained to be explored.

Herein, we demonstrate the tristate ferroelectric memory effect in $\text{Bi}_{1/2}\text{Na}_{1/2}\text{TiO}_3$ (BNT)-based relaxor ferroelectrics. This tristate ferroelectric memory effect utilizes the presence of relaxor state, which serves as an intermediate polarization state between the two ferroelectric remanent states with opposite polarization directions. This is an inherent nature of some modified BNT-based materials, and therefore no complex fabrication techniques are required. We show that this tristate ferroelectric memory effect can be realized in conventionally sintered ceramics. To experimentally verified the tristate ferroelectric effect, the ferroelectric behavior of $\text{Bi}_{1/2}(\text{Na}_{0.8}\text{K}_{0.2})_{1/2}\text{TiO}_3$ (the MPB composition) ceramics is elaborately tailored by Fe, Nb co-doping. Ceramic sample in composition of $\text{Bi}_{1/2}(\text{Na}_{0.8}\text{K}_{0.2})_{1/2}(\text{Ti}_{0.955}\text{Fe}_{0.030}\text{Nb}_{0.015})\text{O}_3$ (BNKTFN) exhibits a slightly pinched P - E hysteresis loop with an obviously non-zero remanent polarization, which is the desired ferroelectric behavior for the tristate ferroelectric memory effect. A “write/read” experiment is performed on the BNKTFN ceramic sample. Results show that the tristate ferroelectric memory can be operated as proposed, and the programmability and retention ability are fairly good. We also propose a phenomenological model for the unique ferroelectric behavior of BNKTFN. This model successfully predicts the polarization change during the write/read operations, and therefore is thought to be useful in the future device design. This study provides a new potential facile way to the multistate ferroelectric memory technology.

1. V. Garcia, M. Bibes, *Nature* **483**, 279 (2012).
2. A.K. Tripathi, A.J.J.M. van Breemen, J. Shen, et al., *Adv. Mater.* **23**, 4146 (2011).
3. D. Lee, S.M. Yang, T.H. Kim, et al., *Adv. Mater.* **24**, 402 (2012).
4. J.H. Lee, K. Chu, K.-E. Kim, et al., *Phys. Rev. B* **93** 115142 (2016).

Structural phase transitions in elpasolite-like fluorides comprising rare earth elements – Raman scattering study

A.N. Vtyurin^{1,2}, A.S. Krylov¹, V.N. Voronov¹, A.S. Oreshonkov¹, S.N. Krylova¹

¹*Kirensky Institute of Physics, Federal Research Center KSC SB RAS, 660036, Krasnoyarsk, Russia*

²*Institute of Engineering Physics and RadioElectronics, Siberian Federal University, 660079, Krasnoyarsk, Russia*
vtyurin@iph.krasn.ru

Crystals of elpasolite-like fluorides A_2BReF_6 (space group of the high symmetry phase is $Fm\bar{3}m$, $Z = 4$) belong to a wide family of perovskites studied intensively for decades. Such interest to fluorides is due to numerous phases and phase transitions observed in this family [1] as well as their perspective applications: normally their transparency window is much wider than that of more traditional oxides while their spectral properties may be varied easily by partial or complete substitution of rare earth ions Re^{3+} .

Most of phase transitions in perovskite-like crystals are induced by displacements of a central ion in ReX_6 octahedrons or by rotations of these octahedrons due to soft phonon modes condensations. Such condensations have been found many times in chlorine-, bromine- and oxygen-containing elpasolites (see, e.g., [2-4]), but only occasionally in fluorides [5]. Here we present Raman scattering investigations of lattice dynamics in several fluorides with elpasolite structures.

Samples have been synthesized from melt as described in [5,6] and cut along crystallographic axes of the cubic phase. Raman spectra have been obtained with Jobin Yvon – Horiba T-64000 spectrometer and Ar^+ laser (514.5 nm, 50 mW), CCD detection with liquid nitrogen cooling, 600 s accumulation time. To interpret results empirical simulations with LADY software and first principle VASP were performed.

High temperature phase of all studied crystals is cubic, and no indications of lattice disorder were found; observed temperature dependences of phonon damping correspond to normal anharmonic decay. Cooling down and shortening of interionic distances result in lowering of the low frequency phonon dispersive branch in $\Gamma-X$ direction and instability of the cubic phase. Eigenvectors of this branch in the cubic phase correspond to rotations of ReX_6 octahedrons, while in the lower temperature monoclinic phase they mix with cations displacements. In crystals with relatively lightweight rare earth ions (Sc, In) temperature dependences of higher frequency phonons correspond to phase transitions of the first order, closer to the second one, while in crystals with heavier ions (Ho, Dy) this intermodal interaction becomes stronger and their cubic phase transforms into the monoclinic one directly by the first order phase transition. In contrast to “classical” soft mode restorations we observed in these crystals strong interactions of main and secondary order parameters fluctuations that reduce the range of the intermediate tetragonal phase for heavier rare earth ions.

1. K.S. Aleksandrov, B.A. Beznosikov, *Perovskite-Like Crystals. Novosibirsk: Nauka*, 320 (1997).
2. W. Buhrer, H. U. Gudel, *J. J. Phys. C*. **20**, 3809 (1987).
3. F. Prokert, K. Aleksandrov, *Phys. Stat. Sol.* **b24**, 503 (1984).
4. G. Baldinozzi, Ph. Sciau, A. Bulou *J. Phys. Condens. Matter*. **7**, 8109 (1995).
5. A.N. Vtyurin, A. Bulou, A.S. Krylov, et. al. *Solid Stat. Phys.* **43**, 2066 (2001).
6. I.N. Flerov, M.V. Gorev, S.V. Melnikova et. al. *Solid Stat. Phys.* **34**, 3493 (1992).

Fabrication and dielectric properties of BaTi_{0.96}Ca_{0.04}O_{2.96}–BiZn_{0.5}Ti_{0.5}O₃ X9R BaTiO₃ based ceramics

Ch. Chen, H. Hao, Ch. Li, Y. Yang, Zh. Yao, M. Cao, H. Liu

*State Key Laboratory of Advanced Technology for Materials Synthesis and Processing, School of Material Science and Engineering, Wuhan University of Technology, Wuhan 430070, Hubei, P. R. China
haohua@whut.edu.cn*

In recent decades, BaTiO₃ (BT) has been the most successfully commercialized dielectric material for XnR (n=7,8,9) capacitors satisfying the capacitance variation below $\pm 15\%$ over temperature ranges of $-55\text{ }^{\circ}\text{C} \sim 125\text{ }^{\circ}\text{C}$, $150\text{ }^{\circ}\text{C}$, $200\text{ }^{\circ}\text{C}$, respectively. Many efforts have been made to optimize the dielectric properties of BT, such as forming solid solution with BiMeO₃, which is relaxor with diffused dielectric peaks and exhibits a plateau ε - T curve above T_m .

In this work, BaTi_{1-x}Ca_xO_{3-x} (BTC100x) ceramics were synthesized via solid-state reaction method, where the Ca substituting Ti site was confirmed by the XRD, TEM analyses and (Vienna Ab-initio Simulation Package) VASP calculation. The BTC4 ceramics exhibited enhanced dielectric constant at low temperature, as shown in Figure 1, which may greatly improve the dielectric constant stability at lower temperature when forming solid solutions with BiZn_{0.5}Ti_{0.5}O₃(BZT) end member. The phase structures, microstructures and dielectric properties of (1-y)BTC4-yBZT ceramics were systematically investigated. The pseudocubic perovskite structure was formed in (1-y)BTC4-yBZT ceramics, the solubility limit of which was around 0.13~0.15. The simultaneous incorporation of Bi³⁺ and Zn²⁺ to occupy A and B sites in the BTC4 lattice induced diffused phase transition which greatly improved dielectric temperature stability over a wide temperature range, as depicted in Figure 2. Of particular significance is that the 0.85BTC4-0.15BZT ceramic is found to exhibit flat dielectric behavior with capacitance variation being less than $\pm 15\%$ over the temperature range of $-55\text{ }^{\circ}\text{C}$ to $200\text{ }^{\circ}\text{C}$, which meets the requirement of X9R capacitor specification.

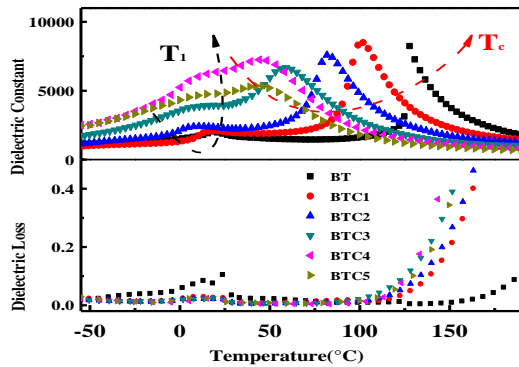


Figure 1. The plot of dielectric constant as the function of temperature of BTC100x ceramics.

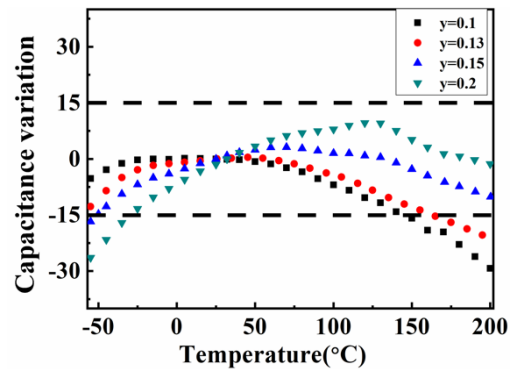


Figure 2. Capacitance variation as a function of temperature for (1-y)BTC4-yBZT ceramics.

1. H. Kishi, Y. Mizuno, H. Chazono, *Japanese J. Appl. Phys.* **42**, 1-15 (2003).
2. B. Xiong, H. Hao, S. Zhang, H. Liu, M. Cao, *J. American Ceram. Soc.* **94**, 3412 (2011).
3. Y.Y. Lu, H. Hao, S. Zhang, et al, *J. European Ceram. Soc.* **37**, 123-128 (2017).
4. L. Zhang, O.P. Thakur, A. Feteira, et al, *Appl. Phys. Lett.* **90**, 142914 (2007).

Integrated magnetoelectric devices based on interfacial magnetoelectric coupling effects

Zh. Hu, J. Wu, Zh. Wang, Z. Zhou, M. Liu

Electronic Materials Research Laboratory, Key Laboratory of the Ministry of Education & International Center for Dielectric Research, School of Electronic and Information Engineering, Xi'an Jiaotong University, Xi'an 710049, China
zhongqianghu@xjtu.edu.cn, mingliu@xjtu.edu.cn

Magnetic properties such as magnetic anisotropy, ferromagnetic resonance, and exchange bias, have been electrically manipulated via magnetoelectric coupling effects, which enable promising applications in electrically tunable magnetic devices. However, these electric field control processes are usually confined at large scale in bulk materials, and the integration of these magnetoelectric materials with semiconductor process in practical devices is still challenging. The interfacial magnetoelectric coupling effects have been reported in thin film heterostructures, which are compatible with the micro-electro-mechanical systems (MEMS) processes. In this work, we design several integrated magnetoelectric devices including tunable magnetic sensors and microwave signal processors, based on the interfacial magnetoelectric coupling effects. High sensitivity and large tunability can be realized with a circuit operation voltage. More importantly, these magnetoelectric devices can be integrated onto flexible substrates for wearable electronics. Our work paves the way toward ultrafast, compact, and power efficient spintronic/electronic devices based on interfacial magnetoelectric coupling.

Superfast domain wall motion and growth of dendrite domains in ferroelectrics. Analogy with crystal growth

V.Ya. Shur, A.R. Akhmatkhanov, A.A. Esin, M.A. Chuvakova

School of Natural Sciences and Mathematics, Ural Federal University, Ekaterinburg, Russia
vladimir.shur@urfu.ru

The experimental study of the formation and growth of dendrite domains and superfast shape transformation of the concave polygonal domain after merging to the convex one in uniaxial ferroelectric will be presented and described. The obtained effects will be considered using analogy between kinetics of ferroelectric domains and crystal growth.

The evolution of the isolated ferroelectric domains during polarization reversal in uniform electric field was studied in congruent lithium niobate LiNbO₃ (CLN) single crystals by *in situ* optical imaging with high temporal resolution. The static domain patterns were imaged at the crystal surface by scanning electron microscopy and in the crystal bulk by confocal Raman microscopy and Cherenkov-type second harmonic generation. Various domain shapes including regular convex polygons, stars and dendrites have been obtained for switching in temperature range and in the samples with artificial dielectric layer.

The growth of dendrite domains has been obtained at the elevated temperatures (above 220 °C) in the plates covered by artificial dielectric layer [3]. The field dependence of the dendrite envelope was revealed. The topological instability leading to appearance of the dendrite shapes was attributed to dominating of the stochastic nucleation in CLN at elevated temperatures [1, 2].

The kinetic approach to domain growth based on generation of steps (pairs of kinks) and motion of kinks along the wall has been applied [4]. It was proposed that the step generation rate and kink motion velocity are determined by the excess of the local value of the sum of the external field and residual depolarization field over the threshold value.

The domain shape change due to screening retardation and formation of the trail of residual charges was demonstrated by computer simulation [4]. It was shown that the determined step generation at the polygonal domain vertices and anisotropic kink motion dominated at temperatures below 200 °C, whereas the stochastic generation is observed at the temperatures above 200 °C. The convex hexagon domain shapes have been observed for effective screening of depolarization field, whereas the irregular polygons and stars screening retardation leads to the.

The first detail experimental study of the transformation of the concave polygonal domain appeared after merging to the convex one, named as “shape stability effect”, has been realized [5]. The convex growth of hexagonal domains was governed by the slowest domain walls, while the concave growth after domain merging – by superfast walls with three orders of magnitude higher velocity. The analysis of convex and concave domain growth allows reconstructing experimentally the v -plot (kinetic Wulff plot) for domain wall motion [6].

The equipment of the Ural Center for Shared Use “Modern nanotechnology” Ural Federal University was used. The research was made possible by Russian Science Foundation (Project № 19-12-00210).

1. V.Ya. Shur, A.R. Akhmatkhanov, *Phil. Trans. R. Soc. A* **376**, 20170204 (2018).
2. V.Ya. Shur, D.S. Chezganov, M.S. Nebogatikov, I.S. Baturin, M.M. Neradovskiy, *J. Appl. Phys.* **112**, 104113 (2012).
3. V.Ya. Shur, M.S. Kosobokov, E.A. Mingaliev, D.K. Kuznetsov, P.S. Zelenovskiy, *J. Appl. Phys.* **119**, 144101 (2016).
4. V.Ya. Shur, *J. Mater. Sci.* **41**, 199 (2006).
5. V.Ya. Shur, A.I. Lobov, A.G. Shur, E.L. Rumyantsev, K. Gallo, *Ferroelectrics* **360**, 111 (2007).
6. A.A. Esin, A.R. Akhmatkhanov, V.Ya. Shur, *Appl. Phys. Lett.* **114**, 192902 (2019).

AFM domain patterning in structurally disordered ferroelectric crystals

T.R. Volk¹, R.V. Gainutdinov¹, Ya.V. Bodnarchuk¹, Xiaoyong Wei², Xin Liu²

¹*Shubnikov Institute of Crystallography of FSRC “Crystallography and Photonics” RAS, Moscow, Russia
Volk-1234@yandex.ru*

²*Electronic Materials Research Laboratory, Key Laboratory of the Ministry of Education & International Center for Dielectric Research, Xi’an Jiaotong University, 710049, Xi’an, China*

At present, crystals of the solid solutions $\text{Pb}(\text{Mg}_{1/3}\text{Nb}_{2/3})\text{O}_3 - x\text{PbTiO}_3$ (PMN- x PT) are under intensive investigations due to their excellent piezoelectric characteristics. Studies in the domain engineering are of importance for an insight into contribution from the domain formation and resulting domain-wall density to the piezoelectric coefficients.

We present the results of domain writing by dc AFM-tip voltages in the tetragonal PMN-0.4PT crystals.

The application of AFM domain patterning is known to be restricted by the formation of so-called “anomalous” domains [1-3]. Recall, in the “anomalous” domains, observed for the first time in BaTiO_3 [1] and found later in various ferroelectrics (for refs see [3]) a small central area is polarized oppositely to the poling field. According to the currently accepted model [2, 3], this anomalous switching is caused by the charge carrier injection from the tip and subsequent formation of a space-charge field E_{sc} directed oppositely to the poling field.

We analyzed the problem of anomalous domains on the example of PMN-PT crystals [4].

Two types of domain were formed in these crystals under AFM-tip voltages. The occurring anomalous ones and “normal” (uniformly polarized along the poling field) ones are presented in Figure 1 (the upper and lower images, respectively). The domain shape is distributed randomly over the surface and is non-reproducible even for the identical exposure conditions (as exemplified by Fig. 1)

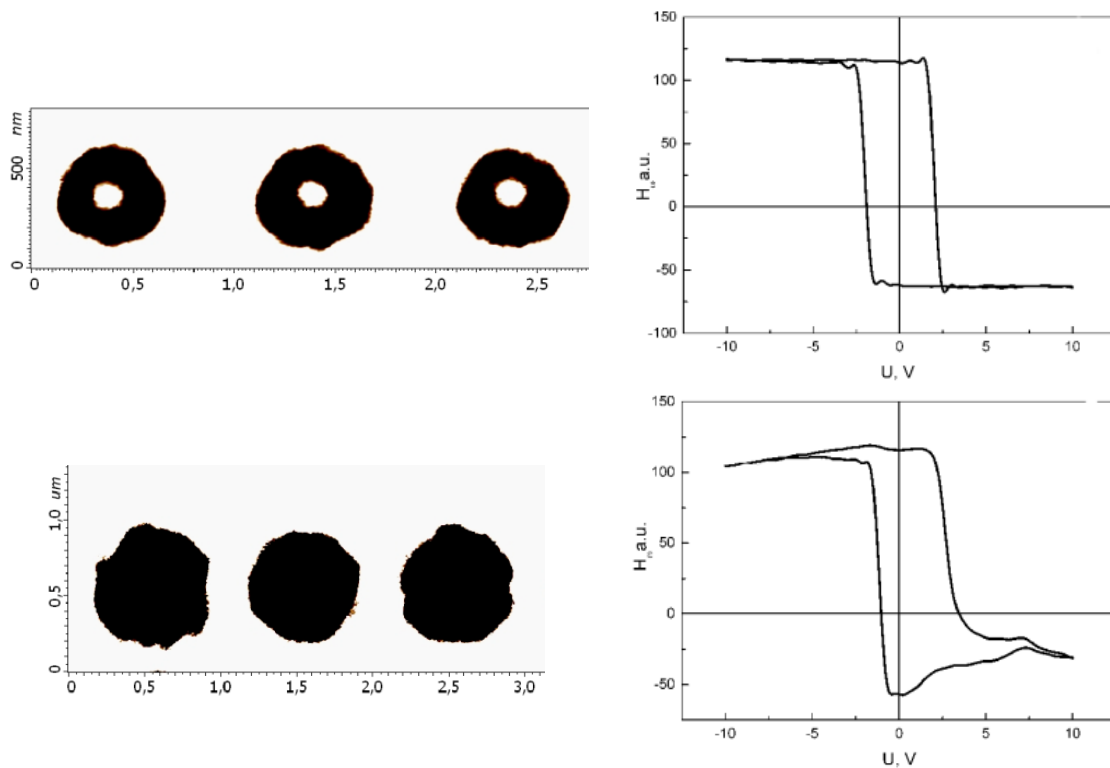


Figure 1. On the left: PFM images of the domain rows written at identical exposure conditions ($U_{tip} = 50$ V, $t_p = 100$ ms) in two closely spaced surface regions; the anomalous (upper) or normal (lower) domains arise.

On the right: the local piezoelectric hysteresis loops measured in these regions; the normal domains occur in the regions showing strongly biased loops (the higher bias voltage U_b); the anomalous domains are characteristic for the regions with lower U_b .

The domain shape was found to correlate with the local piezoelectric hysteresis loops $H_\omega-U_{tip}$. Namely, the larger is the local bias voltage U_b , the higher is the tip voltage U_{tip} at which the anomalous domains appear. In the case that the loop is strongly biased (the lower loop), the formed domains are normal. In the framework of the injection model [2, 3] this means that the necessary condition of the anomalous domain formation is $E_{sc} > E_b$ (where E_{sc} is the local space charge field under a tip, caused by the charge injection, and E_b is the local bias field). This conclusion was confirmed in other disordered ferroelectrics.

The relaxation kinetics of anomalous domains depends on the exposure conditions; the domains written by high U_{tip} are completely stable in a qualitative agreement with the model [2, 3]. The normal domains are decaying significantly faster than the anomalous ones, the decay kinetics depending on the domain spacing

The exposure characteristics of the domain diameter D are independent of the domain shape, i.e. being identical for the normal and anomalous domains. For a given t_p , $D(U_{tip})$ is described by a unified linear function in the whole U_{tip} range. The curves $D(t_p)$ follow a power law $D \sim t_p^k$ with the exponent k very weakly varying with U_{tip} .

1. M. Abplanalp, J. Fousek, P. Gunter, *Phys. Rev. Lett.* **86** 5799 (2001).
2. S. Buhlmann, E. Colla, P. Muralt, *Phys. Rev. B* **72**, 214120 (2005).
3. A.L. Kholkin, I.K. Bdikin, V.V. Shvartsman, et al., *Nanotechnology* **18**, 095502 (2007).
4. V. Gainutdinov, Ya.V. Bodnarchuk, T.R. Volk, et al., *J. Appl. Phys.* (2019) in press.

Atomic force microscopy of layer-doped triglycine sulfate ferroelectric crystals

R.V. Gainutdinov¹, A.L. Tolstikhina¹, A.K. Lashkova¹, B.S. Roshchin¹,
D.A. Zolotov¹, V.E. Asadchikov¹, V.N. Shut², I.F. Kashevich³, S.E. Mozzharov²

¹FSRC "Crystallography and Photonics" of Russian Academy of Sciences, 119333, Moscow, Russia
radmir@crys.ras.ru

²Institute of Technical Acoustics, National Academy of Sciences of Belarus, 210027, Vitebsk, Belarus

³Vitebsk State University, 210032, Vitebsk, Belarus

Despite the long history of the study, ferroelectric crystals of triglycine sulfate $(\text{N}^+\text{H}_3\text{CH}_2\text{COOH})_2(\text{N}^+\text{H}_3\text{CH}_2\text{COO}^-)\text{SO}_4^{2-}$ (TGS) continue to attract the attention of researchers both as model objects and as potential materials for IR detectors, piezoelectric sensors, pyrovidicones, etc. The introduction of impurities makes it possible to modify effectively the properties of TGS. Thus, chromium (interstitial impurity), although slightly distorts the lattice, but affects significantly the physical properties of crystal. An additional tool for influencing the properties of TGS is the regularly inhomogeneous introduction of Cr^{3+} impurity into the growing crystal by periodically changing the composition of crystallization solution. In this way, the periodic growth structure of alternating stripes of TGS and TGS+Cr with different density of domain walls (impurity layers are characterized by a specific finely dispersed domain structure) and presumably possessing different conductivity is formed. Striped crystals TGS – TGS+Cr are distinguished by high unipolarity and stability of ferroelectric characteristics.

In this work domain structure and impurity distribution in TGS – TGS+Cr crystals was studied with different electrical AFM methods: microscopy of piezoelectric response (PFM), scanning capacitance force microscopy (SCFM), Kelvin probe force microscopy (KPFM), conducting AFM (c-AFM). Also, the nanorelief and mechanical properties of crystals with AFM. The search of new opportunities for local diagnostics of the domain and defect structure of ferroelectrics determined our interest to the work. Also the crystals were studied with X-ray fluorescence (XRF) analysis method, since it provides complete and reliable information about the elemental composition of heterogeneous samples.

The object of study was triglycine sulfate single crystals with a profile distribution of chromium ion impurities (Cr^{3+}) obtained at the Institute of Technical Acoustics. The crystals were grown by a velocity method at a constant growth temperature of 31.4 °C (Curie temperature of TGS = 49.15 °C), the supersaturation of the pure solution was 0.1 °C, the solution with an admixture was 0.5 °C. A periodic change in composition was achieved by incrementing the seed alternately in solutions of different composition – in a nominally pure and containing dopant of chromium ions. The concentration of chromium in the solution was in the range 5-6 wt.%. The growth time of the seed in one cycle was 1.5 hours in a clean solution, and 4.5 hours in an impurity solution.

For AFM investigations samples (1.5-2 mm thick) were obtained by fresh cleavage along the (010) plane, for which the bars with the major axis parallel to the ferroelectric axis b were cut from the growth pyramid of the face m. All experiments on the preparation and precision study of the surface of samples were carried out under strictly controlled conditions of the TRACKPORE ROOM-05 measuring complex, a class of purity of 5 ISO (100) with a humidity of 35 ± 1 rel.% and temperature of 24 ± 0.05 °C, which is especially important in the study of the electrical characteristics of ferroelectrics, the results of which can be significantly affected by water adsorbed on the surface of the sample. The crystals were investigated with NTEGRA Prima scanning probe microscope (NT-MDT SI) using Si tip with Pt coating HA_FM/Pt (Tipsnano, Estonia). Tip curvature radius was $R = 35$ nm; the cantilever stiffness $k \sim 3.5$ N/m, and resonance frequency $f \sim 77$ kHz.

For X-Ray Fluorescence Analysis the TGS – TGS+Cr crystal sample was installed in a DRSh diffractometer. The sample was mounted on an adjusting table so as to make the growth strips lie in the horizontal plane along the incident X-ray beam. The size of the sample surface area exposed to the beam was ~ 150 μm in the vertical direction and ~ 5 mm in the horizontal direction.

Then the fluorescent detector was tuned to measure the intensity of the $K\alpha$ chromium line, and the dependence of the intensity on the vertical sample position, i.e., the position of the area exposed to the X-ray beam at the side crystal face, was recorded. The sample displacement step was ~ 0.1 mm, and the measurement range was from 0 to 6.5 mm. Simultaneously, the intensity I of the radiation transmitted through the crystal and falling onto a scintillation detector was determined as a function of the exposed spot position on the sample.

While PFM (Fig. 1a) and KPFM (Fig. 1c) allows to observe only domain structure in SCM contrast (Fig. 1b) are formed both on domain walls and on impurity bands. It was shown that the capacitance image contrast is formed in the impurity gradient regions, on domain walls. The SCM technique, which is based on measuring the capacitance spatial variation and is highly sensitive to the presence of impurities, allowed us to observe growth impurity strips in the ferroelectric crystal independent of the domain structure and establish a correlation between the defect and domain structures. The SCM technique was shown to be a promising tool for studying the heterogeneous ferroelectric surface, which makes it possible to detect simultaneously images from impurity gradient regions and domain walls and gain insight into the correlation between the domain and defect structures.

XRF analysis was used for the first time to analyze quantitatively the composition of ferroelectric TGS crystals with growth impurity strips. This technique allowed us to determine with a high accuracy the Cr concentration in strips and reveal a periodic impurity distribution. The difference between the chromium concentrations in pure and impurity strips was found to be ~ 0.08 wt.%, which yielded a difference of 0.17% between the capacitance image contrasts.

This work was supported by the Ministry of Science and Higher Education within the State assignment FSRC «Crystallography and Photonics» RAS.

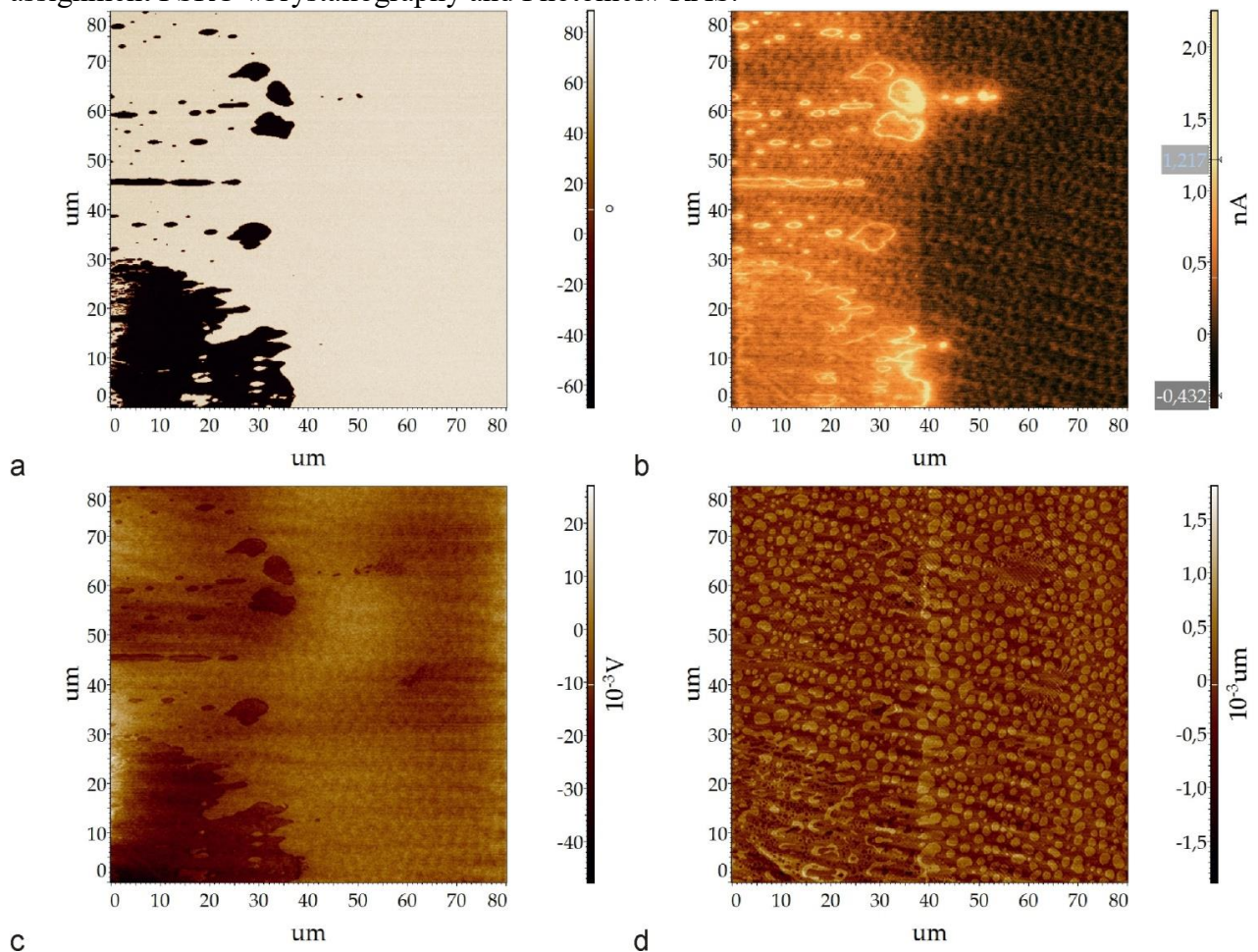


Figure 1. The image of the same surface area of TGS-TGS + Cr crystal with the TGS + Cr stripe (left) and TGS (right): (a) PFM, (b) SCM, (c) KPFM, (d) AFM contact mode, topographic image. The size is $100 \times 100 \mu\text{m}$.

Enhanced coupling of electromagnons in Nd-doped BiFeO₃ nanoparticles near morphotropic phase boundaries

J. Wang, Y. Zhang

*School of Materials Science and Engineering, Xiangtan University, Xiangtan 411105, Hunan, P. R. China
jbwang@xtu.edu.cn*

Multiferroics, displaying multiple ferroic orders, have pushed the development of advanced electrically and magnetically controlled applications in recent years, owing to their strong magnetoelectric (ME) coupling [1, 2]. As the apparent consequence of dynamic ME effects, the electromagnons have been widely investigated. The electromagnons are considered as the origin of the giant magnetodielectric and magnetocapacitance effects, and their coupling strength also directly relates to the magnitude of these effects [3, 4]. Therefore, in this work, the electromagnons of Bi_{1-x}Nd_xFeO₃ ($x = 0\sim 0.2$) are studied by terahertz time-domain spectroscopy, and the effects of doping concentrations on electromagnons are discussed. The results show that the Bi_{1-x}Nd_xFeO₃ exhibits phase change mediated electromagnon effects. The coupling weight is gradually increased at polar *R3c* structures and then come down at antipolar *Pbam* phase, where the weight at antipolar phase is less than that of pure *R3c* phase. Interestingly, the colossal coupling of electromagnons is observed at the polar-antipolar and antiferromagnetic-ferromagnetic phase boundaries. Our work offers an avenue for designing and choosing materials with better performances of magnetodielectric and magnetocapacitance.

1. W. Eerenstein, N.D. Mathur, J.F. Scott, *Nature* **442**, 759 (2006).
2. T. Kimura, T. Goto, H. Shintani, K. Ishizaka, T. Arima, Y. Tokura, *Nature* **426**, 55 (2003);
M.P.V. Stenberg, R. de Sousa, *Phys. Rev. B* **80**, 094419 (2009).
3. M. Cazayous, Y. Gallais, A. Sacuto, R. de Sousa, D. Lebeugle, D. Colson, *Phys. Rev. Lett.* **101**, 037601 (2008).
4. A.B. Sushkov, R.V. Aguilar, S. Park, S.W. Cheong, H.D. Drew, *Phys. Rev. Lett.* **98**, 027202 (2007).

Investigation of phase transitions in multiferroics $\text{HoFe}_{3-x}\text{Ga}_x(\text{BO}_3)_4$ and $\text{TbFe}_{3-x}\text{Ga}_x(\text{BO}_3)_4$ solid solution with huntite structure

A. Krylov^{1,*}, E. Moshkina¹, I. Gudim¹, S. Krylova¹, A. Vtyurin^{1,2}

¹Kirensky Institute of Physics FRC KSC SB RAS, Krasnoyarsk, Russia

²Siberian Federal University, 660041 Krasnoyarsk, Russia
shusy@iph.krasn.ru

Crystals of the $\text{RFe}_3(\text{BO}_3)_4$ family with a structure like natural mineral huntite were reported to possess multiferroic features, demonstrating both structural and magnetic phase transitions [1-3], where transition points may be varied by substituting as rare earth element as a magnetic ion. We present the Raman spectroscopy result of the investigation of single crystals and a solid solution of $\text{HoFe}_{3-x}\text{Ga}_x(\text{BO}_3)_4$ and $\text{TbFe}_{3-x}\text{Ga}_x(\text{BO}_3)_4$.

Temperature measurements were performed in the temperature range 10-400 K. This study aims to investigate the possible existence of a soft mode related to structural order parameter and effects of magnetic transitions on Raman spectra. Analysis of the experimental Raman spectra, temperature dependences of the provisions of the centers of lines, their width and relative intensity was carried out, as well as theoretical temperature approximation for some lines. Some anomalies in the temperature dependences of the spectral lines associated with the occurrence of magnetic order. It was found that significant changes are observed in the spectrum of low-frequency range (below 100 cm^{-1}) – there is a mode corresponding to two-magnon scattering. The structural phase transition accompanied condensation of soft mode (Fig. 1).

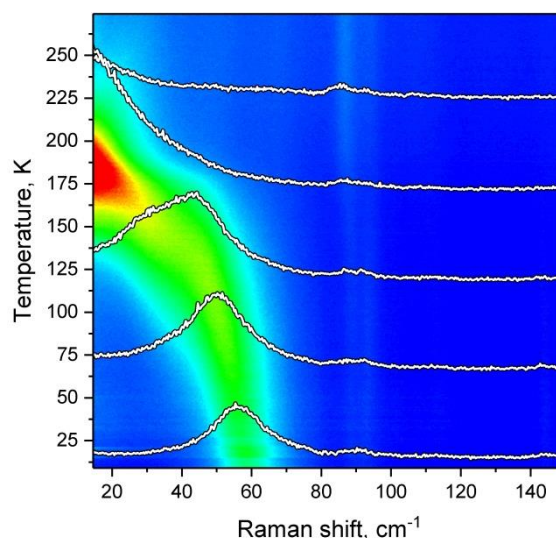


Figure 1. Raman intensity map and spectra transformation of soft mode condensation at $\text{HoFe}_2\text{Ga}(\text{BO}_3)_4$.

The phase diagram Temperature – Composition has been acquired for $\text{HoFe}_x\text{Ga}_{3-x}(\text{BO}_3)_4$ solid solution. Structural transitions manifest clearly by soft mode restoration, and abnormal changes of line position indicate a temperature of magnetic ordering.

The most promising composition for future extensive investigation is $\text{TbFe}_{2.5}\text{Ga}_{0.5}(\text{BO}_3)_4$. This solid solution has magnetic and structural phase transition below 45 K. The strong coupling between these the two ferroic orders expected.

RFBR funded the reported study according to the research project № 18-02-00754.

1. A.S. Krylov et al. *Solid State Commun.* **174**, 26 (2013).
2. E. Moshkina et al. *Cryst. Growth. Des.* **16**, 6915 (2016).
3. A.S. Krylov et al. *Journal of Advanced Dielectrics* **8**, 1850011 (2018).

Flexible piezoelectric ultrasonic energy harvester array using KNN-based lead free composite

L. Jiang^{1,2}, J. Zhu^{1,*}, Q. Zhou^{2,*}

¹College of Materials Science and Engineering, Sichuan University, Chengdu 610064, China

²Roski Eye Institute, Keck School of Medicine, University of Southern California, Los Angeles, CA 90033, USA

*nic0400@scu.edu.cn; qifazhou@usc.edu

Potassium sodium niobate (K,Na)NbO₃(KNN) lead-free ceramics have drawn vast amount of attention as one of the effective alternatives to lead-based ones. This talk reviews the main obtained results [1-3] in authors laboratory on how to enhance the piezoelectric properties of KNN-based ceramics, including the ions or compounds substitution, the constructing and types of phase boundaries near room temperature, the investigation of other tools (sintering aids, synthesis technique, poling conditions) on properties. A flexible piezoelectric ultrasonic energy harvester (PUEH) array was designed and fabricated by integrating a large number of piezoelectric active elements with multilayered flexible electrodes in an elastomer membrane. The developed flexible PUEH device can be driven by the ultrasonic wave to produce continuous voltage and current outputs on both planar and curved surfaces, reaching output signals of more than 2 V_{pp} and 4 μA, respectively. Potential applications of using the flexible PUEH to charge energy storage devices and power commercial electronics were demonstrated.

1. J. Xing, T. Zheng, J. Wu, D. Xiao, J. Zhu, *J. Adv. Dielectr.* **8**, 1830003 (2018).
2. T. Zheng, J. Wu, D. Xiao, J. Zhu, *Progress in Materials Science*, **98**, 552 (2018).
3. K. Xu, J. Li, X. Lv, et al., *Adv. Mater.* **28**, 8519 (2016).
4. L. Jiang, Y. Yang, R. Chen, et al., *Nano Energy* **56**, 216 (2019).

Structure, ferroelectric and local piezoelectric properties of KNN- based perovskite ceramics

E.D. Politova¹, G.M. Kaleva¹, A.V. Mosunov¹, N.V. Sadovskaya¹, D.A. Kiselev²,
A.M. Kislyuk², S.Yu. Stefanovich^{1,3}, P.K. Panda⁴

¹*L.Ya.Karpov Institute of Physical Chemistry, Moscow 105064 Russia, politova@nifhi.ru*

²*National University of Science and Technology "MISiS", Moscow 119991 Russia,*

³*Lomonosov Moscow State University, Moscow 119992 Russia,*

⁴*National Aerospace Laboratories, Kodihalli, Bangalore-560017 India*

Lead-free ferroelectric materials continue to be intensively studied in order to replace widely used lead-based ones [1-4]. We studied influence of cation substitutions and preparation conditions on structure, microstructure, ferroelectric, and local piezoelectric properties of solid solutions in the systems on the base of sodium-potassium niobate ($\text{K}_{0.5}\text{Na}_{0.5}\text{NbO}_3$ (KNN) with perovskite structure [5-7].

Ceramic samples in the KNN-based systems were prepared by the two-step solid-state reaction method at temperatures of 900-1500 K. Solid solutions with Ba^{2+} , Li^+ , Ca^+ in A- and with Cu^{2+} , Mn^{3+} , Ni^{2+} , Fe^{3+} cations in B-sites of perovskite lattice were prepared. To improve density of ceramics overstoichiometric additives (KCl, LiF and ZnO) were used.

To characterize the samples, complex of physico-chemical methods was used: the X-ray Diffraction, Scanning Electron Microscopy (SEM), Second Harmonic Generation (SHG), Dielectric Spectroscopy (DS), and Atomic Force Microscopy in Piezoresponse Force Mode (PFM) methods.

The observed unit cell volume changes in modified KNN-based ceramics depended on ionic radii of substituting cations. Mean size of grains changed from ~3 till ~20 μm in compositions containing low melting additives KCl and LiF. Ferroelectric phase transitions at ~400 and near 700 K were confirmed using the DS and SHG methods. At temperatures higher than ~900 K effects of dielectric relaxation caused by formation of oxygen vacancies were observed in ceramics with aliovalent substitutions.

Increase in the spontaneous polarization value while non monotonous changes in dielectric permittivity values and were revealed for modified ceramics at the room temperature. Ferroelectric polarization switching at nanoscale was observed using PFM method, and in KNN-based ceramics high values of effective d_{33} piezoelectric coefficient 200-300 pm/V reached. The results obtained confirm the statement of prospects of creating new lead-free materials on the base of modified KNN- based compositions.

Acknowledgment. The work was supported by the Russian Foundation for Basic Research (Projects 16-53-48009, 18-03-00372).

1. I. Coondoo, N. Panwar, A. Kholkin, *J. Adv. Dielectr.* **3**, 1330002 (2013).
2. P.K. Panda and B. Sahoo, *Ferroelectrics* **474**, 128 (2015).
3. D. Alikin, A. Turygin, A. Kholkin and V. Shur, *Materials* **10**, 47 (2017).
4. J. Rödel and J. Li, *MRS Bulletin* **43**, 576 (2018).
5. E.D. Politova, G.M. Kaleva, N.V. Golubko, et al., *Ferroelectrics* **489**, 147 (2015).
6. E.D. Politova, E.A. Fortalnova, M.G. Safronenko, et al., *Ferroelectrics* **518**, 109 (2017).
7. E.D. Politova, N.V. Golubko, G.M. Kaleva, et al., *J. Adv. Diel.* **8**, 1850004 (2018).

Strain and structural evolution in lead-free NBT-based piezoceramics

X. Liu, B. Shen, J. Zhai*

School of Materials Science & Engineering, Tongji University, 4800 Caoan Road, Shanghai, China

High-performance $(\text{Na}_{0.5}\text{Bi}_{0.5})\text{TiO}_3$ (NBT) lead-free incipient ceramics are promising piezoactuator materials, but the high driving field limits their practical applications. Herein, we report a large piezostain (d_{33}^*) of 810 pm/V at a low field of 4 kV/mm in the $(0.94-x)(\text{Na}_{0.5}\text{Bi}_{0.5})\text{TiO}_3-0.06\text{Ba}(\text{Zr}_{0.05}\text{Ti}_{0.95})\text{O}_3-x(\text{Sr}_{0.8}\text{Bi}_{0.1}\text{Y}_{0.1})\text{TiO}_{2.95}$ solid solution with $x=0.05$ (SBT5). The dopant induces a randomly distributed local polarization field, which boosts the ferroelectric instability and favors a more disordered relaxor structure. The driving field is notably reduced compared with other NBT-based ceramics, while its strain maintains at a high level along with a high thermal stability. The high strain in SBT5 is due to a field-induced reversible relaxor-ferroelectric phase transformation, while the reduced driving field results from two synergistic effects: remanent quasi-ferroelectric order as the seed for the growth of polar domains helps the system skip nucleation process; the local defects further facilitate the growth of ferroelectric domains. The composition, temperature and electric-field dependence of structural evolutions were systematically elucidated from micro- and macroscopic view. This study opens up a feasible and effective way for achieving a giant electrostrain in lead-free actuator materials.

Tilt control of the charged domain walls in lithium niobate

A.R. Akhmatkhanov, A.A. Esin, V.Ya. Shur

School of Natural Sciences and Mathematics, Ural Federal University, 620000, Ekaterinburg, Russia
Andrey.Akhmatkhanov@urfu.ru

Precise control of the domain structure in ferroelectric single crystals is one of the most important and challenging tasks in physics of ferroelectrics. So far, main part of investigations in this area was aimed at realization of high efficiency nonlinear optical interactions, such as second harmonic generation (SHG) and optical parametric oscillation. These applications require precise spatial variation of the spontaneous polarization, which distribution within the crystal is determined by the positions and orientations of the domain walls (DWs). Recently, the scientific attention has turned from the domains to the DWs themselves: these movable unit-cell-thick interfaces were proposed as the building blocks for reconfigurable nanoelectronics devices, because their properties can differ drastically from the bulk parent material [1, 2]. In particular, it has been shown that conductivity of the charged domain walls (CDWs) in ferroelectrics is many orders of magnitude higher, than that in the single domain state [3]. The utilization of the CDW as nanoelectronics devices requires three technological aspects to be developed: (1) controllable creation, (2) geometry tuning, and (3) removal.

We present the experimental study of the CDW formation in congruent lithium niobate single crystals during polarization reversal using liquid and solid-state electrodes, as well as their combination [4]. It was shown that material of the electrode applied to the Z-polar surface is crucial. It was shown that CDW can be formed by two alternative procedures: (1) by forward switching for liquid electrode at Z+ polar surface and solid electrode – at Z- one, (2) by backward switching for solid electrode at Z+ polar surface and liquid electrode at Z- one. The obtained domain structure was investigated in the bulk of the crystal using scanning Cherenkov-type SHG microscopy [5]. For both used procedures the CDWs were formed when domains grew from Z+ polar surface covered by solid or liquid electrode towards Z- surface covered by solid electrode. Thus, existence of the solid electrode on Z- surface is the necessary condition for CDW formation. The created CDW can be transformed to almost neutral domain wall by application of the field pulse of the reverse polarity for both procedures. As a result, the tilt of the formed CDW can be tuned reversibly in the range from 0.2 to 1.2 degrees resulting in change between almost isolated and highly conductive states. When the tilt exceeded 1.2 degrees the CDW became jugged due to formation of additional spikes. For the second procedure the unusual partial backward switching during forward polarization reversal was revealed. Moreover, we have demonstrated that the created CDW can be used as a nanoelectronics channel for local electrolysis opening the additional possibilities for the ferroelectric lithography.

The equipment of the Ural Center for Shared Use “Modern nanotechnology” Ural Federal University was used. The research was made possible in part by RFBR (grant 18-32-00641_mol_a).

1. A. Crassous, T. Sluka, A.K. Tagantsev, N. Setter, *Nat. Nanotechnol.* **10**, 614 (2015).
2. P. Sharma, Q. Zhang, D. Sando, C.H. Lei, Y. Liu, J. Li, V. Nagarajan, J. Seidel, *Sci. Adv.* **3**, e1700512 (2017).
3. V.Ya. Shur, I.S. Baturin, A.R. Akhmatkhanov, D.S. Chezganov, A.A. Esin, *Appl. Phys. Lett.* **103**, 102905 (2013).
4. A.A. Esin, A.R. Akhmatkhanov, V.Ya. Shur, *Appl. Phys. Lett.* **9**, 092901 (2019).
5. Y. Sheng and A. Best, *Optics Express* **18**, 16 (2010).

Defects on the ferroelectric and photocatalytic properties of La³⁺ ions doped SrBi₂Nb₂O₉ materials

Q. Lou^{1,2}, J. Zeng¹, L. Zheng¹, Zh. Man¹, W. Wang³, A. Kassiba⁴,
C.H. Park⁵, E.D. Politova⁶, G. Li¹

¹Key Laboratory of Inorganic Functional Materials and Devices, Shanghai Institute of Ceramics, Chinese Academy of Sciences, 200050, Shanghai, China

²University of Chinese Academy of Sciences, 100049, Beijing, China

³State Key Laboratory of High Performance Ceramics and Superfine Microstructures, Shanghai Institute of Ceramics, Chinese Academy of Sciences, 200050, Shanghai, China

⁴Institute of Molecules and Materials, UMR6283-CNRS, 72000, Le Mans University, Le Mans, France

⁵Department of Physics Education, Pusan National University, 46241, Gumjung, Pusan, South Korea

⁶Karpov Institute of Physical Chemistry, 105064, Moscow, Russia

The effect of La doping on the efficiency of the photocatalysis of SrBi_{2-x}La_xNb₂O₉ ferroelectric powders and the ceramics synthesized by the solid state method is investigated. It is found that the photocatalysis efficiency is not always correlated to the polarization. As the content of La³⁺ ions increases, Raman spectra reveals that the La³⁺ ions prefer to occupy the Bi-sites in the Bi₂O₂ layers at a low doping content and they also replace Sr²⁺ in the A sites of the perovskite blocks (SrNb₂O₇) with further increasing La content. The leakage current decreases for the low La content x=0.02, but it increases significantly for higher x. The trend of the photocatalytic efficiency is correlated to the photocurrent and both are increased by the low La-doping of x=0.02, whereas they are decreased by the heavier doping of La, although the spontaneous polarization increases continuously with the La-doping. It is suggested that the role of the defects such as oxygen vacancy, Sr-vacancy, and various impurity states for the carrier transport plays the more important role than the spontaneous polarization in the heavily La-doped ferroelectric ceramics.

Tailoring quasi-two-dimensional high conductivity and superconductivity areas at the interfaces of ferroelectric/dielectric heterostructures

R.F. Mamin

*Zavoisky Physical-Technical Institute, FRC Kazan Scientific Center of RAS, 420029, Kazan, Russia
mamin@kfti.knc.ru*

The creation of quasi-two-dimensional electron gas at the interface and the ability to control such states by magnetic and electric fields is impossible without the use of new materials and without the development of new design interfaces. Unique properties of functional materials are achieved due to the effects associated with the complex composition of the interface structure. Such new materials include oxide heterointerfaces between two nonconducting oxides in which, owing to strong electronic correlations, unique transport properties are observed. A high-mobility electron gas was first observed in 2004 [1] at the interface of heterostructure LaAlO_3 (LAO) and SrTiO_3 (STO). Such heterointerfaces involving two insulating nonmagnetic oxides were comprehensively studied. In particular, it was found that the metallic phase (quasi-two-dimensional electron gas, 2DEG) is formed in the STO layers at the LAO/STO interface when the number of LAO layers is larger than three [2]. Such a system undergoes a transition to a superconducting state at temperatures below 300 mK [3].

We investigate the properties of 2DEG at the interface between ferroelectric oxide and insulating oxide in heterostructures, isostructural to $\text{BaTiO}_3/\text{LaMnO}_3$. The numerical simulations of the structural and electronic characteristics of the $\text{BaTiO}_3/\text{LaMnO}_3$ ferroelectric-antiferromagnet heterostructure have been performed. The temperature dependence of the electrical resistance has been studied for heterostructures formed by antiferromagnetic LaMnO_3 single crystals of different orientations with epitaxial films of ferroelectric $\text{Ba}_{0.8}\text{Sr}_{0.2}\text{TiO}_3$ (BSTO) deposited onto them. The measured electrical resistance is compared to that exhibited by LaMnO_3 (LMO) single crystals without the films. It is found that, in the samples with the film, for which the axis of polarization in the ferroelectric is directed along the perpendicular to the surface of the single crystal, the electrical resistance decreases significantly with temperature, exhibiting metallic behavior below 160 K [4]. The transition to the state with 2DEG at the interface is demonstrated. The effect of a magnetic field on heterostructure BSTO/LMO has been investigated. It is shown that magnetic field change the resistivity properties of the interface BSTO/LMO very strong. The new properties of the interfaces of some other heterostructure will have been presented.

The reported study was funded by Russian Scientific Foundation, research project No. 18-12-00260.

1. A. Ohtomo, and H. Hwang, *Nature* **427**, 6973 (2004).
2. S. Thiel, G. Hammerl, A. Schmehl, et al., *Science* **313**, 1942 (2006).
3. N. Reyren, S. Thiel, A.D. Caviglia, et al., *Science* **317**, 1196 (2007).
4. D. P. Pavlov, I.I. Piyanzina, V.I. Muhortov, et al., *JETP Letters* **106** (7), 440 (2017).

Lead-free piezoelectric low-dimension nanomaterials: controllable growth, performance optimization and exploration on micro energy harvesting devices

L. Jiang, Z. Wang, Y.M. Hu, J. Xiong, H.S. Gu

Hubei Key Laboratory of Ferro- & Piezo-electric Materials and Devices, Faculty of Physics and Electronic Sciences, Hubei University, 430062, Wuhan, P.R. China
guhsh@hubu.edu.cn

Since piezoelectric effect was first noticed by Curie brothers in 1880, piezoelectric materials have attracted a huge amount of attention of researchers in the worldwide. Piezoelectric effect enables the transformation from mechanical energy to electrical energy, which is able to collect the energy produced by human movements and be used to construct self-power wearable devices and pace-makers. To achieve this assumption, ZnO-based and PZT(Pb(Zr,Ti)O₃)-based piezoelectric nanogenerators were implanted in mice and cows respectively, both of which generate voltage signals from somatic movements. However, limitations still exist since ZnO possess relatively poor piezoelectric response, while PZT contains the toxic element lead. In contrast with these two materials, KNN((K,Na)NbO₃)-based materials have been the most promising materials in piezoelectric field because of their good biocompatibility, excellent performance and nontoxic character.

In recent years, more and more researches were reported as energy problem has been one urging challenge to resolve. However, most of these relative studies mainly focused on bulk materials such as ceramics, while several of them were associated with low-dimension materials such as nanorods, nanowires, and nanoparticles. In our study, KNN nanorod arrays were synthesized by hydrothermal method, and the influences of reaction time on sizes, morphology, phase and piezoelectric performance of nanorods were explored. Besides, axial and radial piezoelectric responses were tested with PFM mode of atomic force microscopy, the highest radial response d_{33} is 64 pm/v. Furtherly, performance optimization was achieved after annealing in oxygen atmosphere at high temperature, which results in passivating oxygen vacancies of the surface.

However, although piezoelectric response improved a lot via annealing, it is still hard to be comparable with lead-based materials while the highest axial response d_{33} was 360pm/V after annealing at 800°C. Scholars put up an idea to improve responses by constructing MPB (morphotropic phase boundary) at room temperature. Researches pointed out that doping KNN with lithium and tantalum can decrease T_{O-T} (orthorhombic-tetragonal temperature) to room temperature. In our study, KNN nanorods doped with lithium and tantalum were synthesized successfully on the STO(SrTiO₃) substrates, and effects of doping content on morphology, phase and piezoelectric responses of nanorods were studied. According to the results, the radial response can be as high as 83 pm/V, which authentically improved a lot compared with pure KNN.

After systematic researches on materials synthesizing, KNN nanogenerators were assembled on the base of KNN nanorod arrays, which could output a voltage signal as high as 10V while pressed by a human finger. Furtherly, micro energy harvesting under solid conditions, energy harvesting in microfluidics and applications in soft wearable devices were accomplished.

Raman opalescence and central peak scattering near phase transition point in crystals

V.S. Gorelik^{1,2}

¹*P.N. Lebedev Physical Institute of the Russian Academy of Sciences, 119991, Moscow, Russia*

²*Bauman Moscow State Technical University, 105005, Moscow, Russia*
gorelik@sci.lebedev.ru

The investigations of the peculiarities in light scattering near the phase transitions in media are important direction of the modern physics. Because of the strong fluctuations increase near the phase transition point, the opalescence effect, i.e. the sharp growth of light scattering intensity, has been observed. At the beginning of the twentieth century Smolukhovsky, Keesom, Ornstein and Zernike have investigated opalescence near phase transition points of liquids. Later A. Yakovlev, L.M. Mikheeva, and T.S. Velichkina [1,2] have observed the opalescence in crystalline quartz within a narrow temperature interval of the α - β phase transition ($T_C = 846$ K).

Besides, so-called central peak, corresponding to a sharp spectral intensity increase in light, slow neutron, and X-ray scattering in the region of structural phase transitions, was detected in several crystals: Nb₃Sn, SrTiO₃, KMnF₃, KNbO₃, Pb₅Ge₃O₁₁ and others. Today numerous works [3-8] are devoted to the investigations of light scattering laws near the phase transition points in condensed media. In this paper, we present an experimental and theoretical investigation of Raman scattering intensity sharp increase, named as Raman opalescence, for some crystals near the phase transition point.

We have used the new experimental technique for Raman opalescence revealing, based on analysis of so called isofrequency temperature dependencies at low frequency spectral region. We have observed the sharp increase of the isofrequency peak spectral Raman intensity at low frequency Raman shift if the crystal temperature was approaching to the phase transition point. The experimental results are presented for different crystals, including ferroelectrics (LiTaO₃, LiNbO₃, Pb₅Ge₃O₁₁, Ba₂NaNb₅O₁₅) and ferroics (SiO₂, SrTiO₃). Central peak scattering has been observed in isofrequency temperature light scattering dependencies at the vicinity of phase transition point.

The theory of central peak scattering, based on the strong interaction between soft mode and low frequency, good quality, nonfundamental oscillator has been developed. The effect of Hyper Raman opalescence as sharp increase of light scattering at the spectral range of the second harmonic generation near the phase transition point in crystals is described.

This work was supported in part by RFBR grant 18-02-00181.

1. I.A. Yakovlev, L.M. Mikheeva, T.S. Velichkina, *Reports of the Academy of Sciences of the USSR* **107**, 675 (1956).
2. I.A. Yakovlev, L.M. Mikheeva, T.S. Velichkina, *Kristallografiya* **1**, 123 (1956).
3. A.A. Anikev, V.S. Gorelik, B.S. Umarov, *Sov. Phys. Sol. State* **26**, 1679 (1984).
4. V.S. Gorelik, P.P. Sverbil, A.I. Vodchits, et al., *Bulletin of the Russian Academy of Sciences: Physics* **82**, 57 (2018).
5. V.S. Gorelik, A.Yu. Pyatyshev, *Bulletin of the Russian Academy of Sciences: Physics* **82**, 299 (2018).
6. A.A. Anikiev, M.P. Umarov, *Optics and Spectroscopy* **125**, 22 (2018).
7. A.A. Anikev, M.P. Umarov, J.F. Scott, *ATP Advances* **8**, 115016 (2018).
8. N. Lagakos, H.Z. Cummins, *Physical Review B* **10**, 1063 (1974).

Piezoelectric strain tuned magnetic sensor

Zh. Wang, Zh. Hu, M. Liu

Xi'an Jiaotong University, 710049, Xi'an, China
zgwang18@xjtu.edu.cn

Anisotropic magnetoresistive sensors with high sensitivity and stability have been widely used in various industrial applications, including navigation, current sensing, position and rotation sensing, and biosensing. Traditional linear anisotropic magnetoresistive sensors used barber-pole electrodes to rotate the current direction by 45 degree in order to obtain a linear electrical output as a function of external magnetic field. However, the adoption of barber-pole electrodes greatly reduced the working area of the sensor, i.e., the part of strip beneath the barber-pole electrodes could not contribute to the magnetoresistive signal.

Here we report an anisotropic magnetoresistive sensor with antiferromagnetic layer to regulate the magnetization-current angle instead of barber pole electrodes. The proposed sensor design, thereby, could fully use the magnetostrictive area, and the stabilized magnetization could help suppressing magnetic noise, enhancing stability and improving linearity. Moreover, we have fabricated AMR sensors on piezoelectric PMN-PT single crystals to investigate the strain effect on the magnetoresistance of the sensor. With strain tunable magnetic permeability and therefore the sensitivity of the magnetic sensor, we have demonstrated a novel magnetic sensor with tunable measurement range and tunable sensitive direction.

Scanning capillary microscopy: new achievements and opportunities

I.V. Yaminsky

*Lomonosov Moscow State University, 119991, Moscow, Russian Federation
yaminsky@nanoscopy.ru*

*Advanced Technologies Center, 119311, Moscow, Russian Federation
Energy Efficient Technologies, 119234, Moscow, Russian Federation*

Scanning probe microscopy has proven to be an effective tool for visualizing biomacromolecules, bacteria, living cells and tissues in the natural environment with unprecedented spatial resolution. Scanning probe microscopy makes successful steps in the development of molecular diagnostic methods for personalized medicine, in particular, for the early detection of biological agents and markers of various diseases. Methods of scanning probe microscopy demonstrated the detection of a bacterium, a virus [1], a protein, and even a single atom [2]. An effective method for the rapid detection of bacterial resistance to antibiotics was developed and demonstrated in [3]. Highly sensitive detection of viral particles at low concentrations in liquid solutions was shown in [4].

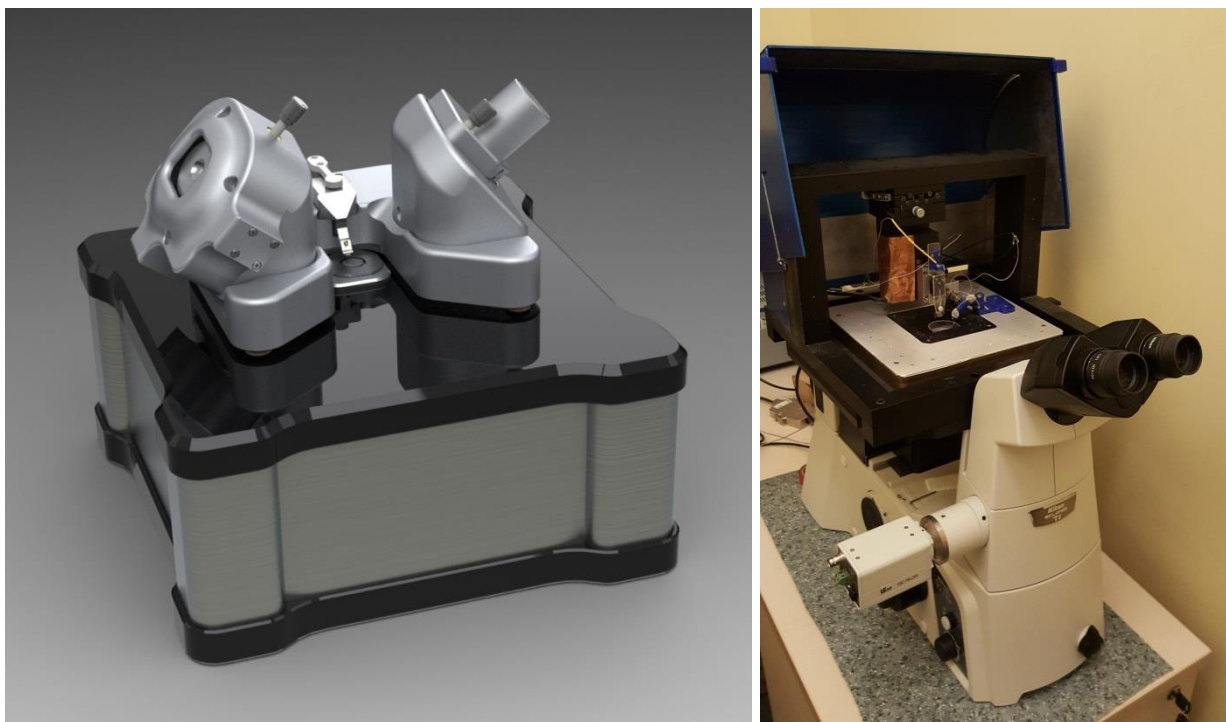


Figure 1. FemtoScan X high-speed scanning probe microscope (left) and scanning capillary microscope combined with Nikon Ti- U inverted optical microscope (right).

Modern scanning capillary microscopy plays a crucial role in various biomedical applications. A capillary probe or a nanopipette of a scanning capillary microscope can act as a device for delivering drugs, an electrochemical sensor, a pH biosensor, a test system for detecting metal ions and many others. Capillaries with two or more channels also allow the directed mass transfer of substances, biomacromolecules (peptides, proteins, nucleic acids, etc.) to the surface of biological objects or inside their volume. In our studies, we use a device embedded in an inverted microscope, so that data from optical and probe microscopy can be obtained and analyzed simultaneously [5]. For example, erythrocytes were observed using a scanning capillary microscope, and an analysis of the results showed that their surface roughness was in the range of 20 nm [6]. In this paper, we use the term “capillary microscopy” because it combines much more functions and methods of use compared to the name “scanning ion-conducting microscopy (SIPM)”, which has traditionally been used previously. Scanning capillary microscopy is successfully developing due to the effective use of multichannel capillaries for directional surface modification and 3D printing. It is possible to predict the further widespread use of scanning capillary microscopy in biomedical applications, in the testing of drugs using only one cell, and

not their cultures. A promising application of capillary microscopy is stereolithography. Art print using fluorescent proteins was first demonstrated in [7]. This work opens up new unique opportunities for the use of multi-channel capillaries for various technological and biomedical applications. The present and future of scanning capillary microscopy for 3D printing and stereolithography is the subject of discussion.

Modern scanning probe microscopy continues to grow rapidly. An important modern trend is to increase the speed and amount of data. Many scientific groups and companies are successfully working in this direction. At present, we have implemented a data acquisition system based on 18-20 bit DACs and ADCs at an operating frequency of 1 MHz. In this case, a frame with a size of 1000x1000 points is taken in 1 sec. However, this is far from the limit for probe microscopy. We are currently developing multichannel electronic data acquisition systems operating at a frequency of 100 MHz – 1 GHz.

Combined techniques are successfully developed when scanning probe microscopy is used with ultra-high-resolution optical microscopy, optical tweezers, optical spectroscopy, etc. Chemical analysis of the surface by recording the absorption of infrared radiation using a probe microscope are one of new techniques. In this method, one can distinguish chemically inhomogeneous areas in biological objects with a resolution of up to 10 nm [8].

Software plays an important role in the development of scanning probe It allows not only to obtain data, but what is very important, to efficiently and effectively process data, to present it in a visual and convenient form. These functions are largely performed by the FemtoScan Online software [9,10]. The FemtoScan Online software integrates the reading of files from most manufacturers of scanning probe microscopes. The development of probe microscopy occurred in such a way that almost all microscope developers used their unique recording data formats, which are implemented into FemtoScan Online software.

The author is grateful for the financial support of Russian Foundation of Basic Research (projects N 17-52-560001 and 16-29-06290).

1. A. Gupta, D. Akin, R. Bashir, *Appl. Phys. Lett.* **84**, 1976 (2004).
2. K. Jensen, K. Kim, A. Zettl, *Nature Nanotechnology* **3**, 533 (2008).
3. G. Longo, L. Alonso-Sarduy, L. Marques Rio, et al., *Nature Nanotechnology* **8**, 522 (2013).
4. P.V. Gorelkin, A.S. Erofeev, Kiselev, et al., *Analyst* **140**, 6131 (2015).
5. I. Yaminsky, A. Akhmetova, G. Meshkov, et al., *Nanoindustry* **1**, 44 (2018).
6. E. Makarova, D. Bagrov, P. Gorelkin, et al., *Nanoindustry* **2**, 42 (2015).
7. K.T. Rodolfa, A. Bruckbauer, D. Zhou, et al., *Chem. Int. Ed Engl.* **44**, 6854 (2005).
8. M. Pilling, P. Gardner, *Chemical Society Reviews* **45**, 1935 (2016).
9. I.V. Yaminsky, A.I. Akhmetova, G.B. Meshkov, *Nanoindustry*, **6**(85), 414 (2018).
10. A.S. Fiolonov, I.V. Yaminsky, A.I. Akhmetova, et al., *Nanoindustry* **5**(84), 339 (2018).

AFM adhesion imaging as a prospective tool in the detection of cell's abnormalities and diseases

M.E. Dokukin^{1,2}, I. Sokolov^{2,3,4}

¹Sarov Physical and Technical Institute, National Research Nuclear University MEPhI,
607186, Sarov, Nizhegorodskaya region, Russia
MEDokukin@mephi.ru

²Department of Mechanical Engineering, ³Department of Biomedical Engineering, ⁴Department of
Physics, Tufts University, 02155, Medford, MA, USA

Despite considerable advances in understanding the biological and biochemical nature of human diseases, many biophysical aspects of changes in tissue, cells and pericellular coat are still unclear. Here we report an approach based on nanoscale-resolution scanning of surfaces of cells which can be applied to study and diagnostic imaging of various diseases.

Using a combination of resonance and sub-resonance atomic force microscopy tapping modes, ringing mode [1], and machine learning analysis we demonstrated that surface parameters, which are typically utilized in engineering to describe surfaces, can be applied to classify physical alterations of the surface of human epithelial cells. We found that the stepwise in vitro development of cancer (from normal to immortal (pre-malignant), to malignant) could be associated with the emergence of simple fractal geometry on the cell surface [2, 3]. Further, we applied this method for the detection of bladder cancer by using cells collected from urine samples. Diagnostic accuracy of 94% achieved when examining five cells per patient's sample. It is a statistically significant improvement ($p < 0.05$) in diagnostic accuracy compared to the currently used clinical standard, cystoscopy, as verified on 43 control and 25 bladder cancer patients [4].

This method can also be applied for the detection of other cancers, in which cells or body fluid are available for analysis without the need for invasive biopsy, e.g., upper urinary tract, urethra, colorectal and other gastrointestinal, cervical and aerodigestive cancers. Furthermore, the described approach can be extended to detect cell abnormalities beyond cancer as well as to monitor cell reaction to various drugs (nanopharmacology).

1. M.E. Dokukin, I. Sokolov, *Scientific Reports* **7**, 11828 (2017).
2. M.E. Dokukin, N.V. Guz, C.D. Woodworth, et al., *New Journal of Physics* **17**, 033019 (2015).
3. N.V. Guz, M.E. Dokukin, C.D. Woodworth, et al., *Nanomedicine: NBM* **11**, 1667 (2015).
4. I. Sokolov, M.E. Dokukin, V. Kalparathi, et al., *PNAS* **115**, 12920 (2018).

Piezoelectric, ferroelectric, optoelectronic and photo-catalytic phenomena from defect levels in hydroxyapatite by first-principles

V.S. Bystrov¹, J. Coutinho², L.F. Avakyan³, A.V. Bystrova^{1,4}, E.V. Paramonova¹

¹*Institute of Mathematical Problems of Biology, Keldysh Institute of Applied Mathematics, RAS, 142290 Pushchino, Moscow region, Russia*
vsbys@mail.ru

²*Department of Physics & I3N, University of Aveiro, Campus Santiago, 3810-193 Aveiro, Portugal*

³*Physics Faculty, Southern Federal University, Rostov-on-Don 344090, Russia*

⁴*Institute of Biomedical Engineering and Nanotechnologies, Riga Technical University, Riga, Latvia*

Hydroxyapatite (HAp) is an important component of mammal bones and teeth, being widely used in prosthetic implants [1]. However, despite the importance of HAp in medicine (exciting applications involving this material as a high biocompatible materials [1]), several promising new applications involving this material (e.g., in photo-catalysis [2]), depend on how well we understand its fundamental properties. Recent experiments and theoretical studies have shown that HA exhibits piezoelectricity, pyroelectricity, and ferroelectricity [3-8]. A number of theoretical studies of the structure and properties of HA have been carried out [3-6]. It shown the value of the d_{33} piezoelectric coefficient as 15.7 pC N^{-1} in good agreement with the experimental study as described in [7, 8]. Further, experimental evidence suggests that oxygen vacancies play a critical role in the production of surface radicals upon exposure of HAp to ultraviolet (UV) light. However, very little is known about the underlying physical and chemical details.

A hybrid density functional theory (DFT) study of the structural and electronic properties of oxygen vacancies in large HAp supercells within the plane-wave formalism was presented in this work. The vacancies were investigated in large supercells, from which formation energies and electronic transition energies were calculated. The calculations were carried out using DFT, as implemented by the VASP [9]. The exchange-correlation potential was evaluated either using the generalized gradient approximation according to PBE functional or the three-parameter hybrid B3LYP functional, which incorporates a fraction of exact exchange with local and semi-local functional [10]. These methods are also applied to the calculation of defect levels [11].

We found that the vacancies essentially occur in two distinct forms, either as a simple vacant oxygen site (referred to as structures I-IV), or as an oxygen atom replacing two neighbouring oxygen vacancies (bridge structures A-C). The former type of vacancies are deep donors, while the latter are shallow donors with rather low ionization energies. No acceptor states (stable negatively charged defects) were found. Vacancy structures I-IV are more stable in the neutral charge state, while bridge structures A-C are preferred in the double plus charge state. This means that the oxygen vacancy adopts rather different configurations on samples where the Fermi energy is in the upper or the lower half of the band gap. From inspection of the one-electron Kohn-Sham levels, combined with the transition levels obtained from total energies, we find that electron promotion from the valence band top to the donor state of the positively charged structures, involves a zero-phonon absorption of 3.6-3.9 eV.

This transition leads to a spontaneous breaking of either a P-O bridge-bond or an O-H bond, and most likely explains the 3.4-4.0 eV absorption onset for the observation of photocatalysis under persistent UV illumination.

The use of B3LYP allows to consider both electronic excited states of electrons and optical properties, as well as the energy of formation of defects at a high and precise level.

This is not unexpected, since this functionality was developed earlier for the description of molecules, and the studied material based on the hexagonal HAp crystal lattice has a similar molecular structure: it contains isolated PO_4 tetrahedra, columns of calcium atoms and OH hydroxyl channel.

The resulting electronic structure of the band of the top of the valence band turns out to be rather flat, which also confirms the “molecular-like” nature of the internal structure of the HAp.

The effectiveness of the use of the exchange-correlation functional B3LYP in the calculations for pure HAP and defect levels in HAP. Further development and more accurate calculation of these electronic properties and optical photoexciting and photocatalytic processes can be made by correct calculations of the electron – electron correlation of the excited electron states taking into account the Frank-Condon relaxation.

Thus, it is the way for future work. The authors thank the Russian Foundation for Basic Researches (RFBR grant 19-01-00519 A) and to the Fundação para a Ciência e a Tecnologia (FCT) through project UID/CTM/50025/2013.

1. A. Iulian ed. *Bioceramics and Biocomposites: From Research to Clinical Practice*. (John Wiley & Sons, Hoboken, New Jersey), 149 (2019).
2. V.S. Bystrov, C. Piccirillo, D.M. Tobaldi, et al., *Applied Catalysis B: Environmental* **196**, 100 (2016).
3. V.S. Bystrov, J. Coutinho, A.V. Bystrova, et al., *J. Phys. D: Appl. Phys.* **48**, 195302 (2015).
4. A. Slepko, A.A. Demkov, *Phys Rev B: Condens Matter*. **84**, 134108 (2011).
5. V.S. Bystrov, *Ferroelectrics* **475** (1), 148 (2015).
6. V.S. Bystrov, *Ferroelectrics*, doi:10.1080/00150193.2019.1574638 (2019).
7. S.B. Lang et al., *Sci. Rep.* **3**, 2215 (2013).
8. S.B. Lang, *Phase Transitions* **89** (7-8), 678 (2016).
9. *Vienna Ab Initio Simulation Package (VASP)* <https://www.vasp.at/> (access 23.04.2019).
10. L.A. Avakyan, E.V. Paramonova, J. Coutinho, et al., *J. Chem. Phys.* **148**, 154706 (2018).
11. V.S. Bystrov, L.A. Avakyan, E.V. Paramonova, et al., *J. Chem. Phys. C*. **123** (8), 4856 (2019).

Magnetic resonance force microscopy of planar ferromagnetic nanostructures

V.L. Mironov

Institute for Physics of Microstructures RAS, 603950, Nizhny Novgorod, GSP-105, Russia
mironov@ipmras.ru, <http://mrfm.ipmras.ru/>

We report the investigation of microwave resonant properties of ferromagnetic nanostructures using magnetic resonance force microscope (MRFM). The home-made MRFM based on “Solver-HV” scanning probe microscope [1-3] was applied for the measurements of ferromagnetic resonance (FMR) in multilayer thin-film structures Co/Pt and spin-wave resonances in the individual microstripes NiFe. All results are supported by micromagnetic modeling of the MRFM response, as well as the calculations of MRFM spectra and spatial distributions of the resonant oscillations of the magnetization.

The peculiarities of magnetic interaction between probe and sample in MRFM experiments are analyzed. Some perspectives of MRFM application for the investigation of spatially modified magnetic nanostructures are discussed.

This work is supported by contract # 0035-2019-0022-C-01, Presidium RAS program # 0035-2018-0016 and Russian foundation for basic researches (project # 18-02-00247).

1. E.V. Skorokhodov, M.V. Sapozhnikov, A.N. Reznik, et al., *Instrum. Exp. Tech.* **61**, 761 (2018).
2. E.V. Skorokhodov, M.V. Sapozhnikov, R.V. Gorev, et al., *Phys. Solid State* **60**, 2254 (2018).
3. A.P. Volodin, C. Van Haesendock, E.V. Skprpkhodov, et al., *Appl. Phys. Lett.* **113**, 122407 (2018).

Electrochemical Strain Microscopy of Li-ion battery cathodes

D.O. Alikin^{1,2}, K.N. Romanyuk^{1,2}, B.N. Slautin¹, D. Rosato³,
V.Ya. Shur¹, A. Tselev², A.L. Kholkin^{1,2}

¹*School of Natural Sciences and Mathematics, Ural Federal University, 62000 Ekaterinburg, Russia*

²*Department of Physics & CICECO – Aveiro Institute of Materials, 3810-193 Aveiro, Portugal*
kholkin@ua.pt

³*Robert Bosch GmbH, 70839 Gerlingen-Schillerhoehe, Germany*

Electrochemical strain microscopy (ESM) can provide useful information on the ionic processes in materials at the local scale. This is especially important for ever growing applications of Li-batteries whose current performance is limited by various intrinsic and extrinsic degradation mechanisms. In this context, ESM is indispensable because it helps uncovering these mechanisms on the nanoscale. However, the ESM method used so far [1] has been only qualitative due to multiple contributions to the measured ESM signal.

In this work, we provide a viable approach for the local probing of ionic concentration and diffusion coefficients based on the low frequency dependence of the ESM signal. A theoretical basis considering the dynamic behavior of ion migration and relaxation and change of ion concentration profiles under the action of the electric field of the ESM tip is developed [2]. We argue that several parasitic contributions to the ESM signal recently discussed in the literature [3] can be thus eliminated. The analysis of ESM images using the proposed approach allows a quantitative mapping of the ionic diffusion coefficients and concentration in ionic conductors (Fig. 1). The results are validated on Li-battery cathodes (LiMn₂O₄) extracted from commercial Li-batteries and provide novel possibilities for their development and further insights into the mechanisms of their degradation after prolonged use. The ESM results are complemented by the micro Raman microscopy investigations [4] that confirm the conclusions provided by ESM.

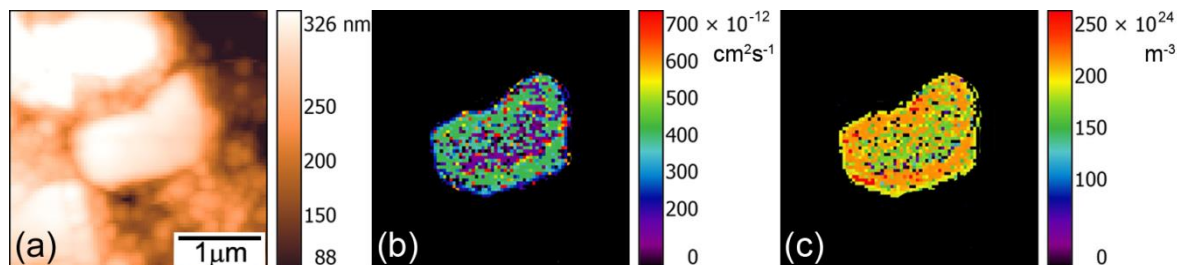


Figure 1. Topography (a), diffusion coefficient (b) and ionic concentration (c) maps of the LiMn₂O₄ cathode extracted from commercial battery.

The work was financially supported by the Portuguese Foundation for Science and Technology (FCT) within the project PTDC/CTM-ENE/6341/2014. The equipment of the Ural Center for Shared Use “Modern nanotechnology” UrFU was used.

1. N. Balke, S. Jesse, A.N. Morozovska, et al., *Nat. Nanotechnol.* **5**, 749 (2010).
2. D.O. Alikin, K.N. Romanyuk, B.N. Slautin, et al., *Nanoscale* **10**, 2503 (2018).
3. D.O. Alikin, A.V. Ievlev, S.Y. Luchkin, et al., *Appl. Phys. Lett.* **108**, 113106 (2016).
4. D. Alikin, B. Slautin, A. Abramov, et al., *Materials* **12**, 1416 (2019).

Investigation of ferroelectric behavior of $\text{Bi}(\text{Fe},\text{Sc})\text{O}_3$ multiferroics using piezoresponse force microscopy

V.V. Shvartsman¹, A.N. Salak², D.D. Khalyavin³

¹*Institute for Material Science, University of Duisburg-Essen, Essen, Germany
vladimir.shvartsman@uni-due.de*

²*Department of Materials and Ceramic Engineering/CICECO, University of Aveiro, Aveiro, Portugal*

³*ISIS Facility, Rutherford Appleton Laboratory, Chilton, Didcot, UK*

Bismuth ferrite (BFO) has attracted an immense attention as a rare room-temperature single-phase multiferroics. The magnetic and ferroelectric structure of BFO can be tuned by cationic substitutions, however the single phase existence range is limited. It can be extended using the high-pressure synthesis method. In particular, this method was applied to sinter $\text{BiFe}_{1-x}\text{Sc}_x\text{O}_3$ ceramics [1,2]. The material appears in different polymorphs. The phase obtained by quenching under pressure is antipolar. However, thermal cycling at normal pressure irreversibly turns this phase into a polar one. The resulting modification is a rare example of coexistence of canted ferroelectric and ferromagnetic states.

Relatively large conductivity and complications to sinter dense ceramics make difficult study and even verification of macroscopic ferroelectric properties. These obstacles can be overcome implementing piezoresponse force microscopy (PFM) addressing ferroelectric behavior at the local scale. The post-annealed $\text{Bi}(\text{Fe}_{0.5}\text{Sc}_{0.5})\text{O}_3$ ceramics show a strong PFM signal and possess a well-developed domain pattern typical of a ferroelectric state. The quenched ceramics, however, demonstrate no piezoresponse that is in line with its antiferroelectric state. We found that this state can be transferred to a ferroelectric one by application of a strong enough electric field. In $\text{Bi}(\text{Fe}_{0.6}\text{Sc}_{0.4})\text{O}_3$ ceramics a coexistence of ferroelectric and antiferroelectric grains was observed. In latter a ferroelectric state could be induced by electric poling. The temporal and temperature stability of the induced states was studied. Mechanisms of antiferroelectric-ferroelectric transformation are discussed.

This work was supported by the TUMOCS project that has received funding from the European Union's Horizon 2020 research and innovation programme under the Marie Skłodowska-Curie grant agreement No 645660.

1. D.D. Khalyavin, A.N. Salak, N.M. Olekhovich, et al., *Phys. Rev. B* **89**, 174414 (2014).
2. A.N. Salak, D.D. Khalyavin, E. Eardley, et al., *Crystals* **8**, 91 (2018).

Polarization-dependent conductivity of grain boundaries in BiFeO₃ thin films

D.O. Alikin^{1,2}, Y. Fomichov³, S.P. Reis^{4,7}, A.S. Abramov¹, D.S. Chezganov¹, V.Ya. Shur¹,
E. Eliseev⁵, A. Morozovska⁶, E.B. Araujo⁴, A.L. Kholkin^{1,2}

¹*School of Natural Sciences and Mathematics, Ural Federal University, 620000, Ekaterinburg, Russia*
Denis.Alikin@urfu.ru

²*Department of Physics & CICECO-Aveiro Institute of Materials, University of Aveiro, Portugal*

³*Faculty of Mathematics and Physics, Charles University in Prague, Prague 8, 180 00, Czech Republic*

⁴*Department of Chemistry and Physics, São Paulo State University, Ilha Solteira – SP, Brazil*

⁵*Institute for Problems of Materials Science, National Academy of Sciences of Ukraine, Kyiv, Ukraine*

⁶*Institute of Physics, National Academy of Sciences of Ukraine, 03028 Kyiv, Ukraine*

⁷*Federal Institute of Education, Science and Technology of São Paulo, 15503-110 Votuporanga, Brazil*

Many efforts have been devoted so far to achieve the control of interfaces in ferroelectric materials based on their polarization. These efforts resulted in the discovery of a variety of different phenomena such as polarization-dependent tunneling effect, resistive switching, symmetry breaking, etc. [1, 2] In particular, domain wall conductivity [3], formation of topological defects [4], phase boundaries [5] and ferroelectric-insulator interfaces [6] have been studied. Charge transport across the interfaces in complex oxides attracts a lot of attention because it allows creating novel functionalities useful for device applications. In particular, it has been observed that movable domain walls in epitaxial BiFeO₃ films possess enhanced conductivity that can be used for reading out in ferroelectric-based memories [3]. In this work, the relation between the polarization and conductivity in sol-gel BiFeO₃ films with special emphasis on grain boundaries (GBs) as natural interfaces in polycrystalline ferroelectrics is investigated. The grains exhibit self-organized domain structure in these films (Fig. 1), so that the “domain clusters” consisting of several grains with aligned polarization directions are formed. Surprisingly, GBs between these clusters (with antiparallel polarization direction) have significantly higher electrical conductivity in comparison to “inter-cluster” GBs, in which the conductivity was even smaller than in the bulk. As such, polarization-dependent conductivity of the GBs was observed for the first time in ferroelectric thin films. The results are rationalized by thermodynamic modelling combined with finite element simulations of the charge and stress accumulation at the GBs giving major contribution to conductivity.

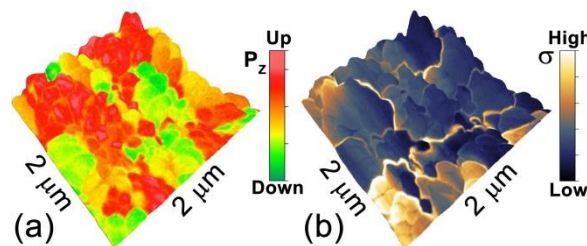


Figure 1. (a) Domain structure and (b) current response in BiFeO₃ sol-gel thin films.

This work was developed within the scope of the project CICECO-Aveiro Institute of Materials, FCT Ref. UID/CTM/50011/2019, financed by national funds through the FCT/MCTES. The equipment of the Ural Center for Shared Use “Modern nanotechnology” UrFU was used. For the financial support, we also express our gratitude to the Brazilian agencies: FAPESP (Project N° 2017/13769-1) and CNPq (Research Grant 304604/2015-1 and Project N° 400677/2014-8). This project has received funding from the European Union’s Horizon 2020 research and innovation program under the Marie Skłodowska-Curie grant agreement No 778070.

1. T. Eshita; W. Wang, K. Nomura, K. Nakamura, et al., *Jpn. J. Appl. Phys.* **57**, 11UA01 (2018).
2. A.Q. Jiang, Y. Zhang, *NPG Asia Mater.* **11**, 2 (2019).
3. J. Seidel, L.W. Martin, Q. He, Q. Zhan, Y-H. Chu et al., *Nat. Mater.* **8**, 229 (2009).
4. N. Balke, I. Bdikin, S.V. Kalinin, A.L. Kholkin, *J. Am. Ceram. Soc.* **92**, 1629 (2009).
5. Y. Heo, L.J. Hong, L. Xie, X. Pan, C-H. Yang, J. Seidel, *NPG Asia Mater.* **8**, e297 (2016).
6. Y. Zhang, H. Lu, L. Xie, X. Yan, T.R. Paudel, et al., *Nat. Nanotechnol.* **13**, 1132-1136 (2018).

THz time-domain spectroscopic ellipsometry with simultaneous measurements of orthogonal polarizations

Q. Guo¹, Y. Zhang², Zh. Lyu¹, D.-W. Zhang¹, Y.-D. Huang³, C. Meng⁴,
Z.-X. Zhao¹, J.-M. Yuan^{1,5}

¹College of Liberal Arts and Sciences, National University of Defense Technology, 410073, Changsha, Hunan, China

jmyuan@nudt.edu.cn

²School of Materials Science and Engineering, Xiangtan University, 411105, Hunan, China

³Advanced Interdisciplinary Technology Research Center, National Innovation Institute of Defense Technology, 100071, Beijing, China.

⁴Xi'an Research Institute of High-tech, 710025, Xi'an, Shaanxi, China

⁵Graduate School of China Academic of Engineering Physics, 100193, Beijing, China

Terahertz (THz) spectroscopy covers numerous interactions in physical, chemical, and biological systems. For opaque materials in the THz band, spectroscopy is generally performed with THz time-domain reflection spectroscopy (THz-TDRS), which compares the relative amplitudes and phases of reflected THz waveforms from a sample with those from a reference. The reference is often a flat metal mirror. This method is straightforward but the front surfaces of the reference and the sample must be positioned, within a fraction of a micron, in exactly the same location to obtain the accurate phase of the reflection. Such precise *in situ* positioning is difficult, although various methods have tried to overcome phase uncertainty [1-3].

Spectroscopic ellipsometry is a promising way to solve this problem and there have been attempts to establish THz time-domain spectroscopic ellipsometry (THz-TDSE) [4,5]. Here, we present a new instrumentation for THz ellipsometer, THz-TDSE with simultaneous measurements of orthogonal polarizations, which extends the reliable frequency range with a low dynamic range photoconductive antenna THz source. In order to realize simultaneous measurement of orthogonal polarizations, the method of splitting the circularly polarized probe laser pulses was employed [6]. This method made the apparatus capable of measuring orthogonal polarizations with very high extinction ratios and without rotating the polarizer. In the calibration, the TDSE response function was obtained via the simultaneous polarization measurements reflected by a flat metal mirror, adapted in conventional TDRS, and used here for THz-TDSE without problems of position accuracy. The calibration could be used to determine accurate ellipsometric parameters with a high tolerance of imperfect polarizer extinction ratios and of non-ideality in the THz reflection components. As a proof of principle demonstration, results were presented for an opaque, heavily p-doped Si (0.01~0.05 $\Omega \cdot \text{cm}$) wafer and highlighted the advanced potential of our THz-TDSE for reflection-based measurements.

The optical layout of our THz-TDSE system is shown in Figure 1a for simultaneous measurements of p- and s-polarizations. The THz pulses, generated from a photoconductive-antenna radiated by a commercial Ti:sapphire laser, were collimated and focused into the reflection module with an incident angle of 60°, which was similar to a periscope, for easy placement of the sample. In the detection part, the probe pulses were then split by a 5:5 non-polarizing beam splitter (NPB) into a detector for the X-polarized electric field (DX) and a detector for the Y-polarized electric field (DY). With proper azimuths of half-wave plates ($\lambda/2$), DX and DY could simultaneously measure THz waveforms with different polarizations. The frequency-dependent ellipsometric parameters ($\tan \Psi$ and Δ) of the Si wafer are shown in Figure 1b. The measured results (red circles and blue rectangles) are consistent with the Drude fitting (red solid lines and blue dashed lines). Figure 1c presents the relative errors of $\tan \Psi$ measured by simultaneous and non- simultaneous measurements of orthogonal polarizations. The relative errors of $\tan \Psi$ (magenta pentagrams) measured by our system were below 1% over the entire frequency range, because of the one-run detection of the two polarized components, which meant that the flicker noise of the system was greatly reduced. In contrast, limited by the low dynamic range of the THz source in the high frequency range, the relative errors in the normal THz-TDSE increased quickly with frequency beyond 1THz. The simultaneous measurements rejected significant common-mode

noise from the laser, and it extended reliable THz spectra into the frequency range with a low dynamic range of a photoconductive-antenna THz source, which is a fundamental breakthrough for reflection-based measurements and overcomes the hurdle of phase uncertainty.

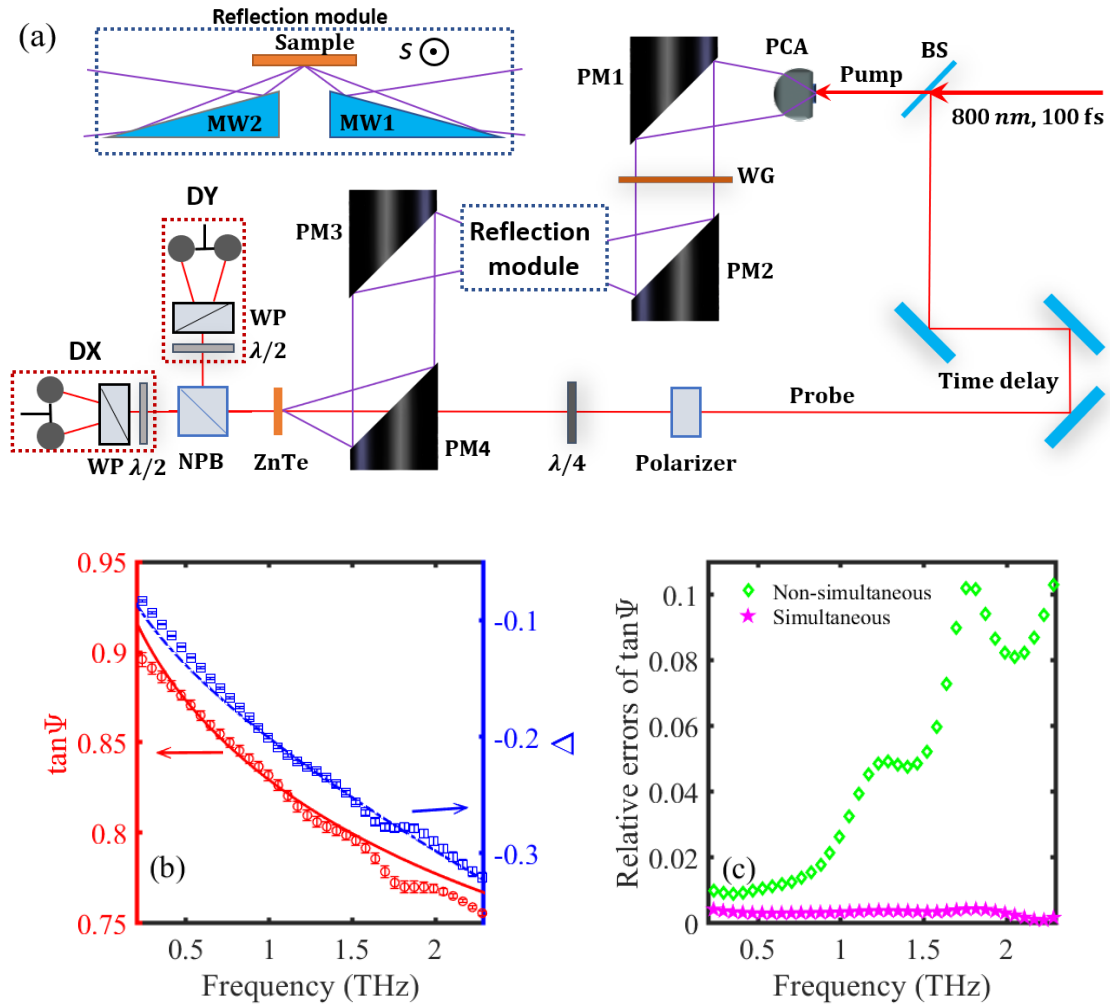


Figure 1. (a) Optical diagram of the THz-TDSE. (b) Ellipsometric parameters ($\tan \Psi$ and Δ) of the Si wafer. The red circles and blue rectangles are experimental data. The red solid lines and blue dashed lines are the Drude fitting results. (c) The relative errors of $\tan \Psi$ were calculated from the simultaneous and non-simultaneous measurements of two orthogonal polarizations. The relative error was defined as the relative standard deviation.

1. A. Pashkin, M. Kempa et al., *Review of Scientific Instruments* **74**, 4711 (2003).
2. S. Nashima, O. Morikawa et al., *Applied Physics Letters* **79**, 3923 (2001).
3. Hikaru Igawa, Tatsuya Mori et al., *Japanese Journal of Applied Physics* **53**, 05FE01 (2014).
4. Mohammad Neshat and NP Armitage, *Optics Express* **20**, 29063 (2012).
5. Nicholas Karl, Martin S Heimbeck et al., *Applied Physics Letters* **111**, 191101 (2017).
6. Nick C. J. van der Valk, Willemine A. M. van der Marel et al., *Optics Letters* **30**, 2802 (2005).

Dielectric breakdown of polymer composites: Experiments and phase-field simulations

Y. Shen¹, J.Y. Jiang¹, Z.H. Shen¹, L.Q. Chen²

¹*School of Materials Science and Engineering, State Key Lab of New Ceramics and Fine Processing, Tsinghua University, Beijing, 100084, China*

²*Department of Materials Science and Engineering, Pennsylvania State University, University Park, Pennsylvania 16802, United States*

Polymer nanocomposites, which combines high dielectric permittivity (ϵ_r) of ceramics and high breakdown strength (E_b) of polymers, are promising dielectrics for high power electrostatic capacitors. Capable of delivering ultrahigh power, they are the major enabler for a number of modern electrical and electronic devices. Tremendous efforts have been made to break the adverse coupling between ϵ_r and E_b and raise their low energy density, make them viable for energy storage applications. Experimental results indicate that the interfaces between inorganic fillers and polymer matrix play critical roles in determining the E_b of the composites. Phase-field models are employed to simulate the complicated dielectric breakdown process in composites. It is revealed that aspect ratio and orientation of inorganic fillers are critical factors that could substantially change the distribution of local electric field and affect the propagation of breakdown path. Simulation results also show that breakdown paths are originated mostly at the interface between composite and electrodes as a result of charge injection from the electrodes under high electric field. Fillers of large energy band gap is capable of raising the energy barrier and suppressing the detrimental charge injection. In light of these findings, optimal structure designs of polymer composites with low loss are proposed and demonstrated.

1. X. Zhang, Y. Shen et.al., *Adv. Mater.* **27**, 819 (2015).
2. X. Zhang, Y. Shen et.al., *Adv. Mater.* **28**, 2055 (2016).
3. Z.H. Shen, Y. Shen et.al., *Adv. Mater.* **30**, 1704380 (2018).

Photoinduced dynamics in ferroelectric semiconductor $\text{Sn}_2\text{P}_2\text{S}_6$

N.E. Sherstyuk¹, K.A. Brekhov¹, G.Kh. Kitaeva², E.D. Mishina¹

¹MIREA – Russian Technological University, 119454, Moscow, Russia
nesherstuk@mail.ru

²Lomonosov Moscow State University, 119991, Moscow, Russia

The possibility of switching the order parameter in ferroics by means of an electromagnetic pulse is currently one of the most studied topics in the field of interaction of laser radiation with matter. The application of this technology to ferroic materials will probably allow the creation of new high-speed and non-volatile storage devices. If the switching of the magnetization by a single femtosecond laser pulse has already been demonstrated, the problem of the ultrafast ferroelectric switching of the order parameter has not yet been solved. It is established that ultrafast switching of magnetization is determined by spin-orbit and exchange interactions. There are no such mechanisms in ferroelectric materials.

Currently, there are several works in which attempts are made to switch the ferroelectric polarization using medium infrared pulses [1,2]. One of the first steps towards all-optical magnetic order parameter switching was photo-induced excitation of spin oscillations at the magnetic resonance frequency near the phase transition θ . The study of the excitation of photoinduced phonon soft modes in ferroelectric materials is a similar step to the all-optical control of the ferroelectric order parameter.

The class of ferroelectric semiconductors is very important for such studies. One of the most typical representatives of this material is tin hypophosphite $\text{Sn}_2\text{P}_2\text{S}_6$ (SPS). Studies of the effects of femtosecond laser pulses on an SPS crystal were presented by us earlier [3,4] The first experimental results of photoinduced excitation of phonon modes in an SPS crystal were presented by us in [5]. It was shown that two phonon modes can be excited in an SPS crystal with femtosecond laser pulses with the energy of 3.1 eV at room temperature. One of them was attributed to the phonon acoustic mode with a frequency of 20 GHz. The other, with a frequency of 0.89 THz, was attributed to the soft mode. The latter belongs to A' symmetry group in the ferroelectric phase and transforms into the B_u symmetry mode in the paraelectric phase. In addition, we demonstrated [6] that the effect of femtosecond laser pulses on SPS did not lead to a local crystal heating or a change in the Curie temperature in the time range up to 10 ps.

Here we present the results of a study of the phonon mode parameters and other photorefractive effects inducing in an SPS single crystal by femtosecond laser pulses in the vicinity of the phase transition and at room temperature. It is shown that the response of a crystal to a laser pulse reminds a soft mode near the phase transition. However, the observed decrease in the frequency of oscillations in the vicinity of the Curie temperature T_c is much weaker than previously reported. This can be explained by the shading of pure soft mode by its interaction with other photo-induced modes.

This work was partly supported by the Russian Ministry of Science and Higher Education (grant 3.7500.2017/9.10) and Russian Foundation of Basic Research (grant 18-32-20047). The studies were performed using the equipment of the Joint Center for Collective Use RTU MIREA.

1. R. Mankowsky et al., *Phys. Rev. Lett* **118**, 197601 (2017).
2. A. Subedi, *Phys. Rev. B* **92**, 214303 (2015).
3. K.A. Grishunin, K.A. Brekhov and O. V. Samotokhin, *Russian Technol. J.* **2**, 134 (2015).
4. P.A. Prudkovskii et al., *JETP Lett.* **105**, 158 (2017).
5. K.A. Brekhov et al., *JETP Lett.* **102**, 372 (2015).
6. K.A. Brekhov et al., *Phys. Solid State* **60**, 31 (2018).

Ferroelectric relaxor properties characterized by dynamic mechanical analyses

X. Wang, Y. Chen, X. Yao

School of Materials Science and Engineering, Tongji University, Shanghai 201804, China
xs-wang@tongji.edu.cn

Relaxation makes ferroelectrics a critical component in sensors, actuators and ultrasound devices, with large electromechanical coupling effects. Although various studies of ferroelectric relaxation have been undertaken, much remains to be investigated regarding the related the electric properties and mechanisms. In this study, an alternative mechanical method using a dynamic mechanical analyzer (DMA) was applied to investigate the low frequency relaxor behavior of ferroelectric PZT and BaTiO₃ ceramics, compared with conventional electric method. Ferroelectric to paraelectric phase transitions were clearly detected and an obvious low frequency relaxor behavior was characterized, induced by Debye relaxation. The activation energy of each relaxation peak and relaxation limit time was theoretically analyzed using the Arrhenius relationship.

The DMA is suited for characterizing low frequency relaxor behavior of ferroelectrics, it is sensitive to internal structural changes. In contrast, no low frequency relaxor behavior was detected by dielectric measurements. This study deepened the current knowledge on relaxor ferroelectrics, and offered the potential for provide new insights into the investigation of low frequency relaxor characterization.

Switching processes in ferroelectric superlattices

A.S. Sidorkin¹, L.P. Nesterenko¹, Y.Gagou², P.Saint-Gregoire³,
A.Yu. Pakhomov¹, E.V. Vorotnikov¹, N.G. Popravko¹

¹Voronezh State University, 394018, Voronezh, Russia
sidorkin@phys.vsu.ru

²Universite de Picardie Jules Verne, 80039 Amiens Cedex, France

³ICGM, C2M, 34095 Montpellier Cedex, France; University of Nimes, 30021 NIMES Cedex 01, France

In present work the studies of switching processes were carried out on perovskite ferroelectric superlattices with alternating BaZrO₃/BaTiO₃ (BZ/BT) layers with a superlattice period of $\Lambda = 13.32$ nm that was layered by pulsed laser sputtering.

To study repolarization processes of samples by switching currents, we used rectangular shape stimulating switching signal with amplitude from 50 mV to 8 V at 10 kHz. We used an arbitrary form signal generator Waveform Generator 2571 to apply the same duration equally spaced bipolar rectangular periodic voltage pulses with a rise time of the switching voltage of not more than 10 ns to the samples.

Similarly to ferroelectric films, the full switching curve in superlattices has two sections – the initial, so-called activation section or region of “weak” fields, where the indicated dependence of the switching current on the applied field strength is close to the exponent, and the subsequent linear section, region of “strong” fields, or section slip, in which the dependence of the maximum switching current is proportional to the field $i_{max} \approx const E$.

The boundary between the regions of activation and nonactivation modes of switching, the so-called threshold or critical field of E_{crit} , determined by switching currents, approximately corresponds to the coercive field, determined by the dielectric hysteresis loop. The threshold field decreases as the ferroelectric phase transition temperature is approached.

A detailed study of switching currents under the action of rectangular field pulses in weak fields less than the coercive field showed that the integral characteristics of the switching do not obey the strictly exponential dependence on the field strength. This leads to the appearance of a dynamic indicator μ for the power dependence of the switching current on the electric field strength, the magnitude of which is less than unity. The selection of the power index μ for the activation region shows that in the superlattices compared to ferroelectric films, this indicator has a much smaller value and is practically independent of temperature.

Tilt angle of the switching current field dependence in the area of strong fields decreases with increasing temperature, which indicates a decrease in the mobility of the domain boundaries as the transition temperature to the non-polar phase decreases, apparently due to an increase in the switching time here.

The presence of an activation region in the regularities of switching ferroelectric superlattices indicates that repolarization processes here are most likely carried out by moving the domain boundaries.

ORAL PRESENTATIONS



Flat bands, scanning tunneling microscopy, and the violation of time-reversal symmetry

V.R. Shaginyan

Petersburg Nuclear Physics Institute, NRC Kurchatov Institute, Gatchina 188300, Russia

The topological fermion condensation of quantum phase transition (FCQPT) paves a new avenue in modern physics. Such a transition belongs to the unique type of quantum phase transitions the originators of the theory of instabilities omitted, and leads to the topological reconstruction of the Fermi surface. We discuss the modification of the systems under the action of FCQPT, representing the "missed" instability, which allows the development of an entirely new approach to or a "second edition" of condensed matter theory, presenting this physics as a completely new method for studying many-body objects.

Tunneling differential conductivity (or resistivity) is a sensitive tool to experimentally test the non-Fermi liquid (NFL) behavior of strongly correlated Fermi systems. In the case of common metals the Landau Fermi liquid (LFL) theory demonstrates that the differential conductivity is a symmetric function of bias voltage V . This is because the particle-hole symmetry is conserved in LFL state. When a strongly correlated Fermi system turns out to be near the topological fermion condensation quantum phase transition, its LFL properties disappear so that the particle-hole symmetry breaks making the differential tunneling conductivity to be asymmetric function of V . This asymmetry can be observed when a strongly correlated metal is in its normal, superconducting or pseudogap states. We show that the asymmetric part of the dynamic conductance does not depend on temperature provided that the metal is in its superconducting or pseudogap states. In normal state the asymmetric part diminishes at rising temperatures. Under the application of magnetic field the metal transits to the LFL state and the differential tunneling conductivity becomes a symmetric function of V . These findings are in good agreement with recent experimental observations.

We argue that existing theories based either on model calculations within Hubbard and Kondo models simulations, based actually on the more complicated versions of the same models, were not able to explain the destruction of asymmetric conductivity in sufficiently high magnetic fields. To the best of our knowledge, the presented FC theory is the only one capable to explain the above experimental puzzles. Moreover, our approach suggests that FCQPT is intrinsic to strongly correlated substances and can be viewed as the universal cause of their NFL behavior.

1. V.R. Shaginyan, A.Z. Msezane, G.S. Japaridze, V.A. Stephanovich, Y.S. Leevik, *JETP Lett.* **108**, 335 (2018).

Influence of condensation enhancement effect in nanocapillaries at hydrophilic surface on AFM image contrast

I.S. Mukhin^{1,2}, M.V. Zhukov¹, A.M. Mozharov^{1,2}, A.O. Golubok^{1,3}

¹*ITMO University, 197101, St. Petersburg, Russia, imukhin@yandex.ru*

²*St. Petersburg Academic University, 194021, St. Petersburg, Russia*

³*Institute for Analytical Instrumentation RAS, 198095, St. Petersburg, Russia*

In order to improve spatial resolution and contrast of atomic force microscopy (AFM) images standard silicon probes could be modified with nanostructures like nanotubes, diamond-type carbon and metal-carbon whiskers and nanowires. Hydrophobicities (hydrophilicities) of the probe and the sample have essential influence on obtained AFM data [1-4]. Phenomenon of the surface features height difference between AFM images (up to contrast inversion) taken with oscillating Si cantilevers corresponding to tapping and noncontact modes was reported in [5-7].

In this work we investigate differences in AFM imaging of nanopores and nanochannels located on the hydrophobic and hydrophilic surfaces obtained using conventional Si probes and Si probes modified with Pt/C wires. In contrast to [5-7] the inversion phenomenon observed in AFM images is associated with effect of enhanced vapor condensation in the nanopores and nanochannels on hydrophilic surfaces. We found that enhanced vapor condensation in nanopores affects on AFM contrast and spatial resolution of hydrophilic surfaces at normal conditions.

For AFM study of surface features on hydrophilic porous samples, two types of probes, namely standard Si cantilever and cantilever modified with single Pt/C nanowire (NW) were used. NWs were produced on the top of silicon cantilevers NSG01 by depositing Pt/C material under focused electron beam in presence of precursor gases in vacuum chamber of scanning electron microscope.

Standard Si probe and Pt/C NW probe approach/retract curves to hydrophilic Au layer deposited on Si wafer were measured in order to obtain data related to the adhesion properties of the probes used. It was shown experimentally that Pt/C NW probe had better adhesion to hydrophilic gold surface and more hydrophilic properties in comparison with standard Si probe.

Hydrophilic surface of different samples (including porous K8 glass, erythrocyte membrane, patterns in PMMA and SU-8 resists) was visualized using both standard Si probe as well as Pt/C NW modified probe in tapping and constant force modes under the same operating conditions. It was shown that use of conventional Si probes provides an inversion of real contrast whereas use of probes modified with hydrophilic Pt/C nanowires provides adequate imaging when mapping objects with dimensions smaller than critical on hydrophilic surface using AFM. The phenomenon of AFM contrast inversion and reasons of the spatial resolution improvement in case of probes modified with nanowires are based on the fact that liquid meniscus shape depends on dimensions of nanochannel [8].

We conclude that handling the AFM data requires to consider the possibility of contrast inversion phenomenon occurrence. The latter may be obtained when using standard Si cantilevers at normal conditions in tapping and contact modes due to the condensation of vapor in the nanochannels and nanopores on hydrophilic surfaces. This phenomenon takes place only when lateral size of surface feature (pore or channel) is less than the critical value of 100 nm which is associated with liquid meniscus shape changing [8]. Unlike standard Si probes the modified probes with Pt/C NW allow to eliminate artefacts in AFM imaging of nanochannels and nanopores on hydrophilic surfaces that leads to improvement in spatial resolution and contrast of AFM images.

1. A. Opitz, M. Scherge, S. Ahmed, et al., *J. Appl. Phys.* **101** (6), 064310 (2007).
2. A. Gil, J. Colchero, M. Luna, et al., *Langmuir* **16** (11), 5086 (2000).
3. M. Luna, J. Colchero, A. Gil, et al., *Appl. Surf. Sci.* **157** (4), 393 (2000).
4. P. Miranda, L. Xu, Y. Shen, et al., *Phys. Rev. Lett.* **81** (26), 5876 (1998).
5. S. Van Noort, K. Van der Werf, B. De Grooth, et al., *Ultramicroscopy* **69** (2), 117 (1997).
6. A. Kuhle, A. Sorensen, J. Zandbergen, et al., *Appl. Phys. A* **66**, 329 (1998).
7. P. Rahe, R. Bechstein, J. Schutte, et al., *Phys. Rev. B* **77** (19), 195410 (2008).
8. P. Kim, H. Kim, J. Kim, et al., *Lab on a Chip* **9** (22), 3255 (2009).

Structural-mechanical AFM study of inhomogeneous stiff nanocoating of softpolymer substrate

I.A. Morozov¹, A.S. Kamenetskikh²

¹*Institute of Continuous Media Mechanics UB RAS, 614013, Perm, Russia, ilya.morozov@gmail.com*

²*Institute of Electrophysics UB RAS, 620016, Ekaterinburg, Russia*

Modification of polymer surfaces with low-energy gas plasma (nitrogen, argon, oxygen, acetylene) is used to change the wettability of the surface and, as a consequence, to control the interaction with biological objects [1]. As a result of such treatment, a carbonized surface nanolayer [2] is formed on a wide class of polymers. Polyurethane is one of the most widespread polymers. This is the two-phase material consisting of soft and stiff blocks. The structure and fraction of the hard phase depend on the recipe and manufacturing conditions. In this work, the soft elastic polyurethane (initial elastic modulus is 30 MPa) was studied; the stiff phase of which forms a percolation thread-like network (Fig. 1). The AFM indentation of this polymer showed heterogeneous surface stiffness up to the depth of 10 nm; at higher indentation depth the stiffness becomes homogeneous.

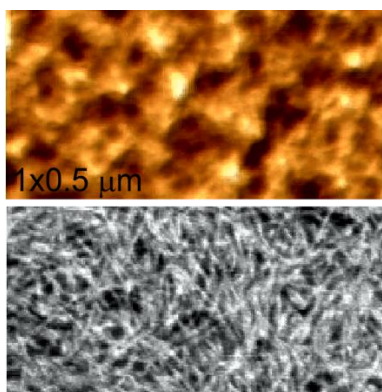


Figure 1. AFM images of relief and phase of the untreated polyurethane.



Figure 2. Indentation imprints of the treated surface.

Plasma treatment was performed in the vacuum chamber of the plasma unit. Argon and nitrogen partial pressures were set at $2 \cdot 10^{-3}$ Torr and a glow discharge with a current of 2 A was ignited in the source of a low-energy electron beam and an accelerating voltage of 100 V was set. Injection of electrons into the chamber provided generation of Ar-N₂ plasma, the particles of which interacted with the surface of the samples. Treatment time was regulated in the range of 0.5-2 minutes.

As a result of treatment, the surface acquires a rough granular structure. The obtained samples were indented with a probe with high spring constant of the cantilever and indentation imprints (Fig. 2) were observed on the surface. At the same time, the untreated polymer is recovered elastically after the similar indentation. Thus, the measured depth of the imprint was used to estimate the thickness of the hard layer (6-9 nm). The modified layer is locally inhomogeneous: its thickness depends on the surface area. The AFM study in force modulation regime established heterogeneous stiffness of the activated surfaces. The average value of stiffness increases with the treatment time, but the thickness of the layer increases to a certain limit and then does not change. All these features are related to the heterogeneous surface features of the initial polyurethane.

In addition to the structural-mechanical properties, the surface energy also changes (inversely proportional to the treatment time). Which, in turn, influences the sorption of blood proteins. The properties of such a heterogeneous stiff coatings must be taken into account when designing deformable products which surface could be damaged under certain loading conditions.

The work is supported by the RSCF grant 17-79-20042.

1. D.J. Wilson, N.P. Rhodes, R.L. Williams, *Biomaterials* **24**, 5069 (2003).

2. L. Calcagno, G. Compagnini, G. Foti, *Nucl. Instrum. Meth. B* **65**, 413 (1992).

Evaluation of mechanical and electrical parameters of individual polyaniline nanoparticles

N.A. Davletkildiev^{1,2}, I.A. Lobov¹, D.V. Sokolov¹

¹OSC SB RAS, 644024, Omsk, Russia

LI__87@mail.ru

²Dostoevsky Omsk State University, Omsk, 644077 Russia

The desire to reduce the size of electronic devices to the nanoscale makes new demands on the materials from which they are made. During the transition from the bulk structure to a separate nanoparticle, the properties of the material change significantly. Polyaniline (PANI) is one of the most important conductive polymers, which is widely used in various electronic applications. The most important characteristics of conductive polymers are mechanical and electrical parameters, the magnitudes of which largely depend on the production conditions. The properties of PANI have been investigated only with respect to its bulk state. Measurements, as a rule, are carried out on the polymer massive layers, therefore, the results are influenced by the contact interactions between PANI molecules. This paper presents the results of measurements of the electron work function, dielectric constant and elastic modulus of individual PANI nanoparticles containing a small number of molecules. The measurements were carried out in a single experiment using two methods of scanning force microscopy.

PANI was obtained via chemical oxidative polymerization of aniline [1]. The PANI nanoparticles were separated from the bulk polymer by sonication in ethanol. A suspension of nanoparticles was deposited on a freshly split HOPG. Measurements of individual PANI nanoparticles using electrostatic force microscopy (EFM) and contact atomic force microscopy (AFM) were obtained using AFM MFP-3D (Asylum Research). The electron work function was determined from the magnitude of the positive phase shift in the EFM images using the technique described in [2]. We are using the negative phase shift measured from EFM images and the model described by [3] to measure the dielectric constant for nanoparticles of PANI. The magnitudes of the Young's modulus were determined by fitting the model curve constructed using the Hertz model for a conical probe to the force-indentation curves using the Asylum Research MFP-3D Hertz analysis tool.

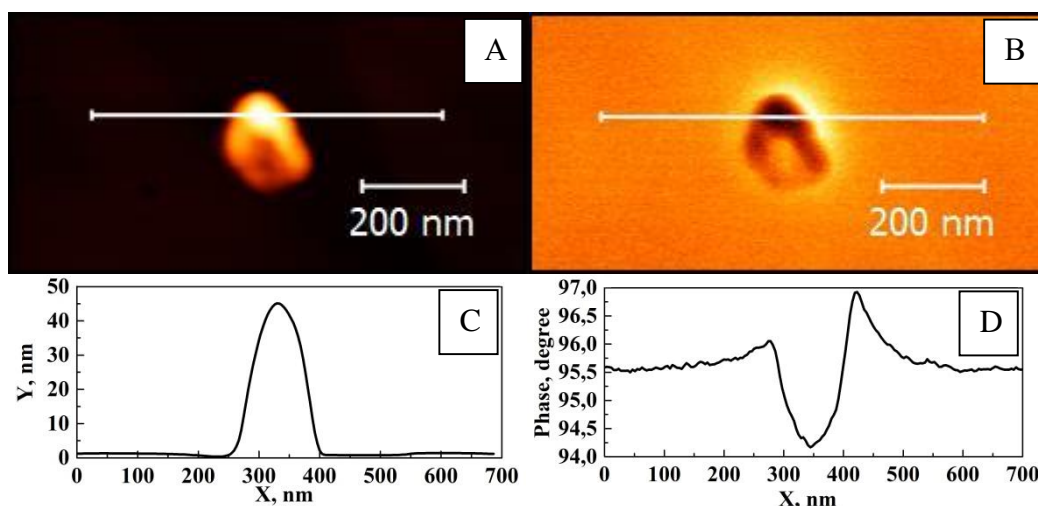


Figure 1. (a) AFM image, (b) EFM image of PANI nanoparticle, and (c,d) their cross-sections along line.

Figures 1a,b show an example of AFM and EFM images of a PANI nanoparticle consisting of several polymer macromolecules, as well as their cross-sectional profiles showing the characteristic particle size of PANI (Fig. 1c) and the contrast feature of its EFM image (Fig. 1d). An increase in the EFM signal (oscillation phase of the cantilever) around the nanoparticle indicates the presence of conductivity in it.

Figure 2a shows the parabolic dependence of the tangent of the EFM positive phase shift on the magnitude of the tip voltage. The position of the dependence minimum on the voltage axis corresponds to the contact potential difference between the tip and the PANI nanoparticle. The average electron work function of PANI nanoparticles calculated on the basis of such dependences was $W = 4.88$ eV. This value is consistent with the magnitude of the work function we obtained earlier on the PANI monolayer films.

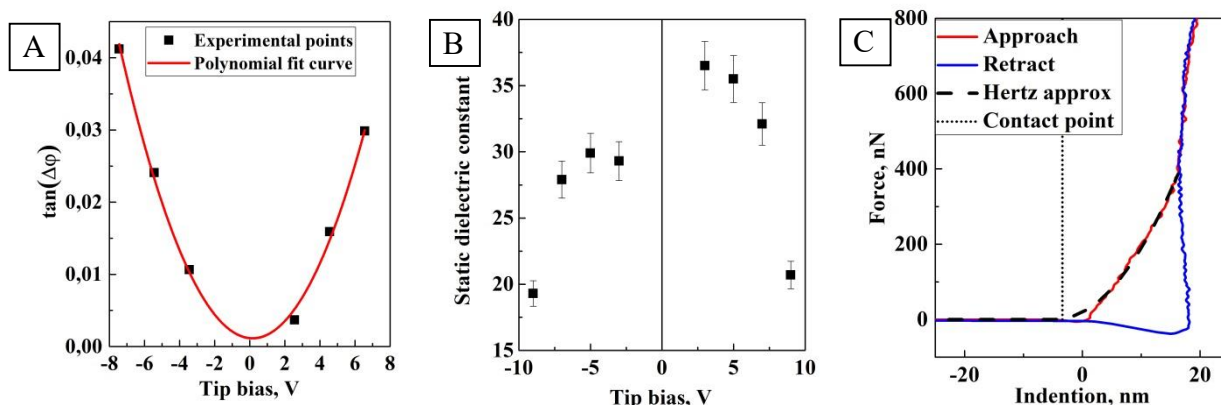


Figure 2. Typical dependences of the tangent of the EFM positive phase shift (a) and the dielectric constant (b) of the PANI nanoparticle on the applied tip voltage; (c) experimental indentation curve of a PANI nanoparticle and its approximation by the Hertz model.

Figure 2b shows the dependence of the calculated value of the static dielectric constant of the PANI nanoparticle on the applied voltage. With increasing voltage, the dielectric constant decreases, this shows a decrease in the polarizability of PANI molecules with increasing electric field strength. The obtained values of the PANI nanoparticles dielectric constant are in the value range of the PANI layers dielectric constant with different degrees of protonation [4].

Figure 2c shows a typical PANI nanoparticle indentation curve with an AFM probe, built on the basis of force curves, its approximation by a model curve constructed on the basis of solving the Hertz model for a conical probe. When calculating the elastic modulus, we used the Poisson's ratio for PANI $\nu = 0.38$ from [5]. The average value of the Young's modulus of the PANI nanoparticles was $E = 4.42$ GPa. The obtained value corresponds to typical values of the elastic modulus of the PANI layers [6].

The work was carried out according to the state task of the Omsk Scientific Center SB RAS (project registration number AAAA-A17-117041210227-8).

1. I.A. Lobov, I.K. Shulus, *Omsk scientific bulletin* **3** (159), 98 (2018).
2. N.A. Davletkildeev, D.V. Stetsko, V.V. Bolotov, et al., *Materials Letters* **161**, 534 (2015).
3. C. Staii., A.T. Johnson Jr., N.J. Pinto, *Nano Letters*. **4**, 859 (2004).
4. H.H.S. Javadi, K.R. Cromack, A.G. MacDiarmid, et al., *Physical Review B* **39** (6), 3579 (1989).
5. J. Nunes Pereira, P. Vieira, A. Ferreira, et al., *J. Polym. Res* **19**, 9815 (2012).
6. J. Nunes Pereira, H. Gholami, A. Shakeri, et al., *Current Chemistry Letters* **6**, 151 (2017).

Automation of topography and phase contrast measurements in tapping mode

Y.A. Bobrov¹, V.A. Bykov^{1,2}, S.I. Leesment¹, V.V. Polyakov¹

¹*NT-MDT Spectrum Instruments, 124460, Zelenograd, Moscow, Russia*
 polyakov@ntmdt-si.com

²*Moscow Institute of Physics and Technology, 141700, Dolgoprudny, Moscow, Russia*

The idea to use oscillating cantilever for topography measurements was proposed simultaneously with AFM invention. The beginning of wide use and popularization of tapping mode (often called “semicontact mode” in Russian language) should be referred to appearance of publications [1-3]. A bit later it was accidentally found that the phase of cantilever oscillations can also be imaged in tapping mode, in some cases giving valuable contrast of material properties [3]. Dozens of AFM modes were introduced since that time, but tapping (incl. phase imaging) still remains the most frequently exploited one. Tapping mode also serves as the basis for a variety of more complex AFM modes like Kelvin probe force microscopy (KPFM), electric force microscopy (EFM), magnetic force microscopy (MFM), etc. as well as for rapidly growing family of optical nanospectroscopy methods like scattering scanning near-field optical microscopy (s-SNOM) in visible, infrared and terahertz spectral ranges.

At the same time, our analysis shows that more than one fifth of AFM images published in peer-reviewed journals contain typical artefacts associated with switching from attractive to repulsive regimes of interaction of cantilever and surface, probe parachuting effect and incorrect setting of feedback gain value. This disheartening situation motivated the development of “ScanTronic” system which allows to automatically adjust the amplitude of cantilever oscillations, scan rate, set point and feedback gain values in tapping mode AFM to provide reliable artifacts-free results.

Parachuting effect (Fig. 1a) that occurs at sudden detach or collision of cantilever with the sample cause the most prevalent artifacts in both topography and phase images in tapping mode. It becomes extremely critical if high aspect ratio probes are used. Analysis of this effect shows allowable ranges of cantilever oscillations amplitude, scan rate, set point and feedback gain values – following these limitations, one avoids artifacts of this kind. We also propose simple yet highly effective way (Fig. 1b) to compensate parachuting artifacts in AFM images by use trace and retrace scan lines.

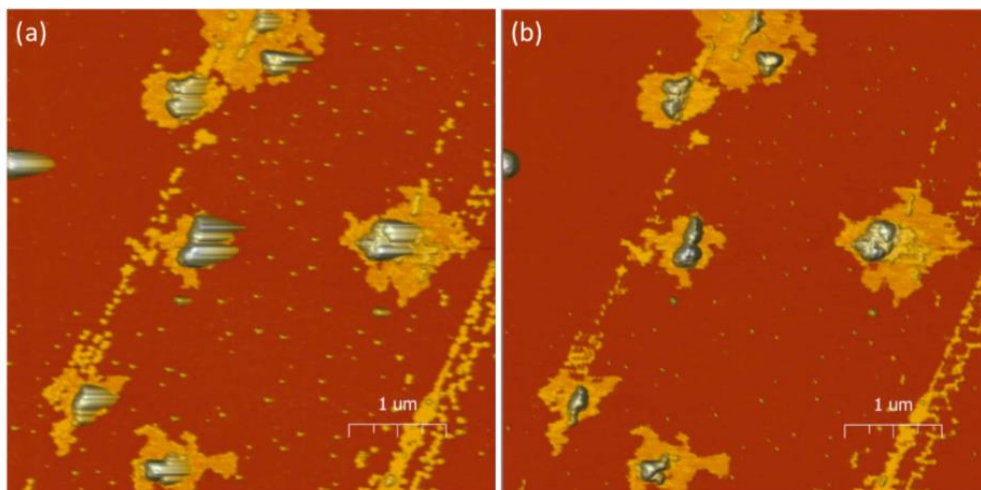


Figure 1. Fluoroalkanes F14H20 on Si imaged in tapping mode: (a) parachuting artefacts, (b) *in-situ* parachuting artefacts compensation using trace and retrace scan lines.

General consideration of AFM feedback system operation gives quite elementary but very representative relation between the error signal value $e(x)$ and feedback gain k_{FB} , scan speed dx/dt and topography gradients dH/dx : $e(x) \sim k_{FB} \cdot (dx/dt) \cdot (dH/dx)$. This relation yields that error signal can be decreased while scanning rough topographies by adaptive control of scan speed. This option, that we implement in our microscopes under “safe probe” name, allows to minimize the

risk of damage of the probe and consequently decrease average cantilever consumption per single measurement session.

Switching between attraction and repulsive regimes [4] is another often source of artefacts in tapping mode. It is well known that phase signal can be used to recognize the type (sign) of interaction between cantilever and a surface that take place during experiment. We show the way of automated control and pre-adjustment of interaction regime in tapping mode and demonstrate its effectivity.

This considerations form the basis of algorithms realized in our “ScanTronic” module. One of numerous examples of “ScanTronic” applications for studies of sPS-PVDF structure is shown in Figure 2.

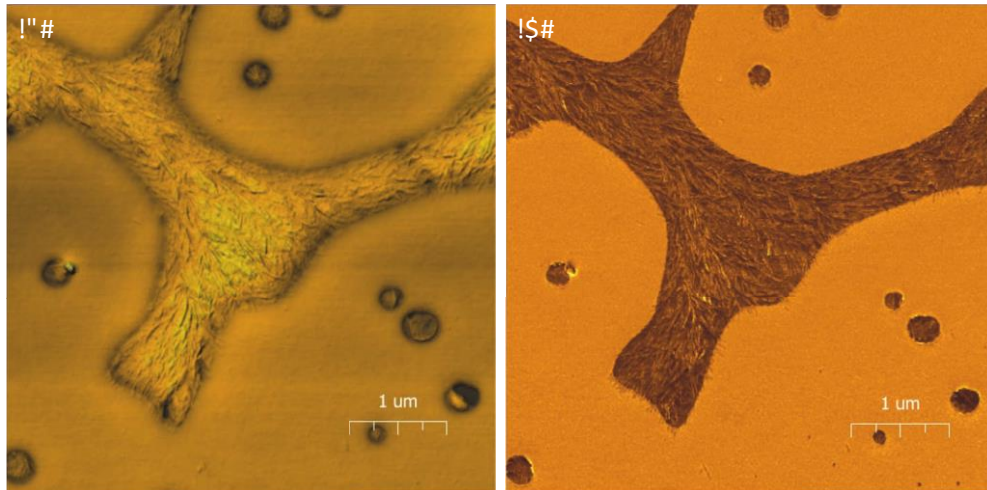


Figure 2. sPS-PVDF topography and phase contrast. Cantilever oscillations amplitude, scan rate, set point and feedback gain values are adjusted automatically by “ScanTronic”.

Thus the system for automated adjustment of scanning parameters in tapping mode is developed and corresponding physical principles are discussed. We present a number of examples showing that these principles and measures combined with linear control theory techniques and machine learning algorithms make it possible to literally completely automate the adjustment of scanning parameters in tapping mode. This approach drastically increases the quality of phase contrast images as well.

Further development of “ScanTronic” will allow to automate the adjustment of scanning parameters in more complex AFM modes for automated imaging of electrical, magnetic and other properties of surfaces with (sub-)nm level spatial resolution.

1. Q. Zhong et. al., *Surf. Sci.* **290**, 688 (1993).
2. H.G. Hansma, et al., *Scanning* **15**, 296 (1993).
3. S.N. Magonov, V.B. Elings, M. Whangbo, *Surf. Sci.* **375**, 385 (1997).
4. R. Garsia, R. Perez, *Surf. Sci. Rep.* **47**, 197 (2002)

New developments in AFM cantilevers fabrication methods

E.V. Lisov¹, A.B. Shubin²

¹*ScanSens GmbH, 28359, Bremen, Germany.
sales@scansens.com*

²*Ostek Art-Tool, 121087, Moscow, Russia*

(1) Polysilicon AFM cantilevers: technology of separate preparation of polysilicon bulk and silicon tip. Method of polysilicon bulk deposition to achieve accurately defined lever's resonance and stiffness parameters. AFM cantilevers with pencil-shape tips of Etalon Premium series for high quality AFM topography measurements.

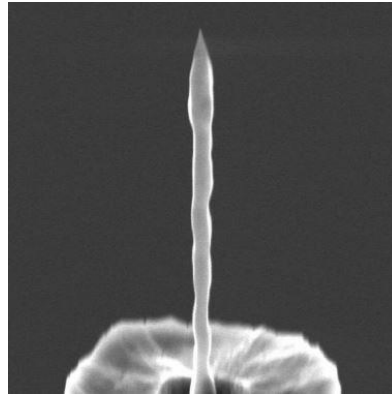


Figure 1. Pencil-shape tip of cantilevers of Etalon Premium series.

(2) Chemical stable metal W_2C coating which demonstrates stability under high force loads and currents, as the result of special technology of tip's coating conservation.

(3) AFM cantilevers with full diamond (FD) tips. Comparison of wear off velocity between full diamond and standard silicon tips using a special test structure of hemi-spherical grains. Application of FD cantilevers for investigations of topography of sticky samples.

Atomic force microscopy in polymeric chemistry's studies

T.S. Sazanova, K.V. Otvagina, I.V. Vorotyntsev

*Nizhny Novgorod State Technical University n.a. R.E. Alekseev, 603950, Nizhny Novgorod, Russia
yarymova.tatyana@yandex.ru*

Atomic force microscopy (AFM) is a unique method for polymeric surfaces visualization not only because of high lateral and vertical resolutions, but also its ability of gaining quantitative three-dimensional information about surface topography and roughness without destruction of a soft surface. Nowadays this method is oftentimes used to obtain only surface images, but polymeric surfaces contain much the largest information. Therefore it is relevant to open up AFM opportunities.

This work was aimed to develop a new approach based on AFM that allowed to establish a surface structuring mechanism of polymers during their modification (on the example of chitosan-based copolymers with polyacrylonitrile (PAN) and polystyrene (PS) modified with ionic liquids (ILs) with various anions) [1], to find out a dependence of polymers wettability, mechanical, and other functional properties on their surface structure (in particular on their roughness) (on the example polymeric films based on polysulfone (PSU), cellulose triacetate (CTA) and polyvinyl alcohol (PVA) obtained on glass substrates with different roughness), and to estimate a phase distribution at surfaces of polymer-based materials (on the example of the chitosan copolymers).

In the part of experiments with the chitosan copolymers, surface structuring features of chitosan (CS) graft and block copolymers with PAN and PS modified with ILs based on a cation of 1-butyl-3-methylimidazolium (bmim) with various anions ([BF₄], [PF₆] and [Tf₂N]) at each stage of modification were studied by step-by-step AFM scanning, and stability study of surface structure of the CS copolymers was estimated by mathematical statistics methods.

In the part of experiments with PSU, CTA, and PVA, an approach based on AFM combined with wettability measurements and mechanical testing was used. PSU, CTA and PVA polymer films were obtained by corresponding polymer solution casting using automatic coating machine MemcastPlus (Porometr, Belgium) onto three inert supports from borosilicate glass. The glass supports surface and the polymers surface were studied by a scanning probe microscope SPM-9700 (Shimadzu, Japan) using contact and tapping modes respectively. According to comparative analysis of the obtained AFM, mechanical testing, and wettability measurements results, it was found that (1) the higher intermolecular rotation freedom of a polymer, the more its surface reflects a support structure and its roughness (at significant values of supports roughness, this effect is brought to nothing); (2) polymers wetting decreases with an increase in their surface roughness because surfaces with significant roughness tend to be superhydrophobic and not wetted by most liquids; and (3) the nature of changes in polymer mechanical properties depends on their chain flexibility.

All this extensive information obtained by the proposed AFM-based approaches can be used to control polymers' functional properties by varying their surface roughness with regard to their chemical nature. This is important to develop a technique for formation of "smart" materials with given characteristics.

This work was supported by the RSF (project No. 18-19-00453).

1. T.S. Sazanova, K.V. Otvagina, I.V. Vorotyntsev, *Polymer Testing* **68**, 360 (2018).

SPM characterization of large samples

V.S. Neudachina

*Intertech Corporation, 119049 Moscow, Russia
vsn@intertech-corp.ru*

Asylum Research, a division of Oxford Instruments and a manufacturer of the quietest AFM in the market, Cypher™, has introduced a novel instrument – **Jupiter XR**, the first and only large-sample AFM to offer both high-speed imaging and extended range in a single scanner. The novel instrument provides complete 200 mm sample access and delivers higher resolution, faster results, a simpler user experience, and the versatility to excel in both academic research and industrial R&D laboratories.

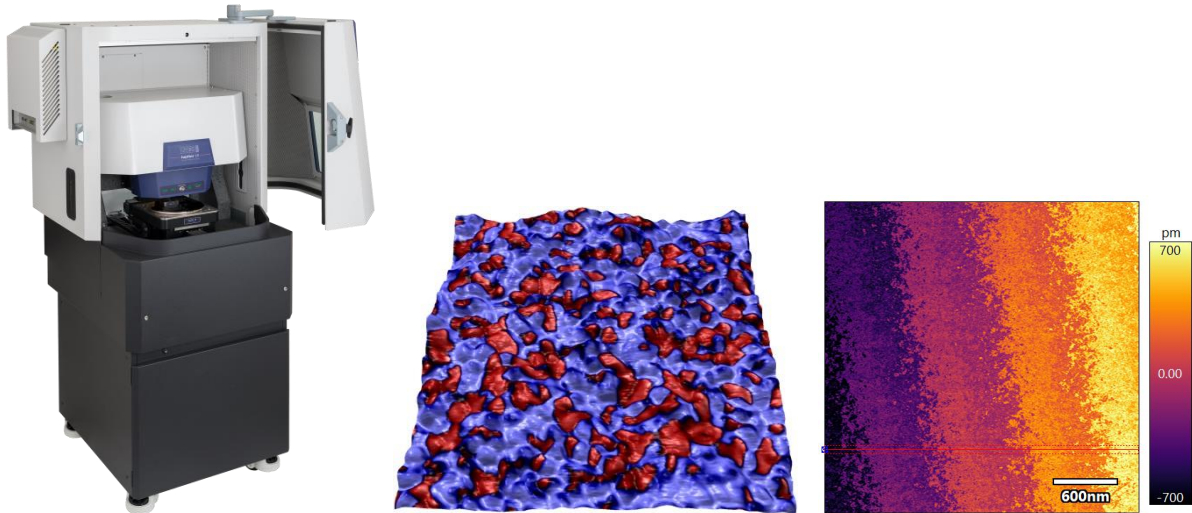


Figure 1. (Left) General view of Jupiter XR AFM; (Center) DART PFM image of a sol-gel piezoelectric film; (Right) Detailed AFM image of a SiC wafer surface with ≈ 500 pm steps.

The instrument offers higher resolution than any other large-sample AFM currently available in the market and implements the exclusive blueDrive tapping mode to improve the stability and ensure longer tip times, even with fast scanning. It also features a fully motorized laser and detector setup, sharp diffraction limited top-view optics to help locate precise regions of interest, and allows going from atomic resolution to large $100\ \mu\text{m}$ scans in any imaging modes. The concept of modular design implemented in this instrument makes it fast and simple to add accessories and future upgrades. Multisite imaging can be fully automated for both real-time measurements and subsequent offline analysis.

Jupiter XR has the lowest noise floor (below 25 pm) of any large-sample AFM and allows the researchers to routinely capture images in under 1 minute, at least 5x faster than most other AFMs. The instrument features unique LVDT position sensors that are inherently linear and never require recalibration. Low-noise X-Y sensors enable distortion-free closed-loop imaging, while ultra-low-noise Z sensor (<35 pm noise) makes measurements more accurate and repeatable.

The basic instrument configuration includes multiple scanning, nanomechanical, nanoelectrical and electromechanical modes (over 40 various modes).

Advanced integrated solutions based on atomic-force microscopy

Yu.E. Vysokikh¹, S.Yu. Krasnoborodko¹, D.A. Kozodaev²

¹MTEON, Moscow, Zelenograd, 124617, Russia
krasnoborodko@mteon.ru

²NT-MDT BV, Apeldoorn, The Netherlands kozodaev@ntmdt.nl

Atomic force microscopy (AFM) with modern techniques and combination with advanced optical methods continue to be one of the most powerful tools for advanced materials analysis at nano-scale. The NT-MDT Group (NT-MDT BV – The Netherlands; NT-MDT LLC and MTEON LLC – Russian Federation) produce Atomic-Force Microscopes and AFM based multi-method tools which are used to obtain comprehensive information about sample surface characteristics including topography, rigidity, adhesion forces mapping, spreading resistance, surface potential, magnetic domain structure etc.

| | |
|--|---|
| New generation of digital AFM controller | Implementation of all existing and perspective AFM techniques Improved fast scanning algorithms Raster Nanomechanics Analysis (RNMA mode) Direct access to more than 12 AFM signals (with no additional hardware) |
| Full automation of AFM head alignment | Automation measurement processes for routine research Possibility to adjust measuring head via software (including operation in vacuum) |
| New generation of AFM optical head | Outstanding level of AFM and optical methods combination in all new design with possibility of high efficiency laser illumination in “side”, “bottom” and “top” scheme. |
| Powerful Raman spectrometer | Spectrometer with automated switch between up to 5 lasers and cover whole optical range from UV to near IR Fast laser scanning using galvano-mirrors Coherent spectroscopy of combination anti-Stokes light scattering (CARS) |
| High resolution magneto-optical microscopy | Novel design of Si aperture probe helps to achieve efficient illumination, focusing. Light collection with possibility of independed detecting XY polarization direction |
| LTEM | Combination of AFM and laser terahertz emission microscopy |

The team has more than 20 years' experience in the development and production of atomic force microscopes. The NT-MDT group provide maintenance, service support and upgrade of all AFM based devices which were produced under the NT-MDT brand name - installed in Russia and world-wide.

Scienta-Omicron high-end UHV SPM modern instrumentation

M.A. Trusov, M.G. Minin

*IMC Group Ltd., Russia 117638, Moscow
minin@imc-systems.ru*

Scienta-Omicron is the leading innovator in Surface Science. The company provides top capabilities for the research community through its UHV technology leadership in scanning probe microscopy, electron spectroscopy, and thin film deposition. Scienta-Omicron was always known as the innovative manufacturer of scanning probe microscopes providing leading edge technology for forefront research and science, including unrivalled quality and reliability standards to enable the customers to do successful research.

Today Scienta-Omicron offers a wide variety of SPM techniques for UHV at variable temperatures (from 25 K to 1500 K), for low temperature applications (down to 0.5 K), for high-magnetic field research (up to 3T), or for large samples (up to 4" in diameter). These instruments are available as stand-alone components, within turn-key UHV SPM systems, and also as parts of multi-technique solutions tailored to the customer needs from one source with worldwide sales and service groups.

In this talk we will consider new UHV SPM technologies and instruments from Scienta-Omicron, both for basic STM and spectroscopy, and for AFM with QPlus and beam-deflecting techniques for hi-end surface research.

Water adsorption and polar properties of self-assembled diphenylalanine nanotubes

P. Zelenovskiy^{1,2}, E. Domingues³, M. Kornev¹, V. Slabov³, A. Nuraeva¹, S. Vasilev^{1,4},
V. Yuzhakov¹, S. Kopyl³, F.M.L. Figueiredo³, V. Shur¹, A. Kholkin^{1,3}

¹*School of Natural Sciences and Mathematics, Ural Federal University, 620000, Ekaterinburg, Russia*

²*Department of Chemistry & CICECO–Aveiro Institute of Materials, University of Aveiro,
3810-193, Aveiro, Portugal
zelenovskiy@urfu.ru*

³*Department of Physics & CICECO–Aveiro Institute of Materials, University of Aveiro,
3810-193, Aveiro, Portugal*

⁴*Chemical Department, University of Limerick, Castletroy Limerick, Ireland*

Self-assembled micro- and nanotubes of diphenylalanine dipeptide (H-Phe-Phe-OH, FF) represent promising functional biomaterial for new medical and energy harvesting devices [1] due to its outstanding piezoelectric [1, 2], pyroelectric [3] and mechanical [4] properties. After the self-assembly in aqueous solution water molecules remain captured inside the nanochannels, stabilize its structure [5] and modify physical properties. Here we studied water adsorption in FF nanochannels, its structure and polar properties.

Room temperature nitrogen and water adsorption measurements showed that the specific surface area of FF nanotubes is comparable with that of polymers of intrinsic microporosity, several kinds of metal-organic frameworks and porous carbons. Single-crystal X-ray diffraction and computer modeling revealed the reconstruction of the bound water layer at low temperatures, whereas the peptide shell remains almost the same. Temperature of this reconstruction corresponds to a phase transition observed recently at 230 K by dielectric measurements [6]. Ab-initio calculations showed that all analyzed water structures are polar, and the direction and values of their dipole moments were obtained. For all temperatures the dipole moment is mainly oriented along the nanotube's axis and is opposite to the dipole moment of the peptide shell, thus reducing the total polarization of the nanotube. However, the direct piezoelectric measurements demonstrated non-monotonous decrease of the piezoelectric coefficient with water removing. The origin of this contradiction is not clear yet.

Experimental part of this work was performed within the scope of the project CICECO-Aveiro Institute of Materials, FCT Ref. UID/CTM/50011/2019, financed by national funds through the FCT/MCTES. Theoretical part of the work was supported by Russian Science Foundation (Grant No. 18-72-00052). S.K., P.Z. and A.K. are grateful to FCT project PTDC/CTM-CTM/31679/2017. P.Z. is grateful to FCT project PTDC/QEQ-QAN/6373/2014. S.K and A.K are grateful to joint Portugal-Turkey project (TUBITAK/0006/2014).

1. A. Kholkin, N. Amdursky et al., *ACS Nano* **4**, 610 (2010).
2. S. Vasilev, et al., *J. Phys. Chem. Solids* **93**, 68 (2016).
3. A. Esin, et al., *Appl. Phys. Lett.* **109**, 142902 (2016).
4. I. Azuri, L. Adler-Abramovich et al., *J. Am. Chem. Soc.* **136**, 963 (2014).
5. T. Andrade-Filho, T. Martins et al., *Theor. Chem. Acc.* **135**, 185 (2016).
6. F. Salehli, D. Chovan et al., Submitted *Adv. Funct. Mater.* (2019).

Smart hybrid nanostructures for cancer treatment

N.D. Thorat¹, C. Silien^{2,3}, S.A.M. Tofail^{2,3}, J. Bauer¹

¹*Department of Bioengineering, Faculty of Fundamental Problems of Technology, Wroclaw University of Science and Technology, 50-370 Wroclaw*

²*Department of Physics, University of Limerick, Limerick, V94 T9PX, Ireland*

³*Bernal Institute, University of Limerick, Limerick, V94 T9PX, Ireland*

In last decade, the smart hybrid nanostructures (SHN) have been proposed for the theranostic of various types of human cancers. This includes technologies that enable simultaneous diagnosis, primary and if necessary secondary treatment, as well as monitoring of the therapy outcomes. Numerous SHN are nowadays used as remotely triggered modalities, such as organic and inorganic nanostructures, organic-inorganic conjugates, polymer micelles, liposomes etc. These SHN can be administrated directly or indirectly into tumors and respond to different external physical stimuli e.g. ultraviolet, visible or near-infrared light, radiofrequency waves, X-ray, alternating magnetic field or ultrasound waves. Among of all SHN, the nanocomposites that may be stimulated by light and used as remote triggers to exert anti-tumor activity through irradiation are of particular interest. Currently, the light-mediated cancer theranostic is more likely to apply near infrared radiation (NIR) than ultraviolet (UV) or visible light (VIS), which is related to greater and deeper NIR penetration into the tissues and less scattering, however the exact light used depends on the type of the nanomaterial and therapeutic modality [1, 2].

Light-stimulated nanotheranostics are usually combined with various types of therapies, such as photodynamic therapy (PDT), photothermal therapy (PTT), photo-triggered chemotherapeutics (PTCH) or two-photon triggered therapy (TPTT) [3]. They are frequently integrated into a single multifunctional nanoplatform, that may use different light triggered co-therapy modalities by designing smart multifunctional materials that combine different types of imaging and therapeutic agents. A number of new strategies have recently been developed to enhance the overall therapeutic effect of SHN, e.g. oxygen self-enriching photodynamic therapy (Oxy-PDT) where the photosensitizer is stuffed into perfluorocarbon nanodroplets to optimize tumor oxygenation or decorating platinum nanozymes on photosensitizer integrated metal organic frameworks (MOFs) to enhance PDT. New methods of increasing light penetration into tissues are also being tested, such as wireless photonic activation, which enables on-demand light excitation of photosensitizers for therapeutic dosimetry. On the contrary, in case of sensitive human organs the wireless systems for metronomic cancer treatment (long-term low-dose PDT) are proposed to offer an alternative way of tumors treatment. Correspondingly, the innovative optical technologies, that provide more efficient light penetration into deeply located tissues with much less attenuation using new transparency regions NIR-III (1600-1870nm) and NIR-IV (2100-2300 nm) are developed [4, 5].

Concluding, the current generation of tumor theranostic strategies seek to strengthen both, therapy and diagnosis using multifunctional smart hybrid nanostructures coupled with minimally invasive biomedical devices that maximize the permeability of the drug to the tumor and interaction with applied physical stimuli to effectively treat cancers.

The project leading to this work has received funding from the European Union's Horizon 2020 research and innovation programme under the Marie Skłodowska-Curie grant agreement No 751903.

1. R.A Bohara, N.D. Thorat, *Hybrid nanostructures for cancer theranostic*, Elsevier, (2019).
2. Sonali, V.M. Viswanadh, R.P. Singh, et al., *Nanotheranostics* **2**, 70 (2018).
3. H. Kim, K. Chung, S. Lee, et al., *Wiley Interdiscip. Rev. Nanomed. Nanobiotechnol.* **8**, 23 (2016).
4. N.D. Thorat, H. Townely, G. Brennan, et al., *ACS Biomater. Sci. Eng.* **5**, **6**, 2669 (2019).
5. J. Shi, P.W. Kantof, R. Wooster, O.C. Farokhzad, *Nat. Rev. Cancer.* **17**, 20 (2017).

Resistive switching phenomena in thin ferroelectric films

N.V. Andreeva¹, A. Petraru³, A. Petukhov², A.V. Batueva¹

¹*Saint Petersburg Electrotechnical University "LETI", 197376, Saint Petersburg, Russia
nvandr@gmail.com*

²*Nanoelektronik, Technische Fakultät, Christian-Albrechts-Universität zu Kiel, D-24143 Kiel, Germany*

³*St. Petersburg State University, Saint Petersburg, Russia*

We investigate the mechanisms of electron transport relating to resistive switching effects in BaTiO₃ thin ferroelectric films. For this purpose, we varied the thickness (in the range of 3-12 nm) and the structure (epitaxial, nanocrystalline and polycrystalline) of BaTiO₃ thin film in the STO/LSMO/BTO systems. Thin ferroelectric films were characterized by means of piezoresponse force microscopy, tunneling atomic-force microscopy and XRD measurements. Ferroelectric and resistive properties of heterostructures were measured in the temperature ranging from 40 K to room temperature. Low temperature measurements were done under ultra-high vacuum conditions.

We suppose that the specificity of transport mechanisms in BaTiO₃ ultrathin films is defined by the ratio of film thickness and the mean free path of injected electrons. We conclude that for thin epitaxial ferroelectric films below the certain thickness (less than ≈ 3.5 nm) a dominant contribution in a current through the structure arose from elastic tunneling. *I-V* characteristics of these structures are nonlinear, symmetrical without hysteresis [1].

Increasing the thickness or changing the structure of a thin ferroelectric film (from epitaxial to polycrystalline) leads to an impact from non-elastic, trap-assisted tunneling in current (traps are presented by oxide defects). An appearance of *I-V* curve hysteresis at voltages close to the coercive voltage of the ferroelectric film is observed. Partially, this hysteresis could be explained by an impact of currents, related to the repolarization of ferroelectric film. An analysis of experimental *I-V* curves for ferroelectric thin films with thicknesses in the range of 3.5-12 nm suggests an influence of space charge limited currents on a transport mechanism through the structures. Study of the local electrical properties of polycrystalline ferroelectric films by means of tunnel atomic-force microscopy justifies that the resistive switching is driven by the bulk properties of crystallites, but not by its boundaries.

The results of low temperature measurements evident the correlation of the *I-V* curve hysteresis with the ferroelectric properties of thin films: cooling down of the samples causes increase in the value of voltages at which *I-V* curve hysteresis appeared (compatible with the temperature dependence of ferroelectric film coercive voltage [2]).

Cycling measurements of the resistive switching effects in BaTiO₃ thin film under UHV conditions revealed the shift of the voltage referred to the development of *I-V* curve hysteresis to the lower values with the number of switching cycle. After 10-15 switching cycles in UHV, the voltage at which *I-V* curve hysteresis appeared is stabilized to a certain value. This fact could indicate on the role of oxygen vacancies in the resistive switching phenomena in thin ferroelectric films.

Concluding, we assume that the switching of the resistance in thin ferroelectric films is originated from the reciprocal influence of the built-in electric field (due to the polarization) and the specificity of electron transport, implying the trap-assisted tunneling and space charge limited current.

1. N. Andreeva, A. Petrov, A. Petraru, et al., *Mater. Res. Express* **6**, 026427 (2019).

2. N. Andreeva, M. Tyunina, A. Filimonov, et al., *Appl. Phys. Lett.* **104** (11), 112905 (2014).

The investigation of the time characteristic of local polar inhomogeneities in paraelectric phase in relaxors and ferroelectric crystals: on the example of $\text{Sr}_x\text{Ba}_{1-x}\text{Nb}_2\text{O}_6$ crystals with different chemical composition

I.V. Zaytseva, A.M. Pugachev

Institute of Automation and Electrometry SB RAS, 630090, Novosibirsk, Russia
ZaytsevaIV@iae.sbras.ru

Local polar inhomogeneities arising in the paraelectric phase in certain temperature range are a unique feature of relaxors and some ferroelectrics. Dynamic of these inhomogeneities are different in relaxor and ferroelectric crystals. It is known that these regions effect on temperature behavior of a central peak associated with the fluctuations of order parameter (polarization). The anomalies of elastic modules (sound velocity) in the paraelectric phase also appear due to the presence of local polar inhomogeneities. However, the relationship between anomalies of the elastic moduli and local polar inhomogeneities in ferroelectric crystals and relaxors remains unstudied now.

In present work the temperature behavior of elastic modules in $\text{Sr}_x\text{Ba}_{1-x}\text{Nb}_2\text{O}_6$ (SBN- x) crystals with chemical compositions $x = 0.33, 0.5, 0.61, 0.75$, BaTiO_3 and PMN crystals were investigated by Brillouin light scattering using six-passed Fabry-Perot interferometer. The central peak was measured by Raman scattering using spectrometer TriVista 777. The temperature dependencies of position (elastic module) and FWHM of longitudinal acoustic mode (LA mode) and central peak were investigated in mentioned above samples. Acoustic anomalies of an elastic module in a wide temperature range were observed. Assuming the existence of local piezoelectric effect inside polar inhomogeneities a relaxation time τ fluctuations was determined. Obtained relaxation time was being compared with that of the central peak.

The reported study was funded by RFBR according to the research projects No. 18-02-00399 and State assignment No AAAAA17-117052410033-9. The experiments were performed in the multiple-access center “High-Resolution Spectroscopy of Gases and Condensed Matter” in IA&E SBRAS (Novosibirsk, Russia).

Optical and electrophysical properties of Ce-doped Gd₃Al₂Ga₃O₁₂

V.M. Kasimova^{1,2}, N.S. Kozlova¹, O.A. Buzanov³, A.P. Kozlova¹, E.V. Zabelina¹

¹National University of Science and Technology MISiS, 119049, Moscow, Russia

²FRC "Crystallography and Photonics" of the Russian Academy of Sciences, 119333, Moscow, Russia

³JSC Fomos-Materials, 107023, Moscow, Russia
kasimovavalya@mail.ru

Scintillators are used to detect ionizing radiation and particles of high and low energies. New challenges of modern science and technology demand new scintillation materials. Nowadays oxide crystals appear to be the most popular materials for scintillation detectors. One of such crystals is cerium-doped gadolinium-aluminum-gallium garnet (Gd₃Al₂Ga₃O₁₂:Ce, GAGG:Ce), it was first synthesized in 2011 [1]. GAGG:Ce is garnet type crystal with cubic group of symmetry, space group Ia₃d [2].

This crystal is a non-hygroscopic, chemically stable material with high density (6.63 g/cm³) and the highest light yield among oxygen-containing scintillators (40–60)×10³ photon/MeV, with high radiation hardness and transparent to its own radiation [2, 3]. GAGG:Ce is considered for use in medical visualization equipment such as a sensor element in a positron emission tomograph (PET) due to the properties required for PET detectors [4].

Though physical properties of these crystals have been investigated for previous 8 years, the fundamental optical properties still have been studied slightly. For instance, refractive indices are reported in few manuscripts [5, 6] and vary considerably. Moreover the literature review showed the absence of information about Gd₃Al₂Ga₃O₁₂:Ce electrophysical properties.

Therefore the aim of the research is the determination of optical and electrophysical parameters of GAGG:Ce.

The investigated GAGG: Ce crystals are grown by the Czochralski method in the company JSC Fomos-Materials. In the Accredited Testing Laboratory "Single Crystals and Stock on their Base" of NUST "MISiS" the optical parameters were studied by spectrophotometric methods: transmittance and reflectance, absorbance and refractive indices. Two methods for the refractive indices determination are implemented on a spectrophotometer "Cary 5000" with the universal measuring accessory "UMA" (Agilent Technologies): the method of reflection at near-normal incidence and the Brewster method.

The spectral dependences of GAGG: Ce are non-monotonic with the characteristic absorption bands with maxima $\lambda \approx 440$ nm, $\lambda \approx 340$ nm, $\lambda \approx (300-310)$ nm, $\lambda \approx 270$ nm, $\lambda \approx 230$ nm. The estimation of the optical band gap of these crystals by the Tauc method showed a value of 5.88 ± 0.05 eV.

The electrophysical properties were investigated by the special equipment for measurement of thermal dependences of electrical conductivity.

1. K. Kamada, T. Yanagida, T. Endo, et al., *IEEE NSS/MIC*, 1927(2011).
2. M. Tyagi, F. Meng, M. Koschan, et al., *J. Phys. D: App. Phys.* **46** (47), 475302 (2013).
3. V. Alenkov, O. Buzanov, G. Dosovitskiy, et al., *Nucl. Instrum. Methods Phys. Res., Sect. A.* **916**, 226 (2019).
4. B. Seitz, A.G. Stewart, K. O'Neill, *IEEE NSS/MIC* (2013).
5. N.S. Kozlova, O.A. Buzanov, E.V. Zabelina, et al., *Crystals Crystallography Reports*, **61**, 474 (2016).
6. K. Kamada, Y. Shoji, V.V. Kochurikhin, et al., *J. Crystal Growth* **452**, 81 (2016).

Progressive prediction using instrumental variable for accurate prediction of band gap of ABO₃ perovskites

Ch. Li¹, H. Hao¹, G. Zhao¹, H. Liu^{1*}, B. Xu^{2*}

¹State Key Laboratory of Advanced Technology for Materials Synthesis and Processing and International School of Materials Science and Engineering, Wuhan University of Technology, Wuhan 430070, P.R. China

²State Key Laboratory of New Ceramics and Fine Processing School of Materials Science and Engineering, Tsinghua University, Beijing 100084, P.R. China

*lxhxp@whut.edu.cn; xuben@mail.tsinghua.edu.cn

Perovskite-type oxide materials have been extensively used in many technologically applications due to their unique physical and chemical properties [1, 2]. The band gap is a key parameter that governs the conductivity of superconductor and the efficiency of perovskite solar cells. And it is usually measured by experiments or quantum mechanics calculations, but the drawbacks of expensive and time-consuming make the screening of possible compounds impractical [3, 4]. Therefore, a rapid and accurate method for predicting band gap of perovskites is urgently required. In this work, we proposed a robust machine-learning framework with instrumental variable – formation energy – to predict the band gap of perovskites progressively. An optimal feature set containing 24 attributes was established, and the modulus of bond-valence vector sum [5] on three sites (A, B and O site) were chosen to represent the structural distortion. After establishing a robust formation energy regression model ($R^2:0.964$), the predicted value was used as an instrumental variable to predict the band gap, and a tremendous precision ($R^2:0.857$) was obtained. A structure-property relationship mapping perovskites band gap is concurrently excavated that the number of electrons in d orbital, formation energy and modulus of bond-valence vector sum on O site are the three most crucial and relevant predictors.

Figure 1 shows the overall workflow of the progressive learning method. Schematic presents the details of perovskite compounds collection and the outlines of progressive learning workflow, including E_f prediction, instrumental variable generation, E_g prediction and results analysis.

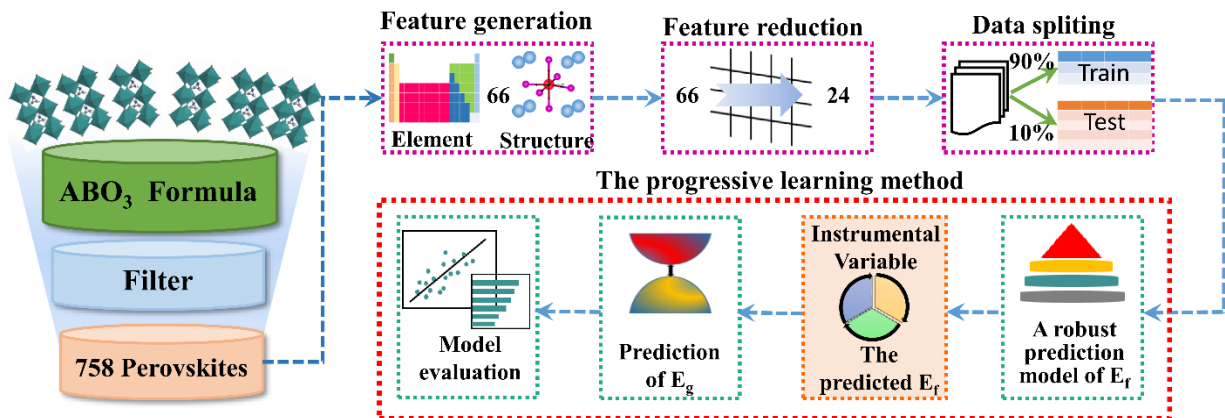


Figure 1. Overall workflow of the progressive learning method.

1. G. Pilia, P.V. Balachandran, J.E. Gubernatis, T. Lookman, *Acta Crystallographica Section B: Structural Science, Crystal Engineering and Materials* **71**, 507 (2015).
2. C. Ablitt, S. Craddock, M.S. Senn, A.A. Mostofi, N.C. Bristowe, *npj Computational Materials* **3**, 44 (2017).
3. P. Geerlings, F.D. Proft, W. Langenaeker, *Chemical Reviews* **103**, 1793 (2003).
4. E. Kim, K. Huang, S. Jegelka, E. Olivetti, *npj Computational Materials* **3**, 53 (2017).
5. Y. Qi, S. Liu, I. Grinberg, A.M. Rappe, *Physical Review B* **94**, 134308 (2016).

The study on AZO based hybrid transparent electrode and its application in perovskite solar cells

J. Xiong, W.H. Zhang, J.J. Zou, H.S. Gu

Hubei Key Laboratory of Ferro- & Piezo-electric Materials and Devices, Faculty of Physics and Electronic Sciences, Hubei University, 430062, Wuhan, P.R. China
guhsh@hubu.edu.cn

The presentation will focus on improving the performance of the perovskite solar cells via fabricating novel transparent electrode with superior photoelectrical properties and selecting as well as modifying the electron transport material, and carried out the following works:

(1) A triple-layered transparent conductive film, AZO/Pd/AZO (APA), was deposited via magnetron sputtering on glass substrate at room temperature. The resistivity of APA film annealed in hydrogen atmosphere rapidly decreased. Optical measurements indicated that the optical band gap (E_g) of APA films varies from 3.37 eV to 3.69 eV with adjusting annealing temperature from 200 °C to 500 °C. The very low resistivity of $4.8 \times 10^{-4} \Omega \text{ cm}$ with a sheet resistance of 45 Ω/sq , a transmittance of 83.2% and a figure of merit value of $3.53 \times 10^{-3} \Omega^{-1}$ were obtained after hydrogen annealing at 400 °C.

(2) ITO/Ag grid/AZO hybrid electrode was used for low-temperature planar perovskite solar cell with the electron transport-layer of ZnO nanoparticles. The results demonstrate that neither a mesoporous scaffold nor any high-temperature processing steps were required and the PCE as high as 13.86% was achieved. ITO/Ag grid/AZO hybrid electrode with the optimized Ag grid of $15 \times 100 \mu\text{m}$ showed an extremely low sheet resistance of 3.8 Ω/sq and a relatively high transparency of 89.6% at the wavelength of 550 nm. A very high FOM of $8.8 \times 10^{-2} \Omega^{-1}$ was achieved by combining outstanding electrical properties of ITO and excellent optical properties of AZO.

Domain engineering in relaxor-PT ferroelectric single crystals

C. He, J. Xiong, X. Long

Fujian Institute of Research on the Structure of Matter, Chinese Academy of Sciences, 350002, Fuzhou, China

hechao@fjirsm.ac.cn, lxf@fjirsm.ac.cn

Domain engineering is an important and effective technique for enhancing piezoelectric properties in ferroelectric single crystals. The <001>-oriented rhombohedral relaxor-PT ferroelectric single crystals, such as PMN-PT and PZN-PT, exhibit ultrahigh piezoelectric properties due to engineered domain configuration. This engineered-domain configuration technique makes use of the anisotropy of the ferroelectric single crystals as a function of the crystallographic orientation. For example, the [001] poled orthorhombic BaTiO₃ crystals with the engineered domain configurations exhibited d_{33} of over 500 pC/N and k_{33} of over 85%. For relaxor-PT ferroelectric single crystals, there are several ways to manipulate engineered-domain configuration for enhancement the piezoelectric properties, such as applying nanocomposite electrodes, modifying the pattern of electrodes and utilizing different poling methods. Recently, Yamamoto and Yamashita et al. reported an alternating current poling (ACP) method that can enhance the dielectric and piezoelectric properties of PMN-PT crystals.

The ACP method may be an effective domain engineering technique for enhancing piezoelectric properties of relaxor-PT ferroelectric single crystals. The reported work about the ACP focused on the PMN-PT crystals with low coercive field. The smaller of the coercive field is, the easier of the domain reverse. It is not clear the effect of domain engineering for relaxor-PT ferroelectric single crystals with high Curie temperature and large coercive field. In this work, PIN-PT single crystals were grown by top-seeded solution method, new poling method for domain engineering was used to enhance the piezoelectric properties of PIN-PT crystals. The d_{33} of PIN-PT single crystal is 1050 pC/N, 1450 pC/N after DCP and ACP at room temperature respectively. The d_{33} after ACP was equivalent to the value after DCP at high temperature. The d_{33} after ACP was not satisfied due to high coercive field of PINT (8-12 kV/cm, which is 3-4 times larger than that of PMNT single crystal). We modified the poling process, the optimal piezoelectric coefficient was 2350 pC/N obtained by tuning the steady-state time. The steady-state time was crucial for the poling the ferroelectric single crystals with high large coercive field.

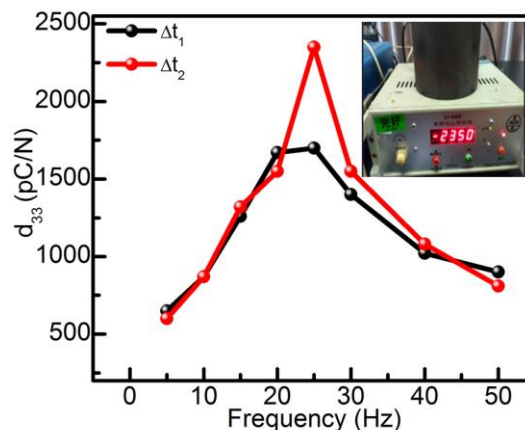


Figure 1. Frequency dependence of d_{33} of PINT ferroelectric single crystals under different steady time.

1. C. He, X. Li, Z. Wang, et al, *J. Alloys Compd.* **539**, 17 (2012).
2. Y. Yamashita, N. Yamamoto, Y. Hosono, K. Itsumi, U.S. patent: US 2015/0372219 A1.
3. J. Xu, H. Deng, Z. Zeng, et al, *Appl. Phys. Lett.* **112**, 18290 (2018).

Effect of titanium in LiNbO₃ on domain growth during *e*-beam writing

L.S. Kokhanchik¹, S.M. Shandarov², T.R. Volk³

¹*Institute of Microelectronics Technology and High Purity Materials RAS, 142432, Chernogolovka, Russia*
 mlk@iptm.ru

²*Tomsk State University of Control Systems and Radioelectronics, 634050, Tomsk, Russia*

³*A.V. Shubnikov Institute of Crystallography, FSRC 'Crystallography and Photonics' RAS, 119333, Moscow, Russia*

Lithium niobate (LiNbO₃) is a basic material for optical integrated circuits of quantum photonics. Periodic domain structures in combination with nonlinear optical waveguide layers on lithium niobate make it possible to realize with high efficiency quasi-phase-matching (QPM) radiation conversion. The *e*-beam writing of domains is an alternative approach of non-contact creation of periodical domain structures and provides a possibility to fabricate domains on the non-polar surfaces of LiNbO₃. In addition, this non-polar geometry of *e*-beam writing is accessible for 3D characterization of the created domains [1].

We present our results on domain growth investigation in titanium doped LiNbO₃ crystals. The early observed specificity of domain emerging in Ti:LiNbO₃ waveguides [2, 3] has revealed necessity of more detailed understanding of the titanium influence on the domains emerging by *e*-beam writing.

The samples under study were optically polished LiNbO₃ plates of non-polar orientation. The following compositions were investigated and compared: a nominally pure LiNbO₃ of congruent composition (CLN); LiNbO₃ doped with 0.5 mol.% TiO₂ (CLN-0.5Ti); and Ti:LiNbO₃ waveguide, obtained by high-temperature titanium diffusion. Near the Ti: LiNbO₃ surface a concentration of titanium was ~ 7.6 at.%, and then C_{Ti} gradually decreased to 0.5-0.8 at.% in 4-5 μm depth.

The *e*-beam writing of single domains and periodical gratings of planar type was carried out at the different SEM accelerating voltages. A comprehensive investigation of individual domains and periodical structures was performed by using chemical etching and the nondestructive low voltage SEM and SHG microscopy. Three-dimensional (3D) structure of the planar domain gratings in Ti:LiNbO₃ waveguide was observed depending on the *e*-beam writing conditions. The features of domain growth on non-polar Y cuts in CLN, CLN-0.5Ti and in the waveguide Ti:LiNbO₃ were investigated. The differences revealed in the domain sizes as well in the domain structure characteristics of upper and bottom of the domain gratings are discussed in the framework of the current model of intrinsic defect structure of LiNbO₃ and an increase of conductivity along the Ti:LiNbO₃ depth related to the C_{Ti} variations.

The results obtained show ways to match the conditions of *e*-beam irradiations to the waveguide thickness in order to optimize the grating position, uniformity of domains and waveguide quasi-phase-matching SHG [4].

1. T.R. Volk, L.S. Kokhanchik, R.V. Gainutdinov, et al., *J. Adv. Dielectrics* **8**, 1830001 (2018).
2. C. Restoin, C. Darraud-Taupiac, J.L. Decossas, et al., *J. Appl. Phys.* **88**, 6665 (2000).
3. L.S. Kokhanchik, M.V. Borodin, N.I. Burimov, et al., *Phys.Sol.St.*, **52**, 1722, (2010).
4. S.M. Shandarov, L.S. Kokhanchik, T.R. Volk, et al., *Quant.Electr.* **48**, 761 (2018).

Electron beam periodical poling in [001]c-poled PMN-39PT single crystal

D.S. Chezganov¹, E.O. Vlasov¹, L.V. Gimadeeva¹, E.A. Pashnina¹, P.S. Zelenovskiy¹,
E.D. Greshnyakov¹, X. Liu², Y. Zhao², Q. Hu², X. Wei², V.Ya. Shur¹

¹*School of Natural Sciences and Mathematics, Ural Federal University, 620000, Ekaterinburg, Russia*
chezganov.dmitry@urfu.ru

²*Xi'an Jiaotong University, 710049, Xi'an, P.R. China*

The Pb(Mn_{1/3}Nb_{2/3})O₃-PbTiO₃ (PMN-PT) ferroelectric single crystal is a very attractive material for nonlinear optical application due to the estimated nonlinear-optical coefficients. This requires methods of precise control of domain wall positions for the creation of precise periodical domain structures [1].

We have used charge injection by controlled e-beam irradiation [2] of the artificial surface dielectric layer covering PMN-PT single crystal to create the tailored domain structure. The domain formation has been studied experimentally. The results explained in terms of kinetic approach [3].

We revealed the switching of *c*-domains leading to formation of the tailored domain structures. We have measured the dose dependence of the shape and size of isolated domain as a result of dot irradiation. The switched domain area demonstrates the typical linear dose dependence up to 50 pC while at higher doses goes to saturation with a large dispersion (Fig. 1a). The linear dependence can be attributed to screening of depolarization field by injected charge. The obtained saturation is caused by electrostatic interaction of domain walls or influence of *a*-domains. The domain shape changes with dose increase from circular (Fig. 1b) to irregular.

We used the line and stripe irradiation mode for creating 1D periodical patterns (Fig. 1c). The increase of the width of stripe domains at the irradiated surface with dose has been revealed. The appearance of the fingers at domain walls oriented mainly at the angle close to 45° relative to [100] direction was revealed at the highest doses.

We have demonstrated the ability to create the stripe domains along arbitrary direction as well as ring-shaped domains (Fig. 1d). Since any area element consists of discrete points the circle domain shape upon dot irradiation at low doses is the key point which allows us to produce domain patterns with arbitrary geometry. The width of stripe domains was independent on direction. The confocal Raman microscopy modified for PMN-PT was used for domain imaging in the crystal bulk [4]. We have shown that domain grew down to 200 μm while periodical pattern conserved down to 30 μm. The obtained knowledge can be used for creating elements with periodical domain structures for light frequency conversion.

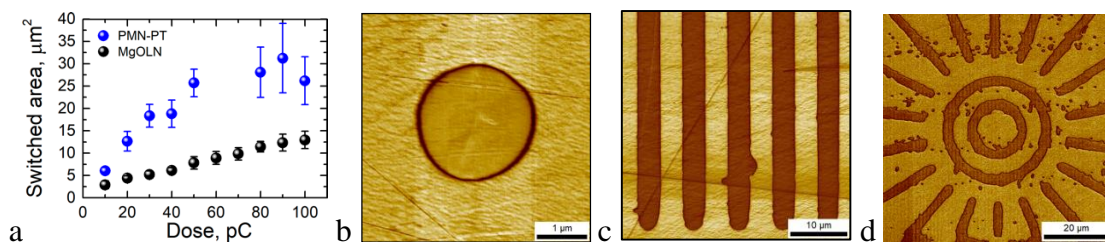


Figure 1. (a) The dose dependence of switched domain area for MgOLN and PMN-PT crystals, PFM images of *c*-domain structure created by: (b) dot irradiation, (c) stripe irradiation along [100] direction with period of 8 μm, (d) irradiation along arbitrary directions.

The equipment of the Ural Center for Shared Use “Modern Nanotechnology” UrFU has been used. The research was made possible in part by RFBR (grant 17-52-80116-BRICS_a).

1. V.Ya. Shur, A.R. Akhmatkhanov, and I.S. Baturin, *Appl. Phys. Rev.* **2**, 040604 (2015).
2. V.Ya. Shur, D.S. Chezganov, et al., *Appl. Phys. Lett.* **106**, 232902 (2015).
3. V.Ya. Shur, *J. Mater. Sci.* **41**, 199 (2006).
4. P. Zelenovskiy, E. Greshnyakov, D. Chezganov, et al., *Crystals* **9**, 65 (2019).

High-field nonlinear properties and characteristics of domain wall motion of Fe₂O₃ doped PMnS-PZN-PZT ceramics

H. Zhang, W. Jin, J. Zhou, J. Shen, J. Zhou, W. Chen*

State Key Laboratory of Advanced Technology for Materials Synthesis and Processing, School of Materials Science and Engineering, Wuhan University of Technology, Wuhan 430070, P. R. China
*chenw@whut.edu.cn

High-power piezoelectric devices, such as ultrasonic motors, underwater acoustic transducers, piezoelectric transformers, etc., require ceramics with large piezoelectric responses and, particularly, low losses [1, 2]. In our previous work, Fe₂O₃ doped Pb(Mn_{1/3}Sb_{2/3})O₃-Pb(Zn_{1/3}Nb_{2/3})O₃-Pb(Zr, Ti)O₃ (PMnS-PZN-PZT) ceramics was found to possess a relatively high piezoelectric property ($d_{33} = 356$ pC/N) and an extremely low dielectric loss ($\tan \delta = 1.2 \times 10^{-3}$) [3], showing that the ceramics are promising for high-power applications. From a fundamental point of view, understanding the origin of the low losses of this excellent material is of scientific interest, which would offer important clues for the development of piezoelectric ceramics with more superior high-power performance. Generally, the domain wall motion is the dominant loss origin for dense piezoelectric ceramics [4]. Therefore, the characterization of domain wall motion is the key to the understanding of loss properties. For the Fe₂O₃ doped PMnS-PZN-PZT ceramics, however, the characteristics of the domain wall motion are still remained to be clarified.

In this study, the high-field dielectric and piezoelectric nonlinearities of Fe₂O₃ doped PMnS-PZN-PZT piezoelectric ceramics are investigated. To characterize the domain wall motion, the electric field dependent dielectric and piezoelectric constants are analyzed in terms of Rayleigh law. Results show that with the increase of electric-field level, both the dielectric and piezoelectric constants deviate their low-field values and exhibit increase trends, due to the enhanced domain wall motion at high field. Rayleigh analysis reveals the contribution from lossless reversible domain wall motion to the high-field nonlinear dielectric and piezoelectric properties in Fe₂O₃ doped PMnS-PZN-PZT ceramics. This behavior could be associated with the orderly distribution of defect pinning centers, and is thought to be responsible for the low losses of the ceramics. The effects of temperature on high-field dielectric nonlinearity is also investigated. It is found that the high-field dielectric nonlinearity is enhanced with the increase of temperature. This phenomenon is explained with the increase of the mobility of the oxygen vacancies and the randomization of the defect pinning centers at elevated temperatures.

1. S. Zhang, J.B. Lim, H.J. Lee, et al., *IEEE Trans. Ultrason. Ferroelect. Freq. Contr.* **56**, 1523 (2009).
2. K. Uchino, J.H. Zheng, Y.H. Chen, et al., *J. Mater. Sci.* **41**, 217 (2006).
3. J. Mao, J. Zhou, H. Zheng, et al., *J. Synth. Cryst.* **39**, 72 (2010).
4. G. Liu, S. Zhang, W. Jiang, et al., *Mater. Sci. Eng. R* **89**, 1-48 (2015).

Formation of dendrite domain structures in single crystals of lithium niobate

M.A. Chuvakova¹, A.R. Akhmatkhanov¹, E.D. Saveliev¹, V.S. Sursyakov¹,
A.A. Esin¹, D.S. Chezganov¹, D.O. Alikin¹, M.S. Nebogatikov¹, A.I. Lobov¹,
P.K. Galenko², D.V. Alexandrov¹, A.L. Korzhenevskii³, V.Ya. Shur¹

¹*School of Natural Sciences and Mathematics, Ural Federal University, 620000 Ekaterinburg, Russia*
M.A.Chuvakova@urfu.ru

²*Otto Schott Institut für Materialforschung, Friedrich-Schiller-Universität, 07743 Jena, Germany*

³*Institute for Problems of Mechanical Engineering, RAS, 199178, St. Petersburg, Russia*

The surface shape instability leading to self-organized formation of complicated patterns under homogenous external conditions being the attribute property of nonequilibrium systems has been spotlighted as a potential bottom-up technology for fast and parallel creation of useful nanoscale patterns [1]. It has been shown previously that the realization of domain wall shape instability effect in uniaxial ferroelectrics leading to dendrite domain growth requires two conditions: strong input of the stochastic nucleation and the bulk screening retardation [2-4]. These conditions can be realized in lithium niobate single crystals with artificial dielectric layer during polarization reversal at high temperature.

In the present work, the formation of the dendrite domain structures was studied in congruent lithium niobate single crystalline Z-cut plates covered by silicon dioxide film with thickness from 150 to 900 nm. The transparent indium tin oxide (ITO) electrodes were used for polarization reversal with simultaneous *in situ* visualization and recording of the switching current. The ITO electrodes were circular at Z+ polar surface and completely covered Z- polar surface. The sample was placed in the temperature-controlled microscope stage THMS600 (Linkam, UK) at 250 °C.

The main stages of domain structure evolution for polarization reversal in the “middle” field range (7-9 kV/mm) were revealed: (1) the appearance of domain nuclei, (2) the growth of the six main branches, (3) growth, splitting and branching of the main and secondary branches. In the “low” fields range (5-7 kV/mm) the growth of only three main branches along Y+ crystallographic directions with following splitting and branching was observed. The individual domain shape followed C_{3v} crystal symmetry. The growth velocity of main branches remained constant through the most part of switching process with some deceleration at the very beginning.

The imaging of the static domain structures by scanning electron and optical microscopies allowed to reveal that they consist of three (for low fields) or six (for high fields) main branches oriented close to Y crystallographic directions. The structure of secondary branches is discussed.

The phase-field simulation was used to verify the analogy between self-organized growth of the domains and new phase during the first order phase transition [5]. The similarity of the simulated and experimentally observed shapes of isolated domains confirmed the proposed model.

The equipment of Ural Center for Shared Use “Modern Nanotechnology” Ural Federal University was used. The research was made possible by Russian Science Foundation (Project № 19-12-00210).

1. J.V. Barth, G. Costantini, K. Kern, *Nature* **437**, 671 (2005).
2. V.Ya. Shur, A.R. Akhmatkhanov, *Phil. Trans. R. Soc. A* **376**, 20170204 (2017).
3. V.Ya. Shur, A.R. Akhmatkhanov, M.A. Chuvakova, M.A. Dolbilov, P.S. Zelenovskiy, A.I. Lobov *J. Appl. Phys.* **121**, 104101 (2017).
4. V.Ya. Shur, D.S. Chezganov, M.S. Nebogatikov, I.S. Baturin, M.M. Neradovskiy, *J. Appl. Phys.* **112**, 104113 (2012).
5. A.R. Akhmatkhanov, A.I. Lobov, M.A. Chuvakova, E.D. Saveliev, V.Ya. Shur., *IOP Conf. Ser.: Mat. Sci. Eng.* **256**, 012027 (2017).

Chemically engineered multiferroic Morphotropic Phase Boundary in BiFeO₃-based single phase multiferroics

J. Zhuang^{1*}, A.A. Bokov^{2,1}, N. Zhang¹, J. Zhang¹, W. Ren¹, Z.-G. Ye^{2,1}

¹Electronic Materials Research Laboratory, Key Laboratory of the Ministry of Education & International Center for Dielectric Research, Xi'an Jiaotong University, 710049, Xi'an, P. R. China
jzhuang@xjtu.edu.cn

²Department of Chemistry and 4D LABS, Simon Fraser University, V5A 1S6, Burnaby, Canada

As the reach points of different phases with complex structural features, morphotropic phase boundary (MPB) in ferroelectric and ferromagnetic solid solutions can significantly enhance the piezoelectric performance and magnetostrictive response, respectively. Recently, the phase-change functional responses related to the multiferroic MPB are proposed to be a promising way to enhance the magnetoelectric coupling in BiFeO₃-based single phase multiferroics [1]. In this work, we verify the tunable magnetic ordering and the construction of multiferroic MPB by engineering the chemical concentrations of the ferroelectric PbTiO₃ or magnetic DyFeO₃ end member in the BiFeO₃-DyFeO₃-PbTiO₃ ternary solid solution system. Based on the results obtained in our lab [2-3] and reported in the literature [4-6], the structure-ferroic properties phase diagram of BiFeO₃-DyFeO₃-PbTiO₃ ternary system is established (see Fig. 1), where a compositional region with coexisting ferroelectric polarization and ferromagnetic moment is found. More importantly, a multiferroic MPB line separating two chemical regions with distinct crystal structures and ferroic orderings is discovered in the phase diagram. The phase changing nature of MPB compositions with temperature and compositions are investigated from room temperature to high temperature paraelectric phase. This work could provide a promising system to explore the highly desired colossal effects on magnetoelectric coupling in single phase multiferroics by phase-change functional responses.

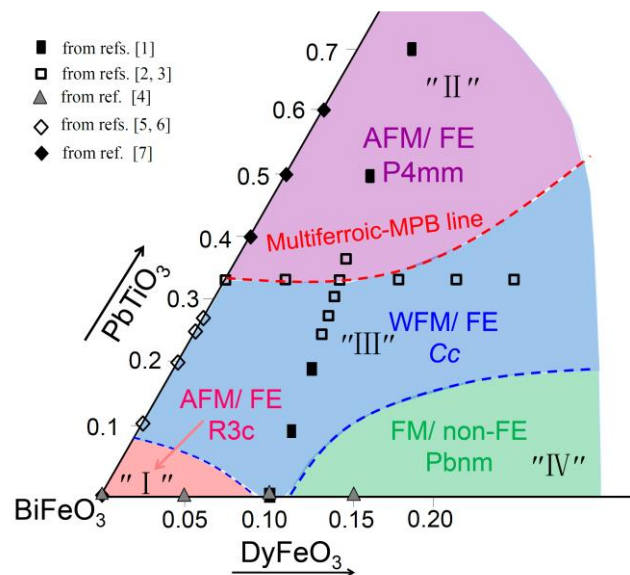


Figure 1. The sketched structure-ferroic properties phase diagram of the BiFeO₃-DyFeO₃-PbTiO₃ ternary system, indicating the following phase regions: FE = Ferroelectric Phase, non-FE = Non-ferroelectric Phase, FM = Ferromagnetic or Ferromagnetic Phase, AFM = Antiferromagnetic Phase, and showing a multiferroic-MPB line.

1. Diéguez O., Íñiguez J., *Phys. Rev. Lett.* **107**, 057601 (2011).
2. J. Zhuang, J. Lu, N. Zhang, *et. al.*, *J. Appl. Phys.* **125**, 044102 (2019).
3. J. Zhuang, L.-W. Su, H. Wu, *et. al.*, *Appl. Phys. Lett.* **107**, 182906 (2015).
4. S. Bhattacharjee, D. Pandey, *J. Appl. Phys.* **107**, 124112 (2010).
5. S. Bhattacharjee, A. Senyshyn, H. Fuess, D. Pandey, *Phys. Rev. B*, **87**, 054417 (2013).
6. W.-M. Zhu, H. Y. Guo, Z.-G. Ye, *Phys. Rev. B*, **78**, 014401 (2008).

Frozen superparaelectric state of the local polar domains in GdMn_2O_5 and $\text{Gd}_{0.8}\text{Ce}_{0.2}\text{Mn}_2\text{O}_5$

B.Kh. Khannanov, V.A. Sanina, E.I Golovenchits, M.P. Scheglov

Ioffe Institute, 194021, St. Petersburg, Russia
khannanov@mail.ioffe.ru

The results of a comparative study of the magnetic and dielectric properties, as well as the electric polarization of GdMn_2O_5 (GMO) and $\text{Gd}_{0.8}\text{Ce}_{0.2}\text{Mn}_2\text{O}_5$ (GCMO) multiferroics have been studied in the temperature range 5-330 K. These compounds belong to the class of multiferroics, in which the ferroelectric ordering with Curie temperatures $T_C = 30-35$ K is induced by a special type of magnetic ordering with close magnetic ordering temperatures [1]. GMO and GCMO have a central symmetry at room temperature (space group Pbam), which forbids the existence of electrical polarization. To explain the observed low-temperature ferroelectric ordering, an exchange striction model caused by the alternation of the nearest pairs of Mn^{3+} and Mn^{4+} ions with ferromagnetic strong double exchange and weak antiferromagnetic indirect exchange was proposed. The exchange striction along the b axis violates the lattice central symmetry, inducing ferroelectric ordering with polarization along the b axis [2]. The close temperatures of magnetic and ferroelectric ordering provide the appearance of a strong magnetoelectric coupling and the ability to control the state of GMO and GCMO both by magnetic and electric fields, which is attractive from an applied point of view. However, it is desirable to have such properties at higher temperatures. It has been found that the local polar domains exist in the multiferroics under study due to the phase separation process. The local phase separation domains occur due to the presence of the same number of Mn^{3+} and Mn^{4+} ions in GMO and in GCMO the number of Mn^{3+} ions prevail over Mn^{4+} ions due to the doping of GMO with Ce^{4+} ions. As a result, the same phase separation domains appear in GCMO, but their concentration is higher compared to GMO. The phase separation domains exist in the studied multiferroics in a wide temperature range from the lowest to room temperature. It was of interest to compare the results of electrical polarization studies in GMO and GCMO having different concentrations of polar domains of the same nature. The Mn^{3+} ions contain $3t_{2g}$ and $1e_g$ electrons on the $3d$ shell, while the Mn^{4+} ions have only $3t_{2g}$ electrons and an empty orbital doublet. The final probability of $1e_g$ electrons tunneling between Mn^{3+} and Mn^{4+} ions and deformations of the octahedra into which Mn^{3+} ions fall upon the recharging of Mn^{4+} ions by the $1e_g$ electrons lead to the energetic advantage of forming phase separation domains in which Mn^{3+} and Mn^{4+} ion pairs and their recharging electrons are accumulated. This process is similar to that which takes place in manganites with colossal magnetoresistance LaAMnO_3 ($A = \text{Sr}, \text{Ca}, \text{Ba}$) [3]. The phase separation domains in GMO and GCMO turned out to be polar and have ferromagnetic correlations, i.e. multiferroic ones. These domains form the superparaelectric state, which at temperatures $T \leq T_{\text{fr}} \gg T_C$ represents the frozen superparaelectric state, in which electric polarization loops with residual polarization were observed. Such type state was previously considered theoretically [4], but was not observed experimentally. The temperatures T_{fr} correspond to the condition $kT_{\text{fr}} \approx E_A$, where E_A is the activation barrier at the boundaries of the phase separation domains [4, 5]. It turned out that the polarization and T_{fr} temperature values were differed for GMO and GCMO. Polarizations were greater, but temperatures of them existence were lower in GCMO. Electric polarization was measured by two different methods: the method of thermally stimulated pyro-current and the method of hysteresis loops (PUND – positive up negative down-method). It made it possible to separate the contributions to the polarization of the low-temperature polar order of the exchange-striction nature and the frozen superparaelectric state of the local polar domains. This also made it possible to understand the properties of polarizations of local polar domains, which arise at different ways of applying an external electric field in these two methods (when measuring static and dynamic polarization). The PUND method of measuring hysteresis loops allows one to subtract the parasitic contribution of the local conductivity of the phase separation regions. The influence of the magnetic field H on the polarization induced by the phase separation domains was found. The magnetic field increased the polarization and the temperature T_{fr} , to which hysteresis loops were observed. It was also found that a uniform, single-domain polar order occurs at $T < T_C$

in a strong internal field of the staggered field type without the application of an external electric field (at $E = 0$), which was first established by us when measuring the polarization by the pyro-current method without preliminary polarization of the sample in the E field $\neq 0$. The field E began to influence only near T_C , when the internal field sharply decreased and fluctuations appeared.

This work was supported by RFBR (Grant N 18-32-00241).

1. Y. Noda, H. Kimura, M. Fukunaga, et al., *J. Phys. Condens. Matter* **20**, 434206 (2008).
2. J. van den Brink and D.I. Khomskii, *J. Phys. Cond. Matter* **20**, 434217 (2008).
3. M.Yu. Kagan and K.I. Kugel', *Phys. Usp.* **44**, 553 (2001).
4. M.D. Glinchuk, E.A. Eliseev, A.N. Morozovska, *Phys. Rev. B* **78**, 134107 (2008).
5. V.A. Sanina, B.Kh. Khannanov, E.I. Golovenchits, et al., *Phys. Solid State* **60**, 537 (2018).

Optical properties of ferroelectric photonic structures

D. Bi¹, V.S. Gorelik^{1,2}

¹*Bauman Moscow State Technical University, 105005, Moscow, Russia*

²*P.N. Lebedev Physical Institute of the Russian Academy of Sciences, 119991, Moscow, Russia*
gorelik@sci.lebedev.ru

Ferroelectric materials have been an important issue in physical research since their discovery. Their optical properties have attracted the interest of many researchers. A ferroelectric photonic structure can be fabricated by filling a ferroelectric substance into a mesoporous photonic crystal, which can enhance the possibility of observing optical phenomena in the ferroelectric structure [1]. This paper presents the research results of the optical properties of ferroelectric photonic structures.

The initial samples studied in this work are opal matrices, constructed from highly packed amorphous silica nanoglobules. The opal matrix was formed by self-assembly [2] of silica nanospheres prepared by the Stober's method [3]. Ferroelectric substances (NaNO₂, KNO₃, etc.) were filled into the cavity of the photonic crystal by placing mesoporous photonic crystals into the ferroelectric substance solution and evaporation with heating.

In the reflection spectra of photonic crystals, there are strong reflective areas of light, i.e., photonic stop band [4-6]. The positions of the stop band depend on the refractive index, the crystal lattice constant of the constituent material, etc. After introducing different ferroelectric substances into the cavity of the photonic crystal, the formed composite ferroelectric photonic structures have different dielectric constants. Therefore, for the photonic composite structures made from different ferroelectric materials and the same initial photonic crystal, the shifts in stop band positions are different. The shift in stop band positions of the composite photonic structure is also related to the amount of ferroelectric material filled.

Raman spectra of composite ferroelectric photonic structures and their corresponding ferroelectric materials were observed in this work. To reduce the influence of the fluorescence spectrum of opal matrix, the exciting laser of Raman scattering is chosen to be 785 nm. When the incident light of the Raman spectrum was close to the stop band position of the composite photonic crystals, the density of the photonic states was greatly enhanced [7]. In addition, there was also Mie scattering in the opal matrix with large-sized particles, which also caused a sharp increase in the density of photonic states [8]. Thus, the Raman spectral intensity of the ferroelectric composite photonic crystal was increased. Such optical property of composite opal photonic crystals can be used to increase the probability of occurrence of other optical phenomena in them, such as second harmonic generation [9] and others [10, 11]. This plays an important role in expanding the application of ferroelectric materials.

Thus, it is very important to prepare new ferroelectric photonic composite structures and study their optical properties. It can help to find new applications of ferroelectric materials in optical or other aspects.

This study was supported by the RFBR (№ 18-02-00181) and the China Scholarship Council.

1. Y. Almohamed, R. Barille, A.I. Vodchits, et al., *JETP Lett.* **101**, 365 (2015).
2. C.K. Liau, Y.K. Huang, *Expert Systems with Applications* **35**, 887 (2008).
3. W. StoBer, A. Fink, E. Bohn, *J. Colloid Interface Sci.* **26**, 62 (1968).
4. E. Yablonoitch, *Phys. Rev. Lett.* **58**, 2059 (1987).
5. S. John, *Phys. Rev. Lett* **58**, 2486 (1987).
6. V.S. Gorelik, *Laser Physics* **18**, 1479 (2008).
7. V.S. Gorelik, P.P. Sverbil, V.V. Filatov, et al., *Photonics Nanostructures: Fundam. Appl.* **32**, 6 (2018).
8. C. van de Hulst, *Light scattering by small particles* (N.Y.: Wiley), 470 (1957).
9. K.I. Zaytsev, S.O. Yurchenko, *Appl. Phys. Lett.* **105**, 269 (2014).
10. S.O. Yurchenko, K.I. Zaytsev, E.A. Gorbunov, et al., *J. Phys. D: Appl. Phys.* **50**, 055105 (2017).
11. V.S. Gorelik, *Eur. Phys. J. Appl. Phys.* **49**, 33007 (2010).

Fermi level pinning study at the surface of GaP nanowires

V.A. Sharov^{1,2}, P.A. Alekseev², V.V. Fedorov¹, A.D. Bolshakov¹

¹*Saint-Petersburg Academic University, 194021, Saint-Petersburg, Russia*

²*Ioffe Institute RAS, 194021, Saint Petersburg, Russia*

vl_sharov@mail.ru

Semiconductor nanowires (NWs) are prospective building blocks for next generation nanoscale electronic devices. In this case, understanding NWs transport properties is of great importance. It is well known, that surface effects in quasi one-dimensional nanostructures are strong due to high surface to volume ratio. In particular, surface Fermi level pinning in NWs leads to a surface band bending and to a formation of the near surface depleted area. Such a depletion decreases conductivity of the NW. Width of the depletion area is governed by doping level, NW diameter and position of Fermi level pinning. To quantitatively analyze transport properties of the GaP NWs, one should obtain a position of the surface Fermi level pinning (work function). This parameter can be measured with Kelvin probe microscopy, as was reported previously with III-As NWs [1]. Worth noting, that GaP NWs can be grown with wurtzite (WZ) crystal structure. Such NWs draw an attention due to quasi direct band gap and possible optoelectronic applications. However, surface electronic properties of the WZ GaP NWs are not sufficiently studied. The aim of this work is to measure a position of the surface Fermi level pinning in WZ and zinc blende (ZB) GaP NWs.

The studied undoped gallium phosphide NWs were grown using molecular beam epitaxy on (111) silicon substrate. The NWs possess average length of approximately 5 μm and tapered shape with the diameter decreased from about 350 nm near the base to about 150 nm near the top. TEM study revealed that NWs had ZB crystal structure with 500 nm WZ insert near the tip. However, the very end of the NW also exhibited ZB structure. The formation of WZ segments in the NW top part is strongly related with the catalytic droplet consumption during Ga-limited growth regime and subsequent changes of the droplet contact angle promoting GaP nucleation at the triple phase (vapor-liquid-solid) line.

The Fermi level pinning position was determined by amplitude-modulated Kelvin probe force microscopy (AM-KPFM). At each scanning point the surface potential given by $V_s = \Phi_{\text{tip}} - \Phi_{\text{sample}}$ is measured as well as topography. Φ_{tip} and Φ_{sample} are the work functions of AFM tip and sample surface respectively. Before each measurement the work function of the probe was calibrated using freshly cleaved highly oriented pyrolytic graphite (HOPG), whose work function (Φ_{HOPG}) is well defined as 4.48 eV [2]. Then the work function Φ_s can be expressed as $\Phi_s = 4.48 + (V_{\text{HOPG}} - V_s)/e$, where V_{HOPG} is the surface potential of the HOPG measured by the same probe as V_s , and e is the electronic charge.

NWs were separated from the growth substrate and dispersed on silicon substrate for AFM measurements. KPFM mapping of a single NW revealed the difference between WZ and ZB GaP work function: a 500 nm region between its very end and middle region demonstrated lower surface potential. The position of the decreased potential region is in a perfect agreement with the location of WZ insert obtained upon TEM images analysis. Using the abovementioned formulas, WZ and ZB GaP work function were calculated to be 4.2 and 4.18 eV respectively. As the value of electron affinity in GaP is 3.08 eV, one can conclude that the surface Fermi level is in the middle of bandgap.

This work was supported by the Russian Science Foundation (Grant 18-72-00231).

1. P.A. Alekseev, M.S. Dunaevskiy, G.E. Cirilin, et al., *Nanotechnology* **29**, 314003 (2018).
2. W.N. Hansen, G.J. Hansen, *Surface Science* **481**, 172 (2001).

Domain structure evolution in (111)-cut rhombohedral PMN-PT single crystals during polarization reversal

A.D. Ushakov¹, A.A. Esin¹, A.R. Akhmatkhanov¹, Q. Hu²,
X. Liu^{1,2}, Y. Zhao^{1,2}, A.A. Andreev¹, X. Wei², V.Ya. Shur¹

¹ School of Natural Sciences and Mathematics, Ural Federal University, 620000, Ekaterinburg, Russia
andrey.ushakov@urfu.ru

² Electronic Materials Research Laboratory, Key Laboratory of the Ministry of Education & International Center for Dielectric Research, Xi'an Jiaotong University, 710049, Xi'an, China

Lead magnesium niobate-lead titanate $(1-x)\text{Pb}(\text{Mg}_{1/3}\text{Nb}_{2/3})\text{O}_3-x\text{PbTiO}_3$ (PMN-PT) solid solution attracts a great attention due to its prominent piezoelectric properties used for actuator, sensor, transducer and energy harvesting applications [1]. Moreover, PMN-PT is considered as a potential candidate for non-linear optical and photonic devices. It implies that deep understanding of the physical fundamentals of domain structure evolution and polarization reversal process is essential for the creation of domain patterns for promising applications in this material.

In the present work, we studied the domain kinetics during polarization reversal in rhombohedral [111]-oriented PMN-PT crystal by *in situ* optical microscopy domain visualization and interferometric profilometry at different stages of switching accompanied by analysis of the switching current data (Fig. 1). It allowed us to distinguish different domain types from the revealed optical contrasts and to define the domain structure evolution stages from initial $c\uparrow$ -domain state with small number of $a\uparrow$ -domains and $2a$ -CDW: (I) nucleation and growth of $a\uparrow$ -domains and $2a$ -CDW; (II) nucleation and growth of $c\downarrow$ -domains (with opposite direction of spontaneous polarization). The effect of light scattering on $2a$ -CDW with field-controlled density was revealed. The estimated “optical current” [3] obtained by analysis of the optical images correlated with the switching current data in both cases. The undesirable effect of the partial backswitching during electric field decrease was attributed to the clamped switching conditions.

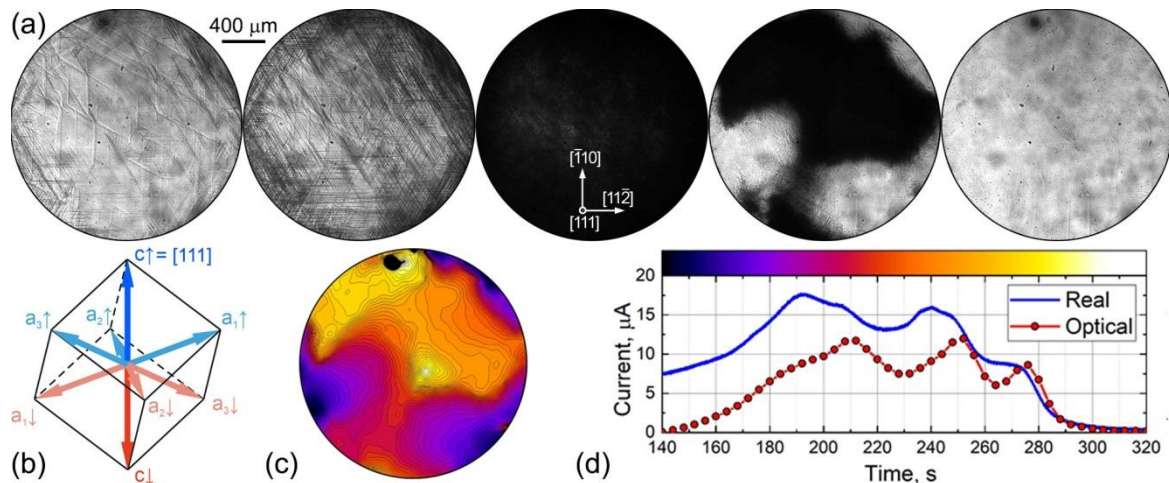


Figure 1. (a) Optical images of instantaneous domain states during polarization reversal in (111)-cut rhombohedral PMN-PT single crystal. (b) Polarization directions for [111]-oriented pseudocubic cell. (c) Kinetic map and (d) the real switching and optical currents.

The equipment of the Ural Center for Shared Use “Modern Nanotechnology” UrFU has been used. The research was made possible in part by RFBR (grant 17-52-80116-BRICS_a).

1. E. Sun, W. Cao, *Prog. Mater. Sci.* **65**, 124 (2014).
2. A.D. Ushakov, A.A. Esin, A.R. Akhmatkhanov et al., *Appl. Phys. Lett.* **113**, 112902 (2018).
3. V.Ya. Shur, E.V. Nikolaeva, E.I. Shishkin, et al., *Appl. Phys. Lett.* **79**, 3146 (2001).

Nanoscale investigation of domain evolution behavior in rhombohedral $\text{Pb}(\text{Mg}_{1/3}\text{Nb}_{2/3})\text{O}_3\text{-PbTiO}_3$ relaxor ferroelectric single crystal

Q. Hu¹, D.O. Alikin², P.S. Zelenovskiy², D.S. Chezganov², Y. Zhao¹, X. Liu¹, P. Luan¹, W. Zhao¹, Y. Zhuang¹, X. Fu¹, Zh. Li¹, F. Li¹, Y. Tian¹, L. Jin¹, Zh. Xu¹, V.Ya. Shur², X. Wei¹

¹*Electronic Materials Research Laboratory, Key Laboratory of the Ministry of Education & International Center for Dielectric Research, School of Electronic Information, Xi'an Jiaotong University, Xi'an 710049, China*

wdy@mail.xjtu.edu.cn; xuzhuo@mail.xjtu.edu.cn

²*School of Natural Sciences and Mathematics, Ural Federal University, Ekaterinburg 620000, Russia*

vladimir.shur@urfu.ru

Domains and domain walls play key roles in determining the properties of ferroelectric materials. Investigations on domain evolution behaviors with external temperatures and electric fields are of significant scientific value and meaningful for practical applications. Scanning probe measurements are performed in this paper to study the domain evolutions under external temperatures and local electric fields at nanoscale. Results by the piezoresponse force microscopy (PFM) demonstrate that the domain structure clearly changes during phase transitions, which is also in accordance to the macroscopic dielectric behavior. Kelvin probe microscopy is introduced to study dynamics of artificially created domains. Experimental results show that the artificially created domains are stable during the testing time range. Moreover, the time-dependent surface potential decay of artificially created domains can be classified into three groups by the temperature range upon heating, which is also correlated to the phase structure of the crystal at each temperature region. We believe that our work can deepen the understanding on domain kinetics of the PMN-PT single crystals and also provide instruction on the application of such relaxor ferroelectric single crystals on digital memory devices.

Giant piezoelectric response in textured piezoceramics with tetragonal tungsten bronze structure

M.A. Bunin, O.A. Bunina, Yu.A. Kuprina, V.P. Zavyalov

*Research Institute of physics, Southern Federal University, 344090, Rostov-on-Don, Russia
bunin.m.a@gmail.com*

High-density textured ceramics samples $K_2Sr_4Nb_{10}O_{30}$ with the large dielectric anisotropy were sintered by the hot-pressing technique. Its crystallographic characteristics obtained by the X-ray powder diffraction method were analyzed and compared with the data for isotropic ceramics. Lattice parameters and relative uniform deformations were determined for crystallites which axes are oriented parallel (*c*-oriented) or perpendicular (*a*-oriented) relative to the texture axis. It was shown that *a*-oriented crystallites are under tensile deformations along the *c*-axis and compression along the *a*-axis without changing cell volume, while *c*-oriented crystallites are stretched along the *a*-axis with enlarged cell volume.

The amplitudes of the surface piezoresponse (PR) of the textured samples turned out to be abnormally large, which was not observed for an isotropic ceramics sample. The relative piezomodulus d_{33} were estimated from the PR magnitudes. It turned out to be $\sim(67-98)$ or $\sim(85-146)$ times greater (depending on the sample orientation relative to the texture axis) than for the isotropic sample. The piezomodules measured for bulk samples are in a similar ratio. One of the possible reasons of the giant surface PR can be attributing to the deformations anisotropy in the *a*- and *c*-oriented crystallites in textured ceramics. Because of this, the different types of crystallites have different lattice parameters. During the dense ceramics fabrication, an interface arises between different types of crystallites, on which the direction of the spontaneous polarization vector becomes less stable. It increases the sensitivity of the ceramics surface to an external electric field, which can greatly magnify the PR amplitude. Its value should depend on the sample orientation relative to the texture axis, in consistency with the difference in the estimated values of the relative d_{33} above. The possible influence of domain walls and polar nanoregions on the giant piezoelectric response in hot-pressed potassium-strontium niobate ceramic is discussed.

This work was supported by the Ministry of Education and Science of the Russian Federation (research projects No. 3.1649.2017/4.6 and № 3.6439.2017)

Research progress in novel poly-silicon aromatic alkyne based composite with ultra high permittivity

X. Yao, H. Peng, H. Lin

Key Laboratory of Inorganic Functional Material and Device, Shanghai Institute of Ceramics, Chinese Academy of Sciences, Shanghai, China
yaoxiaogang@mail.sic.ac.cn

The modern information revolutions, such as 5G mobile communication, large capacity satellite, wearable electronics, etc. demand billions of laminates with high dielectric constant and low dielectric loss to transmit electrical signals at high frequency as well as high temperature resistance. In this study, a high performance composite for microwave circuit application has been fabricated by filling a thermosetting poly-silicon aromatic alkyne (PSAA) matrix with $\text{Ca}_{1-x}\text{La}_{2x/3}\text{TiO}_3$ -based (abbreviated as CLT) ceramic fillers. Firstly, the performance of CLT ceramics were improved by doping with a proper amount of Al_2O_3 (0.28~1.11 mol.%). Particularly, the anti-reduction mechanism of Ti^{4+} in $\text{Ca}_{0.9}\text{La}_{0.067}\text{TiO}_3$ ceramic was carefully investigated. The $\text{Ca}_{0.9}\text{La}_{0.067}\text{TiO}_3$ ceramic doped with 1.11 mol.% Al_2O_3 exhibited good microwave dielectric properties: $\epsilon_r = 141$, $Q \times f = 6848$ GHz. Secondly, highly dense and spherical ceramic fillers were produced by granulation followed with sintering process. The particle size distributions of the fillers were 20~50 μm and could be well controlled. At last, a composite was fabricated by filling PSAA matrix with high performance CLT ceramic fillers. The results showed that large-size spherical fillers distributed well throughout the PSAA matrix. The 0.5PSAA-0.5CLT composite exhibited ultra-high dielectric constant of ~ 16.0 , low dielectric loss of 2.5×10^{-3} (at 10 GHz) and kept intact even under temperature of 450 $^\circ\text{C}$.

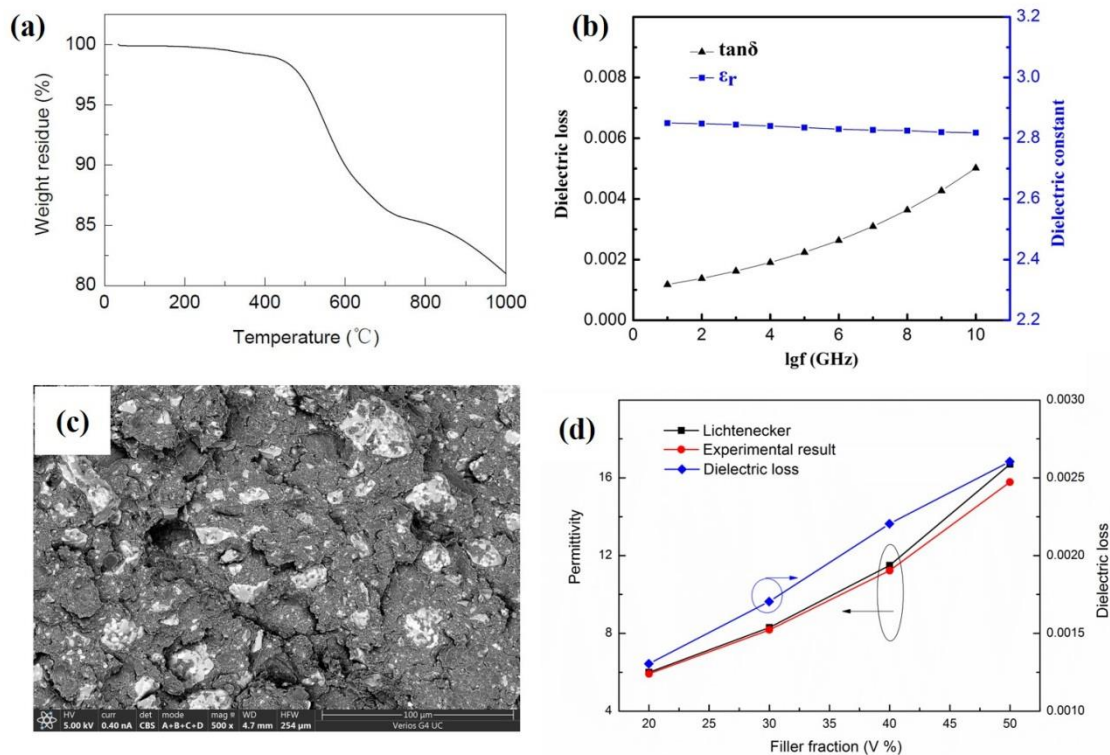


Figure 1. (a) Thermo-gravimetric curve of thermosetting PSAA resin. (b) Dielectric properties of thermosetting PSAA resin with the variation of frequency. (c) SEM photograph of the cross section of 0.5PSAA-0.5CLT composite. (d) Dielectric properties of 0.5PSAA-0.5CLT composite at high frequency.

Dielectric characterization of erythrocytes by electrostatic force microscopy

N.A. Davletkildiev^{1,2}, D.V. Sokolov¹, E.Yu. Mosur^{1,2}, A.A Lopandina²

¹*Omsk Scientific Center, Siberian Branch, Russian Academy of Sciences, Omsk, 644024 Russia
stezko@obisp.oscsbras.ru*

²*Dostoevsky Omsk State University, Omsk, 644077 Russia*

The human cells have unique biophysical and biochemical properties that ensure interaction with the surrounding physiological environment to realize of specific functions. The study of mechanical, electrical and optical parameters of cells is important for clinical diagnostics.

The electrical properties of cells investigate generally by measuring a response of cells on external electric field [1]. The electric response depends on the shape, size, internal structure and conductivity of cell, and susceptibility of cellular components. It should be noted that the registration of response is usually performed on large cell populations that leads to average of measured parameters. In this case, the properties of individual cells are not taken into evaluation that lead to limited of measurement accuracy. The study of individual cells allows to determinate the heterogeneity of their characteristics within a cells population and to measure of samples containing cells of various types without the need for their separation [2]. Using of electrostatic force microscopy (EFM) to determine the dielectric response of individual bacterial cells with high precision and reproducibility was demonstrated in [3].

In this work, the object of study was red blood cells (RBC) that perform a fundamental physiological function of living organisms – transport of respiratory gasses. RBC were separated by centrifugation of whole blood, and then thrice washed with isotonic solution. In the next step, RBC were fixed of a 2%-paraformaldehyde solution for 2 h, then transferred to deionized water to achieve concentration equal to 10^8 cells/ml. Aqueous suspension of RBC (15 μ l) was deposited on a freshly cleaved surface of highly oriented pyrolytic graphite (HOPG) and incubated for 30 min. Then the samples were washed in deionized water to remove non-adsorbed cells and air-dried at room temperature. The HOPG surface with immobilized RBC was scanned by atomic force microscope MFP-3D SA (Asylum Research) by EFM-method at various applied voltages. The conductive cantilevers of the ETALON HA_FM series (NT-MDT SI, Russia) with Pt coating were used, having the following parameters: $k \sim 3.4$ N/m, $Q \sim 234$, $R \sim 35$ nm.

Figure 1a shows an example of image and corresponding EFM-contrast (Fig. 1b) for an individual RBC on HOPG surface at +3 V on probe. Figure 1c presents the phase shift ($\Delta\Phi$) between RBC and HOPG surface on EFM-profile.

Figure 2 demonstrates the EFM measurements for quantitative analysis of experiment data. RBC is modeled as disc shape with height H and a dielectric constant ϵ is located on the HOPG. The probe is a spherical shape with radius of curvature R that is at a fixed height h above the sample.

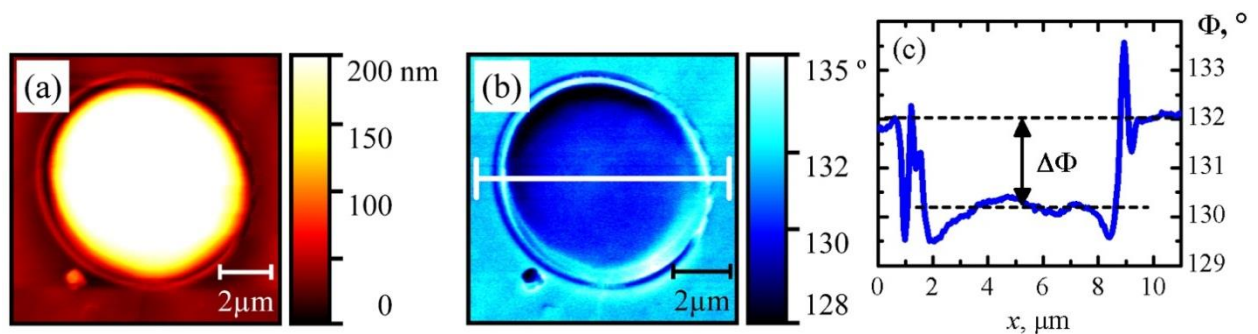


Figure 1. 2D-images of individual RBC on HOPG in first (a) and second (b) passes ($h = 100$ nm), and the corresponding profile of the EFM-image (c).

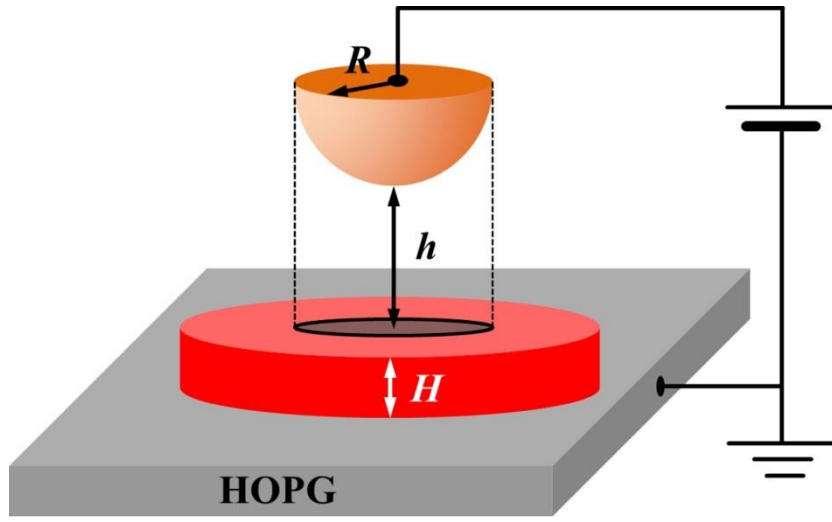


Figure 2. Scheme of EFM experiment (probe placed in the center under the RBC).

The dependence of phase shift tangent on square of the applied voltage for studied samples is linear. This indicates that the contrast of EFM-images for RBC is determined only by the capacitive coupling of the probe-sample.

Modeling of the EFM-profiles was performed according to the method described in [4]. To calculate the phase shift between RBC and the probe, the second derivative of the probe-RBC-HOPG capacitance was calculated using the equation:

$$\frac{\partial^2 C}{\partial z^2} = 4\varepsilon_0 \int_0^R \int_{y_1}^{y_2} \left[h + R - \sqrt{R^2 - x^2 - y^2} + \frac{H}{\varepsilon} \right]^{-3} dx dy,$$

where ε_0 – vacuum permittivity, ε – dielectric permittivity of individual RBC, $y_1 = -\sqrt{R^2 - x^2}$, $y_2 = +\sqrt{R^2 - x^2}$ – the limits of integration along the y-axis.

By fitting the model phase shift to the experimental one, the mean value and range of the dielectric permittivity of individual RBC were determined, equal to 2.6 ± 0.8 . Since the volume of the erythrocyte is filled with proteins, which, according to the literature, have dielectric permittivity values of 2-4 [3], the obtained value of ε is adequate.

The work was carried out according to the state task of the Omsk Scientific Center SB RAS (project registration number AAAA-A17-117041210227-8).

1. E. Du, S. Ha, M. Diez-Silva, et al., *Lab Chip* **13** (19), 3903 (2013).
2. M. Brown, C. Wittwer, *Clinical Chemistry* **46** 8(B), 1221 (2000).
3. D. Esteban-Ferrer, M.A. Edwards, L. Fumagalli, et al., *ACS nano* **8**, 9843 (2014).
4. N.A. Davletkil'deev, D.V. Sokolov, V.V. Bolotov, et al., *Tech. Phys. Lett.* **43**, 205 (2017).

Experimental assessments of metallic and metal oxide nanoparticles toxicity

L.I. Privalova¹, B.A. Katsnelson¹, M.P. Sutunkova¹, I.A. Minigalieva¹, V.B. Gurvich¹,
S.N. Solovyeva¹, S.V. Klinova¹, O.G. Makeyev², I.E. Valamina², R.R. Sakhautdinova¹,
T.V. Bushueva¹, V.Ya. Shur³, I.V. Zubarev³, E.V. Shishkina³

¹The Yekaterinburg Medical Research Center for Prophylaxis and Health Protection in Industrial Workers, 620014, Yekaterinburg, Russia
privalovali@yahoo.com

²The Central Research Laboratory of the Ural State Medical University, 620028, Yekaterinburg, Russia

³School of Natural Sciences and Mathematics, Ural Federal University, 620000, Yekaterinburg, Russia

Toxicity of nanoparticles (NPs) of Fe₃O₄ produced by a chemical technique and nanoparticles of Ag, Au, CuO, NiO, Mn₃O₄, PbO, ZnO, TiO₂, SiO₂, Al₂O₃ generated through laser ablation was investigated with the help of a single intra-tracheal and repeated intra-peritoneal injections in non-lethal doses. Besides, we carried out long-term inhalation experiments with low concentrations of Fe₂O₃-NP, SiO₂-NP or NiO-NP and *in vitro* experiments on established cell lines with NPs of NiO, Mn₃O₄, PbO, CuO and CdO.

It was proved that these NPs are much more toxic compared to their fine micrometric or even submicron counterparts and are usually the more toxic the smaller their dimensions within the nano-scale range. We found also that toxicity of Me-NPs strongly depends on their chemical nature, solubility and mechanisms of action specific for a particular metal. Solubilization of Me-NPs in biological milieus plays an important role in their toxicokinetic which can prevail over that of the physiological mechanisms controlling their distribution, retention and elimination. On the other hand, thanks to the high activity of these mechanisms, the organism is not defenseless against the impact of Me-NPs.

The nonspecific responses of the organism to the impact of Me-NP included: changes in the cytological and some biochemical characteristics of the bronchoalveolar lavage fluid caused by the deposition of particles in the lower airways; various manifestations of systemic toxicity including always significant damage to the liver and kidneys; some cytological signs of a likely onset of hyperergic inflammation; moderate neurological disturbances associated with possible penetration of Me-NP into the brain from the blood as well as from the nasal mucous membrane along the olfactory pathway; a paradoxically low manifestation of pulmonary pathology due to low chronic retention of nanoparticles in the lungs; a genotoxic effect on the organism level.

As a protective measure, the toxicity and even genotoxicity of Me-NPs can be significantly attenuated by adequately composed combinations of some bioactive agents in innocuous doses.

Detection of proteins, viruses, bacteria using scanning probe microscopy

A.I. Akhmetova, I.V. Yaminsky

*Lomonosov Moscow State University, 119991, Moscow, Russian Federation
akhmetova@nanoscopy.ru*

*Advanced Technologies Center, 119311, Moscow, Russian Federation
Energy Efficient Technologies, 119234, Moscow, Russian Federation*

The use of probe microscopy techniques for the detection of biological macromolecules is a relatively new direction. In the works [1, 2] we propose biosensor for viruses, bacteria and proteins detection. In particular, the sialic acids were used for detection of influenza A virus as the biospecific recognition reagents to bind to hemagglutinin of the virus. For bacterial cells detection, the antibodies against surface antigenic determinants of the cells are placed on the sensory layer surface. Detection of biological agents in the biosensor is carried out by registration of the amplitude, phase, frequency and the quality factor of the mechanical vibrations of the piezoceramic biochip.

The biosensor includes a flow cell with a piezoceramic biochip, a peristaltic pump, and a control unit. Data processing is carried out on a personal computer using original software. To maintain a given constant temperature in the flow cell, a thermistor is installed, which simultaneously serves both to measure temperature and to heat the fluid in the cell. The biochip is a miniature piezoceramic disc with sensor layers on opposite sides. When the influenza virus or microalbumin is attached to the biochip sensor surface, the resonant frequency of the biochip changes. As a result of the pathogens interaction with the receptor layer, the effective mass and rigidity of the biochip changes, which is recorded by the shift of the biochip resonant frequency. The biochip design was successfully patented (patent # 2636048 Biosensor device for the detection of biological micro- and nano-objects).

To test the biochip's performance, an experiment was conducted to test the activity of antibodies on microalbumin. When comparing the results of measurements of different concentrations of specific antibodies to albumin (50 $\mu\text{g/ml}$ and 5 $\mu\text{g/ml}$), it was found that when the concentration of antibodies immobilized on a piezoceramic disk decreases, the range of changes in the resonance frequency decreases, which confirms the results obtained by ELISA.

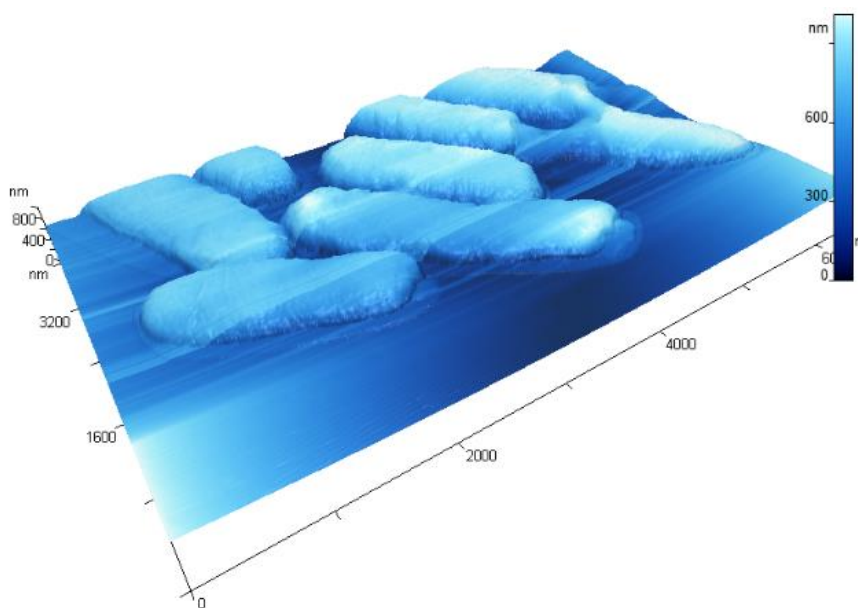


Figure 1. An image of the *E.coli* bacteria obtained using a FemtoScan scanning probe microscope and FemtoScan Online software.

1. A.I. Akhmetova, N. Gutnik, G. Meshkov, et al., *Nanoindustry* **70** (8), 22 (2016).
2. A.I. Akhmetova, I. Nazarov, G. Presnova, et al., *Nanoindustry* **49** (8), 44 (2017).

Hybrid piezoelectric and biodegradable polymer-based scaffolds for biomedical applications

R.V. Chernozem, M.A. Surmeneva, R.A. Surmenev

Tomsk Polytechnic University, 634034, Tomsk, Russia
rsurmenev@mail.ru

There is a growing interest in piezoelectric materials due to their potential of providing electrical stimulation to cells to promote repair of the damaged tissues without external energy source used. A recent study has shown that the most significant effect on fibroblasts has been revealed in case of scaffolds with the largest piezoelectric constants such as polyvinylidene fluoride [1]. Polyhydroxybutyrate (PHB) is biodegradable and piezoelectric polymer [2]. However, PHB possesses reduced piezoelectric properties compared with PVDF. Polyaniline (PANi) is conductive biocompatible polymer and increase piezocharge constants of piezoelectric materials [2]. To the best of our knowledge, the piezoelectric PHB-based scaffolds with PANi are lack studied. Thus, the present study is aimed to fabricate and investigate piezoelectric properties, chemical and phase compositions of hybrid biodegradable scaffolds based on piezoelectric PHB and conductive PANi polymers.

Polymer scaffolds were fabricated using electrospinning. PHB was dissolved in chloroform with PANi mixed as follows: pure PHB (100-0), PHB-1% PANi (99-1), PHB-2% PANi (98-2), PHB-3% PANi (97-3) [2].

The morphology of the scaffolds was characterized by scanning electron microscopy (SEM). Fourier transform infrared spectroscopy (FTIR) spectra were recorded using a Nicolet 5700 FT-IR Spectrometer (Thermo Electron Corporation, USA). To study the phase composition and structure, X-ray diffraction was used (XRD-6000, Shimadzu, Japan) with Cu K α radiation ($\lambda = 0.154$ nm) in the 2θ range from 5° to 90° with a step size of $0.02^\circ/2\theta$ at 40 kV and 30 mA. The piezoelectric charge coefficient (d_{33}) of the prepared scaffolds was tested using a Wide-Range d_{33} Tester Meter. Surface electric potential of the scaffolds was measured under mechanical loading using a custom-made set contained: two electrodes, oscilloscope and power amplifier (Fig. 1).

Figure 2a represents FTIR spectra of PHB and PHB-PANi scaffolds. PHB-3% PANi spectrum exhibited new bands at ~ 1603 and ~ 1589 cm^{-1} (an insert in Fig. 2a) attributed to the aromatic ring [3] and C=N stretching of the quinoid diimine unit correspond to PANi, respectively [4]. At the same time, XRD analysis confirmed the presence of the PANi in the structure. Besides, SEM analysis showed the decrease of the average fiber diameter at the increase of PANi mass fraction in PHB [2]. Finally, it can be seen that the trend was the same for d_{33} and surface electric potential (Fig. 2b), i.e. the maximum of the d_{33} and surface electric potential were observed at the 2% PANi mass fraction in the scaffolds [2].

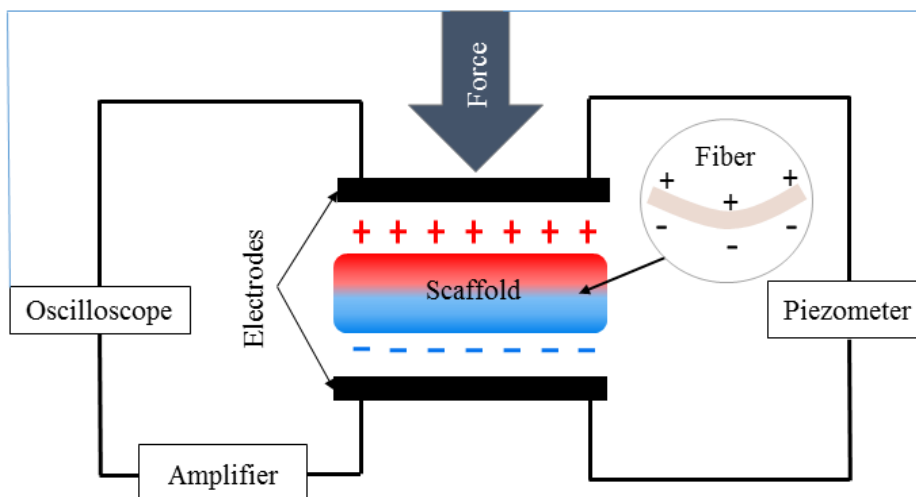


Figure 1. Schematic illustration of the measurements of d_{33} and surface potential.

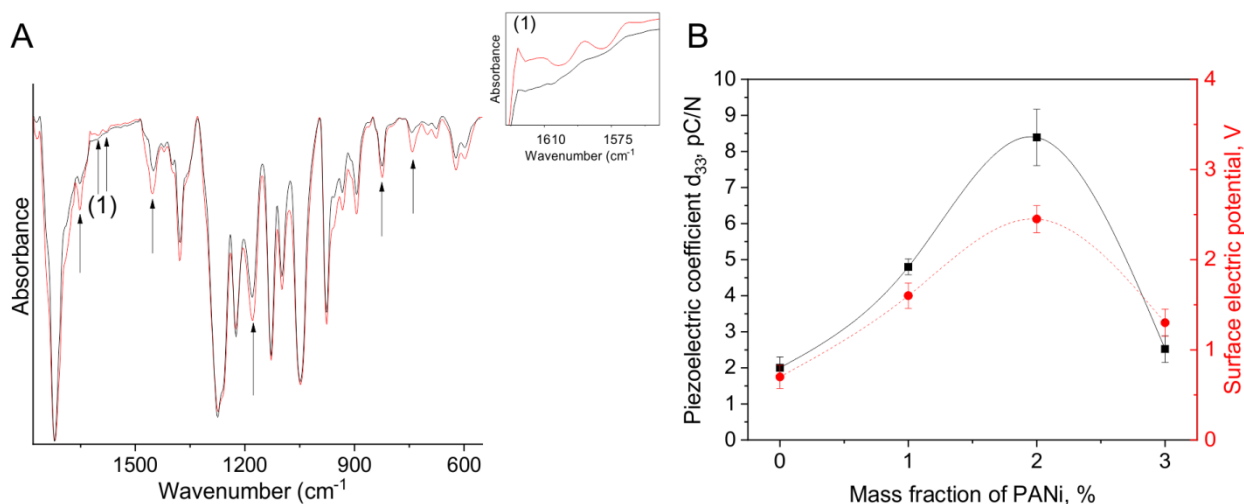


Figure 2. (a) FTIR spectra of the pristine PHB (black) and PHB-3% PANi (red) scaffolds; (b) The dependence of the piezoelectric coefficient/surface potential on PANi content in PHB.

Fibrous scaffolds based on PHB and PANi can be successfully fabricated via electrospinning technique. Doping of PANi leads to decreasing of the average fibers diameter as well as significantly increased the piezoelectric charge coefficient and surface electric potential of PHB scaffolds. The maximum increase of the piezoelectric coefficient and surface electric potential was observed at the PANi mass fraction of 2%. Thus, the results of the present study can be successfully applied to fabricate a hybrid biodegradable material with improved piezoelectric properties for regenerative medicine.

The authors thanks to Mr. A. Anyugin and A. Zviagin for the assistance with experiments. The authors acknowledge the financial support from the Russian Science Foundation (project #18-73-10050).

1. H.-F. Guo, Z.-S. Li, S.-W. Dong, et al., *Colloids Surf. B: Biointerfaces* **96**, 29 (2012).
2. R.V. Chernozem, M.A. Surmeneva, R.A. Surmenev, *Mater. Lett.* **220**, 257 (2018).
3. Z. Ping, *J. Chem. Soc. Faraday Trans.* **92**, 3063 (1996).
4. P.L.B. Araujo, C.R.P.C. Ferreira, E.S. Araujo, *eXPRESS Polymer Lett.* **5**, 12 (2011).

Creation of nanoparticles and surface nanostructures of aluminum oxides by hot water treatment

A. Makaev, V. Shur, E. Mingaliev, D. Kuznetsov, D. Chezganov, I. Kozheletova, V. Pryakhina
School of Natural Sciences and Mathematics, Ural Federal University, 620000, Ekaterinburg, Russia

Metal oxide nanostructures (MONSTRs) and nanoparticles (MONPs) produced by treatment of the metal surface have unique physical and chemical properties. Recently, MONSTRs have been used in electronic [1], optical [2, 3] and sensitive [2] devices of an evidence-based concept; however, their synthesis methods have several obstacles that limit their large-scale production. Recently, a simple hot water treatment (HWT) process has been used to produce MONSTRs on surface of various metals, their compounds and alloys by a one-step, scalable, low-cost, and eco-friendly technique [4]. But, up to date there are no systematic studies of MONSTRs formation. Here we present the results of investigation the formation of aluminum oxide nanostructures during HWT at different water temperatures and treatment durations. Moreover, we show that this technique can be used for synthesis of water suspension of metal oxide nanoparticles.

It was shown that at the temperatures below 70 °C the nanostructure formation didn't occur. After HWT at higher temperatures the surface of aluminum plate has been covered by nanostructures with uniform spatial distribution. The density of nano-sheet structure monotonously increased with water temperature. Treatment of plate in boiling water leads to appearance of additional cavitation holes in the plate surface.

The investigation of the nanostructures formed after HWT at fixed temperature (85 °C) for different treatment duration from 2 to 30 minutes allowed to reveal the islet growth character. After 4 minutes treatment the nanostructures locally covered sample surface. The covered area increased with treatment time and after 16 minutes the surface was completely covered by aluminum oxide nanostructures. Investigation The mean thickness of nanostructures about 450 nm does not depend on the temperature.

It was shown that aluminum oxide nanostructures lead to significant change on sample surface wettability. The wetting angle of untreated sample surface was 69°. The aluminum surface became superhydrophilic at temperature range from 70 to 95 °C with almost zero wetting angle. The relaxation of this state becomes very slow with temperature increase and remained close to zero for above 400 hours after HWT at 95 °C.

It was shown that HWT leads also to formation of water solution of nanoparticles Al_2O_3 with mostly spherical shape and mean sizes about 30 nm and large dispersion, which didn't depend on the treatment temperature. The obtained results have been attributed to creation of the aluminum oxide molecules in the water during HWT [4]. This effect leads to formation of the microstructures at the metal surface and nanoparticles in the water. The similar results were obtained for laser ablation [5].

The obtained effects can be used for modification of the metal surface wettability and to creation of the water suspension of metal oxide nanoparticles.

The equipment of the Ural Center for Shared Use "Modern Nanotechnology" UrFU was used. The work was supported by Government of the Russian Federation (Act 211, Agreement 02.A03.21.0006).

1. J. You, et al., *Nat. Nanotechnol.* **11**, 75 (2016).
2. K. Al-Mayalee, et al., *J. Phys. Chem. C*, **122**, 23312 (2018).
3. X. Yu et al., *Nat. Mater.*, **15**, 383 (2016).
4. N. Saadi, L. Hassan, T. Karabacak, *Sci. Rep.*, **7**, 7158 (2017).
5. V. Piriya Wong et al., *J. Nanomater.*, **2012**, 2 (2012).

Raman spectroscopy during indentation measurements

I.I. Maslenikov, A.S. Useinov, M.A. Doronin

¹FSBI “Technological institute for superhard and novel carbon materials”, 108840, Troitsk, Moscow, Russia

i.i.maslenikov@gmail.com

A transparent indenter objective described elsewhere [1] allows to observe in real time surface beneath the tip during the measurement placement and monitor its deformation during an indentation. The indenter is diamond-made cylinder faced at the both ends in the shape of the Berkovich pyramid in the way that the top-end pyramid is rotated vs bottom-end pyramid by 60 degrees. The shape allows the parallel beam of light passing through an indenter’s face to remain parallel and maintain direction, having only a linear shift vs its original line of propagation. Thus an image observed directly through the objective consists of the three sectors, which form a connected image if the linear translation is applied.

The invention not only saves the time for the movement between indenter and optical objective, but also allows to conduct the spectroscopic measurements during an indentation. An example of phase transformations occurring during the loading and unloading of silicon is given in [2]. In this work we made a measurements of DLC covered silicon specimen. The specimen was loaded up to 40 N and then unloaded back to 30 N after which Raman surface mapping was performed. Corresponding spectra shows a DLC, diamond and Si different phases peaks. Particular peak position depends on the local pressure applied, so one can construct a map for example for the pressure distribution in the DLC coating, which is shown on the Figure 1.

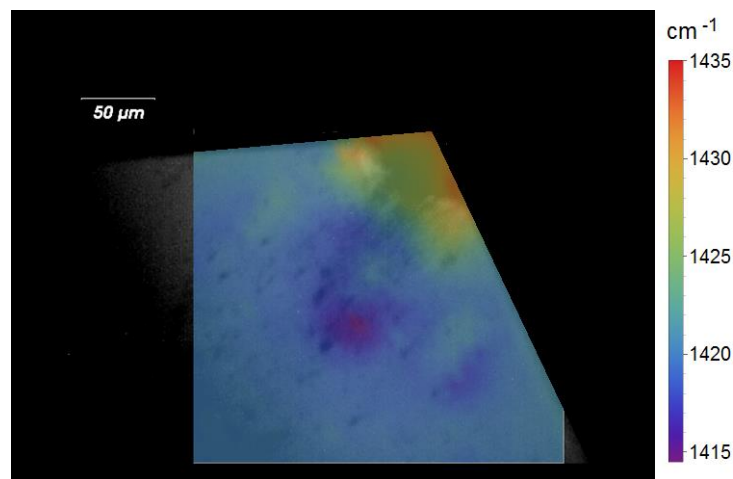


Figure 1. DLC Raman peak position map, 30 N applied.

The map is given for the one out of the three visible sectors and shows that the pressure is bigger within the contact area, particularly below the indenter’s edges. One can also observe a dark stains out of the area of indentation, which can be ascribed to the fact that the DLC coatings delaminates from the Si surface, which tends to protrude out of its original position as the radial cracks develops.

The obtained spectra can also be used to create a map for the Si-I/DLC or Si-II/Si-I peak intensity ratio. Conducted experiment shows a possibility to perform a local simultaneous mechanical and spectrum analysis, which can be particular useful for the a sophisticated heterogeneous structures which the phases that undergoes phase transformation under pressure.

1. I.I. Maslenikov, V.N. Reshetov, A.S. Useinov, et al., *Instruments Exp. Tech.*, **61** (5), 719 (2018).
2. I.I. Maslenikov, V.N. Reshetov, A.S. Useinov, *Mater. Trans.* **60** (8), 1433 (2019).

Studies of morphology and magnetic properties of island magnetic metamaterials

L.A. Fomin¹, V.A. Berezin¹, A.V. Chernykh, B.A. Loginov², A.B. Loginov³

¹*Institute of Microelectronics Technology and High Purity Materials RAS, 142432, Chernogolovka, Russia*

fomin@iptm.ru

²*National Research University of Electronic Technology 124498, Zelenograd, Moscow, Russia*

³*Faculty of Physics M.V.Lomonosov Moscow State University 119991, Moscow, Russia*

At present, magnetic nanocontacts and tunnel structures with spin-polarized current flowing through them are among the interesting objects of research in spintronics [1]. Spin injection by a current through a nanocontact or a tunnel junction can lead to a significant nonequilibrium spin accumulation in the region immediately near the contact. In particular, the inverse population of the spin subbands of a ferromagnet can occur due to the injection of hot electrons which are non-equilibrium in the spin. In this case, radiative spin-flip transitions of conduction electrons will occur, which can be stimulated indirectly through *s-d*-exchange interaction with an electromagnetic wave. The frequency of radiation is determined by the energy of the effective exchange splitting of the spin subbands and lies in the terahertz range. For the manufacture of such contacts, technically sophisticated lithographic methods are mainly used [2]. We have proposed a method for making a multitude of contacts by growing island films.

The combination of in situ electrical measurements and ex situ atomic force research allowed us to develop a technology for growing by pulsed laser deposition on a dielectric substrate (sapphire, MgO) unpercolated island films of ferromagnetic metals (Fe, Ni, Co) to create magnetic metamaterials based on them. In the metamaterials metallic nanocrystals (10-200 nm in size) are separated by a thin layer of a dielectric, a normal metal, or an antiferromagnet.

The influence of growth temperature and growth rate on the morphology and size of islands was studied. It was found that in regimes with low supersaturation: at high temperatures of 400-600 °C and low repetition rates of laser pulses of 1-10 Hz, a stable, reproducible dependence of the morphology of island films on growth conditions is observed, which makes it possible to obtain island films and metamaterials with desired properties.

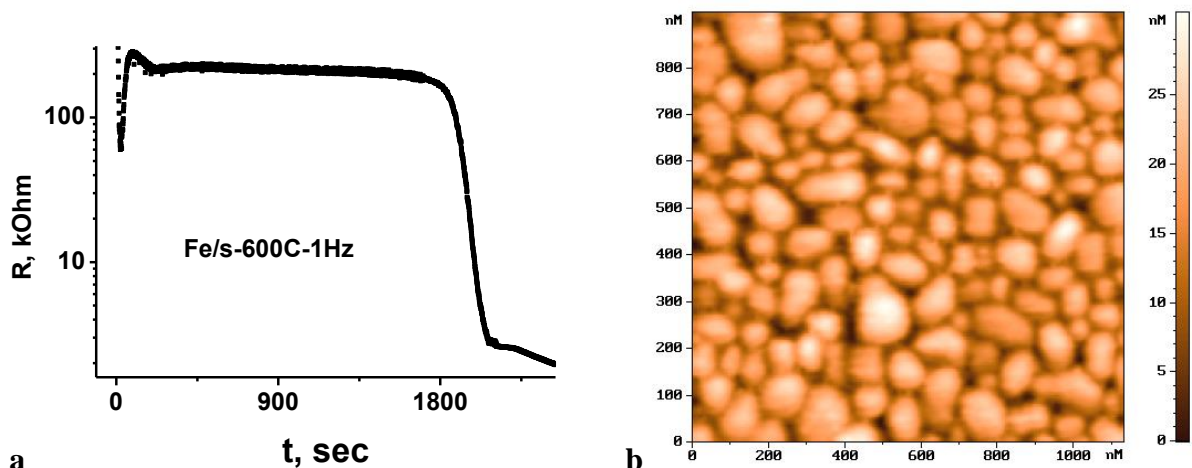


Figure 1. (a) Typical dependence of island film resistance on thickness during growth and (b) an AFM image of unpercolated islands.

Atomic force and magnetic force microscopy made it possible to investigate the morphology and magnetic structure of ferromagnetic and ferromagnet/antiferromagnet structures, in which the use of annealing in a magnetic field above the Neel temperature forms a unidirectional exchange anisotropy. Magnetic force experiments accompanied by micromagnetic calculations and magnetoresistive measurements made it possible to determine the spatial distribution of magnetization and interpret the magnetic states of metamaterials from ferromagnetic and

antiferromagnetic metals. Real AFM images were used for calculating magnetization distribution of islands by means of OOMMF software [3]. The simulated MFM contrast obtained from that micromagnetic calculations was compared with experimental MFM images.

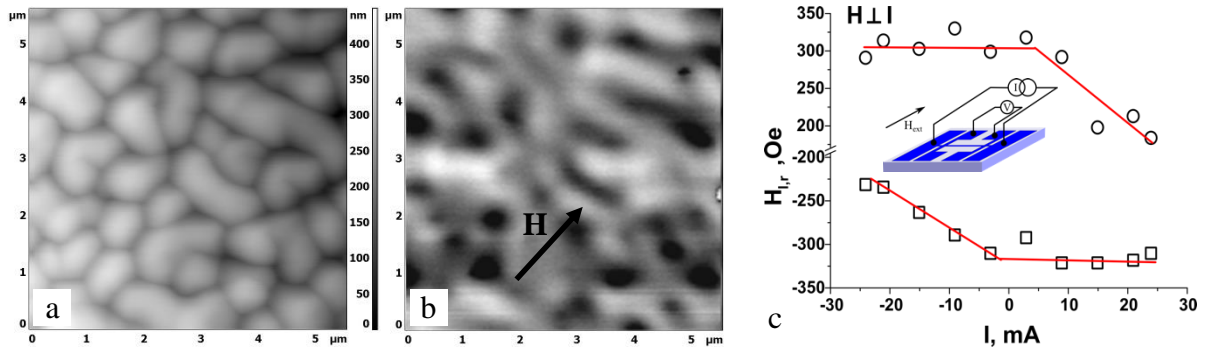


Figure 2. (a) AFM and (b) MFM images of Fe islands covered with FeMn film in presence of external magnetic field $H = 672$ Oe (shown by an arrow). (c) The dependence of the position change of the left, H_l and right, H_r peaks on the magnetoresistance curve of the Ni/FeMn metamaterial. In the inset in (c) the measurement setup is shown.

In the Figure 2a and 2b the surface morphology and MFM contrast of Fe islands covered with FeMn film in presence of external magnetic field are shown. The lateral dimensions of the islands were about $1 \mu\text{m}$, and in height they were about 250 nm . MFM measurements showed that at such sizes the islands behave like separate magnets. At the same time, for small island sizes (100 nm), the characteristic features in the MFM contrast are markedly larger than the island size. MFM measurements in an external magnetic field allow us to state that small islands are magnetically coupled.

In the metamaterial films in the form of Ni islands, covered with a continuous antiferromagnetic FeMn film, strong current effects in anisotropic magnetoresistance were detected. In bridges made of such films and annealed in a magnetic field acting in the sample plane perpendicular to the axis of the bridge, the position of the maxima of the anisotropic magnetoresistance curve depends on the magnitude of the flowing current. This dependence can be explained by the influence of the magnetic field of the transmitted current on the magnetic structure of the ferromagnetic nickel islands of the metamaterial. In the Figure 2c the experimental dependences of the positions of the right H_r and left H_l peaks in the magnetoresistance curve in the Ni/FeMn metamaterial are shown. At low measurement currents, the hysteresis curve for the film and, accordingly, the magnetoresistance curve exhibits an exchange bias [4] in a magnetic field perpendicular to the current. When a sufficiently large current flows in the forward direction, it creates a positive magnetic field that is aligned with the external field at its positive values, and thereby overcome a domain wall pinning and shifts the right peak on the magnetoresistance curve H_r . When it flows in the opposite direction the magnetic field of the current does not allow it to overcome a domain wall pinning and affect the position of the right peak H_r . The same reasoning is valid for the left peak H_l . However, such reasoning cannot give a full explanation of the observed effect. Further research is required.

1. J. Walowski and M. Munzenberg, *J. Appl. Phys.* **120**, 140901 (2016).
2. V. Korenivski, A. Iovan, A. Kadigrobov, et al., *Europhys. Lett.* **104**, 27011 (2013).
3. <https://math.nist.gov/oommf/>
4. W.H. Meiklejohn, *J. Appl. Phys.* **33**, 1328 (1962).

Changing the domain structure of CoNi particles under mechanical stress

A.P. Chuklanov, D.A. Biziyayev, A.A. Bukharaev, N.I Nurgazizov

Zavoisky Physical-Technical Institute, FRC Kazan Scientific Center of RAS, 420029 Kazan, Russia
 achuklanov@kfti.knc.ru

The Villari effect (or the magnetoelastic effect – when the magnetic properties of a solid changes under mechanical stress) can be used for detection of a mechanical tension in the planar ferromagnetic particles or in a near-surface layer of the substrate where those particles are fabricated. The lateral resolution of this technique will be close to the lateral sizes of the particles. Usually the square planar particle has four-domain structure with equal domain sizes. In the presence of mechanical tension the area of domains with a magnetization perpendicular to direction of the tension were increased. The size increasing is caused by the negative magnetostriction of ferromagnetic material from which the particles were made. The length of the “bridge” between two antiparallel domains can be chosen for the characterization of the changing of the particle magnetic properties. The length of this “bridge” can be easily measured by magnetic force microscopy (MFM) and used to characterize the mechanical stress in the particle.

Studies were carried out on array of the planar CoNi (Co 18%, Ni 82%) particles with the size of $25 \times 25 \mu\text{m}^2$ and $8 \times 8 \mu\text{m}^2$. The particles were fabricated on a thin glass substrate. Heights of particles were varied for different samples in range 20-50 nm. Particles were prepared by electron beam evaporation under ultrahigh vacuum conditions by using a “Multiprobe P” setup (Omicron). An array of identical particles was formed by sputtering through a metal grid placed on the surface substrate. After sputtering, the sample was annealed at 300 °C during 15 min to reduce the stresses generated in the particles during sputtering.

To create the stressed particles substrate was elastically curved. For this purpose, the flat holder was used. The thin metal wire was placed under the center of a sample and the edges of a sample were clamped. The tension of particles was varied by changing the diameter of the wire under the sample's center. The scanning probe microscope (SPM) Solver HV and P47 (NT-MDT) were used. The magnetic cantilevers “Multi75M-G” (BudgetSensor) were used for MFM measurements. The obtained MFM images were compared with the computer modeling to determine a magnetic structure of the particles. The calculations were carried out by the OOMMF [1] and “Virtual MFM” [2] software. The size and shapes of particles obtained by SPM were used for modeling.

It has been shown that uncompressed 25- μm particles have a multidomain structure. Under the mechanical tension, the particle has quasi-uniformly structure with direction of magnetization perpendicular to tension. The uncompressed 8- μm particles have four-domain structure, with domains of equal sizes. A uniaxial tension of particle leads to increasing the sizes of domains with direction of magnetization perpendicular to the tension. The increasing of domain sizes leads to form a characteristic “bridge” between them, which is clearly observed on the MFM images. The direction of a bridge is perpendicular to the tension direction. The length of the bridge is directly proportional to the magnitude of the tension. Thus, the CoNi particles under study with the lateral size $8 \times 8 \mu\text{m}^2$ can be used as the detector of the mechanical stress.

The work was partly supported by RFBR 17-08-00915.

1. M.J. Donahue, D.G. Porter: (<http://math.nist.gov/oommf/>).
2. D.V. Ovchinnikov, A.A. Bukharaev, *Technical Physics* **46**, 1014 (2001).

Study of inelastic electron tunneling in the Pt-Au tunnel junction in ultra-high vacuum STM

D.V. Lebedev^{1,2}, I.S. Mukhin^{3,4}, V.A. Shkoldin³, A.M. Mozharov⁴, A.O. Golubok²

¹*Saint Petersburg State University, 199034, St. Petersburg, Russia*
denis.v.lebedev@gmail.com

²*Institute for Analytical Instrumentation RAS, 198095, St. Petersburg, Russia*

³*ITMO University, 197101, St. Petersburg, Russia*

⁴*St.Petersburg Academic University, 194021, St. Petersburg, Russia*

In recent years fabrication of the compact light sources operated under external applied voltage is important task in connection with development of the concept of electro-optical chips and optical computers. A promising compact light source is a tunnel junction formed between two metal surfaces located at a subnanometer distance. The phenomenon of light emission from a metal-insulator-metal (MIM) tunnel contact was first experimentally demonstrated in the work of Lambe and McCarthy [1]. Photon generation was interpreted in terms of inelastic electron tunneling and the excitation of surface plasmon waves propagating along the metal-dielectric interface. An increase in the quantum efficiency of this process can be achieved by using a tunnel gap between STP tip and metal surface in an scanning tunnel probe (STM) microscope [2, 3]. The scanning tunnel spectroscopy in a ultra-high vacuum conditions allows to investigate processes of the generation of photons under STM tip without direct collecting and detecting of photons. Analysis of the second derivative of the current – voltage characteristics ($I-V$) of a tunnel junction allows indirectly investigating the processes of light emission in a tunnel junction.

This work is devoted to a research of tunnel spectra of nanocontact "Pt/Ir STM tip – gold film" in ultra-high vacuum conditions that is relevant to creation of the local sources of optical radiation operated by external electric potential.

To study the Pt-Au tunnel junction, in this work atomically smooth gold surfaces were used. Preparation of crystal Au (111) films on the surface of mica was made in several stages. Freshly cleaned mica plates $K_2O-Al_2O_3-SiO_2$ (TipsNano Co, Estonia) were placed in a vacuum chamber of a thermal evaporation system (Boc Edwards Auto 500, United Kingdom). After that, the system was pumped to a pressure of 10^{-7} mbar. Next, the samples were heated to a temperature of 200 °C. Then a gold film was deposited on the heated sample at a speed of (6-7) nm/min. To register the current-voltage characteristics of the Pt/Ir-Au tunnel contact, samples with gold films were loaded into an Omicron SPM Probe ultra-high vacuum system (Germany). In all STM experiments, Pt/Ir probes DPT10 (Bruker, USA) were used. Typical STM images of the sample surface is shown in Figure 1a. It should be mentioned, that the grain step height was 0.2 nm, which corresponds to the literature data for 1 layer of gold atoms [4].

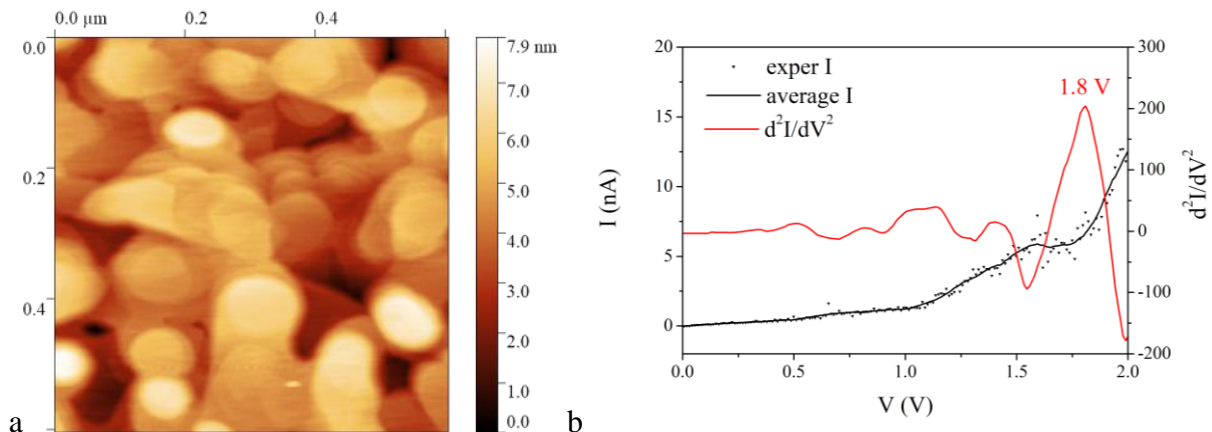


Figure 1. (a) STM image of Au (111) film on mica surface, (b) $I-V$ curve of the Pt/Ir tip/Au film system and its second derivative.

It is well known that the process of inelastic tunneling of electrons is accompanied with the appearance of characteristic peaks on d^2I/dV^2 dependence. Figure 1b shows a typical $I-V$ characteristic, as well as its second derivative, which we obtained for the Pt/Ir-Au tunnel junction. On the second derivative curve, there is an obvious peak at 1.8 V. These data indicate the presence of inelastic processes and as a result of radiation from a tunnel junction. In addition, there is an interesting area of the current-voltage curve corresponding to voltages of 1.6-1.8 V. In this range weak reduction of current at increase in voltage is observed. This fact indicates the presence of negative differential resistance, which confirms the existence of a resonant energy level in the tunneling electron transport [5]. Thus, the analysis of $I-V$ curves of tunnel gap allows to study the process of inelastic electron tunneling and investigate the process of photon generation with direct optical signal collection.

This work was carried out with the support of the Russian Science Foundation (Grant 17-19-01532).

1. J. Lambe, S. McCarthy, *Physical Review Letters* **37**, 923 (1976).
2. F. Bigourdan, et al., *Physical Review Letters* **116**, 106803 (2016).
3. R. Berndt, R. James, et. al., *Physical Review Letters* **67**, 3796 (1991).
4. K. Krupski, et al., *Materials* **8**, 2935 (2015).
5. J.M. Beebe, et al., *Physical Review Letters* **97**, 026801 (2006).

The role of uncompensated electric charges in the polarization dynamics induced by femtosecond high-intensity infrared laser pulses

V.A. Abalmasov

*Institute of Automation and Electrometry, Siberian Branch of the Russian Academy of Sciences,
630090, Novosibirsk, Russia
abalmasov@iae.nsc.ru*

Fast control over polarization is essential for many applications of ferroelectrics. Recently it was proposed to switch the polarization by an ultra-short laser pulse which frequency is in resonance with an infrared-active phonon mode Q_{IR} nonlinearly coupled to the ferroelectric soft mode Q_P [1]. The follow-up experiment [2] has indeed shown that a 150 fs midinfrared laser pulse with a fluence above 60 mJ cm^{-2} switches polarization in an irradiated part of LiNbO_3 crystal but then very fast, after about 0.2 ps, the polarization returns back to its initial value.

To model the soft mode dynamics in [1,2] a potential $V(Q_{IR}, Q_P)$ obtained ab-initio for different values of Q_{IR} and Q_P in unrelaxed lattice was used. We use instead the Landau thermodynamic potential $F(Q_{IR}, Q_P)$ which is crystal symmetry-invariant and known to describe well the soft mode dynamics [3]. Thus, we solve numerically the system of equations for two phonon coordinates:

$$\ddot{Q} + \gamma \dot{Q} + \partial F / \partial Q = 0.$$

The solution of these equations for the parameters values as in the experiment [2] shows the polarization return, Figure 2, only if we take into account an electric field \mathbf{E} due to uncompensated electric charges determined by the polarization difference ($\mathbf{P}_b - \mathbf{P}_d$), Figure 1a, which appear during the very fast switching.

We argue that uncompensated electric charges can also be responsible for the polarization which appears in quantum paraelectric SrTiO_3 [4] after minutes of repeating ultra-short midinfrared excitation pulses in the experimental conditions similar to [2]. These charges, Figure 1b, gradually grow when polarization appears just after the pulses due to induced strains and then they slowly recombine on a time scale of hours or much faster if illuminated by ultraviolet light.

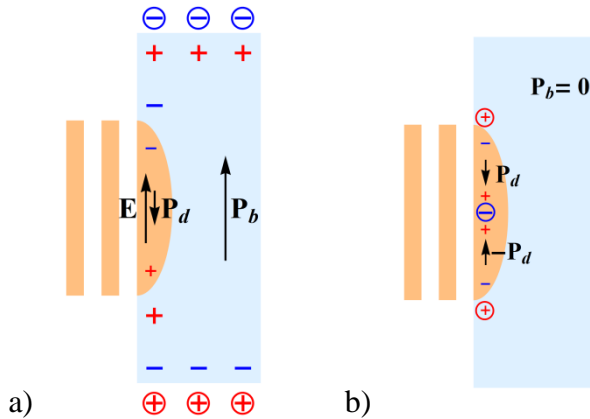


Figure 1. Scheme for free electric charges (in circles) and polarization-bound charges as in the experiments with (a) LiNbO_3 [2] and (b) SrTiO_3 [4].

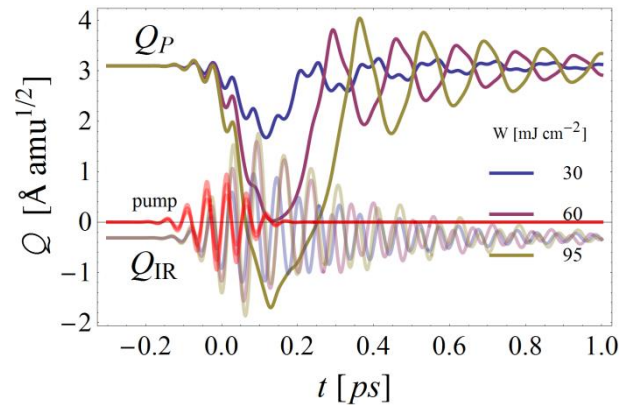


Figure 2. Numerical solution for the polarization dynamics in LiNbO_3 in conditions of the experiment [2].

1. A. Subedi, *Phys. Rev. B* **92**, 214303 (2015).
2. R. Mankowsky, A. von Hoegen, M. Först, A. Cavalleri, *Phys. Rev. Lett.* **118**, 197601 (2017).
3. V. Ginzburg, A. Levanyuk, A. Sobyenin, *Physics Reports* **57**, 151 (1980).
4. T.F. Nova, A.S. Disa, M. Fechner, A. Cavalleri, arXiv:1812.10560 (2018).

Resistive switching and ferroelectricity in HfO₂ thin films

N. Lyapunov, H.M. Yau, J.Y. Dai

Department of Applied Physics, The Hong Kong Polytechnic University, Hung Hom, Kowloon, Hong Kong

jiyan.dai@polyu.edu.hk

HfO₂ is a unique material that can demonstrate resistive switching and ferroelectricity in thin films. Resistive switching is observed in metal-insulator-metal structures and strongly depends on the choice of electrode materials. Resistive switching occurs due to formation and rupture of conductive filaments in the insulating layer. According to the choice of electrode materials conductive filaments can be made of oxygen vacancies or metallic. HfO₂ thin films for observation of resistive switching are traditionally amorphous. For observation of ferroelectricity in HfO₂ thin films, they, conversely, should be crystalline, and the effect does not depend that much on the choice of electrode materials as resistive switching does.

For observation of the resistive switching effect in HfO₂ thin films, Pt and TiN are traditionally chosen as electrode materials. With such a choice of electrode materials (inert Pt and active TiN) conductive filaments are made of oxygen vacancies. Al₂O₃ thin layer deposited by Atomic Layer Deposition (ALD) can be introduced between Pt and HfO₂ layers to enhance the resistive switching effect [1]. In our case the basic device structure is Pt/HfO₂/TiN. Pt and TiN are deposited by magnetron sputtering, HfO₂ is ALD deposited. The ALD deposition temperature varies from 150 to 250 °C, different thicknesses from 5 to 25 nm are investigated. Different annealing temperatures (up to 300 °C) and times (up to 30 min) of annealing of the resistive switching layer in oxygen are also investigated. Bipolar resistive switching behavior with positive set and negative reset has been found (the bottom electrode is grounded). Although the switching voltage varies from device to device, the overall uniformity level is found to be acceptable. Different compliance current levels during set process and different stop voltage levels during reset process are implemented to achieve different resistance states.

As it was mentioned before, ferroelectricity in HfO₂ thin films does not depend that much on the choice of electrode materials as resistive switching does, but, as the film should be crystalline in this case, not amorphous, it strongly depends on the crystallinity of the underlying layer. Another thing that greatly affects the effect is doping of HfO₂ thin films with different dopants at different doping concentrations. Thus, recently Wei et al. discovered a ferroelectric rhombohedral phase in well-oriented Hf_{0.5}Zr_{0.5}O₂ thin film [2], showing the presence of ferroelectricity in other phase besides the well-known orthorhombic polar phase (Pca21) [3, 4]. In the present study, the epitaxial growth of Al-doped HfO₂ on different oriented La_{0.7}Sr_{0.3}MnO₃/SrTiO₃ substrates is reported. The well-oriented films, which under the compressive/tensile strains depend on the lattice change, show different piezoresponse by piezoresponse force microscopy (PFM). The film growth on (111)-oriented substrate shows the largest electromechanical effect, and no wake-up cycling is required. The results, with the analysis of structure characterizations, explore the possible ferroelectric phase and the corresponding properties in Al:HfO₂ thin film.

1. Z. Chen, F. Zhang, B. Chen, et al., *Nanoscale Research Letters* **10**, 130 (2015).
2. Y. Wei, P. Nukala, M. Salverda, et al., *Nature Materials* **17**, 1095 (2018).
3. J. Muller, T.S. Bosccke, U. Schroder, et al., *Nano Letters* **12**, 4318 (2012).
4. M.H. Park, T. Schenk, C.M. Fancher, et al., *Journal of Material Chemistry C* **5**, 4677 (2017).

The energy-storage performances in $(1-x)(\text{Na}_{0.5}\text{Bi}_{0.5})\text{TiO}_3-x\text{SrZrO}_3$ ceramics

J. Li, Sh. Yang, Q. Hu, Y. Zhuang, Zh. Xu, F. Li*

Electronic Materials Research Laboratory, Key Laboratory of the Ministry of Education and International Center for Dielectric Research, Xi'an Jiaotong University, Xi'an 710049, China
*ful5@xjtu.edu.cn

In step with the development of energy storage technology and the power electronics industry, dielectric materials with high energy density are in high demand. In this work $(1-x)\text{Na}_{0.5}\text{Bi}_{0.5}\text{TiO}_3-x\text{SrZrO}_3$ (NBT–SZ) ceramics were synthesized by conventional solid state sintering method range from 1100 to 1250 °C. Their crystal structure, microstructure, dielectric, ferroelectric and energy storage properties were investigated and compared. Results show that all prepared sample are single phase without secondary phase. Meanwhile, those grain size decrease with increasing doping SZ content. It was found that those ceramics dielectric permittivity decrease with increasing SZ content, meanwhile exhibiting relaxor behavior. The highest recoverable energy density of 1.7 J/cm³ under 20 MV/m was achieved in the sample with 6 mol.% SZ content, which also displayed good energy-storage stability in the temperature range from room temperature to 150 °C. Simultaneously, the leakage current was largely reduced due to the addition of SZ.

Periodical poling in congruent lithium niobate with slanted polar axis

E.A. Neradovskaia^{1,2}, M.M. Neradovskiy^{1,2}, M.A. Chuvakova^{2,3}, A.R. Akhmatkhanov^{2,3},
P. Baldi¹, R. Maksimenka⁴, N. Forget⁴, V.Ya. Shur^{2,3}

¹*Institute de Physique de Nice, Université Côte d'Azur – CNRS, 06180, Nice, France*
neradovskaia.elizaveta@ya.ru

²*School of Natural Sciences and Mathematics, Ural Federal University, 620000, Ekaterinburg, Russia*

³*Labfer Ltd, 620014, Ekaterinburg, Russia*

⁴*Fastlite Ltd, 06600, Antibes, France*

Periodically poled lithium niobate (PPLN) crystals are widely used in nonlinear optics as frequency mixers for wide wavelength range [1]. The typical thickness of such optical element ranges from 0.5 to 1.0 mm. The development of femtosecond lasers with high average and peak power (> 10 W) boosted the interest to large aperture (~ 1 cm) frequency mixers. Formation of periodical domain structure in 1-cm-thick Congruent Lithium Niobate (CLN) crystals is a challenging task due to threshold field about 21 kV/mm [2]. Alternative solution is the so-called “slanted poling” technique [3], which represents formation of periodical domain structure in nonpolar cut plate. For optimal cut, the angle between polar Z-axis and crystal surface is 25° and X-axis is parallel to sample surface. In this case the pump beam propagates with extraordinary polarization along X-axis thus realizing the maximum nonlinear coefficient d_{33} . However, the CLN wafers with optimal cut are rare on the market and quite costly.

Here we propose to apply the concept of slanted poling on CLN wafers with widespread cuts for surface acoustic wave applications (slanted CLN), which are much more affordable.

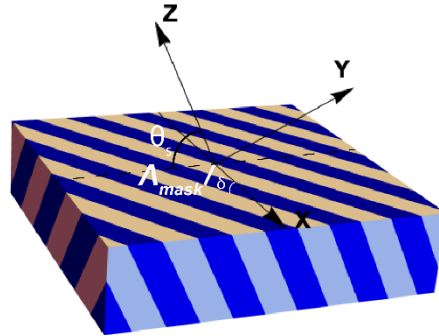


Figure 1. Scheme of periodically poled slanted CLN. θ_s is a slant angle. Λ_{mask} is a mask period. δ is angle between mask direction and X-axis.

The large-aperture frequency mixers were designed for: 36° Y-cut and 64° Y-cut. The slanted crystals are oriented, so the Y-axis is in the crystal surface and an angle between polar Z-axis and surface sample is called slant angle θ_s (Fig. 1). The flat domain walls in CLN crystal with C_{3v} symmetry can be parallel to one of two YZ-planes inclined relative to the sample surface [4].

The poling mask period was calculated using angular quasi-phase matching (AQPM) conception [5] for optical parametric amplification (OPA) process for: $\lambda_{\text{pump}} = 1030$ nm, $\lambda_{\text{signal}} = 1542$ nm, $\lambda_{\text{idler}} = 3100$ nm. We considered that all interacting beams are collinear. The mask period $\Lambda_{\text{mask}} = 33.2$ μm at an incident angle $\theta_i \approx 35^\circ$ and the angle between an incident plane and X-axis located in the sample plane $\alpha = 270^\circ$ for 36° Y-cut; and $\Lambda_{\text{mask}} = 18.3$ μm at $\theta_i \approx 45^\circ$ and $\alpha = 270^\circ$ for 64° Y-cut. The area covered by periodical mask was 2×2 mm^2 .

The periodical domain structure was produced by electrical field poling using liquid (saturated aqueous solution of LiCl) and metal electrodes combination [6]. The photoresist mask was created by photolithography on Z_s^+ surface using photoresists with thickness ranging from 1.8 to 3.8 μm . The instantaneous domain images during poling visualized by optical microscopy were recorded by high-speed CMOS camera (Photron Mini UX100, Japan) with frame rate up to 1000 fps. The field pulses with magnitude ranged from 21.5 to 34.5 kV/mm were applied. The thickness of the samples was ranged from 265 to 500 μm .

The period of photoresist pattern was varied from 40.2 down to 18.3 μm . It was demonstrated that the 64° Y-cut wafers demonstrate better poling results with formation of more homogeneous structures with small number of imperfections. It was shown that decrease the poling period leads to decrease of structure switching time, increase of the field required for polarization reversal and increase of the density of imperfections. The influence of sample and photoresist thickness on the poling quality has been discussed.

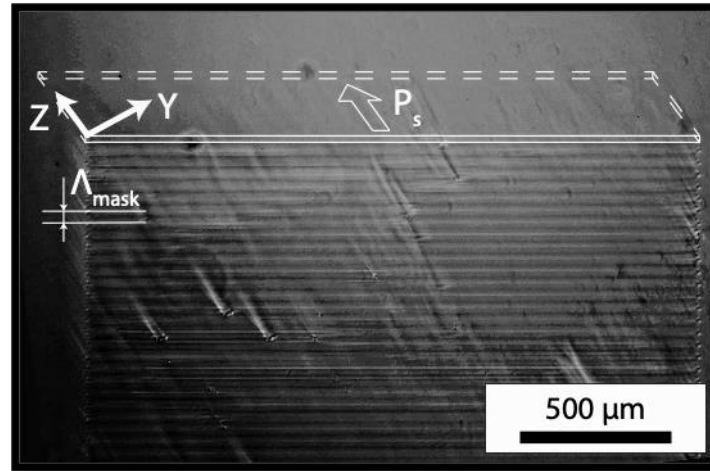


Figure 2. Optical image of the domain structure with period 40.2 μm in 0.5mm-thick 64° Y-cut CLN.

The OPA process efficiency was measured in periodically poled 500- μm -thick 64° Y-cut CLN with $\Lambda_{\text{mask}} = 18.3 \mu\text{m}$ and 265- μm -thick 36° Y-cut CLN with $\Lambda_{\text{mask}} = 33.2 \mu\text{m}$ using 1030 nm fs-laser with pulse duration 350 fs, frequency 100 kHz and average power 11 W. Broadband seed beam with wavelength range from 1200 to 2000 nm was generated using Yttrium Aluminum Garnet (YAG) crystal pumped by the same fs-laser. The diameter of the pump beam was about 400 μm . The maximal OPA gain (≈ 300) was reached for periodically poled 64° Y-cut CLN.

The equipment of the Ural Center for Shared Use “Modern Nanotechnology” Ural Federal University was used. EN is grateful for the financial support of Fastlite Ltd. through the convention n°163967 with CNRS.

1. L. E. Myers et al., *JOSA B*, **12**, 11 (1995).
2. V. Ya. Shur, *J. Mater. Sci.*, **41**, 199 (2006).
3. H. Ishizuki and T. Taira, *Opt. Mater. Express*, **1**, 7 (2011).
4. V. Ya. Shur, *Ferroelectrics*, **340**, 3 (2006).
5. B. Boulanger and J. Zyss, *International Tables for Crystallography* (Springer), 178 (2006).
6. E. A. Neradovskaia et al., *Ferroelectrics*, **541**, 115 (2019).

On joint application of atomic force microscopy and light scattering data for determination of growth rate for fractal solid state surface height

A.E. Rassadin

Laboratory of infinite-dimensional analysis and mathematical physics of Lomonosov Moscow State University, 119991, Moscow, Russia
brat_ras@list.ru

Determination of parameters for kinetic equations is one of the main problems of modern nanoengineering [1]. This report deals with estimation for the rate ν of epitaxial growth of solid state surface in the framework of the simplified Kardar-Parisi-Zhang model:

$$\frac{\partial H}{\partial t} = \nu + \frac{\nu}{2} \cdot (\nabla H)^2, \quad (1)$$

where $H(\vec{x}, t)$ is the height of solid state surface, $\vec{x} = (x_1, x_2)$ is two-dimensional vector of transversal coordinates and ∇ is two-dimensional gradient.

This model differs sharply from the primordial Kardar-Parisi-Zhang model suggested in article [2] because of in equation (1) there are no terms describing the surface diffusion of sputtering substance and the external source of sputtering particles. On the other hand absence of these terms gives one a possibility to solve the following problem namely let initial condition for equation (1) possesses by the next form:

$$H_0(\vec{x}) = h_0(\vec{x}) + \mu \cdot u_0(\vec{x}), \quad (2)$$

where μ is small parameter: $0 < \mu \ll 1$ and $u_0(\vec{x})$ is stationary stochastic two-dimensional field with zero average: $\langle u_0(\vec{x}) \rangle = 0$, generally speaking $u_0(\vec{x})$ being fractal function.

Representation (2) for initial condition means that in order to construct solution of equation (1) one ought to use perturbation theory:

$$H(\vec{x}, t) = h(\vec{x}, t) + \mu \cdot u(\vec{x}, t) + \dots \quad (3)$$

Further if one chooses regular shape $h_0(\vec{x})$ in initial condition (2) as follows:

$$h_0(\vec{x}) = h_* - \frac{\vec{x}^2}{2 \cdot L_*}, \quad (4)$$

(h_* and L_* are constant positive values), then zero order approximation in asymptotic series (3) is equal to:

$$h(\vec{x}, t) = h_* + \nu \cdot t - \frac{\vec{x}^2}{2 \cdot (L_* + \nu \cdot t)} \quad (5)$$

(it is easy to check that function $h(\vec{x}, t)$ is exact solution of equation (1)).

Thus the first order approximation in asymptotic series (3) in accordance with formula (5) ought to obey to the next linear partial differential equation with variable coefficients:

$$\frac{\partial u}{\partial t} + \frac{\nu \cdot \vec{x}}{L_* + \nu \cdot t} \cdot \nabla u = 0 \quad (6)$$

One can derive exact solution of the Cauchy problem for equation (6) with initial condition $u_0(\vec{x})$ by the well-known method of characteristics:

$$u(\vec{x}, t) = u_0 \left(\frac{L_* \cdot \vec{x}}{L_* + \nu \cdot t} \right) \quad (7)$$

It is obvious that $\langle u(\vec{x}, t) \rangle = 0$ therefore $\langle H(\vec{x}, t) \rangle = h(\vec{x}, t)$. It means that one can directly calculate covariance function of total height $H(\vec{x}, t)$ of solid state surface:

$$B(\vec{\xi}, t) = \langle (H(\vec{x}, t) - \langle H(\vec{x}, t) \rangle) \cdot (H(\vec{x} + \vec{\xi}, t) - \langle H(\vec{x} + \vec{\xi}, t) \rangle) \rangle, \quad (8)$$

namely if process of epitaxy lasts from $t = 0$ to $t = t_*$ then it is necessary to measure shapes $H_0(\vec{x})$ and $H(\vec{x}, t_*)$ by means of atomic force microscopy before the beginning and after the end of technological process. Further one should estimate $\langle H_0(\vec{x}) \rangle$ and $\langle H(\vec{x}, t_*) \rangle$ with help of thresholding. Thresholding is known to be a kind of denoising procedure in the framework of wavelet analysis [3].

At last one ought to derive the two-dimensional Fourier-transform from function (8):

$$S(\vec{q}, t) = \int B(\vec{\xi}, t) \cdot \exp(-i \cdot \vec{q} \cdot \vec{\xi}) \cdot d^2 \xi \quad (9)$$

On the other hand one can measure at $t = t_*$ bistatic cross-section σ of monochromatic visible light with fixed polarization on this surface and extract from this value spectral density (9) because of the so-called small-scales approximation in this situation is valid [4].

If these functions are close in some norm then conjecture about validity of equation (1) is true hence in this case using formulae (3) and (7) it is easy to find that

$$B(\vec{\xi}, t) = \mu^2 \cdot K_0 \left(\frac{L_* \cdot \vec{\xi}}{L_* + v \cdot t} \right) + o(\mu^2), \quad (10)$$

$$K_0(\vec{\xi}) = \langle u_0(\vec{x}) \cdot u_0(\vec{x} + \vec{\xi}) \rangle \quad (11)$$

being autocorrelated function of stochastic field $u_0(\vec{x})$.

Thus spectral density for covariance function (10) is equal to:

$$S(\vec{q}, t) = \mu^2 \cdot \left(\frac{L_* + v \cdot t}{L_*} \right)^2 \cdot S_0 \left(\frac{L_* + v \cdot t}{L_*} \cdot \vec{q} \right) + o(\mu^2), \quad (12)$$

where $S_0(\vec{q})$ is spectral density corresponding to autocorrelated function (11) therefore in accordance with small-scales theory [4]:

$$\frac{\sigma_{\vec{q}=0, t=t_*}}{\sigma_{\vec{q}=0, t=0}} = \left(1 + \frac{v \cdot t_*}{L_*} \right)^2 + O(\mu) \quad (13)$$

Formula (13) means that if one can measure bistatic cross-section on this surface before the start of technological process too and determine parameter L_* from expression (4) by fitting of data of atomic force microscopy after thresholding then one can estimate the rate v of epitaxial growth of solid state surface.

Quantum mechanical mechanisms of arising of two-dimensional Weierstrass-like shapes $u_0(\vec{x})$ are also considered according to approaches of article [5].

This work was supported by RFBR, grant N 18-08-01356-a.

1. A.E. Rassadin, et al., *IOP Conf. Ser.: Mater. Sci. Eng.* **443**, 012027 (2018).
2. M. Kardar, G. Parisi, Y.C. Zhang, *Phys. Rev. Lett.* **56**, 889 (1986).
3. N.K. Smolentsev, *Foundations of Wavelet Theory. Wavelets in MATLAB* (DMC Press), 295 (2008) [in Russian].
4. A. Ishimaru, *Wave Propagation and Scattering in Random Media, Vol. 2* (Academic Press), 219 (1978).
5. D. Wojcik, I. Bialynicki-Birula, K. Zyczkowski, *Phys. Rev. Lett.* **85**, 5022 (2000).

Finite element modelling of 1-3 piezoelectric polymer composites with surface effects

G. Iovane¹, A.V. Nasedkin²

¹*University of Salerno, 84084, Fisciano (SA), Italy*

²*Southern Federal University, 344090, Rostov-on-Don, Russia*
nasedkin@math.sfedu.ru

As is known, the properties of nanobodies can significantly differ from similar properties of bodies of ordinary size. To describe this scale effect, a number of different theories and models of nanomechanics were developed. One of such widely used theories is the model of surface elasticity. In turn, among the theories of surface elasticity, the Gurtin-Murdoch model is now more popular. The use of this model leads to the fact that the boundaries of the nanoscale body are covered with elastic membranes, the internal forces in which are determined by surface stresses. Elastic membranes can be placed inside the body with nanoscale inclusions at the interphase boundaries, which also allows modelling imperfect interface boundaries with stress jumps.

The Gurtin-Murdoch model was also transferred to piezoelectric nanoscale bodies. According to this model, the surface constitutive relations were formulated, which are valid on the boundary of the piezoelectric body, and the terms with surface nabla-operators from surface stresses and surface electrical induction were added to the mechanical and electrical boundary conditions. Similarly, on the nanoscale interphase boundaries inside the body, it is also possible to specify surface constitutive relations and interface boundary conditions with surface values. For statements of dynamic problems, taking into account damping effects, the dynamic surface or interface equations can be supplemented by surface damping terms. All of these models reflect dimensional effects and affect on the overall electromechanical state, if the inclusions are only nanoscale.

The described models were used both for the formulation of initial-boundary and boundary-value problems for 1-3 polymer piezoelectric nanostructured composites, and for solving the problems of determining their effective properties. For the numerical solution of these problems, finite element technologies and the ANSYS software package were used. In the simulation, one composite cell with a nanoscale piezoelectric rod in a polymer matrix was considered. The ends of the rod were supposed to be covered with electrodes. Surface effects were set both on the interface lateral surface of the contact between the rod and the polymer matrix, and on the end faces. Finite element modelling of surface effects was carried out by means of shell elements with options of membrane stresses and by using special volume elements with coupled degrees of freedom.

Finite element solutions of static problems, modal problems and problems of steady-state oscillations for various values of surface moduli were obtained. For modal problems, the first frequencies of electric resonances and antiresonances were determined and the dynamic coefficients of the electromechanical coupling were calculated. For a rod with a circular cross section, the approximate analytical solutions were also obtained and these solutions were compared with corresponding numerical solutions. The analysis showed a significant effect of surface moduli and nanoscale thickness on the basic characteristics of the composite structure in static and dynamic operating modes.

This work for second author was supported by the Russian Science Foundation (grant number 15-19-10008-P).

Correlations "interatomic bond strain – Curie temperature" for complex oxides on the perovskite structure quasielastic model base

G.A. Geguzina

*Southern Federal University, Research Institute of Physics, 344090, Rostov-on-Don, Russia
geguzina@sfnu.ru*

The known perovskite structure binary and ternary oxides (PSO) [1], which undergo ferroelectric (FE) or antiferroelectric (AFE) phase transitions (PT) at the corresponding Curie temperatures, T_C are considered. The purpose of the article: to establish qualitative and/or quantitative correlations between the values of the interatomic bond strains $A - O$, δ_{A-O} , or $B - O$, δ_{B-O} , in their structure, on the one hand, the nature and the values T_C , at which their FE or AFE PT occur, on the other hand.

Values of δ_{A-O} or δ_{B-O} can be determined from the proposed by Sakhnenko V.P. and co-authors of the quasi-elastic model of the perovskite structure [1-4], which makes it possible to calculate the theoretical average parameter of the perovskite cell with an accuracy no worse than 1%. The values of the interatomic bond strains can be determined from both the calculated and experimental average parameter, $\bar{a} = \sqrt[3]{V_{per.cell}}$, of the perovskite cell, containing one formula unit. For binary and ternary PSO $\delta_{A-O} = (L_{AO} - L_{AO}^0) / L_{AO}^0$ where L_{AO}^0 is the length of the unstrained (free) interatomic bond $A - O$, and L_{AO} is the length of the strained bond in the complex oxide structure. The L_{AO} values can be determined either from the experimental \bar{a}_{exp} or calculated \bar{a}_{calc} average cell parameter: $L_{AO} = \bar{a} / \sqrt{2}$. The values L_{AO}^0 were calculated [4] by the author from an array of experimental parameters of a reduced perovskite cell of ~1000 known binary and ternary PSO.

The values δ_{A-O} in binary PSO can be both negative, for example, in the structures of ferroelectrics $BaTiO_3$, $PbTiO_3$ and $KNbO_3$, demonstrating the tightness of the bonds $A - O$ in them, as well as can be equal 0, for example, in the structures of some ternary ferroelectrics, showing zero interatomic bond $A - O$ strain. For ternary PSO possessing an FE PT, almost zero or small positive ones are characteristic, and for ternary PSO with an AFE PT, they are much larger. These values indicate that for all FE PSO δ_{A-O} exceed a certain value, above which δ_{A-O} of the AFE PSO are located. Thus, it was possible to separate the FE PSO from the AFE PSO by their δ_{A-O} values. At the same time, the "virtual" FE PSO, for example, $SrTiO_3$ and $KTaO_3$, are located between the FE and the AFE PSO in terms of their δ_{A-O} values.

The correlations between the δ_{A-O} , on the one hand, and FE and AFE PT T_C values, on the other hand, built on diagram (Fig. 1a) for binary PSO, show that the PT temperatures for them among other their composition and structure factors is determined by the interatomic bond strains $A - O$, δ_{A-O} . If for a binary PSO it is $\delta_{A-O} > 0$, the ferroelectric properties are not observed at all, and starting with $\delta_{A-O} > 2\%$ for binary PSO already AFE PT is observed, for example, for AFE PSO $PbSnO_3$ with $\delta_{A-O} = 2$, $PbHfO_3$ with $\delta_{A-O} = 3$ or $PbZrO_3$ with $\delta_{A-O} = 3.6\%$. The $A-O$ bond of AFE PSO $CdTiO_3$ is even more strained – $\delta_{A-O} = 9.1\%$, and $T_C = 1223$ K – maximum T_C for AFE PSO. Then for the binary PSO T_C drops to 630 K for AFE PSO $NaNbO_3$ with $\delta_{A-O} = 15\%$ (Fig. 1c). The ternary PSO in the diagrams c and d with their δ_{A-O} and T_C values are somewhat shifted in the direction of δ_{A-O} increasing and have lower T_C values compared with the FE PT. For ternary AFE PSO, as well as for binary PSO, with the δ_{A-O} growth T_C also grows, but does not reach a pronounced maximum.

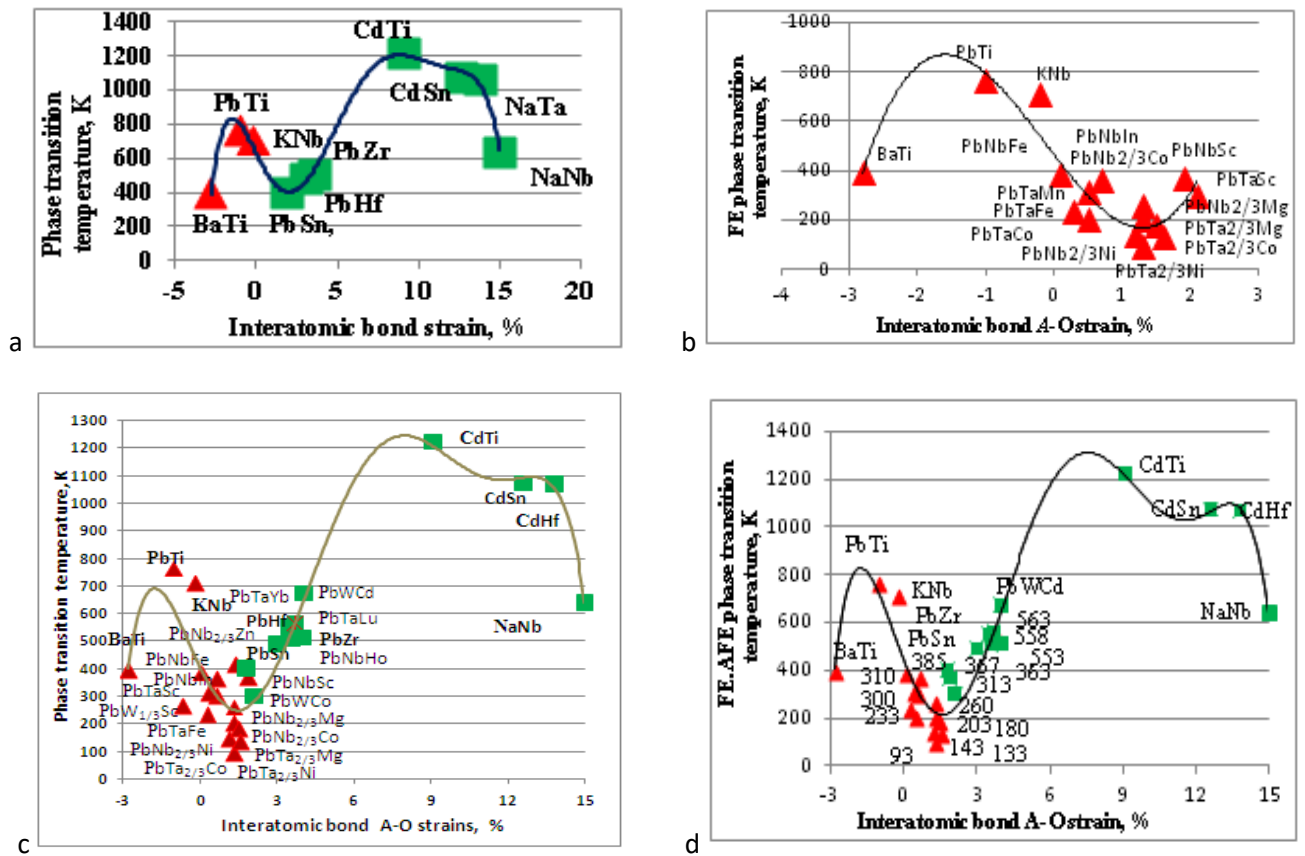


Figure 1. Dependences of the T_C on δ_{A-O} for: (a) FE (triangles) and AFE (squares) binary PSO; (b) binary and ternary FE PSO together; (c) binary and ternary FE and AFE PSO together and (d) the same, but with the corresponding T_C values. Composition formulae are written briefly: there is always no "O3" in them; if the ternary oxide has $\beta_1 = \beta_2 = 1/2$, then these fractions are not indicated; if one of the Bj atoms in the ternary oxide formulae contain the fraction $\beta_1 = 2/3$, then second fraction $\beta_2 = 1/3$ is not indicated, to save space.

For each PT nature there is a certain interval of δ_{A-O} values change and a certain T_C maximum: for the FE PT – 763 K (for PbTiO_3), and for the AFE PT – 1223 K (for CdTiO_3). Ternary PSO have lower PT temperatures than binary PSO. Neither for the FE, nor for the AFE ternary PSO there are no pronounced T_C maxima. For ternary PSO with the following increasing δ_{A-O} after KNbO_3 , T_C drop and quite steeply from 385 K for $\text{PbNb}_{1/2}\text{Fe}_{1/2}\text{O}_3$ to 93 K for $\text{PbTa}_{2/3}\text{Ni}_{1/3}\text{O}_3$, which is minimal for ternary PSO at $\delta_{A-O} = 2\%$. With a further δ_{A-O} increasing in the diagrams **c** and **d** (Fig. 1) for ternary AFE PSO values T_C increase as grows along with T_C of binary AFE PSO, and this process continues until $\text{PbW}_{1/2}\text{Cd}_{1/2}\text{O}_3$ with $T_C = 673$ K and $\delta_{A-O} = 4\%$. Thus, in diagrams **c** and **d** (Fig. 1) T_C of both binary and ternary PSO has a general tendency to change its values with a change of the δ_{A-O} in their structures regardless of their composition features. Constructed correlations can be taken into account in the directed search for new solid solution compositions between different PSO with special properties.

1. E.G. Fesenko. Semeistvo perovskita i segnetoelektrichestvo. (Moscow: Atomizdat), 1972. [in Russian]
2. V.P. Sakhnenko, E.G. Fesenko, A.T. Shuvaev, et al., *Kristallographiya* **17**, 316 (1972).
3. V.P. Sakhnenko, N.V. Ter-Oganessian, *Acta Crystallogr. B.* **74**, 264 (2018).
4. G.A. Geguzina, N.V. Dergunova, V.P. Sakhnenko, et al., *Specvypusk «Nautchnaya mysl Kavkaza»* (Suppl. to Magazine «Izvestiya Severo-Kavkazskogo nautchnogo centra»), 13 (2002).

Phase composition distribution simulation of titanium oxide nanosize structures obtained by the local anodic oxidation method

O.G. Karen'kih, V.I. Avilov, V.A. Smirnov, R.V. Tominov, N.A. Sharapov, N.A. Polupanov

*Southern Federal University, Institute of Nanotechnologies, Electronics and Equipment Engineering,
344006 Taganrog, Russian Federation
AvilovVI@sfedu.ru*

Nanostructures controlled formation is one of the most important tasks of modern nanotechnology. This task is particularly relevant for the memristor structures formation, since their characteristics are influenced not only by the geometric dimensions, but also by the phase composition distribution in the oxide nanosize structure volume, which is the basis for the memristor manufacture [1]. Therefore, the purpose of this work is to develop a mathematical model that allows to calculate the phase composition distribution in the oxide nanosize structure volume obtained by the local anodic oxidation method using a scanning probe microscope.

Modeling the phase composition of oxide nanosize structures obtained by the metal local anodic oxidation method is a multi-step process and involves the generation of oxygen ions in humid air due to the decomposition of water molecules under the influence of an external electric field; oxygen ions mass transfer from the air into the oxide volume and to the metal-oxide boundary; an increase in the oxide volume in the metal oxidation process; metal oxide phase transitions due to the supply of an additional oxidizing agent to the previously formed oxide volume.

Thus, to solve the problem, it is necessary to solve the system of differential equations:

$$\begin{cases} \nabla(\varepsilon\varepsilon_0\nabla\varphi) = -\rho(N) \\ \nabla(-\mu N\nabla\varphi + D\nabla N) = R(\varphi) \end{cases}$$

where φ and N are electric potential and oxygen vacancies distribution in the oxide volume, $\varepsilon\varepsilon_0$ is the medium dielectric constant, $\rho(N)$ is the oxygen ions volume charge density, μ and D are oxygen ions mobility and diffusion coefficient, $R(\varphi)$ is the generation rate oxygen ions in the air.

The joint solution of the presented system of equations will allow one to obtain the oxygen ions distribution in the oxide volume and the oxygen ions flow to the surface. The obtained results are necessary for calculating the phase transitions in the oxide and the oxide growth rate during local anodic oxidation.

On the basis of the developed model, a numerical simulation of the LAO titanium film process was carried out using the MATLAB application software package using the *Partial differential equation* module algorithms, which allows solving systems of nonlinear differential equations in partial derivatives. For this, the electrochemical cell geometry was considered, including an AFM probe, an air medium, an oxide, and a metal film, for which the solution of a given differential equations system was found. Then, the oxygen ion flux distribution over the metal surface and the oxide growth rate were determined, and phase transitions in the oxide volume were calculated.

As a result, the distributions of the TiO, Ti₂O₃ and TiO₂ phases were obtained (Fig. 1), the analysis of which showed that the TiO phase forms near the oxide-metal interface, the Ti₂O₃ phase is in the oxide volume, and the TiO₂ phase is present near the oxide surface. The results obtained can be explained by the fact that in the process of LAO diffusion of oxygen ions takes place through the oxide layer to the metal surface and, accordingly, the ion concentration decreases from the air medium to the metal. Thus, under conditions of oxygen lack, the TiO phase is formed, and under conditions of high oxygen concentration, the oxide is oxidized to TiO₂.

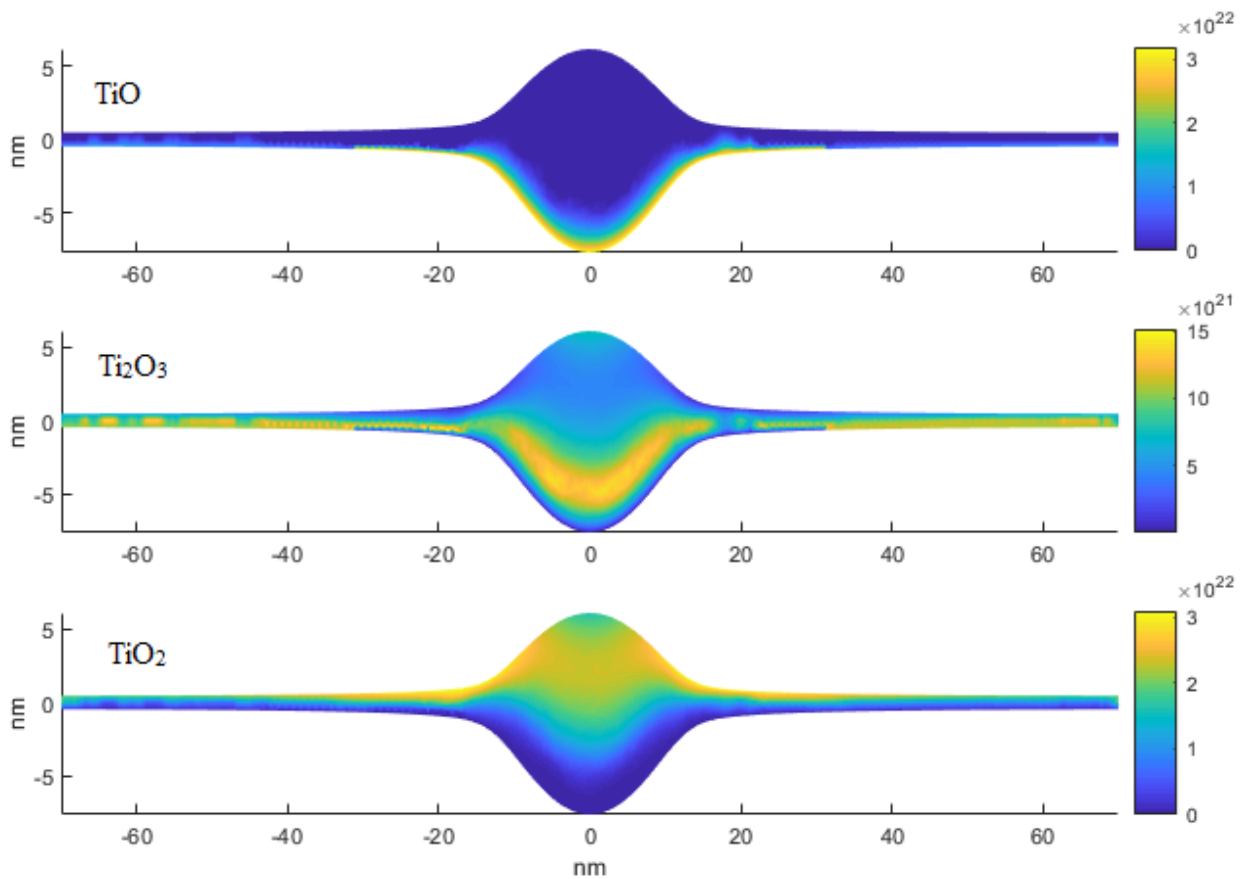


Figure 1. The titanium oxide phases concentration in the volume of the oxide nanosize structure formed by the local anodic oxidation method

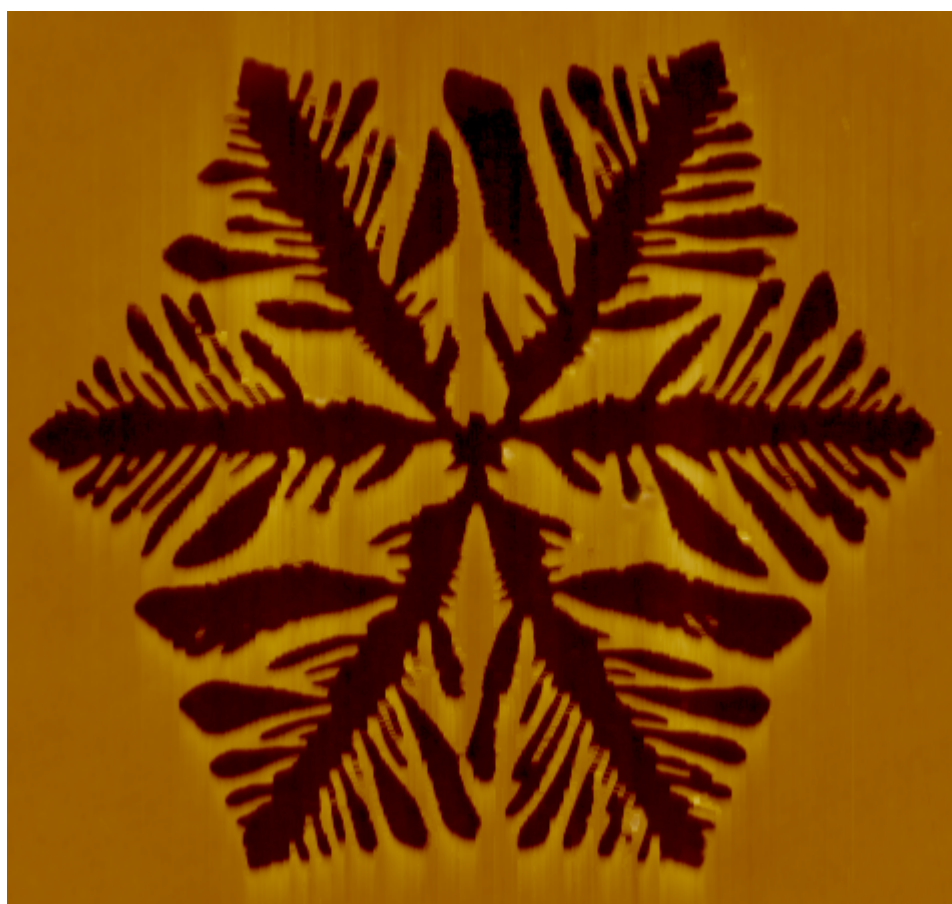
The results obtained correlate well with the experimental results of titanium oxide nanosize structures phase composition XPS analysis on the surface and by ion etching into the oxide [2].

The obtained results can be used in the development of technological processes for the fabrication of the RRAM element base based on titanium oxide nanostructures.

This work was supported by Grant of the President of the Russian Federation No. MK-2721.2018.8. and by RFBR according to the research project № 18-37-00299.

1. V.I. Avilov, V.A. Smirnov, A.A. Fedotov, et al., *IOP Conf. Series: Mat. Sci. Eng.* **443**, 012012 (2018).
2. V.I. Avilov, O.A. Ageev, B.G. Konoplev, et al., *Semiconductors* **50**, 601 (2016).

POSTER PRESENTATIONS



Local polarization reversal in polycrystalline BiFeO₃-based solid solutions

A.S. Abramov¹, D.O. Alikin^{1,2}, A.P. Turygin¹, S. Latushko³, A. Zheludkevich³,
D. Zheludkevich³, A. Pakalniškis⁴, R. Skaudžius⁴, V.Ya. Shur¹, D. Karpinsky^{3,5},
A.L. Kholkin^{1,2}

¹*School of Natural Sciences and Mathematics, Ural Federal University, 620000 Ekaterinburg, Russia
alexander.abramov@urfu.ru*

²*Department of Physics & CICECO – Aveiro Institute of Materials, University of Aveiro, Portugal*

³*Scientific-Practical Materials Research Centre of NAS of Belarus, Minsk, Belarus*

⁴*Institute of Chemistry, Vilnius University, Vilnius, Lithuania*

⁵*Nanoceramics Spolka Akcyjna, Wroclaw, Poland*

Searching of lead-free materials with the electromechanical characteristics comparable to lead zirconate titanate is an actual topic during recent decades due to the increasing demands of ecology in production and recycling. One of the important materials is bismuth ferrite (BiFeO₃, BFO) possessing large polarization and thereby promising for electromechanical performance [1]. The main problem of BFO is poor phase stability due to existence of secondary phases after synthesis and high leakage current [2]. Different methods are used to improve phase stability and realize morphotropic phase boundary (MPB) conditions, such as doping by rare earth elements leading to formation of coexistence of rhombohedral and orthorhombic phases [3]. The solid solution of BFO with stable perovskites, such as barium titanate (BaTiO₃) allows to achieve phase stabilization.

Here, we implemented this doping strategy and investigated relationship between structural state and local piezoelectric properties. Series of the samples were prepared by conventional solid-state sintering and by sol-gel sintering from liquid phase. Macroscopic X-ray diffraction (XRD) revealed gradual lattice transformation from the rhombohedral symmetry (Bi-rich side) to the pseudocubic and tetragonal symmetry. It was shown that despite trend to develop pseudocubic lattice symmetry BFO-BTO demonstrates large piezoelectric response, which can be attributed to coexistence of nanoscale polar and non-polar phases. We suggested that XRD shows the average symmetry of solid solutions correspondent to the non-polar lattice ordering. Whereas, the local study with high spatial resolution by piezoresponse force microscopy allowed revealing the nanoscale polar phase regions. The change of the domain structure geometry from domain maze to lamellar domains with increasing of BTO content was revealed. Local phase transformation was shown to be part of polarization reversal process. Thus, PFM-based studies of phase composition, domain and phase field-induced dynamics are crucial for comprehensive characterization of BFO-based solid solutions.

The equipment of the Ural Center for Shared Use “Modern Nanotechnology” Ural Federal University was used. The study was funded by RFBR (grant No. 19-52-04015) and BRFFR (grant No. F19RM-008). This work was developed within the scope of the project CICECO-Aveiro Institute of Materials, POCI-01-0145-FEDER-007679 (FCT Ref. UID/CTM/50011/2013), financed by national funds through the FCT/MEC and when appropriate co-financed by FEDER under the PT2020 Partnership Agreement. This project has received funding from the European Union’s Horizon 2020 research and innovation program under the Marie Skłodowska-Curie grant agreement No 778070.

1. S. Fujino, M. Murakami, et al., *Appl. Phys. Lett.*, **92**, 202904 (2008).
2. J. Walker, P. Bryant, et al., *Acta Mater.*, **83**, 149 (2015).
3. J. Walker, H. Simons, et al., *Sci. Rep.*, **6**, 19630 (2016).

Effect of the degree of a diffuse phase transitions on the behavior of polarization switching processes and elastic properties in multicomponent ceramics based on PZT

A.V. Skrylev¹, G.M. Akbaeva², A.I. Burkhanov³, A.V. Sopit³, E.M. Panchenko²

¹*Institute of High Technologies and Piezotechnics Southern Federal University, 344090, Rostov-on-Don, Russia*

²*Research Institute of Physics Southern Federal University, 344090, Rostov-on-Don, Russia*
gakbaeva@mail.ru

³*Volgograd State Technical University, 400005, Volgograd, Russia*

The study of a number of ferroelectric-soft ceramics based on PZT shows that they exhibit properties characteristic of ferroelectrics-relaxors [1]. However, unlike relaxors they exhibit pronounced ferroelectric properties under certain conditions, as shown, for example, in [2]. Since multicomponent complex perovskite systems have structural disorder, the properties of such materials can exhibit features associated with the inhomogeneity of the phase state over a wide temperature range.

The purpose of this study is to investigate effect of the degree of a diffuse phase transitions on the behavior of polarization switching processes and elastic properties in multicomponent ceramics based on PZT:



in a wide temperature range, including the region of phase transitions between two polar phases and the main phase transition from the ferroelectric phase to the cubic phase.

Figure 1 presents temperature dependence of the effective dielectric constant $\epsilon'_{eff} = P/\epsilon_0 E$ (P – the polarization determined by Sawyer-Tower method, E – the amplitude of the measuring field) in materials at frequency 1 Hz in wide range of temperatures of the diffuse phase transaction.

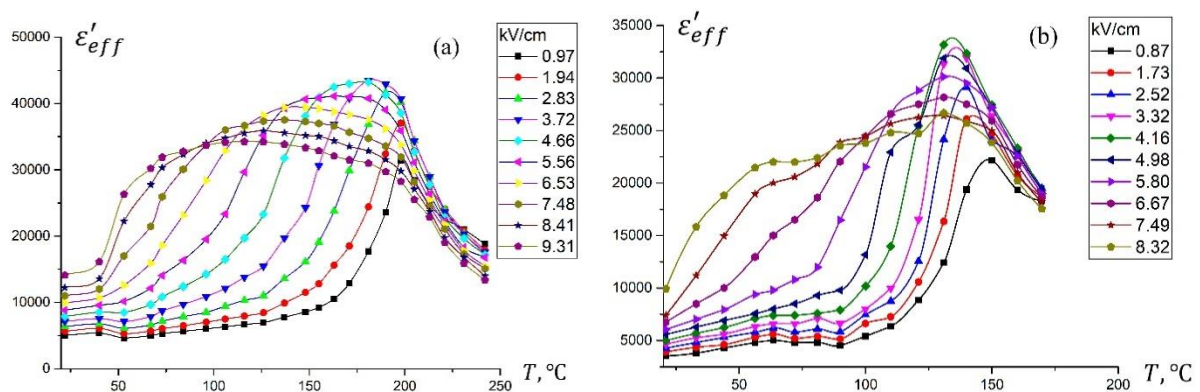


Figure 1. Temperature-frequency dependence ϵ'_{eff} , (a) – composition 1 and (b) composition 2.

1. A.A. Bokov, Z.-G. Ye, *J. Mater. Sci.* **41**, 31 (2006).

2. A.V. Skrylev, A.I. Burkhanov, G.M. Akbaeva, A.E. Panich, *Bull. Russ. Acad. Sci. Phys.* **82**, 372 (2018).

Polarization reversal in Rb:KTP and KTA single crystals

A.R. Akhmatkhanov, M.A. Chuvakova, A.A. Esin, E.V. Shishkina, E.V. Pelegova, V.Ya. Shur

School of Natural Sciences and Mathematics, Ural Federal University, 620000, Ekaterinburg, Russia
Andrey.Akhmatkhanov@urfu.ru

The periodically poled crystals of potassium titanyl phosphate (KTP) family are one of the popular nonlinear optical materials. The KTP family includes crystals with various composition and doping. Among them the Rb doped KTP (Rb:KTP) and potassium titanyl arsenate (KTiOAsO₄, KTA) crystals possess the properties outperforming the basic KTP crystals. Rb:KTP crystals have lower bulk conductivity and KTA crystals have wider transparency range up to 5.5 μm. Realization of highly efficient nonlinear optical interaction requires the creation of precise periodical domain structure in the crystal. Despite the interest to creation of tailored domain structures in these perspective representatives of KTP family the systematical study of domain structure evolution and domain wall motion has not been published yet. In this work we present the study of domain structure evolution and domain wall motion in Rb:KTP and KTA single crystals.

The studied Rb:KTP and KTA Z-cut 1-mm-thick plates with bulk conductivity at room temperature about $2 \cdot 10^{-7}$ Ohm⁻¹cm⁻¹ were grown by top-seeded solution method. The polarization reversal was carried out using liquid electrodes.

In situ visualization of domain kinetics during polarization reversal allowed revealing the formation and fast growth of large number of narrow domain streamers oriented along [010] direction with about ten times higher velocity (6-60 mm/s) than the domain walls (2-5.5 mm/s). Study of the static domain structures demonstrated that the streamers are formed by [100] and [010]-oriented domain walls. The minimal streamer width was about 500 nm and minimal distance between the neighboring streamers – about 100 nm. The switching currents were approximated using the modified Kolmogorov-Avrami approach [2] taking into account the abrupt decrease of the growth dimensionality when the streamers reach the opposite electrode edge.

The polarization reversal in the temperature range allows to reveal the increase of the input of fast and superfast domain walls [3] and noticeable domain elongation with temperature. The domain wall velocities were measured, and corresponding activation energies were extracted.

The equipment of the Ural Center for Shared Use “Modern nanotechnology” Ural Federal University was used. This research was made possible in part by President of Russian Federation Grant for young scientists (grant No. MK-1217.2019.2).

1. V.Ya. Shur, A.R. Akhmatkhanov, *Phil. Trans. R. Soc. A* **376**, 20170204 (2018).
2. V.Ya. Shur, E.L. Romyantsev, S.D. Makarov, *J. Appl. Phys.* **84**, 445 (1998).
3. V.Ya. Shur, A.A. Esin, M.A. Alam, A.R. Akhmatkhanov, *Appl. Phys. Lett.* **111**, 152907 (2017).

Mapping charge carrier mobility at nanoscale

A. Alekseev^{1,2}, A. Yedrissov^{2,3}, S. Kharintsev⁴

¹National Research University "MIET", 124498, Moscow, Russia
alalrus@gmail.com

²National Laboratory Astana, Nazarbayev University, 010000, Kazakhstan

³Karaganda State University, 100028, Karaganda, Kazakhstan

⁴Kazan Federal University, 420008, Kazan, Russia

Charge carrier mobility is important characteristic of semiconductors, which determine performance of the nanoelectronic devices. There are several methods for determination of average macroscopic mobility. One of the most widespread methods is based on space charge limited current (SCLC) measurements, which are performed on thin semiconductor films with flat electrodes. In case of monopolar injection, the Mott-Gurney equation is used for average mobility calculations over macroscopic area (typically few mm²) [1]. The attempts to use conductive atomic force microscopy (AFM) probe as localized top electrode and, thus, provide nanoscale SCLC measurements, lead to significantly higher mobility values. This fact is explained by complicated geometry of the electrodes when AFM probe is used on thin semiconductor films. O. Reid et al. [2] have derived semi-empirical equation for SCLC measurements in organic semiconductors by conductive-AFM (C-AFM). Here, we report on SCLC measurements of semiconducting polymer PTB7 by using C-AFM and following quantification of nanoscale hole mobility. It was shown that nanoscale current distribution is nonuniform and these nanoscale changes of current may be connected to existence of the crystallites in polymer, discovered by XRD methods earlier. It was also shown that SCLC takes place in all our samples and then measured C-AFM current density is proportional to the polymer hole mobility. The current density on film thickness dependence was determined and modification of Reid-Ginger equation [2] based on obtained data was offered. For local mobility mapping the I - V curves were measured at each point of scan. It is concluded that careful estimation of built-in voltage V_{bi} is required at each point, since the value of V_{bi} is not constant on surface. The value of V_{bi} estimated from C-AFM measurements was significantly higher than built-in voltage in macroscopic SCLC measurements (up to 2 V). Finally, the map of hole mobility in PTB7 was calculated from modified Reid-Ginger model [2] adapted to our results by using measured I - V curves and estimated map of V_{bi} (Figure 1). It is seen that the hole mobility map has features of both current map $I(x,y)$ and $V_{bi}(x,y)$, i.e. in general the current image does not directly correlate with the mobility map due to variations of V_{bi} on surface.

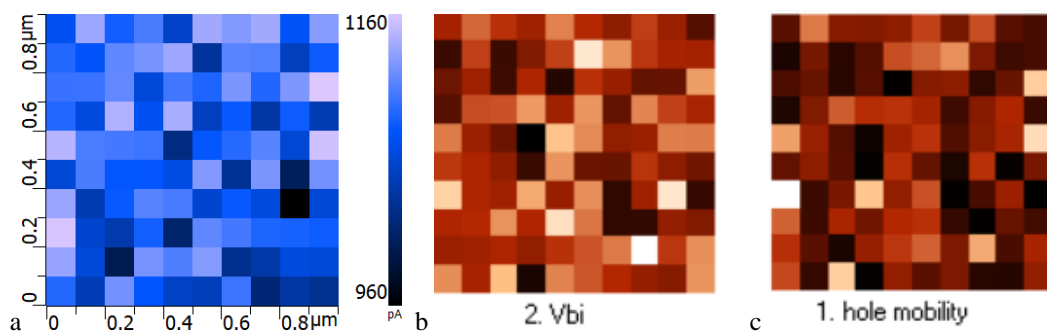


Figure 1. (a) cross-section of I - V curves on PTB7 film at 3 V, (b) distribution of V_{bi} , (c) hole mobility map. Brighter colors correspond to higher values.

This work was supported by Federal Target Program of MES of Russian Federation, contract 14.575.21.0149 (RFMEFI57517X0149).

1. M.A. Lampert, P. Mark, *Current Injection in Solids* (Academic Press), 363 (1970).
2. O.G. Reid, K. Munechika, D.S. Ginger, *Nano Lett.* **8**, 1602 (2008).

The SPM study of oligonucleotides consisting of repeated nucleotide sequences

T.I. Sharipov¹, R.R. Garafutdinov², I.T. Amangulova¹, R.Z. Bakhtizin¹

¹Bashkir State University, 450076, Ufa, Russia

²Institute of Biochemistry and Genetics RAS, 450054, Ufa, Russia
sha-t@yandex.ru

The physical properties of DNA molecules, both natural double-stranded and synthesized single-stranded, are currently being actively studied. Thanks to the invention of scanning tunneling (STM) and atomic force microscopes (AFM) it became possible to study various nanoobjects at the molecular and submolecular levels. Obviously, that DNA molecules, and in particular oligonucleotides, are no exception. Synthesized single-stranded DNA sequences consisting of only one type nucleotides, in which the nitrogen base is only adenine, thymine, guanine or cytosine are of particular interest.

The interest in the processes of charge transport in DNA molecules is very high, due to prospects of using these molecules in nanoelectronics. Attempts to measure the electrical resistance of DNA give contradiction results [1-3]. The ambiguity of the results is influenced by the experimental conditions and the type of DNA molecules under study [4], namely: length, nucleotide composition, different sequence of nucleotides in the DNA chain, the number of chains in the molecule.

We can measure the current-voltage curve of a biomolecule using STM. For this, the molecule must be placed between two electrical contacts, one of which is a conducting probe of the microscope, and the other – the substrate surface fragment.

We set the task of performing the series of experiments to study the conductivity of oligonucleotides depending on their nucleotide composition. In the report we will present the results of STM/STS studies of oligonucleotides consisting of repeated nucleotide sequences of only one type, for example, thymine – $d(T)_n$, where n is the number of such nucleotides.

First, we obtained a silver substrate by thermal spraying of silver in vacuum on the mica surface. Next, the obtained substrate was coated with the studied molecules. Then we carried out STM study of the silver surface with immobilized oligonucleotide molecules by the constant tunneling current mode. In addition to obtaining a number of STM images and identifying oligonucleotides on them, the current-voltage curves of single molecules have been measured. In this case, the current-voltage curve is the dependence of the tunneling current on the applied voltage between the probe and the silver substrate. The current-voltage curves were measured several times at each point, and then the data were averaged.

The work was performed with financial support of the grant of the Republic of Bashkortostan for the young scientists for 2019, contract № 29GR.

1. H.W. Fink, C. Schonberger, *Nature* **398**, 407 (1999).
2. D. Porath, A. Bezryadin, S. De Vries, et al., *Nature London* **403**, 635 (2000).
3. T.I. Sharipov, R.Z. Bakhtizin, *IOP Conf. Series: Mat. Sci. Eng.* **256**, 012009 (2017).
4. M. Iijima, T. Kato, S. Nakanishi, et al., *Chemistry Letters* **34** (8), 1084 (2005).

Evidence of surface structure of the cultured astrocytes and glioblastoma cell culture after exposing β -amyloids (A β 1-40, A β 1-42, tau-protein) isolated from the aged human brain with Alzheimer's disease

A.N. Astashonok¹, Z.B. Kvacheva², N.N. Poleshchuk¹, L.V. Lipatova³

¹*The Republican Research and Practical Center for Epidemiology and Microbiology, 220114, Minsk, Belarus
micro.87@mail.ru*

²*Institute of Biophysics and Cell Engineering of National Academy of Sciences of Belarus, 220072, Minsk, Belarus*

³*St. Petersburg V.M. Bekhterev Psychoneurological Research Institute, 192019, Saint Petersburg*

The main characteristic traits of Alzheimer's disease (AD) are the violation of the metabolism of amyloid precursor protein (APP), deposition of amyloid-beta (A β) plaques and neurofibrillary tangles in the brain tissue, neuronal death and the loss of synapses. All of these signs contribute to cognitive decline in a progressive manner up to total disintegration of memory, speech and visually-spatial properties of the person. Understanding the contribution of these pathological events has been a focus of intensive research study from the last decades. However, our progress in this area has been limited by the difficulties in generating in vitro specific models that recapitulate this pathology. Here we described the nanoscale evaluation of the structural changes of cytoplasmic membrane of macroglial and glioblastoma cell line under the action of various nano-sized pathological forms of A β -amyloids, tau-protein which isolated from brain tissue of patients who had died from AD.

For atomic force microscopy (AFM) investigations, we study the rat C6 glioma cell line and mouse EPNT-5 glioblastoma cells collected from Institute of cytology of the Russian Academy of Science (St. Petersburg). All cell lines were maintained in Dulbecco's modified Eagle's medium supplemented with 10% fetal bovine serum, 100 units/ml penicillin G, 0.1 mg/ml streptomycin (37 °C with 5% CO₂). The isolation of pathological proteins (A β -amyloids, tau-protein) was performed according to the protocols of A. Rostagno, J. Ghiso, 2009 [1] and V. M. Lee, J. Wang, 1999 [2]. The treatment of experimental cultures (C6, EPNT-5) β -amyloids, tau-protein was carried out in the logarithmic growth phase by adding 40 μ l of purified brain fraction (concentration \sim 0.4 mmol/ml, the dilution steps – 10⁻¹-10⁻⁵). The culture flasks were incubated at 37 °C for 48 hours, daily observing the integrity, density of the cell monolayer and morphology. AFM analysis was done at room temperature in tapping mode using Si₃N₄ with a resonant frequency of 190-315 kHz.

AFM investigations of the analyzed cell cultures revealed a considerable range of morphologies of transforming cells as comparison of intact cell cultures (Fig.1 a-f) The untreated cells (C6, EPNT-5) showed a conventional cellular shape with distinct boundaries and centrally located two or three nuclei. When (C6, EPNT-5) cells were exposed to β -amyloids for 12 hours, obvious apoptotic changes, such as aggregation, micronucleated cells and floating cells, were observed. Interestingly, the cell membranes were severely damaged. These changes also included increases in the fluctuation of the surface components of the cell membrane, increase in shrinkage, the absence of pores, formation of giant rounded cells with the loss of lamellopodia.

Analysis of the surface roughness parameters (R_a , R_q) cytoplasmic membranes showed that intact cells differ by a much larger arithmetic average and root-mean-square roughness ($R_a = 76 \pm 14$ nm, $R_q = 118 \pm 14$ nm, $p < 0.01$) compared to with experimental cultures ($R_a = 252 \pm 15$ nm, $R_q = 204 \pm 14$ nm, $p < 0.01$). Thus, it has been shown that A β -amyloids affect the cellular cytoplasmic membrane, changing its structure and its spatial organization.

In order to obtain more complete information about the structure of the cytoskeleton, force spectroscopy and measurement of the local values of the Young's modulus were used both in intact astrocytes and in experimental cultures. The force curves were taken at points located along selected lines (10 or 20 points per line). It was shown that on intact astrocytes, the range of values of the Young's modulus had a large scatter (1.4-7.8 kPa), which is typical of most active proliferating eukaryotic cells. At the same time, the Young's modulus subjected to the

transformation with A β -amyloids was significantly higher (~17.9 kPa). This is likely to indicate that bundles of fibrils of cells transformed with β -amyloids more closely adhere to their cytoskeleton, which increases the local rigidity of these cells.

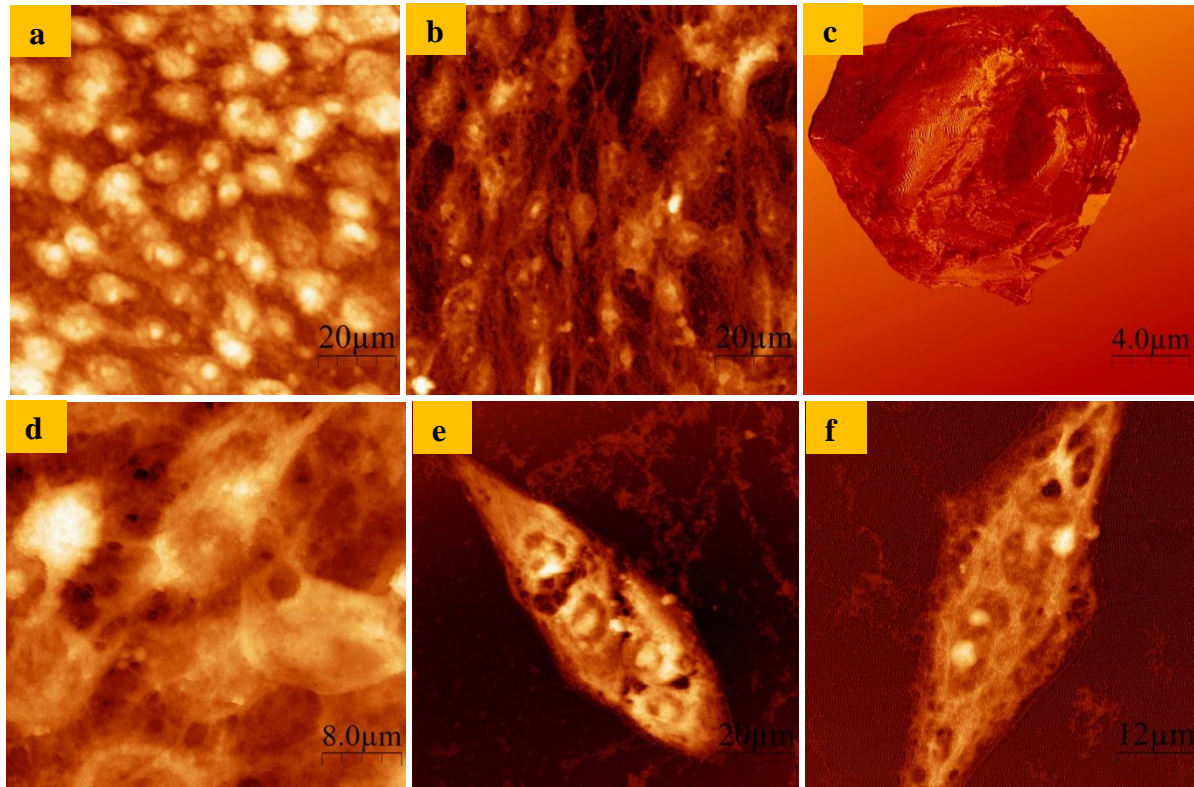


Figure 1. AFM images of topography of the normal (a,d) and treated C6 (b,c), EPNT-5 cell cultures (e, f) with β -amyloids and tau-protein which were isolated from brain tissue of patients with Alzheimer's disease.

Besides, another marker (tau-protein, concentration 0.05 mg/ml) was found to disrupt the cell membrane, not similar to β -amyloids. We revealed more crude morphological changes in astrocytes and glioblastoma (protrusions and loss of filopodia, local fragmentation of the cytoplasmic membrane, the releasing of the contents of the cytoplasm into the intercellular space). Also we have found significant differences in the morphological features between untreated and experimental EPNT-5 cells. We found a very small number of giant cells against the background of destroyed cells, which retained three or four nuclei and well-defined components of the cytoskeleton. These cells are likely to meet specific forms of glioblastomas that contribute to the survival of cancer in the host. However, their role is currently virtually unknown.

1. A. Rostagno, J. Ghiso, *Curr. Protoc. Cell Biol.* **1**, 1 (2009)
2. V.M. Lee, J. Wang, *Methods Enzymol.* **309**, 81 (1999).

Nanoscale organization of the normal human dermal fibroblasts and mesenchymal stem cells isolated from adipose tissue

A.G. Polesko¹, Z.B. Kvacheva¹, A.N. Astashonok²

¹*Institute of Biophysics and Cell Engineering of National Academy of Sciences of Belarus, 220072, Minsk, Belarus*

²*The Republican Research and Practical Center for Epidemiology and Microbiology, 220114, Minsk, Belarus, micro.87@mail.ru*

Stem cells are an immature cells which are the source of a large number of other cell types. It is well known that they are classified as embryonic stem cells, pluripotent stem cells and adult stem cells. The most important population of adult stem cells are mesenchymal stem cells (MSC). At first, these cells were detected and isolated from the bone marrow. It was believed that the bone marrow-derived mesenchymal stem cells are a source for updating and restoring such connective tissues like bone, skin, cartilage and fat. Nowadays, bone marrow MSCs analogues are detected in all other tissues. In this work we summarize our data concerning nanoscale organization of human mesenchymal stem cells and dermal fibroblasts to study their potential role in the regeneration and transplant processes.

Skin biopsies were obtained during mammoplasty surgery with *patient-informed consent*. Tissue fragments (explants) were placed in plastic petri dishes with addition specific nutrient medium. The medium was replaced every 3-4 days. The cells were harvested when grown to 80% confluence and dispersed in a new plastic culture bottles. Mesenchymal stem cells were obtained from human adipose tissue according to protocol S. Schneider et al., 2017 [1]. AFM images were obtained in tapping mode using silicon cantilevers with a resonant frequency of 190-315 kHz. All measurements were performed at room temperature.

AFM analysis revealed variations in structural organization of the analyzed cell types. Dermal fibroblasts (the average sizes – 15-20 μm) (fig. 1a) exhibited a very distinguishable actin cytoskeleton organization – a lot of cross-linking actin filaments and larger fibers (like stress fibers) in filopodia. Conversely, MSCs (fig.1a) exhibited a smooth surface and almost no stress fibers but had a very large variation in size that exceeded 60-70 μm .

To characterize the elasticity of these cells, mean Young's modules were calculated. The results reveal that there are significant differences between the fibroblasts-like cells (Young's modulus) collected from human skin (value – 1.4-7.8 kPa) than human adipose tissue (value – 5.2-6.4 kPa). This is probably due to a large variety of cells of the surface epithelium, which are highly specialized and occupy certain tissues niches.

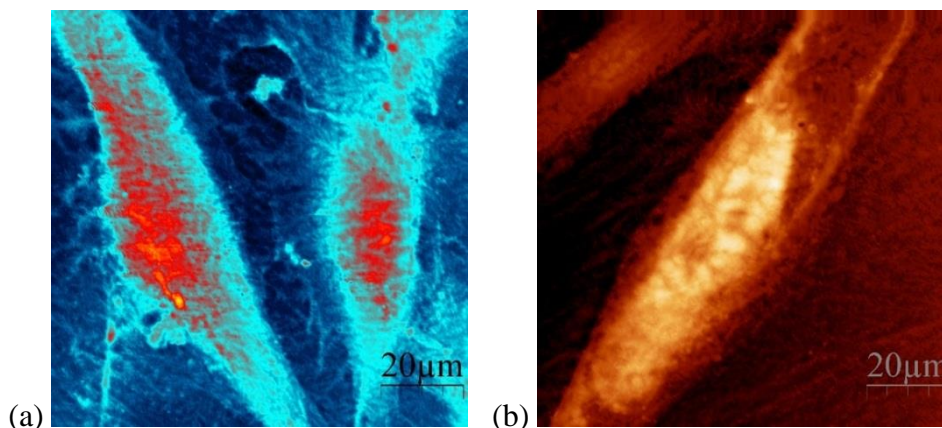


Figure 1. Typical surface topography of the analyzed cell types. AFM tapping-mode images of (a) human dermal fibroblasts and (b) mesenchymal stem cells.

In summary, our study showed morphometric and biophysical features of dermal fibroblasts and mesenchymal stem cells. We improved understanding of the physical characteristics of different cell types. The obtained results can be used to understand their general biological significance and to search for their specific potential and other properties in regenerative medicine and transplantology.

1. S. Schneider et al. *Eur. J. Med. Res.* **22**, 17 (2017).

Atomic force microscopy of titanium oxide nanosize structures resistive switching

V.I. Avilov, V.A. Smirnov, R.V. Tominov, N.A. Sharapov, A.A. Avakyan

*Southern Federal University, Institute of Nanotechnologies, Electronics and Equipment Engineering, 344006 Taganrog, Russian Federation
AvilovVI@sfnu.ru*

Modern microelectronics development is associated with the development of new energy efficient, high-speed memory elements that can be built on the memristor structures basis that switching between high and low resistance states [1, 2]. However, for the introduction of such memory elements into production it is necessary to conduct comprehensive studies of the time stability of their resistive switching.

Experimental studies were carried out on a titanium film with a about 20 nm thickness, obtained by the magnetron sputtering method on a dielectric substrate SiO₂. For this purpose, using a scanning probe microscope, nanolithography was carried out using local anodic oxidation (LAO), which resulted in the oxide nanosize structures formation with lateral dimensions of 3×3 μm² and a thickness of 5 nm on the thin titanium film surface. Studies of current-voltage characteristics showed that the structure obtained exhibits a memristor effect and switches between high and low resistance states (Fig. 1).

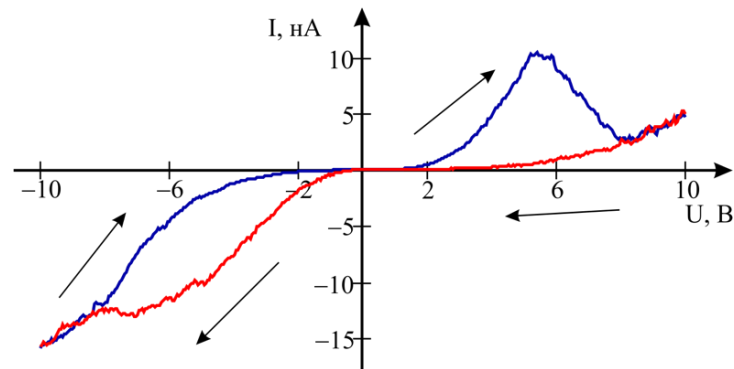


Figure 1. Volt-ampere characteristic of titanium oxide nanosize structure formed by LAO method.

Measurement and analysis of current-time characteristics (Fig. 2) showed that in the initial state, when positive voltage pulses are applied, there is no current through the memristor structure, which corresponds to the HRS state. When negative voltage pulses are applied, the current through the structure is of the order of 0.3 nA, which corresponds to the LRS state. The results obtained correspond to the memristor effect based on the modulation of the width of the potential barrier at the electrode/oxide interface.

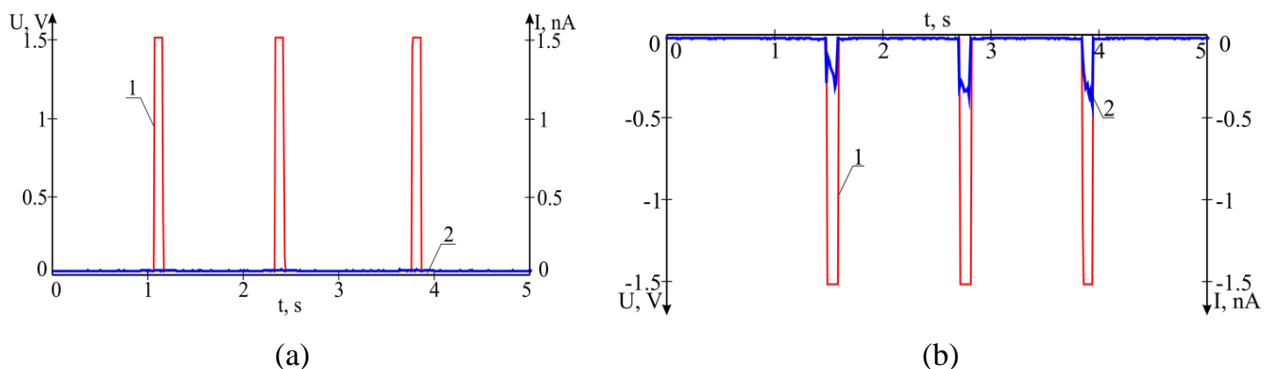


Figure 2. The current-time characteristics of the memristor structure based on the titanium ONS, obtained by applying voltage pulses (1) and current (2) of different polarity: (a) positive; (b) negative.

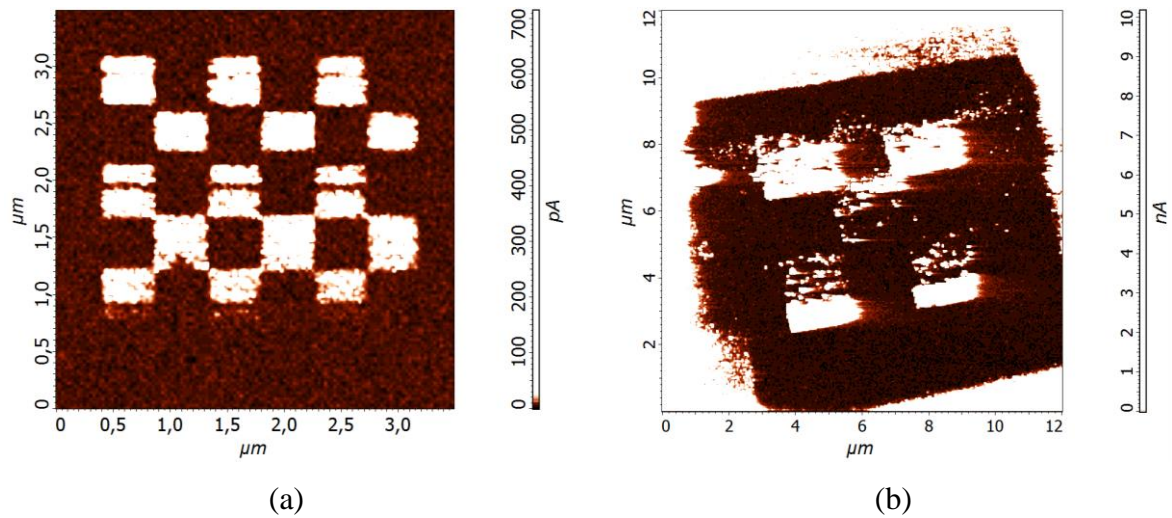


Figure 3. AFM images of the current distribution of test areas in the LRS state on the surface of the memristor structure: (a) after formation; (b) after 75 days.

To study the time of information storage in memristor structures on the ONS surface using AFM the test area was formed and its resistive switching to the LRS state by applying negative voltage pulses with an amplitude of -6 V. Scanning in the spreading resistance mode with the application of 1.5 V voltage pulses allowed us to construct a map of the current distribution of this test area on the surface in the LRS state (Fig. 3a). Then, after 75 days, the structure was scanned in the spreading mode, which showed that the test areas were saved in the LRS state (Fig. 3b).

Thus, it was shown that oxide nanoscale structures of titanium, formed by the method of local anodic oxidation, exhibit a stable memristor effect for a long time. The obtained results can be used in the development of technological processes for manufacturing the elemental base RRAM based on oxide nanosized titanium structures using probe nanotechnology.

This work was supported by RFBR according to the research project № 18-37-00299 and by Grant of the President of the Russian Federation No. MK-2721.2018.8.

1. V.I. Avilov, V.A. Smirnov, A.A. Fedotov, R.V. Tominov, N.A. Sharapov, N.A. Polupanov, *IOP Conf. Series: Mat. Sci. Eng.* **443**, 012012 (2018).
2. R.V. Tominov, V.A. Smirnov, V.I. Avilov, A.A. Fedotov, V.S. Klimin, N.E. Chernenko, *IOP Conf. Series: Mat. Sci. Eng.* **443**, 012036 (2018).

Effect of the lithium ions on the structure formation of the ceramics based on sodium niobate

E.V. Barabanova, O.V. Malyskina, A.I. Ivanova, E.S. Tesnikova, M.S. Vahrushev

Tver State University, 170002, Tver, Russia
pechenkin_kat@mail.ru

The structure of sodium, potassium and lithium niobate ceramics and complex oxides based on them was studied. Ceramic samples were prepared by solid-phase synthesis method from alkali metal carbonates KCO_3 , $NaCO_3$, $LiCO_3$ and niobium pentoxide Nb_2O_5 by traditional ceramic technology. Sintering was carried out at a temperature of 1100 °C except of potassium niobate (700 °C). The ceramics structure was studied by scanning electron microscope (SEM) JEOL JSM 6610 LV in the secondary electron mode. Studies of the domain structure and local piezoelectric loops were carried out by piezoresponse force microscopy (PFM) at room temperature on a SolverNano (NT-MDT).

These oxides are octahedral type oxides with the general formula ABO_3 , where the position of A can be occupied by ions of Li, Na, K. As can be seen in Figure 1, the shape and size of the grains depend on the type of ion in position A. In the case of potassium niobates the shape is cubic, as well as for solid solution of potassium sodium niobate. The main difference is the grain size (Fig. 1a,e). The lithium niobate ceramics grains have irregular shape (Fig. 1c), as a result they contact more closely. And sodium niobate ceramics grains have spherical shape (Fig. 1b).

The addition of 10% lithium ions to $KNaNb_2O_6$ ceramics leads to a strong increase in the size of the grains (Fig. 1e,f), but they retain their cubic shape. In the case of addition of 10% lithium ions to $NaNbO_3$ ceramics grains remain spherical (Fig. 1d). Furthermore, the addition of lithium to both the $KNaNb_2O_6$ and $NaNbO_3$ ceramics leads to an increase the density and hardness of ceramics samples. At the same time the presence of potassium ion in position A is associated with the cubic shape of grains.

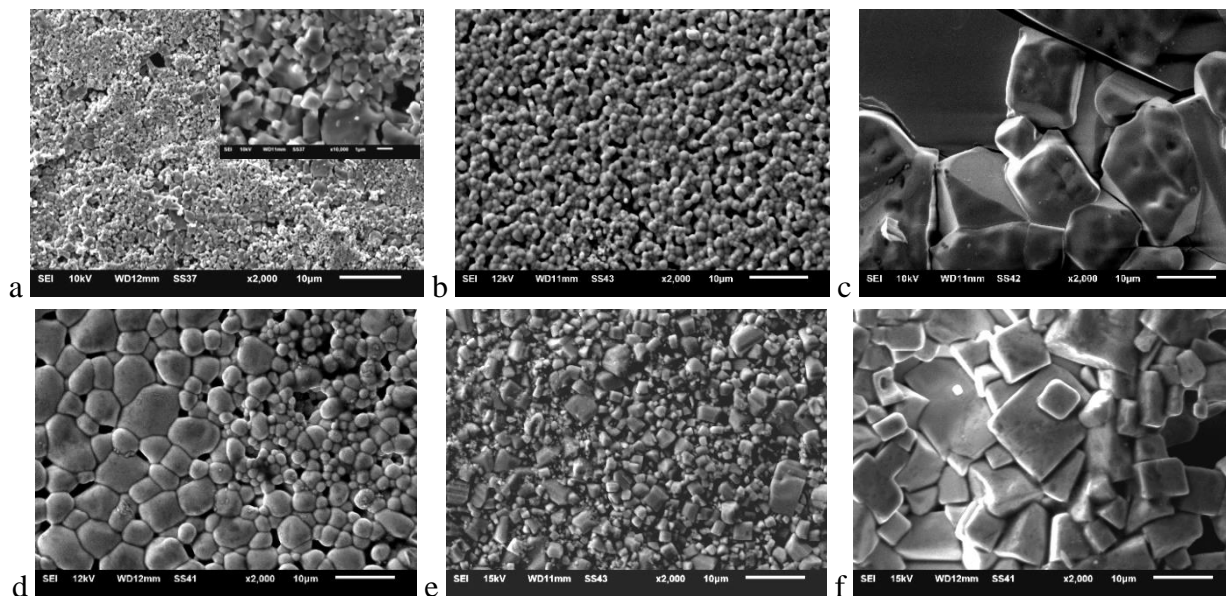


Figure 1. SEM image of (a) $KNbO_3$, (b) $NaNbO_3$, (c) $LiNbO_3$, (d) $Li_{0.1}Na_{0.9}NbO_3$, (e) $KNaNb_2O_6$, (f) $Li_{0.1}(NaK)_{0.9}Nb_2O_6$ ceramics. Scale 10 μm : (a) inset scale 1 μm .

IR spectra of polystyrene-based composite films

E.V. Barabanova, Ya.V. Vorob'eva, A.M. Ivanov, O.V. Malyshkina

Tver State University, 170100, Tver, Russia
pechenkin_kat@mail.ru

In the work, the transmission spectra of polystyrene-based polymer films with a filler of lead zirconate titanate (PZT) ceramics were studied by IR spectroscopy. The films were produced from a solution of polystyrene in toluene. The ferroelectric ceramics were ground to a particle size of not more than 4 μm . The filler was introduced in volume concentrations of 10, 20, 35, and 50%.

Except transmittance of composite films were investigated pure polystyrene films obtained from a solution in toluene and industrially from the melt (test sample to the spectrometer). As can be seen from fig. 1 the spectrum of a polystyrene film obtained from a solution is less transparent than a reference film obtained from a melt. This can be explained by the scattering of incident radiation on the pores formed during solidification of the film from the solution by evaporation of toluene. Also to the absorption bands of polystyrene in the film obtained from the solution added to the absorption band of toluene. The most intense is the band at 1072 cm^{-1} .

As a result, even a small amount of ceramics in the polymer turns out that the film becomes completely opaque with the exception of a small area in the area of "fingerprints" [1, 2]. The transmission peaks are clearly located between the absorption bands of polystyrene and toluene and correspond to 449, 889, 935, and 1228 cm^{-1} . But their intensity is low and decreases with increasing filler concentration. Consequently, the region of transparency of the PZT is superimposed on the region of the characteristic frequencies of polystyrene. This leads to the transmission of the composite film in a narrow frequency range. However, at high concentrations of filler light is scattered by the pores and grain boundaries. This makes the composite completely opaque.

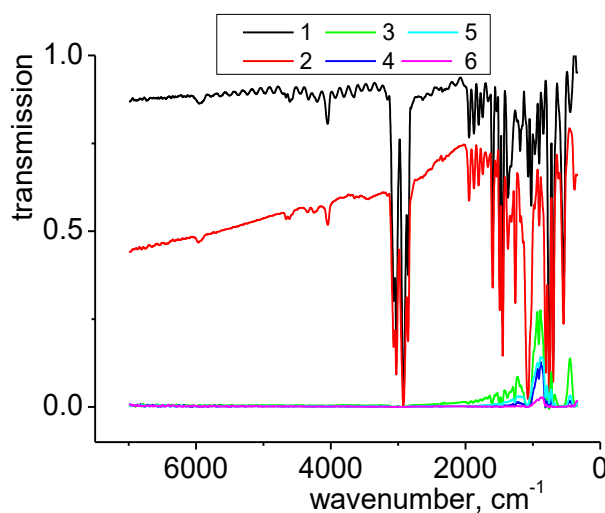


Figure 1. Transmission spectra for a films of pure polystyrene obtained from melt – 1 and from solution – 2, a composite with a filler content of 10% – 3, 20% – 4, 35% – 5, 50% – 6.

1. S. Krimm, *Infrared Spectra of High Polymers* (Fortschritte Der Hochpolymeren-Forschung), 51 (1960).
2. R.A. Hoult, B. Perston, R.A. Spragg, *Spectroscopy* **28**, 2 (2013).

Investigation of the properties of magnetocaloric $\text{Mn}_{1-x}\text{Fe}_x\text{NiGe}$ ($0.05 \leq x \leq 0.30$) films

T.M. Tkachenko¹, V.I. Mityuk², S.M. Baraishuk¹, A.I. Turovets¹

¹Belarus State Agrarian Technical University, 220053, Minsk, Belarus
bear_s@rambler.ru

²State Scientific and Production Association «Scientific-Practical Materials Research Centre of the National Academy of Sciences of Belarus», 220072, Minsk, Belarus

MnNiGe-based solid solutions are currently positioned as “green” magnetocaloric materials, promising for use in magnetic refrigerators [1-3]. The magnetic behavior of the MnNiGe system is strongly dependent on doping, special heat treatment, pressure imposition, etc. One of the most important factors determining the magnetic behavior of the system is the state of the sample – film or massive.

The purpose of the work is to study the microstructure, surface topography and magnetic properties of the samples of solid solutions $\text{Mn}_{1-x}\text{Fe}_x\text{NiGe}$ ($0.05 \leq x \leq 0.30$) in the state of the film. Polycrystalline samples of solid solutions $\text{Mn}_{1-x}\text{Fe}_x\text{NiGe}$ were synthesized in a single-zone resistance furnace, followed by quenching in water. The resulting alloys were powdered with a grain size about 0.1-0.3 mm. Then using the obtained precursor according to the “flash” method [4], thin films of $\text{Mn}_{1-x}\text{Fe}_x\text{NiGe}$ images were deposited ($0.05 \leq x \leq 0.30$). The glass slides $18 \times 18 \times 0.5 \text{ mm}^3$ in sizes were used as substrates. The films were studied by atomic force microscopy (microtest machines NT-206, tips Mikromasch CSC 38) in contact mode. To evaluate the surface, at least 5 scanning sites were selected from different sections of the surface with a size of $20 \times 20 \mu\text{m}^2$ and $5 \times 5 \mu\text{m}^2$, which allowed averaging the parameters of the relief. The processing of the obtained data was carried out with the help of the program “SurfaceXplorer” according to the technique described in [5].

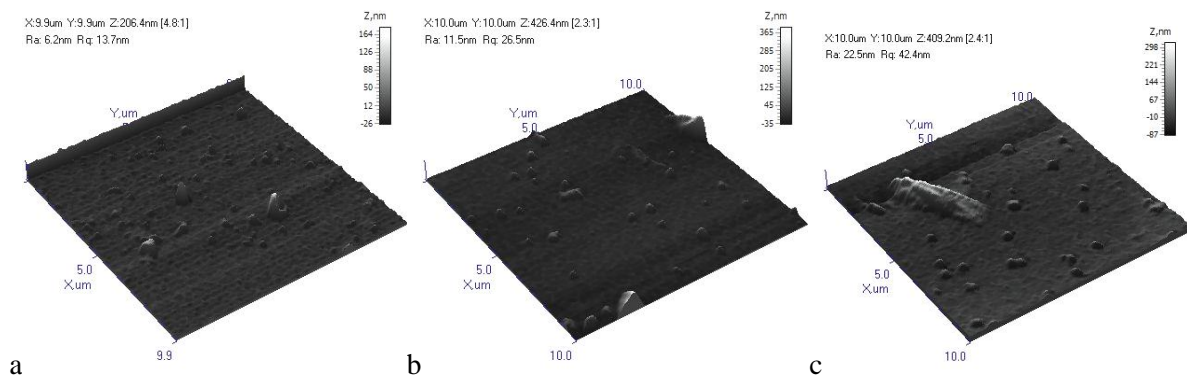


Figure 1. The surface topography of the $\text{Mn}_{1-x}\text{Fe}_x\text{NiGe}$ thin film when scanning on a $10 \times 10 \mu\text{m}^2$: (a) $x = 0.1$; (b) $x = 0.2$; (c) $x = 0.3$.

AFM studies have shown that the typical surface of thin films of $\text{Mn}_{1-x}\text{Fe}_x\text{NiGe}$, for different values of x , has a similar relief. With a scan area size of $10 \times 10 \mu\text{m}^2$ (Fig. 1), uniformly distributed round-shaped structural formations with a size of 0.1-0.3 μm in diameter with an average height of 0.1-0.2 μm are observed on the surface, which can be seen from the section profile (Fig. 2). The distribution of heights for these sites is presented in Figure 2b, there is also an analysis of the orientation of the surface structures 2c, which indicates the presence of a weakly expressed orientation of the formations on the surface. The arithmetic average surface roughness, averaged over 5 different scans, with the specified site selection for $\text{Mn}_{0.95}\text{Fe}_{0.05}\text{NiGe}$ systems is $R_a = 8.1 \text{ nm}$, mean square $R_q = 11.0$. The ratio of the projective surface area to the full one is 0.984. The values for the other combinations of the composition are given in Table 1.

The thickness of the applied coating was estimated by the ratio of the mass of the deposited layer to the density of the substance (X-ray density is used) and surface area of the deposited layer. The results of determining the thickness of the coatings are presented in Table 1.

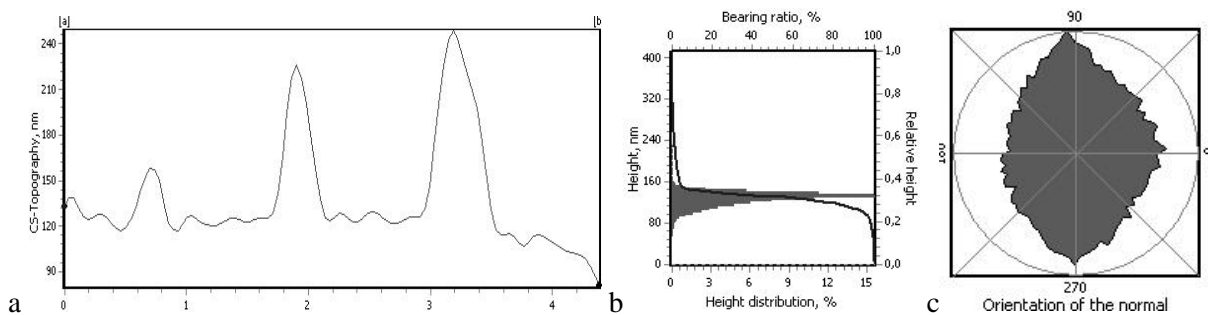


Figure 2. The surface topography of the $\text{Mn}_{0.95}\text{Fe}_0$ thin film when scanning on a $10 \times 10 \mu\text{m}^2$: (a) cross section; (b) height histogram; (c) orientation of formations on the surface.

Table 1. Parameters of the obtained films.

| No | Sample | Thickness, nm | The ratio of the projective surface area to the full | R_a , nm | R_q , nm |
|----|---|---------------|--|------------|------------|
| 1 | $\text{Mn}_{0.95}\text{Fe}_{0.05}\text{NiGe}$ | 705 | 0.984 | 8.1 | 11.0 |
| 2 | $\text{Mn}_{0.90}\text{Fe}_{0.10}\text{NiGe}$ | 744 | 0.987 | 15.2 | 29.0 |
| 3 | $\text{Mn}_{0.85}\text{Fe}_{0.15}\text{NiGe}$ | 784 | 0.974 | 11.5 | 14.7 |
| 4 | $\text{Mn}_{0.80}\text{Fe}_{0.20}\text{NiGe}$ | 868 | 0.991 | 9.2 | 20.4 |
| 5 | $\text{Mn}_{0.75}\text{Fe}_{0.25}\text{NiGe}$ | 554 | 0.992 | 5.1 | 13.7 |
| 6 | $\text{Mn}_{0.70}\text{Fe}_{0.30}\text{NiGe}$ | 896 | 0.986 | 12.1 | 26.6 |

Using the AFM images, the multifractal dimension of the surface was calculated using the horizontal section method (area – perimeter). When calculating the fractal dimension, the systematic deviation characteristic of the method of horizontal sections was taken into account [6]. Analysis of the fractality of the studied sites by 500 sublayers gives an average value of the fractal dimension 2.57 the coefficient of self-similarity of 0.785 for 0.75 that change to 3.00 and 0.995 for x 0.95, respectively. As can be seen from the table and Fig. 1, as x increases, the surface roughness grows, as well as more massive structures are formed on it, more than 1.5 microns in length, 1.5 microns in diameter and from 0.3 to 1 micron in height. In this case, the average value of the fractal dimension of the sites studied increases somewhat in comparison with the main relief and reaches from 2.57 to 3.00, which indicates a developed "bulk" surface.

To determine the phase composition, parameters, and volume of the crystal cell of the samples, X-ray structural studies were performed in Cu $K\alpha$ radiation at room temperature. We assume the existence of a connection between the magnetic properties of the films and the morphology of their surfaces. At present, the magnetic and magnetocaloric properties of the films are being investigated. The work is in progress.

1. V.I. Val'kov, I.F. Gribov, B.M. Todris, et al., *Phys. Solid State* **60**, 1125 (2018).
2. A.P. Sivachenko, V.I. Mityuk, V.I. Kamenev, et al., *Low Temp. Phys.* **39**, 1051 (2013).
3. M. Budzynski, V.I. Val'kov, A.V. Golovchan, et al., *Phys. Solid State* **57**, 2410 (2015).
4. A.I. Galyas, T.M. Tkachenko, RF Patent No. 2901 (2006).
5. I.S. Tashlykov, S.M. Baraishuk, *Russ. J. Non-ferrous Metals* **49**, 303 (2008).
6. W. Zahn, A. Zösch, *Fresenius J. Anal. Chem.* **365**, 168 (1999).

Determination of the dominant factor affecting the change of the phase transition point in thin ferroelectric films

O.S. Baruzdina, O.G. Maksimova, O.S. Piskunov, A.V. Maksimov

Cherepovets state university, 162600, Cherepovets, Russia
olgabaruzdina91@mail.ru

Size effects in nanoscale ferroelectrics lead to a significant change in their properties compared with bulk ferroelectric materials. The manifestation of the size effect consists of both in a change of the value of the dielectric constant and in the displacement of the phase transition point.

The purpose of the work is to determine the factor that has the greatest influence on the phase transition in thin ferroelectric films. In this work, the Ising model is used to describe the ferroelectric phase transition. The calculations were carried out by the Monte Carlo method. The solution of the task consists of 4 stages:

(1) Investigation of the influence of boundary conditions on the phase transition point. The plotted temperature dependences of the heat capacity of a ferroelectric film under various boundary conditions show a shift of the phase transition point, but this effect is significant only for films with a thickness of about 2-3 unit cells. However, experimental techniques allowed to detect the size effects for ferroelectric film with a thickness of 10 unit cells [1].

(2) Investigation of the influence of the correlation effects on the phase transition point in thin ferroelectric films. At this stage, it was taken into account that the distance between the dipoles will change depending on the temperature. A shift in the phase transition point was also observed. However at this stage the critical size was not detected.

(3) Investigation of the influence of the depolarizing field on the phase transition point. The inclusion of a depolarizing field leads to a decrease in the Curie point. Similar results for ferroelectric composites with spherical ferroelectric inclusions were obtained in work [2]. Taking into account this factor has been shown that the polarization in sufficiently thin films is not observed even at low temperatures. This is explained by the fact that its thickness is less than two values of the thicknesses of the "dead" layer. The double thickness of the "dead" layer is considered as the critical size of ferroelectric films, which disappear its ferroelectric properties.

(4) In conclusion, the study of the influence of all factors on the shift of the Curie point was conducted.

As a result of modeling, it was shown that the dominant factor that has the greatest influence on the phase transition in thin ferroelectric films is the depolarizing field.

The study was supported by the Russian Foundation For Basic Research, Project № 19-32-50032.

1. J. Junquera, P. Ghosez, *Nature* **422**, 506 (2003).
2. B. Darinskii, A. Sidorkin, A. Sigov, N. Popravko, *Materials* **11**, 85 (2018).

Molecular modeling of ZnO nanoclusters interacting with various dopant and PVDF

V.S. Bystrov^{1,*}, I.K. Bdikin,² B. Sigh², B. Kumar³

¹*Institute of Mathematical Problems of Biology, Keldysh Institute of Applied Mathematics, RAS, 142290 Pushchino, Moscow region, Russia*
vsbys@mail.ru

²*TEMA-NRD, Mechanical Engineering Department and Aveiro Institute of Nanotechnology (AIN), University of Aveiro, 3810-193 Aveiro, Portugal*

³*Crystal Lab, Department of Physics & Astrophysics, University of Delhi, Delhi-110007, India*

Zinc oxide (ZnO) is a versatile material, which has unique optical, semiconducting and most important piezoelectric properties [1]. Alternatively, poly(vinylidene fluoride) (PVDF) and PVDF-trifluoroethylene (TrFE) (i.e., its copolymer) are piezoelectric polymers, has been used for dynamic strain sensing and energy harvesting [2]. Ideally, piezoelectric materials should possess high piezoelectricity, while remaining conformable and flexible like piezo-polymers. One of the method for simultaneously achieving improved piezoelectric and mechanical performance is by embedding piezoelectric ZnO nanomaterials into PVDF polymer matrices for enhancing piezoelectricity of such composite architectures [3]. Similarly is possible to enhance piezoelectric property in ZnO structures by doping it's crystals by various atomic dopants [4]. The goal of this study is to perform the estimation of the ZnO crystal cluster models, "ZnO+PVDF" and "ZnO+A" composite structures and properties using molecular modeling and computational physical properties calculations. We take out the initial unit cell crystal structure of ZnO crystal in the hexagonal P63m group [6-8] from CCDC data base (lattice constant $a = 3.249 \text{ \AA}$ and $c = 5.204 \text{ \AA}$) [6] and reconstruct it to the HyperChem [9] workspace, where built first a minimal ZnO cluster (from 18 atoms) and second a nanorod ZnO model cluster (from 72 atoms). Then we construct here the "ZnO+PVDF" and "ZnO+A" models with various atoms. Computational molecular models of ZnO cluter, PVDF chain and composite of "ZnO+PVDF" were considered and performed in this study using HyperChem software by various semi-empirical methods PM3, MNDO/d in restricted/unrestricted Hartree-Fock (RHF/UHF) approximation [9, 10]. For "ZnO+A" the *ab initio* methods was used with various basis set (3-21G with 675-735 primitive Gaussians, and 6-31G* with ~1200 Gaussians) [9], depending of the atom "A". Distance between "A" and cluster's centre of mass $\sim 3.5 \text{ \AA}$. Initial pure ZnO model were calculated using both approaches. Models are presented on Figure 1, results in Table 1.

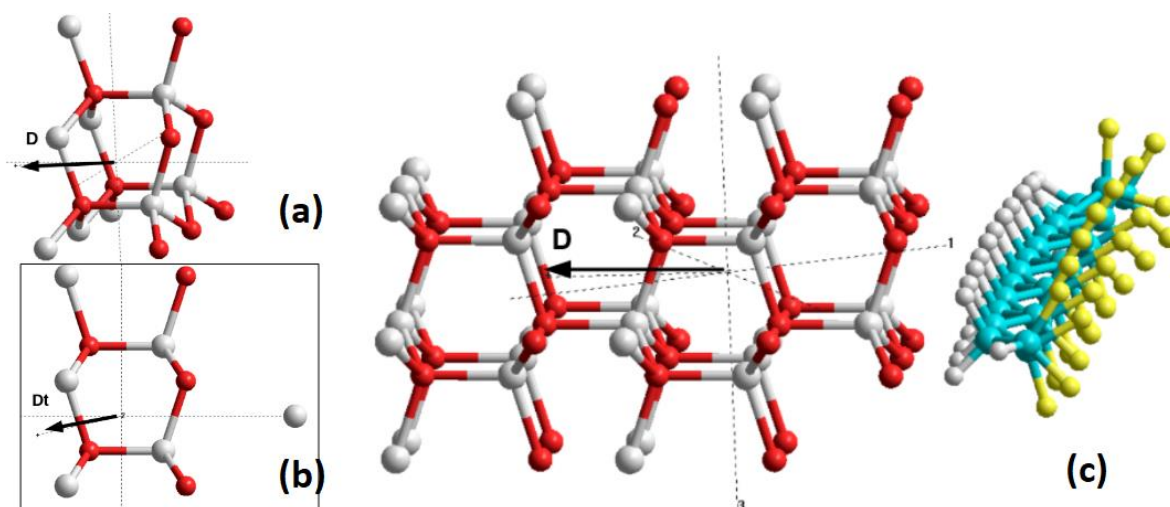


Figure 1. ZnO cluster model: (a) ZnO initial minimal cluster, (b) ZnO nanoparticle interacting with atom "A", (c) ZnO nanorod interacting with PVDF chain in composite structure model.

Table 1. Polarization characteristics of “ZnO+PVDF” composite cluster, obtained by various methods.

| Model | Parameters | Methods (in RHF/UHF) | | | Other data | | |
|--------------------|--|----------------------------|----------------------------|--------------------|--|---------------------|----------|
| | | PM3 | MINDO-d | Ab initio 3-21G | Calculat. P, C/m ² [7,8] | Experimental [1,5] | |
| | | | | | | P, C/m ² | d*, pm/V |
| ZnO-18 | Dipole, Debye | 17.728 | 15.123 | 16.1815 | | | |
| | Polarization, C/m ² | 0.1032 | 0.0885 | 0.0947 | 0.07-0.08 | | 9.9-12.4 |
| ZnO-72 | Dipole, Debye | 13.441 | 11.739 | | | | |
| | Polarization, C/m ² | 0.0944 | 0.0825 | | 0.07-0.08 | | 9.9-12.4 |
| ZnO-18 + Cr | Dipole, Debye | | | 11.8837 | | | |
| | Polarization, C/m ² | | | 0.0669 | | 0.0618 | 120 |
| ZnO-18 + V | Dipole, Debye | | | 4.627 | | | |
| | Polarization, C/m ² | | | 0.0258 | | 0.02 | 110 |
| ZnO-18 + Mg | Dipole, Debye | | | 15.245 | | | |
| | Polarization, C/m ² | | | 0.08535 | | 0.002 | 54 |
| ZnO-18 + Y | Dipole, Debye | | | 6.0831 | | | |
| | Polarization, C/m ² | | | 0.0339 | | | 420 |
| PVDF12 | Dipole, Debye | 25.12 | 29.971 | | | | |
| | Polarization, C/m ² | 0.167 | 0.199 | | 0.1 | 0.1 | 20-40 |
| PVDF12 + ZnO-72 | Dipole/ at distance between, Debye / Å | 45.082/10.0 45.338/10.5 | 51.927/10.0 47.844/11.5 | | | | |
| | Polarization, C/m ² | 0.154 0.155 | 0.1775 0.1634 | | | | |

Data obtained show good agreements with experimental data. However, it is only first step of our calculations and work will be continued further, similarly as in our previous calculations of the piezoelectric coefficients in PVDF and Graphene-based polymer ferroelectrics [9-11]. Authors wish to acknowledge the Russian Foundation for Basic Researches (RFBR) grant # 19-01-00519 A.

1. N. Sinha, S. Goel, A.J. Joseph, et al., *Ceram. Int.* **44**, 8582 (2018).
2. V.M. Fridkin, S. Ducharme, *Ferroelectricity at the Nanoscale* (Springer), 30 (2014).
3. T. Furukawa, M. Date, E. Fukada, *J. Appl. Phys.* **51**, 1135 (1980).
4. J.S. Dodds, F.N. Meyers, K.J. Loh, *IEEE Sensors Journal* **12**(6), 1889 (2012).
5. K. Batra, N. Sinha, S. Goel, et al., *J. Alloy. Compd.* **767** 1003 (2018).
6. K. Kihara, G. Donnay, *Canadian Mineralogist* **23**, 647 (1985).
7. P. Gopal, N.A. Spaldin, *J. Electron. Mater.* **35**(4), 538 (2006).
8. S.-H. Park, D. Ahn, *Appl. Phys. Lett.* **87**, 253509 (2005).
9. *HyperChem 8.0, Professional Edition.* (Gainesville: Hypercube. Inc.) (2010).
10. V.S. Bystrov, I.K. Bdikin, M. Silibin, et al., *J. Mol. Mod.* **23**, 128 (2017).
11. V.S. Bystrov, I.K. Bdikin, M.V. Silibin, et al., *Ferroelectrics* **541**, 17 (2019).

Effects of doping site and concentration on upconversion luminescence of Er³⁺ doped Ba(Mg_{1/3}Nb_{2/3})O₃

J. Shen, Y.Y. Cheng, J. Zhou, W. Chen

*State Key Laboratory of Advanced Technology for Materials Synthesis and Processing, School of Materials Science and Engineering, Wuhan University of Technology, Wuhan 430070, P. R. China
chenw@whut.edu.cn*

Upconversion (UC) luminescence of rare earth ions doped perovskite-structure materials has been investigated extensively in recent years due to their widespread applications in solar battery, biomedical sensing and optical lasers [1-3]. The complex perovskite Ba(Mg_{1/3}Nb_{2/3})O₃ (BMN) compounds is a peculiar microwave dielectric material and it has different site symmetries of Ba-site (C_{3v} and D_{3d}) [4]. Its high structural diversity and tolerance provide adjustable crystal site points for rare-earth ions. But there is very limited knowledge about the influence of the site symmetry of Er³⁺ doped BMN on its photoluminescence (PL) properties.

In this work, BMN perovskite upconversion (UC) phosphors doped with 1.0, 2.0, 3.0, 4.0, 5.0 mol.% of Er³⁺ were synthesized by a well-designed sol-gel method. The prepared powders were characterized by scanning electron microscopy (SEM), X-ray diffraction (XRD), ultraviolet visible spectrophotometer and photoluminescence (PL) spectra. SEM results demonstrate that BMN: Er phosphors are uniform spherical nanostructures with a mean diameter of 20 nm. Structural analysis results show that the powder possesses hexagonal structure and Er³⁺ ions enter the Ba-sites of BMN crystal structure. Under the excitation of 980 nm infrared light, BMN: Er³⁺ show bright green emission near 524 nm and 548 nm generated by the ²H_{11/2}/⁴S_{3/2}→⁴I_{15/2} transition, relatively weak red emission is observed near 662 nm due to the ⁴F_{9/2}→⁴I_{15/2} transition. When the doping concentration of Er increases, the intensity of the green light present earlier increase and later decrease trend whereas the red light almost has no change. According to the analysis of Judd-Ofelt and hypersensitive transition theory, it is related to the symmetry of doping site. The results demonstrate that the site symmetry plays an important role in the intensity of PL. Different green to red ratio is attributed to the local symmetry influence on the emission bands. Hence, it is reasonable to conjecture that characteristics of luminescence (i.e. green to red ratio) can be modulated by adjusting doping site and concentration.

1. T. Dilbeck, K. Hanson, *Journal of Physical Chemistry Letters* **9**, 5810 (2018).
2. S. Chen, A.Z. Weitemier, X. Zeng, et al. *Science* **359**, 679 (2018).
3. Y. Liu, Y. Lu, X. Yang, et al. *Nature* **543**, 229 (2017).
4. S. Janaswamy, G.S. Murthy, E.D. Dias, et al. *Materials Letters* **55**, 414 (2002).

Microscopic investigation and magnetic properties of metal nanowires

D. Bizyaev¹, A. Bukharaev¹, D. Cherkasov², I. Doludenko^{2,3}, D. Panov^{2,3}, D. Zagorskiy²

¹*Kazan Institute of Physics and Technology named after E.K. Zavoisky, Federal, Russia Research Center “Kazan Research Center of the Russian Academy of Sciences”, 420008, Kazan, Russia
dzagorskiy@gmail.com*

²*Shubnikov Institute of Crystallography of Federal Scientific Research Centre “Crystallography and Photonics” of Russian Academy of Sciences, 119333, Moscow, Russia*

³*National Research University Higher School of Economics, 101000, Moscow, Russia*

Arrays of nanowires (NWs) from metals of the iron group have unique properties, including magnetic ones. Possible applications of such structures are for micromagnets, for sensors, for surfaces for magnetic recording with high density (including three-dimensional [1]). One of the ways to obtain such structures is matrix synthesis using porous templates [2, 3]. There are several different ways to measure their magnetic characteristics. Thus, the measurement of hysteresis loops on a Magnetometer and the study of the Mössbauer spectra (for iron-containing samples) provides integral information about the whole NWs ensemble. Recently, some works were started on the study of the properties of individual NWs. These include measurements on SEM microscopy, TEM microscopy (Lorentz microscopy) and MFM [4, 5], in which single NWs isolated from an array were studied. In the present work, NWs arrays were obtained by the method of galvanic deposition (template synthesis) of metals into the pores of matrices – track membranes and porous alumina. The arrays of homogeneous NWs (from one metal) and the so-called layer NWs are obtained. Layer NW consists of alternating layers of Ni/Cu and Co/Cu. Preliminary study of the obtained NWs was carried out by the SEM method (Fig. 1).

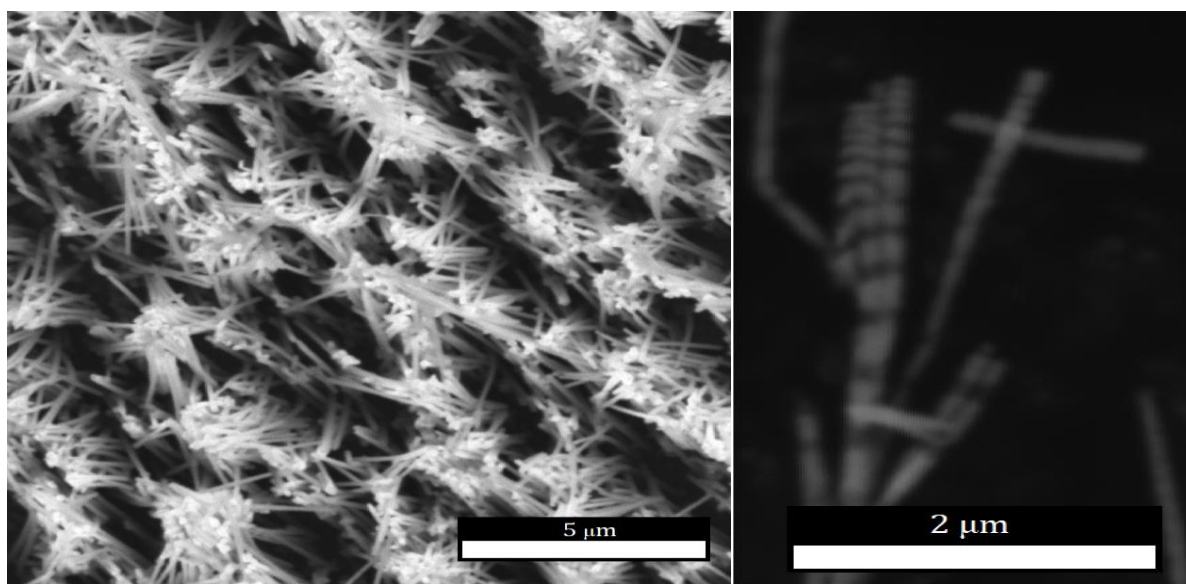


Figure 1. SEM images of layer NWs.

It is shown that NWs grown in the track membrane completely fill the pore channels, and their diameter is somewhat higher than the pore diameter. The TEM study (conducted earlier in [6] for Ni/Cu nanoparticles) made it possible to determine the thicknesses of alternating layers (from 30 to 250 nm). Elemental analysis showed that alternating layers consist of pure copper and nickel-copper alloy (up to 20% copper). For probe microscopy Solver P47 Pro with cantilevers Multi75M-G (BudgetSensor) was used. For AFM measurements, NW suspension in water was deposited on the holder by the “irrigation” method, followed by drying and then covered by a thin layer of metal (by thermal sputtering). For MFM measurements, the one-pass technique was used in order to avoid the influence of neighboring NWs on each other. Figure 2a shows the AFM images of the topography of a single layer Co /Cu NW, Figure 2b shows the MFM image of the same NW, and Figure 2c shows the MFM image after an external magnetic field 16 mT was applied along the NW axis.

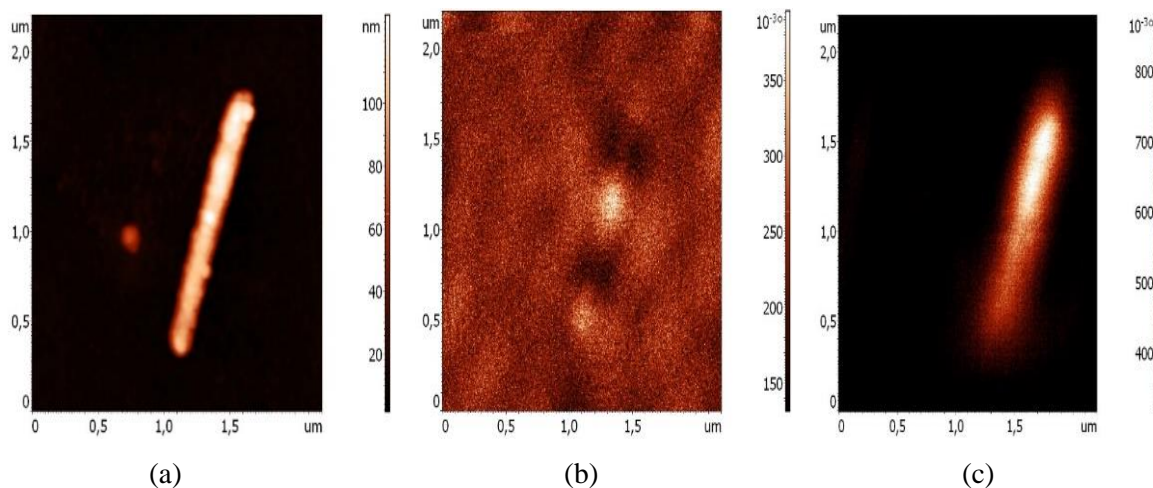


Figure 2. (a) an AFM image of a layer NW (Co/Cu), (b), (c) an MFM images of the same NW (b – without field, c – with application of an external field).

It is seen that the NW is divided into regions of different magnetization, and the application of the external field changes this state. AFM/MFM measurements of NWs grown in the pores of the Alumina Oxide (POA) matrix were also performed. Measurements were done at the cut of the POA. The results are presented and discussed.

So, the fragmentation of NWs into domains was demonstrated and the influence of NWs to each other was concluded.

This work was partially supported (NWs synthesis) by Grant № 18-32-01066. The authors thanks P.Yu. Apel (JINR, Dubna) for providing polymeric matrices, to K.S. Napolsky (Chemical fac. MSU) for providing samples of NWs grown in pores of the POA.

1. Yu.P. Ivanov, A. Chuvilin, S. Lopatin, H. Mohammed, J. Kosel. *ACS Appl. Mater. Interfaces* **9**, 16741 (2017).
2. M. Va'zquez, *Magnetic Nano- and Microwires: Design, Synthesis, Properties and Applications* (Woodhead Publishing Elsevier), (2015).
3. A. Davydov, V. Volgin, *Electrochemistry*, **52**, 905, (2016).
4. Yu.P. Ivanov, A. Chuvilin, L.G. Vivas, et al. *Sci. Rep.* **6**, 23844 (2016).
5. E. Berganza, M. Jaafar, C. Bran, et al. *Sci. Rep.* **7**, 11576 (2017).
6. O.M. Zhigalina, D.N. Khmelenin, I.M. Ivanov, et al. *J. Nanomaterials and Nanostructures – XXI Century* **2(9)**, 23 (2018).

Domain patterning on non-polar cut lithium niobate by focused ion beam

D.S. Chezganov, A.P. Turygin, E.O. Vlasov, E.A. Pashnina, A.S. Nuraeva, V.Ya. Shur

*School of Natural Sciences and Mathematics, Ural Federal University, 620026, Ekaterinburg, Russia
chezganov.dmitry@urfu.ru*

The domain evolution on the polar surfaces of lithium niobate (LN) during switching by various techniques is well studied whereas the forward growth stage of domain evolution mostly remained hidden. The domain interaction during the stage is one of the key problems for the creation of the periodical domain structures with short periods. The focused ion beam (i-beam) irradiation controlled by the lithographic system was shown to be a promising method for short-pitch domain poling due to highly localized nanosized field source induced by injected charges [1]. The study of domain switching by i-beam on the nonpolar cuts allows revealing the features of domain intergrowth along the polar direction. From a practical point of view, the geometry of the X-cut LN plates provides direct access to the largest nonlinear-optical and electro-optical tensor elements that promises a smaller size of devices.

We have studied the domain formation at the Y-cuts of 5 mol.% MgO-doped LN induced by injected charges during focused Ga^+ ion irradiation in the vacuum chamber of dual-beam Auriga Crossbeam workstation (Carl Zeiss, Germany) equipped by the i-beam lithographic system (Elphy Multibeam, Germany). The irradiation of isolated dot rows with various distances was used. The static domain structures were visualized by piezoresponse force microscopy (PFM), optical microscopy and scanning electron microscopy (SEM) after selective chemical etching.

The dependences of domain sizes (length, top width, aspect ratio) on the irradiated charge, beam current and ion energy were measured. It was shown that length of needle-like domains depends linearly on dose (irradiated charge) (Fig. 1a) while domain width (width of needle top) depends as a square root. The fact was explained by the external screening of the depolarizing field by the injected charges [2]. The domain length is independent on beam current whereas the domain width demonstrated weak dependence which can be attributed to the increase of beam spot with the current.

The interaction of isolated needle-like domains was studied. It was shown that the domain length depends on the periods of the irradiated dot row. There are two distinguished situations: (1) relative large periods ($> 3 \mu\text{m}$), where decrease of domain length observed at edges of rows due to lower total electric field caused by the absence of adjacent dots (Fig. 1b), (2) short period ($< 3 \mu\text{m}$), where the interaction of charged domain wall was observed (Fig. 1c). The measurement of domain length in irradiated dot row for various spacing allowed to reveal three main regimes: (1) uniform, (2) intermitted quasiperiodic, (3) chaotic. The similar behavior was previously observed during switching by the biased tip of a scanning probe microscope [3].

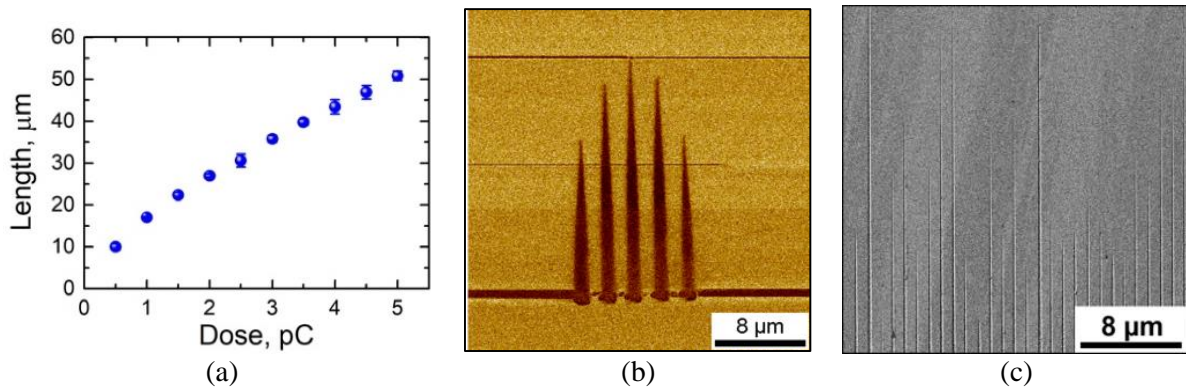


Figure 1. (a) The dependence of domain length on dose, (b) PFM image of needle-like domains, (c) SEM images of domain comb structure with 1 μm spacing.

Obtained results give a new insight in the problem of the domain interaction during forward growth and can provide useful basis for application of the nanodomain engineering in development of non-linear optical frequency converters, data storage, and computing devices.

The equipment of the Ural Center for Shared Use “Modern nanotechnology” Ural Federal University was used. The research was made possible by the Russian Science Foundation (grant № 19-72-00091).

1. D.S. Chezganov, V.Ya. Shur, E.O. Vlasov et al., *Appl. Phys. Lett.* **110**, 082903 (2017).
2. D.S. Chezganov, E.O. Vlasov, E.A. Pashnina et al., *Appl. Phys. Lett.* (2019), (in press).
3. A.P. Turygin, D.O. Alikin, M.S. Kosobokov et al., *ACS Appl. Mater. Interfaces* **10**, 36211 (2018).

SEM-investigating microstructure of cast AlNiCuFeCo high entropy alloys formations a liquid-phase separation

O.A. Chikova, D.S. Chezganov, V.S. Tsepelev, V.Yu. Ilyin

Ural Federal University, 620002, Ekaterinburg, Russia
chik63@mail.ru

The FeCoNi(CuAl)_x ($x = 0-1.2$, in molar ratios) high-entropy alloys (HEAs) has a combination of superior magnetic and mechanical properties have been investigated. The liquid-phase separation it is known that to has taken place when the undercooling is equal or greater than 100 K [1]. Crystallographic structures of FeCoNi(CuAl)_x HEAs transform from single face-centered cubic (FCC) phase for $0 \leq x \leq 0.6$ to body-centered cubic (BCC) phase combined with minor FCC phase for $0.9 \leq x \leq 1.2$, whereas FCC plus BCC duplex phases are found in the range of $0.7 \leq x < 0.9$. TEM images of FeCoNi(CuAl)_{0.8} alloy show large numbers of the FCC Cu-rich nano-precipitates disperse in the BCC matrix [2].

The samples AlCuNiCoFe alloy of equiatomic composition were obtained by vacuum arc melting at laboratory. High purity metals, i.e., aluminum of A999 special purity grade, 99.9%, copper of the Mk00 brand (99.98%) and carbonyl iron (special purity grade, 99.98%), were applied as initial materials. The kinematic viscosity was measured using by the oscillating cylinder method during heating and subsequent cooling. A metallographic study was carried out on a Carl Zeiss Auriga CrossBeam scanning electron microscope using the function energy dispersive spectroscopy (EDS). Scanning electron microscope Auriga CrossBeam (Carl Zeiss, Germany) was equipped with the EDS system IncaEnergy (Oxford Instruments, UK) with 350 X-Max X-ray detector with spatial resolution about 1 μm and spectral resolution of 125 eV at K α line of Mn. The SEM was used for visualization of surface morphology and structural defects in secondary electron mode with the resolution down to 2 nm. The EDS was applied for revealing of elemental composition of defects and inclusions. The EDS data collection and processing were made by means of IncaEnergy software.

The liquid-phase separation in a AlCuNiCoFe high entropy alloy of equiatomic composition has by study investigated by viscometric method. Melt overcooling before crystallization 80 K was recorded. It is interesting to note values of viscosity for studied melt during cooling were equal to or more than the corresponding values recorded by heating. The most significant increase in the viscosity at low temperatures (near liquidus).

Microstructure of ingots homogeneous over the cross section and consist of dendrites and the interdendritic layers of multi-phase composition. According to SEM-microscopy can distinguish the multiple phases in the dendrites and the interdendritic space. In ingot AlCuNiCoFe of equiatomic composition the dendrites consist of a ternary eutectic ($\alpha\text{-Al} + \text{CuAl}_2 + \text{Cu}_4\text{NiAl}_7$) and large primary crystals isomorphic compounds CoCu_2Al_7 and FeCu_2Al_7 . Interdendritic space contains small primary crystals Cu_4NiAl_7 [3]. A substantial of interdendritic porosity occurs.

The equipment of the Ural Center for Shared Use “Modern nanotechnology” Ural Federal University was used.

1. T. Guo, J. Li, J. Wang, Y. Wang, H. Kou, S. Niu, *Intermetallics*. **110**, 86 (2017).
2. Q. Zhang, H. Xu, X.H. Tan, X.L. Hou, S.W. Wu, G.S. Tan, L.Y. Yu, *J. Alloy Compd.* **1061**, 693 (2017).
3. M. Kivy, Z. Beyramali, M. Asle, S. Lekakh, *Mater. Design.* **224**, 127 (2017).

Study of structure-property relationship in polycrystalline steels based on analysis of EBSD data

O.A. Chikova^{1,2}, D.S. Chezganov², N.I. Sinitsin²

¹*Ural State Pedagogical University, 620017, Ekaterinburg, Russia
chik63@mail.ru*

²*Ural Federal University, 620002, Ekaterinburg, Russia*

The structure-property linkages are central to the development and deployment of advanced materials in emerging technologies [1]. In this work, we formulate novel, data-driven, assays for exploring the structure-property linkages for structural steel. These assays are built on recent advances in low-dimensional quantification of material structure using correlations and principal analyses of EBSD data, as well as in the mechanical characterization using nanoindentation [2-4]. These novel protocols are demonstrated on a steel 110Г13Л that exhibits rich polycrystalline microstructures.

The comparative analysis of EBSD data obtained for different samples cut made of manganese steel 110Г13Л and received by various methods was made. High-manganese austenitic wear-resistant steel 110Г13Л (Hadfield steel) has the following chemical composition, wt.%: C(0.95-1.50)-Mn(11.5-15.0). The sample surface was studied by method EBSD. The study was made by scanning electron microscope Auriga CrossBeam (Carl Zeiss, Germany) equipped with the EBSD analysis system HKL Channel 5(Oxford Instruments, UK). The EBSD data acquisition was made by Flamenco Acquisition software (Oxford Instruments, UK). The accelerating voltage of 20 kV and electron beam current of 8 nA were used during scanning. The areas with a size of 20×20 μm² were scanned with a step size of 80 nm. The obtained data was processed and analyzed by Tango software (Oxford Instruments, UK).

Analysis of the diffraction patterns of backscattered electrons allows us to estimate the proportion of low-angle and special grain (CSL) boundaries of a material, to construct a Schmidt factor map and a misorientation histogram of the grains [2, 3]. Uncorrelated misorientations indicate misorientations between randomly selected points in the data set. Correlated misorientations display data between adjacent points, in other words, the angular distribution of grain boundaries. The theoretical curve shows what can be expected from a random set of orientations. The difference between uncorrelated misorientations and the theoretical curve arises, as a rule, due to the strong texture. The presence of a larger specific fraction of low-angle boundaries indicates high plasticity and corrosion resistance of sample. It is known that low-energy and special boundaries of metal grains are highly resistant to destruction. From a materials science perspective, it is important to determine both the ratio of the boundaries of CSL and their distribution in metal. Schmidt factor maps are used to determine the degree of homogeneity of a possible deformation. The Schmidt factor maps were constructed for a slip system typical for FCC crystals: {111} <110> with loading direction parallel to OZ axis. It was previously established that if almost all the boundaries low-angle, the texture is stronger, then the Young's modulus and crystallite hardness, determined by the nanoindentation method, are lower. The decrease in the modulus of elasticity, due to high material texture significantly reduces additional pressure and improves formation mechanical workability of ingot [3].

The equipment of the Ural Center for Shared Use “Modern nanotechnology” Ural Federal University was used.

1. A. Khosravani, A. Cecen, S.R. Kalidindi, *Acta Materialia* **123**, 55 (2017).
2. A.V. Belonosov, O.A. Chikova, V.V. Yurovskikh, D.S. Chezganov, *Russ. J. Nondestruct. Test.* **49**, 196 (2013).
3. O.A. Chikova, A.N. Konstantinov, E.V. Shishkina, D.S. Chezganov, *Russian Metall.* **7**, 535 (2013).
4. D.S. Chezganov, O.A. Chikova, M.A. Borovykh, *Phys. Metals Metallogr.* **118**, 857 (2017).

MFM study of switching magnetization in particles with configurational anisotropy obtained by the microsphere lithography

D.A. Bizyaev, A.A. Bukharaev, A.P. Chuklanov, N.I. Nurgazizov

*Zavoisky Physical-Technical Institute, Federal Research Center "Kazan Scientific Center of RAS"
420029, Kazan, Russia
dbiziaev@inbox.ru*

The triangular or square ferromagnetic particles with configurational anisotropy of shape can be in several quasi-homogeneous stable states of magnetization. The states are separated by rather high energy barriers that ensure their stability in time. It is possible to use such the particles for creating magnetoelastic random access memory cells – MeRAM [1]. The memory cell of this type can store not one, but several bits of information [2]. Previously the magnetic properties of the particles with configurational anisotropy made by scanning probe lithography were studied in our laboratory [3].

In this work, the quasi-homogeneous states of triangular permalloy particles was studied by magnetic force microscopy with depend on particles size and shape. The particles were made by the microsphere lithography technique. The lithographic mask was a monolayer of close-packed microspheres diameter 2.35 and 5 μm . This lithographic method makes it possible to form particles of identical size and shape with concave sides.

The particular attention was paid to the switching of the magnetization of particles from one quasi-homogeneous state to another under external magnetic field. The values of the switching fields and processes of magnetization reversal of ferromagnetic particles of two types were compared. The particles of first type were made by scanning probe lithography [3] while the particles of second type prepared by microsphere lithography.

It is established that particles obtained by using microspheres with a diameter of 5 μm have a vortex magnetization structure. The particles obtained by using microspheres with a diameter of 2.35 μm , have a quasi-homogeneous magnetization. In addition, the magnetization reversal of such particles in an external magnetic field always occurs through an intermediate quasi-homogeneous state of magnetization.

For the similar particles that were made by scanning probe lithography the magnetization reversal occurred stepwise without transition to the intermediate quasi-homogeneous state [3]. When the magnetization reversal of particles occurs through the intermediate stable state the magnitude of switching field are increases. This is probably due to the magnetic interaction between particles made by microsphere lithography. The magnitude of interaction is determined by the distance between particles and close packing of microspheres.

This work was partially supported by the RFBR grant 18-02-00204.

1. A.A. Bukharaev, A.K. Zvezdin, A.P. Pyatakov, Yu.K. Fetisov, *Phys. Usp.* **61**, 1175 (2018).
2. M. Salehi-Fashami, N. D'Souza, *J. Magn. Magn. Mater.* **438**, 76 (2017).
3. D.A. Bizyaev, A.A. Bukharaev, A.P. Chuklanov, N.I. Nurgazizov, *Phys. Solid State* **60**(11), 2194 (2018).

The effect of optical cooling of the SPM probe in the optomechanical resonator

M.S. Dunaevskiy¹, P.A. Alekseev¹, V.A. Sharov¹, A. Baranov²

¹*Ioffe Institute, 194021, Saint-Petersburg, Russia*
Mike.Dunaeffsky@mail.ioffe.ru

²*IES, University of Montpellier, CNRS, 34095, Montpellier, France*

The optomechanical resonator is a connected system consisting of an optical resonator and a mechanical resonator. The simplest example of an optomechanical resonator is a Fabry-Perot resonator in which one mirror is stationary, and the second is attached to a spring and can oscillate. However, there are a huge number of other various designs of optomechanical resonators. In the last decade, studies of processes in optomechanical resonators have been actively carried out [1, 2]. Ongoing studies indicate the possibility of substantial optical cooling of microscopic mirrors in optomechanical resonators down to the ground state [3, 4]. This opens up a number of new research opportunities in the field of precision measurements of ultra-small forces [5], quantum computing [6], as well as in other areas. In this paper, we will study optomechanical resonators formed by the surface of an emitting semiconductor laser and the reflective surface of an SPM cantilever. The use of scanning probe microscopy techniques will allow a detailed study of the properties of such optomechanical resonators. The results of the work (optical cooling) can be used to significantly increase the sensitivity of the SPM during the detection of small forces.

The possibility of forming an optomechanical resonator “semiconductor laser - SPM probe” was experimentally investigated using single-mode ridge lasers with a well-known shape of an outgoing light beam. Optimal conditions were found (probe size and shape, probe coating, probe-surface distance) to achieve the best Q-factor of the optomechanical resonator.

There are determined and separated contributions from two mechanisms of optomechanical coupling: (i) – light pressure on the SPM probe, (ii) – heating the SPM probe. These two mechanisms can lead to a different sign of the oscillation frequency shift of the SPM probe in the optomechanical resonator, which can be experimentally verified. It was determined for which types of SPM probes one or another of the above mentioned mechanisms dominates.

The effect of optical cooling of an SPM probe in an optomechanical resonator was investigated by measuring the spectra of thermal vibrations of an SPM probe. Minimal achievable temperatures of SPM probe cooling were experimentally established.

1. T.J. Kippenberg et al., *Science* **321**, 1172 (2008).
2. S. Groblacher et al., *Nature* **460**, 724 (2009).
3. A. Schliesser, et al., *Nat. Phys.* **4**, 415 (2008).
4. J. Chan et al., *Nature* **478**, 89, (2011).
5. LIGO Collaboration, *Nat. Phys.* **7**, 962 (2011).
6. K. Stannigel, et al., *Phys. Rev. Lett.* **105**, 220501 (2010).

Magnetic field effect on the TGS:Cr dielectric properties and real structure

A.P. Ereemey^{1,2}, R.V. Gainutdinov¹, E.S. Ivanova¹, E.A. Petrzhik¹, A.K. Lashkova¹

¹FSRC «Crystallography and Photonics» RAS, 119333, Moscow, Russia

²Faculty of Physics Moscow State University, 119991, Moscow, Russia
xxx8336@yandex.ru

We present the effect of a constant magnetic field on the dielectric properties of a ferroelectric, its domain structure, and distribution of defects in it. The nominally pure triglycine sulfate single crystal with specially introduced chromium impurity (TGS:Cr) was studied. The samples were kept in a constant magnetic field $B = 2T$ for 20 minutes, and the magnetic induction vector \mathbf{B} was perpendicular to the axis \mathbf{Y} of spontaneous polarization. To study the anisotropy of the effect, two orientations of the samples in a magnetic field were examined – $\mathbf{B} \parallel \mathbf{X}$ and $\mathbf{B} \parallel \mathbf{Z}$. The dielectric properties were controlled by measuring the dielectric hysteresis loops P - E and the temperature dependence of the dielectric constant $\varepsilon'(T)$ near the phase transition. The domain structure and topography of the polar (010) cleavage were studied by the methods of the atomic force microscopy (AFM).

The significant changes in the properties of the samples after magnetic exposure were found. Figure 1 shows the dependences of the relative change in the maximum of the dielectric constant in the heating and cooling modes. It is seen that the magnetic field influence is a long-term post-effect. About a day after the magnetic exposure, an increase in the dielectric constant near the phase transition by 27% was observed, and a return to the initial value took place after 10 days.

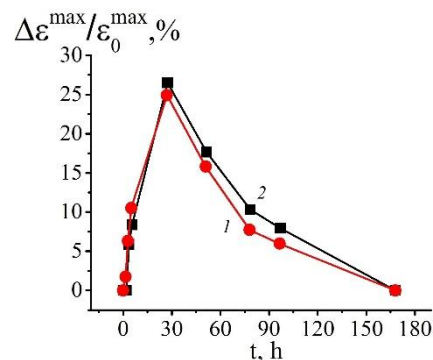


Figure 1. The dependences of the relative change in the maximum of dielectric constant of TGS:Cr crystal on the time after exposure to a constant magnetic field in the heating (1) and cooling (2) modes.

Similar time changes were observed in the defect structure of crystal. According to [1], the criterion for a defect state of TGS is the density and distribution of the nanorelief elements (rounded islands and pits of submicron lateral sizes on the polar (010) cleavage). The exposure of TGS:Cr in a constant magnetic field led to a significant change in the distribution of the nanorelief elements. The maximum decrease in the average size of nanorelief elements was observed approximately a day after the magnetic effect, as in the case of the dielectric properties change.

The comparison of the results obtained by various methods allows to suggest that the observed changes are associated with magnetostimulated transformation of defects, which are the centers of pinning of the domain walls. The changes in the defect subsystem of crystals under the action of magnetic field have been studied in detail when investigating the magnetoplastic effect in nonmagnetic crystals (see, for example, review [2]).

1. N. V. Belugina et al., *Crystallogr.* **56**, 1070 (2011).

2. V.I. Alshits et al., *Dislocations in Solids* **14**, 333 (2008).

Study of growth temperature effect on wetting layer during In/GaAs droplet epitaxy

M.M. Eremenko¹, S.V. Balakirev^{1,2}, N.E. Chernenko^{1,3}, O.A. Ageev¹, M.S. Solodovnik^{1,2}

¹Research and Education Center "Nanotechnologies", Southern Federal University, 347922, Taganrog, Russia
eryomenko@sfnu.ru

²Department of Nanotechnologies and Microsystems, Southern Federal University, 347922, Taganrog, Russia

³Department of Radio Engineering Electronics, Southern Federal University, 347922, Taganrog, Russia

Controlling the characteristics of nanostructures is a key task for improving the functional parameters of existing devices based on semiconductor heterostructures. Droplet epitaxy, due to the separate deposition of components, allows to significantly expand the possibilities in the field of control and variation of the parameters of the obtained nanostructures. However, the formation of a wetting layer during the deposition of metal droplets still insufficiently studied.

In this paper we present the results of the experimental investigation of temperature dependence of wetting layer formation during droplet epitaxy of In/GaAs(001) nanostructures grown at various temperatures and deposition thicknesses using X-ray photoelectron spectroscopy technique.

From the presented data (Figure 1a,b) it is clear that the intensity of the In3d5A line on curve 1 (low-temperature sample without droplets) drops to zero much earlier than the lines on curve 2 (high-temperature sample with droplets) – by 360 s and 840 s, respectively. This may indicate a different thickness of the deposited material on the samples (a change of 2 times). The conventionally monotonous nature of the decrease in the intensity of the In3d5A spectral line in the first case indirectly indicates the relatively homogeneous structure of the In wetting layer. The complex nature of the intensity curve in the second case is due to the complex structure on the surface. It should be noted that the 3-fold difference in this case also correlates with the previously obtained experimental data [1].

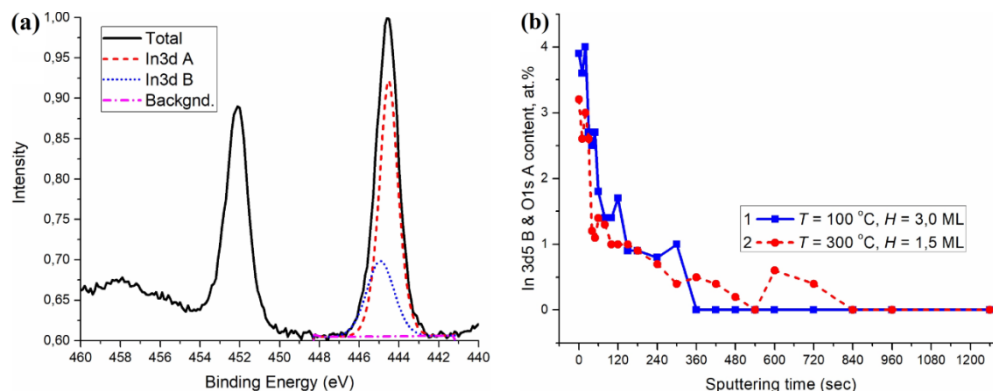


Figure 1. (a) XPS spectra from samples obtained at $T = 100\text{ }^{\circ}\text{C}$, $H = 3\text{ ML}$ and $T = 300\text{ }^{\circ}\text{C}$, $H = 1.5\text{ ML}$ and (b) change of In3d5A line intensity during etching of sample surfaces.

The results of X-ray photoelectron spectroscopy of In/GaAs samples formed under different conditions confirm an increase in the wetting layer thickness with a decrease in the formation temperature of the systems.

This work was supported by the Russian Science Foundation Grant No. 15-19-10006. The results were obtained using the equipment of the Research and Education Center and Center for Collective Use "Nanotechnologies" of Southern Federal University.

1. S.V. Balakirev, M.S. Solodovnik, O.A. Ageev, *Phys. Status Solidi B* **255**, 1700360 (2018).

Dielectric permittivity enhancement by formation of charged domain walls in stoichiometric lithium niobate

A.A. Esin, A.R. Akhmatkhanov, V.Ya. Shur

*School of Natural Sciences and Mathematics, Ural Federal University, 620000, Ekaterinburg, Russia
Alexander.Esin@urfu.ru*

In the recent years, a growing attention is paid to the modification of the properties of the ferroelectric materials by the charged domain wall (CDW) engineering. These intrinsic interfaces are considered as an alternative to the conventional chemical doping to achieve the nanoscale tailored structure. Currently, the influence of CDWs on the conductivity [1, 2] and piezoelectric coefficient [3] has been revealed. The dielectric properties can be effectively improved by formation of the domain structures with the high concentration of CDWs [4]. Two mechanisms of this effect have been considered: the motion of domain walls under applied electric field and stationary contribution that arises irrespective of any lateral displacement of the wall.

We have revealed the significant increase of low-frequency dielectric permittivity of the stoichiometric lithium niobate (SLN) as a result of CDW formation. The self-assembled structure consisting of spike-like domains with CDWs was formed during the polarization reversal at 145 °C by application of the rectangular high field pulse using uniform metal electrodes. The electrical impedance was measured in the frequency range 10 Hz-100 kHz immediately after polarization reversal. The dielectric permittivity has increased up to one order of magnitude at the lowest frequencies, whereas no changes were observed at frequencies above 10 kHz. The created increase of the dielectric permittivity relaxes to the single domain state value. The acceleration of this relaxation by application of the DC bias has been revealed.

The effect of dielectric permittivity enhancement has been attributed to the vibration of the individual steps on the CDW. Slow bulk screening of the depolarization fields leads to stabilization of the steps and decrease of the dielectric response. Acceleration of the relaxation under DC bias was attributed to intensification of the stabilization process.

The presented effect can be used for increasing of dielectric permittivity by the formation of CDWs. The creation, displacement and erase of CDWs [5] provide a route to develop new nanoelectronic devices.

The equipment of the Ural Center for Shared Use “Modern nanotechnology” Ural Federal University was used. The research was made possible in part by RFBR (grant 18-32-00641_mol_a).

1. A. Crassous, T. Sluka, A.K. Tagantsev, N. Setter, *Nat. Nanotechnol.* **10**, 614 (2015).
2. V.Ya. Shur, I.S. Baturin, A.R. Akhmatkhanov, D.S. Chezganov, A.A. Esin, *Appl. Phys. Lett.* **103**, 102905 (2013).
3. T. Sluka, A.K. Tagantsev, D. Damjanovic, M. Gureev, N. Setter, *Nat. Commun.* **3**, 748 (2012).
4. V.Ya. Shur, E.L. Rummyantsev, E.V. Nikolaeva, E.I. Shishkin, *Appl. Phys. Lett.* **77**, 3636 (2000).
5. A.A. Esin, A.R. Akhmatkhanov, V.Ya. Shur, *Appl. Phys. Lett.* **9**, 092901 (2019).

Domain structure of BaTiO₃ ceramics before and after poling

L. Gimadeeva¹, D. Alikin^{1,2}, A. Abramov¹, Q. Hu³, D. Chezganov¹, X. Wei³, V. Shur¹

¹*School of Natural Sciences and Mathematics, Ural Federal University, 620000, Ekaterinburg, Russia*
lv.gimadeeva@urfu.ru

²*Department of Physics & CICECO - Aveiro Institute of Materials, University of Aveiro, 3810-193, Aveiro, Portugal*

³*Electronic Materials Research Laboratory, Key Laboratory of the Ministry of Education & International Center for Dielectric Research, Xi'an Jiaotong University, 28 Xianning West rd., Xi'an, China*

Barium titanate (BaTiO₃, BTO) is an extensively studied ferroelectric with large polarizations and dielectric permittivity [1]. As a lead-free environmentally friendly material it is considered as a candidate for capacitors, resistors with positive temperature coefficient, ultrasonic transducer and piezoelectric devices [2]. BTO at room temperature has a tetragonal distorted perovskite unit cell allowing to consider it as a model material for studying the domain structure evolution in an electric field [1]. The domain walls significantly impact macroscopic properties [3, 4]. Piezoelectric performance can be estimated to be above 70% and consists of contributions of reversible and irreversible wall motion [5, 6] in heterogeneous multi-axial materials of grain and phase boundaries and defects [7]. The role of grain boundaries in polarization reversal has not been understood despite of long study. Thus, the microscopic studies of domain structure and local piezoelectric response in BTO ceramics by piezoresponse force microscopy (PFM) and complementary methods is useful for understanding the polarization reversal in polycrystalline materials. The BTO ceramics sintered by conventional solid-state path was studied by 3D-PFM to determine polarization direction in individual grains [8]. The domain structure imaging before and after poling allowed to study the domain evolution during polarization reversal. Complementary electron backscattered diffraction mapping was used for inspecting sizes and orientations of grains. The domain wall motion and interaction with grain boundaries are discussed and conditions for transgranular domain formation are formulated.

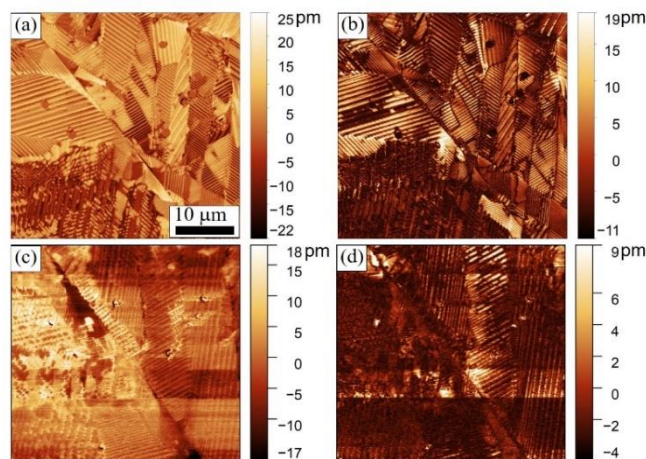


Figure 1. PFM domain images in BTO: (a,c) vertical and (b,d) lateral piezoresponse, (a,b) before and (c,d) after poling.

The research was made possible by President of Russian Federation grant for young scientists (MK-3653.2019.2). The equipment of the Ural Center for Shared Use “Modern Nanotechnology” Ural Federal University was used.

1. D. Hennings, *Int. J. High Technol. Ceram.* **3**, 91 (1987).
2. G.H. Haertling, *J. Am. Ceram. Soc.* **82**, 797 (1999).
3. Z. Zhao, V. Buscaglia et al., *Phys. Rev. B* **70**, 024107 (2004).
4. C.A. Randall, N. Kim et al., *J. Am. Ceram. Soc.* **81**, 677 (2005).
5. G. Arlt, *Ferroelectrics* **76**, 451 (1987).
6. S. Wada, K. Yako, H. Kakemoto et al., *J. Appl. Phys.* **98**, 014109 (2005).
7. D.M. Marincel, H. Zhang, et al., *Adv. Funct. Mater.* **24**, 1409 (2014).
8. S.V. Kalinin et al., *Microsc. Microanal.* **12**, 1 (2006).

Microscopic investigation of nanoscale coesite crystals in ultra-high pressure silica glass from impactites

Ye.A. Golubev, T.G. Shumilova, S.I. Isaenko

*Institute of Geology of Komi SC of Uralian Branch of RAS, 167982 Syktyvkar, Russia
golubev@geo.komisc.ru*

Substances forming under ultrahigh pressures and high temperatures (UHPHT) raise an interest for understanding of some fundamental problems of matter state under extremely high PT conditions with a potential to new functional materials. In diamond-bearing impactites of the 70 Ma old Kara astrobleme (Polar Ural, Russia) HP post-impact liquation glasses with coesite have been discovered [1, 2], which may be interesting for understanding of general regularities in the formation and stability of crystalline-noncrystalline systems under extreme conditions. Microscopic methods, including AFM belong to the most effective methods for studying of nanoscale structure features of glass solids [3, 4].

For this work we collected vein-like UHPHT glasses from natural outcrops at banks of the river Kara. The chemical composition, phase state and local microstructure were determined by the methods of EDS, SEM and Raman spectroscopy. Nanoscale topography was detected by AFM and SEM. The surface morphology has been characterized by AFM measurements in tapping and phase contrast mode using an Integra Prima (NT-MDT, Russia) with super sharp silicon cantilevers of SSS-NCH (Nanosensors). The surfaces of the polished specimens were studied with a SEM Tescan MIRA3.

UHPHT glasses have fluidal microstructure and are composed of an amorphous matter with feldspar composition with small droplets of coesite-containing silica glass. Using the methods of microscopy, generally AFM, we have shown that the aluminosilicate glass matrix has a homogeneous nanostructure with rounded densely packed clusters of about 50-60 nm in size. Coesite crystals are clearly distinguished within amorphous matrix of silica droplets, both on SEM images and by the phase-contrast AFM method. Their sizes vary from 50 nm to several micrometers. The silica matrix in droplets has a homogeneous nanostructure consisting of elongated clusters with sizes of 15-30 nm. In this way, microscopic images of UHPHT impactites demonstrate a result of initial impact melt differentiation to bisilicate phase and aluminosilicate by liquation and crystallization processes with the following solidification sequence at the melt cooling: (1) coesite; (2) silicate glass; (3) aluminosilicate glass.

The study was supported by the Russian Science Foundation (project #17-17-01080).

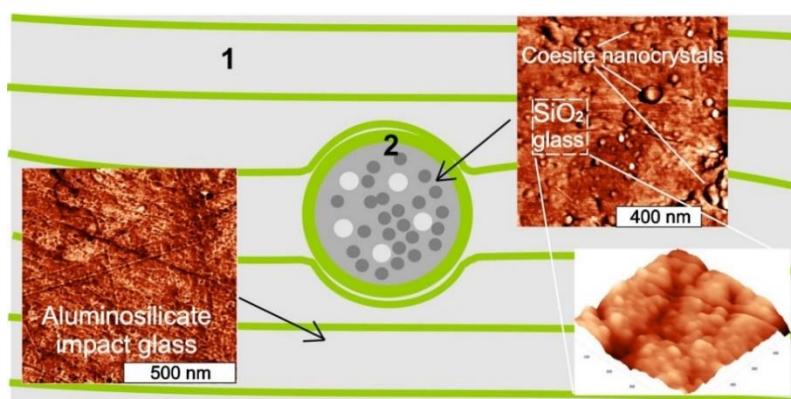


Figure 1. Schematic representation of the UHPHT impact glass microstructure: (1) aluminosilicate glass matrix; (2) a drop of coesite-containing silica glass within surrounding aluminosilicate glass matter.

1. T.G. Shumilova, V.P. Lutoev, S.I. Isaenko, et al, *Sci. Rep.* **8**, 6923 (2018).
2. T.G. Shumilova, S.I. Isaenko, B.A. Makeev, et al, *Doklady Earth Sciences* **480**, 595 (2018).
3. Ye.A. Golubev, T.G. Shumilova, S.I. Isaenko, et al, *J. Non-Crystalline Solids.* **500**, 388 (2018).
4. Ye.A. Golubev, T.G. Shumilova, S.I. Isaenko, *IOP Conf. Series: Mat. Sci. Eng.* **443**, 012008 (2018).

Features of combining of scanning probe microscopy with optical and scanning electron microscopy

I. Sapozhnikov, O. Gorbenko, M. Felshtyn, M. Zhukov, A. Golubok

*Institute for Analytical Instrumentation RAS, 198095, Saint Petersburg, Russia
aogolubok@mail.ru*

There are two main experimental approaches to visualizing the structure or mapping the properties of objects with nanometer spatial resolution. In one case, a focused beam of particles or radiation interacts with the sample under study. In this case, the beam source is far from the sample, while in another case a sharp solid-state probe close to the surface under study interacts with the sample. Since the interaction of focused beams and sharp probes with the sample surface has a different nature, the combination of beam and probe approaches in one device [1-5] provides more complete information about the object under research. The report discusses the features of combining a scanning probe microscope (SPM) with an optical (OM) or scanning electron microscope (SEM).

The requirements for compatibility of SPM with OM and SEM are discussed. It is shown that when a piezo-inertial displacement systems will be used a sufficiently compact SPM units, easily compatible both with the OM lens and the SEM goniometer may be created. The compact design of the piezo-inertial movers is due to the absence of complicated mechanical components and the possibility to easy controlled a piezo-inertial mover by asymmetric pulses of electrical voltage. In addition, to simplify the design and reduce the size of the SPM units, we used as a probe sensor the piezoresonance and piezoresistive cantilevers, which, unlike standard cantilevers, do not require an optical scheme to measure their deflection. The peculiarities of working of piezoresonance and piezoresistive cantilevers are discussed.

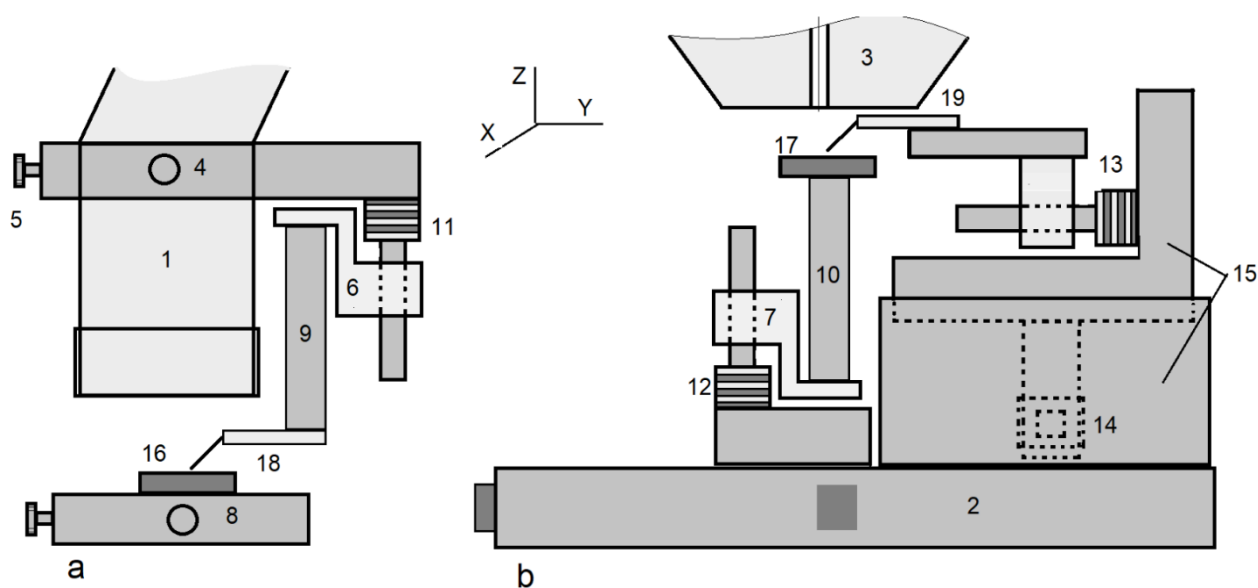


Figure 1. The scheme of SPM combination with optical microscope (a) and with scanning electron microscope (b). 1 – optical lens; 2 – SEM goniometer; 3 – pole piece of the SEM objective lens; 4,5 – screws for alignment of the probe under the optical beam; 6,7 – 1D piezo-inertial movers; 8 – 2D stage of OM; 9,10 – piezotubes for X, Y- scanning by the probe (sample); 11,12,13,14 – stack multilayer piezo actuators; 15 – 2D piezo-inertial mover; 16,17 – samples; 18,19 – probe sensors.

Figure 1a shows a scheme of SPM unit combined with the OM lens (1). Figure 1b shows a scheme of the SPM unit located on the goniometer (2) of the SEM under the pole piece (3) of the SEM objective electron lens. The gap between sample surface and the pole piece of the objective lens is 7 mm. In the case of a combination of SPM-OM the probe (18) moves in the (X,Y) plane under the OM light beam using screws (4,5). It is sufficient to use only 1D piezo-inertial mover (6) to capture the interaction between the probe (18) and the sample (16). To choose the place on the sample (16) a 2D OM stage (8) is used. The piezotube (9) is used for scanning by the probe

(18) at X,Y directions. The stack multilayer piezo actuator (11) is used both for fine scanning by the probe (18) at Z direction and for coarse approach of the probe (18) to the sample (16) using the 1D piezo-inertial mover (6). In the case of a SPM-SEM combination, a 2D piezo-inertial mover (15) is used to move the probe (19) under the electron beam. To select a region on the sample (19) surface the SEM goniometer (2) is used. In this case, the piezotube (10) is used to scan the sample (17) at the X,Y directions, and the stack multilayer piezo actuator (12) is used both for fine scanning the sample (17) at the Z direction and for coarse approach of the sample (17) to the probe (19) using the 1D piezo-inertial mover (7).

The performance data of the 1D and 2D piezo-inertial movers are given. The combinations of SPM with OM and SEM at the different measurement modes are discussed. Examples of visualization of objects of different nature by methods of beam and probe microscopy in combined systems SPM-OM and SPM-SEM, as well as an examples of probe nanolithography performed under the control of SEM are given (Fig. 2).



Figure 2. SEM image of a result of a dynamic force nanolithography performed under electron beam control in SPM combined with SEM. (on the left the W-probe used for probe nanolithography is seen, scanning area $6 \times 7 \mu\text{m}^2$).

1. A.O. Golubok, V.A. Timofeev, *Ultramicroscopy* **42-44**, 1558 (1992).
2. U. Stahl, C.W. Yuan, A.L. de Lozanne, et al., *Appl. Phys. Lett.* **65**, 2878 (1994).
3. J. Kreith, T. Strunz, E. J. Fantner, G. E. Fantner, M.J.Cordill, *Rev. Sci. Instrum.* **88**, 053704 (2017).
4. AFM SEM/FIB Integrated Nanoscale Characterization, Nanonics Imaging Ltd., see <http://www.nanonics.co.il/products/spm-for-sem-fib>
5. LensAFM – AFM for optical microscopes, Nanosurf company, see <https://www.nanosurf.com/en/products/lensafm-afm-for-optical-microscopes>

Low temperature resistive elements integrated into superconductive NbN nanowires produced under ion beam irradiation

B.A. Gurovich¹, B.V. Goncharov¹, L.V. Kutuzov¹, K.E. Prihodko^{1,2},
D.A. Komarov¹, A.G. Domantovsky¹, M.M. Dementeva¹

¹NRC "Kurchatov Institute", 123098, Moscow, Russia
Bvgoncharov@gmail.com

²National Research Nuclear University "MEPhI", 115409, Moscow, Russia.

Traditional lift-off technique of Ti-Au resistive elements deposition has a number of disadvantages: relatively large sizes of the elements, a large number of technological operations required for sputtering.

New methods for the fabrication of integrated resistive functional nanoelements based on superconducting thin NbN films have been developed at the NRC "Kurchatov Institute" for the creation of cryoelectronic devices for various applications, due to controlled changes in the chemical composition and modification of the properties of nanomaterials under ion beam irradiation.

These methods have the following advantages: low number of necessary technological operations; the possibility of creating integrated elements of small size (<100 nm); by controlling the size of the irradiated region, the radiation dose and the beam composition, various functional elements (resistors, capacitances, inductances) can be created.

To create the resistors ultrathin NbN films with thickness of 5 nm, obtained by cathode sputtering on SiO₂ substrates were used. Formation of structures for electrical measurements was performed by electron lithography and plasma-chemical etching.

Modification of NbN films was performed by composite 0.1-4 keV ion beam of H⁺ and OH⁻ ions, through the open windows in the PMMA mask of the required geometry.

In this paper, integrated resistors were built into low-temperature superconducting current lines of NbN with different resistances in the range 1 Ω-1 MΩ. The different values of resistivity was obtained by varying the geometry of irradiated area integrated into the superconductive line.

Irradiation based technique to form integrated resistive elements can be used during different design cryogenic circuit production.

The work was supported by the NRC "Kurchatov Institute" (№1639).

1. B.A. Gurovich, K.E. Prihod'ko, M.A. Tarkhov, et al., *Nanotechnol. Russia* **10**, 530 (2015).
2. B.A. Gurovich, M.A. Tarkhov, K.E. Prihod'ko, et al., *Nanotechnol. Russia* **9**, 386 (2014).
3. B.A. Gurovich, K.E. Prihod'ko, E.A. Kuleshova, et al., *J. Exp. Theor. Phys.* **116**, 916 (2013).

Creation of thin superconducting MoCN covering by cathode sputtering technique as a basis film for functional cryogenic nanoelements

B.A. Gurovich¹, B.V. Goncharov¹, L.V. Kutuzov¹, K.E. Prihodko^{1,2}, E.D. Olshansky¹

¹NRC “Kurchatov Institute”, 123098, Moscow, Russia

Bvgoncharov@gmail.com

²National Research Nuclear University “MEPhI”, 115409, Moscow, Russia

At present, studies of thin superconducting films as a basis for nanoscale electronic devices (such as single-photon detectors) are of great interest in connection with high values of critical current densities (3-6 MA/cm²) and relatively high superconducting transition temperatures (12-14 K). Nowadays many type of thin film superconductive materials (NbN, MoN, MoC) are used to build up SSPD and HEB devices. However, with the rapid development of cryoelectronics, the search for new materials remains urgent.

Films made by cathode sputtering were used to create molybdenum carbonitride (MoCN) of various thicknesses on SiO₂ substrates using a Mo and C mosaic target. Sputtering carried out in a nitrogen atmosphere at temperature of 800 °C. Formation of structures for electrical measurements was performed by electron lithography and plasma-chemical etching, followed by deposition of Ni-Pt contacts.

The dependence of resistance on the temperature was measured in the temperature range 4.2-300 K. It was found that the obtained material showed superconducting properties. It was investigated the dependence of superconducting state transition temperature dependence on the film thickness as well as the dependence of the transition critical current on the temperature in the temperature range 4.2-13 K.

The thicknesses of the films was measured by bright-field TEM technique on the FIB cut cross-section samples. Chemical elements depth distribution profiles were measured by EELS technique in STEM mode of transmission electron microscope with accuracy of the electron probe size (~0.15 nm). We used 0.5 nm step size to get the chemical elements depth distribution profiles.

The work was supported by the NRC “Kurchatov Institute” (№1639).

1. B.A. Gurovich, K.E. Prihod'ko, M.A. Tarkhov, et al., *Nanotechnol. Russia* **10**, 530 (2015).
2. B.A. Gurovich, M.A. Tarkhov, K.E. Prihod'ko, et al., *Nanotechnol. Russia* **9**, 386 (2014).
3. B.A. Gurovich, K.E. Prihod'ko, E.A. Kuleshova, et al., *J. Exp. Theor. Phys.* **116**, 916 (2013).
4. K.E. Prihodko, B.A. Gurovich, D.A. Komarov, et al., *Nucl. Instr. Meth. Phys. Res. B* **326**, 273 (2014).
5. J.F. Ziegler, M.D. Ziegler, J.P. Biersack, *Nucl. Instr. Meth. Phys. Res. B* **268**, 1818 (2010).
6. A. Gilewicz, R. Jedrzejewski, A.E. Koshmanska, B. Warcholinski., *Thin Solid Films* **577**, 94 (2015).

Charged domain walls in lithium tantalate with compositional gradients produced by VTE process

E.D. Greshnyakov, B.I. Lisjikh, V.I. Pryakhina, M.S. Nebogatikov, V.Ya. Shur

*School of Natural Sciences and Mathematics, Ural Federal University, 620000 Ekaterinburg, Russia
evgeny.greshnyakov@urfu.ru*

We investigated the shape of charged domain walls (CDWs) in LiTaO₃ (LT) single crystals with inhomogeneous spatial distribution of Li concentration along polar axis. Vapor Transport Equilibration process (VTE) was used for changing the Li concentration from congruent (48.8 mol.%) to stoichiometric (50 mol.%) composition. Spatially inhomogeneous distributions were obtained for various durations of VTE at 1100 °C (far above Curie temperature) [1, 2].

The spatial distribution of Li concentration was measured by confocal Raman spectroscopy (Alpha AR300, WITec). CDWs were visualized at the surface using optical (BX61, Olympus, Japan) and scanning electron (Merlin, Carl Zeiss) microscopes after selective chemical etching and in the bulk using Cherenkov-type Second Harmonic Generation microscopy (Ntegra Spectra, NT-MDT) and confocal Raman microscopy.

The geometry of the initial domain structure formed during cooling below Curie temperature after VTE depends on the spatial distribution of LT composition. The wide polydomain layer appeared in the volume with congruent composition and single domain layers appeared near polar surfaces. The polydomain layer represent 3D maze domain structure with head-to-head and tail-to-tail CDWs. The increase of VTE duration resulted in Li concentration increase and thinning of polydomain layer. The narrow CDW was formed for long enough VTE due to presence of built-in fields produced by gradient of Li concentration [1-3].

The subsequent cooling to room temperature resulted in change of CDWs morphology and formation of the domain bumps under the action of the pyroelectric field. Moreover, the isolated non-through domains with diameter below 5 μm appeared in the volume between polar surfaces and CDW. The shape of domain cross-section changed with depth from hexagonal close to the surface layer with stoichiometric composition to trigonal for congruent composition in the bulk.

The equipment of Ural Center for Shared Use “Modern Nanotechnology” Ural Federal University was used. The research was made possible by Russian Science Foundation (Project № 19-12-00210).

1. V.I. Pryakhina, E.D. Greshnyakov, B.I. Lisjikh, A.R. Akhmatkhanov, D.O. Alikin, V.Ya. Shur, A. Bartasyte, *Ferroelectrics* **525**, 47 (2018).
2. V.I. Pryakhina, E.D. Greshnyakov, B.I. Lisjikh, M.S. Nebogatikov, V.Ya. Shur, *Ferroelectrics* **542**, 13 (2019).
3. V.Ya. Shur, E.L. Rummyantsev, *J. Korean Phys. Soc.* **32**, S727 (1998).

Shape change of metal oxide nanoparticles produced by laser ablation in liquid

E.V. Gunina, V.I. Pryakhina, E.V. Shishkina, D.K. Kuznetsov, E.D. Greshnyakov, V.Ya. Shur

*School of Natural Sciences and Mathematics, Ural Federal University, 620000, Ekaterinburg, Russia
ekaterina.gunina@urfu.ru*

The shape variation of the nanoparticles (NPs) is important for several applications including creation of the antibacterial coatings and nanotoxicological research. Currently, the expansion of the study of nanoparticle toxicity needs production of the stable colloids (water suspensions) of high metal oxide concentration with model pure NPs of given composition, sizes and shapes [1,2]. The laser ablation in water (LAW) gives the unique ability to produce the colloids of spherical NPs. Moreover, the NPs can be transformed from octahedron to spherical shape by non-focused laser irradiation in a liquid in short time. However, other morphologies such as hollow particles, cubes, rods, spindles, tubes, disks, plates and sheets also have been fabricated with the assistance of external factors and directly by LAW.

The formation of metal oxide NPs and nanostructuring of the target surface by LAW and hot water treatment have been studied using Pb as a model metal. The pulse Yb fiber laser (Fmark-20 RL, Laser technology center Ltd) with 1062 nm wavelength, 100 ns pulse duration and repetition rate about 21 kHz has been used for laser ablation. The 2-mm-thick Pb target of 99.99% purity with diameter 46 mm at the bottom of the glass Petri dish was covered by 5 mm layer of deionized water. The water volume was about 40 ml. The focused laser beam (fluence 80 J/cm², spot diameter 40 μm) has been scanned over the target area about 16 mm² with linear velocity 270 mm/s. The typical duration of the ablation process was about 240 s. The water temperature near the target surface was measured by thermocouple. Various target surface preparations have been used: (1) aging by long exposure at ambient conditions, (2) cleaning by LAW and subsequent ultrasonification, (3) etching by CCP oxygen plasma, (4) treating by hot deionized water [3].

It was found that the laser ablation of the targets aged at ambient conditions, cleaned by LAW and treated by hot water leads to appearance of nonspherical 2D (plates) and 3D (octahedra and rods) NPs in suspension and at the target surface. The NPs of the classical spherical shape appeared in suspension immediately after LAW and their shape changes rapidly in the heated water. It was found that the octahedra and rods appeared at the target surfaces immersed in the water with temperature about 70 °C after several minutes even without laser ablation. Thus, the noticeable role of the unavoidable hot water treatment during LAW in formation of the nonspherical micro- and nanoparticles was proved.

The equipment of the Ural Center for Shared Use “Modern Nanotechnology” UrFU was used. The work was supported by Government of the Russian Federation (Act 211, Agreement 02.A03.21.0006).

1. I. Minigalieva, B. Katsnelson, L. Privalova, V. Gurvich, V. Shur, E. Shishkina, A. Varaksin, V. Panov, T. Slyshkina, E. Grigorieva, *Toxicol. Lett.* **238**, S279 (2015).
2. A.E. Tyurnina, V.Y. Shur, R.V. Kozin, D.K. Kuznetsov, V.I. Pryakhina, G.V. Burban, *Phys. Solid State* **56**, 1431 (2014).
3. V.Ya. Shur, E.V. Gunina, A.A. Esin, E.V. Shishkina, D.K. Kuznetsov, E.A. Linker, E.D. Greshnyakov, V.I. Pryakhina, *Appl. Surf. Sci.* **483**, 835 (2019).

Investigation of the effect of upper electrode material on the memristor properties of strained carbon nanotubes

A.V. Guryanov, M.V. Il'ina, O.I. Il'in, O.A. Ageev

*Southern Federal University, Institute of Nanotechnologies, Electronics and Electronic Equipment Engineering, 347922, Taganrog, Russian Federation
guryanov@sfnu.ru*

Silicon technology is used as the basis for the creation of micro- and nanoelectronics storage devices. However, this technology has serious limitations for further miniaturization and reduction of energy consumption. Research is carried out to find an alternative technology for the formation of storage devices. One of the promising directions in this area is the development of memristor structures [1]. Special attention to the creation of memristor structures is attend to vertically aligned carbon nanotubes (VA CNT), which demonstrate high performance and scalability [2]. However, research in this area is at an early stage and requires further research.

The aim of this work is an experimental study of the upper electrode material effect on the memristor properties of carbon nanotubes.

An array of vertically aligned carbon nanotubes grown by PECVD on the lower TiN electrode was used as the test sample. The parameters of the nanotubes were determined using a scanning electron microscope Nova Nanolab 600 and were: diameter 54 ± 6 nm, length 1130 ± 110 nm, density $72 \mu\text{m}^{-2}$ (Fig. 1). Experimental studies were carried out by scanning tunneling microscopy (STM) in current spectroscopy mode at a tunnel gap of 1 nm using a scanning probe microscope Solver (NT-MDT, Russia). STM probes of W, Pt and graphite were used as the upper electrode. Sawtooth voltage pulses with amplitude from ± 1 to ± 8 V was applied between the STM probe localized on a single VA CNT and the sample. A VA CNT deformation occurred under the action of the local electric field during the measurement [2, 3]. Current-voltage characteristics (CVC) a strained VA CNT obtained from amplitude at ± 4 and ± 7 V are shown in Figure 2 and 3, respectively.

The analysis of the obtained results showed that the use of a graphite probe as the upper electrode of a VA CNT memristor structure leads to significant decrease a total resistance of the structure at low voltages compared to Pt and W probes (Fig. 2). This is due to the close values of the work function of graphite and VA CNT. However, when increasing the amplitude of the applied voltage to ± 7 V or more, degradation of the graphite probe is observed, which is due to its evaporation under the action of high field strength (Fig. 3a). The use of probes made of refractory Pt and W can solve this problem (Fig. 3b,c).

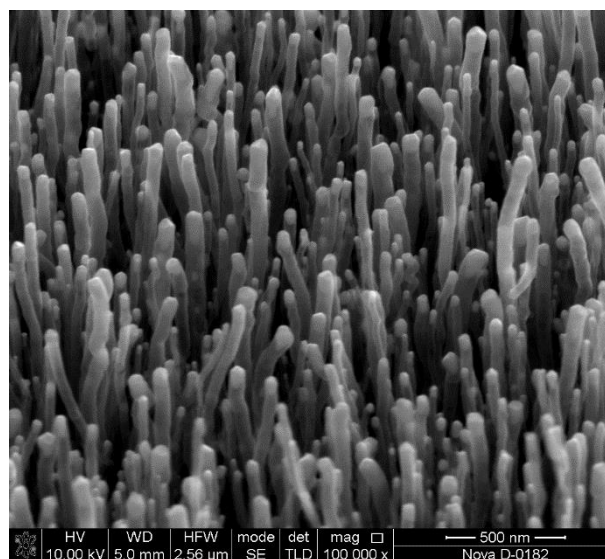


Figure 1. SEM-image of the VA CNT experimental sample.

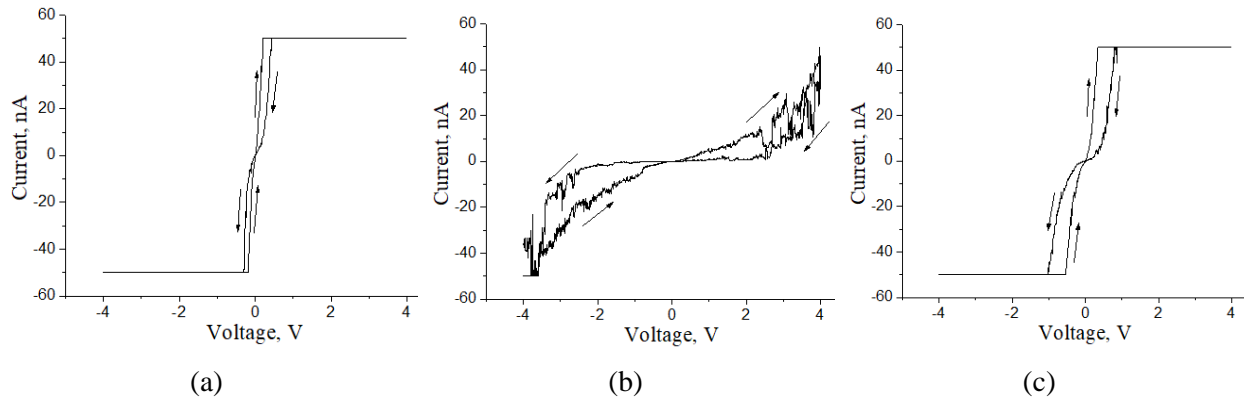


Figure 2. CVC of a single VA CNT obtained by current spectroscopy at ± 4 V voltage for: (a) graphite probe, (b) Pt probe, (c) W probe.

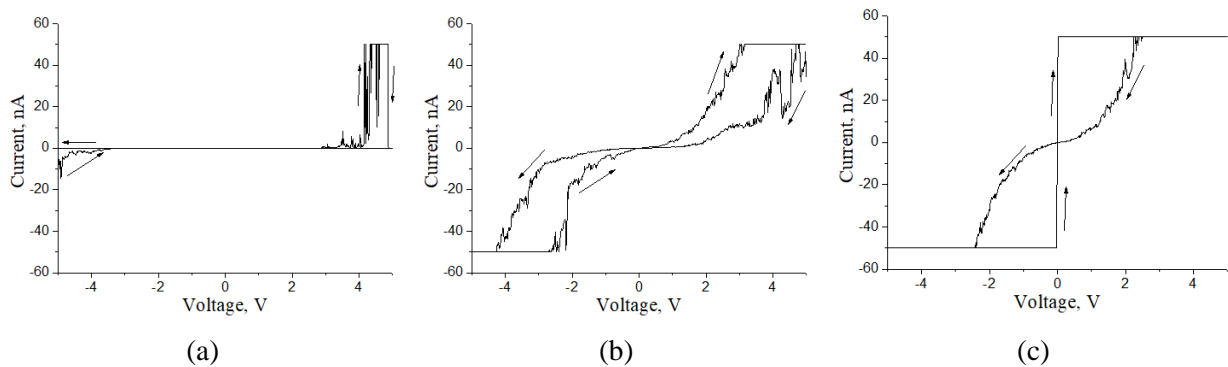


Figure 3. CVC of a single VA CNT obtained by current spectroscopy at ± 7 V voltage for: (a) graphite probe, (b) Pt probe, (c) W probe.

Analysis of the CVCs obtained by Pt and W probes showed that the highest value of the ratio in the high- and low-resistance states of VA CNT is observed when using the W probe due to the minimum resistance in the low-resistance state both at small (Fig. 2b,c) and at higher voltages (Fig. 3b,c). This dependence is also associated with a lower work output W (4.5 eV) than Pt (5.3 eV).

Thus, in this paper an experimental study of the effect of the upper electrode on the memristor properties of strained carbon nanotubes was carried out. It is shown that the material of the upper electrode affects the switching voltage of the memristor structure based on VA CNT. The best results are shown by the W upper electrode. The obtained results can be used to create non-volatile storage devices based on aligned carbon nanotubes. The results were obtained using the equipment of the Research and Education Center and the Center for collective use "Nanotechnologies" of Southern Federal University.

The reported study was funded by RFBR according to the research project No. 16-29-14023 ofi_m.

1. J.S. Meena, S.M. Sze, U. Chand, T.-Y. Tseng, *Nanoscale Research Letters* **9**, 1-33 (2014).
2. M.V. Il'ina, O.I. Il'in, Yu.F. Blinov, et al., *Carbon* **123**, 514 (2017).
3. M.V. Il'ina, O.I. Il'in, Yu.F. Blinov, V.A. Smirnov, O.A. Ageev, *Tech. Phys.* **63**, 1672 (2018).

Polarization switching effects in thin BZT films

E.V. Guschina¹, V.V. Osipov^{1,2}, B.R. Borodin¹, M.S. Dunaevskiy¹

¹Ioffe Institute, 194021, Saint-Peterburg, Russia
katgushch@yandex.ru

²Herzen University, 191186, Saint-Peterburg, Russia

Thin ferroelectric films of barium zirconate titanate $\text{Ba}(\text{Zr}_{1-x}\text{Ti}_x)\text{O}_3$ (BZT) solid solutions are promising materials for microwave devices [1, 2]. These materials are of interest due to the fact that when Ti atoms are replaced by Zr atoms, microwave losses and leakage currents can be reduced [3]. In this paper, using the methods of contact scanning probe microscopy (SPM) and piezoelectric microscopy, the processes of local charging and repolarization of BZT films, as well as the storage times of the created domains were investigated.

We studied $\text{Ba}(\text{Zr}_{1-x}\text{Ti}_x)\text{O}_3$ 100 nm thick films (with x from 0.2 to 0.65), obtained by plasma deposition with a double system of crucibles. The main task of SPM research was to investigate the features of the structural and ferroelectric properties of these films. Also in this work, experiments were carried out to create ferroelectric domains, to establish the effect of annealing on the ferroelectric properties and to determine the lifetime of the domains.

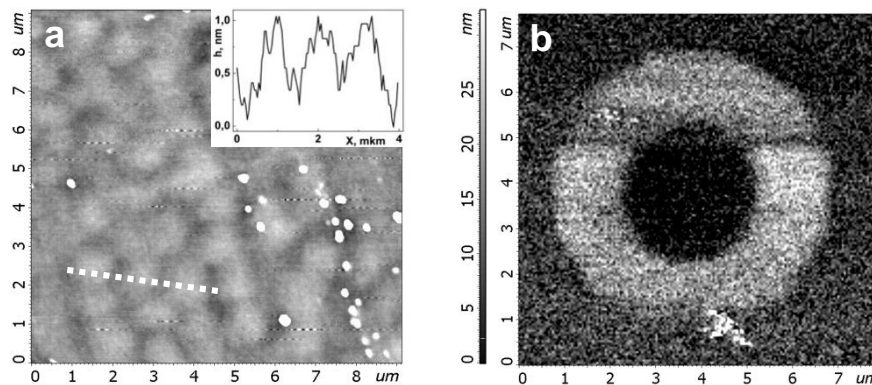


Figure 1. (a) Typical SPM topography of BZT film, inters – profile along dotted line; (b) PFM image of polarized BZT film: +10 V (“light” donut-shaped area), -10 V (“dark” round area in the center).

Figure 1a shows the typical topography of one of the studied BZT films. The inset shows the profile along the characteristic topographic features of the relief. It can be seen that the sample is quite smooth, the characteristic z -height of the relief is 1 nm, while the lateral size of the topographic features is about 1 micron. Figure 1b shows a PFM image obtained by scanning an area of BZT film with “ $-z$ polarized” (“dark” round area in the center of Fig. 1b) and “ $+z$ polarized” (“light” donut-shaped area in the Fig. 1b) regions. In the “light”/“dark” region, the polarization vector is directed outside/inside the film. Outside there is a region with intermediate polarization (between “ $+z$ ” and “ $-z$ ”).

It has been established that the lifetime of the created domains is at least several hours. Also a local hysteresis loop of the BZT films has been measured with the SPM technique. It was established that thermal annealing of BZT films does not lead to the complete disappearance of the domains, but it reduces their lifetime and the average value of residual polarization.

This work was supported by the RFBR grant N 18-32-00092_mol-a.

1. O.G. Vendik, *Phys. Solid State* **51**, 1529 (2009).
2. S. Gevorgian, *Ferroelectrics in microwave devices, circuits and systems* (Springer London), 396, (2009).
3. H. Chen., C. Yang, J. Zhang, B. Wang, H. Ji, *Appl. Surf. Sci.* **255**, 4585 (2009).

Electron beam processing of silicon carbide substrate to obtain graphene-like carbon films

E.Yu. Gusev, M.P. Karmanov

*Southern Federal University, Institute of Nanotechnologies, Electronics and Equipment Engineering, Research and Education Centre "Nanotechnologies", 347922, Taganrog, Russia
eyugusev@sfedu.ru*

Nanostructured carbon films: graphene and graphene-like films are considered as future electronics materials for applications in nanoelectronics and carbon electronics [1]. Therefore, achieving their quality synthesis is in demand. Among the various methods of its obtaining the most interesting is the synthesis directly on silicon carbide substrates [2], e.g. thermal decomposition [3, 4]. Recently, various approaches using a irradiation technique or particle beam (laser, ion and electron beams) were extensively paid attention due to high precision, efficiency, mature control method, and fast speed [2, 5, 6]. The application of particle beam irradiation on graphene obtaining could present obvious advantages, including suitability for a large-scale production of graphene.

In this paper, we present our first result on graphene-like films fabrication by electron beam processing of silicon carbide substrate.

Several pieces of 35-42 mm² were cut from a 6H-SiC substrate and chemically cleaned. One sample was served as reference and other samples were then electron beam processed (EBP) for synthesis of graphene. EBP was carried out on a specialized electron beam system based on laboratory vacuum with the Pierce electron gun. An electron current of 50 to 180 mA and beam rate of a few mm/s were applied to heat the samples in pressure of 0.3-0.5 mTorr, so corresponding temperature were in the range of 1680 to 2000 K. The as-received layers as well as initial substrate surfaces on reference sample were characterized by Raman spectroscopy and atomic force microscopy.

A series of {0001} 6H-SiC samples were electron beam processed and nanostructured carbon films were available on the sample surfaces. Raman spectra of some samples are shown in Figure 1.

The D, G and 2D peaks as well as D/G (0.17-0.88) and 2D/G (0.70-0.89) ratios are detected. The FWHM of 2D peaks are 61-81. Temperature effects are discussed.

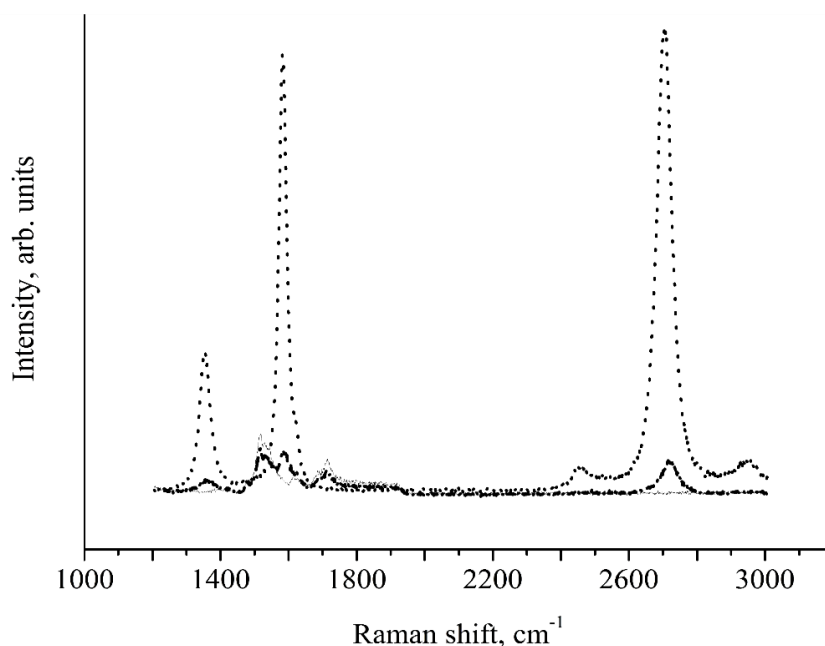


Figure 1. Raman spectra of reference (solid gray line) and electron beam processed (dashed and pointed black lines) 6H-SiC samples.

Comparison of the obtained results with known Raman spectra's and atomic force microscopy data [1-5, 7-9] allows us to assume that nanostructured carbon films, from monolayer to multilayer graphene and turbostratic graphite with various degrees of defects, are formed under the conditions of electron-beam processing.

It is expected that further optimization of the processing conditions will allow to fabricate required nanostructured carbon films.

Different nanostructured carbon films have been synthesized on {0001} 6H-SiC by electron beam processing. The preparation of graphene on silicon carbide substrates by EBP will be promising method in carbon electronic applications.

This study was financially supported by Southern Federal University. The results were obtained using the equipment of the Research and Education Center "Nanotechnologies" of Southern Federal University.

1. H.C. Lee, W.W. Lie, S.P. Chai, A.R. Mohamed, C.W. Lai, C.S. Khe, C.H. Voon, U. Hashim, N.M.S. Hidayah, *Procedia Chemistry* **19**, 916 (2016).
2. N. Mishra, J. Boeckl, N. Motta, F. Iacopi, *Physica Status Solidi A* **213**(9), 2277 (2016).
3. A.A. Lebedev, I.S. Kotousova, A.V. Lavrent'ev, S.P. Lebedev, P.A. Dement'ev, V.N. Petrov, A.N. Smirnov, A.N. Titkov, *Phys. Solid State* **52**(4), 855 (2010).
4. R.V. Konakova, O.F. Kolomys, O.B. Okhrimenko, V.V. Strelchuk, E.Yu. Volkov, M.N. Grigoriev, A.M. Svetlichnyi, O.B. Spiridonov, *Semiconductors* **47**(6), 812 (2013).
5. J. Kim, M. Park, H.K. Shin, J. Choia, B. Panta, P.S. Saud, T. An, S.-H. Chae, H.-Y. Kim, *Materials Letters* **149**, 15 (2015).
6. E.Yu. Gusev, S.P. Avdeev, *J. Phys.: Conf. Ser.* **1124**, 022026 (2018).
7. W. Strupinski, K. Grodecki, P. Caban, P. Ciepielewski, I. Jozwik-Biala, J.M. Baranowski, *Carbon* **81**, 63 (2015).
8. L.M. Malard, M.A. Pimenta, G. Dresselhaus, M.S. Dresselhaus, *Phys. Rep.* **473**, 51 (2009).
9. T. Hu, H. Bao, S. Liu, X. Liu, D. Ma, F. Ma, K. Xu, *Carbon* **120**, 219 (2017).

Uncertainty of tunneling microscopy measurements of the field emission from multilayer nanostructures

E.V. Panfilova¹, A.B. Syritskii², A.R. Ibragimov¹

¹Department of Electronic Technologies in Mechanical Engineering, Bauman Moscow State Technical University, 105005, Moscow, Russia
zotaak@mail.ru

²Department of Metrology and Interchangeability, Bauman Moscow State Technical University, 105005, Moscow, Russia

The paper presents the results of scanning tunneling microscopy (STM) investigation [1] of electron field emission (FE) from multilayer nanostructures based on silica opal film Cr-SiO₂-Au-C. Opal film was deposited in colloidal solvent [2], other films – by vacuum deposition [3, 4]. We discuss the problem of uncertainty of measurements of the field enhancement factor or gain coefficient k by using the current I versus applied voltage V characteristics of the emission [5]. k factor is defined as the ratio of the electric field at the nano-edge to the applied to the gap electric field. A large k factor allows emitters operate at a small applied voltage.

Uncertainty of measurements has been estimated according to ISO/IEC GUIDE 98-3:2009 Uncertainty of measurement – Part 3: Guide to the expression of uncertainty in measurement (GUM:1995). In the experiment the k factor was calculated by means of the graph of FE in Fowler–Nordheim coordinates. The FE regime was observed for higher applied voltage (Fig. 1).

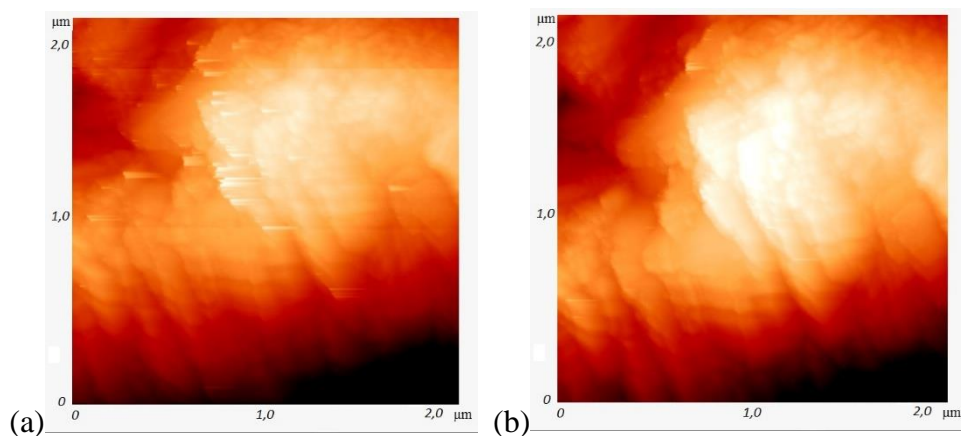


Figure 1. The dependence of STM-images on the regimes of the current I versus applied voltage V curve: (a) tunneling regime, (b) FE regime.

Type A uncertainty was calculated from a series of observations and measurements of the tangent of inclination of the FE graph. Type B uncertainty was evaluated using available information in handbooks and technical passport. At specified level of confidence of 95% the value of estimated expanded uncertainty was approximately 10%. The phenomenon of uncertainty in STM measurements of k factor is mainly related to the reproducibility of the films deposition process and unevenness of multilayer structure. The main application of this methodology is laboratory testing of the emission nanostructures.

1. A.S. Komshin, S.R. Orlova, *Meas. Tech.*, **59**, 589 (2016).
2. V.L. Kuleshova, E.V. Panfilova, E.P. Prohorov, *2018 International Russian Automation Conference (RusAutoCon)*, 1-5 (2018).
3. S.V. Sidorova, M.A. Pronin, A.A. Isaeva, *2018 International Russian Automation Conference (RusAutoCon)*, 1-4 (2018).
4. Y.V. Panfilov, L.L. Kolesnik, V.T. Ryabov, S.V. Sidorova, *J. Phys.: Conf. Series*, **872**, 1 (2017).
5. A.B. Syritskii, E.V. Panfilova, *IOP Conf. Series: Mat. Sci. Eng.* **443**, 012035 (2018).

Optimization of the photonic crystal colloidal films deposition by means of atomic force microscopy

E.V. Panfilova¹, A.B. Syritskii², A.R. Ibragimov¹

¹*Department of Electronic Technologies in Mechanical Engineering, Bauman Moscow State Technical University, 105005, Moscow, Russia*
zotaak@mail.ru

²*Department of Metrology and Interchangeability, Bauman Moscow State Technical University, 105005, Moscow, Russia*

This article describes the results of optimization of the colloidal photonic crystal (PhC) opal films deposition by means of atomic force microscopy investigation. The main factors affecting the quality of the PhC films are studied. Ordered structure is critical for the formation of the photonic band gap (PBG) because Bragg diffraction occurs in the periodic distribution of colloidal spherical particles.

For preparing samples authors used a colloidal solution of polystyrene monodisperse latex of particles diameters ranging from 220 nm to 330 nm and siall substrates. The original technology of opal matrices fabrication by vertical lifting from a colloidal solution [1] is described. The structure of the obtained films was monitored by measuring the relative area of ordered structure by means of scanning atomic force microscope Solver Next (NT-MDT, Russia) in semi-contact mode [2]. The photonic crystal properties were monitored by measuring the reflectance at the PBG by means of Epsilon spectrophotometer (IZOVAC, Belorussia). It was found that lifting velocity and solution concentration are the most significant factors for obtaining an ordered structure of photonic crystals.

Full factorial experiment was used to optimize the effect of the above-mentioned factors. The revealed dependences allowed to determine the optimal conditions for obtaining high photonic crystalline quality of opal film: the highest values of the relative area of ordered structure and reflectance at the PBG. Figure 1 shows an AFM-image of the obtained at optimal conditions opal film surface. This film has closest packed structure consisting of hexagonal close packed layers.

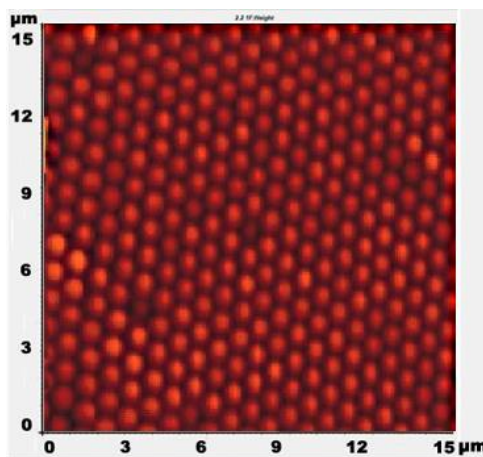


Figure 1. AFM-image of 220 nm polystyrene particles opal film fabricated at 0.3 mm/min lifting velocity and 5% concentration of solution.

The presented results may be used for the development of the colloidal monolayer technology for microsphere lithography.

1. V.L. Kuleshova, E.V. Panfilova, E.P. Prohorov, *2018 International Russian Automation Conference (RusAutoCon)*, 1-5 (2018).
2. A.B. Syritskii, E.V. Panfilova, *IOP Conf. Series: Mat. Sci. Eng.* **443**, 012035 (2018).

Study of the electromechanical properties of aligned carbon nanotubes coated with ZnO using atomic force microscopy

M.V. Ili'na, A.V. Guryanov, O.I. Il'in, Z.E. Vakulov, A.A. Fedotov, O.A. Ageev

*Southern Federal University, Institute of Nanotechnologies, Electronics and Electronic Equipment Engineering, 347922, Taganrog, Russia
mailina@sfedu.ru*

Aligned carbon nanotubes (CNTs) are one of the most promising materials for creating nanoelectronics and nanopiezotronics devices due to the unique memristive and piezoelectric properties [1, 2]. Studies of the effect of a piezoelectric coating on the properties of CNTs are of particular interest. Moreover, the study of electromechanical parameters of aligned CNTs by scanning probe microscopy is a nontrivial task due to their mobility during scanning [3].

The aim of this work is to study the effect of a conformal ZnO coating on the geometric parameters and the piezoelectric response of aligned carbon nanotubes by atomic force microscopy (AFM).

As the experimental sample was used vertically aligned CNTs array grown by plasma enhanced chemical vapor deposition on a silicon wafer with TiN bottom electrode on the surface. The diameter, height and density CNTs in array were 42 nm, 2.6 μm and 82 μm^{-2} , respectively (Fig. 1a). The conformal deposition of the ZnO films was carried out at laser radiation energy of 160 mJ and a pulse number of 10 000 with a repetition rate of 10 Hz using a Pioneer 180 (Neocera Co., USA). Surface studies of the CNT array were performed by the AFM in the semicontact mode using the Ntegra probe nanolaboratory (NT-MDT, Russia). A commercial cantilever with a platinum coating NSG11/Pt was used as the AFM probe. The AFM images of the CNT array before and after the deposition of ZnO are shown in Fig. 1b and Fig. 1c respectively. Studies of the piezoelectric response of CNTs were carried out on the basis of the previously developed technique [2]. The results of the study of the piezoelectric response of CNTs before and after ZnO coating are shown in Fig. 2.

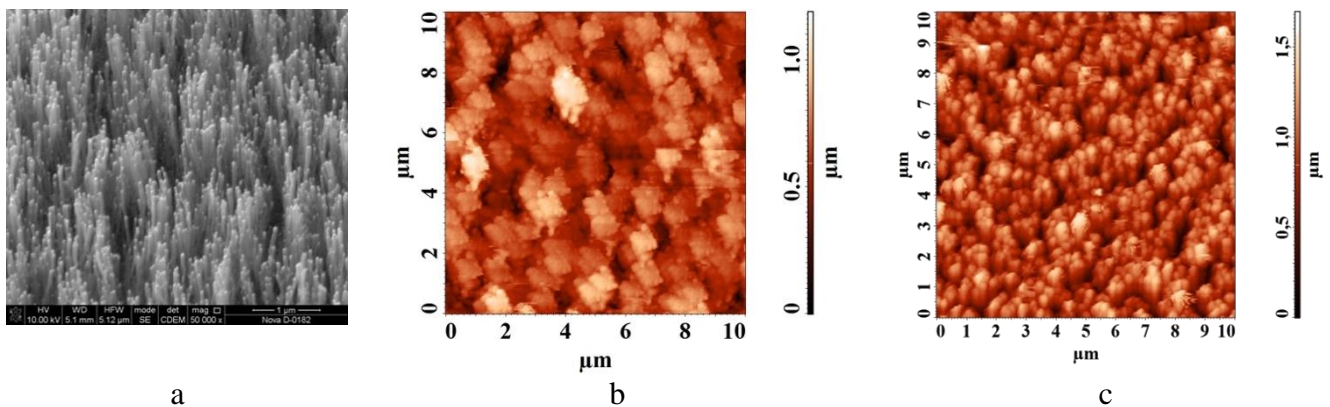


Figure 1. Experimental sample of vertically aligned CNT array: (a) SEM image; (b, c) AFM images before and after ZnO coating, respectively.

Studies of the experimental sample by the scanning electron microscopy showed no visible changes before and after the deposition of the ZnO film, which suggests that the deposition is conformal. In this study by the AFM method showed clear differences. Thus, the analysis of AFM images obtained before and after the deposition of ZnO showed that pure CNTs are combined into bundles with a diameter of 1 μm under the action of van der Waals forces when scanning in the semicontact mode (Fig. 1b). When scanning CNTs coated with ZnO bundling does not occur (Fig. 1c). This is due to the simultaneous decrease in the van der Waals forces arising between CNTs conformally coated with ZnO and an increase in bending stiffness of CNTs due to the coating. As a result, the elastic forces arising in the nanotubes during the formation of the bundle become larger than the van der Waals forces and no bundles are formed.

Studies of the piezoelectric response of CNTs before and after deposition of ZnO have shown that in both cases a piezoelectric current arises when the nanotube is deformed (Fig. 2). In this

case, prior to deposition, a piezoelectric current of up to 14 nA is detected immediately upon approaching a CNT bundle (Fig. 2a), due to the fact that nanotubes have strain when combined into a bundle [2]. The current value slightly increases (up to 17 nA) during a further deformation of a CNT bundle by the force spectroscopy AFM. The piezoelectric current is absent when approaching a CNT conformally coated with ZnO (Fig. 2b). However, a current of up to 22 nA arises with further deformation of the coated CNT (Fig. 2b). The magnitude of the detected current increases as compared with pure CNTs, which may be due both to a change in the type of deformation of the CNT from bending to compression, and to the influence of the ZnO piezoelectric coating.

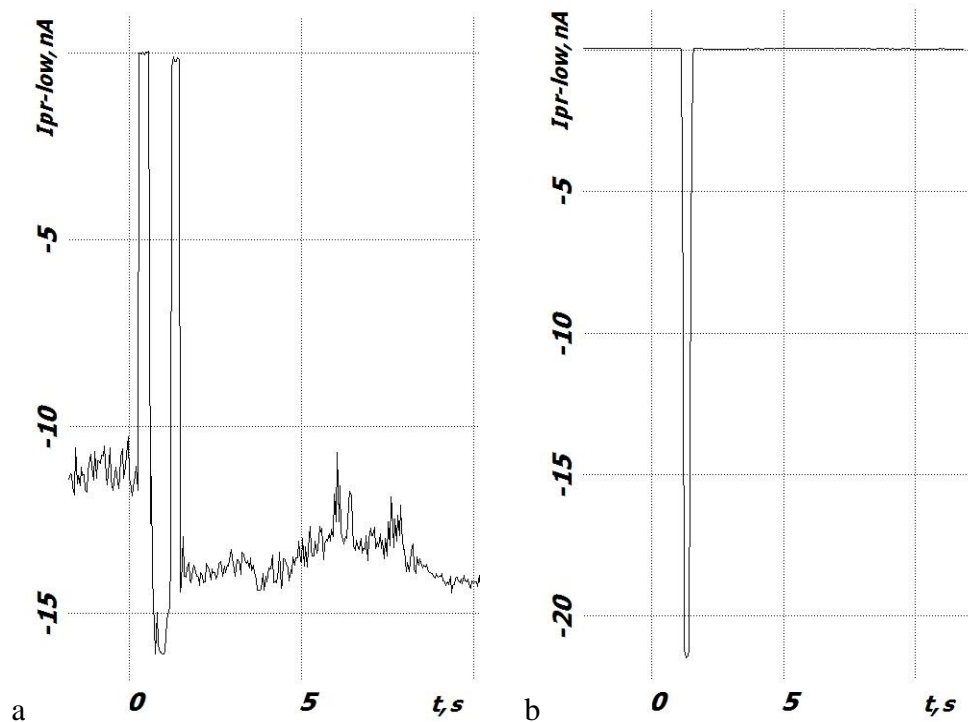


Figure 2. The current-time dependences of the deformation process of CNTs before (a) and after (b) coating with ZnO.

Thus, it has been shown that the conformal coating of ZnO leads to an increase in the bending stiffness of CNTs, as a result of which CNT bundles are not formed during the AFM scanning. In this case, the piezoelectric response of CNTs is increased by more than 35%. The obtained results can be used to develop and creation of nanoelectronics devices based on vertically aligned CNTs in particular sensors and adhesion coatings. The results were obtained using the equipment of the Research and Education Center and the Center for collective use "Nanotechnologies" of Southern Federal University.

The reported study was funded by RFBR according to the research projects No. 18-32-00652 mol_a, No.18-29-11019 mk and by grant of the Southern Federal University (project No. VnGr-07/2017-26).

1. M.V. Il'ina, O.I. Il'in, Yu.F. Blinov, et al., *Carbon* **123**, 514 (2017).
2. M.V. Il'ina, O.I. Il'in, Y.F. Blinov, et al., *Materials* **11**, 638 (2018).
3. M.V. Il'ina, O.I. Il'in, V.A. Smirnov, Yu.F. Blinov, B.G. Konoplev, O.A. Ageev, *Scanning Probe Techniques for Characterization of Vertically Aligned Carbon Nanotubes*, in: *Atomic-force Microscopy and Its Applications*, eds. T.Tański, M.Staszuk, B. Ziębowicz (IntechOpen), (2018).

Recording and light scattering on dynamic holographic gratings in $\text{Sr}_{0.61}\text{Ba}_{0.39}\text{Nb}_2\text{O}_6:0.002 \text{ wt.}\% \text{ CeO}_2$ crystal

L.I. Ivleva¹, P.A. Lykov¹, D.A. Nikolaev¹, V.B. Tsvetkov^{1,2}

¹Prokhorov General Physics Institute of the Russian Academy of Sciences, 119991 Moscow, Russia; ivleva@lst.gpi.ru

²National Research Nuclear University MEPhI, Moscow 115409, Russia.

The crystals of strontium-barium niobate solid solutions $\text{Sr}_x\text{Ba}_{1-x}\text{Nb}_2\text{O}_6$ (SBN:x) belong to highly efficient non-linear photorefractive media. These crystals can be considered as a promising material for recording of three-dimensional holographic grating, which is of the interest for practical applications such as optical memory.

We present the results of studying of the scattering properties of dynamic holographic gratings being demonstrated with lasers with different spectral output. The gratings were written in photorefractive SBN crystal sample by second harmonic of CW Nd:YAG laser ($\lambda = 532 \text{ nm}$, $W_{out} \approx 200 \text{ mW}$, intensity $\sim 3 \text{ W/cm}^2$, the beam divergence $\sim 0.8 \text{ mrad}$) while using the loop scheme.

The parallelepiped shaped SBN:Ce sample ($a \times b \times c = 8 \times 6 \times 8 \text{ mm}^3$) was used in experimental study. The element was prepared from the photorefractive crystal of $\text{Sr}_{0.61}\text{Ba}_{0.39}\text{Nb}_2\text{O}_6:0.002 \text{ wt.}\% \text{ CeO}_2$ which was grown from the melt by modified Stepanov technique. The special die of capillary type was used to produce profiled crystal of high optical quality. The poling process was carried out by applying the DC electric field ($E \sim 8 \text{ kV/cm}$) along c-axis of the crystal within 24 h at room temperature. As a probe light source the lasers CW Nd:YAG laser ($\lambda = 1064 \text{ nm}$), CW He-Ne ($\lambda = 632.8 \text{ nm}$) (with output power being up to 3 W and 50 mW, respectively) and pulse-periodic alexandrite laser (pulse energy $\sim 50 \text{ mJ}$) were used. Experimental dependences of the reflection coefficient R of probe beams on variations of angle of incidence $\Delta\phi$ with respect to the Bragg angle (angular scattering spectrum) as well as spectral characteristics of incident and scattered radiation were investigated.

Maximum value of the reflection coefficient $R_{max} \sim 50\%$ was achieved for fundamental mode of He-Ne laser. The width of angular scattering spectrum $\Delta\phi$ was less than 1 mrad (FWHM) and well corresponded to the signal beam divergence of $\sim 0.7 \text{ mrad}$. It is worth noting that R_{max} did not exceed 3% for multimode He-Ne laser with full divergence $\sim 2.5 \text{ mrad}$.

In the case of alexandrite laser ($\lambda \approx 748 \text{ nm}$) with spectral width of 4.25 nm the spectral narrowing of the scattering light was observed depending on the signal beam divergence. Maximum value of the reflection coefficient $R_{max} \sim 6\%$ was achieved for laser beam divergence $\sim 1 \text{ mrad}$ with spectral width of the scattered light being 2.2 nm (FWHM). In this case wide wings, which are spectral characteristic of laser radiation, did not observe in the spectrum of scattered radiation. To increase the reflectivity efficiency of the gratings, the SBN sample was placed into an additional linear resonator. In this case, the power of scattered radiation was about 25% of the radiation power of the probe laser.

Experiments with using of CW TEM₀₀ Nd:YAG laser ($\lambda = 1064 \text{ nm}$) and beam divergence 0.75 mrad (FWHM) showed that maximum value of the single pass reflection coefficient was $R_{max} = 5\%$. This value was not depended on the probe beam power in the range of 0.2–3 W. Thus, the Nd:YAG laser emission did not provide the erasing action on the holographic gratings.

This work was supported by VolkswagenStiftung, Grant No. Az. 90.261 and Presidium RAS Program No. 5: "Photonic technologies in probing inhomogeneous media and biological objects".

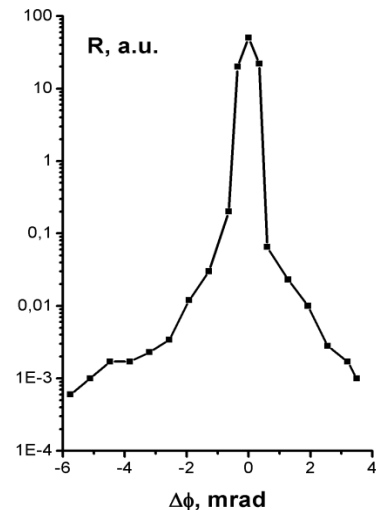


Figure 1. The angular spectrum of the scattering of Nd:YAG beam on holographic grating recorded in SBN:Ce crystal.

Experimental dependences of the reflection coefficient R of probe beams on variations of angle of incidence $\Delta\phi$ with respect to the Bragg angle (angular scattering spectrum) as well as spectral characteristics of incident and scattered radiation were investigated.

Functionalized PPO and polyolefin low dielectric thermosetting blend

W. Hu, J. Zhou*, J. Shen, W. Jin, W. Chen

*State Key Laboratory of Advanced Technology for Materials Synthesis and Processing, School of Materials Science and Engineering, Wuhan University of Technology, Wuhan 430070, P. R. China
zhoujing@whut.edu.cn*

Polyphenylene ether (PPO) resin is widely used as matrix resin for the production of printed circuit boards (PCBs) in the electronics industry because it has high comprehensive properties, including excellent dielectric properties, outstanding mechanical properties and good resistance against acids and alkalis [1]. However, there are weaknesses for PPO such as difficulty in processing, poor resistance to organic solvents and insufficient thermal resistance, which limits its applications in the field of microelectronic devices. To overcome these barriers, many efforts have been made to modify PPO, such as compounding with other thermosetting resins, especially epoxy resin [2]. But the introduction of polar group of these thermosetting resins, leading to poor dielectric properties. Hence, it is significant to develop a facile and effective method to reinforce the properties of PPO while retaining excellent dielectric properties.

Polyolefin has a very weak polarity and groups capable of crosslinking, so it can be used as an effective curing agent to blend with PPO. In this work, a modified PPO curing system were obtained by introducing functional groups containing double bonds to both ends of PPO and copolymerizing the functionalized PPO with polyolefin at a high temperature in the presence of a peroxide. In order to improve the processing properties of PPO, low molecular weight PPO, which can dissolve easily at room temperature, was used as raw material. The result indicated that by adding Polyolefin, the organic solvent resistance and thermal stability of the resulting blend was significantly improved, while good dielectric performance was retained. With the amount of polyolefin increased, the dielectric constant of the thermosetting blend decreased, but excessive addition of the polyolefin reduced the thermal stability of the blend. When the mass ratios of polyolefin in the composite were 0.4, the curing system displayed low dielectric constant of less than 2.75 and high thermal decomposition temperature (more than 400 °C).

1. Y.Q. Wang, Y.Q. Tao, J.F. Zhou, et al., *ACS Sustainable Chem. Eng.* **6**, 9277 (2018).
2. C.H. Chen, K.W. Lee, C.H. Lin, et al., *Polymers* **10**, 411 (2018).

In situ supported VO_x on carbon nanotubes for the low-temperature selective catalytic reduction of NO with NH₃

W. Jin¹, B. Jiao¹, W. Chen^{2,*}, M. Li¹, J. Zhao¹, X. Zhang¹

¹State Key Laboratory of Silicate Materials for Architectures, Wuhan University of Technology, Wuhan 430070, P. R. China

²State Key Laboratory of Advanced Technology for Materials Synthesis and Processing, School of Materials Science and Engineering, Wuhan University of Technology, Wuhan 430070, P. R. China
chenw@whut.edu.cn

Selective catalytic reduction (SCR) of NO_x with NH₃ is nowadays considered as the most promising technology for the elimination of NO_x [1]. As a typical commercial NH₃-SCR catalyst, V₂O₅-WO₃(MoO₃)/TiO₂ catalysts are commonly used due to the high catalytic activity and SO₂ tolerance [2]. However, there are some unavoidable disadvantages in commercial V-Ti catalysts. For example, the active component is unevenly dispersed and easily detached from the surface of the carrier under the scouring of the flue gas, thus shortening the service life of the catalyst. In addition, the operating temperature of the V-Ti catalyst is relatively high, about 300-400 °C, and its catalytic activity is poor at low temperature. Therefore, it is extremely urgent to develop a SCR catalyst with high low temperature activity and good stability.

In order to solve the above problems, vanadium oxide was supported on the surface of the carbon nanotube by in-situ growth because the introduction of carbon nanotubes can improve the low temperature catalytic activity of the catalyst. And the in situ synthesis method can enhance the interaction between VO_x and the carrier, thus enhancing the dispersion of VO_x. In our work, the VO_x were in situ supported on carbon nanotubes (CNTs) by a Cetylpyridinium Chloride (CPC) assisted reflux route. It was found that the in situ prepared catalyst exhibited better NH₃-SCR activity at low temperature, better stability, higher SO₂-tolerance and improved water-resistance than that of the catalysts prepared by impregnation or a mechanically mixed method. The EDS-mapping results indicated that the vanadium oxide species had good dispersion on the CNTs surface. The XPS results demonstrated that there were lower valence vanadium species (V⁴⁺ and V³⁺) and chemisorbed oxygen species. According to the literatures, vanadium oxides with low valence states can easily adsorb oxygen to generate active oxygen species during SCR reaction, which is important to the low temperature SCR activity [3]. The H₂-TPR results suggested that there was a strong interaction between the vanadium oxide on the surface of CNTs. The NH₃-TPD results demonstrated that the catalysts presented a larger acid amount and stronger acid strength. The in situ prepared VO_x/CNTs catalyst could be considered as a promising candidate for the low-temperature SCR of NO with NH₃.

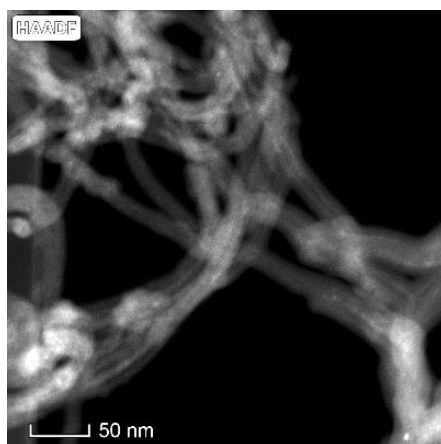


Figure 1. EDS-mapping of V₂O₅/CNTs catalyst.

1. D.S. Zhang, L. Zhang, L.Y. Shi, et al., *Nanoscale* **5**, 1127 (2013).
2. X.M. Zhou, X.Y. Huang, A.J. Xie, et al., *Chemical Engineering Journal* **326**, 1074 (2017).
3. H.F. Chen, Y.Xia, R.Y. Fang, et al., *Applied Surface Science* **459**, 639 (2018).

Resolution of the etching method of graphene/SiC using FIB

I.L. Jityaev, A.M. Svetlichnyi, A.S. Kolomiitsev

*Southern Federal University, Institute of Nanotechnologies, Electronics, and Equipment Engineering,
347900, Taganrog, Russia
izhityaev@sfnu.ru*

Modern electronics is aimed at reducing the size of the elements. This improves the performance of integrated circuits. An important aspect is the use of modern materials with improved electrophysical properties. Graphene is a two-dimensional carbon material. New areas of its use are constantly emerging. The prospect of its use in electronics is associated with its high mobility of charge carriers at room temperature, electrical and thermal conductivity, and mechanical strength.

In this study, the method of thermal destruction of silicon carbide in vacuum was used for graphene growth. This method allowed us to obtain graphene films directly on an isolated substrate without additional transfer operations, which contribute to the appearance of additional defects in the graphene films. Semiinsulating silicon carbide 6H-SiC was used as the substrate. Silicon carbide is a promising substrate for micro- and nanoelectronic devices, since it is a material with high thermal conductivity, mechanical strength, and is highly resistant to aggressive environments in a wide temperature range [1]. However, certain difficulties appear when profiling SiC substrates due to its high strength and stability. The use of liquid etchants for silicon carbide requires additional high-temperature heating. Also, with liquid etching, there is a limit on the minimum size of the formed elements.

In this work, in order to eliminate the indicated limitations, the method of focused ion beams was used for etching graphene films on silicon carbide. An important advantage of the method is high accuracy and reproducibility of processing, the possibility of maskless etching of structures, the formation of nanoscale elements [2, 3].

The purpose of this work is to study the resolution of the FIB method in the processing of graphene/silicon carbide. This task is relevant in the formation of elements of nanoelectronics [4-6]. A large influence on the parameters of the local processing area is influenced by the ion beam current. Therefore, in this work, an array of recess in the graphene/SiC structure was formed for different values of the ion beam current.

The AFM method was used to study the local areas of experimental samples after FIB treatment. The dependence of the number of detected areas after exposure to an ion beam on the sample surface on the ion beam current was plotted on the basis of the AFM-images. Detection of the treated areas at small values of the ion beam current was difficult. It is revealed that the decrease in the resolution of the method occurs with an increase in the ion beam current. The use of an ion beam in the range of 10-100 pA is optimal for the formation of nanoscale structures.

1. I.L. Jityaev, O.A. Ageev, A.M. Svetlichnyi, et al., *J.Phys.: Conf. Series* **741**, 012011 (2016).
2. I.L. Jityaev, A.M. Svetlichnyi, V.I. Avilov, et al., *IOP Conf. Series: Mat. Sci. Eng.* **443**, 012012 (2018).
3. V.I. Avilov, O.A. Ageev, I.L. Jityaev, et al., *Proc. SPIE* **10224**, 10224T (2016).
4. I.L. Jityaev, A.M. Svetlichnyi, A.S. Kolomiitsev, et al., *IOP Conf. Series: Mat. Sci. Eng.* **256**, 012021 (2017).
5. R.V. Konakova, O.B. Okhrimenko, A.F. Kolomys, et al., *J. Superhard Mater.* **38**, 235 (2016).
6. R.V. Konakova, O.B. Okhrimenko, A.M. Svetlichnyi, et al., *Semiconductors* **49**, 1242 (2015).

Self-assembly of hollow bismuth ferrite spheres

A.V. Dmitriev, E.V. Vladimirova, M.V. Kandaurov

Institute of Solid State Chemistry, Urals Branch of the Russian Academy of Sciences, 620990, Ekaterinburg, Russia
dmitriev@ihim.uran.ru

The development of novel approaches to the control of the architecture of nanoparticle sets by means of affecting self-assembling is the crucial task of modern science. This can be achieved using the theory of self-organization in dissipative systems, thus providing a basis for creating future prospective materials. The identification of contributions of various factors in self-assembly processes and physical modeling can assist in developing approaches of expectable impact a reacting system to design modern materials with outstanding properties and morphology.

In this paper, we promote the novel technique of controllable self-assembly during ultrasonic spray-pyrolysis. This method allows for obtaining spherical particles consisting of different materials. In particular, we evaluate ultrasonic spray-pyrolysis for the production of BiFeO₃ (BFO) microspheres due to recent attention to this material.

The theory of the spray-pyrolysis is based on the model of drying droplet containing given insoluble content. The reaction system holds two contrary processes while the solvent is evaporating from the droplet surface. The first process is connected with the decrease of droplet size; the second consist of the alignment of content concentration within droplet due to diffusion. Depending on the leading process described above there can be formed solid agglomerates or hollow spheres which also can have both close and open porous. However, adjustment of drying temperature and solution concentration are not the only factors to affect the phase morphology. To the best of our knowledge metal ions tend to form chelate compounds with tartaric acid. Moreover, the presence of complex metalorganic compounds in a reaction system leads to the significant decreasing of the ion diffusion velocity and as a result, there can be obtained spherical particles with a thin wall.

We synthesized BFO powders by the spray-pyrolyzing of the water solution of iron and bismuth nitrates with tartaric acid. Prepared samples were characterized as single-phase due to X-ray analysis. The morphology of obtained BFO powders seems to be dependent on drying temperature. Furthermore, morphology tends to vary if solution concentration or the amount of tartaric acid is adjusted.

Morphology seems to affect the magnetic properties of BFO powders. Physical parameters such as wall thickness, the package density of crystallite units, and the grain size in agglomerates appear to be crucial that define the magnetic behavior of BFO powder.

This research was carried out under the financial support of the Russian Foundation for Basic Research №17-08-00893.

Synthesis and magnetic properties of $\text{BiFe}_{1-x}\text{Co}_x\text{O}_3$ ($x = 0-0.07$)

M.V. Kandaurov, A.V. Dmitriev, E.V. Vladimirova

*Institute of Solid State Chemistry, Urals Branch of the Russian Academy of Sciences
620990, Ekaterinburg, Russia
mukaejib@gmail.com*

In recent years there has been growing interest in multiferroic materials, in particular to bismuth ferrite. BiFeO_3 (BFO) exhibit multiferroic properties at room temperature that is leading to prospective applications in various fields (microelectronics, spintronics, medicine, etc.).

The big part of current researches is devoted to BFO magnetic properties. Of particular interest is their enhancing. BiFeO_3 is known to be anti-ferromagnetic with a G-type magnetic structure. The decreasing crystallite size leads to the exhibition of soft ferromagnetic behavior due to cycloid canting. However, ferromagnetic behavior can be achieved through the partial substitution of Fe-ions in B-sublattice that is described in large scientific data. Moreover, magnetic properties are strongly connected with the synthesis technique and the morphology of obtained samples.

The purpose of this research consists in the identification of Co-substituted bismuth ferrite samples obtained through such methods as self-combustion (Pechini) and ultrasonic spray-pyrolysis. These methods provide the opportunities of nanostructured BiFeO_3 fabrication with a distinct morphology. In particular, the utilizing of ultrasonic spray-pyrolysis leads to the formation of spherical agglomerates with outstanding properties due to the specific interface of particles.

Owing to little data on the Co-doping of BFO B-site Co was chosen as a dopant. Synthesis of single-phase samples was challenging due to the appearance of $\text{Bi}_{25}\text{FeO}_{40}$, $\text{Bi}_2\text{Fe}_4\text{O}_9$, and $\text{Bi}_{13}\text{Fe}_{6.5}\text{Co}_{6.5}\text{O}_{40}$ impurities. To the best of our knowledge the addition of chelating agents can assist in annealing temperature decreasing and uniform dopant distribution. Tartaric acid meets these requirements, thus it was added in ratio 1:1, 2:1, and 3:1 to metals.

Obtained samples constitute the porous spheres of BiFeO_3 which is confirmed with SEM and helium pycnometry. Samples exhibit soft ferromagnetic response due to the results of magnetic measurements. The value of remnant magnetization increases with the amount of Co-substitution as well as with the amount of TA used. Moreover, the substantial leap of remnant magnetization is observed for spray-pyrolyzed BFO in comparison to samples obtained through the Pechini method due to lesser crystalline size.

This research was carried out under the financial support of the Russian Foundation for Basic Research №17-08-00893.

Electric polarization induced by phase separation domains in multiferroics of RMn_2O_5 ($\text{R} = \text{Gd}, \text{Bi}$)

B.Kh. Khannanov, V.A. Sanina, E.I. Golovenchits, M.P. Scheglov

Ioffe Institute, 194021 str., St. Petersburg, Russia
khannanov@mail.ioffe.ru

A comparative study of the electric polar states in multiferroics GdMn_2O_5 and BiMn_2O_5 with a common subsystem of Mn ions (in equal ratios of Mn^{3+} and Mn^{4+} ions), but strongly differing in their properties of R ions, was carried out. Ion Gd^{3+} (ground state $^8\text{S}_{7/2}$), which is a strongly magnetic ion with spin $S = 7/2$, but weakly interacting with the lattice. Ion Bi^{3+} is a non-magnetic ion containing $6s^2$ electrons, which cause a strong non-central local distortion of the lattice. The long-range ferroelectric order having an exchange-striction magnetic nature had been observed at low temperatures ($T \leq T_C = 30\text{-}35$ K).

The homogeneous single-domain GdMn_2O_5 the maximal ferroelectric polarization, as compare with other RMn_2O_5 , was observed due to the strong homogeneous Gd-Mn exchange. In BiMn_2O_5 , the lattice distortions near the Bi ions changed the distances between pairs of ions Mn of different valences, violating the homogeneity of the internal field of the exchange striction. As a result, the polarization induced by the exchange striction, was in 20 times less. Along with this, an electrical polarization of a different nature had been found at temperatures $T \gg T_C$ in both studied crystals [1]. A generally accepted point of view is that RMn_2O_5 has sp.gr. *Pbam* (at room temperature) not admitting the existence of a polar order. We believe that the high-temperature polarization we observed was caused by the frozen superparaelectric state, which was formed by the restricted polar domains resulting from phase separation and charge carrier self-organization. Charge ordering in RMn_2O_5 and the e_g electron transfer between $\text{Mn}^{3+}\text{-Mn}^{4+}$ ion pairs are key factors responsible for polar electric states of these multiferroics at all temperatures. The double exchange between $\text{Mn}^{3+}\text{-Mn}^{4+}$ ions induces the phase separation in RMn_2O_5 which is similar to phase separation in LnAMnO_3 ($A = \text{Sr}, \text{Ba}, \text{Ca}$) manganites containing Mn^{3+} and Mn^{4+} ions as well. Phase separation exists at all temperatures and makes the formation of local conductive domains containing $\text{Mn}^{3+}\text{-Mn}^{4+}$ ion pairs with ferromagnetically oriented spins energetically favorable. The polar phase separation domains are located in a dielectric antiferromagnetic (paramagnetic) matrix of the original crystal, forming at sufficiently low temperatures the frozen superparaelectric state. Such type state was considered theoretically in the system of isolated ferroelectric nanoscale domains in a dielectric matrix [2]. In this state, hysteresis loops and remanent polarizations are observed. The frozen superparaelectric state turns into the conventional superparaelectric one near T^* ($T^* = 100\text{-}330$ K), in which the hysteresis loops are destroyed. The T^* values correspond to the temperatures at which the potential barriers of the restricted polar domain reorientations become equal to the kinetic energy of the itinerant electrons (leakage). The polarization magnitudes, its anisotropy, and the temperatures T^* were very different for GdMn_2O_5 and BiMn_2O_5 . The magnetic field H increased the barriers at the phase separation domain boundaries due to the double exchange growth, thus increasing the T^* . The electric hysteresis loops were measured using the version of the PUND method presented in [3], which was adapted to studies of the local polar domains. The emergence of the local phase separation domains was confirmed in the high-sensitivity 3-crystal X-ray diffractometer measurements and in the permittivity and conductivity investigations. We revealed correlations between properties of the local phase separation domains and hysteresis loops.

This work was supported by RFBR (Grant N 18-32-00241).

1. B.Kh. Khannanov, V.A. Sanina, E.I. Golovenchits, M.P. Scheglov *J. Magn. Magn. Mater.* **421** 326 (2017).
2. M.D. Glinchuk, E.A. Eliseev, A.N. Morozovska, *Phys. Rev. B* **78** 134107 (2008).
3. S.M. Feng, Y.S. Chai, J.L. Zhu, et al., *New J. Phys.* **12**, 073006 (2010).

Piezoelectric actuation of graphene-based polar structures: frequency and geometry effects

A. Ushakov¹, M. Kosobokov¹, A. Akhmatkhanov¹, I. Kravchenko², V.Ya. Shur¹, A.L. Kholkin^{1,3}

¹*School of Natural Sciences and Mathematics, Ural Federal University, 620000 Ekaterinburg, Russia*

²*Center for Nanophase Materials Sciences, Oak Ridge National Laboratory, Oak Ridge, Tennessee 37831, United States*

³*Department of Physics & CICECO – Aveiro Institute of Materials, 3810-193 Aveiro, Portugal*

Ferroelectric materials based on lead zirconate titanate (PZT) are widely used in sensors and actuators because of their strong piezoelectric activity and compact design. However, their application is limited because of high processing temperature, brittleness, lack of conformal deposition and, more importantly, limited possibility to be integrated with micro- and nano electromechanical systems (MEMS and NEMS). Recent studies on piezoelectricity in 2D materials have demonstrated their great potential in these applications, essentially due to their flexibility and integrability with MEMS and NEMS [1]. In this work, we deposited a few layer graphene (FLG) on amorphous Si₃N₄ membranes and studied their electromechanical response by sensitive laser interferometry and rigorous FEM calculations. Modal analysis by FEM and comparison with experimental results show that the driving force for piezoelectric-like response can be the polar interface layer formed between residual oxygen in Si₃N₄ and FLG. The response reaches about 14 nm at resonance and could be further enhanced by adjusting geometry of the device. These phenomena are fully consistent with the earlier Piezoresponse Force Microscopy (PFM) results on free-standing graphene on SiO₂ grating substrates [2] and open up an avenue for using graphene-based structure in MEMS, NEMS and microenergy harvesting applications [3].

The work was financially supported by the Russian Foundation for Basic Research within the project 16-29-14050 ofr. The equipment of the Ural Center for Shared Use “Modern nanotechnology” of UrFU was used.

1. H.H. Perez Garza, E.W. Kievit, G.F. Schneider, U. Staufer, *Nano Letters* **4**, 4107 (2014).
2. G. da Cunha, P. Zelenovskiy, K. Romanyuk, S. Luchkin, Ya. Kopelevich, A. Kholkin, *Nature Communications* **6**, 7572 (2015).
3. J.P.G. Tarelho, M.P.S. dos Santos, J.A.F. Ferreira, A. Ramos, S. Kopyl, S.-O. Kim, S. Hong, A. Kholkin, *Materials Today* **21**, 1019 (2018).

Conductive Atomic Force Microscopy study of local resistive switching by a complex signal in the yttria stabilized zirconia films

D.O. Filatov, M.N. Koryazhkina, D.A. Antonov, I.N. Antonov,
D.A. Liskin, M.A. Ryabova, O.N. Gorshkov

National Research Lobachevsky State University of Nizhny Novgorod, 603950, Russia
dmitry_filatov@inbox.ru

In recent years, the investigations of resistive switching (RS) have attracted much attention [1]. The effect of RS consists in the bistable (or multistable) switching of the resistance of a thin (from several nanometers to several tens nanometers in thickness) dielectric films sandwiched between two conductive electrodes under the external voltage applied between the electrodes [2]. The electronic devices, the functioning of which is based on the RS are called memristors [3]. Today's understanding of the RS mechanism in the metal oxides is based on the concept of forming the conductive filaments consisting of the oxygen vacancies between the conductive electrodes in the electric field between the electrodes [4]. The switching of a memristor from the low resistance state (LRS) to the high resistance one (HRS) is achieved by the rupture of the filament by a voltage pulse (the RESET process). The filament can be restored by a voltage pulse of the opposite polarity that results in the switching from the HRS back to LRS (the SET process). The memristors are considered to be promising for application in the next generation non-volatile computer memory (Resistive Random Access Memory, ReRAM) [5], in the neuromorphic computers [6], etc. However, at present the application of the memristors is limited by an insufficient stability of the memristor parameters, which is a fundamental property of the RS [7]. The origin of the RS instability is the stochastic nature of the rupture and restoring of the filaments in the functional dielectric layer: a very limited (countable) number of oxygen vacancies are involved into the RS [8]. Traditional approaches to the improvement of the RS stability include the appropriate choice of the insulator and electrode materials, the engineering of the grain boundaries in the functional insulator, the application of electric field concentrators inside the insulator, etc. [9-11]. The alternative approaches include the circuit solutions, the application of adaptive switching protocols, etc. [12].

In the present work, the local RS in the yttria stabilized zirconia (YSZ) films was investigated using Conductive Atomic Force Microscopy (CAFM) [13] using the triangular switching voltage pulses with superimposed sinusoidal high-frequency (HF) signal. The YSZ films (~12 mol.% Y_2O_3) of ≈ 4 nm in thickness were deposited onto the Si(001) substrates with pre-deposited SiO_2 (500 nm), Ti (25 nm), and TiN (25 nm) layers by magnetron sputtering at 300 °C using Torr International[®] 2G1-1G2-EB4-TH1 vacuum setup. The RS was investigated performed using Omicron[®] UHV AFM/STM LF1 in ultra high vacuum ($\sim 10^{-10}$ Torr) in the contact mode (Fig. 1). The NT-MDT[®] NSG-11 DCP[™] probes were used.

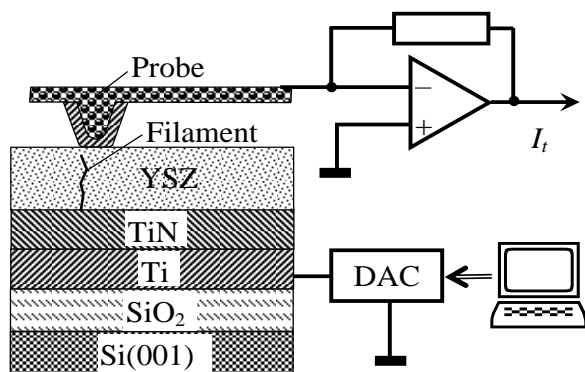


Figure 1. Scheme of the experimental setup.

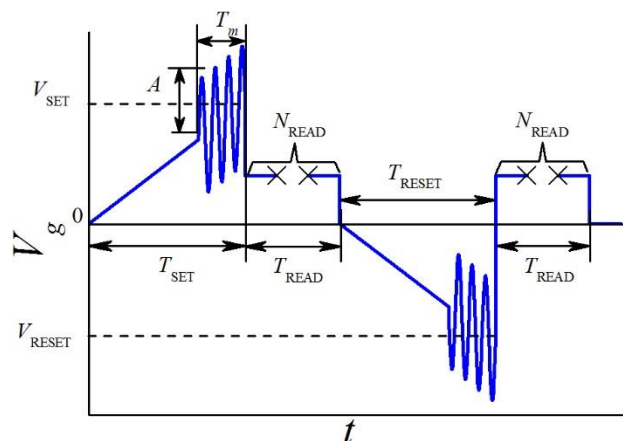


Figure 2. The RS protocol.

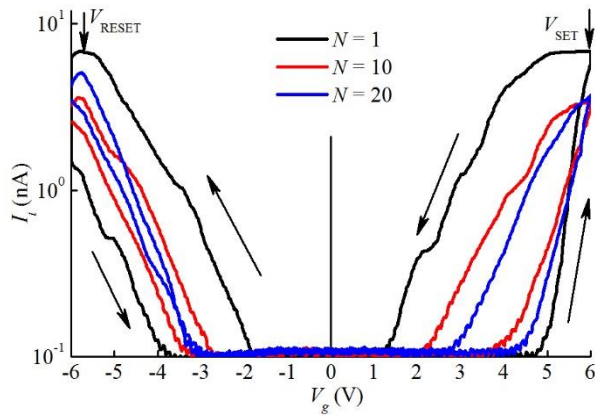


Figure 3. Cyclic I - V curves of the virtual memristor. N is the number of switching cycles.

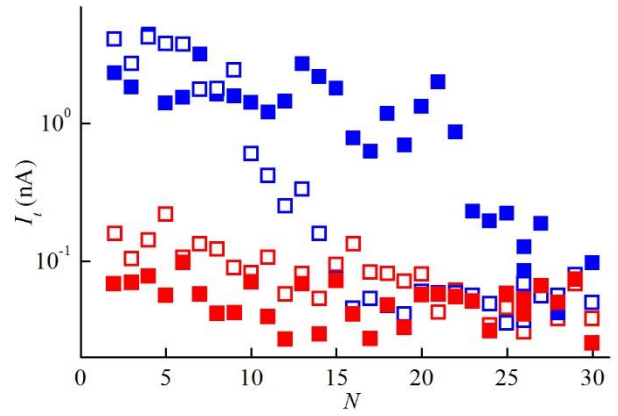


Figure 4. Endurance diagram for a virtual memristor ($\blacksquare, \square - I_{ON}$, $\blacksquare, \square - I_{OFF}$) with ($\blacksquare, \blacksquare$) and without (\square, \square) HF sinusoidal signal ($A = 0.2$ V, $f = 6.5$ kHz).

The bias voltage V_g applied between the CAFM probe and the TiN sublayer was supplied by the digital-to-analog converter (DAC) of NT-MDT® Solver Pro™ AFM controller. The endurance of the probe currents in the LRS and HRS I_{ON} and I_{OFF} , respectively to the multiple cyclic write/erase operations was investigated. The switching/measurement protocol is shown in Figure 2. After the triangular switching voltage pulses with an amplitudes $V_{SET} = 5$ V and $V_{RESET} = -6$ V, the values of I_{ON} and I_{OFF} were recorded at read voltage $V_{READ} = 3$ V. The HF sinusoidal signal with the amplitude $A = 0.2$ V and frequency $f = 6.5$ kHz (matching the frequency of the O^{2-} ion jumps to the nearest neighboring oxygen vacancies in YSZ at 300 K [14]) was superimposed onto the triangle V_g pulses.

A pronounced hysteresis typical for the bipolar RS was observed in the cyclic current-voltage (I - V) curves of the CAFM probe contact to the YSZ film composing a virtual memristor (Fig. 3). The hysteresis magnitude decreased with increasing number of switching cycles N that was the manifestation of the virtual memristor degradation. Accordingly, the I_{ON} values approached I_{OFF} with increasing N (Fig. 4). The adding of the HF sinusoidal signal to the triangular switching pulses led to an increase in the local RS stability: the decrease in I_{ON} began at larger N values than in the case of switching by triangular pulses without the HF sinusoidal signal. The observed effect was attributed to the resonant activation of the O^{2-} ion migration via the oxygen vacancies under the external alternating electric field.

This work was supported by RFBR (18-42-520059p_a).

1. D. Ielmini, R. Waser, *Resistive Switching: From Fundamentals of Nanoionic Redox Processes to Memristive Device Applications* (Wiley-VCH), (2016).
2. R. Waser, M. Aono, *Nature Materials* **6**, 133 (2007).
3. D.B. Strukov, G.S. Snider, D.R. Stewart, R.S. Williams, *Nature* **453**, 80 (2008).
4. I. Riess, *J. Electroceram.* **39**, 61 (2017).
5. J. Ouyang, *Emerging Resistive Switching Memories* (Springer), (2016).
6. A. James, *Memristor and Memristive Neural Networks* (IntechOpen), 314 (2018).
7. W. Yi, S.E. Savel'ev, G. Medeiros-Ribeiro, et al, *Nature Commun.* **7**, 11142 (2016).
8. P. Parreira, G.W. Paterson, S. McVitie, D.A. MacLaren, *J. Phys. D: Appl. Phys.* **49**, 095111 (2016).
9. Y. Sun, C. Song, J. Yin, et al, *ACS Appl. Mater. Interf.* **9**, 34064 (2017).
10. M. Trapatseli, S. Cortese, A. Serb, et al, *J. Appl. Phys.* **121**, 184505 (2017).
11. W. Wu, H. Wu, B. Gao, N. Deng, H. Qian, *J. Appl. Phys.* **124**, 152108 (2018).
12. F. Alibart, L. Gao, B.D. Hoskins, D.B. Strukov, *Nanotechnology* **23**, 075201 (2012).
13. M. Lanza, *Materials* **7**, 2155 (2014).
14. S. Tikhov, O. Gorshkov, I. Antonov, A. Morozov, M. Koryazhkina, D. Filatov, *Adv. Cond. Mat. Phys.* **2018**, 2028491 (2018).

Multimodal characterization of broadband, polycrystalline silver halide fibre bundle for confocal laser scanning microscopy in the near-mid infrared spectra

E.A. Korsakova¹, S., Markham², A.A. Mani², A.S. Korsakov¹,
L.V. Zhukova¹, C. Silien², J. Bauer³, S.A.M. Tofail²

¹*Scientific Laboratory of Fiber Technologies and Photonics, Ural Federal University named after the first President of Russia B.N. Yeltsin, 620002, Yekaterinburg, Russia*
korsakovaea@mail.ru

²*Department of Physics and Bernal Institute, University of Limerick, V94 T9PX, Limerick, Ireland*

³*Department of Biomedical Engineering, Wrocław University of Technology, 50-377, Wrocław, Poland*

Polycrystalline silver halide fibre bundles have been found to possess high transparency in the near to mid infrared (MIR) spectra and, as such, can expand the capability of conventional silica fibre based confocal laser scanning microscopy in the visible spectra to near and mid infrared microscopy within the same field of view. Such an extended capability can be enhance real time, large area imaging needs in burgeoning additive manufacturing industry, biological imaging especially for histopathology and cytology. These fibres can be also used in endoscope-based imaging. Making these fibres is difficult and requires high purity raw materials, specialized techniques and robust process control.

Maintaining the orientation of polarization of IR along the fibre is important for many applications, including confocal laser scanning microscopy (CLSM), where optical fibre bundles can be used as delivery channels. We have recently reported that $\text{AgCl}_{0.25}\text{Br}_{0.75}$ fibres can transmit IR but between 1 to 9 μm wavelength the fibres affect the polarization of the transmitted IR [1]. Here we use multimodal characterization underpinned by Multiphysics modelling the impact of materials and processing on the orientation of polarization of IR as it passes through such silver halide polycrystalline fibres.

Single crystals of silver halide solid solutions are isotropic. They have cubic NaCl lattice structure and have the same properties along all the axes. Depending on the shape and spatial orientation of the grains, polycrystalline silver halides may be anisotropic for IR radiation. The wavelengths propagated inside the optical fibres are in the range of 0.46-4.21 μm (for the wavelength range of 1-9 μm) [2]. Through scanning electron microscopy and scanning probe microscopy, we observe that a significant portion of these polycrystalline fibres is actually nanocrystalline. The structure is organized at two levels: microscopic grains with dimensions of 1-3 μm , and, nanocrystalline subgrains of 70-250 nm size. We conduct further scanning probe microscopy to understand the role of such nanocrystallinity and anisotropy in defining the local and global optical rotation.

This work was supported by the Russian Science Foundation under grant No. 18-73-11063.

1. S., Markham, A.A. Mani, E.A. Korsakova, A.S. Korsakov, L.V. Zhukova, C. Silien, J. Bauer, S.A.M. Tofail, *Proc of Photonics Ireland Conference 2018, Ireland*. 20 (2018).
2. A. S. Korsakov, D. S. Vrublevsky, A. E. Lvov, L. V. Zhukova, *Optical Material* **64**, 40 (2017).

Dependence of pyroelectric response on inter-electrode capacitance for integrated-optical circuits utilizing x -cut LiNbO_3 chips

S.M. Kostritskii,¹ A.V. Yatsenko,² Yu.N. Korkishko,¹ V.A. Fedorov¹

¹*RPC Optolink Ltd, Zelenograd, Moscow, Russia*
skostritskii@optolink.ru

²*Physics and Technology Institute, Simferopol, Russia*

The pyroelectric response of integrated-optical circuits (IOC) has been studied for IOCs utilizing x -cut LiNbO_3 chips with different topologies of electrodes. The schematic sketch of the IOC chip is given in Fig. 1. Each IOC contains the coplanar Au/Cr electrodes, consisting of an electro-optic modulator on main $-x$ surface (placed near center of bottom part of chip). The pyroelectric response was measured by the method which had been described in previous paper [1], i.e. the pyroelectric voltage U_{in} was directly recorded while changing the temperature T of the sample in the range from 295 to 380 K. The range of temperature scanning rate $V = dT/dt$ covered the interval from ≤ 0.1 to 1.5 K/min. A measuring resistor ($R_m = 1.06 \text{ G}\Omega$) was wired in parallel to the one of modulator electrodes and amplifier input, thus U_{in} appeared on this electrode and amplified by factor of 5 was measured with an electrometer. Two extra In-Ga electrodes were deposited on $+z$ and $-z$ surfaces of chip's lateral edges and one extra electrode was grounded. According to the previous finding [2], such a conductive coating must decrease the pyroelectric response, that is undesirable phenomenon at practical application of IOC [2, 3].

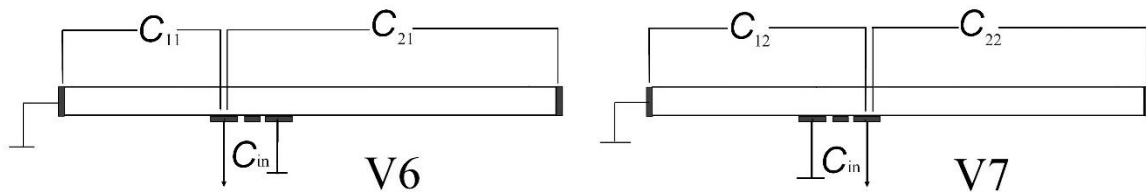


Figure 1. Schematic diagrams of the different topologies for IOC electrical connection. C_{in} is input integral capacitance of modulator and amplifier for measuring circuit, C_{ij} are capacitances of different parts of IOC chip. One of modulator electrodes is connected with C_{in} .

It has been experimentally established, that pyroelectric voltage U_{in} is proportional to the temperature scanning rate V (Fig. 2), and a magnitude of U_{in} depends on electrodes connection topology (Figs. 1,2).

A physical model is proposed in Figure 1. Here the intent is to choose the simplest model possible that will adequately describe the transient effect. The pyroelectric crystal (in conjunction with the electrodes) acts as a capacitor. When the crystal experiences a change in

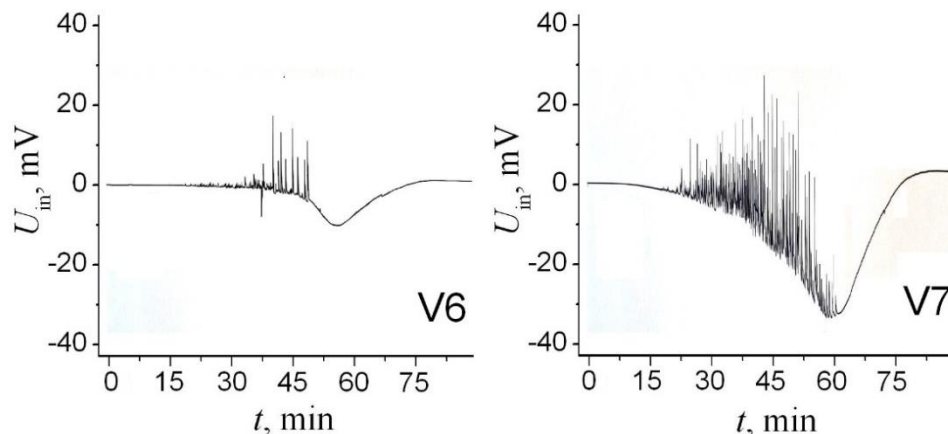


Figure 2. Pyroelectric voltage U_{in} measured for the two different electrodes connection topologies (see Fig. 1) as functions of scanning time t during heat-up of IOC. Rate $V = dT/dt$ of temperature change was gradually increased from $V \leq 0.1$ K/min (at $t \leq 5$ min) to the maximum value of 1.5 K/min at $53 \leq t \leq 62$ min, after V decreased and $V = 0$ at $t \geq 84$ min. Sharp pulses in the electrometer output are related to electric discharges over the IOC's surface.

temperature, it frees electric charges that appear on the extra electrodes deposited on the polar surfaces of lateral edges of IOC chip. The pyroelectric LiNbO₃ crystal is oxide, and it has very high resistance [1-3]. Thus, these accumulated charges cannot leak through the material. Thus, under homogeneous change in temperature, the pyroelectric LiNbO₃ crystal acts as a charge generating capacitor [4].

A simple circuit composed of capacitances is chosen to model how the charge distribution, and thus the electric field, may depend on the electrode connection topology. The scheme given in Fig. 1 divides the IOC capacitance into different contributions. Direct measurement of the capacitances of different parts of IOC chip gave the following results: $C_{11} \cong 5.1$ pF, $C_{22} \cong 2.6$ pF, $C_{21} \cong 4.1$ pF, and $C_{21}^* \cong 1.9$ pF. C_{21} and C_{21}^* are capacitances measured, when a second modulator electrode is ungrounded and grounded, respectively. The ratio of the capacitances for the different-length inter-electrode gaps scales roughly with the gaps length ratio. Note, that a simple evaluation of C_{21}^* and C_{21} capacitances ratio cannot be directly made because the shape of the field lines should be substantially different in these cases. Thus, the pyroelectric voltage U_{in} depends on capacitance C_{ij} of a chip part between the modulator electrode, which is connected to measuring circuit, and ungrounded extra electrode deposited on right edge of IOC (Fig. 1).

To estimate quantitatively a ratio between U_{in} magnitudes at the different electrodes connection topologies, we consider that during the temperature increase at a rate V the change of the charge q at an effective capacitor C_{ij} in the time is given by the difference of the charge released due to pyroelectric effect and the charge transferred through the measuring circuit. The voltage U_{in} across C_{in} equals to the voltage across the corresponding capacitor of the IOC chip:

$$U_{in} \sim R_{in} C_{21}^* \frac{dq}{dt}, \text{ and } U_{in} \sim R_{in} C_{22} \frac{dq}{dt},$$

for V6 and V7 electrodes connection topologies (Fig. 1), respectively. $\frac{dq}{dt} \sim \gamma \times V$, where γ is pyroelectric coefficient [1].

In fact, the experimental results obtained (Fig. 2) is consistent with our simple model of the IOC as the charge generating capacitor divided into the different contributions, according to the electrodes topology. Besides, these results show that a further suppression of undesirable pyroelectric response is possible by decrease of appropriate contributions in IOC capacitance, that may be achieved by increase of the inter-electrode gap or/and IOC chip width. Moreover, some additional suppression would be possible by decrease of a chip thickness and optimization of electrodes configuration [5].

At the other hand, we can apply the two-component model [3] for qualitative explanation of the pyroelectric response of IOC. The two components are: (1) pyroelectric: unscreened bound charge buildup occurs on z surfaces of lateral edges, and (2) electrostatic: capacitive loading of modulator electrodes causes the potential of these electrodes to change much less than the potential of the rest of the $-x$ surface, leading to a large potential difference between the modulator electrodes. Considering the close proximity of electrodes to bound charges, very large field may be generated between electrodes.

1. S.V. Evdokimov, R.I. Shostak, A.V. Yatsenko, *Sol. State Phys.* **49**, 1866 (2007).
2. K.W. Shafer et al., *US patent 612842A4* (2000).
3. P. Skeath et al., *Appl. Phys. Lett.* **49**, 1221 (1986).
4. A. Hossain, M.H. Rashid, *IEEE Transact. Indust. Appl.* **27**, 824 (1991).
5. R.A. Becker, *Opt. Lett.* **10**, 417 (1985).

Direct laser writing of periodic structures in a Cu-doped near-surface layer on z -cut LiNbO_3 crystals

P.P. Basnin¹, I.M. Chirkova¹, O.G. Sevostyanov¹, S.M. Kostritskii²

¹Phys. Dept., Kemerovo State University, Russia

²RPC Optolink Ltd, Zelenograd, Moscow, Russia
skostritskii@optolink.ru

In this work we demonstrate the possibility to form periodic homogeneously-altered refractive index structure in a Cu-doped near-surface region of lithium niobate crystals using direct laser writing technique. To increase photosensitivity the selective Cu-doping of a thin near-surface layer (0.25-0.5 μm) was applied, utilizing the ion exchange in the molten palmitic acid mixed with small amount of copper carbonate. A cw Ar^+ -laser was used for fine controllable modification of the near-surface layer. This laser produces radiation at wavelengths of 488 and 514.5 nm. A laser beam was focused into the sample surface by a microscope objective (100 \times , NA= 0.9). To form the regular periodic structure (Fig. 1), the samples were translated by two linear stages with velocity 10-260 $\mu\text{m/s}$ in X-Y plane.

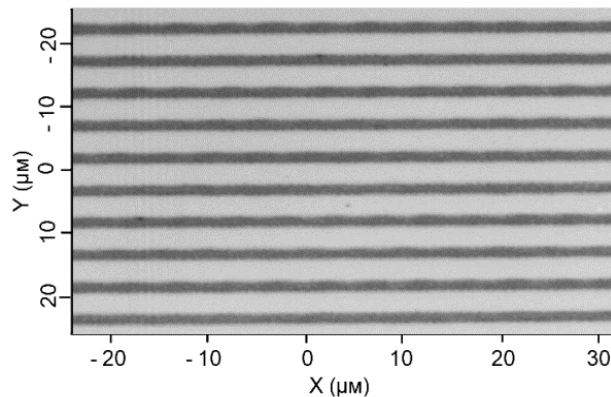


Figure 1. Microscopic image (reflection mode) of periodic structure written by focused laser beam in a near-surface layer of LiNbO_3 wafer doped by Cu with ion exchange technique.

The heavy Cu-doping and, hence, the strong absorption (optical density ≥ 1.5) of laser radiation within near-surface layer provide a marked heating (≥ 100 $^\circ\text{C}$) of the illuminated area. It causes thermally-induced out-diffusion of H^+ ions from this area in a space-charge field, and, thus, formation of a self-fixed structure with spatially-modulated refractive index, Fig. 1. The bulk photovoltaic and pyroelectric effects [1] are assumed to be the main contributing factors to the space charge field, spatial modulation of the $\text{Cu}^+/\text{Cu}^{2+}$ ratio and optical absorption. Note, that this self-fixed laser-induced refractive index change can be by one-two orders of magnitude higher than values reached with the standard holographic technique in a bulk of crystals doped with photorefractive ions. It allows for fabrication of highly effective Bragg gratings for the various integrated photonics applications.

Considering the significant temperature gradient within micro-regions with modified crystal structure, very large fields may be generated under surface well in excess of the coercive field strength. This transient field has pyroelectric origin and its strength may be enough for local reversal of spontaneous polarization and for formation of a periodic domain structure [2]. Additionally, we show that with different ion exchange algorithms a sufficient control on topological charge separation can be achieved in micrometer scale that lets implement the well-controlled recording procedures in lithium niobate waveguides.

This work is funded by Volkswagen Foundation/Trilateral Project "Investigation of the domain wall conductivity in uniaxial ferroelectrics".

1. L.B. Schein, P.J. Cressman, L.E. Cross, *J. Appl. Phys.* **49**, 798 (1978).

2. J. Imbrock, H. Hanafi, M. Ayoub, C. Denz, *Appl. Phys. Lett.* **113**, 252901 (2018).

Effect of surface ligands on fluorescence properties and stability of all-inorganic CsPbI₃ perovskite quantum dots

S. Kou, M. Wang, Zh. Yang

Electronic Materials Research Laboratory, Key Laboratory of the Ministry of Education International Center for Dielectric Research & Shaanxi Engineering Research Center of Advanced Energy Materials and Devices, Xi'an Jiaotong University, Xi'an 710049, China
mqwang@mail.xjtu.edu.cn

In recent years, with the rapid increase in the external quantum efficiency of perovskite LED luminescence, the perovskite materials and the device has attracted the attention of researchers from all over the world, and it has become a new research hotspot in the field of display materials and devices. Although the research on perovskite LED devices has made great progress, the stability of the device cannot meet the requirements of industrialization. Therefore, the challenge is to further improve device performance and seek technological breakthroughs to achieve long device lifetimes.

The design of new thermal injection schemes includes injection temperature, organic solvent, precursor species, optimization of synthesis process conditions from the perspective of synthesis methods, which will be improvement of quantum yield and luminescence stability of quantum dots. The surface modification of CsPbI₃ quantum dots was studied. The multi-ligand strategy was used to study the effects of ligand types and addition amounts on quantum dot dispersion stability and fluorescence quantum yield. The surface doping of CsPbI₃ quantum dots is studied for the influence of element type, doping amount and quantum dot size on the phase stability of CsPbI₃ quantum dots. Perovskite materials with different fluorescence bands were prepared, and their microstructure, fluorescence spectra and fluorescence quantum yield were characterized by SEM and steady-state transient fluorescence spectrometer. The CsPbI₃ quantum dots have an average grain size of 10-20 nm, a size distribution of less than 5%, a fluorescence emission wavelength of 450-700 nm, a fluorescence peak half-height width of less than 30 nm, and a fluorescence lifetime of more than 50 ns. The solution fluorescence quantum yield is higher than 95%, and the solution is stored in a closed container for more than one month.

Kinetics of photo-stimulated adsorption of enzyme molecules onto *n*- and *p*-type silicon

A.V. Kozłowski, S.V. Stetsyura

Saratov State University, 410012, Saratov, Russia
kozłowski@bk.ru

Atomic force microscopy (AFM) is an effective method for monitoring the deposition of functional organic layers on a silicon substrate [1]. Enzyme molecules (for example, glucose oxidase (GOx)) can be used to fabricate a receptor layer on the surface of an ion-sensitive semiconductor transducer. The adsorption of enzyme molecules onto the semiconductor surface is due to electrostatic interaction. Thus, the conductivity type of a semiconductor substrate, as well as a change in surface charge density induced by illumination, can influence the number of adsorbed enzyme molecules.

In our work, AFM was used to study the kinetics of photo-stimulated adsorption (PSA) of GOx molecules onto the surface of both *p*- and *n*-type silicon.

The experiments were performed with single-crystal silicon wafers of *n*-type ($\rho = 4 \Omega \text{ cm}$) and *p*-type ($\rho = 8 \Omega \cdot \text{cm}$). Initially, the substrates were boiled in a peroxide–ammonia solution and rinsed in deionized water (resistivity $18.2 \text{ M}\Omega \cdot \text{cm}$). This treatment leads to “reconstruction” of a native oxide layer while the silicon surface acquires negative charge in deionized water due to activation of OH-groups. GOx molecules from *Aspergillus niger* was used as enzyme molecules. In a wide pH range of the solution, the GOx molecule has an effective negative charge. The size of the GOx molecule is $6.0 \times 5.2 \times 7.7 \text{ nm}^3$ [2]. A cationic polyelectrolyte polyethylenimine (PEI) with a molecular weight of 25 kDa was used to increase the adsorption of negatively charged GOx onto silicon substrates. The PEI molecules were adsorbed on silicon substrates from the 1 mg/ml aqueous solution during 10 min followed by rinsing in water during 10 min and drying. The photo-assisted layer-by-layer adsorption technique suggested in [3] was used to adsorb GOx from the 0.5 mg/ml aqueous solution onto covered with PEI silicon substrates. The adsorption time varied between 10 min and 60 min.

The topography of the films was measured using AFM by NTEGRA Spectra (NT-MDT Spectrum Instruments, Russia). Scanning was performed under ambient conditions at a frequency of 0.5 Hz in tapping mode using HA_NC/W₂C cantilevers of ETALON series. The Gwyddion software for statistical analysis of AFM data was used.

According to the AFM images, the surface coverage of substrate by GOx molecules taking into account the GOx size and the limitations of the measurement method was determined. The surface coverage with GOx molecules calculated as a percentage of area covered with GOx from the total substrate area. It was obtained that, for the *p*-Si type, the surface coverage value decreases, while for *n*-Si, it increases with adsorption time at fixed illumination level.

Thus, using the method of scanning probe microscopy, the quantitative results of the GOx adsorption process as a function of illumination, adsorption time, and the conductivity type of Si substrate were obtained.

The work was supported by the German–Russian Interdisciplinary Science Center (G-RISC) funded by the German Federal Foreign Office via the German Academic Exchange Service (DAAD), Project No. P-2018a-10.

1. S.V. Stetsyura, A.V. Kozłowski, *Tech. Phys. Lett.* **43**(3), 285 (2017).
2. H.J. Hecht, H.M. Kalisz, J. Hendle, R.D. Schmid, D. Schomburg, *J. Mol. Biol.* **229**, 153 (1993).
3. I.V. Malyar, D.A. Gorin, S. Santer, S.V. Stetsyura, *Appl. Phys. Lett.* **110**, 133104 (2017).

A technique of creating of ferroelectric regular domain structures using highly dissipative liquids at room temperature

V.V. Krutov, A.S. Sigov, A.A. Shchuka

MIREA – Russian technological University, Moscow, 119454 Russia
v_krutov@mirea.ru

A number of applications of ferroelectric regular domain structures (RDS) as photonic and phonon crystals are known. Recently, Chinese scientists have found a new application of ferroelectric RDS as actuators with improved characteristics. The authors of the article [1] presented an actuator (with a giant deformation) based on RDS in PZT ceramics, as well as its multilayer modification [2].

At the same time, at the present stage of development it is not enough to develop devices and technologies, focusing only on the physical aspects of solving the problem, and it is advisable to go to the most economical technological solution, reducing the duration of the technological cycle, which is especially important in the mass production of products. In this regard, it is promising we develop “double pulse heterothermal” technique with extremely short duration of the technological cycle among peers [3-5]. It should be noted that in contrast to existing methods using standard equipment, a completely new technique is being developed that requires the use of electroacoustic modules with interfering (at a given angle) ultrasonic beams.

The report is devoted to the phenomenon of RDS formation in ferroelectrics under the action of a uniform electric field and a temperature lattice induced by interfering elastic waves. The possibilities of creating ferroelectric RDS with a period $d \approx 40\text{-}100 \mu\text{m}$ using ultrasonic waves at frequencies close to the lower boundary of the microwave range ($f \approx 300 \text{ MHz}$) are considered with the help of computer modeling. Such RDS are used, for example, in acoustoelectronics in the manufacture of acoustic filters and resonators with improved characteristics, as well as generators of terahertz waves [6]. The model describes the effect of interfering ultrasonic waves on the ferroelectric through a thin layer of a liquid electrode with a thickness δ less than half a period of the formed domain structure. Efficiency of use as liquid electrodes of electrically conductive liquids with a high value of the A coefficient of the frequency dependence of the absorption index $\alpha = A f^2$ in the specified frequency range was shown. The results of estimation calculations of the main technological parameters for liquid electrodes based on ionic liquids with a high A coefficient are presented.

It was shown, that the use of highly dissipative ionic liquids such as 1-butyl-3-methylimidazolium bis(trifluoromethylsulfonyl)imide (the synonym is [C₄mim][NTf₂]) and 1-hexyl-3-methylimidazolium bis(trifluoromethylsulfonyl)imide (the synonym is [C₆mim][NTf₂]) creates favorable conditions for the application of the technique at room temperature.

A low acoustic loss material with isotropic properties (fused quartz) is used in the model. Recommendations on the choice of ultrasound frequency and angles of incidence on the quartz-liquid interface providing necessary spatial period of RDS are given. The work was supported by RFBR (grant 19-07-00469).

1. F. Li, Q. Wang, H. Miao, *J. Appl. Phys.* **122**, 074103 (2017).
2. Q. Wang, F. Li, *Sensors and Actuators A: Physical* **272**, 212 (2018).
3. V.V. Krutov, A.S. Sigov, A.A. Shchuka, *Ferroelectrics* **476**, 69 (2015).
4. V.V. Krutov, V.G. Mikhalevich, A.S. Sigov, A.A. Shchuka, E.A. Zasovin, *Phys. Solid State* **54**, 965 (2012).
5. V.V. Krutov, A.S. Sigov, A.A. Shchuka, *Applied Physics* **3**, 53 (2018).
6. G.Kh. Kitaeva, S.P. Kovalev, I.I. Naumova, A.N. Tuchak, P.V. Yakunin, Y.-C. Huang, E.D. Mishina, A.S. Sigov, *Laser Phys. Lett.* **10**, 055404 (2013).

Raman spectroscopy study of the switchable phases metal-organic frameworks DUT-8(Ni)

A. Krylov¹, I. Senkovska², V. Bon², S. Kaske^{1,2}, E. Slysareva³, S. Krylova¹, A. Vtyurin^{1,3}

¹Kirensky Institute of Physics FRC KSC SB RAS, Krasnoyarsk, Russia
shusy@iph.krasn.ru

²Technische Universität Dresden, Bergstrasse 66, 01062 Dresden, Germany

³Siberian Federal University, 660041 Krasnoyarsk, Russia

Metal-Organic Frameworks (MOFs) have revolutionized the field of crystal engineering, and solid-state chemistry is unique materials, which can transform their crystal structure from a dense, nonporous to a highly porous, open state and vice versa as a response to external stimuli. They are bistable or multistable crystalline materials with long-range structural ordering, a reversible transformability between crystalline phases, and permanent porosity [1]. MOF exhibit wide variety of properties attractive for a variety of applications.

We report the results of a Raman scattering study of a switchable Metal-Organic Framework DUT-8 (Ni) belonging to the class of pillared layer MOFs [2]. Several samples of DUT-8 series were studied. The Raman spectra comparison showed a significant difference in the low-wavenumber region for open (23 cm^{-1}) and closed (59 cm^{-1}) pore forms of DUT-8(Ni) [3] (Figure 1). This characteristic spectral features can be a basis for rapid, and routinely applicable Raman based technique for characterization of different switchable MOF's phases and for in situ evaluation and analysis of them by the spectral profile.

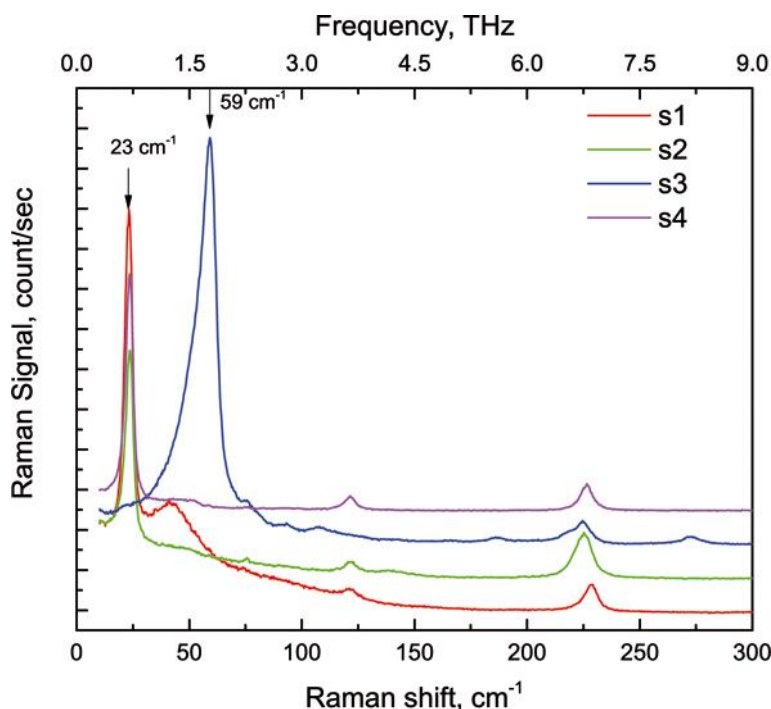


Figure 1. Raman spectra samples of DUT-8(Ni) at open (op) and close (cp) pore form.

Acknowledgments: I.S., V.B., S.K. thank the DFG for financial support (FOR 2433); A.K., S.K., A.V. thank the Russian Foundation for Basic Research for financial support (18-02-00754).

1. A. Schneemann, et al. *Chem. Soc. Rev.* **43**, 6062 (2014).
2. N. Kavoosi, et al., *Dalton Trans.* **46**, 4685 (2017).
3. A. Krylov, et al. *Phys. Chem. Chem. Phys.* **19**, 32099 (2017).

Lattice dynamics of $\text{HoGa}_3(\text{BO}_3)_4$ and $\text{HoFe}_3(\text{BO}_3)_4$ crystals

S.N. Krylova¹, A.S. Krylov¹, E. M. Roginskii^{2,3}

¹Kirensky Institute of Physics FRC KSC SB RAS, 660036, Krasnoyarsk, Russia
slanky@iph.krasn.ru

²Ioffe Institute, 194021, Sankt-Peterburg, Russia

³Faculty of Physics, St Petersburg State University, 194508, St. Petersburg, Russia

The crystals of the huntite family with the general formula $\text{RX}_3(\text{BO}_3)_4$ (R = lanthanide ions, $\text{X} = \text{Al}, \text{Ga}, \text{Fe}, \text{Cr}$) attract the special interest of the investigators. The stability of the huntite crystal structure due to rigidity of the BO_3 polyhedron. The optical nonlinear and multiferroic properties lead to different practical applications of these materials [1-3]. The $\text{HoFe}_3(\text{BO}_3)_4$ crystal undergoes the phase transition at $T_C \approx 366$ K [4]. The low-temperature structure of the $\text{HoFe}_3(\text{BO}_3)_4$ crystal is presented in Fig. 1. The structure of two magnetic ions of different types (3d and 4f) gives rise to magnetic order at low temperatures [5]. Coexistence of structural and magnetic order parameters can open new opportunities to control their physical characteristics. The $\text{HoGa}_3(\text{BO}_3)_4$ crystal exhibits a strong magnetoelectric effect [6]. To interpret mechanisms and value of magnetoelectric relations it is necessary to know the structure of crystal vibrational spectra and mechanisms of them formation.

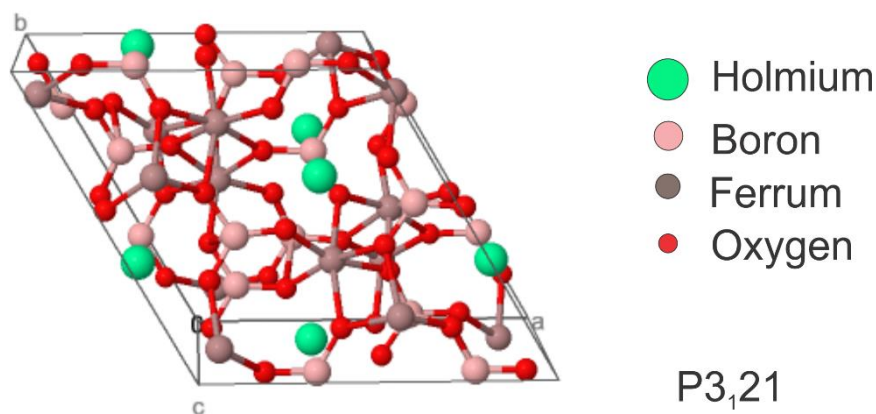


Figure 1. The structure $\text{HoFe}_3(\text{BO}_3)_4$ crystal in the low-temperature phase.

The present work devoted to ab-initio theoretical study of the lattice dynamics of $\text{HoGa}_3(\text{BO}_3)_4$ and $\text{HoFe}_3(\text{BO}_3)_4$ crystals. The calculation is based on the Density Functional Theory (DFT) approach with a plane-wave (PW) basis set using the generalized gradient approximation parameterized by Perdew, Burk and Emzerhop Perdew (GGA-PBE) [7].

This work is financially supported by the Russian Foundation for Basic Research № 18-02-00754.

1. D. Jaque, *J. Alloys Compd.* **204**, 323 (2001).
2. A. Brenier, C. Tu, Z. Zhu, B. Wu, *Appl. Phys. Lett.* **84**, 2034 (2004).
3. X. Chen, Z. Luo, D. Jaque, et al, *J. Phys.: Condens. Matter* **13**, 1171 (2001).
4. N.V. Volkov, I.A. Gudim, E.V. Eremin, et al, *JETP Lett.* **99**, 2, 72 (2014).
5. A.M. Kadomtseva, Y.F. Popov, G.P. Vorob'ev, et al, *Low Temp. Phys.* **36**, 511 (2010).
6. V.I. Zinenko, M.S. Pavlovskii, A.S. Krylov, et al, *J. Exp. Theor. Phys.* **117**(6), 1032 (2013).
7. J.P. Perdew, K. Burke, M. Ernzerhof, *Phys. Rev. Lett.* **77**, 3865 (1996).

Raman scattering study of SrTiO₃: Bi ceramics with higher ($x = 0.16$) bismuth content

S.N. Krylova¹, A.N. Vtyurin^{1,2}, A.S. Krylov¹, X. Wei³, W. Chen³

¹Kirensky Institute of Physics, Federal Research Center KSC SB RAS, 660036, Krasnoyarsk, Russia
slanky@iph.krasn.ru

²Institute of Engineering Physics and RadioElectronics, Siberian Federal University, 660079, Krasnoyarsk, Russia

³Electronic Materials Research Laboratory, Xi'an Jiaotong University, Xi'an 710049, P.R. China

The dielectric properties of 0.1-15 mol.% bismuth doped SrTiO₃ ceramics have been investigated systematically for decades. The temperature dependence of the dielectric permittivity suggests that the ferroelectric behavior at lower impurity content transits to mixed relaxor ferroelectric type when impurity concentration reaches 5 mol.%, and further to relaxor behavior for samples above 10 mol.% Bi content. Because of the impurity in ABO₃ perovskites, dipolar entities form polar nanodomains. In the very dilute limit each domain behaves as a non-interacting polar entity with a local dynamics. At higher concentrations of disorder, however, the domains can interact leading to a more complex relaxation behavior. Among the manifestations of such behavior is the formation of a glass-like relaxor state. Such formation results in a typical modification of low frequency lattice dynamics and should show in low frequency Raman spectra (see e.g. [1]). Yet to our knowledge Raman spectra of such ceramics with higher concentration of bismuth content have not been investigated up to now. So here we report temperature transformation of Raman spectra of Bi_xSr_(1-1.5x)TiO₃, $x = 0.16$ ceramics in a lower frequency range.

Raman spectra have been obtained with Jobin Yvon-Horiba T-64000 spectrometer and Ar⁺ laser (514.5 nm, 50 mW), CCD detection with liquid nitrogen cooling, 600 s accumulation time. The polycrystalline ceramics samples were obtained from conventional mixed oxide powder. High-purity SrCO₃, TiO₂, and Bi₂O₃ powders were mixed for 6 h by ball milling in distilled water. The powders were calcined at 1100 °C for 6 h. After calcination, the powders were pressed at 20 MPa and sintered in a range of 1380-1195 °C in air for 4 h and furnace cooled. Details of sample synthesis and control are given in [2].

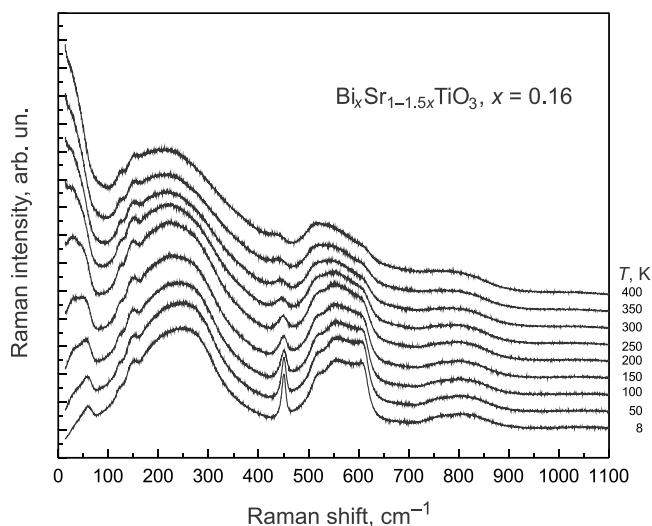


Figure 1. Temperature transformation of Bi_xSr_(1-1.5x)TiO₃ Raman spectra.

Typical temperature transformation of obtained spectra is shown in the figure 1. Results are discussed in comparison with earlier data [1] for ceramics with lower Bi content.

1. A. Almeida, P. Teles, M.R. Chaves, P.M. Vilarinho, J.L. Baptista, *Ferroelectrics* **294**, 49 (2003).
2. W. Chen, X. Yao, X. Wie, *J. Mater. Sci.* **43**, 1144 (2008).

Study of electrical properties of Ni-phylosilicate nanoscrolls with reduced Ni nanoparticles

T.S. Kunkel^{1,2}, A.A. Krasilin^{2,3}, E.A. Straumal⁴, A. Nomine^{3,5}, J. Ghanbaja⁵, A.V. Ankudinov²

¹SPbPU, 195251, Saint-Petersburg, Russia

²Ioffe Institute, 194021, Saint-Petersburg, Russia
tatyana_kunkel@mail.ru

³ITMO University, 197101, Saint-Petersburg, Russia

⁴IFAV RAS, 142432, Chernogolovka, Russia

⁵Université de Lorraine, Institut Jean Lamour, UMR CNRS 7198, Nancy F-54011, France

Catalyst materials consisting of metal (Fe, Co, Ni) nanoparticles placed on an oxide carrier possess great interest for application in a wide range of chemical process [1]. These structures can be strong electric fields sources – a single-isolated metal ball with a radius of 1 nm with a charge of 1 electron creates a field of about 10^9 V/m. Such high fields might have significant influence on chemical reaction potential barrier. Hence, the problem relies in the synthesis of stable catalytically active metallic nanoparticles arrays. One way to create such arrays is laser electrodispersion (LED) [2]. In our work, another method to form isolated metal nanoparticles was implemented: they were reduced out of the Ni-doped phyllosilicate nanoscrolls in hydrogen flow.

The $(\text{Ni}_x\text{Mg}_{1-x})_3\text{Si}_2\text{O}_5(\text{OH})_4$ ($x = 0.67$ and 1) nanoscrolls were prepared by hydrothermal treatment (350 °C, 20 MPa, 12 h, 0.25 M NaOH water solution) of coprecipitated of Mg and Ni hydroxides in the presence of amorphous SiO_2 . Further, the samples were annealed in a reducing medium (hydrogen) in the 400-900 °C temperature range, which made it possible to obtain metal nanoparticles incorporated into a silicate matrix. The samples morphology was studied by the transmission electron microscopy (TEM), Figure 1.

To inject the charge into the sample and to study the charge leakage, the Kelvin probe force microscopy (KPFM) method was used. It was found that, initially, the nanoscroll potential is about 1 mV, and the area around it has a potential of 3 mV (Fig. 2b). After charging by voltage pulse application, the nanoscroll potential increased to 3 mV, and the surrounding area – to 9 mV (Fig. 2c). With time, the potentials slowly decreased to 2 mV and 7 mV, respectively (Fig. 2d, red line).

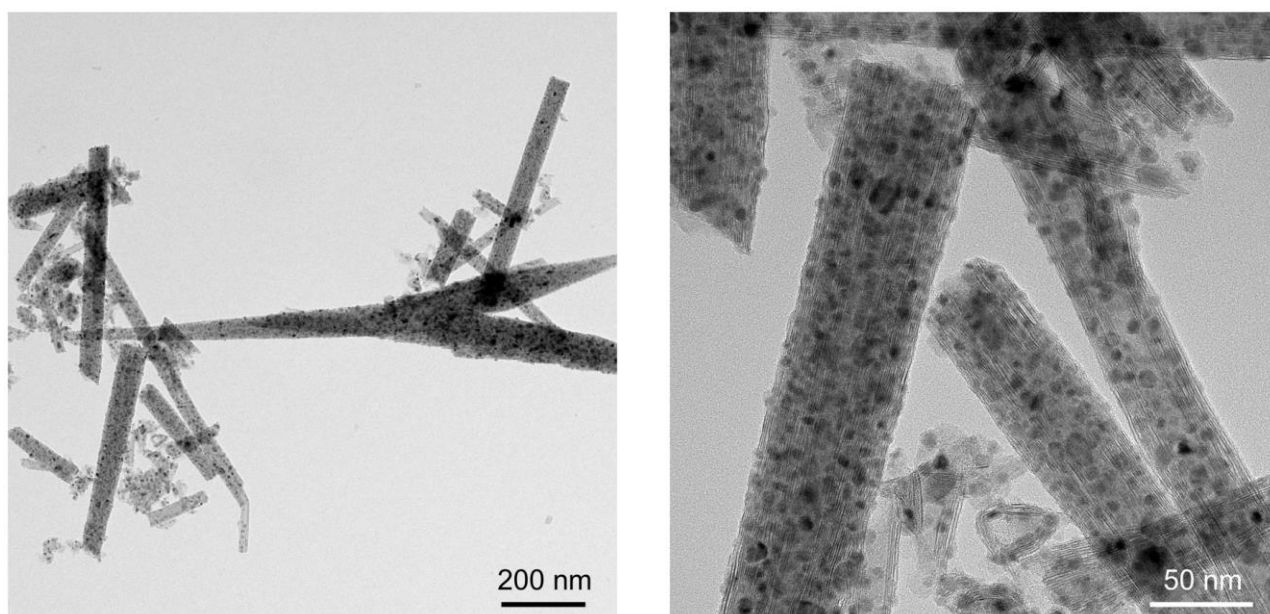


Figure 1. TEM micrographs of $\text{Ni}_2\text{MgSi}_2\text{O}_5(\text{OH})_4$ nanoscrolls after partial reduction of Ni.

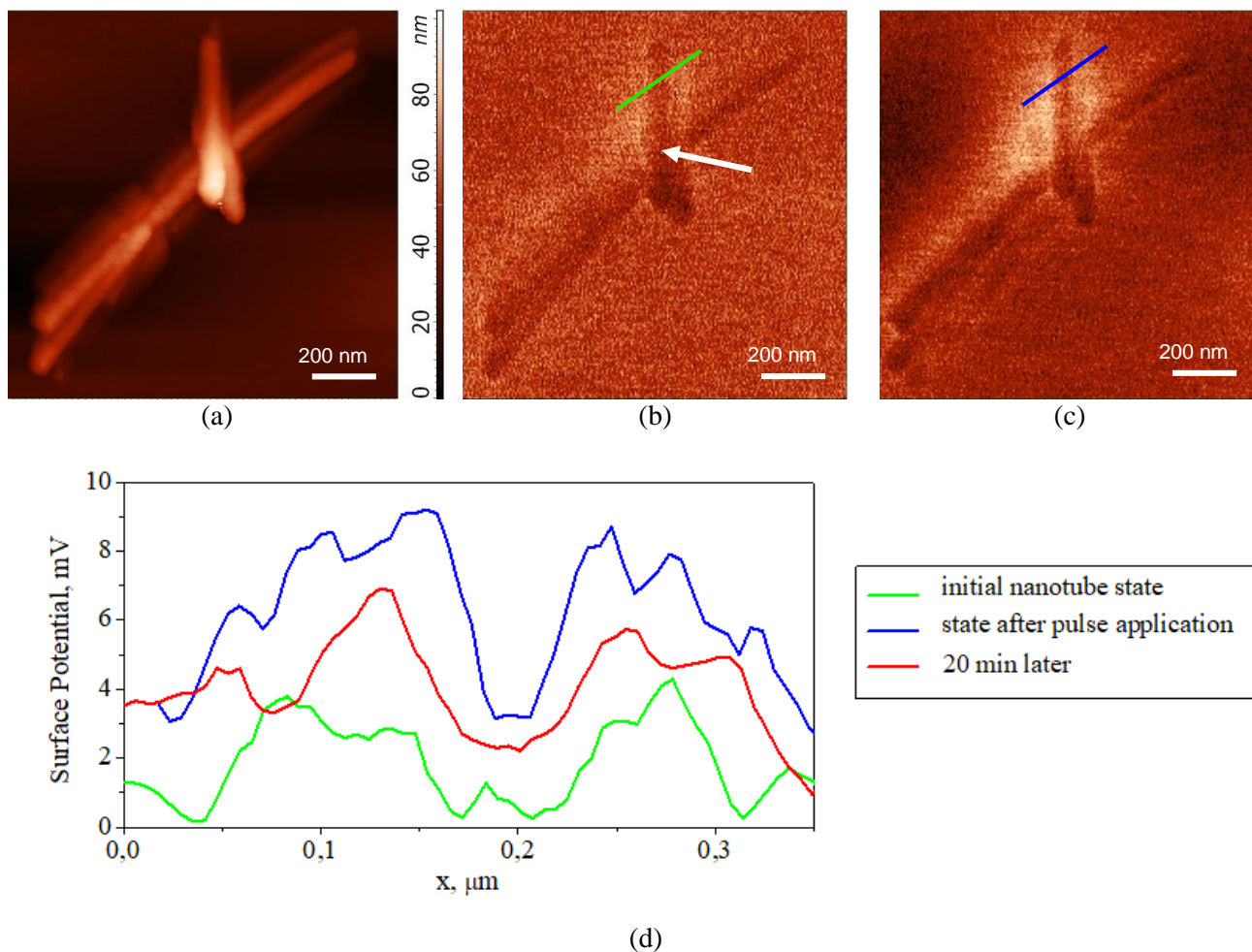


Figure 2. KPFM topography image (a) and surface potential map of the Ni(30 nm)/Si substrate with $\text{Ni}_3\text{Si}_2\text{O}_5(\text{OH})_4$ nanoscrolls before (b) and after (c) rectangular voltage pulse application ($\tau = 30$ s, $U = +10$ V). The surface potential profiles (d) across the uncharged nanoscroll (green), immediately after charge injection (blue) and 20 min later (red). Parameters of visualization: HA_C/W2C+ cantilever, resonant frequency of 17.8 kHz, free / set.point oscillation amplitude of about 8 nm / 5 nm; probe-sample distance at KPFM mode is about 10 nm. Arrows indicate the contact point the charge was injected.

The report will also consider the results of the charge injection experiments (using KPFM and spreading resistance microscopy) for the samples of different Ni, Mg contents as well as annealing temperatures.

1. Q. Yang, Q. Xu, H.L. Jiang, *Chemical Society Reviews*, **118**, 10, 4981 (2017).
2. E.V. Golubina, E.S. Lokteva, K.I. Maslakov, T.N. Rostovshchikova, M.I. Shilina, S.A. Gurevich, V.M. Kozhevnikov, D.A. Yavsin, *Nanotechnologies in Russia*, **12**, 19 (2017).

Hydrothermal growth and piezoelectric response of Li,Ta-doped (K,Na)NbO₃ nanorod arrays

L. Jiang, Z. Wang, Y.M. Hu, H.S. Gu

Hubei Key Laboratory of Ferro- & Piezo-electric Materials and Devices, Faculty of Physics and Electronic Sciences, Hubei University, 430062, Wuhan, P.R. China
guhsh@hubu.edu.cn

Research and development on the Lead-free piezoelectric nanomaterials have attracted great attentions owing to their great potential for the application in energy harvesting and micro/nano-scaled sensors and actuators. Among the lead-free piezoelectric materials, potassium sodium niobite ((K,Na)NbO₃, KNN) have been regarded as the one of the most promising systems due to their high piezoelectric coefficient and energy conversion efficiency. However, piezoelectric performances of pure KNN are not able to be comparable with that of traditional piezoelectric material Pb(Zr,Ti)O₃. Most of the research works are focusing on modifying KNN-based ceramics and improving piezoelectric responses by doping Li(Lithium) and Ta(Tantalum) into the lattice, which can decrease their phase transition temperature TO-T to room temperature. In this work, the Ta-doped KNN nanorods were synthesized through substrate-oriented hydrothermal process. the response of the KNN NRs along radial direction was also studied by PFM method. Until now, typical butterfly-shape curves and reverse-phase curves of synthesized nanorods were attained by PFM examination. In addition, the enlarged lattice spacings because of substitution of Ta were observed according to TEM results, and the EDS results obviously show the existence of Ta. However, these results need farther and more systematic analyses, and this research is under way. In near future, Li,Ta-doped (K,Na)NbO₃ nanorods will be tried to synthesized by hydrothermal method. Moreover, the growth behavior and revolution on the composition, phase and piezoelectric performance with the change of hydrothermal reaction conditions will be systematically studied.

Nano-layered-structure interface and Zinc diffusion of borosilicate glass during sealing process

S.H. Li¹, K.J. Hu¹, J. Wang², J.Y. Liu², X.Y. Shen², Y. Zhang^{1*}

¹Beijing Key Laboratory of Fine Ceramics, State Key Laboratory of New Ceramics and Fine Processing, Institute of Nuclear and New Energy Technology, Tsinghua University, Beijing, 100084 P R China

²Beijing Tsingneng Chuangxin Science and Technology Co.Ltd.

yzhang@tsinghua.edu.cn

The interface microstructure and element diffusion between a borosilicate glass and an AISI3040 steel was investigated. Pre-oxidation of the steel was performed in a low pO_2 atmosphere before sealing process. The oxidation layer is composed of Cr_2O_3 , $MnCr_2O_4$ spinel and SiO_2 . From Energy dispersive X-ray spectra (EDS) analysis, a significant Zinc diffusion between glass and metal has been observed. High resolution images showed that Zinc selectively migrated from the glass to $MnCrO_4$ grains, while no Zinc was detected in Cr_2O_3 grains. Transmission electron microscopy (TEM) studies revealed that there exists a nano-layered-structure with a thickness of about 2 nm in the glass-to-metal interface. Another important feature is the enrichment of potassium and calcium elements in the nano-layer. This may be attributed to the migration of these elements from the glass during sealing process.

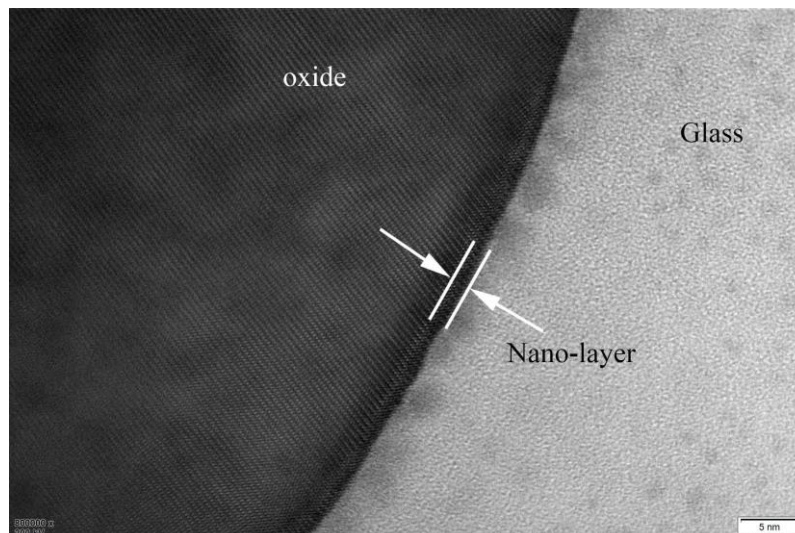


Figure 1. HRTEM image of nano-layered-structure interface between the glass and the metal.

Effects of annealing atmosphere on the dielectric properties of barium strontium titanate glass-ceramics using impedance spectroscopy and thermally stimulated depolarization current technique

X.W. Liang, Z.Y. Zhao, T.Y. Zhang, Y. Zhang*

Beijing Key Laboratory of Fine Ceramics, State Key Laboratory of New Ceramics and Fine Processing, Institute of Nuclear and New Energy Technology, Tsinghua University, Beijing, 100084 P R China
yzhang@tsinghua.edu.cn

Impedance spectroscopy (IS) analysis and thermally stimulated depolarization current (TSDC) study were carried out to investigate the effects of annealing atmosphere on the dielectric properties of barium strontium titanate ((Ba,Sr)TiO₃, BST) glass-ceramics. In the present work, the nitrogen-sintered BST glass-ceramics were annealed in air and oxygen, respectively.

IS analysis reveals the resistivity of air-annealed and O₂-annealed glass-ceramics samples increased by about two orders of magnitude compared to the N₂-sintered samples. An enhancement of insulation property was attributed to the decrease of oxygen vacancy concentration caused by the variation of annealing atmosphere. The activation energy calculated from the dc conductivity, complex impedance and modulus indicates the dielectric relaxation could be ascribed to the motion of dipoles related to oxygen vacancies. The result of TSDC shows the presence of two overlapping peaks which may associated with defect complex (2Ti_{Ti'}-V_{O''}) at lower temperature and space charge polarization at higher temperature. It was found that the current density and the concentration of dipole decreased when samples annealed in oxidation atmosphere. As a result, the decrease in oxygen vacancy concentration results in the decrease of conductivity.

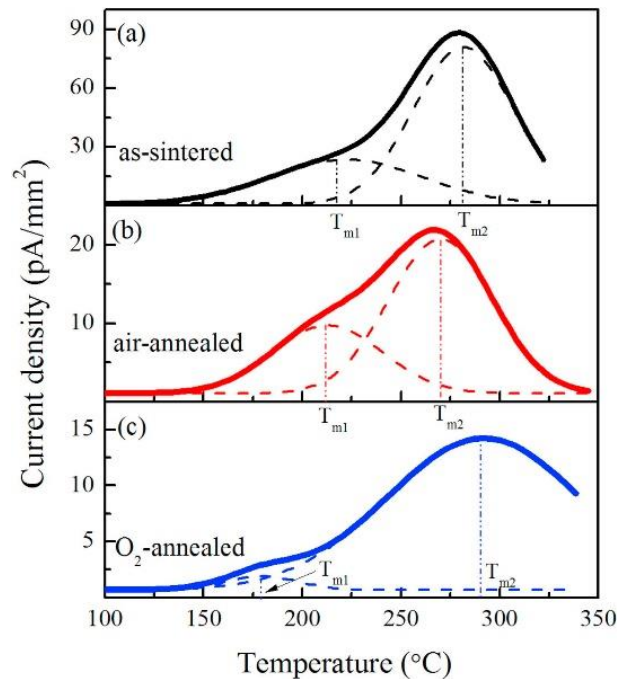


Figure 1. TSDC spectra of the BST glass-ceramics polarized at a dc electric field of 140 V/mm for 20 min at 250 °C: (a) as-sintered, (b) air-annealed and (c) O₂-annealed. Solid lines are experimental curves while dashed lines are fitting curves.

1. X.Z. Song, T.Y. Zhang, Y. Zhang, et al, *Ceramics International* **44**, 5668 (2018).
2. X.Z. Song, T.Y. Zhang, Z.Y. Zhao, et al, *J. American Ceram. Soc.* **102**, 901 (2019).
3. Z. Li, X.Z. Song, Y. Zhang, et al, *J. Appl. Phys.* **121**, 204102 (2017).

Polarization reversal in lithium niobate with compositional gradients

B.I. Lisjikh, E.D. Greshnyakov, V.I. Pryakhina, V.Ya. Shur

School of Natural Sciences and Mathematics, Ural Federal University, 620000 Ekaterinburg, Russia
lisjikh.boris@yandex.ru

The polarization reversal under application of the electric field in LiNbO₃ (LN) single crystals with inhomogeneous spatial distribution of Li concentration along polar axis has been investigated.

Vapor transport equilibration (VTE) process (high temperature annealing in Li-rich atmosphere) was used to change Li concentration from congruent (48.8 mol.%) to stoichiometric (50 mol.%) composition [1]. Z-cut 1-mm-thick plates were annealed at 1050 °C. Spatially inhomogeneous distribution was obtained by variation of VTE duration. The VTE temperature lower than T_C allowed to preserve the initial single domain state.

Two configurations of unilateral gradients were used, SLN@Z+ and SLN@Z-, which presents unilateral gradient with stoichiometric composition at the correspondent polar surface. Both configurations were obtained by polishing of annealed plates to half-thickness. Spatial distribution of Li along polar axis was measured by Confocal Raman spectroscopy (Alpha AR300, Witec) [2].

Polarization reversal was carried out using liquid electrodes (LiCl water solution). Domain kinetics was observed by *in situ* imaging during polarization reversal using polarizing optical microscope with high-speed video camera. Polarization reversal was performed in forward and backward directions, sequentially. Electrical pulses had rectangular shape with constant voltage or triangular with rising by 200 V. After switching in one direction opposite sign voltage pulse was applied.

It was shown that creation of Li concentration gradient in the surface layer resulted in appearance of a built-in bias field E_{bias} . The value of E_{bias} was defined as a difference between «forward» (E_f) and «backward» (E_b) switching fields, required for polarization reversal of complete area under electrode:

$$E_{bias} = \frac{E_f - E_b}{2}. \quad (1)$$

The variation of VTE duration led to different Li concentration gradients (dC_{Li}/dz) and, hence, to different values of E_{bias} . Bias field dependence on dC_{Li}/dz in 100 μm thick surface layer was obtained for all samples – SLN@Z+ and SLN@Z- (Figure 1). The linear dependence was revealed for gradients up to 5 mol.%/mm:

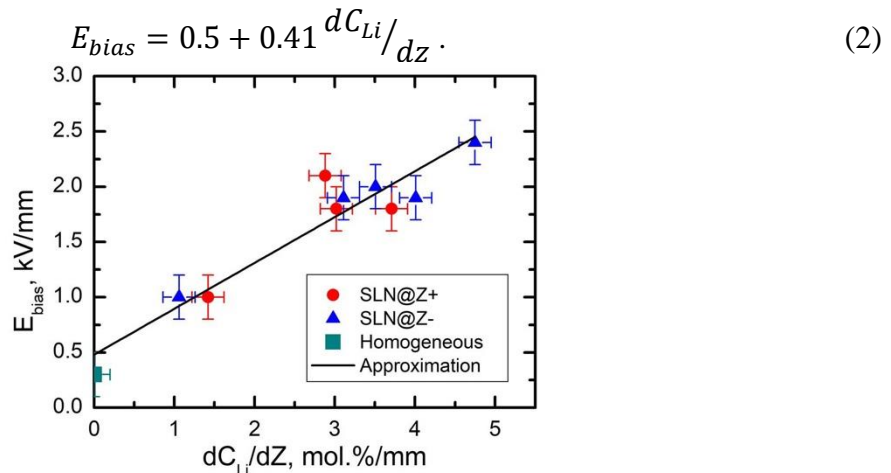


Figure 1. Dependence of the bias field on Li concentration gradient.

The equipment of Ural Center for Shared Use “Modern Nanotechnology” Ural Federal University was used. The research was made possible by Russian Science Foundation (Project № 19-12-00210).

1. D.-L. Zhang, et al, *Cryst. Gr. Des.* **13**, 1793 (2013); Q. Li, et al, *J. Am. Ceram. Soc.* **99**, 3055 (2016).
2. M.D. Fontana, P. Bourson, *Appl. Phys. Rev.* **2**, 040602 (2015).

Study of the domain evolution and transmittance on various temperature in PKN single crystal using in situ method

L. Wenbin

Shanghai Institute of Ceramics, Chinese Academy of Sciences, Shanghai, P.R. China

High quality single crystal of Lead Potassium Niobate (PKN) was fabricated by Bridgman method through spontaneous nucleation and $\langle 001 \rangle$ -oriented slides were obtained. The full width at half maximum (FWHM) measured less than $22''$. Strip-shaped domain observed in PKN single crystal sample by polarizing microscope. The domain and transmittance were investigated by in situ observation under different temperature. The results show that evolution of domains disappearing in heating process and appearing in cooling process gradually, and they are recovered during heating and cooling process. The transmittance influenced by temperature because of the scatter and reflection in domain walls. It is suggested that domains evolution and optical transmittance or absorption, can be employed the phase transition in ferroelectric crystals.

Investigation of high conductivity area at the interface between $\text{Ba}_{0.8}\text{Sr}_{0.2}\text{TiO}_3$ and LaMnO_3 after effect of electric field on $\text{Ba}_{0.8}\text{Sr}_{0.2}\text{TiO}_3$ ferroelectric film

D.P. Pavlov, N.N. Garig'yanov, A.V. Leontyev, T.M. Salikhov, V.V. Kabanov, R.F. Mamin

Zavoisky Physical-Technical Institute, FRC Kazan Scientific Center of RAS, 420029, Kazan, Russia
 mamin@kfti.knc.ru

As it has been shown [1], the high conductivity area (quasi two dimensional electron gas) may be created at an interface due to electric polarization discontinuity [2, 3]. A quasi two dimensional electronic gas (q2DEG) is formed in the STO layers next to the interface which becomes superconducting below a temperature of 300 mK [1, 4]. Remarkably, the superconducting state coexists with a magnetic state being stable up to the room temperature. Ferroelectrics are attractive materials for such purpose. They have a wide range of different distinctive properties, among them: spontaneous polarization switching, high dielectric permeability, dielectric nonlinearity, piezo- and pyro- activity, linear and quadratic electro-optical effects. That can expand the scope of application in nanoelectronics. The direction of such polarization in the ferroelectric film might be switched by an external electric field.

Antiferromagnetic LaMnO_3 (LMO) might be transferred to ferromagnetic state by increasing the concentration of free carriers by injection. The change of domain structure in ferroelectric $\text{Ba}_{0.8}\text{Sr}_{0.2}\text{TiO}_3$ (BSTO) film can change a concentration of free carriers on the interface with LMO means that increasing the free charge carriers might lead to the local ferromagnetic state and magneto-resistivity in a system with q2DEG. Therefore, there is an opportunity to switch conductivity of interface by an electric field in the heterostructure BTO/LMO.

In the present work the thin film of epitaxial BSTO was sputtered on the top of LMO single crystalline samples using the magnetron sputtering technique. Conductivity measurements were performed by a four-point probe method. Measurements were performed before and after effect of electric field on $\text{Ba}_{0.8}\text{Sr}_{0.2}\text{TiO}_3$ ferroelectric film. We have shown that when a non-uniform electric field is applied to a ferroelectric film, we can turn off the state with high conductivity. And under the influence of a uniform electric field on the ferroelectric film, we can turn on the state of high conductivity.

The reported study was funded by Russian Scientific Foundation, research project No. 18-12-00260.

1. A. Ohtomo, and H. Hwang, *Nature* **427**, 6973 (2004).
2. M. K. Niranjan, Y. Wang, S.S. Jaswal, E.Y. Tsymbal, *Phys. Rev. B* **103**, 016804 (2009).
3. K.D. Fredrickson, A. Demkov, *Phys. Rev. B* **91**, 115126 (2015).
4. N. Reyren, S. Thiel, A. Caviglia et al., *Science* **317**, 5842 (2007).

Properties of the barium strontium titanate film on the silicon substrate

R.I. Batalov¹, D.K. Zharkov¹, D.P. Pavlov¹, S.A. Migachev¹, I.V. Lunev², A.S. Elshin³,
A.V. Leontyev¹, A.O. Chibirev², T.S. Shaposhnikova¹, R.F. Mamin^{1,2}

¹Zavoisky Physical-Technical Institute, FRC Kazan Scientific Center of RAS, 420029, Kazan, Russia
dmitry.p.pavlov@gmail.com

²Institute of Physics, Kazan Federal University, Kazan 420008, Russia

³Moscow Technological University, 191454, Moscow, Russia

To improve the properties of solar cells, primarily to increase the absorptivity of solar cells in a wider region of the light spectrum [1], various films are applied to their surface. Also recently, the photovoltaic effect is often used [2], which is the direct conversion of light into electricity and is considered one of the most reliable and abundant sources of renewable and clean energy. A high-mobility electron gas was observed in 2004 [3] at the interface of LaAlO₃/SrTiO₃ heterostructure. In this work we solve these problems by creating such a special state of the interface when applying a thin ferroelectric film on silicon. The properties of barium-strontium titanate (BST) films on a silicon substrate and the possibility of their modification are investigated. The properties of the heterostructures obtained by dielectric and various optical methods are measured and characterized. It was found that changes of the capacity of the heterostructure are related to increase of conductivity through the Si layer with increasing frequency based on the results of the study of the frequency dependences of the BST/Si heterostructure. The reflection spectrum from the BST film was studied. Based on these results, the absorption spectrum was modeled, which has a peak in the region of 3 eV. There is also an inflection in the region of 2.6-2.8 eV, which can correspond to energy from the top of the valence band to the lower levels of the BST film defect system. The photoconductivity of the heterostructure interface and the possibility of modifying the properties of barium-strontium titanate films by the laser annealing method and the ion implantation method are studied. The surface was tested by atomic force microscopy before and after modification. The laser annealing method did not yield any significant results. The most promising method was the modification of barium-strontium titanate films on a silicon substrate by the ion implantation method with the introduction of chromium atoms with energy of 40 keV. The effect of modification on photoconductive properties of the films was revealed. The measurement of the photoconductivity has shown that current at the interface increases substantially when illuminated by the ultraviolet light. This increase is particularly high for samples modified by ion implantation. The possibility of carrier concentration increasing by this way is discussed when exciting the *p/n* junction for use as an operating element in solar batteries.

The reported study was supported of the Russian Foundation for Basic Research, research project No. 18-42-160005. The work is partially performed according to the Russian Government Program of Competitive Growth of Kazan Federal University. A.S. Elshin thanks the Russian Foundation for Basic Research for financial support, project No. 17-32-50047.

1. Ch.S. Solankii, H.K. Singh, *Anti-reflection and Light Trapping in c-Si Solar Cells*. (Singapore, Springer) 2: 186 p. (2017).
2. S.Y. Yang, J. Seidel, S.J. Byrnes, P. Shafer, C.-H. Yang, M.D. Rossell, P. Yu, Y.-H. Chu, J.F. Scott, J.W. Ager III, L.W. Martin, R. Ramesh, *Nature Nanotechnology* **5**, 143 (2010).
3. A. Ohtomo, and H. Hwang, *Nature* **427**, 6973 (2004).

Study of the influence of technological factors on improving the efficiency of ferroelectrically hard piezoceramic material PCR-8, designed for operation in power modes

M.A. Marakhovskiy¹, A.E. Panich¹, M.V. Talanov², V.A. Marakhovskiy¹

¹*Scientific Design and Technological Bureau "Piezopribor", Southern Federal University, 344090, Rostov-on-Don, Russia
marmisha@mail.ru*

²*Research institute of Physics Southern Federal University, 344090, Rostov-on-Don, Russia*

At present, ferroelectric materials intended for working in high-field regimes cause great interest in piezoelectric instrument making. Along with high coefficients of electromechanical coupling, these materials have low dielectric losses, high mechanical quality factor which provides high efficiency of the emitter. Ferroelectrically hard piezoceramic materials are resistant to external influences and have a high temperature stability of the parameters, which allows them to be used in various devices, including those designed for extreme conditions (accelerometers, piezo motors, piezotransformers of power sources of onboard equipment) [1]. To date, commercial piezoceramic materials of various compositions (PZT-8, APC-840, APC-841, PCR-8 [2]) have been created. However, the increase in the functional parameters of ferroelectrically hard materials can be achieved not only by creating new chemical compositions, but also by improving the technology of manufacturing piezoceramics and optimization of technological regimes. Thus, it is important to study the influence of technological factors on the functional parameters of ferroelectrically hard piezoceramic materials. The aim of the work was to establish correlations between the technological regimes of sintering of the well-known ferroelectrically hard piezoceramic material PCR-8 and its functional parameters.

PCR-8 ceramics were produced by solid-phase synthesis and sintered in three different ways: by conventional ceramic technology (chamber furnace at atmospheric pressure), by hot pressing with uniaxial pressure and by Spark Plasma Sintering in vacuum with uniaxial pressure and direct current pulses.

The completeness of the sintering process of piezoelectric ceramics was evaluated by the results of X-ray phase analysis, microstructure images obtained on a scanning electron microscope and the values of the density of sintered piezoelectric ceramics determined by hydrostatic weighing.

As a result of the obtained data analysis, it was found that the use of hot pressing and spark plasma sintering technology contributes to an increase in the density (ρ) and transverse piezoelectric module (d_{31}) by 5 and 60%, respectively. Along with the increase in the main parameters, it was possible to reduce the sintering temperature of the piezoelectric ceramics by 250 °C.

Thus, in the course of the study it was possible not only to increase the efficiency and manufacturability of ferroelectrically hard piezoceramic material PCR-8, but also to reduce energy consumption in the manufacture of final products. As a result, the use of spark plasma sintering technology allows to expand the field of practical application of ferroelectrically hard piezoceramic material PCR-8, to increase the share of the finished product and reduce its cost.

1. V.V. Eremkin, V.G. Smotrakov, M.A. Marakhovskiy, et al. *Materials Science* **10**, 20 (2014).

2. A.J. Danziger, O.N. Razumovskaya, L.A. Reznichenko, S.I. Dudkina. *High-performance piezoelectric materials. Search optimization* (Rostov n/D: Paika), 96 (1994).

The determination of mechanical properties of nanostructured tantalum nitride and tantalum oxynitride films on the glass and stainless steel surfaces by atomic force microscopy

A.S. Petrovskaya¹, G.B. Melnikova¹, T.A. Kuznetsova¹, S.A. Chizhik¹,
A. Zykova^{2,3}, V. Safonov^{2,3}

¹*A.V. Luikov Heat and Mass Transfer Institute of NAS of Belarus, 220072, Minsk, Belarus
agata.petrovskaya@gmail.com*

²*National Science Centre «Kharkov Institute of Physics and Technology», Kharkov, Ukraine*

³*Department of Physical Technologies Kharkov National University, Kharkov, Ukraine*

One of the main advances in the interventional cardiology is the development of metal stents. The requirements for stents are quite strong: high flexibility, plasticity, strength and rigidity, X-ray contrast, biocompatibility with the organism. For the stents production different materials are used such as stainless steel, platinum-iridium alloys, etc. The surface of the stent is covered with various types of ceramic coatings to prevent changing their properties. The study of mechanical properties of tantalum films and the evaluation of its operational properties is an important task because the surface of stents is often subjected to chemical and mechanical effects. The aim of this work is to define the friction coefficient, adhesion force and roughness of tantalum nitride and tantalum oxynitride coatings on the glasses and stainless steel substrates using atomic force microscopy (AFM).

The TaN, TaON coatings were deposited on glass and stainless steel substrates in a high-vacuum system with a turbopump (a base pressure was about 10^{-2} Pa) using Direct Current planar magnetron sputtering (the magnetron power was about 6 kW). The samples were cleaned by standard methods in the ultrasonic bath before the deposition process. The study of the mechanical characteristics of the surface was carried out on NT-206 device (Belarus). Roughness values were determined by AFM-method using CSC 38 cantilevers (Mikromasch, Estonia). The stiffness of cantilevers was 0.03 N/m according to the manufacturer's passport, the radius of curvature – was less than 10 nm. The NCS 11 cantilevers (Mikromasch, Estonia) were used to determine the coefficient of friction and adhesion force. The stiffness NCS 11 was 3 N/m. For determine the friction coefficient the radius of curvature of the cantilever was increased to 100 nm by scanning the silicon surface with high load.

Tantalum nitride and tantalum oxynitride coatings on the glasses and 316L SS stainless steel substrates were studied using AFM. It was found that the microstructure of the surface of coatings is largely determined by the used substrate. The mean square roughness (R_q) of the initial steel was 5 nm, the friction coefficient was 0.072, and the value of the adhesion force was 12.5 nN. After tantalum nitride or tantalum oxynitride films deposited on the steel, R_q increased to 7-8 nm. It should be noted that the roughness of surface of tantalum coatings practically was not change with increasing of scan area. This is indicating about uniformity of the applied coating. The roughness values of glass slides surfaces reduced by 2 times after deposited tantalum oxynitride coatings. The coefficient of friction of coatings on stainless steel substrates decreases in 2-3 times. The use of materials with low friction coefficient as stents is promising, because they allow retaining and not reduce the blood flow along the vessel walls. But it slightly decreased on the surface of the glass, within the confidence interval. So, the tantalum films can be used to produce implanted materials to reduce the formation of blood clots on their surface.

Study the effect of curcumin microparticles on structure and properties of blood cells membranes by the atomic force microscopy

D.L. Radyukevich¹, G.B. Melnikova¹, A.S. Petrovskaya¹, T.N. Tolstaya¹, S.A. Chizhik¹,
N.Th. Binh², N.T. Tinh²

¹A.V. Luikov Heat and Mass Transfer Institute of National Academy of Science of Belarus,
220072, Minsk, Belarus
galachkax@gmail.com

²Institute of Applied Physics and Scientific Instruments of Vietnam Academy of Science and Technology,
Ha Noi, Vietnam

Curcumin has a number of useful pharmacological properties: antioxidant, antibiotic, antiviral, anti-inflammatory. The interaction of curcumin particles and blood cells is an interesting research topic in the pharmacological industry. Atomic force microscopy (AFM) allows determining local changes in structure and mechanical properties of the cell membranes. The aim of the work is to determine influence curcumin microparticles on blood cells properties.

Curcumin microparticles were obtained by spray drying method. For this spray dryer LU-222 Advanced device (Labultima, India) was used, the parameters of the spray drying process: drying air temperature 90 °C, vacuum 1680 Pa, nozzle fluid pressure 4 kg/cm². Microparticles were obtained from 1.25 mass.% suspension of curcumin (Chem-Impex Int'l Inc., Mw 368.38, purity 98.24%) in acetone.

For determine effects of curcumin on cells a suspension of obtained microparticles in physiological solution were used ($C = 1$ mg/ml). Cell samples isolated from the venous blood of healthy patients. Curcumin was incubated with erythrocyte and platelet masses during 60 min at room temperature. Then cells were fixed with glutaraldehyde, washed twice with phosphate buffer and distilled water, formed swab and dried at room temperature on mica substrates.

The effects of curcumin particles on the structure and properties of blood cell membranes were studied by the AFM method (NT-206, produced by MTM, Belarus) and standard silicon probe of V-shaped type CSC 21 B, stiffness 2 N/m, (produced by "Mikromasch", Estonia). Elastic modulus of cells membrane was calculated by the Johnson-Kendall-Roberts model.

It was established, that after effect curcumin microparticles on cells, the elastic modulus of erythrocytes increased from 80.4 to 110.8 MPa, value of adhesion force was halved. An increase in elastic modulus indicates a decrease in cell deformability, as well as their ability to aggregate. The elastic modulus of platelets was decreased, which is associated with an increase in the degree of cells aggregation. Value of adhesion force was not changed.

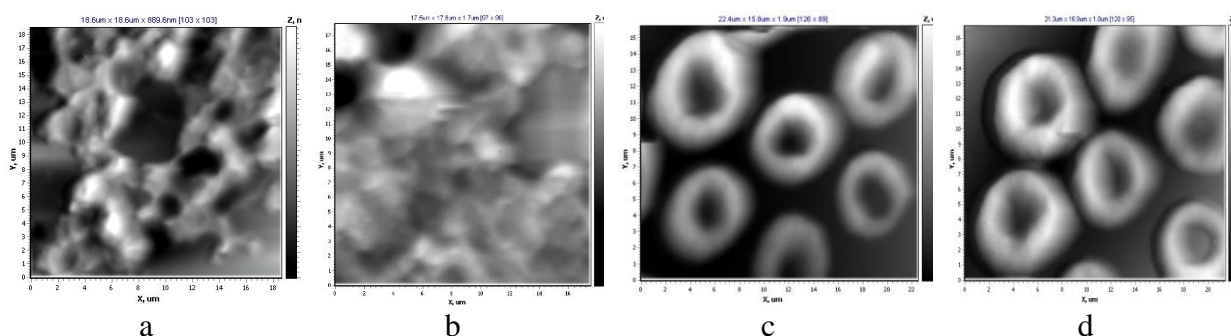


Figure 1. AFM-images of (a, b) initial structure of cells and (b, d) after incubation with curcumin microparticles.

So, by AFM method the changes mechanical properties of two types blood cells after incubation with curcumin microparticles were demonstrated, which can be the result of various biochemical reactions in the process of their interaction.

Scanning probe microscopy investigation of iron garnet films for magnetoplasmonics

A.N. Shaposhnikov¹, S.D. Lyashko¹, A.S. Nedviga¹, A.V. Karavainikov¹, E.Yu. Semuk¹
Yu.E. Vysokikh², T.V. Mikhailova¹

¹V.I. Vernadsky Crimean Federal University, Simferopol, 295007, Russia
taciamic@yandex.ru

²Scientific and Technological Center of Unique Instrumentation of the RAS, Moscow, 117342, Russia
visokih@yandex.ru

Synthesis and investigation of magnetoplasmonic (MP) nanostructures is relevant for construction of micro-dimensional optical isolators, modulators and switches, miniature integrated nanophotonic devices for fast multi-mode and multi-directional control, plasmonic circuit elements controlled by magnetic field [1]. For example, nanostructure “iron garnet (IG) – perforated Au film” experimentally demonstrated the effective modulation of transmission with contrast up to 98% using a weak external magnetic field [2]. Creation of metallic coating on IG films imposes specific surface requirements. Additionally, the films should have definite magnetic and magneto-optical properties [3]. In the work authors present the investigation of topography and domain structures of IG films proposed for magnetoplasmonic applications by scanning probe microscopy methods, including polarization near-field optical microscopy [4].

Films of bismuth-substituted IG with micro and nanoscale thicknesses were synthesized by liquid-phase epitaxy (LPE) and reactive ion beam sputtering (RIBS). Figure 1 (a) and (b) shows the typical surface of LPE film with root mean square surface roughness (rms) of 2.1 nm and its domain structure obtained by magnetic force microscopy with period of 16 μm , respectively. Measurements of various LPE films showed that rms could reach values less than 0.9 nm. Figure 1 (c) demonstrates the surface of deposited film with rms of 7.2 nm, which is determined by the size of polycrystals.

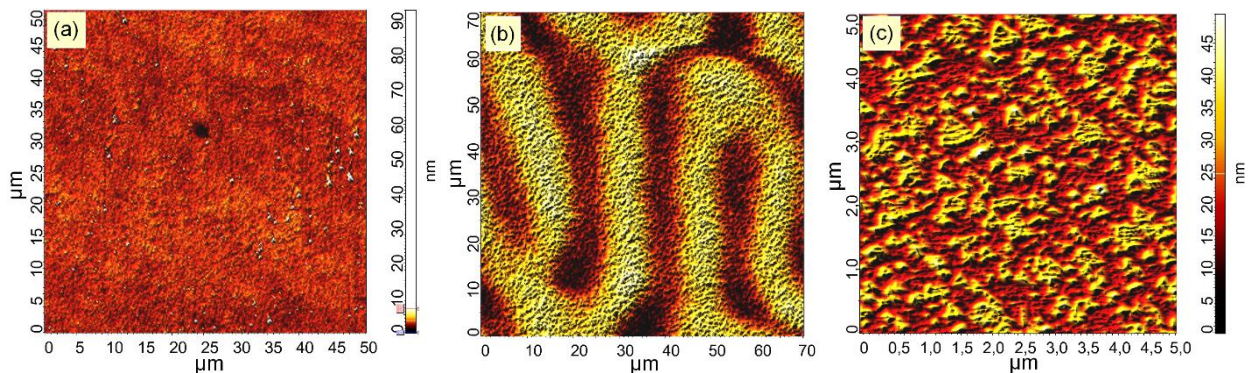


Figure 1. Typical (a) topography and (b) domain structure of LPE IG film and (c) topography of RIBS film.

Considerable attention was paid to minimizing the rms of samples in order to create on them plasmonic meta-surfaces perforated by nanoscale objects. Magnetic and magneto-optical properties of films were discussed also.

Research performed by grant of Russian Science Foundation (project no. 19-72-20154).

1. G. Armelles, A. Cebollada, A. García-Martín, M.U. González, *Adv. Optical Mater* **1**, 10 (2013).
2. G.A. Wurtz, W. Hendren, R. Pollard et al., *New J. Phys.* **10** 105012 (2008).
3. V.N. Berzhansky, A.V. Karavainikov, T.V. Mikhailova, et al., *J. Magn. Magn. Mater.* **440**, 175 (2017).
4. Yu.E. Vysokikh, A.V. Shelaev, A.R. Prokopov, et al, *J. Phys.: Conf. Series* **741**, 012190 (2016).

Dielectric properties of an eco-friendly ferroelectric nanocomposite from cellulose nanoparticles mixed with Rochelle salt

Bich Dung Mai¹, Hoai Thuong Nguyen^{2,3,*}, A.Yu. Milinskiy⁴, S.V. Baryshnikov⁴

¹*Institute of Biotechnology and Food Technology, Industrial University of Ho Chi Minh City, 700000, Ho Chi Minh City, Vietnam*

²*Division of Computational Physics, Institute for Computational Science, Ton Duc Thang University, Ho Chi Minh City, Vietnam*

³*Faculty of Electrical & Electronics Engineering, Ton Duc Thang University, Ho Chi Minh City, Vietnam
nguyenhoaituong@tdtu.edu.vn*

⁴*Faculty of Physics and Mathematics, Blagoveschensk State Pedagogical University, 675000, Blagoveschensk, Russia*

The idea of this study is to develop an eco-friendly ferroelectric nanocomposite based on cellulose nanoparticles (CNP) prepared from cotton waste (Fig. 1a). In [1, 2] the wood was utilized to improve the piezoelectric response of Rochelle salt (RS) or matrix of porous cellulose to synthesize composite with RS. However, due to difficulties in controlling the filling level because of using porous matrices with nanochannels, the influence of RS content on composite properties was not discussed. Besides, ferroelectric properties of RS as phase transition and dielectric relaxation at low frequencies were not reported. To solve these problems, a mixed composite at different composition weight ratios was synthesized in the present study. The composite was carefully characterized to explore the changes of structure and functional groups, and therefore to clarify the interaction of components in the composite (Fig. 1b).

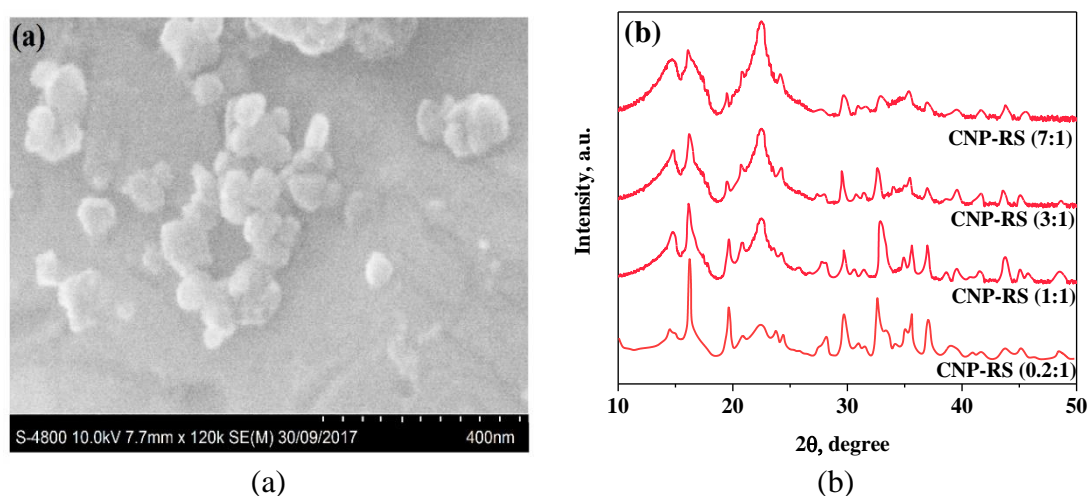


Figure 1. (a) SEM image of the used cellulose grown in near spherical shape and (b) XRD spectra of CNP-RS composite at different composition weight ratios.

The results showed that at low CNP content (CNP:RS = 0.2:1) the upper Curie point (24 °C) characteristic for the RS cluster was observed. For CNP:RS of 0.5:1, 1:1, 3:1 and 5:1, two phase transition points: the lower-temperature one related to RS and the higher-temperature one – to CNP shifted to higher temperatures with increasing CNP content due to the stronger interaction between CNP and RS components were detected. Especially, at CNP:RS ratio of 7:1 and higher CNP content, there was no phase transition detected owing to the maintenance of ferroelectric phase up to decomposition temperature. Besides, a reduction of relaxation frequencies with increasing CNP content was also observed. The strong interaction between hydrogen containing CNP and RS was assumed to be a reason for these mentioned anomalies.

1. E. Lemaire, C. Ayela, A. Atli. *Smart Materials and Structures* **27**, 2 (2018).
2. A.S. Sidorkin, S.D. Milovidova, O.V. Rogazinskaya, Hoai Thuong Nguyen. Patent RU2666857C1 (2018).

Influence of silicon dioxide nanoparticles on dielectric relaxation of triglycine sulfate

B.D. Mai¹, H.Th. Nguyen^{2,3,*}, A.Yu. Milinskiy⁴, S.V. Baryshnikov⁴

¹*Institute of Biotechnology and Food Technology, Industrial University of Ho Chi Minh City, 700000, Ho Chi Minh City, Vietnam*

²*Division of Computational Physics, Institute for Computational Science, Ton Duc Thang University, Ho Chi Minh City, Vietnam*

³*Faculty of Electrical & Electronics Engineering, Ton Duc Thang University, Ho Chi Minh City, Vietnam*

*nguyenhoaituong@tdtu.edu.vn

⁴*Faculty of Physics and Mathematics, Blagoveschensk State Pedagogical University, 675000, Blagoveschensk, Russia*

This study is devoted to clarifying the nature of anomalous phase transition and dielectric relaxation properties of a classical ferroelectric triglycine sulfate (TGS) under the influence of silicon dioxide nanoparticles (SiO_2) at low frequencies of 10^2 - 10^7 Hz in a temperature range from 20 to 120 °C. Although the composite from SiO_2 and TGS has been synthesized already as reported in [1,2], there are several aspects needed to mention: (i) the influence of SiO_2 at different composition weight ratios on properties of TGS was not studied; (ii) the features of dielectric relaxation that plays a leading role for TGS applications at low frequencies were not considered at all. To fill this gap, a composite from silicon dioxide nanoparticles (SiO_2) and triglycine sulfate (TGS) was synthesized at different SiO_2 :TGS weight ratios. X-ray diffraction (XRD) and Fourier-transform infrared spectroscopy (FTIR) techniques were utilized to characterize the synthesized composite samples before utilizing them for dielectric measurements (Fig. 1).

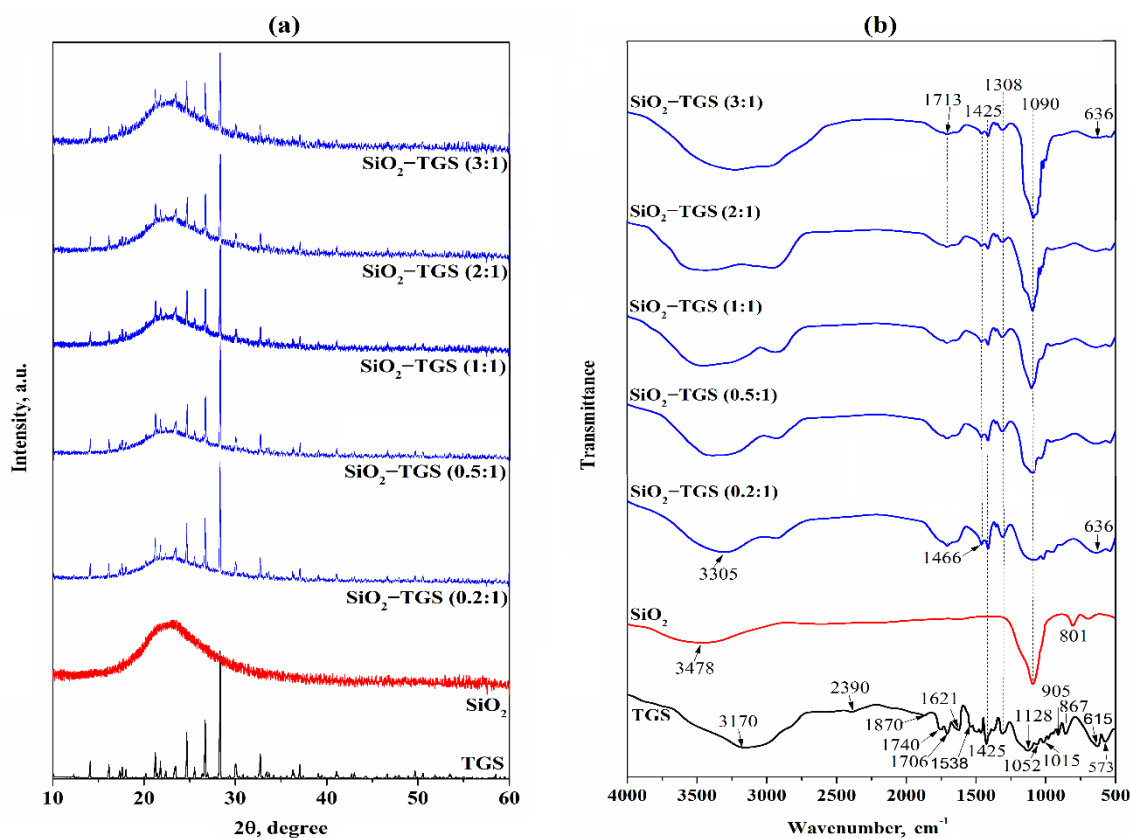


Figure 1. XRD patterns (a) and FTIR spectra (b) for TGS, SiO_2 and for SiO_2 +TGS composite at different composition weight ratios.

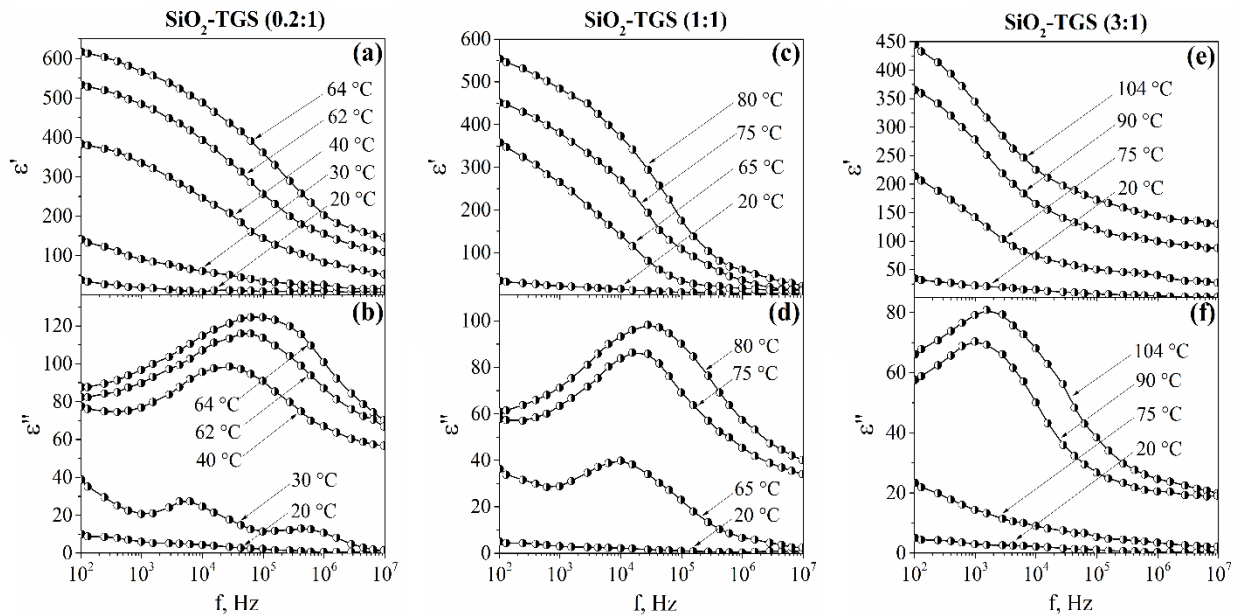


Figure 2. Frequency dependences of the real and imaginary parts of complex dielectric constant for SiO_2+TGS composite at $\text{SiO}_2:\text{TGS}$ weight ratios of 0.2:1 (a, b), 1:1 (c, d) and 3:1 (e, f) at different temperatures in ferroelectric phase.

It was indicated that the relaxation frequencies decreased with increasing SiO_2 content (Fig. 2). In addition, in comparison with Curie point of single crystals TGS, the phase transition temperature in TGS component increased from 15 to 55 °C. The obtained anomalies were thoroughly explained based on the assumption of interaction occurred between composite components through hydrogen bonds.

1. S.D. Milovidova, O.V. Rogazinskaya, A.S. Sidorkin, et al. *Phys. Solid State* **57**, 510 (2015).
2. S.D. Milovidova, O.V. Rogazinskaya, A.S. Sidorkin, et al. *Bull. Russ. Acad. Sci.: Phys.* **74**, 1295 (2010).

The surface piezoresponce and electric potential of the *c*-oriented Sr_{0.5}Ba_{0.5}Nb₂O₆/Pt/Al₂O₃ thin films

M.D. Miruschenko¹, I.A. Donchenko¹, V.A. Yorshin¹, M.A. Bunin¹,
A.V. Pavlenko², D.V. Stryukov², L.I. Kiseleva²

¹Research Institute of physics and Physical faculty, Southern Federal University, 344090, Rostov-on-Don, Russia
miruschenko98mail@yandex.ru

²Southern Scientific center of the Russian Academy of Sciences, 344006, Rostov-on-Don, Russia

The barium-strontium niobate thin films Sr_xBa_{1-x}Nb₂O₆ (SBN, 0 < x < 1) are one of the most promising practically significant lead-free ferroelectric materials with good piezoelectric characteristics, for example, to create a ferroelectric RAM. The SBN lattice is of the tetragonal tungsten bronze (TTB) type and comparing to the cubic oxides with a perovskite structure allows for a greater variety of possible atomic positions in the cell. The only component of the vector of spontaneous polarization is directed along the *c*-axis.

The changing of the domain structure depending on the thin film thickness is considered for the Sr_{0.5}Ba_{0.5}Nb₂O₆ (SBN-50). For this purpose, X-ray diffractometry data, measurements of the piezoelectric response and surface potential were obtained.

The films were deposited on a Pt/Al₂O₃ substrate on a Plasma-50-SE station with the method of HF sputtering of stoichiometric ceramic target at oxygen pressures 0.45-0.55 Torr. The RF discharge power 125-195 W was chosen so as to obtain equally oriented films, which were then studied by X-ray diffractometry (diffractometer DRON-3). The surface piezoresponce and potential images were obtained on the VeecoMultimodeVS SPM using standard methods. Probe SCM-PIC, $k = 0.2$ N/m, $V_{ac} = 2-4$ V, the probe pressure force ~ 102 nN. The potential was recorded using the Kelvin probe method.

The SBN-50 films thickness was 150-230 nm. X-ray diffraction data showed characteristic reflections from the (001), (002), (211), and (311) planes. The change in the relative intensity of the (311) reflection characterizes the degree of the film texturing. The film obtained at the lowest discharge power had the smallest thickness, the highest degree of texturing, and the greatest degree of preferential orientation of the *c*-axes.

The crystallites size forming the films surface was 120-450 nm. Information on the domain structure obtained from the piezoelectric image showed that the fraction of *c*-domains decreases with increasing film thickness. The boundaries of the crystallites do not always coincide with the domains boundaries; they often divide crystallites into parts, pertaining to domains with opposite direction of the spontaneous polarization vector. In the domain boundary region, the potential amplitude is $\sim 60-100$ mV, and its width is ~ 50 mV.

The Fourier filtering method was used to study small-sized peculiarities of the piezoelectric image. It represent an information about the details that usually are hardly distinguishable, but can provide a very important information, for example, about polar nanoregions in relaxors, to which the SBN films belongs. It turned out that for SBN-50 film such areas are located mainly on domain boundaries. Its characteristic size is 3-4 nm.

This work was supported by the Ministry of Education and Science of the Russian Federation (research projects No. 3.1649.2017/4.6 and No. 3.6439.2017).

Effect of the hydrophilicity degree of silicon substrate on the morphology of the triglycine film

A.S. Morozova^{1,2}, S.A. Ziganshina¹, A.A. Bukharaev¹, M.A. Ziganshin²

¹Zavoisky Physical-Technical Institute, FRC Kazan Scientific Center of RAS, 420029, Kazan, Russia
morozova_anna_s@mail.ru

²Kazan Federal University, 420008, Kazan, Russia

The influence of silicon substrates with different surface properties on the self-organization of tripeptide based on glycine in the film was studied using atomic force microscopy.

The formation of organic crystals and studying of their properties are among the actual problems of nanotechnology [1]. Wherein the methods for producing of micro- and nanocrystals with physicochemical properties determined by the surface morphology are being actively developed [2]. One of the methods for formation of organic crystals is the self-assembly of amorphous films deposited on various substrates after interaction with the vapors of organic compounds. Variation of organic vapors or substrate type allows to obtain organic structures with different geometric parameters [3]. At the same time, the directed self-assembly of molecules in thin films and predicting the possible morphology of the film surface and crystals grown is still a challenge [4].

The popular objects for such studies are the oligopeptides, since micro- and nanostructures based on them are currently used in various technologies [5]. A feature of oligopeptides is the ability to self-assemble with the formation of various structures [6]. The simplest oligopeptide from the variety is the dipeptide glycylglycine, formed from the residues of the simplest amino acid – glycine. Glycine being a part of many proteins and biologically active compounds has a high biological activity [7], so the structure and properties of its crystals are rather well studied [8]. But the properties of glycine-based oligopeptide crystals have not been sufficiently studied. Di- and triglycine are of great interest in connection with the possibility of their use in the production of biologically active and medicinal drugs [9].

Earlier we found that the nature of the substrate has a significant effect on the morphology of the initial film of tripeptide (glycyl-glycyl-glycine, GGG) [10], as well as on the morphology of the films after the interaction with organic vapor.

In the present work, the attempt to evaluate the effect of the hydrophobicity degree of silicon substrate on the morphology of GGG film before and after interaction with vapors of organic compounds and water was made. For creation of the silicon surface with hydrophobic properties a special treatment of hydrophilic silicon with a 5% solution of hydrofluoric acid for 40 minutes was used.

Films on the substrate surface were formed by dropping of the freshly prepared tripeptide solution (40 μ l, 1 mg/ml) in a methanol/water mixture followed by solvent evaporation. The extended crystals of GGG on the surface of hydrophilic silicon after spontaneous evaporation of the solvent were formed. The dendrite-like structures of GGG are formed on hydrophobic silicon. Apparently, the crystal structure of silicon promotes the self-assembly of the GGG film with the formation of crystalline structures. On the surface of silicon plate there are oxides and hydroxyl groups which are capable to effective adsorb of the tripeptide molecules. These groups also can orient the GGG molecules in space through interaction with charged carboxylate ($-\text{COO}^-$) and ammonium ($-\text{NH}_3^+$) groups which are in the plane (001) of the GlyGly crystal.

To study the process of self-assembly and the formation of nanostructures and crystals with different shapes and sizes, it is necessary to obtain amorphous films on the surface of the substrates. Since the amorphous films, being metastable from the point of view of thermodynamics, possess excess energy and can be transferred to an ordered state (nanostructures, crystals) under the influence of external factors [11]. Therefore, a technique for producing an amorphous GGG film by quickly evaporation of the solvent was developed.

The saturation of films by the organic compounds vapors (alcohols, chloroform, dichloromethane, benzene, acetonitrile, pyridine) and water was carried out for 2-3 hours at room

temperature. It was found that only strong proton donors (alcohols) and proton acceptor (pyridine) affect the GGG film deposited on hydrophilic silicon. Well-cut rectangular crystals were found on the surface. The results obtained show that hydrophilic silicon prevents the formation of structures on the surface of the amorphous GlyGly film under the interaction with weak (dichloromethane, chloroform, acetonitrile, benzene) proton donors and proton acceptor. In this case, the properties of hydrophilic silicon are similar to those of mica. The morphology of the film deposited on hydrophobic silicon was changed by both strong (alcohols, water and pyridine) and weak (dichloromethane, chloroform, acetonitrile, benzene) proton donors and proton acceptors. For example, the action of dichloromethane vapors on the GG film deposited on hydrophobic silicon leads to the formation of small, interconnected, crystalline structures. In this case, the properties of hydrophobic silicon are similar to those of highly oriented pyrolytic graphite.

Thus, the paper demonstrated the influence of the hydrophilicity degree of a silicon substrate on the surface morphology of GGG films after interaction with vapors of organic compounds.

The results obtained can be useful in developing methods for the controlled assembly of short-chain peptides on solid surfaces by rational choice of substrate and vapor or for explaining the reasons for the formation of various shapes nanostructures based on short peptides when different substrates are used.

1. X. Yang, A.S. Myerson, *Cryst. Eng. Comm.* **17**, 723 (2015).
2. J. Li, C.J. Tilbury, S.H. Kim, M.F. Doherty, *Progress in Materials Science* **82**, 1 (2016).
3. J.S. Lee, J. Ryu, C.B. Park, *Soft Matter* **5**, 2717 (2009).
4. F. Punzo, *J. Molecular Struct.* **1032**, 147 (2013).
5. S. Kim, J.H. Kim, J.S. Lee, C.B. Park, *Small* **11**, 3623 (2015).
6. M. Zelzer, *Chem. Soc. Rev.* **39**, 3351 (2010).
7. Y. Lu, X. Zhu, J. Li, *Biochemical Pharmacology*. **123**, 40 (2017).
8. V. Vijayalakshmi, P. Dhanasekaran, *J. Cryst. Growth*. **506**, 117 (2018).
9. M. Liakopoulou-Kyriakides, *Studies in Natural Products Chemistry* **27**, 793 (2002).
10. А.С. Морозова, С.А. Зиганшина, А.А. Бухараев, М.А. Зиганшин, *Труды XXIII Международного симпозиума «Нанозелектроника» 11–14 марта 2019 г., Нижний Новгород*. **1**, 373 (2019).
11. P.G. Debenedetti, F.H. Supercooled, *Nature* **410**, 259 (2001).

Significant influence of metal surface morphology on photon emission from a local tunnel junction at ambient conditions

I.S. Mukhin^{1,2}, V.A. Shkoldin^{1,2}, D.V. Permyakov¹, K.S. Ladutenko¹, A.A. Vasiliev²,
A.V. Uskov⁴, A.A. Bogdanov¹, A.O. Golubok^{1,3}, A.K. Samusev¹

¹*ITMO University, 197101, St. Petersburg, Russia*
imukhin@yandex.ru

²*St.Petersburg Academic University, 194021, St. Petersburg, Russia*

³*Institute for Analytical Instrumentation RAS, 198095, St. Petersburg, Russia*

⁴*P.N. Lebedev Physical Institute Russian Academy of Sciences, 119991, Moscow, Russia*

Modern computational devices are based on conventional integrated circuits, where data transfer is organized via electronic signals. Nowadays performance of these devices is close to their theoretical limit. One of the promising ways to overcome the current limitations is based on a transition to optical platform with photonic integrated circuits, which may provide increase of operating frequencies along with the reduced Joule heating.

For real implementation of the integrated optoelectronic circuits, development of electrically driven localized photonic and plasmonic emitters is required. Tunnel electrical contact is one of the promising ways to develop sub-micron optical emitters. According to Lamb and McCarthy the light emission is governed by inelastic electron tunneling in a planar metal-insulator-metal structure with a thin potential barrier. According to the results of several theoretical and experimental works [5], light emission in this system is related to quantum oscillations of the tunnel current. An enhanced photon emission in a tunnel contact between a metal tip of scanning tunneling microscope (STM) and a metal layer was demonstrated by Gimzewski et al. [6]. This effect occurs due to the increase of the local density of optical states (LDOS) in the tunnel gap under the STM probe. In this system, the tunnel gap has a few nanometer size and can be considered as electrically driven subwavelength optical source.

We study light emission from a tunnel contact between thin Au film on a cover glass and STM W probe covered with Au layer. At ambient conditions we investigate the dependence of the photon emission intensity on Au film surface morphology, namely on geometrical parameters of constituent nanometer-scale Au grains. AIST-NT CombiScope – STM with integrated inverted optical microscope was used to study the light emission in tunnel junction. The emission was collected under the substrate covered with Au. The photon emission was observed when STM operated in “threshold” mode with excited feedback [3]. In this mode the system promotes fast approach of the probe to the sample and when the current flow occurs the feedback system immediately brakes the contact moving the probe from the sample. As a result, oscillations of the gap occur leading to the tunnel current fluctuations while the total integral current value remains. It was demonstrated experimentally that this regime provides maximum photon emission efficiency. Analysis of the experimental data reveals that photon emission is more efficient with decrease of grain height and increase of grain width. The atomically flat monocrystalline Au sample allows to achieve maximum efficiency of photon emission. In the same STM regime, one could tailor the emission efficiency in four orders of magnitude range by changing the surface morphology. The observed phenomena are explained by the fact that the effective area of tunnel contact is inverse proportional to the square of the grain aspect ratio.

The obtained results demonstrate the critical influence of nanometer surface roughness of the sample on the efficiency of photon emission from tunnel junction. Due to low quantum yield of the emission in the tunneling process our results would have important value for development of effective single photon emitters which could be the basic of optoelectronic components.

1. F. Bigourdan, J.-P. Hugonin, F. Marquier, C. Sauvan, J.-J. Greffet. *Phys.Rev. Lett.* **116**, 106803 (2016).
2. J. Kern, R. Kulloock, J. Prangmsma, M. Emmerling, M. Kamp et al. *Nature Photonics* **9**, 582 (2015).
3. B. Rogez, S. Cao, G. Dujardin, G. Comtet, E. Le Moal et al. *Nanotechnology* **27**, 465201 (2016).

SEM and SPM studies of friction composite materials based on carbon graphitized fibers

T.I. Muravyeva, A.G. Shpenev, D.L. Zagorskiy, I.V. Shkalei

Ishlinsky Institute for Problems in Mechanics RAS, 119526, Moscow, Russia
 muravyeva@list.ru

Carbon composites based on graphitized fiber and pitch matrix demonstrate high wear resistance and heat resistance, which makes them an ideal material for the manufacture of brake discs in the aircraft industry. The influence of the microstructure of graphitized fiber on the structure and wear resistance of friction composite materials was investigated and discussed.

Two samples of materials – type №1 (reference) and type №2 – were tested. The only difference in the production technology of these materials was the different composition of fiber impregnation (apret) before their graphitization. However, the samples showed a significant difference in wear resistance during friction testing. Samples were studied after tests carried out at the IM-58 friction machine. In order to estimate the effect of the microstructure of the fibers and the structure of the finished materials on their wear resistance, investigations were carried out using optical (OM), scanning electron (SEM) and scanning probe microscopy (SPM) methods. High resolution images of the friction surface of the samples were obtained using the SPM Smart SPM TM. AIST-NT cantilevers (fpN10), operated in tapping mode with beam stiffness – 10-20 N/m and resonant frequency 200-300 kHz were used. The maximum scanning field was 100x100 μm .

The tribological tests showed that the wear resistance of samples of type №2 is much lower. This was explained by the SEM and AFM investigations. Figure 1 shows the SEM images of single fibers of composite materials (samples of type №1 and type №2).

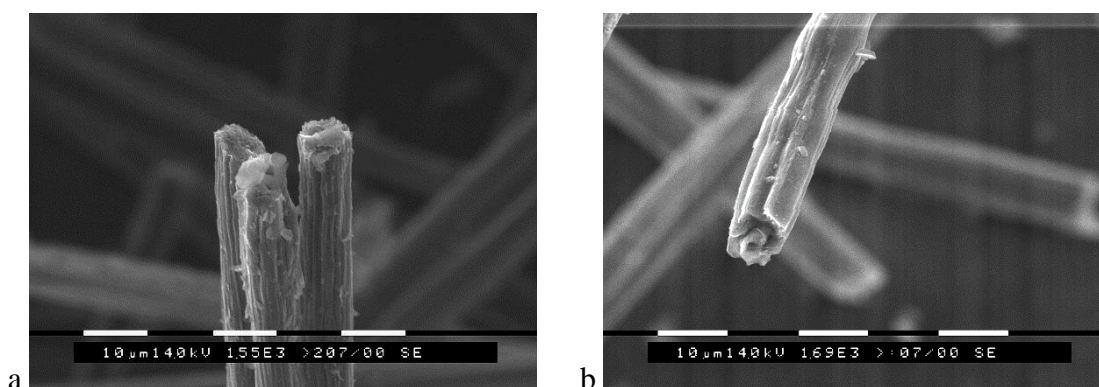


Figure 1. SEM-images of single fibers of composite materials: (a) sample of type №1 (reference), (b) type №2.

It is clearly seen that the structure of fiber (sample of type №1) consists of a large number of even plates, which are crystalline layers of graphite. The fiber sample of type №2 consists of a smaller number of thicker layers, which also have an uneven shape along the fiber axis. This leads to significant changes in the shape of the lateral surface of the fiber. The lateral surface of the fiber of reference sample type №1 has smooth fins of crystalline graphite layers, while the fiber of sample type №2 has an irregular shape with cracks and depressions. Changes in the surface structure of the fiber lead to changes in the layers of the matrix adjacent to the fibers. During the formation of the pitch matrix, carbon layers are formed around the fibers during the pyrolytic decomposition of the oil pitch. The structure of the layers of the matrix surrounding the fiber depends on the structure of the surface of the fiber. This leads to a change in the entire layered structure of the composite material.

SPM studies were carried out for a detailed study of the layers of the matrix surrounding carbon fibers. Figure 2 shows SPM images of the surface of composite materials of two samples after friction tests.

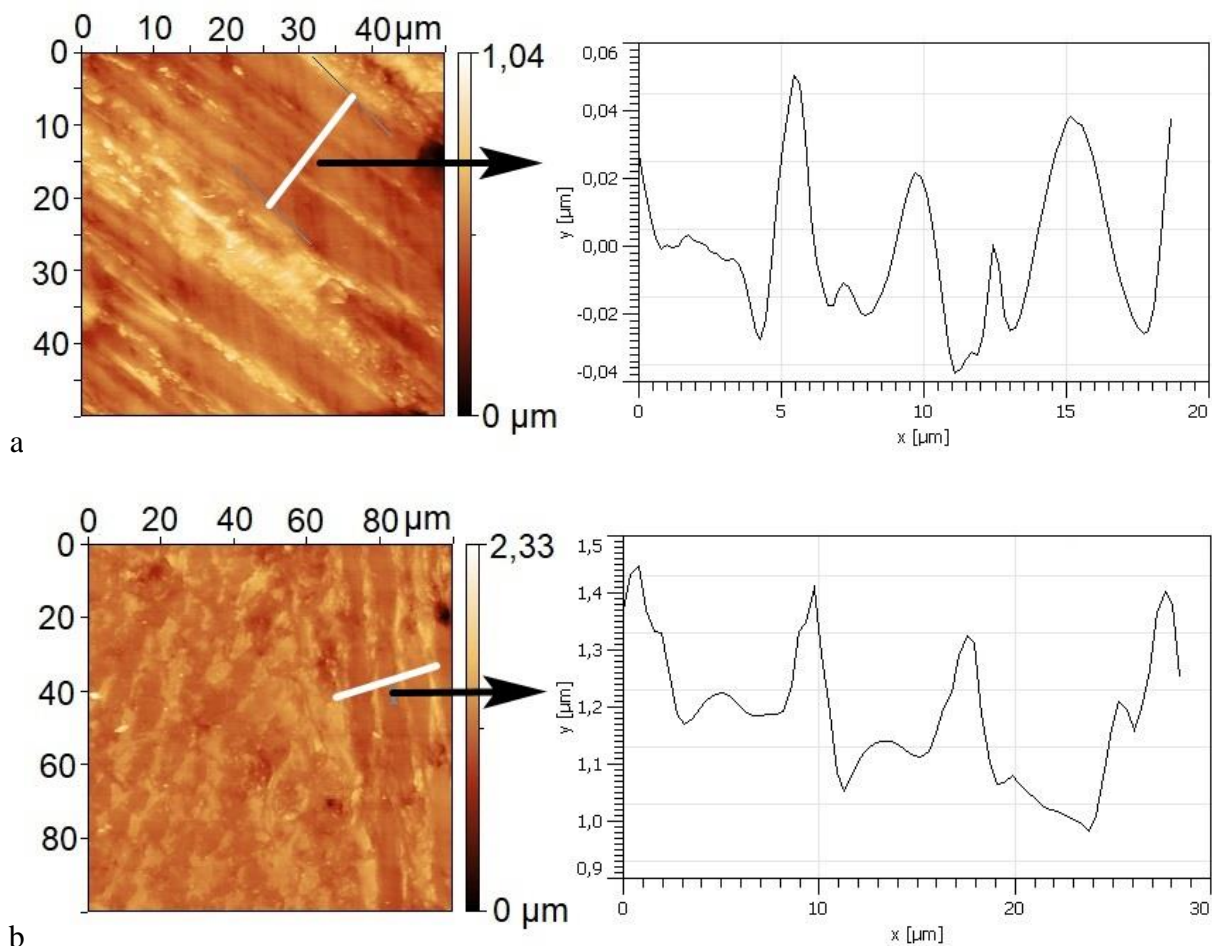


Figure 2. SPM-images of the surface of composite materials: (a) the morphology of material of samples of type №1 and the section profile; (b) the morphology of the material of samples of type №2 and the profile of the secant.

Analyzing profilograms of friction surfaces obtained using the SPM method, we can draw conclusions about the properties of the fiber and the matrix and their relative position. An important feature of the material of samples type №1 (Fig. 2 a) is that the difference of the levels of the surface around the underlying fiber are small – they are of the order of $0,01 \mu\text{m}$, that is, the fibers are actually flush with the matrix. This means that the wear rates of the fiber and the matrix are almost identical, which ensures optimum wear resistance of the material as a whole. In materials of sample №2, the fibers lie noticeably below the level of the matrix – by $0,3\text{--}0,4 \mu\text{m}$ (Fig. 2 b). This means that, firstly, the wear resistance of the fibers of sample №2 is lower than the wear resistance of the matrix, and hence the wear resistance of the reference fibers. Secondly, the increased roughness causes an additional increase of wear by the abrasive mechanism.

The results obtained allow us to conclude that small changes in the production technology of fibers lead to significant changes in the structure and properties of the finished fibers. These changes effect on the wear resistance of the composite material as a whole.

The work was supported by the Russian Scientific Foundation (project no. 19-19-00548).

Influence of surface treatment on the structure and properties of proton-exchanged waveguides in lithium niobate

S.S. Mushinsky¹, I.V. Petukhov^{1,2}, V.I. Kichigin^{1,2}, O.P. Semenova², A.B. Volyntsev²

¹PNPPK, 614990, Perm, Russia
sergey.mushinsky@gmail.com

²Perm State University, 614000, Perm, Russia

Lithium niobate (LN) surface condition greatly influences proton exchange (PE) process which in turn influences the structure and properties of PE-waveguides. Influence of several types of surface treatment on the structure and properties of waveguides in congruent LN (X-cut) was investigated in this work.

In particular, it was found that surface treatment in the mixture of sulfuric acid and hydrogen peroxide (Piranha solution) or in the mixture of ammonium hydroxide and hydrogen peroxide (RCA-1) leads to increased value of extraordinary refractive index change at the surface of the crystal (Δn_e) after PE and annealing. This may be explained by a better cleaning of the surface of lithium niobate.

On the other hand, surface treatment in oxidizing media containing fluoride ions (mixture of hydrofluoric and nitric acids) leads to decreased values of Δn_e after PE and annealing. After such treatment, surface composition of LN crystal may change (more specifically, niobium ions depletion and oxygen ions enrichment may occur) which lead to PE inhibition. Since proton concentration in the molten benzoic acid is extremely small, PE happens probably due to hydrogen ions resulting from dissociative adsorption of benzoic acid molecules on the surface of LN.

Congruent LN contains up to 4% lithium vacancies. Moreover surface layer may contain sufficient number of defect structures formed during wafer manufacturing, e.g. cutting, lapping, polishing. Surface treatment in molten eutectic mixture of LiNO_3 37.5 mol.%, KNO_3 44.5 mol.% and NaNO_3 18.0 mol.% (the mixture was also used for reverse proton exchange (RPE)) could "heal" defects of the surface layer. Nevertheless, LN surface treatment during 1 hour at 330 °C does not influence subsequent PE. This may be caused by great changes of LN surface during proton exchange process initiated by lithium ion substitution with hydrogen ions. This is why preliminary changes in composition of thin surface layer caused by treatment in lithium-rich melt are rapidly mitigated during proton exchange.

Influence of RPE on waveguide characteristics was studied. RPE rate is greater for unannealed waveguides rather than annealed ones. Structural phase transition rate is greater for RPE than for annealing at the same temperature (330 °C). RPE does not lead to formation of κ_1 -particles which form during post-PE annealing [1].

The research was supported by RFBR (project No. 17-43-590309 p_a).

1. S.S. Mushinsky, V.I. Kichigin, I.V. Petukhov, M.A. Permyakova, D.I. Shevtsov, *Ferroelectrics* **508**, 40 (2017).

Analysis of porosity influence on the effective moduli of ceramic matrix PZT composite based on the simplified finite element model

A.B. Kudimova, A.V. Nasedkin

*Southern Federal University, 344090, Rostov-on-Don, Russia
nasedkin@math.sfedu.ru*

To improve the efficiency of piezoelectric materials, composites based on piezoceramics are being actively created during the last years. So, to improve the mechanical properties, more rigid crystallites can be added to piezoceramics at the sintering stage and a piezoceramic – crystallite composite can be obtained. In reality, such a composite is three-phase, consisting of a piezoceramic matrix, elastic inclusions and pores, mostly located at the boundaries between piezoceramics and inclusions. The total porosity in ceramic-matrix composites can be both small and large enough. In this regard, when designing such composites, it is desirable to take porosity into account either as the third phase, or as the boundary of a loose contact of the main phases.

This paper considers the problem of determining the full set of effective moduli of granular piezocomposites, taking into account both the distributed microporosity in the ceramic matrix and the mesoporosity on some of the contact boundaries of elastic granules with piezoceramics, i.e. taking into account pores comparable in size to the size of inclusions. The homogenization problems were solved using the effective moduli method of the mechanics of composites. All stages of modelling and computing were implemented in the ANSYS finite element package.

A cube uniformly divided into cubic cells was considered as a representative volume element. Each cell consisted of finite elements in the form of rectangular parallelepipeds with the properties of dense PZT ceramics, material of elastic inclusions or pores. Some cells consisted of eight finite elements, with only the main cubic elements provided with properties of inclusions by random number sensor (painted in turquoise in Fig. 1 and 2). The finite elements adjacent to the faces with the elements - inclusions, by a random number sensor were endowed with the properties of pores (painted in purple in Fig. 1 and 2). The remaining elements of the structure (painted in red in Fig. 1 and 2) had the material properties of the PZT ceramic matrix. The choice of the relative sizes of inclusions and pores, as well as the number of elements of inclusions and pores, was determined on the basis of the specified volume concentrations of inclusions and pores.

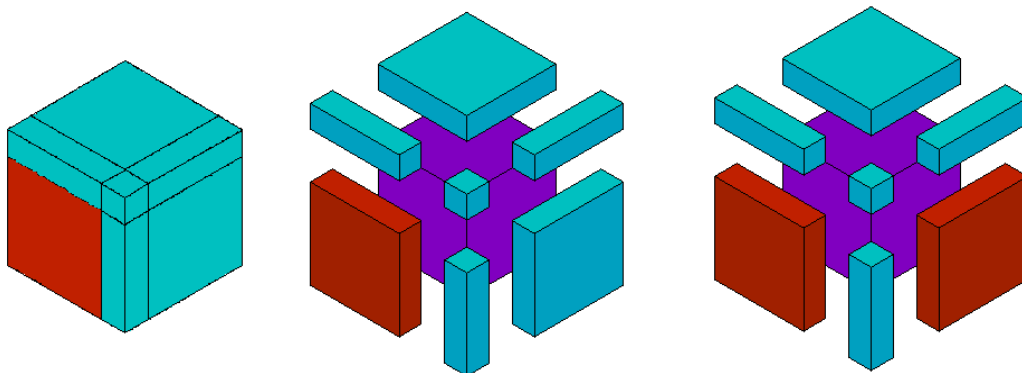


Figure 1. Example of the composite unit cell.

Figure 1 shows an example of a single ceramic matrix composite cell with inclusion and pores. The cell itself is shown on the left, the disassembled cell with one pore in the center, the disassembled cell with two pores on the right.

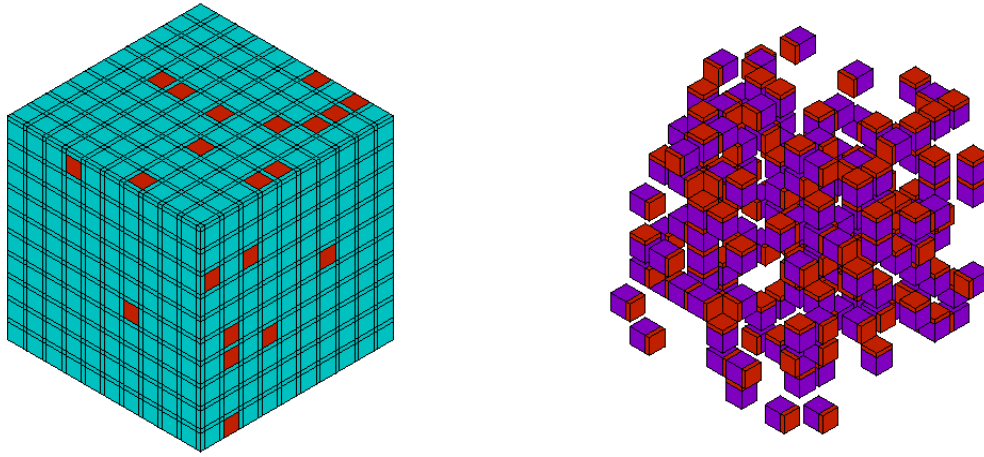


Figure 2. Example of a representative volume of the composite.

Figure 2 shows an example of a representative volume of the composite in which each inclusion has one pore nearby. The entire representative volume is shown on the left, and the elements with properties of inclusions and pores are shown on the right.

The described technique of constructing representative volumes was applied to composites with mesoporosity. The microporosity accounting was carried out in two stages. At the first stage, structures of representative volumes of microporous PZT ceramic material were built using a similar technology without elastic inclusions and its effective moduli were determined. At the second stage, the ceramic-matrix composite with micro- and mesoporosity was studied as a three-phase: the first phase were piezoelectric ceramics with effective moduli of the microporous material found at the first stage, the second phase were elastic inclusions, and the third phase were mesopores.

As an example, calculations of effective moduli of composites consisting of a piezoceramic matrix of PCR-1 and with inclusions of α -corundum were carried out. The analysis of effective moduli was carried out depending on the proportion of inclusions and the presence or absence of micro- and mesoporosity. The resulting dependences of the effective moduli on the content of inclusions and pores were as expected. Since the inclusions were more rigid than piezoceramics, the effective moduli of stiffness increased with the increase in the proportion of inclusions. In addition, since the inclusions were absolutely elastic with low dielectric permittivities, the effective piezomoduli and dielectric permittivities decreased in absolute value with an increase in the fraction of inclusions. The accounting of the porosity reduced the effective stiffness as well as piezomoduli and dielectric constants. At the same time, mesoporosity had a more significant effect compared to micro porosity, since, in the presence of mesopores, the boundaries of incomplete fit of inclusions with a ceramic matrix were also taken into account. The results obtained allow to estimate the effective moduli of ceramic matrix piezocomposites for different proportions of inclusions, pores, and their sizes.

The work was carried out as part of project No. 9.1001.2017 / 4.6 of the competitive part of the state task of the Ministry of Science and Higher Education of Russia.

Crystal structure and growth kinetics of self-assembled microtubes with different chirality

A.S. Nuraeva¹, P.S. Zelenovskiy^{1,2}, S. Kopyl³, S.G. Arkhipov⁴, S.G. Vasilev^{1,5}, V.S. Bystrov⁶, D.A. Gruzdev⁷, M. Waliczek⁸, V. Svitlyk⁹, V.Ya. Shur¹, L. Mafra², A.L. Kholkin^{1,3}

¹*School of Natural Sciences and Mathematics, Ural Federal University, 620000 Ekaterinburg, Russia
alla.nuraeva@urfu.ru*

²*Department of Chemistry & CICECO–Aveiro Institute of Materials, University of Aveiro, 3810-193 Aveiro, Portugal*

³*Department of Physics & CICECO–Aveiro Institute of Materials, University of Aveiro, 3810-193 Aveiro, Portugal*

⁴*Novosibirsk State University, 630090 Novosibirsk, Russia*

⁵*Department of Chemical Science, University of Limerick, V94 T9PX Limerick, Ireland*

⁶*Institute of Mathematical Problems of Biology, Keldysh Institute of Applied Mathematics, RAS, 142290 Pushchino, Moscow region, Russia*

⁷*Postovsky Institute of Organic Synthesis, Russian Academy of Sciences (Ural Branch), Ekaterinburg, 620990, Russia*

⁸*Faculty of Chemistry, University of Wroclaw, 50-383 Wroclaw, Poland*

⁹*European Synchrotron Radiation Facility, 38043 Grenoble, France*

Chirality is an intrinsic universal property of matter inherent to many organic molecules as amino acids, sugars, etc. Chirality has a major influence in engineering of new nonlinear optical materials [1] and recently became a central concept in spintronics [2]. Detailed study of chirality-dependent material properties needed for practical applications. The simplest objects for this investigation are peptides due to their wide range of self-assembled structures such as thin films, nanobelts, vesicles, nanospheres, fibers, nano- and microtubes etc. [3]. These structures possess chirality at different hierarchical levels of organization and are considered as advanced functional materials for nanotechnological and biomedical applications since they possess many attractive properties, such as inherent biocompatibility, structural and functional flexibility, biodegradability, availability and cost-effectiveness.

Diphenylalanine (H-Phe-Phe-OH, FF) is the simplest aromatic dipeptide and the most studied self-assembled peptide for now [4]. Intensive research of FF-based nanotubes (NTs) and microtubes (MTs) in last years showed their unique assembly characteristics and remarkable physical properties such as high rigidity [5] notable thermal stability [6] interesting electronic [7] nonlinear optical [8] and photoluminescent [9] properties as well as exceptional piezoelectric effect [10] and pyroelectricity [11]. However, despite of the numerous studies on the FF self-assembly, physical properties and applications, the role of chirality in its structure and properties is still poorly studied and understood.

Since FF is a chiral molecule it can exist in two enantiomeric forms: H-L-Phe-L-Phe-OH (L-FF) and H-D-Phe-D-Phe-OH (D-FF). Recent study by molecular modeling had shown that α -helix NTs of L-FF and D-FF possess different total energies and dipole moments [12]. In this way, here could be the differences in structure and properties of L-FF and D-FF NTs and MTs.

Therefore, this work is aimed to perform an experimental and theoretical study of the structure and growth kinetics of L-FF and D-FF microtubes. Better understanding the role of chirality in the growth process will allow improving the methods for NTs and MTs fabrication, their better implementation in various functional devices, and may assist in developing new drugs and biomaterials. It was shown that L-FF and D-FF MTs simultaneously grown under identical ambient conditions have quite different morphology. L-FF MTs have a tendency to branching and their length is almost twice comparison to D-FF MTs. Along with this fact, the diameter of L-FF MTs is 20% lower than that of D-FF MTs (Table 1). The *in-situ* study of MTs growth showed that both L-FF and D-FF MTs have similar growth kinetics with small difference. The average growth rate of L-FF MTs, taken from the linear regression slope considering all experimental points, is significantly lower than that of D-FF (0.5 $\mu\text{m/s}$ for L-FF vs. $\sim 2 \mu\text{m/s}$ for D-FF). At the same time, step-like growth behaviour in case of L-FF MTs is not that pronounced as in case of D-FF MTs, which means that in nonregular plateaus the length of D-FF MTs almost does not change.

Table 1. Comparison of morphologies of L-FF and D-FF MTs.

| Enantiomer configuration | Mode length, μm | Median length, μm | Diameter, μm |
|--------------------------|----------------------------|------------------------------|-------------------------|
| L-FF | 860 ± 230 | 1089 | 1.9 ± 0.6 |
| D-FF | 490 ± 120 | 610 | 2.3 ± 1.0 |

The X-ray diffraction study showed L-FF tubes belong to $P6_1$ space group which leads to right-handed helix for L-FF NTs, while D-FF MTs belong to $P6_5$ space group which leads to left-handed helix for D-FF NTs. Obviously, this symmetry difference is attributed to FF monomer chirality.

In order to understand the differences in morphology and growth kinetics, the total energy of six-molecule FF rings – structural units of the nanotubes, and the interaction energy between two FF rings for both forms were calculated using experimentally determined data. The obtained total energy for L-FF ring appears to be higher than that for D-FF ring, however this difference does not depend on the distance and the direction of removal of one FF monomer. The interaction energy between two FF rings was calculated along either c -axis or a -axis, thus simulating the interaction at growing and side facets of the MT, respectively. For arrangement of the rings along c -axis the values of interaction energy are almost the same for both L-FF and D-FF rings. At the same time, for arrangement of the rings along a -axis the value of interaction energy for D-FF rings is about 25% higher than that for L-FF rings. Thus, this difference could shed light on the origin of different morphology and growth kinetics of L-FF and D-FF MTs.

It was found for the first time that L-FF and D-FF microtubes have different crystal structure and demonstrate their different growth kinetics, regardless of the chemically identical composition of these L- and D- enantiomers. L-FF microtubes demonstrate gradual continuous growth leading to almost doubling their lengths with respect to D-FF, showing a step-like growth. The essential difference in interaction energies of the rings at side facets of the growing L-FF and D-FF microtubes was found which satisfactorily explains the observed effects. These effects can be considered in the design of biocompatible electronic components and biosensors, where the enantiospecific interaction between the sensor and the analyte can take place.

The measurements of microtubes growth kinetics and morphology analysis were done in Ural Federal University (UrFU) and made possible by Russian Science Foundation (Grant No. 18-72-00052). The equipment of the Ural Center for Shared Use “Modern nanotechnology” UrFU was used. Computer simulation was performed under the support of Russian Foundation for Basic Research (Grant No. 19-01-00519 A). X-ray diffraction data were collected under the experiment SC-4587 at the European Synchrotron Radiation Source (ESRF, Grenoble, France). S.K., P.Z., L.M. and A.K. are grateful to FCT project PTDC/CTM-CTM/31679/2017. P.Z. and L.M. are grateful to FCT project PTDC/QEQ-QAN/6373/2014. S.K and A.K were also supported by the joint Portugal-Turkey project (TUBITAK/0006/2014). Part of this work was developed within the scope of the project CICECO-Aveiro Institute of Materials, FCT Ref. UID/CTM/50011/2019, financed by national funds through the FCT/MCTES.

1. T. Verbiest, S. Van Elshocht, M. Kauranen, L. Helleman, et al., *Science* **282**, 913 (1998).
2. R. Naaman, D.H. Waldeck, *Annu. Rev. Phys. Chem.* **66**, 263 (2015).
3. J. Wang, K. Liu, R. Xing, X. Yan, *Chem. Soc. Rev.* **45**, 5589 (2016).
4. L. Adler-Abramovich, E. Gazit, *Chem. Soc. Rev.* **43**, 6881 (2014).
5. P. Zelenovskiy, I. Kornev, S. Vasilev, A. Kholkin, *Phys. Chem. Chem. Phys.* **18**, 29681 (2016).
6. P.S. Zelenovskiy, A.O. Davydov, A.S. Krylov, A.L. Kholkin, *J. Raman Spectrosc.* **48**, 1401 (2017).
7. B. Akdim, R. Pachter, R.R. Naik, *Appl. Phys. Lett.* **106**, 183707 (2015).
8. A. Handelman, S. Lavrov, A. Kudryavtsev, et al. *Adv. Optical Mater.* **1**, 875 (2013).
9. T. Nikitin, S. Kopyl, V.Ya. Shur, Y.V. Kopelevich, A.L. Kholkin, *Phys. Lett. A* **380**, 1658 (2016).
10. A. Kholkin, N. Amdursky, I. Bdikin, E. Gazit, G. Rosenman, *ACS Nano* **4**, 610 (2010).
11. A. Esin, I. Baturin, T. Nikitin, S. Vasilev, et al, *Appl. Phys. Lett.* **109**, 142902 (2016).
12. V.S. Bystrov, S.A. Kopyl, P. Zelenovskiy, O.A. Zhulyabina, V.A. Tverdislov, F. Salehli, N.E. Ghermani, V.Ya. Shur, A.L. Kholkin, *Ferroelectrics* **525**, 168 (2018).

Investigation of the surface of *Chlorella* microalgae by atomic force microscopy in liquid

A.A. Okhotnikova, V.A. Smirnov

*Southern federal university, Institute of Nanotechnologies, Electronics and Equipment Engineering
347928, Taganrog, Russia
ohotnikova@sfnedu.ru*

Recently, an increase in the demand for fuel leads to a significant problem of the modern world - the limited reserves of coal and oil. In addition, the burning of fossil raw materials leads to the release of carbon dioxide, the accumulation of which leads to a deterioration of the ecological situation in the world. Therefore, the development of alternative methods for obtaining renewable and non-polluting harmful substances from the combustion of fuels is the important task of modern science.

A significant role in solving this problem can play microalgae – photosynthetic organisms that use the energy of sunlight to convert carbon dioxide and water into organic matter. This organic substance can be converted into biodiesel and ethanol. Microalgae are not demanding to live conditions, methods of their cultivation are simple and inexpensive. For the effective cultivation of microalgae, it is necessary to study the geometric parameters and the external influences on their life. New opportunities for studying micro- and nanoscale biological objects are provided by AFM, which allows one to study biological objects without their special sample preparation under natural conditions. The aim of this work is to study the geometric parameters of microalgae *Chlorella* by AFM and the seasonal change in their morphology.

Water samples taken from the area of the Taganrog Bay of the Azov Sea in the spring were used. Using an optical microscope of scanning probe nanolaboratory (SPN) Ntegra Vita (NT-MDT) the types of microalgae were identified: dinophyte, green, diatom and blue-green. Of greatest interest were green and blue-green microalgae, the starch product of which is starch, and in conditions of nitrogen deficiency - oil. *Chlorella* prevailed among green algae, which was chosen for study. The optical image of the microalgae data is presented in Figure 1 a.

Then *Chlorella* microalgae were investigated by atomic force microscopy in liquid on SPN. Silicon cantilever of brand NSG 20 was used. Figure 1 b. the AFM image of *Chlorella* microalgae obtained by scanning in sea water is presented. During the experiment, it was found that when scanning in air microalgae were also covered with inorganic elements, which distorted the topology of their surface. This problem was solved with the help of AFM method in liquid, which allows to study microalgae in natural conditions, without preliminary sample preparation.

Using the method of AFM in a liquid, the geometrical parameters of microalgae *Chlorella* were determined. Analysis of the images showed that the length varied from 1.4 to 2.5 μm , its width from 1.1 to 1.45 μm , while in the central part of the microalgae a characteristic deepening was observed from 2 to 41 nm. The results obtained can be used in the development of technological processes for the manufacture of biofuels based on biomass of microalgae.

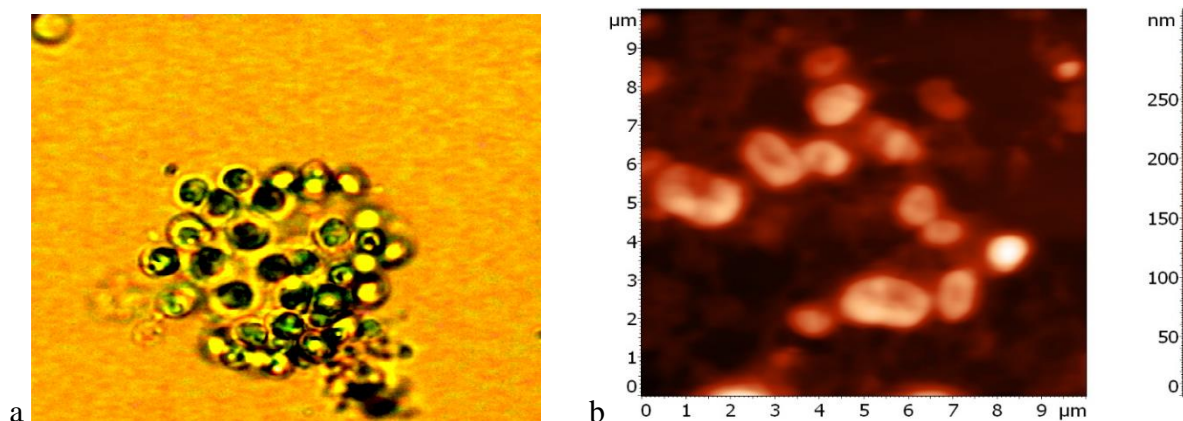


Figure 1. The results of the study of the surface of microalgae *Chlorella*: (a) optical image of microalgae with magnification $\times 1100$; (b) AFM-image of microalgae, obtained in liquid.

Dielectric and repolarization properties of BaTiO₃/BaZrO₃ ferroelectric superlattices

A.S. Sidorkin¹, L.P. Nesterenko¹, Y. Gagou², P. Saint-Gregoire³, |
A.Yu. Pakhomov¹, E.V. Vorotnikov¹, N.G. Popravko¹

¹*Voronezh State University, 394018, Voronezh, Russia*
 sidorkin@phys.vsu.ru

²*Universite de Picardie Jules Verne, 80039 Amiens Cedex, France*

³*ICGM, C2M, 34095 Montpellier Cedex, France; University of Nimes, 30021 NIMES Cedex 01, France*

Ferroelectric superlattices consisting of several alternating layers of different ferroelectrics or ferroelectric and dielectric demonstrate better functional characteristics than single-component thin films or may have new properties that are not observed in individual layers.

In the present work we study multilayer structure consisting of 32 alternating pairs of BaTiO₃/BaZrO₃ epitaxial layers with a period of 13.32 nm on MgO single crystal substrate with the conductive compound LSCO (La_{0.5}Sr_{0.5}CoO₃) sublayer obtained by pulsed laser deposition. The sprayed layers surface quality was controlled by fast electron diffraction technique. The results of X-ray diffraction studies (CoK α radiation) showed structural perfection of superlattices without the presence of impurity phases. According to the X-ray phase analysis, was determined the parameter of the unit cell of the obtained superlattice in the normal to the substrate plane direction: $a = 4.0838 \text{ \AA}$.

Temperature measurements of the main dielectric parameters, such as polarization, coercive field and dielectric constant, have shown the existence of a ferroelectric phase transition at a temperature of 393 °C that is much higher than for BaTiO₃ ferroelectric.

The polarization switching study was conducted by dielectric hysteresis loops and switching currents using the Merz method. According to the switching currents data, the region of weak and strong fields was studied. It is shown that the magnitude of the threshold field separating these regions corresponds to the coercive field and decreases as it approaches the Curie point.

The study of switching currents in weak fields revealed that the integral characteristics of switching, and, consequently, domain boundaries movement speed do not obey a strictly exponential dependence on the field strength. This leads to the appearance of a dynamic indicator μ for the switching current power dependence (the velocity of the domain boundaries) on the electric field strength, which magnitude is less than one and changes slightly when approaching the phase transition point.

On the basis of the switching time for the region of strong fields was calculated the mobility of the domain boundaries at various temperatures. The switching time increases with increasing of the temperature. That means a decrease of the domain boundaries mobility, probably due to the critical deceleration of polarization relaxation near the Curie point.

Probe microscopy for investigation of conical nanowires

D.V. Panov^{1,2}, D. A. Cherkasov¹, D.L. Zagorskiy¹

¹*Shubnikov Institute of Crystallography of Federal Scientific Research Centre “Crystallography and Photonics” of Russian Academy of Sciences, Moscow, Russia
dggamer@mail.ru*

²*National Research University Higher School of Economics, Moscow, Russia*

A large number of studies have been devoted to the preparation of metallic nanowires (NWs) by the matrix synthesis method. It is known that, in addition to the “traditional” cylindrical NWs, the method makes it possible to obtain cone-shaped nanostructures. Such structures are interesting in that their top has a small radius of curvature and can be used for the emission of electrons or ions. Currently, such nanowires with a variable cross section are also of interest as candidate materials for spintronics.

To obtain such structures by matrix synthesis, it is necessary to fabricate a matrix with conical pores and to obtain replicas of these pores. The first problem is solved by etching the pore channels in the irradiated polymer film in an alcohol-alkaline solution. Obtaining conical replicas consists in applying a thin metal contact layer (thermal sputtering of copper in a vacuum), followed by filling of dead-end pores with the required metal; both processes are carried out on one side of the membrane.

The method of probe microscopy was used in the work at two stages – to study the polymer matrix and to study the resulting conical structures. The AFM image of pores in TM allows not only to estimate the size of pores, but also to estimate the degree of inclination of the pore walls. After galvanic deposition, the resulting conical replicas were also studied by the AFM method. Figure presents the image of the topography of a single cone.

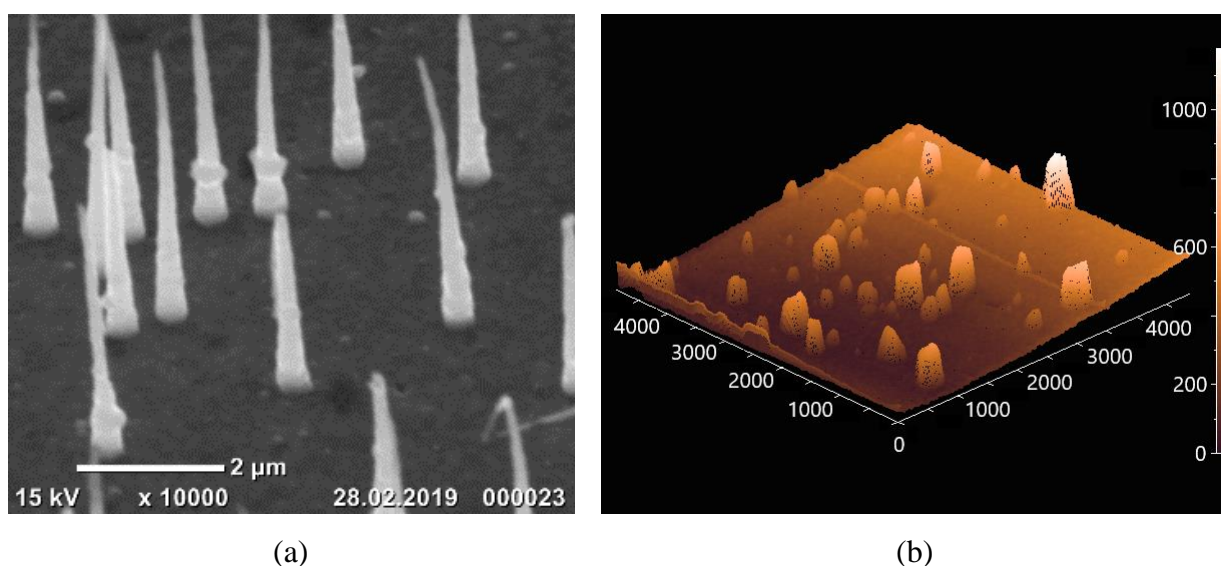


Figure 1. (a) SEM and (b) SPM-image of conical nanowires.

The resulting images demonstrate the correlation of SEM and AFM images. In addition, they allow a detailed assessment of the topography of the tip. Thus, the shape of the tips – different from the cone – suggested that the electrolyte does not completely fill the “bottom” of the conical pore during the electroplating process. To overcome this negative effect, several types of additives have been used. It was shown that the use of the “brightener” gave the best effect.

Poling and annealing of piezoelectric poly(vinylidene fluoride) micropillar arrays

I.O. Pariy¹, A.A. Ivanova¹, V.V. Shvartsman², M.A. Surmeneva¹, R.A. Surmenev^{1*}

¹Physical Materials Science and Composite Materials Centre, National Research Tomsk Polytechnic University, 634050, Tomsk, Russia

*rsurmenev@mail.ru

²Institute for Materials Science and Center for Nanointegration Duisburg-Essen (CENIDE), University of Duisburg-Essen, 45141, Essen, Germany

The effect of annealing and poling processes on the crystalline phase and piezoelectric properties of poly(vinylidene fluoride) (PVDF) micropillar arrays was investigated. PVDF micropillars were prepared by the imprinting method, heated and treated with high-voltage poling. The effect of the treatment conditions on the crystallization behaviour and the piezoelectric properties of the patterned PVDF films were investigated by differential scanning calorimetry (DSC), Fourier transform infrared spectroscopy (FTIR) and piezoresponse force microscopy (PFM). Figure 1 shows the PFM images for the poled and annealed PVDF micropillar arrays and the piezoelectric characterization of the PVDF micropillar arrays.

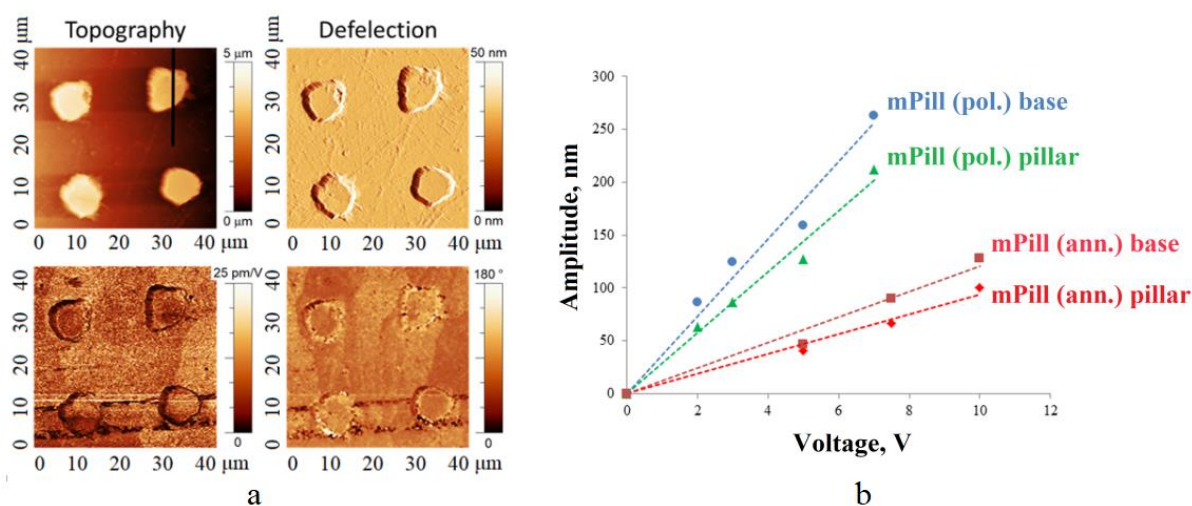


Figure 1. PFM images for the poled and annealed PVDF micropillar arrays on a 40×40 μm area (a) and piezoelectric characterization of the PVDF micropillar arrays (b).

The results of this study demonstrate a qualitative agreement of the β -phase content estimated using FTIR measurements, the degree of crystallinity obtained from DSC data and the intensity of the measured piezoelectric response, which was obtained from PFM analysis. Poled PVDF micropillars were shown to possess the highest crystallinity (22.7%) and β -phase content (42%) among all studied samples, which results in a 2.9-fold increase of the piezoelectric response. The FTIR measurements of poled and non-poled β -PVDF samples reveal that the main effect of the poling process is the partial rotation of molecular chains and the further transformation of the γ into the β phase, leading to an increase in the piezoelectric response, which was confirmed by the PFM results. The developed PVDF micropillar structures can be used as nanotip-based biosensors, nanotip-based tactile sensors, and power nanogenerators.

R.S. acknowledges the financial support from the Russian Science Foundation (project #18-73-10050).

E-beam domain patterning in thin plates of MgO-doped LiNbO₃

E.A. Pashnina, D.S. Chezganov, E.O. Vlasov, L.V. Gimadeeva,
E.D. Greshnyakov, M.A. Chuvakova, V.Ya. Shur

*School of Natural Sciences and Mathematics, Ural Federal University, 620000, Ekaterinburg, Russia
helen.pashnina@gmail.com*

We have studied the formation of periodical domain structure (PPLN) induced by controllable electron beam (e-beam) irradiation in the single-crystalline plates of MgO-doped lithium niobate covered by artificial dielectric layer depending on electron energy, plate and layer thickness. The creation of the through periodic domain structures with vertical domain walls and a period down to 1.5 μm was demonstrated in 1-mm-thick plate [1].

The studied samples represented Z-cut optical grade plates of MgO-doped lithium niobate (MgOLN) of various thicknesses: (1) 1-mm-thick, (2) 100- μm -thick, (3) 7- μm -thick produced by polishing. The irradiated Z⁻-polar surface was covered by AZ nLOF 2020 (MicroChemicals) photoresist layer with thicknesses 1.5, 2, and 2.5 μm . The solid copper electrode was deposited on the opposite surface and grounded during irradiation. The Auriga Crossbeam Workstation (Carl Zeiss NTS) equipped with e-beam lithography system Elphy Multibeam (Raith GmbH) was used for the patterning. The static domain structures at the surface were imaged by piezoresponse force microscopy, scanning electron microscopy (SEM) in backscattered electron channeling mode in a nondestructive manner and secondary electron mode after selective chemical etching. The confocal Raman microscopy was used for domain imaging in the bulk.

The influence of the plate and resist layer thicknesses and the electron energy on the morphology of the produced domains has been studied. It was shown that there were no changes in the domain morphology with reduction of the plate thickness. The dependences of the switched domain area on the dose demonstrated the linear behavior in plates of various thicknesses. The fact was explained by the external screening of the depolarization field by the injected charge. The increase of the domain sizes with the plate thickness was attributed to a shorter stage of the forward domain growth. It was shown that the domain sizes decrease for the distances between the domain walls less than 2- μm for all crystal thicknesses. The fact was attributed to the interaction of charged domain walls. The effect of the suppression of the domain formation in arbitrary positions within the array in the thick plate was attributed to the domain interaction during the forward growth. The variation of the resist layer thickness and the electron energy led to decrease in the domain sizes due to the delocalization of the space charge.

The obtained results allowed revealing the optimal parameters for periodical poling with short periods, which have been used for the creation of through 1D and 2D periodical domain structures with the neutral walls and period down to 1.5 μm on thick and thin plates (Fig.1).

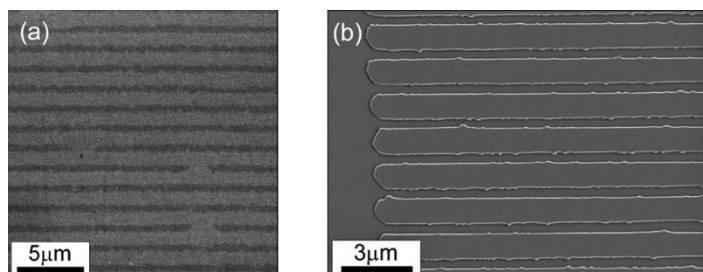


Figure 1. SEM images of PPLN with 1.5- μm -period in (a) 7- μm -thick, (b) 1-mm-thick plates.

The equipment of the Ural Center for Shared Use “Modern nanotechnology” Ural Federal University was used. The research was made possible by the Russian Science Foundation (grant № 17-72-10152).

High temperature superconductivity at the interface $\text{Ba}_{0.8}\text{Sr}_{0.2}\text{TiO}_3/\text{La}_2\text{CuO}_4$

D.P. Pavlov, M.I. Bannikov, N.N. Garig'yanov, T.M. Salikhov, V.V. Kabanov, R.F. Mamin

Zavoisky Physical-Technical Institute, FRC Kazan Scientific Center of RAS, 420029, Kazan, Russia
dmitry.p.pavlov@gmail.com

A high-mobility electron gas was observed in 2004 [1] at the interface of heterostructure LaAlO_3 (LAO) and SrTiO_3 (STO). Such heterointerfaces involving two insulating nonmagnetic oxides were comprehensively studied. In particular, it was found that the metallic phase (quasi-two-dimensional electron gas, 2DEG) is formed in the STO layers at the LAO/STO interface when the number of LAO layers is larger than three [2]. Such a system undergoes a transition to a superconducting state at temperatures below 300 mK [3].

Here we report the tailoring quasi-two-dimensional electron gas (q2DEG) state as well as a high- T_C quasi-two-dimensional superconductivity (HTq2DSC) in heterostructure $\text{Ba}_{0.8}\text{Sr}_{0.2}\text{TiO}_3/\text{La}_2\text{CuO}_4$ consisting of an insulating ferroelectric film deposited by magnetron sputtering on a *non*-atomically-flat surface of an insulator single crystal. We have shown, that the temperature dependence of the electrical resistance for heterostructure formed by antiferromagnetic La_2CuO_4 (LCO) single crystals with epitaxial films of ferroelectric $\text{Ba}_{0.8}\text{Sr}_{0.2}\text{TiO}_3$ (BSTO) deposited onto them has been studied. The measured electrical resistance is compared to that exhibited by LCO single crystals without the films. The interface of that heterostructure shows superconducting behavior with transition temperature T_C is about 30 K, which 100 time larger than T_C in $\text{LaAlO}_3/\text{SrTiO}_3$. The beginning of a transition to superconducting state occurs around 40 K, similar to what is observed in bulk $\text{La}_{2-x}\text{Sr}_x\text{CuO}_4$ single crystals at optimal doping. Important that, when we applied electrodes for resistance measurements on the back side of the heterostructure (from single crystal side, without contact with interface), superconducting state is not observed. Therefore, we conclude that this is not a case of surface superconductivity, and that the oxygen does not penetrate the surface layer during the sputtering of the film. The heterostructure in that case is created by a relatively simple method at the *non*-atomically-flat boundary of the two insulating oxides with different elementary cell structures. It opens up new physics, when a polarization catastrophe is associated not with the polar oxides, but with the ferroelectric oxides. If a weak magnetic field is applied perpendicularly to the interface of the heterostructure, a resistance appears. This confirms a quasi-two-dimensional nature of the superconductive state. The existence of superconducting phase at the interface was confirmed by observation of the diamagnetic susceptibility. The proposed concept promises ferroelectrically controlled interface superconductivity which offers the possibility of novel design of electronic devices.

The reported study was funded by Russian Scientific Foundation, research project No. 18-12-00260.

1. A. Ohtomo, H. Hwang, *Nature* **427**, 6973 (2004).
2. S. Thiel, G. Hammerl, A. Schmehl, C. W. Schneider, J. Mannhart, *Science* **313**, 1942 (2006).
3. N. Reyren, S. Thiel, A. Caviglia et al., *Science* **317**, 5842 (2007).

Effect of magnetic field on high conductivity area at the interface of heterostructure $\text{Ba}_{0.8}\text{Sr}_{0.2}\text{TiO}_3/\text{LaMnO}_3$

D.P. Pavlov, N.N. Garig'yanov, A.V. Leontyev, D.K. Zharkov,
T.M. Salikhov, V.V. Kabanov, R.F. Mamin

Zavoisky Physical-Technical Institute, FRC Kazan Scientific Center of RAS, 420029, Kazan, Russia
dmitry.p.pavlov@gmail.com

A high-mobility electron gas was observed in 2004 [1] at the interface of heterostructure LaAlO_3 (LAO) and SrTiO_3 (STO). It has been shown that analogous to the ionic polar discontinuity, that this state may be created at an interface due to electric polarization discontinuity [2, 3]. A quasi two dimensional electronic gas (q2DEG) is formed in the STO layers next to the interface which becomes superconducting below a temperature of 300 mK [1, 4]. Ferroelectrics are attractive materials for such kind heterostructure creation, because ferroelectrics have an electric polarization. And one of more useful material for that is $\text{Ba}_{0.8}\text{Sr}_{0.2}\text{TiO}_3$ (BSTO). As substrate we use LaMnO_3 (LMO), because antiferromagnetic LaMnO_3 (LMO) might be transferred to ferromagnetic state by increasing the concentration of free carriers by injection. This means that increasing the free charge carriers might lead to the local ferromagnetic state and magneto-resistivity in a system with q2DEG. Therefore, there is an opportunity to switch conductivity by a magnetic field, if the magnetic order will be realized in the interface of heterostructure BSTO/LMO due to screening of ferroelectric polarization. The thin film of epitaxial $\text{Ba}_{0.8}\text{Sr}_{0.2}\text{TiO}_3$ (BSTO) was sputtered on the top of single crystalline LaMnO_3 samples using the magnetron sputtering technique. Conductivity measurements were performed by a four-point probe method. Measurements were performed before and after effect of magnetic field on BSTO/LMO heterostructure. We have shown that when a magnetic field is applied time-by-time to heterostructure during c -axis of LMO, the resistivity is decreasing and maximum of resistivity on temperature shift on more high temperature up to the some temperature of maximum. Thus if at the beginning the maximum was at 160 K in the final case we get the temperature of maximum about 240 K. Under future application of magnetic field the temperature of maximum is not change.

The reported study was funded by Russian Scientific Foundation, research project No. 18-12-00260.

1. A. Ohtomo, H. Hwang, *Nature* **427**, 6973 (2004).
2. M. K. Niranjan, Y. Wang, S.S. Jaswal, E.Y. Tsybal, *Phys. Rev. B* **103**, 016804 (2009).
3. K.D. Fredrickson, A. Demkov, *Phys. Rev. B* **91**, 115126 (2015).
4. N. Reyren, S. Thiel, A. Caviglia et al., *Science* **317**, 5842 (2007).

Heterostructure with ferroelectric: growth and conductivity measurements

D.P. Pavlov¹, A.A. Kamashev¹, I.I. Piyanzina^{1,2}, D.A. Tayurskii², P.F. Mamin^{1,2}

¹Zavoisky Physical-Technical Institute, FRC KazanSC of RAS, 420029, Kazan, Russian Federation

²Kazan Federal University, 420008, Kazan, Russian Federation
i.piyanzina@gmail.com

Oxide heterostructures are in the focus of solid-state research for more than a decade. The intense exploration of the multilayered systems is well justified as electronic reconstruction at the internal interfaces and the surfaces allows for a plethora of phenomena which are otherwise not observed in a single compound. Moreover, the sensitivity of competing or even coexisting phases to external fields and control parameters in the transition metal oxides makes the oxide heterostructures ideal candidates for multifunctional devices - especially since metallic phases may be confined to lateral extensions of a few lattice constants.

In 2004 the astounding phenomenon was found at the interface between two nonmagnetic wide-band-gap insulative oxides LaAlO₃ and SrTiO₃ [1]. A two-dimensional electronic system (2DES) is formed in the SrTiO₃ layers next to the interface which becomes superconducting below a temperature of 300 mK [1, 2]. Remarkably, this superconducting state coexists with a magnetic state being stable up to the room temperature. It was concluded, that the primary mechanism responsible for the 2DES formation is the electronic reconstruction followed by structural reconstruction. Since then two-dimensional conducting state has been later found in other dielectrics. And all of them have in common is that conductivity occurs due to either the polar nature of one of components or due to defects. Later, it has been shown that 2DES can be created at the interface of nonpolar oxides one of which is ferroelectric [3, 4]. The main advantage of using ferroelectrics is a possibility to switch on and off the polarization and thus to control properties of the electron system. Moreover, ferroelectrics have a range of other outstanding properties which might expand the scope of applications in nanoscale electronic devices: spontaneous polarization switching, high dielectric permeability, dielectric nonlinearity, piezo- and pyro- activity, linear and quadratic electro-optical effects.

By means of *ab initio* investigations within DFT calculations we investigated ferroelectric polarization impact onto the conductive properties of the nonpolar BaTiO₃/SrTiO₃ heterostructure and found that polarization towards the interface might induce conductivity [5]. At the experimental part the thin film of epitaxial Ba_{0.8}Sr_{0.2}TiO₃ (BSTO) was sputtered on the top of single crystalline SrTiO₃ substrate using the magnetron sputtering technique. We also investigated bilayer structure Ba_{0.8}Sr_{0.2}TiO₃/Ba_{0.2}Sr_{0.8}TiO₃ on the MgO and Si substrates and Ba_{0.8}Sr_{0.2}TiO₃/LaMnO₃ heterostructure. Capacitance and conductivity measurements were performed by a four-point probe method. In our investigation we present electrical resistivity at different temperature and photoconductivity measurements.

The reported study was funded by RFBR according to the research project № 18-32-00595.

1. A. Ohtomo, H. Hwang, *Nature* **427**, 6973 (2004).
2. N. Reyren, S. Thiel, A. Cavaglia et al., *Science* **317**, 5842 (2007).
3. M.K. Niranjan, Y. Wang, S.S. Jaswal, E.Y. Tsybal, *Phys. Rev. L* **103**, 016804 (2009).
4. K.D. Fredrickson, A. Demkov, *Phys. Rev. B* **91**, 115126 (2015).
5. I.I. Piyanzina, Y.V. Lysogorskiy, D.A. Tayurskii, R.F. Mamin, *Bull. Russ. Acad. Sci.: Phys.*, **82**, 3 (2018).

Study of the surface relief morphology of sheet metal with textured polymer coatings

A.R. Baidganov, A.V. Maksimov, O.G. Maksimova, V.I. Egorov, T.O. Petrova

Cherepovets State University, 162600, Cherepovets, Russia
to_87@bk.ru

Surface roughness is manifested as defects for many types of products. However, in the last decade, there has been a need for new materials with additional design functions, for example, textured polymer sheet coatings of metal sheet. Such coatings ideally give a natural and noble appearance for the building structures (roof, etc.). The surface roughness affects the mechanical and optical properties of the materials. Their accounting is necessary for engineering calculations and industrial exploitation of materials with specific types of coatings. However, a theoretical study of these properties is possible only if the 3D relief function of the distribution of the defects under consideration is known.

Optical microscopy (OM) and scanning probe microscopy (SPM) methods have been used to analyze the surfaces of sheet metal samples with polyester textured coatings. The dependences of the type of defects (grooves), their geometrical parameters and their distribution over the surface of the polyester coating (the concentration of centers of "thickening" paint pigments) have been studied for samples of coatings obtained under different conditions of their formation: temperatures of the primer and front layer, thickness of the front layer, paint batches.

Because the character of the distribution of defects in the textured coating is complex and irregular, it was convenient to use the ideas of fractal geometry in our work. A computer simulation of the relief rough surfaces was based on fractal functions constructed by methods of random walks (diffusion limited aggregation model). New methods for constructing fractal functions in 3D space have been developed. We analyzed the type this functions in depending of their parameters. The value of the fractal dimension of the models is determined. It is shown that modeling at different scales of research requires, different algorithms in order to more detailed investigation of individual surface areas.

At comparison experimental data and fractals constructed by means of the distribution functions of the number and amplitude of defects on the surface of the coating, the method for determining the parameters of fractal functions has been developed is given. The research results will allow to develop a methodology for the convergence for rolled metal with textured polymer coatings, allowing to identify the conformity between the color and texture of sample surfaces and the standard.

Computer modeling of shear strain in the polymer brushes

O.S. Piskunov¹, O.G. Maksimova¹, V.I. Egorov¹, R.A. Gerasimov²,
O.S. Baruzdina¹, A.V. Maksimov¹

¹Cherepovets State University, 162600, Cherepovets, Russia
og62@mail.ru

²Southern Federal University, 344006, Rostov-on-Don, Russia

We conducted the modeling of a shear strain in a thin polymer layer (~15 nm) bonded adhesively to a rigid substrate. The discrete-continuous model of a system of chains with given stiffness and polar groups was developed. The polymer chain was considered within Hurst-Harris model. The polar groups were implemented on the base of the tetragonal lattice model. We suppose that a chain with the given stiffness does not extend beyond the limits of a cylindrical region. Its sizes are determined from the condition of a minimum of Helmholtz free energy F . The average elongation of the macromolecule and its entropy depend on the chain bending stiffness and the radius of the tube. The average elongation was computed by random walk method [1]. It was assumed that the potential of polar groups have the main contribution to the energy of interchain interactions (and this energy was calculated using the Metropolis algorithm). The potential of interactions between the nearest polar groups of chains consists of the energy of dipole-dipole (Keesom) interactions and the Lennard-Jones potential. We consider that possible orientations of the polar groups are determined by the average elongation of the chain. The results of modeling showed that the dependence of the free energy on the interchain distance has two minima. The first minimum is characterized by the orientational ordering of the polar groups, the second one by their disordered state. The depth and positions of the minima depend on the temperature, the bending stiffness of chain, the modulus of the dipole moment of the polar groups and the well depth in the Lennard-Jones potential.

Further, the step-by-step modeling of the shear strain in the polymer layer which initially has an orientationally disordered state was conducted. The dependences of the deforming force f on the shear angle γ were obtained. The tangential force was determined as the derivative of the free energy with respect to the shear angle: $f \sim (\partial F / \partial \gamma)_{T,V}$. The $f(\gamma)$ dependences can be divided into three stages of the sample deformation. The first stage is a reversible elastic deformation, obeying Hooke's law and determined by the entropy component of the deforming force. The second stage is a high-strained elastic deformation, characterized by the mutual movement of the segments of macromolecules and the orientation of the polymer molecules along the selected direction. The third stage is the deformation associated with the distortion of valence angles and interatomic distances. The dependences $f(\gamma)$ for polymer systems with different values of chain stiffness are obtained. These stress-strain curves allow us to estimate the value of the elastic limit, as well as to determine the stresses at the points of phase transitions from the disordered state to the orientationally-ordered one.

R.A.G. acknowledge the financial support by the Russian Science Foundation under grant "Methods of microstructural nonlinear analysis, wave dynamics and mechanics of composites for research and design of modern metamaterials and elements of structures made on its base" (No 15-19- 10008).

1. M. Doi, S. Edwards, *The theory of Polymer Dynamics* (Mir), 440 (1998).
2. V.E. Gul, V.N. Kuleznev, *Structure and mechanical properties of polymers* (Labirint), 367 (1994).

Morphological and kinetic consequences of the scratching of the growing crystal surface

N.N. Piskunova

*Institute of Geology of Komi Science Center Ural Branch of RAS, 167982, Syktyvkar, Russia
piskunova@geo.komisc.ru*

Crystals growing in real mineral-forming system are often exposed to the mechanical impact, the evidence of which is scratches and cracks. Mineralogist sees it not merely as a destruction process, but as an imprint, which allows to reconstruct one of historical stages of the crystal and its environment. With the appearance of atomic-force microscopy (AFM) methods it became possible to experimentally model the processes and observe the response of a growing crystal to the impact on its surface. Moreover, an AFM tip can also be used as a nanoindenter scratching the growing surface. This fact has been used in works studying the processes on the surface after it being affected by the tip [1, 2]. The purpose of the present work was to do an AFM study of the morphological and kinetic consequences of evolution of a growing and dissolving crystal in the area of an intentional scratch on its surface. Model crystals of hydroxymethylquinoxalindioxyde ($C_{10}H_{10}N_2O_4$) were obtained directly in the liquid cell of the microscopy. Different furrows were drawn on the face (100) of dioxydine crystal by means of AFM probe. The force with which it presses the surface during the contact mode is 10^{-8} N. Friction force of the probe and the specimen in a humid condition is equal to stressing force in the 2/3 degree [3]. In the standard mode, with the feedback being on, this interaction force is constantly maintained and the probe does not touch the surface. When scanning is not working and the feedback is off, the probe can be intentionally moved along the surface. Often it makes the mechanical impact on the growing surface that initiates the pits (Fig. 1). We have established that the occurrence of a defect depends on whether the tip moves on or against the direction of growth steps movement. The influence of such short-term contact has important crystal-genetic (morphological and kinetic) consequences and is perceptible even after a long time.

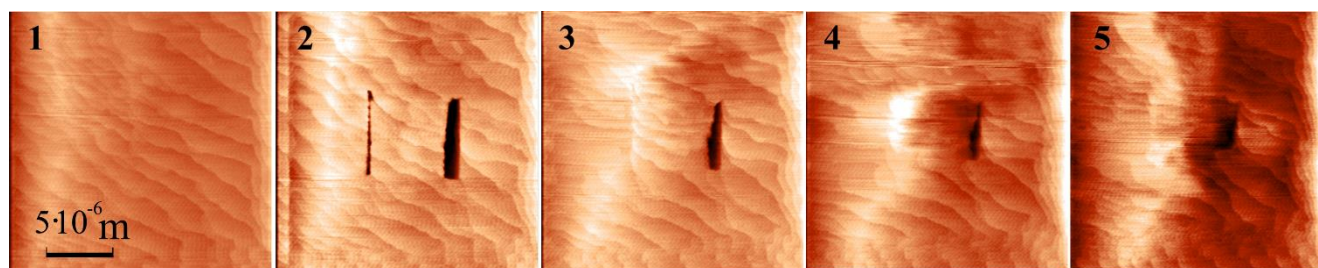


Figure 1. AFM-snapshots of the growing crystal's surface (the part of layer-by-layer growth area) before (1) and after (2-5) being scratched.

We carried out experiments with a mechanical deformation on topographically different parts of a growing crystal. We have studied the difference in the sculpture and the behavior of scratching steps formed by the screw dislocation: near the peak point and far from the peak point (layer-by-layer growth area). This leads to non-linear effects; first, to the loss of morphological stability. We observe the phenomenon of simultaneous growth and dissolution at the neighbouring steps. The tangential velocities of the set of points on the growth steps were calculated with the use of image processing program. The obtained data were subsequently statistically processed. Results were compared with images of the similar spirals growing without a scratch.

This work is supported by RFBR (19-05-00460) and the Program of Basic Researches of the Ural Branch of RAS (18-5-5-44).

1. S. Yanagiya, N. Goto, *J. Surf. Eng. Mater. Adv. Technol.* **2**, 210 (2012).
2. S. Elhadj, A.A. Chernov, J. De Yoreo, *Nanotechnology* **19**, 105304 (2008).
3. S. Rekhviashvili, *Zhurnal Technicheskoy Fiziki* **71**, 10 (2000) [in Russian].

Ab initio insight into the electronic properties of heterointerfaces composed of nonpolar ferroelectric oxides

I.I. Piyanzina^{1,2}, D.P. Pavlov¹, R.R. Zagidullin¹, A.A. Kamashev¹,
D.A. Tayurskii², P.F. Mamin^{1,2}

¹Zavoisky Physical-Technical Institute, FRC KazanSC of RAS, 420029, Kazan, Russian Federation

²Kazan Federal University, 420008, Kazan, Russian Federation

i.piyanzina@gmail.com

Recently, using ab initio calculations it has been predicted that quasi two-dimensional electron system (q2DES) can be created at the interface of nonpolar oxides one of which is ferroelectric [1, 2]. In this case ferroelectric component of the heterostructure causes the electric polarization discontinuity, which leads to the electron transfer from the surface to the interface. Ferroelectrics have a wide range of different distinctive properties which can expand the scope of application in nanoelectronics, among them: spontaneous polarization switching, high dielectric permeability, dielectric nonlinearity, piezo- and pyro- activity, linear and quadratic electro-optical effects.

In the present work *ab initio* investigations were performed for a LaAlO₃/SrTiO₃ heterostructure. We used DFT [3] implemented into the VASP program [4]. We performed method approbation [5], investigated necessary conditions for a q2DES formation, analyzed an impact of oxygen vacancies and hydrogen dopants onto the electronic, structural and magnetic properties [6]. We found that four LaAlO₃ overlayers are required for conductivity at the interface induction. In the case of 3LaAlO₃/SrTiO₃ heterostructure conductivity can be induced by defects (oxygen vacancies or hydrogen dopants) located at the surface or at the interface [6].

Approved method and parameters were used for the modelling of heterointerface composed of ferroelectric oxides. We performed comparative analysis of structural and conductive properties of LaAlO₃/SrTiO₃ and LaAlO₃/BaTiO₃ heterointerfaces, containing polar LaAlO₃. Both heterostructures exhibit similar electronic properties with conductive electrons confined within the TiO₂ layer. We investigated ferroelectric polarization impact onto the conductive properties of the nonpolar BaTiO₃/SrTiO₃ heterostructure. We found that polarization towards the interface induce conductivity. After that other pairs of ferroelectric/dielectric were investigated: LiNbO₃/SrTiO₃ and PbTiO₃/SrTiO₃.

The reported study was funded by RFBR according to the research project № 18-32-00595. The research is carried out using the equipment of the shared research facilities of HPC computing resources at Lomonosov Moscow State University.

1. M.K. Niranjan, Y. Wang, S.S. Jaswal, E.Y. Tsybal, *Phys. Rev. L* **103**, 016804 (2009).
2. K.D. Fredrickson, A. Demkov, *Phys. Rev. B* **91**, 115126 (2015).
3. W. Kohn, A.D. Becke, R.G. Parr, *J. Phys. Chem.* **100**, 31 (1996).
4. G. Kresse, J. Furthmuller, *Phys. Rev. B* **54**, 11169 (1996).
5. I.I. Piyanzina, T. Kopp, Yu.V. Lysogorskiy, D.A. Tayurskii, V. Eyert, *J. Phys.: Condens. Matter* **29**, 9 (2017).
6. I.I. Piyanzina, V. Eyert, Yu.V. Lysogorskiy, D.A. Tayurskii, T. Kopp, *J. Phys.: Condens. Matter* **31**, 295601 (2019).

Experimental investigation of Ba_{0.8}Sr_{0.2}TiO₃ (BSTO)/STO heterointerface

R.R. Zagidullin¹, I.I. Piyanzina^{1,2}, D.P. Pavlov¹, D.A. Tayurskii², P.F. Mamin^{1,2}

¹Zavoisky Physical-Technical Institute, FRC KazanSC of RAS, 420029, Kazan, Russian Federation

²Kazan Federal University, 420008, Kazan, Russian Federation

i.piyanzina@gmail.com

In 2004 the astounding phenomenon was found at the interface between two nonmagnetic wide-band-gap insulative oxides LaAlO₃ (LAO) and SrTiO₃ (STO) [1]. A two-dimensional electronic system (2DES) is formed in the STO layers next to the interface which becomes superconducting below a temperature of 300 mK [1, 2]. Remarkably, this superconducting state coexists with a magnetic state being stable up to the room temperature. It was concluded, that the primary mechanism responsible for the 2DES formation is the electronic reconstruction followed by structural reconstruction.

Since then 2DES has been later found in other non-magnetic dielectrics. And all of them have in common is that the creation of 2DES is due to either the polar nature of one of components or due to defects or dopants. Later, it has been shown that 2DES can be created at the interface of nonpolar oxides one of which is ferroelectric [3, 4]. The main advantage of using ferroelectrics is a possibility to switch on and off the polarization and thus to control properties of the electron system.

By means of ab initio investigations within DFT calculations we investigated ferroelectric polarization impact onto the conductive properties of the nonpolar BaTiO₃/SrTiO₃ heterostructure. We found that polarization towards the interface induce conductivity [5]. At the experimental part the thin film of epitaxial Ba_{0.8}Sr_{0.2}TiO₃ (BSTO) was sputtered on the top of single crystalline STO substrate using the magnetron sputtering technique. We also investigated bilayer structure Ba_{0.8}Sr_{0.2}TiO₃/Ba_{0.2}Sr_{0.8}TiO₃ on MgO substrate. Conductivity measurements were performed by a four-point probe method. In our investigation we present electrical resistivity versus temperature measurements and those results are still under consideration.

The reported study was funded by RFBR according to the research project № 18-32-00595.

1. A. Ohtomo, H. Hwang, *Nature* **427**, 6973 (2004).
2. N. Reyren, S. Thiel, A. Cavaglia et al., *Science* **317**, 5842 (2007).
3. M.K. Niranjan, Y. Wang, S.S. Jaswal, E.Y. Tsybal, *Phys. Rev. L* **103**, 016804 (2009).
4. K.D. Fredrickson, A. Demkov, *Phys. Rev. B* **91**, 115126 (2015).
5. I.I. Piyanzina, Y.V. Lysogorskiy, D.A. Tayurskii, R.F. Mamin, *Bull. Russ. Acad. Sci. Phys.* **82**, 3 (2018).

Structural, electronic and magnetic properties of ferroelectric/dielectric heterostructures

Yu.V. Lysogorskiy^{1,2}, I.I. Piyanzina^{1,2}, M.I. Bannikov¹, D.P. Pavlov¹, A.V. Leontyev¹, I.F. Gilmutdinov², R.V. Yusupov², R.F. Mamin^{1,2}, D.A. Tayurskii², V.V. Kabanov^{1,3}

¹Zavoisky Physical-Technical Institute, FRC KazanSC of RAS, 420029, Kazan, Russian Federation
mamin@kfti.knc.ru

²Kazan Federal University, 420008, Kazan, Russian Federation

³Department for Complex Matter, Jozef Stefan Institute, 1000 Ljubljana, Slovenia

A quasi-two dimensional electronic system (q2DES) was found at the interface between two nonmagnetic wide-band gap insulating oxides LaAlO₃ (LAO) and SrTiO₃ (STO) in 2004 [1]. This astounding phenomenon is formed in the STO layers next to the interface. That state becomes superconducting below a temperature of 300 mK [2]. It was concluded, that the primary mechanism responsible for the q2DES formation is the electronic reconstruction followed by structural reconstruction.

Since then q2DES has been later found in other non-magnetic dielectrics. And all of them have in common that the creation of 2DES is due to either the polar nature of one of components or due to defects or dopants. It has been shown that q2DES can be created at the interface of nonpolar oxides one of which is ferroelectric [3,4]. The main advantage of using ferroelectrics is a possibility to switch on and off the polarization and thus to control properties of the electron system.

One of the most important features related to the 2DEG formation is the local polarity of layers inside the LAO slab. In the present work we have chosen the BaTiO₃/LaMnO₃ (BTO/LMO) and BaTiO₃/La₂CuO₄ (BTO/LCO) heterostructures, where all layers in the simple electronic limit are neutral, but there is a ferroelectric polarization due to the Ti atoms displacements out of octahedron center in the BTO. The direction of such a polarization might be switched by an external electric field. Based on first-principles band structure calculations, we demonstrate the possibility of q2DES formation at the interface composed of perovskite ferroelectric BTO and antiferromagnet manganite LMO or cuprate LCO. We present the results of structural, electronic and optical properties calculations of BTO/LMO and BTO/LCO heterostructures composed of varying number of layers. We analyze a magnetic properties and an impact of ferroelectric polarization onto the q2DES conducting properties by layer-resolved density of states calculations. Experimental results of magnetic field effect on Ba_{0.8}Sr_{0.2}TiO₃/LaMnO₃ heterostructure and of the superconducting state of BaTiO₃/La₂CuO₄ heterostructure are also discussed.

The reported study was funded by Russian Scientific Foundation according to the research project No. 18-12-00260. The work is partially performed according to the Russian Government Program of Competitive Growth of Kazan Federal University.

1. A.Ohtomo, and H.Hwang, *Nature* **427**, 6973 (2004).
2. N. Reyren, S. Thiel, A. Caviglia et al., *Science* **317**, 5842 (2007).
3. M. K. Niranjana, Y. Wang, S.S. Jaswal, E.Y. Tsybal, *Phys. Rev. L* **103**, 016804 (2009).
4. K. D. Fredrickson, A. Demkov, *Phys. Rev. B* **91**, 115126 (2015).

Electrochemical impedance spectroscopy of organic polyiodides with different anion composition and proton disorder

I.D. Yushina, E.V. Bartashevich, F.V. Podgornov

South Ural State University, 454080, Chelyabinsk, Russia
iushinaid@susu.ru

Organic polyiodides are perspective materials for solid-state dye-sensitized solar cells. Therefore, investigation of dielectric properties and conductance mechanisms is critically important for their further applications. As it was demonstrated, the electrochemical impedance spectroscopy (EIS) is appropriate experimental technique for characterization of polyiodide behavior [1].

In the framework of this report, the impedance spectra (IS) of polyiodide crystals with different anions: symmetric I_5^- anion in case of tetramethylammonium pentaiodide (**1**) and symmetric I_3^- anion in diiodobutenyl-bis-thioquinolinium triiodide with disorder in $N-H^+ \dots N$ fragment (**2**) were investigated in frequency range 0.1 Hz – 1 MHz at temperatures 123-298 K. To identify the dielectric relaxation processes and parameters of electric conductivity, different representation such as complex dielectric, electric modulus and conductivity spectra of IS were employed.

Independently on temperature, the exact values of direct current conductivity (σ_{DC}) could not be derived from real part of electric conductivity spectra (σ'). However, one can estimate the upper limits of the DC conductivity for samples **1** and **2** as 5×10^{-12} S/cm and 10^{-12} S/cm, respectively. As follows from the analysis of the imaginary part of the complex conductivities of both samples, they have both drift and hopping mechanisms of electric conductivity.

Dielectric spectra of samples have rather complicated nature and contain information about relaxation processes. As most of these processes are in the low frequency range, it is more convenient to observe and identify them using electric modulus representation. At high temperatures (at $T = 333$ K for **2** and at $T = 298$ K for **1**), one can clearly observe (Fig. 1) three relaxation modes. The first one can be observed at the lowest frequency ($f = \sigma_{DC}/\epsilon_\infty \epsilon_0$) and can be assigned to the electric conductivity. The second one is probably originated due to the relaxation of Maxwell Wagner polarization because of the heterogeneous structure of the samples. The third mode was found in the middle part of the frequency range and was preliminary attributed to the rotation of molecules owing to the coupling of their dipole moments with probing voltage.

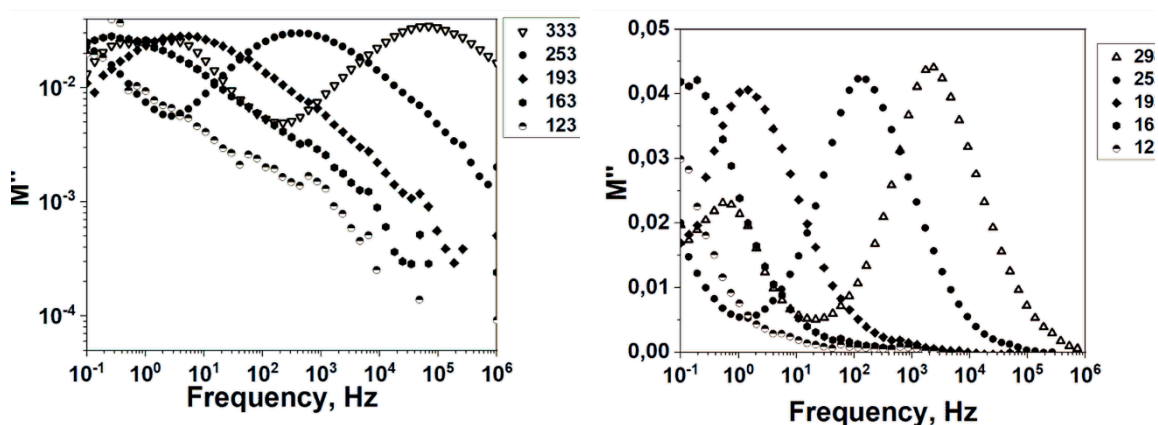


Figure 1. Dependence of the imaginary part of the electric modulus on frequency for tetramethylammonium pentaiodide **1** (right) and diiodobutenyl-bis-thioquinolinium triiodide **2** (left).

Funding for this research was provided by the Ministry of Education and Science 4.1157.2017/4.6.

I. H. Yu, L. Yan, Y. He, H. Meng, W. Huang, *Chem. Commun.* **53**, 432 (2017).

Phase formation and relaxor properties of lead-free perovskite ceramics on the base of sodium-bismuth titanate

E.D. Politova¹, D.A. Strebkov², D.A. Belkova², G.M. Kaleva¹, A.V. Mosunov¹,
S.Yu. Stefanovich^{1,2}, B.A. Loginov², A.B. Loginov³, P.K. Panda⁴

¹*L.Ya. Karpov Institute of Physical Chemistry, Moscow 105064 Russia*
politova@nifhi.ru

²*Lomonosov Moscow State University, Moscow 119992 Russia*

³*National Research University of Electronic Technology MIET,*
Moscow Zelenograd 124498, Russia

⁴*National Aerospace Laboratories, Kodihalli, Bangalore-560017 India*

Lead-free relaxor oxides on the base of rhombohedral perovskite sodium-bismuth titanate ($\text{Na}_{0.5}\text{Bi}_{0.5}\text{TiO}_3$ (NBT)) are being intensively studied in order to replace widely used Pb-based ones [1, 2]. Advantage of the NBT-based compositions comprises presence of polar nanoclusters leading to high mobility of boundaries “domain walls/polar clusters” [3].

We studied influence of A-cations substitutions on structure parameters, microstructure, dielectric, and relaxor ferroelectric properties of solid solutions in the systems $(\text{Na}_{0.5}\text{Bi}_{0.5})_{1-x}\text{B}_x\text{TiO}_3$ with $\text{B} = \text{K}^+, \text{La}^{3+}$, $x = 0-0.1$ [4]. Ceramic samples were prepared by the two-step solid-state reaction method at temperatures $T_1 = 973$ K (6 h), and $T_2 = 1200-1400$ K (2 h).

The samples were characterized using the X-ray Diffraction, Scanning Electron Microscopy, Second Harmonic Generation (SHG), and Dielectric Spectroscopy methods. To improve density of ceramics overstoichiometric KCl and LiF additives were used.

The pseudocubic unit cell parameter increased in modified ceramics in accordance with the ionic radii changes. Main size of grains decreased with x increasing in both systems.

Ferroelectric phase transitions were revealed at as steps near ~ 400 K and as peaks at ~ 600 K in the dielectric permittivity versus temperature curves. Phase transitions near ~ 400 K demonstrate marked relaxor behavior typical for the NBT-based compositions conditioned by the presence of polar nanoregions in a nonpolar matrix [3]. Using the SHG method increase in the spontaneous polarization value was observed in ceramics with $\text{B} = \text{K}$ with x increasing. While decrease in SHG signal in ceramics with $\text{B} = \text{La}^{3+}$ points to enhancement of relaxor properties due to possible decrease in the size of polar nanoregions. In the samples modified by KCl additional anomalies in the $\varepsilon(T)$ dependences were revealed at $T > 900$ K above the ferroelectric phase transition due to formation of vacancies in the oxygen sublattice.

At the room temperature, non monotonous changes of the dielectric parameters were observed in modified compositions studied confirming prospects of new lead-free materials development by modification of NBT-based compositions with aliovalent cation substitutions.

The work was supported by the Russian Foundation for Basic Research (Projects 16-53-48009, 17-03-00542).

1. V.V. Shvartsman, D.C. Lupascu, *J. Amer. Ceram. Soc.* **95**, 1 (2012).
2. Li Ming, H. Zhang, S.N. Cook, et al, *Chem. Mater.* **27**, 629 (2015).
3. W. Kleemann, *Int. J. Mod. Phys. B.* **7**, 2469 (1993).
4. E.D. Politova, D.A. Strebkov, A.V. Mosunov, et al, *Bull. Russ. Acad. Sci. Phys.* **82**, 269 (2018).
5. E.D. Politova et al., *Crystallography Reports* **63**, 266 (2018).

Investigation of profiling of silicon surface by local anodic oxidation nanolithography for memristors crossbar architecture creating

V.V. Polyakova, I.N. Kots, V.A. Smirnov

Southern Federal University, 347922, Taganrog, Russia
vik5702935@yandex.ru

To date the need to improve the lithographic methods in the production of nanoelectronics elements in order to ensure the accuracy and reproducibility of the nanoscaled structures is a fundamental problem in this field. One of the most promising lithographic procedures is local anodic oxidation (LAO) providing high levels of spatial resolution and reproducibility, as well as the direct modification of the substrate surface without the need for supplementary operations typical of photolithography. We offer a methodology for developing a method for creating a crossbar architecture.

The nanoscaled profiling of a silicon 5 (111) n-type substrate surface is studied by the LAO. First, the substrates were subjected to the LAO nanolithography in the atomic force microscopy (AFM) contact mode on an Ntegra probing nanolaboratory (PNL) (NT-MDT, Russia) using NSG 10 cantilevers with a conductive Pt coating. Varying the voltage pulse amplitude from 5 to 12.5 V and the humidity from 30 ± 1 to $70 \pm 1\%$ during the LAO is a promising way to form oxide nanostructures (ONS) with heights from 0.5 ± 0.3 to 2.1 ± 0.1 nm and profiled nanostructures (PNS) with depths from 0.4 ± 0.3 to 1.5 ± 0.2 nm on the substrate (Fig. 1).

The results can be applied to the development of technological processes of the element base of silicon-based nanoelectronics using the probe nanotechnologies.

This work was supported by the FASIE. The work was done on the equipment of Research and Education Centre "Nanotechnology" and Collective Use Centre "Nanotechnology," Southern Federal University.

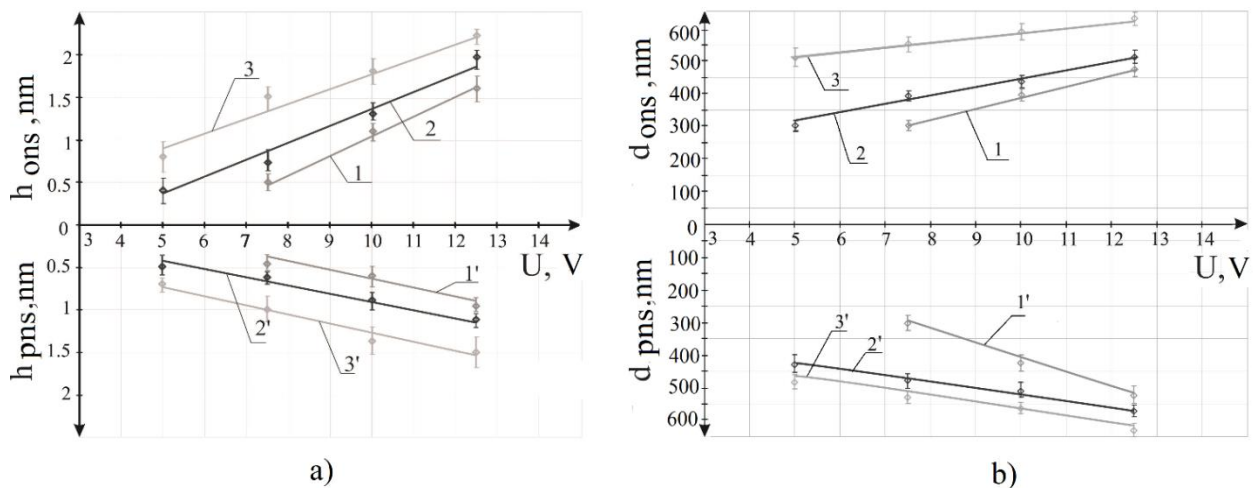


Figure 1. Geometric parameters of nanostructures vs. voltage amplitude during LAO at various values of relative humidity (1, 1', 30 ± 1%; 2, 2', 50 ± 1%; 3, 3', 70 ± 1%): (a) heights of ONSs (1-3) and depths of PNSs (1'-3'); (b) diameters of ONS (1-3) and PNS (1'-3').

**Mossbauer study of cation substitution effect
on the magnetic phase transition temperature
of 0.5AFeO₃-0.5NaNbO₃ (A = Bi, La) solid solutions**

S.I. Raevskaya¹, S.P. Kubrin¹, Jian Zhuang², I.P. Raevski¹,
M.A. Malitskaya¹, I.N. Zakharchenko¹, V.V. Titov¹, V.G. Smotrakov¹

¹Research Institute of Physics and Faculty of Physics, Southern Federal University,
344090, Rostov-on-Don, Russia
sveta.raevskaya@mail.ru

²Electronic Materials Research Laboratory, Key Laboratory of the Ministry of Education and
International Center for Dielectric Research, Xi'an Jiaotong University, 710049, Xi'an, P.R. China

BiFeO₃ is the most widely studied multiferroic due to high temperatures of both ferroelectric and magnetic phase transitions. Recently a possibility of magnetic superexchange between Fe³⁺ ions in BiFeO₃ via the empty 6p states of Bi³⁺ was predicted theoretically [1]. Earlier we showed the role of Pb²⁺ ions which also possess the empty 6p states, in the enhancement of the T_N in perovskite Pb_{1-x}A_xFe_{1/2}Nb_{1/2}O₃ (A = Ca, Ba) solid solutions [2, 3]. However this mechanism of superexchange seems to become noticeable only at high enough dilution of the Fe-sublattice, i.e. in solid solutions.

The 0.5AFeO₃-0.5NaNbO₃ (A = Bi, La) solid solution compositions were prepared by solid phase reactions route from high-purity oxides. The XRD study revealed that the samples are single phase and perovskite structure. Room temperature Mossbauer spectra of both show the quadrupole-split lines. The main reason of quadrupole splitting in such systems is compositional disorder in B-sublattice. All spectra contain 2 or 3 doublets with different values of quadrupole splitting. The isomer shift values of doublets correspond to the Fe³⁺ ions in oxygen octahedron. The presence of 2 or 3 doublets indicates that Fe³⁺ has 2 or 3 different environments in the lattice which may be a fingerprint of B-cations short-range ordering or clusterization [4].

To estimate the temperature of magnetic phase transition (T_N) we performed the measurement of Mossbauer spectrum line intensity under subsequent temperature lowering. Near magnetic phase transition the Mossbauer spectrum transforms from doublet into sextet. This transformation is accompanied by a dramatic decrease of Mossbauer spectrum line intensity I_m . Thus, the abrupt drop in the $I_m(T)$ dependence corresponds to the T_N . Mossbauer studies have shown that while for 0.5BiFeO₃-0.5NaNbO₃ the T_N value is about 150 K, for 0.5LaFeO₃-0.5NaNbO₃ it is only ≈ 20 K. This dramatic difference in T_N values seems to be due to additional contribution of the superexchange between Fe³⁺ ions via the empty 6p states of Bi³⁺ to the overall superexchange in accord with predictions of De Sousa et al. [1].

For both compositions magnetization M studies in the 5-200 K range revealed only a maximum at 20-25 K in the zero-field cooling mode. In the field-cooled mode this maximum was not observed. Such behavior is typical of spin glasses. In PbFe³⁺_{1/2}B⁵⁺_{1/2}O₃ (B⁵⁺ = Nb, Ta) perovskite multiferroics a spin-glass state is known to coexist at low temperatures with the antiferromagnetic state [2, 4]. The absence of the $M(T)$ anomaly at around 150 K for 0.5BiFeO₃-0.5NaNbO₃ composition seems to be due to the strong diffusion of this anomaly. Similar "disappearance" of the $M(T)$ anomaly corresponding to antiferromagnetic phase transition was observed, e.g. for some compositions of the PbFe_{2/3}W_{1/3}O₃-PbTiO₃ and PbFe_{1/2}Nb_{1/2}O₃-PbTiO₃ solid solutions [5, 6].

This work was supported in part by RFBR project 19-52-53030 GFEN_a and by the Ministry of Education and Science of the Russian Federation (research projects 3.1649.2017/4.6 and 3.5346.2017/BP).

1. R. De Sousa, M. Allen, M. Cazayous, *Phys. Rev. Lett.* **110**, 267202 (2013).
2. I.P. Raevski, S.P. Kubrin, S.I. Raevskaya, et. al., *Phys. Rev. B*, **80** (2009).
3. I.P. Raevski, S.P. Kubrin, S.I. Raevskaya, et. al., *Ferroelectrics* **398** (2010).
4. I.P. Raevski, S.P. Kubrin, S.I. Raevskaya, et. al., *Phys. Rev. B* **85** (2012).
5. L. Mitoseriu, D. Marre, A. S. Siri, P. Nanni, *Appl. Phys. Lett.* **83**, 5509 (2003).
6. S.P. Singh, S.M. Yusuf, S. Yoon, et. al., *Acta Mater.* **58**, 5381 (2010).

Dielectric properties of $\text{PbMg}_{1/3}\text{Nb}_{2/3}\text{O}_3$ - PbTiO_3 and BaNb_2O_6 - SrNb_2O_6 solid solution ceramics sintered from mechanochemically synthesized nanopowders

S.I. Raevskaya¹, A.A. Gusev², V.P. Isupov², I.P. Raevski¹,
S.P. Kubrin¹, V.V. Titov¹, O.A. Bunina¹, M.A. Malitskaya¹

¹Research Institute of Physics and Faculty of Physics, Southern Federal University,
344090, Rostov-on-Don, Russia
sveta.raevskaya@mail.ru

²Institute of Solid State Chemistry and Mechanochemistry SB RAS, 630128, Novosibirsk, Russia

Ferroelectric relaxors are widely used as components of various functional materials exhibiting giant dielectric, electrostrictive, pyroelectric, and piezoelectric responses. Recently we have found out that the use of mechanochemical synthesis enables one to modify substantially relaxor properties of ceramics of the disordered perovskites $\text{PbFe}_{1/2}\text{Ta}_{1/2}\text{O}_3$ and $\text{PbMg}_{1/3}\text{Nb}_{2/3}\text{O}_3$ (PMN) [1, 2]. For both substances high-energy mechanical activation of the starting oxides increases the temperature T_m of the dielectric permittivity maximum and reduces dramatically the frequency shift ΔT of T_m . Similar changes of ΔT and T_m were predicted previously, basing on the first-principle calculations, for PMN with an increased degree of a short-range ordering of Mg^{2+} and Nb^{5+} cations [3]. Such explanation is supported by changes in the magnetic phase transition temperature of $\text{PbFe}^{3+}_{1/2}\text{B}^{5+}_{1/2}\text{O}_3$ powders ($\text{B}^{5+} - \text{Nb, Ta}$) obtained by mechanochemical synthesis [4]. In the present study we investigated the effect of mechanochemical synthesis on the dielectric properties of several solid solution ceramics $(1-x)\text{PbMg}_{1/3}\text{Nb}_{2/3}\text{O}_3 - x\text{PbTiO}_3$ (PMN-xPT) and $(1-x)\text{BaNb}_2\text{O}_6 - x\text{SrNb}_2\text{O}_6$ (SBN-x). In both solid solution systems two compositions were studied – one exhibiting good relaxor properties (PMN-0.075PT and SBN-0.75) and the other – a very weak relaxor (PMN-0.33PT and SBN-0.50).

It was found out that high-energy mechanical activation has a very different effect on the dielectric properties of PMN-xPT and SBN-x compositions. While for both usual and mechanoactivated (MA) PMN-0.33PT ceramics ΔT is nearly zero, for MA sample of the relaxor PMN-0.075PT composition the value of ΔT reduces by more than two times as compared to usual ceramics. For both PMN-xPT compositions studied the T_m values of MA ceramics differ by about 10 K from those for the samples obtained by usual method (for PMN-0.075 T_m increases while for PMN-0.33PT it decreases). This difference seems to be due to contamination of the MA samples by iron and formation of the PMN-PT- $\text{PbFe}_{1/2}\text{Nb}_{1/2}\text{O}_3$ solid solution.

For both SBN-x compositions studied T_m values of MA ceramics are lower by more than 50 K while ΔT values are more than twice larger than those reported for single crystals [5] and ceramics obtained by usual method [6]. Similar effects, i.e. lowering of T_m and increase of ΔT values were reported for Fe-doped SBN ceramics [6].

Basing on the comparison of the properties of PMN-xPT, SBN-x and PMN-PFN solid solution compositions fabricated by both the usual solid-state synthesis and by high-energy mechanochemical synthesis one may conclude that the changes in T_m in all the ceramics studied, obtained using high-energy mechanochemical synthesis may be ascribed, at least partially, to the formation of the Fe-containing solid solutions. However the main origin of the ΔT changes observed for MA ceramics seems to be not the incorporation of iron from the milling media into the lattice, but rather the effect of high-energy mechanical activation.

This work was supported in part by RFBR (project 17-03-01293_a) and by the Ministry of Education and Science of the Russian Federation (research project 3.1649.2017/4.6).

1. A.A. Gusev, S.I. Raevskaya, V.V. Titov, et al, *Ferroelectrics* **475**, 41 (2015).
2. S.I. Raevskaya, A.A. Gusev, V.P. Isupov, et al, *Ferroelectrics* **525**, 37 (2018).
3. S. Prosandeev, L. Bellaiche, *Phys. Rev. B* **94**, 180102 (2016).
4. A.A. Gusev, S.I. Raevskaya, V.V. Titov, et al, *Ferroelectrics* **496**, 231 (2016).
5. T. Łukasiewicz, M. A. Swirkowicz, J. Dec, et al, *J. Cryst. Growth* **310**, 1464 (2008).
6. S.H. Kshirsagar, S.R. Jigajeni, A.N. Tarale, et al, *J. Adv. Dielectr.* **5**, 1550001 (2015).

Optical and EXAFS studies of NaNbO_3 - $\text{Gd}_{1/3}\text{NbO}_3$ solid solutions

V.A. Shuvaeva¹, I.P. Raevski¹, A.M. Glazer², S.I. Raevskaya¹, V.V. Titov¹, M.A. Malitskaya¹

¹Research Institute of Physics, Southern Federal University, 344090, Rostov-on-Don, Russia
igorraevsky@gmail.com

²Department of Physics, Oxford University, Oxford, OX1 3PU, UK

NaNbO_3 based solid solutions are prospective environmentally-friendly materials for piezoelectric, pyroelectric, electrostrictive and energy storage applications. In the present work ceramics and flux-grown crystals of $(1-x)\text{NaNbO}_3-x\text{Gd}_{1/3}\text{NbO}_3$ (NNG- x) solid solutions are studied in order to take a further insight into the nature of phase transition diffusion in NaNbO_3 -based solid solutions. At high enough x values NNG- x compositions are known to exhibit a diffuse dielectric permittivity ϵ maxima [1].

Temperature-dependent optical studies of NNG crystals were carried out by the rotating polarizer method, using the Metripol (www.metripol.com) microscope system [2] and a precise heating stage (Linkam HFS91). False-color images showing values of $|\sin\delta| = |\Delta n L 2\pi/\lambda|$ (Δn – birefringence, L – crystal thickness, $\lambda = 600$ nm – light wavelength) and the orientation of the optical indicatrix at every point of the crystals were obtained in the temperature range 20 to 600 °C. Birefringence values were extracted from the $|\sin\delta|$ data.

Optical studies have shown that the value of $|\sin\delta|$ of pure NaNbO_3 exhibits an abrupt jump at 370 °C, corresponding to the well known first-order antiferroelectric phase transition. No such jumps are observed at higher temperatures. High-temperature phase transitions which occur at 480, 520, 575 °C according to the X-ray diffraction studies manifest themselves only through a change in the period of $|\sin\delta|$. Two types of optical extinction – symmetrical and parallel have been observed in two domains of the crystal below the phase transition and only parallel extinction at higher temperatures. This is in a total agreement with the earlier optical studies of NaNbO_3 crystals.

NNG- x crystals also display distinctive changes of birefringence which can be attributed to phase transition, though their dielectric permittivity maxima are diffused substantially. Up to the $\epsilon(T)$ maximum the crystals remained uniform. However in the vicinity of the phase transition spontaneous splitting into small regions less than 0.001 mm in size with diffuse boundaries occurs and the distribution of the birefringence image becomes very messy. The origin for this non-uniformity may be a complicated domain structure arising as a result of the phase transition or coexistence of two phases over a wide temperature range. As the temperature increases the crystal gradually becomes more uniform as seen by the fact that the scale of the non-uniformity increases up to 0.05 mm well above the phase transition point.

Nb K-edge extended X-ray absorption fine structure (EXAFS) spectra of the pure NN and NNG-0.2 ceramics were measured in the transmission mode at the Synchrotron Radiation Source (SRS, Daresbury). Comparison of Fourier Transforms (FT) of Nb K-EXAFS spectra of NN and NNG-20 show that up to 4 Å they are very similar with peak amplitudes just slightly lower for the doped sample, implying that Gd impurities make a subtle effect on the Nb nearest environment. However FT EXAFS of the NN has more distinct peaks comparative to those for NNG-0.2 sample at distances higher than 4 Å from Nb, indicating a breakdown of ordering on the middle-range scale due to Gd impurity.

This study is supported by Russian Science Foundation (project 19-12-00205).

1. I.P. Raevski, L.A. Reznitchenko, M.A. Malitskaya, et al, *Ferroelectrics* **299**, 95 (2004).
2. A.M. Glazer, J.G. Lewis, W. Kaminsky, *Proc. R. Soc. London. Ser. A* **452**, 2751 (1996)

Tuning relaxor and magnetic properties of complex perovskites by varying the compositional ordering degree

I.P. Raevski¹, S.P. Kubrin¹, A.V. Pushkarev², N.M. Olekhnovich², Y.V. Radyush²,
A.A. Gusev³, V.P. Isupov³, S.I. Raevskaya¹, V.V. Titov¹, M.A. Malitskaya¹

¹Research Institute of Physics and Faculty of Physics, Southern Federal University,
344090, Rostov-on-Don, Russia
igorraevsky@gmail.com

²Scientific-Practical Materials Research Centre of NAS of Belarus, 220072, Minsk, Belarus

³Institute of Solid State Chemistry and Mechanochemistry SB RAS, 630128, Novosibirsk, Russia

Ferroelectric ternary perovskite oxides of the $PbB'_{1-m}B''_mO_6$ ($m=1/3$ or $1/2$) type, are widely used as components of various functional materials exhibiting giant dielectric, electrostrictive, pyroelectric, and piezoelectric responses. Dielectric properties of these oxides, especially of the 1:1 type perovskites ($m=1/2$) depend crucially on the long-range ordering degree S of B' and B'' cations. While in the highly-ordered state a sharp ferroelectric or antiferroelectric phase transition takes place, in the disordered state a relaxor state is observed, characterized by a diffuse and frequency-dependent maximum of the dielectric permittivity.

Previously, to change the S values of $PbB^{3+}_{1/2}B^{5+}_{1/2}O_3$ perovskites a long-time annealing was used. Later sintering in the presence of liquid-phase as well as variation of the conditions of either the crystal growth or high pressure synthesis were successfully used to change the ordering degree of B -site ions in $PbB^{3+}_{1/2}B^{5+}_{1/2}O_3$ perovskites with $B^{3+}=Fe, Sc, Yb$; $B^{5+}=Nb, Ta, Sb$ [1, 2]. Recently it was found out that high-energy mechanical activation during mechanochemical synthesis stimulates disordering of B^{3+} and B^{5+} ions in ceramics of some 1:1 type perovskites. In some cases it is possible to vary substantially the S values and correspondingly both the temperature and diffusion of dielectric permittivity maxima in these ceramics by changing the regimes of the mechanochemical synthesis and/or using different starting materials (either oxides or preliminary synthesized $B^{3+}B^{5+}O_4$ precursors) [3]. The parameters of the dielectric spectra of the samples exhibiting a relaxor-like behavior also depend on the conditions of the mechanochemical synthesis. Interestingly, the use of mechanochemical synthesis enables one to modify substantially relaxor properties of ceramics of the disordered perovskites $PbFe^{3+}_{1/2}Ta^{5+}_{1/2}O_3$ and $PbMg_{1/3}Nb_{2/3}O_3$. This effect is believed to be caused by the changes in the degree of the short-range ordering [3].

Ordering of Fe^{3+} and B^{5+} ions in $PbFe^{3+}_{1/2}B^{5+}_{1/2}O_3$ ($B^{5+}=Nb, Ta, Sb$) perovskite multiferroics is believed to have an impact on their magnetic properties, as such ordering changes the number of magnetic neighbors around each Fe^{3+} ion. The effect of compositional long-range ordering on the magnetic phase transition temperature T_N was observed in solid solutions of highly-ordered perovskite $PbFe^{3+}_{1/2}Sb^{5+}_{1/2}O_3$ [2]. On the other hand substantial changes in T_N values of disordered $PbFe^{3+}_{1/2}B^{5+}_{1/2}O_3$ perovskites-multiferroics ($B^{5+}=Nb, Ta$) obtained by mechanochemical synthesis seem to be caused by the changes in the degree of the short-range ordering [4].

This work was supported in part by RFBR (projects 17-03-01293_a and 18-52-00029 Bel_a), Belarussian Republican Foundation for Fundamental Researches (grant T18R-048) and by the Ministry of Education and Science of the Russian Federation (research project 3.1649.2017/4.6).

1. I.P. Raevski, V.Y. Shonov, M.A. Malitskaya et al, *Ferroelectrics* **235**, 205(1999).
2. I.P. Raevski, A.V. Pushkarev, S.I. Raevskaya, et al, *Ferroelectrics* **501**, 154 (2016).
3. S.I. Raevskaya, A.A. Gusev, V.P. Isupov, et al, *Ferroelectrics* **525**, 37 (2018).
4. A.A. Gusev, S.I. Raevskaya, V.V. Titov, et al, *Ferroelectrics* **496**, 231 (2016).

An oscillatory circuit with a ferroelectric capacitor with negative differential capacitance under the action of blocking-generator

A.E. Rassadin

*Laboratory of Infinite-Dimensional Analysis and Mathematical Physics, Lomonosov Moscow State University, 119991, Moscow, Russia
brat_ras@list.ru*

At present intensive studies of ferroelectric systems with negative capacitance are carried out all over the world (see [1] and references therein). The authors of paper [2] were the first who succeeded in obtaining experimentally thermodynamically stable bilayer ferroelectric system of lead zirconate-titanate $\text{Pb}(\text{Zr}_{0.2}\text{Ti}_{0.8})\text{O}_3$ and strontium titanate SrTiO_3 which has a negative differential capacity at room temperature. Three years later the same effect has been found in another nanoscale heterostructure consisting of barium titanate BaTiO_3 and strontium titanate SrTiO_3 [3]. For brevity we shall call these systems by NC-capacitors.

The voltage U_{NC} between the plates of the NC-capacitor depends on its charge q as follows [2,3]:

$$U_{NC}(q) = -\alpha \cdot q + \beta \cdot q^3, \tag{1}$$

where coefficients α and β are considered to be positive [2, 3].

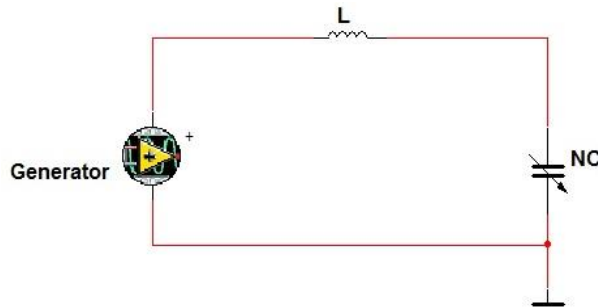


Figure 1. Electrical scheme of oscillatory circuit with NC-capacitor.

Behavior of circuit on Figure 1 under the action of blocking-generator is described by the following Hamilton function:

$$H(x, y, t) = \frac{y^2}{2} - \frac{x^2}{2} + \frac{x^4}{4} - \mu \cdot \tau \cdot x \cdot \sum_{n=-\infty}^{+\infty} \delta(t - n \cdot \tau), \quad 0 < \mu \ll 1, \tag{2}$$

where x and y are dimensionless electrical charge on NC-capacitor and dimensionless electrical current through NC-capacitor respectively, force in this system coincides with voltage (1) in dimensionless form and influence of input voltage from blocking-generator is simulated by series of Dirac delta functions with dimensionless period τ .

In accordance with general approach developed in [4] one can reduce description of dynamical system (2) to investigation of point mapping on semicilinder action I – angle θ variables for system under $\mu = 0$:

$$\begin{cases} I_{n+1} = I_n + \mu \cdot \tau \cdot \frac{\partial x}{\partial \theta}(I_n, \theta_n) \\ \theta_{n+1} = \theta_n + \omega(I_{n+1}) \cdot \tau - \mu \cdot \tau \cdot \frac{\partial x}{\partial I}(I_n, \theta_n) \end{cases} \tag{3}$$

Phase portrait of unperturbed system is presented on Figure 2.

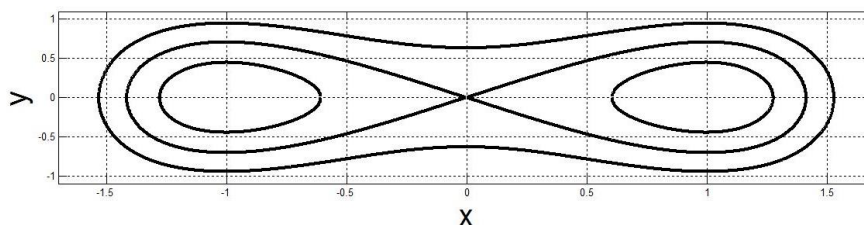


Figure 2. Phase plane of unperturbed system.

Frequency of nonlinear oscillations depending on dimensionless energy h of unperturbed system is equal to [5]:

$$\omega(h) = \begin{cases} \frac{\pi \cdot A(h)}{\sqrt{2} \cdot \mathbf{K}(k_1(h))}, & -\frac{1}{4} \leq h < 0 \\ \frac{\pi \cdot \sqrt{A^2(h) - 1}}{2 \cdot \mathbf{K}(k_2(h))}, & h > 0 \end{cases}, \quad (4)$$

two different expressions corresponding to motion of unperturbed system inside or outside of homoclinic loop on Figure 2. But in mapping (3) frequency (4) depends on action variable I therefore it is required to use the next formulae for this value too:

$$I(h) = \begin{cases} \frac{2}{3 \cdot \pi} \cdot \frac{(2 - k_1^2(h)) \cdot \mathbf{E}(k_1(h)) - 2 \cdot (1 - k_1^2(h)) \cdot \mathbf{K}(k_1(h))}{(2 - k_1^2(h))^{3/2}}, & -\frac{1}{4} \leq h < 0 \\ \frac{4}{3 \cdot \pi} \cdot \frac{(2 \cdot k_2^2(h) - 1) \cdot \mathbf{E}(k_2(h)) - (1 - k_2^2(h)) \cdot \mathbf{K}(k_2(h))}{(2 \cdot k_2^2(h) - 1)^{3/2}}, & h > 0 \end{cases}. \quad (5)$$

In expressions (4) and (5) $k_1(h) = \sqrt{\frac{2 \cdot \sqrt{1+4 \cdot h}}{1 + \sqrt{1+4 \cdot h}}}$, $k_2(h) = \sqrt{\frac{1 + \sqrt{1+4 \cdot h}}{2 \cdot \sqrt{1+4 \cdot h}}}$,

$A(h) = \sqrt{1 + \sqrt{1+4 \cdot h}}$, $\mathbf{K}(k)$ and $\mathbf{E}(k)$ are complete elliptic integrals of the first and the second kind respectively [6].

At last coordinate of unperturbed system is expressed via Jacobi elliptic functions [5]:

$$x(h, \theta) = \begin{cases} A(h) \cdot \operatorname{dn} \left[\frac{\mathbf{K}(k_1(h)) \cdot \theta}{\pi}, k_1(h) \right], & -\frac{1}{4} \leq h < 0 \\ A(h) \cdot \operatorname{cn} \left[\frac{2 \cdot \mathbf{K}(k_2(h)) \cdot \theta}{\pi}, k_2(h) \right], & h > 0 \end{cases}. \quad (6)$$

It is obvious that in formulae (6) instead of dimensionless energy h one ought to use action variable I which can be found as inverse function for expressions (5).

In the report presented dynamics of mapping (3) with different values of its parameters is under investigation. In particular passage of phase point through homoclinic loop on Fig. 2 is taken into account too.

This picture has been compared with picture arising under description of system (2) in the framework of distribution function $f(x, y, t)$ obeying to the Liouville equation [4]:

$$\frac{\partial f}{\partial t} + \frac{\partial H}{\partial y} \cdot \frac{\partial f}{\partial x} - \frac{\partial H}{\partial x} \cdot \frac{\partial f}{\partial y} = 0 \quad (7)$$

1. M.A. Alam, M. Si, P.D. Ye, *Appl. Phys. Lett.* **114**, 090401 (2019).
2. A.I. Khan et al., *Appl. Phys. Lett.* **99**, 113501 (2011).
3. D.J.R. Appleby et al., *Nano Lett.* **14**, 3864 (2014).
4. G.M. Zaslavskii, *Stochasticity of Dynamical Systems* (Nauka), 74 (1984) (in Russian).
5. A.D. Morozov, *Quasi-conservative systems: cycles, resonances and chaos* (World Sci), 123 (1998).
6. H. Bateman, A. Erdelyi, *Higher Transcendental Functions. Vol. 3* (Mc Graw-Hill Book Company), 9 (1955).

Emission arrays based on carbon nanostructures for vacuum electronics

A.A. Rezvan, V.S. Klimin

Southern federal university, 347922, Taganrog, Russia
arezvan@sfnedu.ru

The use of existing methods of formation leads to the degradation of the emission properties of the active region of the structures of vacuum electronics. Based on this, there is the problem of finding technologies for the formation of field emitters based on carbon nanostructures using plasma. In this study, we studied the formation modes of a field emitter with an active region based on carbon structures using plasma etching and deposition technologies to form a model of a field emitter cell.

The experimental model is a small insulating silicon substrate. For the formation of a diffusion barrier, a dielectric layer Si_3N_4 , obtained by plasma chemical deposition from the gas phase [1-4], was used. Using the experimental mode of formation allows you to achieve the growth rate of the dielectric layer $V_G = 11.5 \text{ nm/min}$.

A structure for the growth of carbon nanostructures was formed on the experimental samples. By the method of magnetron sputtering a catalytic nickel layer was obtained. The thickness of the deposited nickel layer varied to about $5 \mu\text{m}$. After that, using the method of plasma chemical vapor deposition, an additional layer of Si_3N_4 dielectric with a thickness of $10 \mu\text{m}$ was formed on the surface of the formed structure. By combining the methods of lithography and plasma chemical etching, a field emitter layout was formed, which provides voltage supply and the formation of the upper electrode, as well as the control electrode. The frame, namely the walls of the field emitter, made of a dielectric material, make it possible not only to protect the active emission region from mechanical impact from the outside, but also to prevent the formation of an electrostatic voltage that prevents the emission current from flowing. Additional modification of the nickel layer relief using plasma techniques allowed us to obtain a vertically oriented array of nickel whiskers, the working surface area of which was set by the etching time and the power of the plasma used. Carbon nanostructures were formed over the array by plasma chemical deposition from the gas phase. The parameters of the growth process were as follows: a temperature of $650 \text{ }^\circ\text{C}$, a gas pressure of 100 mTorr and a working gas velocity of $\text{C}_2\text{H}_2 - 30 \text{ cm}^3/\text{min}$ and $\text{H}_2 - 10 \text{ cm}^3/\text{min}$. After that, electrical contacts were formed over the sensitive layer, which were connected to a signal processing device. The formation time was 5 minutes. On top of the sensitive layer, electrical contacts were formed that connected to a signal processing device.

The experimental models obtained are distinguished by a high degree of adhesion, and the formed array of carbon nanostructures of the active emission region has a sufficient degree of perpendicularity to the substrate, which made it possible to obtain structures with a high aspect ratio. In addition, the data showed that the field emitter based on carbon nanostructures, formed using the above formation modes, is able to achieve the following parameters: the threshold field strength of the onset of emission is $E = 6.7 \cdot 10^8 \text{ V/m}$, the electron work function ranges from 3.1 to 5.3 mA/cm^2 , as well as the field gain coefficient $\beta = 7.9 \cdot 10^7$.

This work was supported by Grant of the President of the Russian Federation No. MK-3512.2019.8 and Southern Federal University (grant VnGr-07/2017-02). The results were obtained using the equipment of the Research and Education Center "Nanotechnologies" of Southern Federal University.

1. V.S. Klimin, A. A. Rezvan, O. A. Ageev, *J. Phys.: Conf. Ser.* **1124**, 022035 (2018).
2. C.G. Morgan, P. Kratzer, M. Scheffler, *Phys. Rev. Lett.* **82**, 4886 (1999).
3. D.A. Murdick, H. N. G. Wadley, X. W. Zhou, *Phys. Rev. B* **75**, 125318 (2007).
4. K. Shiraishi, T. Ito, *Phys. Rev. B* **57**, 6301 (1998).

Formation of vacuum electronics elements by a combination of methods of focused ion beams and plasma layer etching on SiC

A.A. Rezvan, V.S. Klimin, I.N. Kots

Southern federal university, 347922, Taganrog, Russia
arezvan@sfedu.ru

Vacuum electronics is one of the most important areas of development of micro- and nanoelectronics [1-3]. Due to the significant growing of the electronic and microelectronic industry, the need for new materials is increasing dramatically. Particular importance is the reliability of electronic products and their resistance to various environmental influences. It is known that the effectiveness of electronics devices, especially those working in extreme conditions, significantly depends on improving performance, energy saving and reliability of the element base, including the ability of this work. One of the materials on the basis of which it is possible to produce electronic devices that meet such stringent requirements is SiC. Silicon carbide has chemical stability, high resistance to elevated temperatures and radiation, the possibility of doping it with acceptor and donor impurities. In connection with this fact, the development of devices with field emitters based on SiC is relevant.

Experimental samples, which are plates of purified silicon carbide, were placed in the vacuum chamber of the FIB module and oriented so that the flow of accelerated ions would fall on the substrate in the direction of the normal. The working vacuum during the exposure of the beams was maintained at the level of $1 \div 2 \times 10^{-4}$ Pa. At this stage, an array in the form of pointed emitters was formed on the SiC surface.

The carbon nanoscale layer was formed using the atomic layer etching technique in fluoride plasma. SF_6 was used as a fluorine-containing gas, thanks to which it was possible to etch the near-surface SiC layer [4-6]. Moreover, their crystal lattice was used to remove only Si and the formation of a thin carbon layer on the surface of the samples.

The study of the surface topology at each iteration was carried out using scanning electron microscopy and atomic force microscopy.

At the end of a series of experimental studies, it was found that the presented technology for the production of graphene films on the surface of SiC plates by the method of plasma atomic layer etching makes it possible to obtain a carbon structure in accordance with specified parameters at lower temperatures than during thermal destruction of SiC substrates.

This work was supported by Grant of the President of the Russian Federation No. MK-3512.2019.8 and Southern Federal University (grant VnGr-07/2017-02). The results were obtained using the equipment of the Research and Education Center "Nanotechnologies" of Southern Federal University.

1. N. Chekurov, K. Grigoras, A. Peltonen, S. Franssila, I. Tittonen, *Nanotechnology* **20**, 5 (2009).
2. T. Nishinaga, X. Q. Shen, *Appl. Surf. Sci.* **82**, 141 (1994).
3. A. Tseng, *J. Micromech. Microeng.* **14**, R15 (2004).
4. V.S. Klimin, I.N. Kots, V.V. Polyakova, A.A. Rezvan, O.A. Ageev, *Proc. of SPIE* **11022**, 110221R (2019).
5. M. Schmidt, Z. Johari, R. Ismail, H. Mizuta, H. Chong, *Microelectron. Eng.* **98**, 313 (2012).
6. V.S. Klimin, A.A. Rezvan, O.A. Ageev, *J. Phys.: Conf. Ser.* **1124**, 071020 (2018).

Development and research carbon nanotube-based resistive gas sensor

A.A. Fedotov¹, M.V. Kuzhelev², E.G. Zamburg³, N.N. Rudyk¹, O.I. Ilin¹

¹*Southern Federal University, Institute of Nanotechnologies, Electronics and Equipment Engineering, 347922, Taganrog, Russia*

nnrudyk@sfedu.ru

²*Rehm RUS LLC, Moscow, 127018, Russia*

³*National University of Singapore, Department of Electrical & Computer Engineering, Singapore*

In a sophisticated man-made situation and terrorist threat dangerous one of the problems is the necessary for environmental monitoring using gas sensors. The main parameters of gas sensors are sensitivity, selectivity, response and recovery time, dimensions, power consumption. Traditional materials used in resistive sensors (SnO, ZnO, et al.) have good sensitivity, but do not show sufficient selectivity. The long reaction and recovery times, high energy consumption associated with the necessity of heating the sensitive layer [1] are the disadvantages of these sensory materials. Therefore, there is a regular research of new materials which can improve the sensors characteristics. Carbon nanotubes (CNT) are one of the most promising materials for gas sensors, which are designed to eliminate the disadvantages of sensors available on the market [2,3].

The aim of this work is the development and experimental research of the CNT-based resistive gas sensor sensitivity parameters.

The design of the sensor consists of a sital substrate with deposited ITO (100 nm) contact layer by magnetron sputtering using a mask. Then, for the subsequent growth of a CNT-based sensitive layer, was deposited Ni catalyst film (10 nm).

A research of the effect of heating temperature on the formation of catalytic centers (CC) for CNT growth was provide in the range of 700-800 °C. Investigation of the CC parameters of the experimental samples was carried out using a probe nanolaboratory Ntegra (NT-MDT, Russia). It is established (Fig. 1) that the temperature of 750 °C allows the formation of the smallest CC (160 ± 30 nm) with the maximum density (18 μm⁻²).

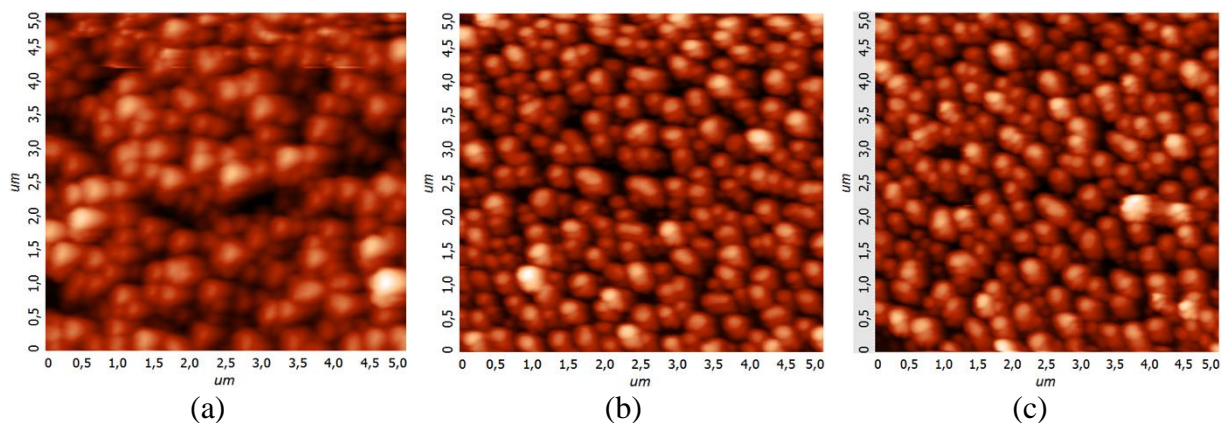


Figure 1. Obtained at a temperature of: (a) 700; (b) 750; (c) 800 °C.

After, a network of disordered CNTs was grown in the NANOFAB PECVD module (Fig. 2). To investigate the work, the gas sensor was placed in a gas measuring stand, where its response to nitrogen, argon and oxygen was checked. The choice and study of the sensor's reaction to the presence of these gases is associated with their potential danger during accumulation in confined spaces.

Measurement of resistance was carried out using a universal ohmmeter B7-78/1. The sensitivity of the device was calculated by the formula:

$$S_k = \frac{R_{gas} - R_{air}}{R_{air}} \cdot 100\% \quad (1)$$

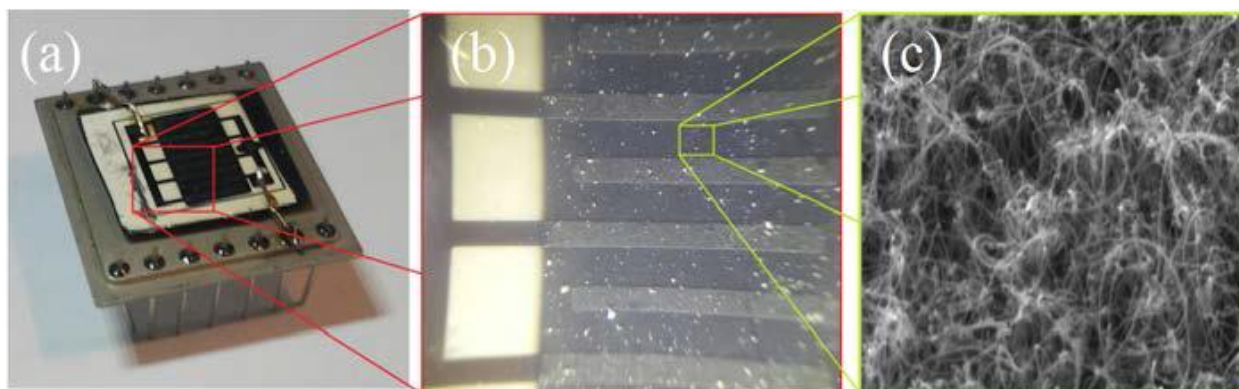


Figure 2. The model of a gas sensor: (a) side view; (b) sensitive layer with interdigital electrodes; (c) SEM-image of CNT film.

The response time was defined as a time interval of 90% of the time required for the release ($R_{gas} - R_{air}$) to a stationary level after injecting a certain concentration of the analyzed gas. Sensor recovery time was defined as the time interval during which the sensor resistance recovers after injection of the analyzed gas to 10% of the maximum value $0.1(R_{gas} - R_{air}) + R_{air}$.

The measurement of the characteristics of the sensitive element was carried out at a temperature in the measuring chamber of 300 K. The initial resistance of the structure was 516 k Ω . From the obtained results, we can conclude that the developed gas sensor sensitive element is characterized by high sensitivity and speed, a distinctive feature of which is the absence of the need to heat the sensitive element for degassing. Figure 3 shows the sensor's response to different gases.

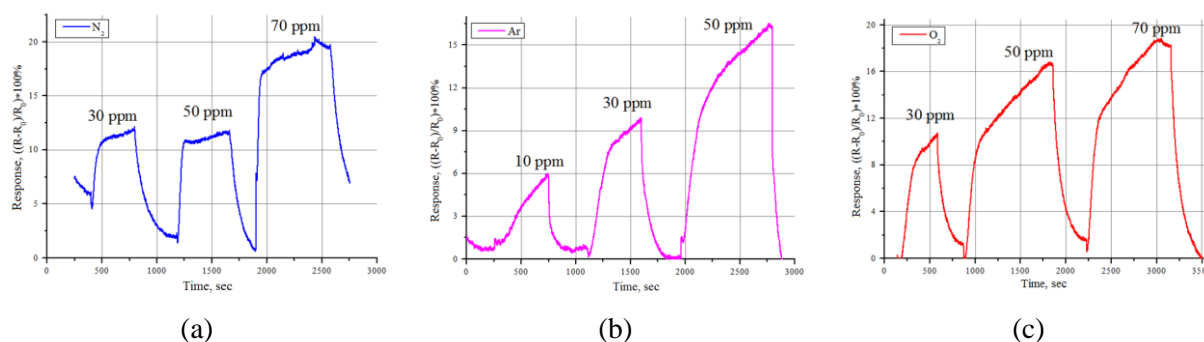


Figure 3. Sensor response in the presence of gases with different concentration: (a) nitrogen; (b) argon; (c) oxygen.

Thus, the measured sensitivity to oxygen, argon, and nitrogen was 18.7%, 16.3%, and 17.2%, respectively, with a response time of 141 s, 186 s, and 153 s respectively.

Obtained results can be used in the development of promising sensor devices based on carbon nanotubes, in particular portable wearable devices as well as multisensor systems, which will expand the range of sensitivity and increase the selectivity of devices.

This work was supported by the Russian Science Foundation under grant № 18-79-00176.

1. F. Rigoni, S. Tognolini, P. Borghetti, et al., *Analyst* **138**, 7392 (2013).
2. K. Chen, W. Gao, S. Emaminejad, et al., *Adv. Mater.* **28**, 4397 (2016).
3. N.N. Rudyk, O.I. Il'in, M.V. Il'ina, et al., *J. Phys.: Conf. Series* **917**, 082008 (2017).

Switching current of the domains ensemble with serrated charged walls

E.L. Rumyantsev, A.R. Udalov

School of Natural Science, Ural Federal University, 620000, Ekaterinburg, Russia
 evgeny.rumyantsev@urfu.ru

We derived an analytical formula describing switching current induced by the ensemble of cone-like domains growing within plane capacitor. In order to make our considerations descriptive and lucid, we restrict ourselves to the simplest case of simultaneous arising of the domains at $t=0$. The solution of the announced problem includes several steps:

(1) **The solution of corresponding electrostatic problem** of the charge induced at the plates of shorted plane capacitor by the dipole placed within it. The solution of this problem follows well-known classical approach [1]. The consideration is carried out for the case of isotropic dielectric permittivity $\varepsilon = 1$. This is done for simplification of the main formulas and for illustrative demonstration of obtained results. The generalization for the case of anisotropic dielectric permittivity is straightforward and will be presented elsewhere. Using obtained solution, the time dependence of the switching current induced by the growing isolated cone-shaped domain is derived. According to setting of an electrostatic problem, the effect of external screening is automatically accounted for, while retarded bulk screening effects for simplicity are totally ignored. The possibility of accounting for bulk screening and its effect upon polarization reversal current are discussed.

(2) **The solution of the stochastic problem** of the average surface of overlapping domains ensemble necessitates modification of Kolmogorov-Mehl-Johnson-Avrami approach. This modification has been carried out following [2,3], where it has been formulated mathematically by introducing the Boolean valued representative functions $u(\mathbf{r}, \mathbf{R}_i, t)$, with the properties: $u(\mathbf{r}, \mathbf{R}_i, t) = 1$ if $\mathbf{r} \in$ domain volume and zero otherwise. Here \mathbf{R}_i is so called representative point – center of nucleation. It is shown that for simultaneous nucleation the solution of statistical averaging over randomly distributed nucleation centers, using representative functions, is based on the formula from the theory of sets: the union of two sets A and B is equal to $A \cup B = A + B - A \cap B$. Combining derived expression for average surface of cone-like domains ensemble with the results of electrostatic problem we arrive to the following formula describing time dependence of the charge induced at the capacitor plates:

$$Q(t) = -2P_s C H(t) \int_0^1 d\alpha (1 - \exp(-\alpha^2 \rho \pi R(t)^2)),$$

where $R(t)$ – radius of cone base, $H(t)$ – cone height, ρ – density of nucleation centers, C – capacitance.

Proposed stochastic approach can be generalized for the description of polarization reversal current of the ensembles comprised of the domains of various shapes. Moreover, the proposed approach to the formulated stochastic problem can be of interest for the description of surface confined reactions.

1. V.V. Batygin, I.N. Toptygin, *Problems in Electrodynamics*, 2 ed., (Academic Press) (1978).
2. K. Sekimoto, *J. Phys. Soc. Jap.* **53**, 2425 (1984); K. Sekimoto, *Phys. Lett. A* **105**, 390 (1984);
 K. Sekimoto, *Physica A* **135**, 328 (1986).
3. E.L. Rumyantsev, *Ferroelectrics* **341**, 75 (2006); I.M. Yaglom, *Kvant* **2**, 13 (1974).

The impact of subchronic intoxication with lead and cadmium oxides nanoparticles on spermatogenesis in rats

Ju.V. Ryabova¹, S.V. Klinova¹, I.V. Zubarev²

¹*The Yekaterinburg Medical Research Center for Prophylaxis and Health Protection in Industrial Workers, 620014, Yekaterinburg, Russia*
vl.ulia@mail.ru

²*School of Natural Sciences and Mathematics, Ural Federal University, 620000, Yekaterinburg, Russia*

The experiment was conducted on the outbred male rats receiving repeated intraperitoneal injections with suspensions of PbO and CdO nanoparticles 3 times a week, for 6 weeks. After the exposure was over, the semen cytological analysis was performed. It revealed an increased percentage of spermatozoa with morphological defects. The type of combined spermatotoxic effects of the nanoparticles was described mathematically. We've shown also that the studied combined toxic effect of PbO and CdO nanoparticles could be attenuated by the background administration of bio-protective agents.

Diffraction methods of investigation of the periodical domain structures with inclined domain walls in lithium niobate

E.N. Savchenkov¹, S.M. Shandarov¹, S.V. Smirnov¹, A.A. Esin²,
A.R. Akhmatkhanov², V.Ya. Shur²

¹Tomsk State University of Control Systems and Radioelectronics, Tomsk, Russia
rossler@mail.ru

²School of Natural Sciences and Mathematics, Ural Federal University, Ekaterinburg, Russia

Periodic domain structures (PDS) in ferroelectric crystals make possible to implement with high efficiency a quasi-phase-matched frequency conversion as well as an electro-optical deflection and switching of laser radiation [1-5]. For the domain sizes in such structures it requires reproducibility with accuracy below 20 nm [6]. It is known that real PDS in a MgO:LiNbO₃ crystal may have a tilt of the domain walls relative to the polar axis reaching as high as 0.2° and more [7, 8]. An effective method for determining the quality of a PDS is the diffraction of light, usually considered for structures with non-inclined domain walls [9-12].

In this report we present the results of an experimental investigation of Bragg diffraction on the PDS with inclined walls, which was produced in a LiNbO₃:5% MgO crystal by electric field poling. The model of perturbations of the optical properties of a crystal by domain walls, which has been used for consideration of such diffraction, should take into account their inclination from the polar axis z to small angle α (Fig. 1).

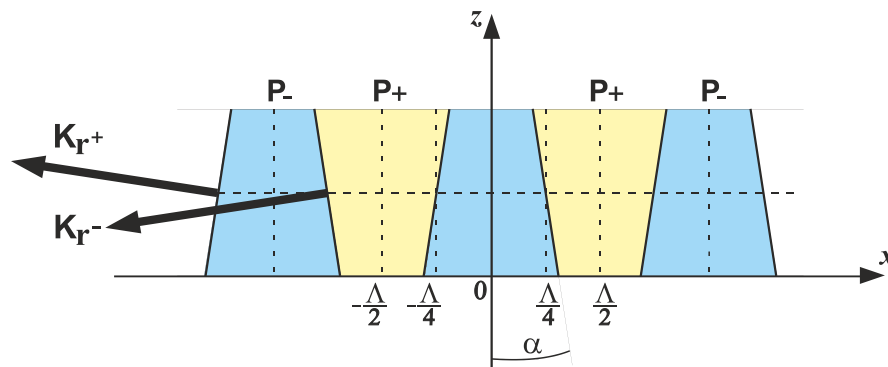


Figure 1. Schematic of the PDS with a spatial period Λ in lithium niobate crystal. Blue and yellow areas indicate the domains with opposite directions of the spontaneous polarization. The grating vectors \mathbf{K}_{r+} and \mathbf{K}_{r-} are shown separately for the two domain wall systems, inclined to the right and left. The angle α determines the inclination of the domain walls to the polar axis z .

We studied experimentally the Bragg diffraction on the PDS with the period $\Lambda = 8.79 \mu\text{m}$ and the angle of inclination estimated as $\alpha = 0.31^\circ$. The sample has a thickness of $h = 1 \text{ mm}$ along the z axis. The interaction length of the light beam propagating in the xy plane at the Bragg angle to the y axis is 2 mm. All measurements are performed with a He-Ne laser beam ($\lambda = 632.8 \text{ nm}$, $P = 1 \text{ mW}$), having a Gaussian intensity distribution and a polarization vector oriented along the z axis. Focusing this beam by the lens with $F = 350 \text{ mm}$ allows to match its waist of 0.29 mm in diameter to the entrance face of the sample placed on the turntable. The position of the waist at the z axis near the middle of sample was chosen so that a symmetric distribution of the intensity in the first diffraction maximum was observed. Figures 2 and 3 show the images of diffraction maxima.

Thus, the analysis of the intensity distribution of the maxima with different orders observed at the Bragg diffraction on the PDS under study (Figs. 2 and 3) allows estimating the tilt angle of inclined domain walls of one.

This work was supported by the Russian Foundation for Basic Research (Grant No 16-29-14046-ofi_m) and by the Ministry of Science and Higher Education of the Russian Federation for 2017- 2019 (State Tasks No 3.1110.2017/4.6 and 3.8898.2017/8.9).

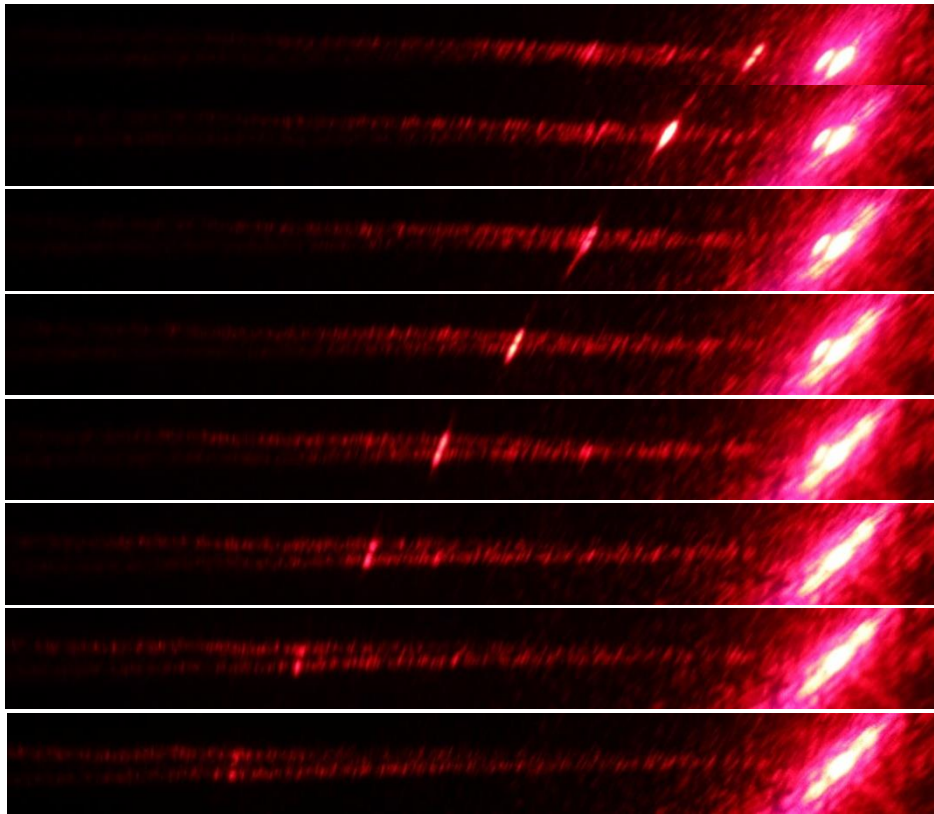


Figure 2. Images of Bragg diffraction maxima for orders from first to eight (from top to down) diverging in the directions specified by the vectors \mathbf{K}_{r+} and \mathbf{K}_r . These images were observed at the distance of 150 mm from the output face of the crystal.

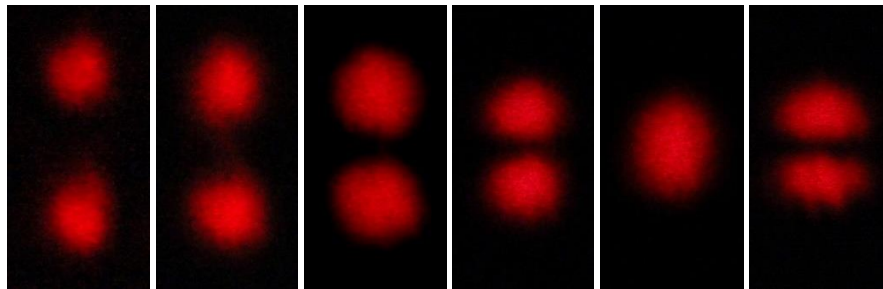


Figure 3. Images of Bragg diffraction maxima with orders from sixth to first (from left to right) observed in the far zone at the distance of 1650 mm from the output face of the crystal. The peaks in the maxima with the orders from 3 to 6 diverge in the directions specified by the vectors \mathbf{K}_{r+} and \mathbf{K}_r .

1. Ferrari P., Grilli S., DeNatale P. (eds.), *Ferroelectric Crystals for Photonic Applications* (Berlin–Heidelberg: Springer-Verlag) (2014).
2. M. Yamada, M. Saitoh, H. Ooki, *Appl. Phys. Lett.* **69**, 3659 (1996).
3. J.A. Abernethy et al., *Appl. Phys. Lett.* **81**, 2514 (2002).
4. I. Mhaouech et al., *Opt. Lett.* **41**, 4174 (2016).
5. H. Gnewuch et al., *IEEE Photon. Technol. Lett.* **10**, 1730 (1998).
6. V.Ya. Shur, A.R. Akhmatkhanov, I.S. Baturin, *Appl. Phys. Rev.* **2**, 040604 (2015).
7. M. Schröder et al., *Adv. Funct. Mater.* **22**, 3936 (2012).
8. C.S. Werner et al., *Sci. Rep.* **7**, 9862 (2017).
9. A.L. Aleksandrovskii et al., *Quant. Electron.* **26**, 641 (1996).
10. M. Müller et al., *J. Appl. Phys.* **97**, 044102 (2005).
11. S.M. Shandarov et al., *Ferroelectrics* **496**, 134 (2016).
12. S.M. Shandarov et al., *Ferroelectrics* **508**, 49 (2017).

Correlation of wall velocity and tip curvature radius of dendrite domain in lithium niobate

E.D. Saveliev, A.R. Akhmatkhanov, D.S. Chezganov, M.A. Chuvakova,
E.D. Matveeva, A.I. Lobov, V.Ya. Shur

School of Natural Sciences and Mathematics, Ural Federal University, 620000 Ekaterinburg, Russia
s-avel@yandex.ru

Recently, the unusual growth of dendritic ferroelectric domains during polarization reversal in uniform field has been demonstrated in single crystals of a uniaxial ferroelectric lithium niobate LiNbO_3 [1]. Two necessary conditions have been realized for dendritic domain growth: (1) existence of the artificial dielectric layer deposited on the polar surface leading to retardation of the bulk screening process and (2) switching at the elevated temperature resulting in stochastic nucleation. It was shown that domain shape depends substantially on the applied electric field.

The presented work is devoted to experimental study of the domain shape evolution in terms of correlation between the curvature radius (ρ) and velocity (v) of the tip of main dendrite branch. The growth rate was measured by analysis of the video record of the domain structure evolution during polarization reversal process recorded with high temporal resolution at z-cut congruent lithium niobate single crystals. The *ex situ* imaging of the static domain structure revealed by selective chemical etching after partial polarization reversal using scanning electron microscopy allowed to measure the curvature radius.

It was shown that well-known stability condition for classical dendrites $v\rho^2 = \text{const}$ [2] does not hold in studied experimental conditions. The obtained fact can be attributed to significant input of the tip-splitting mechanism of dendrite growth [3].

The phase-field simulation of anisotropic dendrite growth for C_{3v} crystal symmetry was used to study the shape transformation and correlation between tip velocity and curvature radius. The modelling was based on the analogy between self-organized growth of ferroelectric domains and new phase during the first order phase transition. The similar behaviour of dendrite shape evolution has been obtained for properly chosen model parameters.

The research was made possible by Russian Science Foundation (Project № 19-12-00210). The equipment of the Ural Center for Shared Use “Modern nanotechnology” Ural Federal University was used.

1. V.Ya Shur, A.R. Akhmatkhanov, *Philos. Trans. Royal Soc. A* **376**, 20170204 (2018).
2. J.S. Langer, H. Müller-Krumbhaar, *Acta Metallurgica* **26**, 1681 (1978).
3. P.K. Galenko, V.A. Zhuravlev, *Physics of dendrites* (World Scientific), (1994).

Atomic force microscopy in the model's development of polymeric functional materials formation on inert supports

T.S. Sazanova^{1,2}, K.V. Otvagina¹, A.E. Rassadin², L.A. Fomin^{2,3}, I.V. Vorotyntsev¹

¹*Nizhny Novgorod State Technical University n.a. R.E. Alekseev, 603950, Nizhny Novgorod, Russia
yarymova.tatyana@yandex.ru*

²*Nizhny Novgorod Mathematical Society, Nizhny Novgorod, 603950, Russia*

³*Institute of Microelectronics Technology and High Purity Materials RAS, 142432, Chernogolovka,
Moscow region, Russia*

The development of polymer-based functional materials with tailor-made structure and properties is closely associated with different physical, chemical and material science problems. Fundamental research of polymers structure and their functional properties is needed for the solution of those problems. Since it is known that physical and physical-chemical properties of polymer-based materials not only depend on their chemical nature but also strongly correlate with their surface structure, the study of this effect is an important task.

For example, in the case of gas separation processes, a non-porous polymeric membrane surface has significant contribution to gas transmission properties. It is due to the fact that first stages in gas separation are deposition of permeating gases on a membrane surface and their absorption. The rougher a membrane surface, the larger will be its actual area, and with the growth of this area, the separation speed also increases, that is, permeable properties are improved.

Thus, functional properties of polymeric materials can be controlled by varying their surface roughness (with due regard to their chemical nature). In this context, the most energy efficient and resource-saving way is mathematical modeling. A mathematical model of the "growth" of polymer films (in particular membranes) on a support could allow to identify the necessary structure and roughness of this support to obtain polymeric materials with tailor-made properties without conducting experiments.

To develop and verify such mathematical "growth" model, a polymeric surface can be assessed by atomic force microscopy (AFM). This method is suitable for such study not only because of high lateral and vertical resolutions, but also its ability of gaining quantitative three-dimensional information about topography without destruction of a soft polymer surface. Also, the results of AFM scanning are presented in digital format, which allows them to be processed using statistics methods [1] and to be used for mathematical modeling [2].

In this work, AFM results were used in the development and verification of a model for polymeric membranes formation on inert supports on the example of a range of membranes based on polysulfone (PSU), cellulose triacetate (CTA) and polyvinyl alcohol (PVA) with different roughness and viscosity.

PSU, CTA and PVA flat sheets were obtained by corresponding polymer solution casting using automatic coating machine MemcastPlus (Porometr, Belgium) onto inert supports followed by solvent evaporation under equilibrium conditions. Solutions of polymers were prepared in the following proportions: 3, 5, and 7.5% PSU in tetrahydrofuran (THF), 0.75, 1.5, and 3% CTA in glacial acetic acid, 0.75, 1.5, and 3% PVA in water. After the polymer films formation, they were easily peeled off the support and desiccated under vacuum for 24 hours. Each of the polymers was cast on three glass substrates.

Borosilicate glass was chosen as an inert support, due to its chemical, thermal and mechanical stability. Before use the glass was chemically treated in order to obtain certain surface roughness. Glass support 1 was exposed in the 5% hydrofluoric acid solution for 10 min, glass support 2 was exposed in the 15% hydrofluoric acid solution containing 50% ammonium fluoride for 5 min and glass support 3 was exposed under etching paste containing 30% HF, 30% NH₄F, and 15% BaSO₄ for 5 min. After etching glass supports were rinsed thoroughly with distilled water in ultrasound bath for 10 min.

The glass supports surface and their roughness were studied by a scanning probe microscope SPM-9700 (Shimadzu, Japan). AFM scanning was performed using a contact mode by silicon

nitride cantilevers OMCL-TR800PSA (Olympus, Japan) with a stiffness coefficient of 0.57 N/m and a typical tip radius of no more than 15 nm (guaranteed - no more than 20 nm), a tip height was 29 microns. The experiments were carried out under ambient conditions. Automatic correction of linear noise was applied during scanning. For checking purposes reproducibility, AFM scanning was carried out on different sites of the studied surfaces. Processing of the obtained AFM images and their analysis were performed by a software SPM Manager ver. 4.02 (Shimadzu, Japan).

The same way, the polymers surface was studied. But since polymeric materials have a loosely-coupled surface structure, AFM scanning was performed using a tapping mode by silicon vibrating cantilevers PointProbe FMR-20 (Nano World Innovative Technologies, USA) with a stiffness coefficient of 1.3 N/m and a typical tip radius of no more than 8 nm (guaranteed - no more than 12 nm), a tip height was 15 microns.

According to the AFM scanning data (height arrays with a dimension of 512×512 pixels) of the supports and the polymer films from the most viscous of the presented solutions (7.5% PSU, 3% CTA, and 3% PVA), a “growth” model as a Kardar-Parisi-Zhang (KPZ) one was developed.

The obtained model takes into account chemical and physico-chemical features of an original polymer solution, including its viscosity, a Kuhn segment of a polymer chain (a flexibility measure of macromolecules) and solvent evaporation rate, as well as support roughness used for film formation.

The viscosity of the polymer solutions was determined using SVM 3001 Stabinger Viscometer (Anton Paar, Austria) at 25 degrees Celsius. The evaporation rate of the solvent from the polymer solutions was defined by measuring changes in the solution mass over time. The Kuhn segments were found by reference data.

The model was successfully verified using the AFM images of the polymer films surface obtained on the same supports from the same polymers (but with a lower initial viscosity), good agreement with experimental data was observed.

This work was supported by the RFBR (project No. 18-08-01356 A).

1. T.S. Sazanova, K.V. Otvagina, I.V. Vorotyntsev, *Polymer Testing* **68** (2018).
2. A.E. Rassadin, T.S. Sazanova, A.V. Stepanov, L.A. Fomin, *IOP Conf. Series: Mat. Sci. Eng.* **443** (2018).

Application of magnetic force microscopy to observe relaxation transformations of the magnetic structure of the ferromagnetic single crystals surface

E.M. Semenova, M.B. Lyakhova, A.I. Sinkevich, A.Yu. Karpenkov, Yu.G. Pastushenkov

Tver State University, 170002, Tver, Russia
semenova_e_m@mail.ru

The paper presents the results of the MFM study of the surface of rare-earth intermetallic compounds. In [1], it was shown that during the preparation of ferromagnetic crystals to study the magnetic domain structure, a mechanically stressed layer is formed on the surface of the samples. Thus, the magnetic structure of the surface is non-equilibrium and does not correspond to the structure of the closing domains. Studies were performed on a scanning probe microscope Solver Next (NT-MDT). The objects of study were rare-earth intermetallic compounds with different types of magnetocrystalline anisotropy. Figure 1 shows the images obtained on the basic surface of a $Y_2(Fe_{0,03}Co_{0,97})_{17}$ single crystal: immediately after polishing the surface (a) and after 24 hours (b). Images were recorded on the same sample site. Figure 1a shows a labyrinth domain structure with an average domain width of less than $1\ \mu m$. As can be seen from the figure 1b, over time, the magnetic structure of the surface transforms. The width and configuration of the domains vary considerably. The average width of the domains is approximately doubled. Domain walls become sinuous. Figure 1b (inset) shows images of the scattering fields of the equilibrium domain structure. Transformation of the domain structure can last from several minutes to several days, depending on the composition of the sample, the method of mechanical surface treatment and temperature.

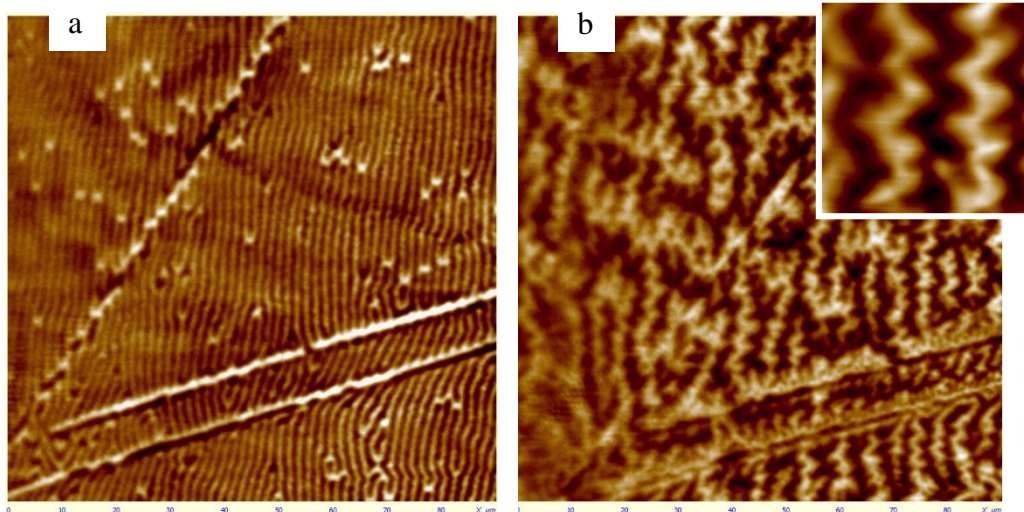


Figure 1. Magnetic domain structure of $Y_2(Fe_{0,03}Co_{0,97})_{17}$ single crystal.

In this paper, we estimated the parameters of the stray fields of a magnetic domain structure based on MFM profiles.

1. Semenova E., Lyakhova M., Karpenkov D., Kuznetsova Yu., Karpenkov A., Skokov K., *EPJ Web of Conferences* **185**, 04027 (2018).

Structure and magnetoelectric coupling of $\text{LiNi}_{1-x}\text{Co}_x\text{PO}_4$ multiferroics

M.A. Semkin¹, N.V. Urusova^{1,2}, M.O. Kalinkin², N.A. Kulesh¹, D.K. Kuznetsov¹,
D.S. Neznakhin¹, A.S. Volegov^{1,3}, D.G. Kellerman^{1,2}, A.N. Pirogov^{1,3}

¹*School of Natural Sciences and Mathematics, Ural Federal University, 620000, Ekaterinburg, Russia*
m.a.semkin@urfu.ru

²*Institute of Solid State Chemistry of the Ural Branch of the RAS, 620990, Ekaterinburg, Russia*

³*M.N. Mikheev Institute of Metal Physics of the Ural Branch of the RAS, 620108, Ekaterinburg, Russia*

Lithium orthophosphates LiMPO_4 , where $M = (\text{Ni}, \text{Co}, \text{Mn}, \text{Fe})$ crystallize to olivine structure, the space group is $Pnma$. They exhibit multiferroic properties with high linear magnetoelectric effect $\alpha \leq 2.0$ pS/m [1, 2]. Excepting LiNiPO_4 , in other LiMPO_4 there is with temperature only a transition from a commensurate antiferromagnetic phase to a paramagnetic state. The polarization arises at the temperature that is equal to the Neel point (T_N) [3]. This fact indicates a strong interaction between magnetic and ferroelectric degrees of freedom. In LiNiPO_4 a polarization exists only in the temperature interval, where the commensurate magnetic phase takes place [4]. Further heating of the sample induces magnetic phase transition to an incommensurate structure at $T_{C-IC} = 20.8$ K and then to the paramagnetic state at $T_N = 21.8$ K. The commensurate antiferromagnetic structure of the orthophosphates LiMPO_4 with $M = (\text{Ni}, \text{Co}, \text{Mn}, \text{Fe})$ is described by the propagation vector $\mathbf{k} = 0$. For example, in the case of the commensurate structure of LiNiPO_4 magnetic moments of Ni ions, located at positions $(0.25 + x, 0.25, -z)$ and $(0.25 - x, -0.25, 0.5 - z)$, are oriented along the c -axis and antiparallel to each other as well as to the moments at sites $(-0.25 - x, -0.25, z)$, and $(-0.25 + x, -0.25, 0.5 + z)$; where $x = 0.026$, $z = 0.018$ [5]. The commensurate structures of other orthophosphates differ from this structure for a mutual orientation of moments or their directions relatively the crystallography axes. For instance, the spins are oriented along the a -axis for LiMnPO_4 , and along the b -axis for LiCoPO_4 [6, 7].

In our work we present the results of structure and magnetic measurements of $\text{LiNi}_{1-x}\text{Co}_x\text{PO}_4$ multiferroic where $x = (0, 0.1, \dots, 0.7)$, and there analysis depend on concentration (x). The $\text{LiNi}_{1-x}\text{Co}_x\text{PO}_4$ multiferroics have been synthesized by a glycerol-nitrate method. X-ray diffraction (XRD) measurements were carried out at room temperature using Shumadzu diffractometer (X-ray source $\text{Cu K}\alpha \lambda = 1.5418$ Å). Structural parameters were refined by Rietveld method using Fullprof program. Morphology of the prepared powder samples was identified by scanning electron microscopy (SEM) AURIGA CrossBeam. The chemical composition ($\text{Ni}_{1-x}\text{Co}_x$) was studied using a full reflection Nanohunter X-ray fluorescence spectrometer. Magnetic measurements were performed with Magnetic Property Measurement System (MPMS XL-7) in the temperature range (2–300) K, under the applied magnetic field of 500 Oe, in the zero field cold (ZFC) mode. The (2–25) K and (25–300) K intervals were investigated with the step ~ 0.1 K and 1 K, respectively.

Figure 1 shows the XRD-patterns for $\text{LiNi}_{1-x}\text{Co}_x\text{PO}_4$ with $x = (0, 0.1, 0.2, 0.3, 0.5, \text{ and } 0.7)$, and SEM-image of the $\text{LiNi}_{0.6}\text{Co}_{0.4}\text{PO}_4$ (for example). All observed reflections correspond to the $Pnma$ space group. The structural parameters have been refined; the lattice constants, and global agreement factor presented in Table 1. The size of the unit cell increases with increasing cobalt concentration in $\text{LiNi}_{1-x}\text{Co}_x\text{PO}_4$. The SEM-image shows that $\text{LiNi}_{0.6}\text{Co}_{0.4}\text{PO}_4$ are homogeneous particles with average size from 0.5 up to 5 μm . Similar SEM-images have been recorded for other samples.

For all samples $\text{LiNi}_{1-x}\text{Co}_x\text{PO}_4$ with $x = (0, 0.1, \dots, 0.7)$ the magnetic phase transitions from the commensurate antiferromagnetic phase to the incommensurate antiferromagnetic state, and to the paramagnetic state are observed. The temperature of the magnetic phase transition from the commensurate to the incommensurate structures (T_{C-IC}) were determined from the temperature dependence of the first derivative of the magnetisation for $\text{LiNi}_{1-x}\text{Co}_x\text{PO}_4$ multiferroics, expected that the magnetoelectric coupling will exist below T_{C-IC} temperature, these values presented in Table 1. The T_{C-IC} temperature decreases in the $\text{LiNi}_{1-x}\text{Co}_x\text{PO}_4$ with increasing the cobalt concentration (x) from 0 up to 0.5, and vice versa increase at concentrations

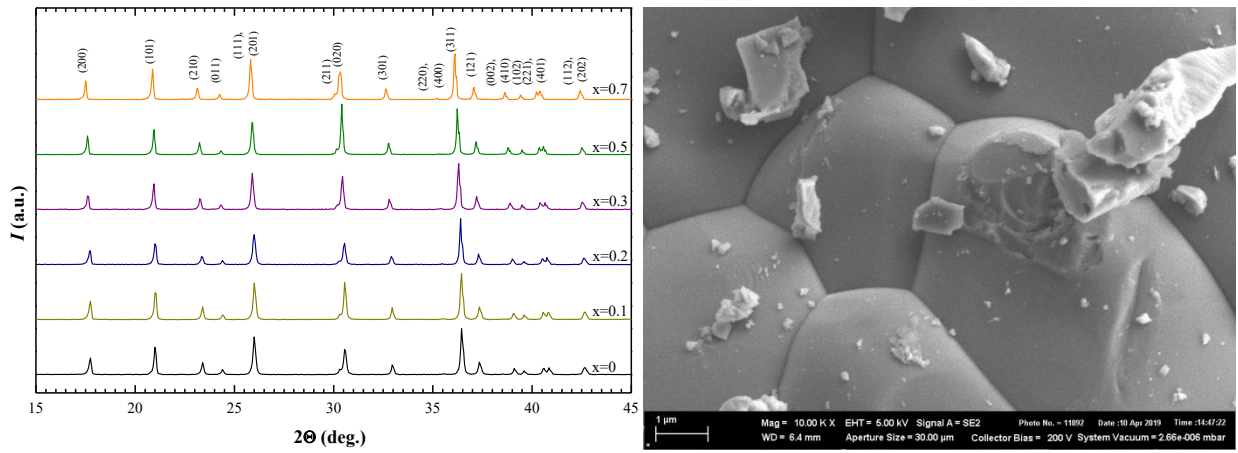


Figure 1. XRD-patterns for $\text{LiNi}_{1-x}\text{Co}_x\text{PO}_4$ (left). SEM-image of $\text{LiNi}_{0.6}\text{Co}_{0.4}\text{PO}_4$ (right).

above 0.5. This behavior of T_{C-IC} in the $\text{LiNi}_{1-x}\text{Co}_x\text{PO}_4$ is explained by the magnetic orderings competition, since in the compounds with $x = (0, 1)$ in which the spins are oriented along the c - and b -axis for LiNiPO_4 , and LiCoPO_4 , respectively.

Table 1. Unit cell parameters of crystal structure of the $\text{LiNi}_{1-x}\text{Co}_x\text{PO}_4$, and their temperature of magnetic phase transition from the commensurate to the incommensurate antiferromagnetic structures.

| x | Sample | a (Å) | b (Å) | c (Å) | χ^2 (%) | T_{C-IC} (K) |
|-----|---|------------|-----------|-----------|--------------|----------------|
| 0 | LiNiPO_4 | 10.0335(6) | 5.8581(3) | 4.6785(3) | 1.77 | 21.81(2) |
| 0.1 | $\text{LiNi}_{0.91}\text{Co}_{0.09}\text{PO}_4$ | 10.0513(6) | 5.8646(3) | 4.6811(3) | 2.01 | 20.47(2) |
| 0.2 | $\text{LiNi}_{0.81}\text{Co}_{0.19}\text{PO}_4$ | 10.0697(6) | 5.8722(4) | 4.6839(3) | 1.59 | 19.10(3) |
| 0.3 | $\text{LiNi}_{0.71}\text{Co}_{0.29}\text{PO}_4$ | 10.0836(6) | 5.8782(3) | 4.6859(3) | 1.61 | 17.58(3) |
| 0.5 | $\text{LiNi}_{0.52}\text{Co}_{0.48}\text{PO}_4$ | 10.1175(4) | 5.8911(2) | 4.6899(2) | 2.41 | 14.50(3) |
| 0.7 | $\text{LiNi}_{0.32}\text{Co}_{0.68}\text{PO}_4$ | 10.1504(5) | 5.9024(2) | 4.6937(2) | 1.96 | 18.13(3) |

This work was supported by MES of RF (contract No. 3.6121.2017/8.9), Act 211 Government of RF (contract No. 02.A03.21.0006), and supported in part by FASO of Russia (theme “Flux” No. AAA-A18-118020190112-8). The equipment of the Ural Center for Shared Use “Modern nanotechnology” SNSM UrFU was used.

1. J.-P. Rivera, *Ferroelec.* **161**, 147 (1994).
2. D. Vaknin, J.L. Zarestky, et. al, *Phys. Rev. Lett.* **92(20)**, 207201 (2004).
3. I. Kornev, M. Bichurin, et. al, *Phys. Rev. B.* **62(18)**, 12247 (2000).
4. R. Toft-Petersen, J. Jensen, et. al, *Phys. Rev. B.* **84**, 054408 (2011).
5. D. Vaknin, J.L. Zarestky, et. al, *Phys. Rev. B.* **60(2)**, 1100 (1999).
6. R. Toft-Petersen, N.H. Andersen, et. al, *Phys. Rev. B.* **85**, 224415 (2012).
7. E. Fogh, R. Toft-Petersen, et. al, *Phys. Rev. B* **96**, 104420 (2017).

Radial non-uniform piezoelectric response of perovskite islands in thin PZT films

S.V. Senkevich^{1,3}, D.A. Kiselev^{2,3}, V.V. Osipov^{1,3}, V.P. Pronin³

¹*Ioffe Institute, 194021, St. Petersburg, Russia*
 SenkevichSV@mail.ioffe.ru

²*National University of Science and Technology «MISiS», 119049, Moscow, Russia*

³*Herzen State Pedagogical University of Russia, 191186, St. Petersburg, Russia*

The structural, ferroelectric and piezoelectric properties of thin polycrystalline $\text{Pb}(\text{Zr},\text{Ti})\text{O}_3$ (PZT) films grown by RF magnetron sputtering have been studied. The films were fabricated in two stage process on Pt/TiO₂/SiO₂/Si substrate. At the first stage, films were deposited at low substrate temperatures (~150 °C) and, at the second stage, ones were annealed and crystallized into perovskite phase at 530-570°C in the conventional furnace. The film thickness was 500 nm.

Microstructure of the films was studied using scanning electron microscope EVO-40 and atomic force microscope MFP-3D SA, Asylum Research and Ntegra Prima. Piezoelectric contact mode (applied alternative voltage 5 V) was used to fix piezoelectric response in the films under study.

Composition of the films corresponded the morphotropic phase boundary with elemental ratio of Zr/Ti = 53.5/46.5. X-ray diffraction results have shown a well-defined <110>- perovskite texture. Microstructure is characterized by spherulite blocks of 10-40 μm in size, according to annealing temperature.

The morphology of the surface and the piezoelectric effect of individual perovskite islands was studied. It was shown the solid-state phase transformation of pyrochlore-perovskite is accompanied by relaxation of mechanical stresses at the interface.

The effect of inhomogeneous distribution of the piezoresponse over the surface of the perovskite island (Fig. 1) - from the maximum response near its boundary to the minimum - to the center of the island was found. It is assumed that the observed effect is caused by the difference in the mechanical clamping of the crystal grains in the periphery of the islets and in the center.

The work was partly supported by the Ministry for Education and Science (Russian Federation) (Grant No 16.2811.2017/4.6) and RFBR (Grant No 18-32-00092_mol-a).

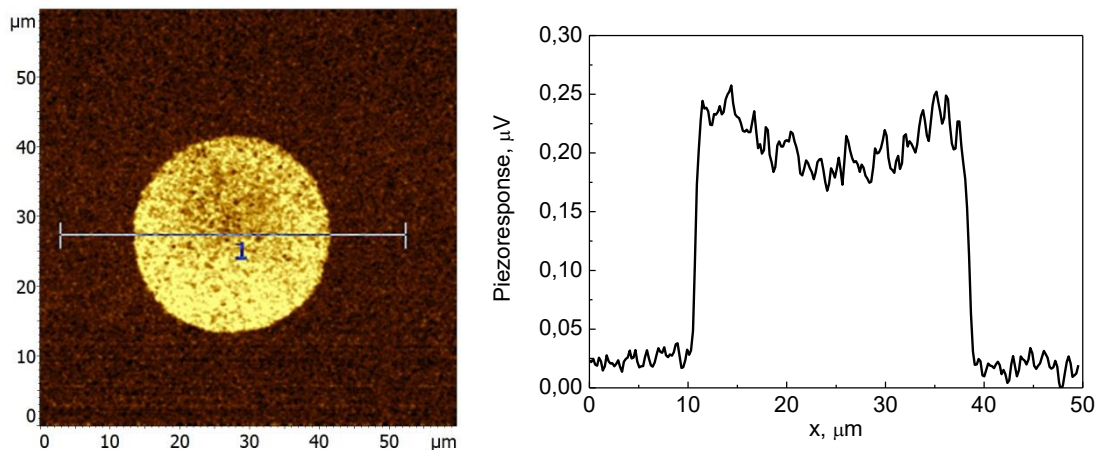


Figure 1. PFM image and profiles of the piezoelectric response of the perovskite island.

Novel technology for fabrication of probe tips for SPM using focused ion beam induced deposition method

N.A. Shandyba¹, I.V. Panchenko¹, A.S. Kolomiytsev¹, S.A. Lisitsyn²

¹*Southern Federal University, Institute of Nanotechnologies, Electronics, and Electronic Equipment Engineering, 347922, Taganrog, Russia
shandyba.nikita@gmail.com*

²*Schooltech, Kvantorium, 414057, Astrakhan, Russia*

Scanning probe microscopy (SPM) is currently one of the main methods for obtaining information about the structure and local properties of the surface. The accuracy and resolution of research using SPM methods is largely determined by the parameters of the probes used. Special SPM methods, such as near-field optical microscopy (SNOM) and vertical wall microscopy (CD AFM), require the use of specialized-shaped probes, the production of which is technologically difficult. Using modern methods of forming nanostructures, it is possible to form the tips of the probes of complex shape. One of the most promising today methods for the formation of nanoscale structures is ion-stimulated deposition of materials from the gas phase using a focused ion beam (FIB) Ga⁺. The FIB method makes it possible to perform technological operations of local ion-beam etching and ion-stimulated deposition of materials under high vacuum conditions without the need for resists, masks and chemical etchants [1].

In the present work, experimental studies of the effect of the parameters of ion-stimulated deposition by the FIB method on the geometric parameters of the formed nanoscale structures are carried out. In the course of experimental studies, the optimal values of the accelerating voltage, the ion beam current, the time of beam impact at a point and the degree of overlap of neighboring impact points (Fig.1), at which the parameters of the formed structures corresponded to the specified, were determined.

Based on the data obtained, probes with high aspect ratios were formed for the AFM and the CD-AFM technique (Fig. 2).

The results obtained in the study can be used in the development of technological processes for the manufacture and modification of special probes for atomic force microscopy, including probes CD-AFM.

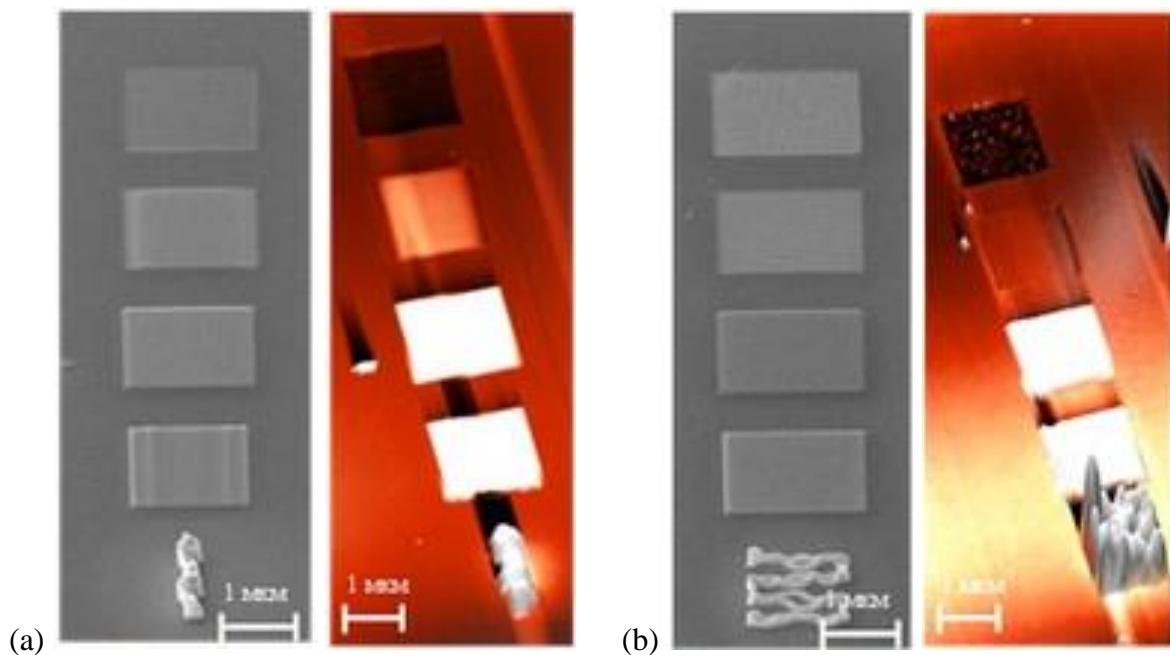


Figure 1. The example of influence of beam overlap on the deposition process (10 ms dwell time, 8 pA beam current): (a) 5 nm, (b) 10 nm.

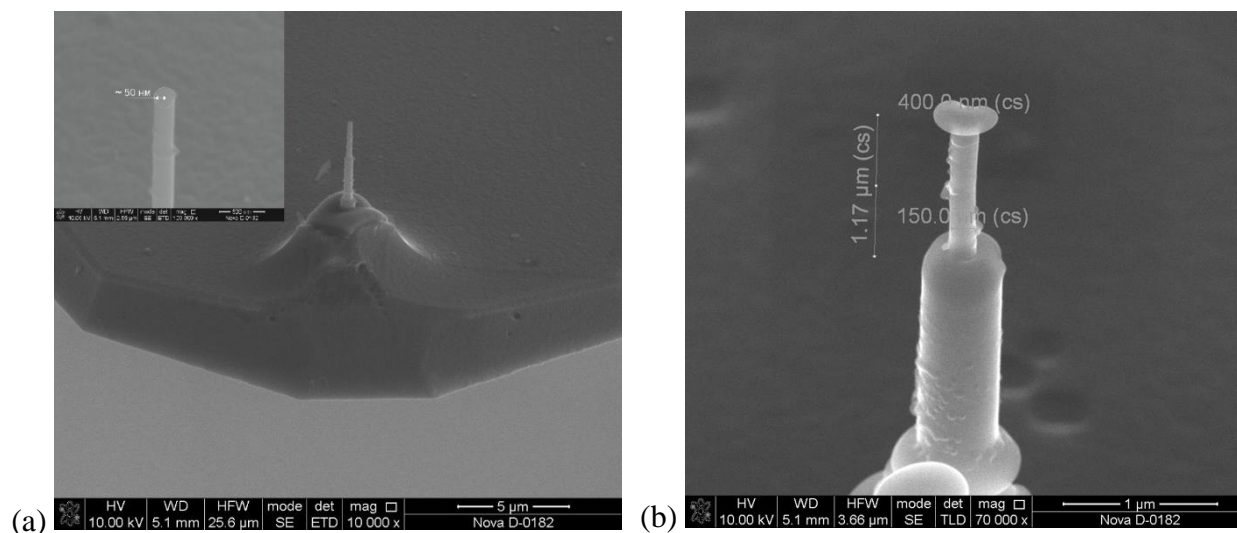


Figure 2. SEM images of AFM (a) and CD AFM (b) probe tips, fabricated by focused ion beam deposition of carbon.

The work was done through a grant from the Russian Science Foundation (project No. 18-79-00175) using the equipment of the Research and Education Center and the Nanotechnology Joint Use Center of the Southern Federal University (Taganrog).

1. O.A. Ageev, A.S. Kolomiitsev, B.G. Konoplev, N.I. Serbu, V.A. Smirnov, *Russ. Microelectr.* **41**, 41 (2012).

Heterogeneous ferromagnetic state in small particles and its connection with ferroelectricity

T.S. Shaposhnikova, R.F. Mamin

Zavoisky Physical-Technical Institute, FRC Kazan Scientific Center of RAS, 420029, Kazan, Russia
t_shap@kfti.knc.ru

Phase transitions in spherical particles of a cubic ferromagnetic were considered in the framework of the Ginzburg-Landau phenomenological theory. Concentrating on depolarizing field effects, we study the competition between states with homogeneous magnetization and vortex structures. For large sphere radii ($R > R_c$), a phase transition to a vortex state is possible, while for $R < R_c$ it can be in a homogeneous state. We obtain the inhomogeneous distribution of the ferromagnetic order parameter in the form of 2D and 3D vortices, for which the absolute value of the local magnetization depends on the distance from the center of the vortex. This approach has meaning for mesoscopic-sized particles. Such softening of the amplitude variations of magnetization was considered, for example, in the papers of Levanyuk [1] in the analysis of the ferroelectric near the phase transition and the Robler et al. [2] in the analysis of the ferromagnet near the phase transition.

It is known that there is a connection between magnetic frustration and ferroelectricity in multiferroics [3]. In multiferroics, the simultaneous existence of magnetic and electric dipoles does not always cause a strong connection between them, since the microscopic mechanisms of ferroelectricity and magnetism are different. A probable microscopic mechanism inducing ferroelectricity in magnetic spirals was discussed, for example, in reference [4]. It involves the antisymmetric Dzyaloshinsky–Moriya (DM) interaction. The DM interaction causes a non-collinear spin ordering. If the magnetic ordering is inhomogeneous, it can lead to polarization [3, 5]. In our work, we compute the polarization caused by ferromagnetic 2D and 3D vortices within the phenomenological approach. The results are used to discuss the formation of "polar clusters".

1. A.P. Levanyuk, R. Blinc, *Phys. Rev. Lett.* **111**, 097601 (2013).
2. U.K. Röbber, A.N. Bogdanov, C. Pfleiderer, *Nature* **442**, 797 (2006).
3. S.-W. Cheong, M. Mostovoy, *Nature Materials* **6**, 13 (2007).
4. I.A. Sergienko and E. Dagotto, *Phys. Rev. B* **73**, 094434 (2006).
5. M. Mostovoy, *Phys. Rev. Lett.* **96**, 067601 (2006).

The delay time of phase transition to the polar phase in relaxors: influence of ultraviolet illumination

S.A. Migachev¹, T.S. Shaposhnikova¹, R.F. Mamin^{1,2}

¹Zavoisky Physical-Technical Institute, FRC Kazan Scientific Center of RAS, 420029, Kazan, Russia
t_shap@kfti.knc.ru

²Institute of Physics, Kazan Federal University, 420008 Kazan, Russia

Relaxors have been subject to intensive research for a long time. Interest in these compounds is determined by a combination of ferroelectric, piezoelectric and optical properties and the possibility of using these materials in data storage systems and optoelectronics. The distinguishing features of relaxors are a strongly diffuse maximum in the temperature behavior of permittivity, the shift of this maximum toward higher temperatures with rising measuring field frequency, and a strong frequency dependence of permittivity at very low frequencies. Numerous experimental data show that the properties of the low-temperature phase depend on the history of samples, therefore, the non-ergodic behavior is observed in the low-temperature phase [1]. In an applied electric field, the transition to a uniform state of polarization is observed in the low-temperature phase after zero-field cooling. Such a phase transition was observed in [1] after a sufficiently long delay time had passed from the beginning of field application. The dependences of delay time t_0 of the phase transition on temperature T and external electric field E were established. The observed regularities have been discussed using an approach [2] developing on the basis of the model of diffuse phase transition in the system with defects [3].

We have investigated the delay time t_0 of the phase transition in $\text{PbMg}_{1/3}\text{Nb}_{2/3}\text{O}_3$ single crystal and in PLZT transparency ceramic sample, and we have found out the influence of ultraviolet illumination on this process. The delay time t_0 of the phase transition have been measured for different temperatures and different applied electric fields. It is shown previously that in the frame of the theoretical approach [2] the delay phase transition in polar phase in relaxors could be explain if the dynamic of electron system would be take in consideration. The photoconductivity properties have been discussed and correlation of observed results with developed model [2, 3] is discussed.

The reported study was partially supported by RFBR, research project No. 18-02-00675a.

1. E.V. Colla, E.Yu. Koroleva, N.M. Okuneva, S.B. Vakhrushev, *Phys. Rev. Lett.* **74**, 1681 (1995).
2. R.F. Mamin, R. Blinc, *Phys.Solid State* **45**, 942 (2003).
3. R.F. Mamin, *Phys. Solid State* **43**, 13141319 (2001).

The investigation of regularities of the memristor effect of oxide nanosized titanium structures from the parameters of local anodized oxidation

N.A. Sharapov, V.I. Avilov

*Southern Federal University, Institute of Nanotechnologies, Electronics and Equipment Engineering, 344006 Taganrog, Russian Federation
nsharapov@sfnu.ru*

One of the priorities for the development of modern nanoelectronics is the development and study of nonvolatile memory elements with high speed. At present, a promising element for creating such a RAM is a memristor, an element of nanoelectronics, whose resistance changes when an external field is applied. A characteristic feature of the memristor is its ability to maintain the value of resistance after the cessation of the external field.

At the same time, an urgent task is to study the patterns of formation of oxide nanoscale structures (ONS) of titanium by the method of local anodic oxidation (LAO) and the manifestation of the memristor effect in them. Therefore, the aim of the work is to study the effect of relative humidity in the chamber on the production of ONS of titanium by the LAO method, exhibiting a memristor effect.

To carry out experimental studies, a thin titanium film 19 ± 0.5 nm thick, obtained on the surface of the SiO₂/Si structure using magnetron sputtering on a multifunctional Auto 500 installation (BOC Edwards, England), was used as the initial substrate. Then, an LAO titanium film with NSG10 brand cantilevers with a conductive Pt coating was carried out using a Solver P47 Pro scanning probe microscope (NT MDT, Zelenograd, Russia), by scanning atomic force microscopy in 3×3 μm areas in a semicontact mode, when applied to the probe system substrate voltage pulses with an amplitude of 10 V, with a probe displacement speed of 3 $\mu\text{m/s}$. The relative air humidity was $30 \pm 1\%$ and $90 \pm 1\%$.

An analysis of the experimental results reflects that with increasing of the relative humidity from 30 to 90%, with LAO, there was a change in the mechanism of resistive switching of the ONS of titanium (Fig. 1). At 30% air humidity the resistance switching of the ONS of titanium proceeded through a mechanism based on the modulation of the Schottky barrier width at the metal/oxide boundary due to the redistribution of oxygen vacancies in the oxide volume. This mechanism can be implemented in the presence of a sufficient number of oxygen vacancies in the oxide volume, which is confirmed by theoretical calculations presented in the first paragraph. The switching mechanism of the resistance of the ONS of titanium obtained by the LAO method at 90% air humidity corresponds to the formation of a conducting channel in the oxide volume, which is possible in case of uneven distribution of oxygen vacancies in the oxide volume in the presence of an area with a low concentration of vacancies which the conducting channel passes through.

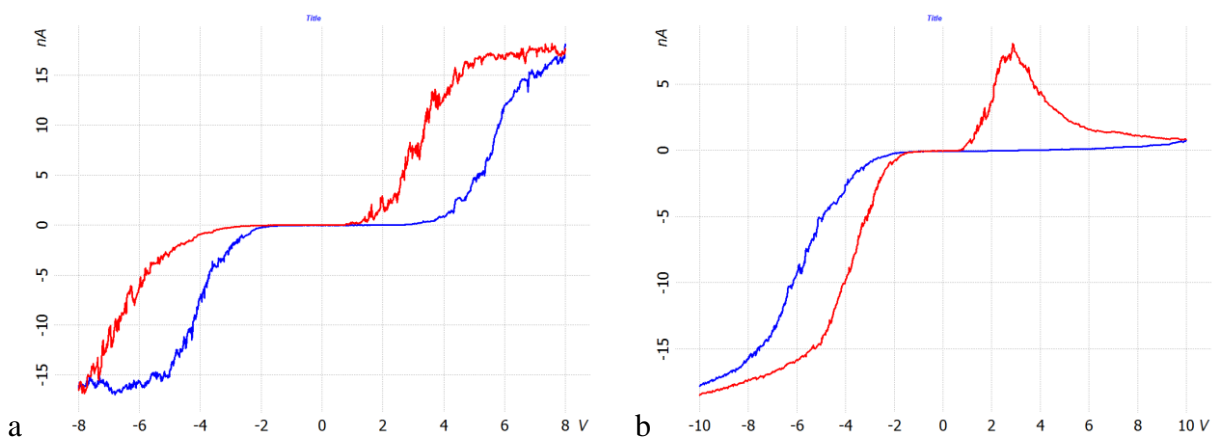


Figure 1. Voltage-current characteristics of ONS titanium obtained at a humidity level in the process chamber (a) 30% and (b) 90%.

Thus, it was shown that the control parameters of the LAO affect the distribution of oxygen vacancies in the volume of the formed ONS, which in turn determines the switching mechanism of the resistance of oxide nanoscale structures of titanium.

The results obtained can be used in the development of technological processes for manufacturing elements of micro- and nanoelectronics based on titanium oxide nanoscale structures by the method of local anodic oxidation.

This work was supported by Grant of the President of the Russian Federation No. MK-2721.2018.8. and by RFBR according to the research project № 18-37-00299.

Conductive AFM study of the electronic properties of vertical GaN nanowires

V.A. Sharov, K.Yu. Shugurov, V.V. Fedorov, A.M. Mozharov

Saint-Petersburg Academic University, 194021, Saint-Petersburg, Russia
vl_sharov@mail.ru

Electronic properties of III-N semiconductors make them important materials for the development of the light-emitting diodes and optoelectronic devices operating in the blue and near-ultraviolet range [1]. One of the problems that III-N-based devices fabrication technology is facing today is the high cost of Al₂O₃ or GaN substrates promoting researchers to develop the nitride compounds growth techniques on more accessible wafers, such as silicon and find new approaches for the defect free epitaxial growth of highly lattice mismatched systems [2]. In this work, we study influence of the Si (111) substrate surface preparation and buffer layer composition on the electronic properties of the GaN NWs synthesized via plasma-assisted molecular beam epitaxy (PA-MBE) in the same growth chamber.

The investigated GaN NWs were grown on Si (111) p-type wafers using Veeco GEN-III machine. Average length and diameter were approximately 500 and 50 nm respectively. Seven samples were grown with different substrate surface preparation and buffer or seeding layer deposition. A comparison study of GaN NWs growth on the bare Si (111) substrate, silicon nitride interlayer, predeposited AlN and GaO_x buffer layers, monolayer thick Ga wetting layer and GaN seeding layer prepared by the droplet epitaxy is performed.

Ntegra Aura (NT-MDT, Russia) setup with built-in current meter and AFM probes with W₂C conductive coating were used to obtain I-V curves of vertical GaN NWs. Grounded atomic force microscope (AFM) probe was used as an electric contact to NW free upper grain. The second contact was established between the highly doped Si substrate and a grounded sample holder of the AFM device. The use of the constant height mode with a stiff cantilever was considered more appropriate than constant force mode for accurate establishing the Tip-NW contact. The AFM probe's deflection was registered by an optical system consisting of a photodetector and a 650 nm laser.

We analyze the obtained I-V curves of the single NW and discuss its morphology and the substrate treatment on the semiconductor properties of the synthesized heterostructures. It is demonstrated that use of AlN buffer or Ga-droplet seeds may lead to the unintentional doping of Si substrate by Al or Ga which deteriorates diode characteristics and increase the reverse current by orders of magnitude. Formation of the vertical NW arrays with random azimuthal orientation was demonstrated on microcrystalline GaO_x wide bandgap semiconductor buffer layer. However, electronic transport of the latter is deteriorated due to high resistance of undoped GaO_x layer.

V.A.S. thanks for support of the heterostructures characterization and K.Yu.S. thanks for support of the experimental data analysis the Ministry of Science and Higher Education of the Russian Federation (Grants 16.2593.2017/4.6 and 3.9796.2017/8.9, correspondingly), V.V.F. and A.M.M. thanks for support of the growth processes the Russian Federation President Council for grants (MK-1204.2019.2 and SP-2324.2018.1, correspondingly).

1. S. Nakamura, *Science* **281**, 956 (1998).

2. K. A. Bertness, N. A. Sanford, A. V. Davydov, *IEEE J.Sel. Top. Quantum Electron.* **17**, 847 (2011).

Local polarization reversal in relaxor SBN single crystals by electron and ion beam irradiation

V.A. Shikhova¹, V.V. Fedorovykh¹, D.S. Chezganov¹, E.O. Vlasov¹, P.S. Zelenovskiy¹, E.D. Greshnyakov¹, M.S. Nebogatikov¹, V.A. Anikin¹, A.L. Kholkin¹, L.V. Ivleva², V.Ya. Shur¹

¹*School of Natural Sciences and Mathematics, Ural Federal University, 620000, Ekaterinburg, Russia*
vera@urfu.ru

²*Prokhorov General Physics Institute, Russian Academy of Sciences, 119991, Moscow, Russia*

The local polarization reversal under the action of medium-energy electron and ion beam irradiation has been studied in barium-strontium niobate single crystals ($\text{Sr}_{0.61}\text{Ba}_{0.39}\text{Nb}_2\text{O}_6$, SBN) with free surface and surface covered by dielectric layer (resist) [1]. SBN single crystals were grown using a modified Stepanov method. The studied plates were cut perpendicular to the polar axis and polished to optical quality.

The scanning electron microscope (Auriga CrossBeam workstation, Carl Zeiss NTS) was used for irradiation with medium-energy electrons and ions [1]. Two types of exposure regimes were used: (1) dot exposure – discrete irradiation by isolated dots with the distances between the points 7 and 100 μm ; (2) stripe exposure – continuous irradiation by stripes with period 7 μm . The stripe exposure was performed along Y crystallographic direction and at 45° to it. Domains were imaged on the surface by piezoelectric force microscopy. Confocal Raman microscopy [2] and Cherenkov type second harmonic generation [3] were used for domain imaging in the bulk.

The ensemble of isolated submicron-size domains appeared in the samples with free surface, whereas the isolated circular domains were revealed in the samples covered by resist. This fact can be attributed to the charge localization in the resist [1]. The circular shape of isolated domains (isotropic domain growth) is caused by step generation at the wall by merging with initial isolated residual nanodomains. It was found that the domains area linearly increases with irradiation dose for distance between dots 100 μm , while the area of domains recorded with 7- μm -distance linearly increases with saturation at dose above 15 pC. The obtained dose dependence of the switched area can be attributed to screening of the depolarization field by injected electrons. The observed domain growth retardation and saturation of the switched domain area for short period is due to the electrostatic interaction of the approaching charged domain walls.

The quasi-regular chains of isolated domains (at doses below 100 $\mu\text{C}/\text{cm}^2$) and stripe domains (at doses above 100 $\mu\text{C}/\text{cm}^2$) were formed as a result of stripe irradiation. The width of the obtained stripe domains linearly increased with irradiation dose and saturated at high doses. The width of stripe domains created by scanning along Y and 45° to Y was almost equal for doses below 250 $\mu\text{C}/\text{cm}^2$. The value of saturation the width of stripe domains oriented along 45° to Y was less than ones oriented along Y, which may be associated with more favorable growth domains along the crystallographic directions. The depth of the created domains on the radiation dose was measured for dot and stripe irradiation. The created domain structures were a stable at room temperature at least for several months. The PFM contrast of created domains decreased with heating and disappeared completely at 120 °C.

The obtained results can be used for creation of the precise domain patterns with arbitrary orientation and shape in SBN single crystals in order to produce the nonlinear optical devices.

The equipment of the Ural Center for Shared Use “Modern Nanotechnology” UrFU was used. The research was made possible by the Russian Science Foundation (grant № 19-72-00008).

1. V.Ya. Shur, D.S. Chezganov, A.R. Akhmatkhanov, D.K. Kuznetsov, *Appl. Phys. Lett.* **106**, 232902 (2015).
2. P.S. Zelenovskiy, V.A. Shikhova, A.V. Ievlev, M.M. Neradovskiy, V.Ya. Shur, *Ferroelectrics* **439**, 33 (2012)
3. Y. Sheng, A. Best, H.-J. Butt, W. Krolikowski, A. Arie, K. Koynov, *Opt. Express* **18**, 16539 (2010).

The role of humidity on the domain growth during local switching in RKTP single crystals

E.V. Shishkina, V.Ya. Shur, E.V. Pelegova, A.R. Akhmatkhanov, M.S. Kosobokov

*School of Natural Sciences and Mathematics, Ural Federal University, Ekaterinburg, Russia
ekaterina.shishkina@urfu.ru*

The domain growth during local switching by conductive SPM tip at controlled humidity has been studied in thin Rb doped potassium titanyl phosphate KTiOPO_4 (RKTP) single crystal.

The 10- μm -thick plate was cut perpendicular to the polar axis and the bottom surface was covered by solid ITO electrode. The local switching was performed by rectangular pulses with duration from 10 ms to 200 s at the controlled relative humidity (RH) from 0 to 70%. The low plate thickness results in formation of the stable intergrown domains with neutral walls. The domains were imaged by piezoresponse force microscopy (PFM). It was shown that the shape of isolated domain changes from rounded nanodomain to the prolate hexagon. The linear voltage dependence of the domain length is typical for local switching in uniaxial ferroelectrics [1]. The pronounced increase of the domain length with RH was revealed. It was revealed that in dry atmosphere the domain size is independent on the pulse duration less than 1 s.

For explanation of the obtained effects we have considered the influence of the RH on the spatial distribution of the local switching field. The sample surface is free of water in dry atmosphere only. In typical ambient conditions (RH = 30%, $T = 20^\circ\text{C}$) and at higher RH values the surface is covered by thin layer of absorbed water leading to broadening of the field distribution caused by formation of the water meniscus at the conductive tip [2]. Moreover, the water layer acting as a solid high-resistant electrode allows to obtain the domains with several micron size because of long-time switching. The calculation of the switching field under the tip and at the domain wall was used for explanation of the obtained experimental data.

To explain the domain evolution, we use the kinetic approach considering the effect of screening retardation. Switching in dry atmosphere shows the independence of the domain size on pulse durations less than 1 s. It means that the nucleated domain reaches the size determined by the spatial distribution of the field produced by the conductive tip faster than 10 ms. Further slower domain growth at the switching times above 1 s is obtained after the essential screening of the depolarization field at the domain wall, since for dry atmosphere the external screening is negligible. The domain shape is determined by field distribution at the domain wall and the nucleation sites at the vertexes of hexagonal domains.

The equipment of the Ural Center for Shared Use “Modern Nanotechnology” UrFU was used. This research was made possible in part by President of Russian Federation Grant for young scientists (grant No. MK-1217.2019.2).

1. B.J. Rodriguez, R.J. Nemanich, A. Kingon, A. Gruverman, S.V. Kalinin, K. Terabe, X.Y. Liu, K. Kitamura, *Appl. Phys. Lett.* **86**, 012906 (2005).
2. A.V. Ievlev, A.N. Morozovska, V.Ya. Shur, S.V. Kalinin, *Appl. Phys. Lett.* **104**, 092908 (2014).

Study of economically alloyed aluminum alloys by SEM and SPM

I.V. Shkalei¹, O.O. Shcherbakova¹, V.A. Lapitskaya²

¹*Ishlinsky Institute for Problems in Mechanics RAS, 119526, Moscow, Russia
ioann_shiva@list.ru*

²*Heat and Mass Transfer Institute of NAS Belarus, 220072, Minsk, Belarus*

Aluminum alloys are promising materials used in various fields of engineering. In particular, they are widely used in the manufacture of bearing assemblies of various machines and mechanisms, where they are gradually replacing costly bronze [1]. In the present work, two economically doped aluminum-based alloys of the following composition were investigated:

No. 1 – Al-5% Si-4% Cu-4% Sn-0.5% Bi-0.5% Pb-0.5% Cd,

No. 2 – Al-5% Si-4% Cu-4% Sn-0.5% Bi-0.5% Pb.

These compositions were selected on the basis of the results obtained in [2].

The alloys were investigated before and after the tribological tests carried out according to the “shoe-roller” scheme (the studied alloy is a counter-body made of «Ст45» structural steel) [3]. The influence of structural changes at the surface during friction on the tribological properties of alloys was evaluated. Methods of scanning electron and probe microscopy were used to study the topography, composition, and properties of the surface and near-surface layers. Studies of the near-surface layers of the pads were carried out on the end sections. The following instruments were used in the work: SEM Quanta-650 (FEI) with analytical equipment EDAX and SPM Dimension FastScan (Bruker). SPM studies of the alloys were carried out in the PeakForce Tapping QNM mode using standard silicon cantilevers of the NSC-11 type (MicroMash) with a probe tip curvature radius of 29 nm and a console force-constant of 99.72 N/m. The probe makes an “approach” to the surface of the sample with recording force curves at each point of the image. Obtaining and recording such curves is the basis of the PeakForce QNM mode, which automatically recalculates the values of mechanical properties (modulus of elasticity and adhesion), taking into account the characteristics of the probe used.

Figure 1 shows the SEM image of a slice of the pads of alloy No. 2 after tribological tests at different pressures.

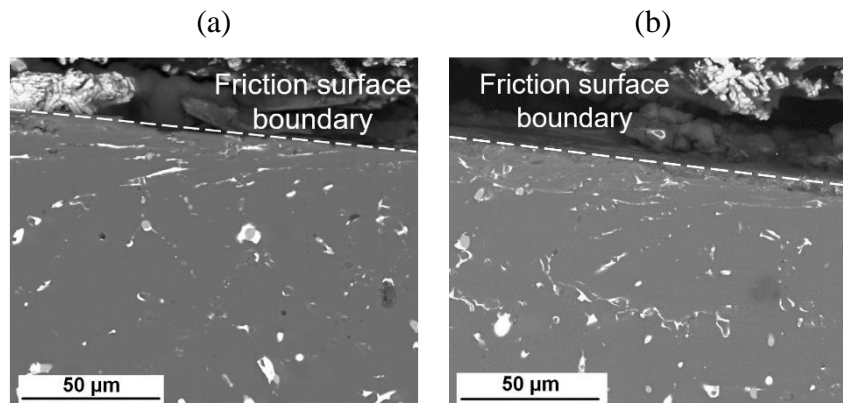


Figure 1. SEM-images of the slice of the block from alloy No. 2 after tribological tests at various pressures: (a) 0.5 MPa; (b) 1 MPa.

When studying sample slices, it can be seen that the structure in the near-surface region differs from structure in bulk. So, the phase components are traced in it in the direction of friction. This is due to the fact that in the process of friction in the surface layers there is a deformation of the dendritic cells of the aluminum matrix, leading to a change in the geometry of these components. The resulting images show that the differences between the alloys are small. The images allow us to estimate the thickness of the deformed layer: for both alloys, this is 20-30 μm (for pressures of 0.5 MPa) and 50-80 μm (for pressures of 1 MPa).

Figure 2 shows the SPM images of the surface morphology of alloy No. 2 after tribological tests.

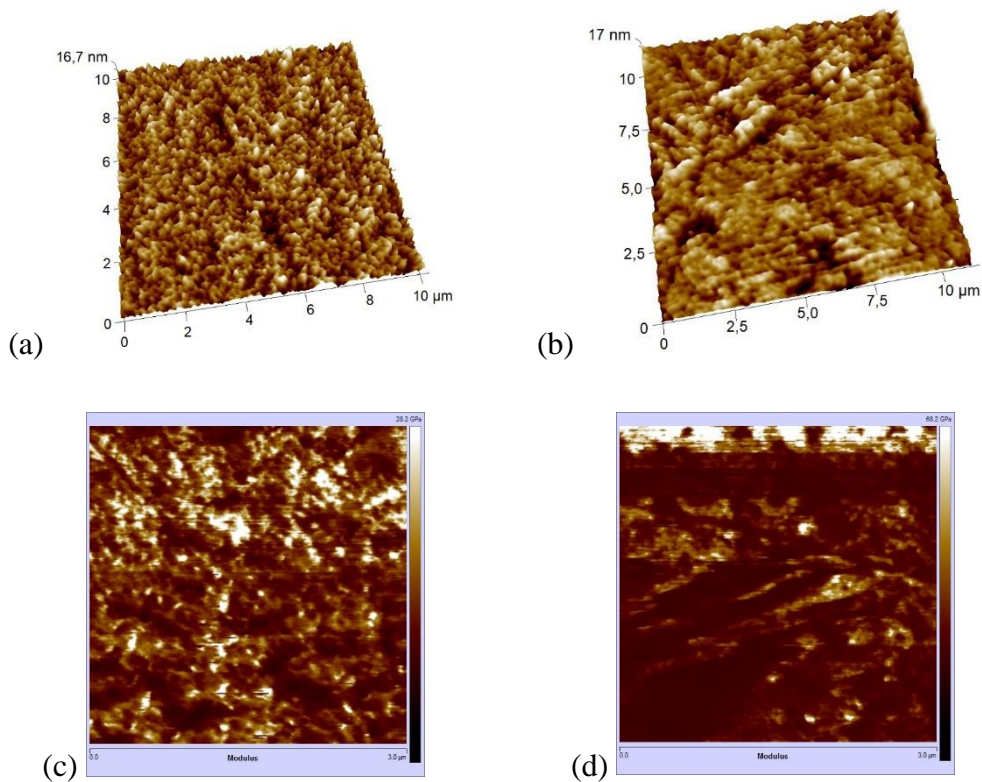


Figure 2. SPM-images of the cut of the surface of the shoe (alloy No. 2) after tribo-testing at a pressure of 1.0 MPa: (a) morphology of the surface layer, (b) morphology in the bulk, (c) modulus of elasticity of the surface layer, (d) modulus of elasticity in volume.

Table 1. The value of the elastic modulus at the cut of the alloy No. 2 at different distances from the boundary of the friction surface after tribological tests 1.0 MPa.

| The distance from the friction boundary, μm | Elasticity modulus E , GPa |
|--|------------------------------|
| 0-20 | 2.7 |
| 20-70 | 1.3 |
| 70-120 | 0.67 |
| 120-180 | 0.59 |
| 180-240 | 0.56 |
| 240-300 | 0.50 |

From Figure 2 and Table 1 it can be seen that the value of the elastic modulus in the near-surface layer of the alloy is significantly higher than in the volume: its values vary from 2,7 GPa to 0,6 GPa. This can be explained by the hardening of the alloy material in the process of friction.

This work was financially supported by the Russian Foundation for Basic Research (projects nos. 18-38-00289) (sample preparation) and partially supported by Grant of President of RF (MK-871.2018.8 No-AAAA-A18-118080290023-0) (microscopy investigations).

1. B.N. Arzamasov, T.V. Solov'eva, S.A. Gerasimov, et al., *Handbook of Structural Materials* (Moscow: Bauman MSTU), 640 (2005).
2. A.O. Yakovleva, N.A. Belov, T.A. Bazlova, I.V. Shkalei, *Phys. Met. Metallogr+* **119**, 35 (2018).
3. B.Ya. Sachek, A.M. Mezrin, O.O. Shcherbakova, et al., *J. Frict. Wear* **39**, 259- (2018).

Magnetron sputtering deposition of ultra-thin tungsten coatings onto amorphous graphite for enhancement of horseradish peroxidase adsorption

I.D. Shumov¹, V.S. Ziborov², Yu.D. Ivanov¹, A.I. Archakov¹, T.O. Pleshakova¹

¹*Institute of Biomedical Chemistry, 119121, Moscow, Russia
shum230988@mail.ru*

²*Joint Institute for High temperatures RAS, 125412, Moscow, Russia*

Atomic force microscopy (AFM) represents a nanotechnological method of molecular detection, which allows one to visualize various nanometer-sized objects, including biological macromolecules, with up to 0.1 nm height resolution [1]. This makes AFM an attractive tool in biochemical research.

To allow their visualization by AFM, the macromolecules under study must be fixed on the surface of a solid support. Regarding biological macromolecules, this can be achieved by their physical adsorption (non-covalent immobilization) onto the AFM support surface. Accordingly, appropriate adsorption efficiency of the macromolecules of interest onto the AFM support is required. Despite this efficiency is strongly affected by electrostatic interactions of the studied macromolecules with the support surface, hydrophobic interactions should also be taken into account, as in a number of cases these very interactions determine the possibility of macromolecules' adsorption [2].

In the present study, the adsorption of horseradish peroxidase (HRP) protein onto the surface of amorphous carbon has been studied by AFM. It has been experimentally demonstrated that modification of amorphous carbon surface by magnetron sputtering deposition of ultra-thin (1.3 nm) tungsten coatings significantly enhances the adsorption of HRP macromolecules onto this surface in comparison with bare carbon.

In our experiments, peroxidase from horseradish (P2088, Sigma, USA) was adsorbed onto amorphous carbon supports (01843-F; Ted Pella, Inc., USA) according to the following procedure: 5 μL of 10^{-7} M to 10^{-6} M HRP solution in Dulbecco modified phosphate buffered saline were incubated on the support surface for 5 min and then washed off with 1 mL of ultrapure deionized water; after that, the AFM support was dried in air. In control experiments, protein-free buffer was used instead of HRP solution.

Ultra-thin tungsten coatings were formed on the surface of graphite AFM supports analogously to the technique described elsewhere [3]. Briefly, Orion-3 magnetron sputtering system (AJA Inc., USA) equipped with tungsten target (thickness 0.25'', diameter 2'', 99.95% purity, Girmet, Russia) was used. Base pressure in the system was not higher than 6×10^{-7} Torr. The sputtering was carried out using argon plasma in DC mode at a constant power of 70 W and 5 mTorr sputtering gas pressure during 10 s. The distance between the target and the specimen was 15 cm. During the sputtering, rotation of the substrate to be coated with constant angle velocity of 40 rpm was provided. The thickness of the so-obtained tungsten films was 1.3 nm as measured by quartz crystal microbalance.

The HRP macromolecules adsorbed on the surface of graphite supports (either coated or not coated with tungsten) were imaged with an NT-MDT atomic force microscope (Zelenograd, Russia) in a semi-contact mode in air with 256×256 resolution.

Figure 1 displays typical AFM images of the surface of graphite supports coated with 1.3 nm tungsten film after their incubation in 10^{-7} M HRP solution (a) and in protein-free buffer (b).

As seen from the image in Figure 1 (a), separate objects with heights of AFM images h from 1 to 3 nm, and a number of objects with $h > 3$ nm are observed on the surface of tungsten-coated graphite after its incubation in 10^{-7} M HRP solution. These data are in agreement with previously reported sizes ($h = 1.5$ nm [4]) of AFM images of HRP (whose molecular weight M_r is 40 kDa [5]), and with the data on the sizes of other proteins with similar M_r (putidaredoxin reductase, $h_{max} = 1.8$ nm [1], $M_r = 45.6$ kDa [6]; adrenodoxin reductase, $h_{max} = 1.8$ nm [7], $M_r = 54$ kDa [8]). Objects with $h > 2$ nm apparently correspond to aggregates formed on the support surface by several HRP macromolecules. It is to be noted that no HRP adsorption was observed in experiments with

bare amorphous graphite without tungsten coating, even in the case with 10-times higher (10^{-6} M) HRP concentration. That is, the adsorption of HRP onto hydrophilic tungsten coating readily occurs, while it is virtually not observed in the case with hydrophobic surface of bare carbon. The control image in Figure 1 (b) indicates that artifact objects are virtually not observed on the support incubated in protein-free buffer, what indicates that the roughness of the obtained coatings is sufficient for imaging protein macromolecules by AFM.

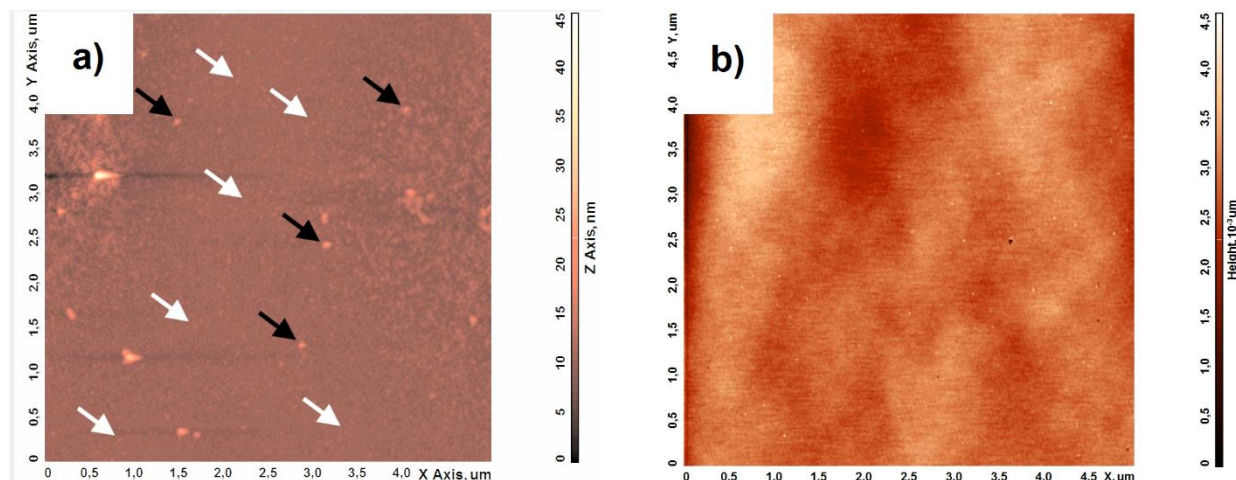


Figure 1. AFM image of amorphous graphite coated with 1.3-nm tungsten film after adsorption of HRP from 10^{-7} M solution (a) and control image (b). Scan size $5 \times 5 \mu\text{m}$. Arrows indicate objects with heights of AFM images h from 1 to 3 nm (white arrows) and $h > 3$ nm (black arrows).

The studies of HRP solutions performed by Ignatenko et al. [9] revealed that HRP forms oligomers in solutions with concentration exceeding 10^{-7} M. Accordingly, the compact objects with $h < 2$ nm observed in Figure 1 (a) can be attributed to HRP monomers, while objects with greater h apparently correspond to HRP oligomers. Accordingly, our data reported herein are in agreement with the literature data [4, 9].

The data obtained in our present study can be used in proteomic studies and in biotechnological research.

The present study was performed in the framework of the Program for Basic Research of State Academies of Sciences for 2013-2020.

1. V.Yu. Kuznetsov, Yu.D. Ivanov, V.A. Bykov et al., *Proteomics* **2**, 1699 (2002).
2. H.P. Felgueiras, *Fundamentals of protein and cell interactions in biomaterials*. In: *Peptides and Proteins as Biomaterials for Tissue Regeneration and Repair* Ed. by M.A. Barbosa and M.C.L. Martins (Woodhead Publishers/Elsevier, Duxford (UK)) 1-27 (2018).
3. I.D. Shumov, S.L. Kanashenko, Yu.D. Ivanov et al., *J. Phys.: Conference Series* **1058**, 012048 (2018).
4. Yu.D. Ivanov, V.V. Danichev, T.O. Pleshakova et al., *Biochemistry (Moscow) Suppl. Series B: Biomedical Chemistry* **7**(1), 46 (2013).
5. P.F. Davies, H.G. Rennke, R.S. Cotran, *J. Cell. Sci.* **49**, 69 (1981).
6. B.P. Unger, I.C. Gunsalus, S.G. Sligar, *J. Biol. Chem.* **261**, 1158 (1986).
7. Y.D. Ivanov, P.A. Frantsuzov, A. Zöllner et al., *Nanoscale Res. Lett.* **6**, 54 (2011).
8. J.-W. Chu, T. Kimura, *J. Biol. Chem.* **248**, 2089 (1973).
9. O.V. Ignatenko, A. Sjolander, D.M. Hushpulian et al., *Adv. Biosens. Bioelectron.* **2**(3), 25 (2013).

Discrete switching during local polarization reversal in ion sliced lithium niobate thin films

B. N. Slautin¹, A. P. Turygin¹, H. Zhu², V. Ya. Shur¹

¹ School of Natural Sciences and Mathematics, Ural Federal University, 620000, Ekaterinburg, Russia
boris.slautin@urfu.ru

² Jinan Jingzheng Electronics Co., Ltd., 250101, Jinan, China

Single-crystalline lithium niobate (LN) thin films are more attractive for optical applications compared to epitaxial and sputtering ones due to absence of light scattering at the grain boundaries. The ion-slicing is useful techniques for producing single-crystalline LN thin bonded to a SiO₂ layer on a LN substrate, called lithium niobate on insulator (LNOI) [1]. LNOI is one of the most effective structure for creation of the integrated optic devices, non-linear light converters and waveguides [2]. Modification of the LNOI films by domain engineering is very perspective topic today for increasing quality and range LNOI-based microelectronic devices.

The domain growth and interaction during local switching have been studied in the LNOI films with bottom electrode [3]. The nanodomain formation in front of the moving domain wall (discrete switching) was recently showed in such films [4]. This effect has been obtained by us in the bulk LN crystals with artificial surface dielectric layer [5]. We repeated the investigation with a wider range of the voltage pulses amplitudes and durations at different humidity. Mechanism of the domain growth and all accompanying effects were described for LNOI films.

We have studied the local domain switching in the LNOI thin films under the biased probe of atomic force microscope. Our investigation was done in the two types of LNOI wafers: (I) with the metal bottom electrode under LN film and (II) with the bottom electrode placed under the SiO₂ layer produced by Jinan Jingzheng Electronics Co (Fig. 1). The qualitative difference of the discrete switching effect in different types of LNOI wafers has been revealed. The regular nanodomain structures appeared in the first type wafers has been attributed to existence of the intrinsic dielectric layer with thickness about 100 nm (Fig. 1a). The irregular structures appeared in the second type wafers are caused by artificial SiO₂ layer blocking the forward domain growth and leading to stronger interaction of the charged domain walls. The influence of the dielectric gap thickness and tilt of the charged domain walls on the distance between main domain and its satellites was studied in detail and numerically modelled for both types of LNOI films.

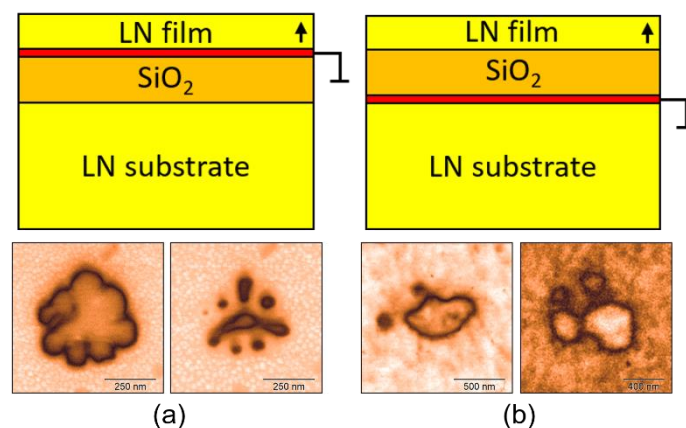


Figure 1. Typical domain shapes and schemes of LNOI wafers (a) first and (b) second types.

The research was made possible by Russian Science Foundation (Project № 19-12-00210). The equipment of the Ural Center for Shared Use “Modern Nanotechnology” UrFU was used.

1. P. Rabiei, P. Gunter, *Appl. Phys. Lett.* **85**, 4603 (2004).
2. H. Han, L. Cai, H. Hu, *Opt. Mater.* **42**, 47 (2015).
3. R.V. Gainutdinov, T.R. Volk, H.H. Zhang, *Appl. Phys. Lett.* **107**, 162903 (2015).
4. W. Ge, H. Zeng, Y. Shuai et al., *Mater. Res. Express* **6**, 035033 (2019).
5. V. Ya. Shur, *J. Mater. Sci.* **41**, 199 (2006).

Gas sensing properties of individual composite nanostructures $\text{TiO}_{2-x}/\text{MWCNT}$ and $\text{SnO}_x/\text{MWCNT}$ measured by scanning force microscopy

N.A. Davletkildeev^{1,2}, D.V. Sokolov¹, E.Yu. Mosur^{1,2}, V.V. Bolotov^{1,2}

¹*Omsk Scientific Center, Siberian Branch, Russian Academy of Sciences, Omsk, 644024 Russia
stezko@obisp.oscsbras.ru*

²*Dostoevsky Omsk State University, Omsk, 644077 Russia*

Composite nanomaterials based on multi-walled carbon nanotubes (MWCNT) and metal oxides are promising materials for gas-sensing application [1]. The trend of miniaturization of electronic devices and the fundamental replacement of massive layers by nanoscale elements attract great interest in the study of electron transport processes in individual nanostructures. Scanning force microscopy is effective method to study the electrical properties of individual nanostructures [2, 3].

MWCNTs synthesized by chemical vapor deposition were used in the work. The concentration of nitrogen in nanotube walls is 3.7 at.% according to X-ray photoelectron spectroscopy data. The functionalization of as-grown MWCNTs was carried out by irradiation with argon ions with energy 5 keV and ion dose 10^{16} cm^{-2} . Composite nanostructures of metal oxide/MWCNTs were fabricated by deposition of non-stoichiometric titanium dioxide (TiO_{2-x}) and tin oxide (SnO_x) on the surface of functionalized MWCNTs using magnetron sputtering method.

Individual MWCNTs, $\text{TiO}_{2-x}/\text{MWCNTs}$, and $\text{SnO}_x/\text{MWCNTs}$ were deposited on microelectrode array from suspensions by spin coating. The suspensions of nanotube and nanostructures was obtained by ultrasonic dispersion of the layers in dichloromethane for 20 min. Conductive atomic force microscopy (C-AFM) and electrostatic force microscopy (EFM) measurements were performed using an atomic force microscope MFP-3D SA (Asylum Research) with conductive cantilevers HA_FM/Pt (NT-MDT) in dry nitrogen (RH ~ 2%) at room temperature. Gas sensing properties were investigated on exposure to a reducing gas (ammonia) and an oxidizing gas (nitrogen dioxide) with concentrations of 1000 ppm.

Optical and atomic-force microscopes were used to detection of individual MWCNTs and composite nanostructures located on two adjacent electrodes (Fig. 1).

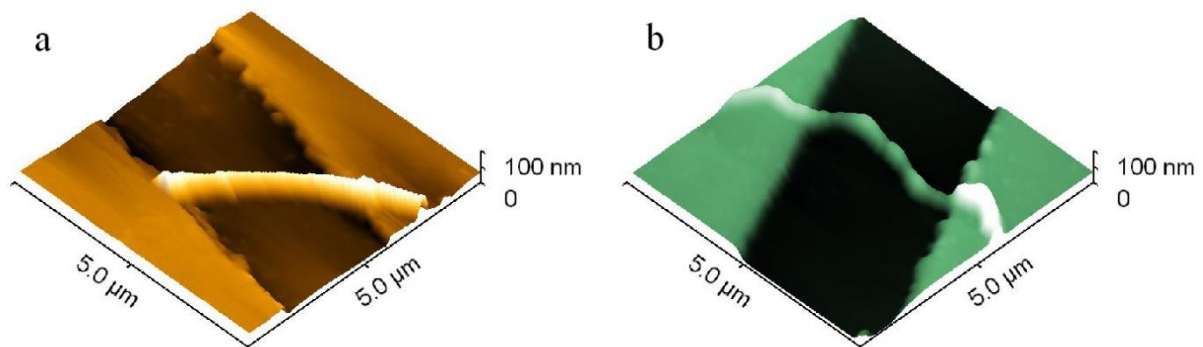


Figure 1. AFM images of individual composite nanostructures located on two adjacent microelectrodes for (a) $\text{TiO}_{2-x}/\text{MWCNT}$ and (b) $\text{SnO}_x/\text{MWCNT}$.

Using the values of work function for the samples obtained by technique [4], the mean values of the Fermi level shift upon adsorption of ammonia and nitrogen dioxide was determined (Fig. 2a).

By comparing the work function values for highly oriented pyrolytic graphite as calibration sample and MWCNTs, it was found that argon ions forms acceptor-like defects in nanotube walls and holes become the major charge carriers in functionalized MWCNTs. During adsorption of the reducing gas, the Fermi level shift in MWCNTs increases slightly due to partial recombination of

holes with electrons. In the case of adsorption of the oxidizing gas, the Fermi level shift decreases significantly, which is caused by an increase the holes concentration in the MWCNT walls.

The Fermi level shift in $\text{TiO}_{2-x}/\text{MWCNTs}$ is like functionalized MWCNTs, but in contrast to MWCNTs, the titanium oxide is an n-type semiconductor and major charge carriers therein are electrons.

In the $\text{SnO}_x/\text{MWCNTs}$ nanostructure the Fermi level shift during gas adsorption is the opposite. Tin oxide is a wide band-gap semiconductor, a space charge region is formed on the band diagram due to surface states, which leads to a pinning of the Fermi level in the depth of band gap. As a result of adsorption of the oxidizing gas, electrons from deep acceptor levels transfer to adsorbate energy levels. The positive charge of surface defect states which occurs after leaving of electrons can partially compensate for the surface negative charge and lead to an increase in the Fermi level shift upwards.

The mean value and range of the conductance of individual MWCNTs, $\text{TiO}_{2-x}/\text{MWCNTs}$ and $\text{SnO}_x/\text{MWCNTs}$ nanostructures upon exposure to gases based on C-AFM measurements was determined (Fig. 2b). The electrical conductance of individual $\text{TiO}_{2-x}/\text{MWCNTs}$ and $\text{SnO}_x/\text{MWCNTs}$ equal in the order of magnitude to the conductance of individual nanotubes that indicates on contribution of the MWCNT walls to the total conductance of composite nanostructures. The changes in conductance during gas exposure correspond to the change in the Fermi level shift for individual MWCNTs, $\text{TiO}_{2-x}/\text{MWCNTs}$ and $\text{SnO}_x/\text{MWCNTs}$ nanostructures.

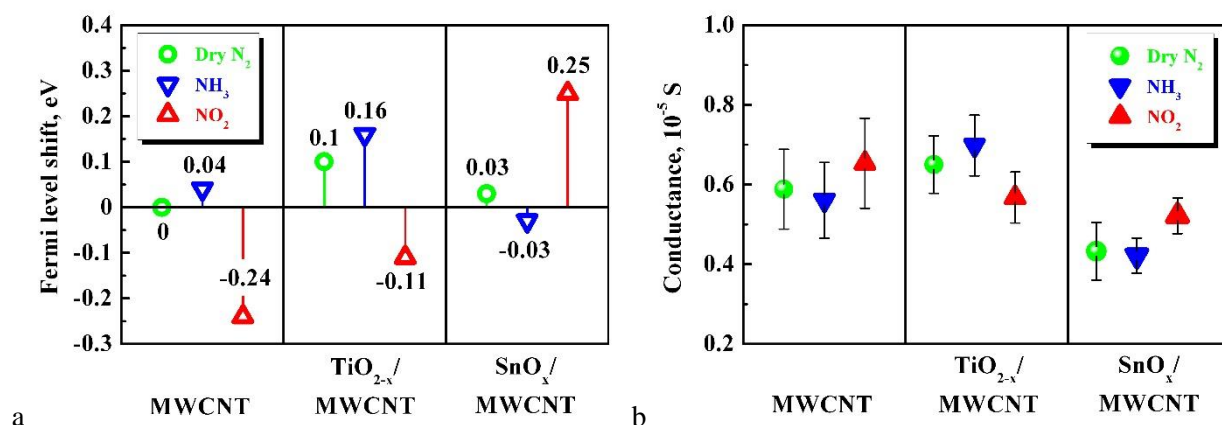


Figure 2. Characteristics of individual MWCNTs, $\text{TiO}_{2-x}/\text{MWCNTs}$ and $\text{SnO}_x/\text{MWCNTs}$ in dry nitrogen, ammonia and nitrogen dioxide: (a) mean on the value of Fermi level shift relative to its position in MWCNT; (b) mean and range on the value of conductance.

The work was carried out according to the state task of the Omsk Scientific Center SB RAS (project registration number AAAA-A17-117041210227-8).

1. E.H. Espinosa, R. Ionescu, B. Chambon, et al., *Sensor. Actuat. B Chem.* **127**, 137 (2007).
2. C. Baldacchini, S. Cannistraro, *Appl. Phys. Lett.* **91**, 122103 (2007).
3. T. Melin, M. Zdrojek, D. Brunel, *Scanning Probe Microscopy in Nanoscience and Nanotechnology*. (Springer-Verlag Berlin Heidelberg), 89 (2010).
4. N.A. Davletkildev, D.V. Stetsko, V.V. Bolotov, et al., *Mater. Lett.* **161**, 534 (2015).

Organism's responses to a long-term inhalation of silica-containing submicron particles (predominantly, nanoscale) of an industrial aerosol

S.N. Solovyeva¹, B.A. Katsnelson¹, M.P. Sutunkova¹, L.I. Privalova¹,
V.B. Gurvich¹, I.A. Minigalieva¹, T.V. Slyshkina¹, I.E. Valamina²,
V. Ya. Shur³, I.V. Zubarev³, D.K. Kuznnetsov³

¹*Yekaterinburg Medical Research Center for Prophylaxis and Health Protection in Industrial Workers, 620014, Yekaterinburg, Russia*
solovyevasn@ymrc.ru

²*Central Research Laboratory of Ural State Medical University, 620028, Yekaterinburg, Russia*

³*School of Natural Sciences and Mathematics, Ural Federal University, 620000, Yekaterinburg, Russia*

Outbred female white rats were exposed for 3 or 6 months, 5 times a week, 4 h a day to an aerosol containing 72% amorphous silica predominantly submicron particles (nanoscale ones included) at an exposure concentration of 2.6 ± 0.6 or 10.6 ± 2.1 mg/m³.

The silica (mostly amorphous) containing submicron particles with a prevailing proportion of those in the nanoscale range induce, when instilled intratracheally, a pulmonary cell response comparable with that to highly cytotoxic and fibrogenic standard quartz powder DQ12. Nevertheless, in long-term inhalation experiment at realistic concentrations, they proved to be of very low systemic toxicity and negligible pulmonary fibrogenicity.

This paradox may be explained by low SiO₂ retention in lungs and other organs due to a relatively high solubility of these nanoparticles in relevant biological and model milieus.

The growth, domain structures, electrical and magnetic properties of BiFeO₃-PbTiO₃ single crystals

Z. Tang,¹ J. Zhuang,^{1*} Y. Fu,¹ A. A. Bokov,^{1,2} N. Zhang,¹ J. Zhang,¹ W. Ren,¹ Z.-G. Ye^{1,2}

¹Electronic Materials Research Laboratory, Key Laboratory of the Ministry of Education & International Center for Dielectric Research, Xi'an Jiaotong University, 710049, Xi'an, P. R. China
jzhuang@xjtu.edu.cn

²Department of Chemistry and 4D LABS, Simon Fraser University, V5A 1S6, Burnaby, Canada

As one of the most popular single-phase multiferroics, the BiFeO₃ based materials attract lots of research interests due to the coexistence of ferroelectric and magnetic orderings above room temperature. Moreover, the extremely high electrostrain in excess of 1% is obtained in La-doped BiFeO₃-PbTiO₃ ceramics recently [1]. In this work, the single crystals of BiFeO₃-PbTiO₃ binary system have been successfully grown using molten-salt method [2]. The as-grown single crystals show dark color and cuboid shape with dimension up to 5 mm, as shown in Figure 1a. X-Ray Diffraction (XRD) results (see Fig. 1b) confirm the formation of pure perovskite structure with *P4mm* symmetry for the as-grown single crystals. The domain structures have been investigated by the Polarized Light Microscope and Piezoresponse Force Microscopy on the (001)_{PC} polished single crystals. In addition, the saturated ferroelectric hysteresis loops are obtained. Finally, the magnetic properties and magnetic anisotropy have been studied by the Physical Property Measurement System and electron Spin resonance technology from room temperature down to 5 K. The results in this work based on BF-PT single crystals are helpful for further understanding of the ferroic couplings in the system.

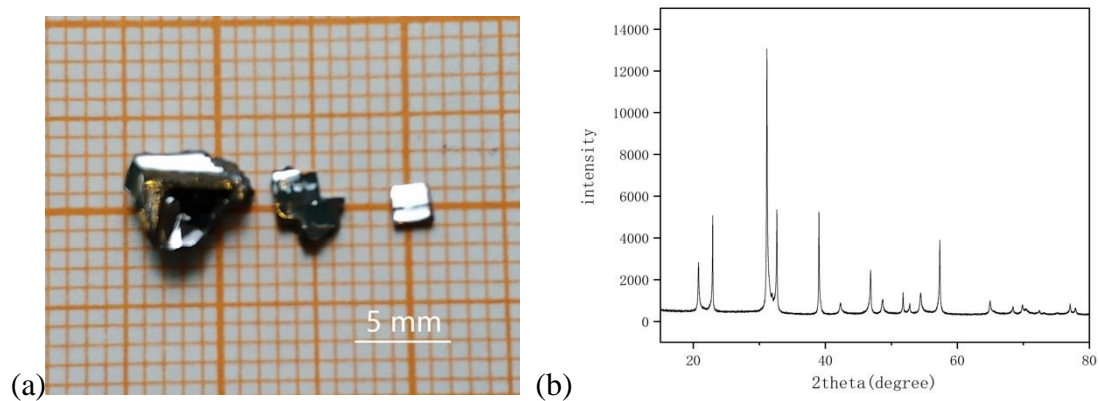


Figure 1. (a) The photographs and (b) the powder XRD pattern of as-grown BiFeO₃-PbTiO₃ single crystals.

1. B. Narayan, J. S. Malhotra, R. Pandey, et. al., *Nature Materials*, **17**, 427 (2018).
2. J. Zhuang, A. A. Bokov, N. Zhang, et. al., *Crystal Growth & Design*, **18**, 4503 (2018).

Investigation of preparation and post processing effects on the topography of ultra-thin Al₂O₃ films

L.P. Guinane¹, E. Ul-Haq¹, J. Kubík², R. Anthony², B.P. Stenson²,
M.N. Morrissey², S. Geary², S.A.M. Tofail¹

¹*Modelling, Simulation, and Innovative Characterisation (MOSAIC), Department of Physics, and Bernal Institute, University of Limerick, V94 T9PX, Limerick, Ireland*
Tofail.syed@ul.ie

²*Analog Devices International (ADI), V94 RT99, Limerick, Ireland*

Alumina (Al₂O₃) thin films are used in a wide range of micro and nanoelectronic applications including protective coatings and diffusion barriers. They have also been used as a series of insulating laminations in integrated magnetic inductors [1]. The thickness and surface state of Al₂O₃, however, is expected to affect exchange coupling, coercivity and anisotropy of the magnetic core of the inductor [2,3]. Additionally, the properties of ultra-thin films of Al₂O₃ are known to be affected by topography and electrostatics of the underlying substrate [4]. Here we report the interplay of substrate condition, deposition parameters, and post processing effects on the topography and electrical properties of Al₂O₃. We fabricated magnetic and nonmagnetic multilayers (Fig. 1) that emulate the vertical architecture and process steps of an integrated inductor. We employ a suite of scanning probe microscopy (SPM) techniques including atomic force microscopy (AFM), Kelvin Probe Force Microscopy (KPFM) and Scanning Spreading Resistance Microscopy (SSRM) using NTEGRA Spectra IITM (NT-MDT Spectrum Instruments, Limerick, Ireland) to determine the presence of pinholes other defects and surface potentials. Additionally, we employ the following techniques; cross-sectional transmission electron microscopy (x-TEM), to verify thickness and structure evolution. Scanning electron microscopy (SEM) revealed islands and pinholes, the density of which was further investigated using an electroplating technique [5] and elemental mapping using energy dispersive X-ray (EDX) analysis. We have also developed a metal-insulator-metal (MIM) capacitor to compare nanoscale properties with macroscopic electrical properties of the ultra-thin films. The capacitor structure has been subject to impedance analysis to determine the electrical permittivity of the insulator. Such a suite of nano and macroscopic analysis allows us to find the interrelation of thickness variation, surface chemistry, topography and electrical properties and can be useful in optimising Al₂O₃ processing for use in laminated magnetic cores.

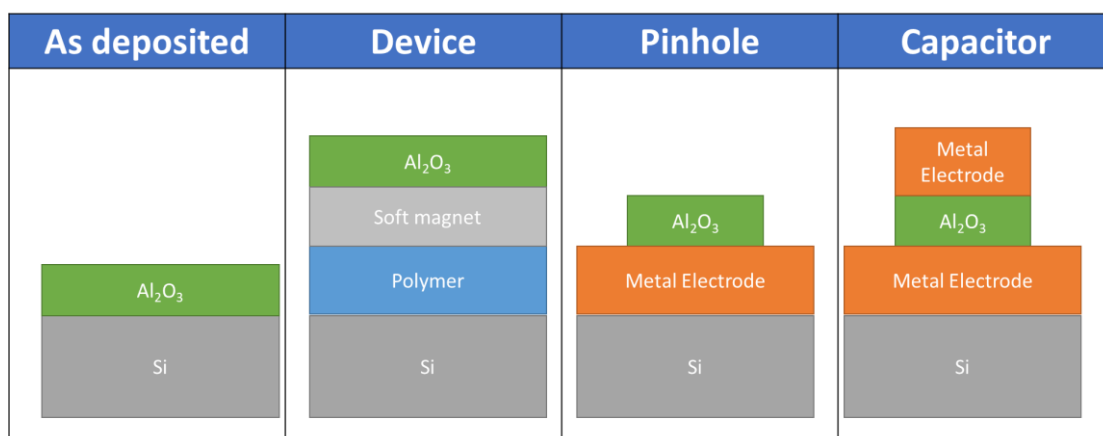


Figure 1. Test structures used for alumina characterisation.

1. C.V. Falub, et al, *AIP Advances* **8**, 048002 (2018).
2. J. C. Slonczewski et al, *IEEE Transactions on Magnetics*, **24**, 2045 (1988).
3. X. Xing et al, *IEEE Transactions on Magnetics*, **47**, 3104 (2011).
4. S. Prasanna et al, *Materials Science in Semiconductor Processing*, **16**, 705 (2013).
5. Y. Zhang et al, *Thin Solid Films*, **517**, 3269 (2009).

PFM studies of ferroelectric phase transition in superprotonic (K_{0.43}(NH₄)_{0.57})₃H(SO₄)₂ crystals

A.L. Tolstikhina, R.V. Gainutdinov, E.V. Selezneva, I.P. Makarova

*Shubnikov Institute of Crystallography of Federal Scientific Research Centre "Crystallography and Photonics" of Russian Academy of Sciences, 119333, Moscow, Russia
alla@ns.crys.ras.ru*

Crystals $M_mH_n(AO_4)_{(m+n)/2} \cdot yH_2O$ ($M = K, Rb, Cs, NH_4, AO_4 = SO_4, SeO_4, HPO_4, HAsO_4$) are of special interest as a potential material for the creation of various electrochemical devices. The proton conductivity is important characteristic of these crystals. Study of temperature behavior of (K_{0.43}(NH₄)_{0.57})₃H(SO₄)₂ crystals at cooling and detection of phase transitions by PFM methods are purpose of this work.

The photo of (K_{0.43}(NH₄)_{0.57})₃H(SO₄)₂ crystals, grown in the Institute of Crystallography, are shown in Figure 1a. Crystals were grown in the K₃H(SO₄)₂–(NH₄)₃H(SO₄)₂–H₂O system [1]. In contrast to the known members of $M_3H(AO_4)_2$ family that have a superprotonic phase transition with an increase in symmetry from monoclinic to trigonal at heating, the crystals of (K,NH₄)₃H(SO₄)₂ with 57% of ammonium grow in the superprotonic phase [2]. X-ray study shows that crystals has trigonal symmetry, space group $R\bar{3}$, $Z = 3$, $a = b = 5.7768(3)$, $c = 22.0983(1)$ Å at $T \approx 23$ C. The trigonal symmetry is conditioned by the K/N occupation ratio and corresponding coordination of NH₄ groups (Fig. 1b). The appearance of the threefold axis leads to disordering of the O atoms involved in hydrogen bonds and as a result to the formation of a dynamically disordered network of hydrogen bonds, and rise of conductivity.

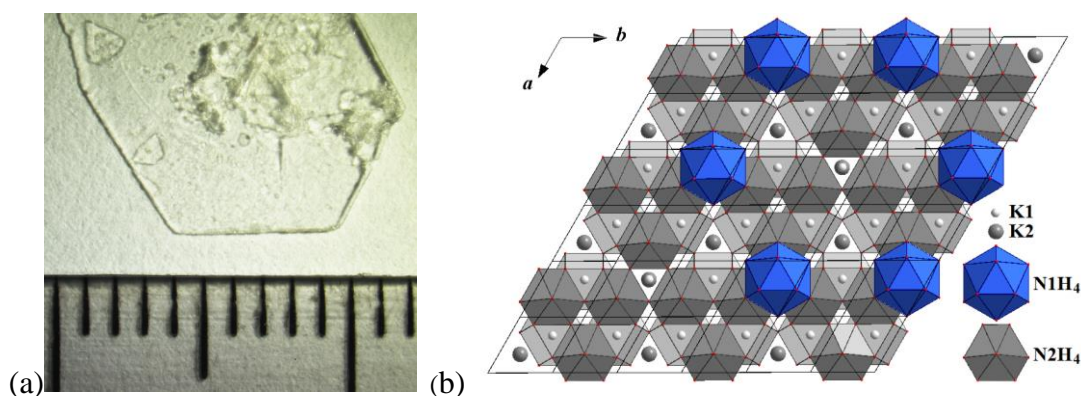


Figure 1. (a) (K_{0.43}(NH₄)_{0.57})₃H(SO₄)₂ crystals. (b) model of the arrangement of K and N atoms in (K_{0.43}(NH₄)_{0.57})₃H(SO₄)₂ crystals: K1 atoms and N1H₄ coordination polyhedra, located in the layers of SO₄ tetrahedra, and K2 atoms and N2H₄ coordination polyhedra, located between the layers, are shown. SO₄ tetrahedra and hydrogen bonds are omitted.

The (K_{0.43}(NH₄)_{0.57})₃H(SO₄)₂ crystal was investigated with two PFM methods using various ways of registration the piezoelectric response. The first one is traditional contact PFM, the second – hybrid PFM. The PFM measurements were carried out with scanning probe microscope NTEGRA Prima (NT-MDT Spectrum Instruments) using NSG01/Pt tip. Also the temperature controller MP6LC which allows to vary temperature (T) from -30 °C to $+120$ °C was used. The maximum interaction force between tip and surface was 160 nN. The temperature varied three times: from 23 ± 0.1 °C to 5 ± 0.1 °C and backwards.

Figure 2 demonstrates the structural changes in the crystal, which occur with a decrease in temperature from 23 °C to 5 °C. Fig. 2a shows the relief of a polished (001) crystal surface. The PFM image (Fig. 2b) shows that at $T = 23$ °C the crystal was in the paraphase. With a decrease in temperature to 9 °C, a transition to the ferroelectric state was observed (Fig. 2c). Small domains with the size about 1 μm are visible on monodomain area. Measurement of mechanical properties allows to observe the small areas with hardness lower than the main template hardness (Fig. 2d). With the temperature decrease to 5 °C, no changes in the structure were observed (Fig. 2e). Repeated temperature change in the range of 5–23 °C showed that the phase transition is reversible.

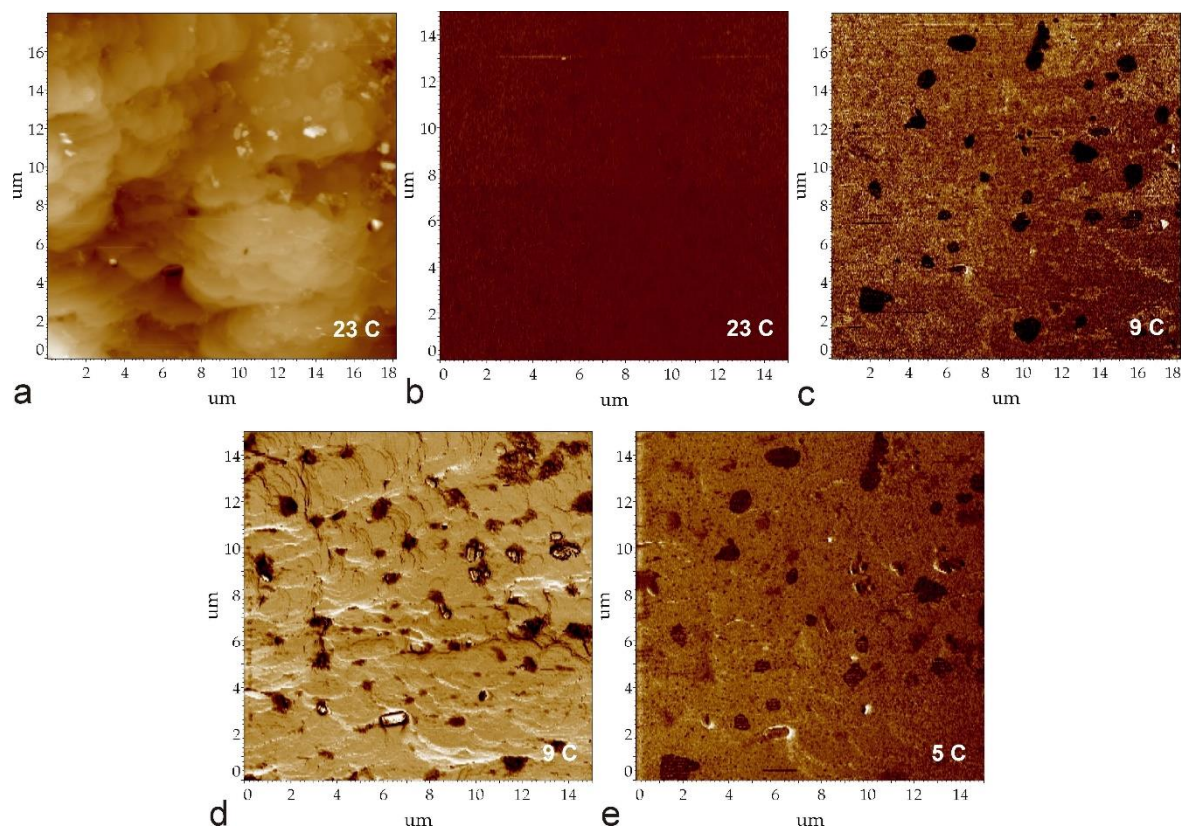


Figure 2. AFM images of $(K_{0.43}(NH_4)_{0.57})_3H(SO_4)_2$ crystal as a function of temperature: (a) topography, contact AFM; (b, c, e) contact in-plane PFM (phase); (d) hybrid mode, hardness (arb. un.).

The PFM method allows first time to observe the phase transition (from paraphase to ferroelectric phase) in $(K_{0.43}(NH_4)_{0.57})_3H(SO_4)_2$ crystal with temperature decrease. The obtained information supplements the structural and dielectric data [2].

We are grateful to V.V. Dolbinina (FSRC “Crystallography and Photonics” RAS, Moscow) for supplying the samples and A.S. Kalinin (NT-MDT Spectrum Instruments, Moscow) for his help.

This work was supported by the Ministry of Science and Higher Education within the State assignment FSRC «Crystallography and Photonics» RAS and the Presidium of the Russian Academy of Sciences, Basic Research Program 1.2.P no. 32.

1. E.V. Dmitricheva, I.P. Makarova, V.V. Grebenev, et al., *Solid State Ionics* **268**, 68 (2014).
2. E.V. Selezneva, I.P. Makarova, I.A. Malyshkina et al., *Acta Cryst. B.* **73**, 1105 (2017).

Investigation of forming-free resistive switching of nanocrystalline hafnium oxide thin films

R.V. Tominov, V.I. Avilov, D.D. Dukhan, V.A. Smirnov

*Southern federal university, Institute of Nanotechnologies, Electronics and Equipment Engineering
347928, Taganrog, Russia
roman.tominov@gmail.com*

Development of the neuromorphic computer systems is the promising direction of microelectronics, which offers great prospersions in unstructured data processing and low power consumption. One of the possible ways of neuromorphic systems is integrated chip (IC) based on neuromorphic structures manufacturing, which are memory elements in the form of cells (neurons) interconnected by data buses (synapses). Such structures can change their electrical resistance between low resistance state (LRS) and high resistance state (HRS) under the influence of an external electric field (effect of resistive switching) and are the basis of non-volatile resistive memory (RRAM) [1-7]. Analysis of the publications showed that films based on binary metal oxides are promising for the manufacture of RRAM [8-10]. Hafnium oxide (HfO_2) is a perspective material, which shows forming-free effect of resistive switching with low power consumption, large HRS/LRS coefficient and high endurance [11-13]. However, for the manufacture of based on forming-free HfO_2 RRAM elements it is necessary to study the regimes of resistive switching in it. Thus, investigation of the effect of resistive switching in HfO_2 films is the aim of this work.

Hafnium oxide thin film was grown using pulsed laser deposition technique. $\text{Al}_2\text{O}_3/\text{TiN}$ as a wafer was used. Deposition performed under the following conditions: wafer temperature: 400°C , target-wafer distance: 50 mm, O_2 pressure: 1 mTorr, pulse energy: 300 mJ. AFM-image of hafnium oxide film surface was obtained using atomic-force microscope Solver P47 Pro (NT-MDT, Russia). Electric measurements were carried out using semiconductor characterization system Keithley 4200-SCS (Keithley, USA) with W probes. During experiment TiN layer was grounded. Current-voltage curves were obtained at -1 to $+1$ voltage sweep. Using the results obtained, resistance of HfO_2 dependence on number of cycle number (endurance test) was built. Curves analyzing was implemented using Origin 8.1 software.

Figure 1 shows experimental investigations of HfO_2 film morphology. It is shown that HfO_2 film surface has a granular structure with $0.25 \pm 0.08 \mu\text{m}$ grain size. The HfO_2 film thickness was measured by scanning of HfO_2/TiN boundary and was equaled $30.25 \pm 5.13 \text{ nm}$. Figure 2 shows electric measurements of TiN/ HfO_2 /W structure. Resistive switching from HRS to LRS (SET) was occurred at $0.62 \pm 0.15 \text{ V}$, and from LRS to HRS (RESET) at $-0.23 \pm 0.04 \text{ V}$. Endurance test shown that HRS was $75.83 \pm 20.61 \text{ k}\Omega$, LRS was $0.74 \pm 0.11 \text{ k}\Omega$ (Figure 1b). It was shown, that HRS/LRS ratio was about 101 at read voltage 0.15 V .

The results can be useful for based on HfO_2 thin films neuromorphic systems manufacturing.

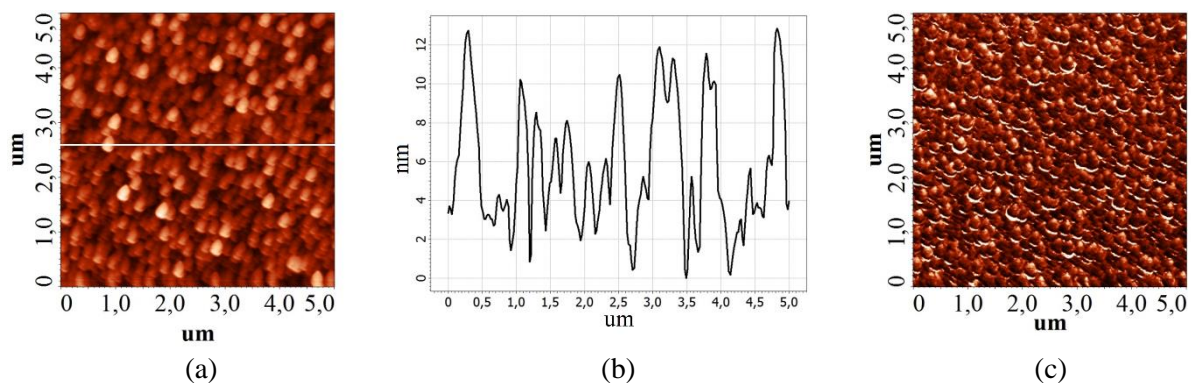


Figure 1. Investigation of nanocrystalline hafnium oxide film morphology:
(a) AFM-image; (b) cross-section profile along white line on (a); (c) phase.

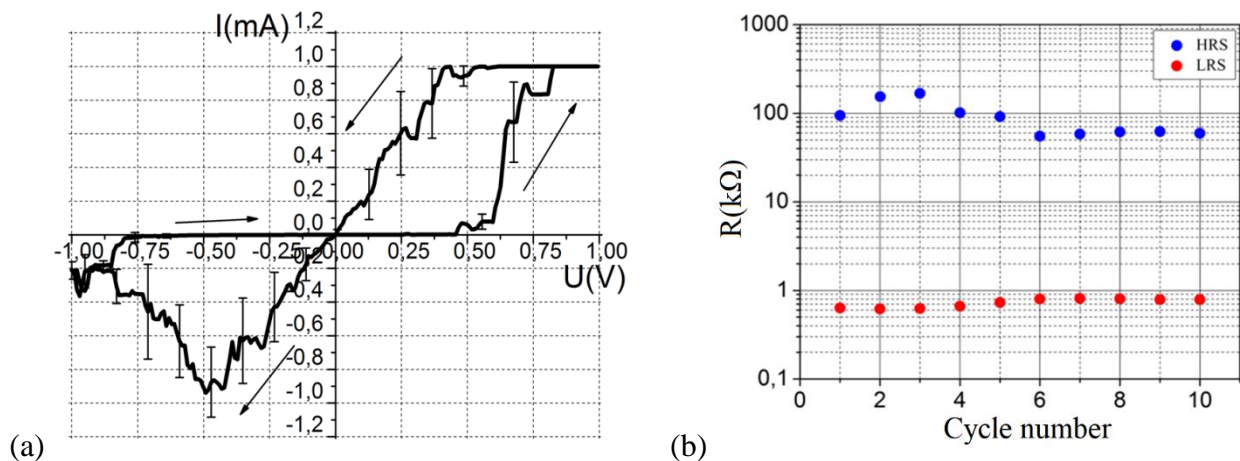


Figure 2. Investigation of effect of resistive switching in forming-free nanocrystalline hafnium oxide film: (a) current-voltage characteristic; (b) endurance test.

This work was supported by Grant of the President of the Russian Federation № MK-2721.2018.8 and RFBR (№ 18-37-00299 mol_a project). The results were obtained using the equipment of the Research and Education Center and Center for Collective Use "Nanotechnologies" of Southern Federal University.

1. D.S. Jeong, H. Schroeder, U. Breuer, R. Waser, *J. Appl. Phys.* **104**, 123716 (2008).
2. V.A. Smirnov, *Nanolithography by Local Anodic Oxidation of Thin Titanium Film*, in: *Piezoelectrics and Nanomaterials: Fundamentals, Developments and Applications*, ed. by I.A. Parinov, 85-103 (2015).
3. O.A. Ageev, N.I. Alyab'eva, B.G. Konoplev, V.V. Polyakov, V.A. Smirnov, *Semiconductors* **44**, 1703 (2010).
4. V.I. Avilov, O.A. Ageev, A.S. Kolomiitsev, B.G. Konoplev, V.A. Smirnov, *Semiconductors* **48**, 1757 (2014).
5. V.I. Avilov, N.V. Polupanov, R.V. Tominov, et al. *IOP Conf. Series: Mat. Sci. Eng.* **256**, 112001 (2017).
6. R.V. Tominov, V.A. Smirnov, V.I. Avilov, et al. *IOP Conf. Series: Mat. Sci. Eng.* **443**, 112036 (2018).
7. N.A. Shandyba, I.V. Panchenko, R.V. Tominov, et al. *J. Phys.: Conf. Series* **1124**, 8 (2018).
8. D.A. Khakhulin, Z. E. Vakulov, V.A. Smirnov, et al. *J. Phys.: Conf. Series* **917**, 9 (2017).
9. R.V. Tominov, E.G. Zamburg, D.A. Khakhulin, et al. *J. Phys.: Conf. Series* **917**, 3 (2017).
10. R.V. Tominov, V.V. Bespoludin, V.S. Klimin, et al. *IOP Conf. Series: Mat. Sci. Eng.* **256**, 012023 (2017).
11. E. Covi, S. Brivio, A. Serb, et al. *IEEE International Symposium on Circuits and Systems (ISCAS)* 393-396 (2016).
12. E. Covi, S. Brivio, M. Fanciulli, S. Spiga, *Microelectronic Engineering* **147**, 41 (2015).
13. B.J. Murdoch, D.G. McCulloch, R. Ganesan, et al. *Appl. Phys. Lett.* **108**, 143504 (2016).

Effect of reactive gas environment on domain structure and local switching of LiNbO₃ thin films deposited on Si(001) by radio-frequency magnetron sputtering

A.P. Turygin¹, A.S. Abramov¹, D.O. Alikin¹, V.A. Dybov², A.V. Kostyuchenko²,
M.P. Sumets³, V.M. Ievlev³, V.Ya. Shur¹

¹*School of Natural Sciences and Mathematics, Ural Federal University, 620000 Ekaterinburg, Russia
anton.turugin@urfu.ru*

²*Voronezh State Technical University, 394026 Voronezh, Russia*

³*Voronezh State University, 394000 Voronezh, Russia*

Lithium niobate LiNbO₃ (LN) is of great interest to engineers and scientists due to its excellent opto-acoustic, electro-optical, pyroelectric, and ferroelectric properties [1]. LN thin films are especially attractive for the applications in the integrated optoelectronics. Variety of devices, such as radiofrequency filters and resonators, surface acoustic wave generators, and opto-acoustic devices, are developed with LN-based heterostructures [2, 3].

In this contribution, we present a study of ferroelectric domain structure and electrical properties of the Si(001)-LN heterostructures formed by RF-magnetron sputtering (RFMS) at different sintering conditions. The 300 nm-thick LN films were fabricated by RFMS of the single-crystalline lithium niobate target in the Ar and Ar(60%)+O₂(40%) environments (0.15 Pa). Wafers of single-crystalline silicon of (001) orientation with n-type conductivity and about 4.5 Ω·cm resistivity were used as the substrates. During RFMS process, the substrates located at the distance of 5 cm over the target erosion zone were heated up to 550 °C. The sputtering was performed with 50 W magnetron power.

Films, fabricated in the pure Ar atmosphere (LN-Ar) with secondary LiNb₃O₈ phase demonstrate low piezoresponse and high conductivity, which makes local switching impossible. Contrary, using the 60% Ar + 40% O₂ gas environment (LN-Ar/O₂) leads to formation of the single-phase LN films with lower conductivity and high piezoelectric response, comparable with bulk LN. PFM measurements reveal the ferroelectric domain structure, which can be switched by electric field. The roughness of both films is almost the same, despite significant differences in morphology. Thermal annealing in air at 750 °C during 2 h led to significant decreasing of surface roughness in LN-Ar film. Contrary, LN-Ar/O₂ film topography and domain structure almost unchanged after annealing.

The obtained results can be used for development of the devices based on LN-film heterostructures.

The equipment of the Ural Center for Shared Use “Modern nanotechnology” UrFU was used. The work was supported by Government of the Russian Federation (Act 211, Agreement 02.A03.21.0006) and by Russian Foundation for Basic Research (Grant 18-32-00959).

1. V.Ya. Shur, *Nano- and microdomain engineering of lithium niobate and lithium tantalate for piezoelectric applications*. In *Advanced Piezoelectric Materials*, 2nd ed.; Uchino, K. (Woodhead Publishing: UK), 235–270 (2017).

2. A. Bartaszyte, S. Margueron, T. Baron, S. Oliveri, P. Boulet, *Adv. Mater. Int.* **4**, 1600998 (2017).

3. M. Sumets, *Lithium Niobate-Based Heterostructures* (IOP Publishing: Bristol, UK), 2018.

Dendrite microstructure of barium strontium titanate based glass-ceramics

A.P. Turygin¹, A.S. Abramov¹, D.O. Alikin¹, D.S. Chezganov¹, I.S. Baturin¹, X. Song²,
T. Zhang², Y. Zhang², K. Hu², Z. Zhao², V.Ya. Shur¹

¹*School of Natural Sciences and Mathematics, Ural Federal University, 620000, Ekaterinburg, Russia*
anton.turygin@urfu.ru

²*Beijing Key Laboratory of Fine Ceramics, State Key Laboratory of New Ceramics and Fine Processing, Institute of Nuclear and New Energy Technology, Tsinghua University, 100084, Beijing, P.R. China*

Glass-ceramics containing ferroelectric grains surrounded by a glass matrix are of significant interest for applications in power electronics due enhanced energy storage capabilities [1]. Glass-ceramics based on barium-strontium titanate (BST) is one of the most promising materials due to its high dielectric permittivity and breakdown strength [2, 3]. The macroscopic properties of BST ceramics are well studied, but the microstructure and morphology of the crystalline phase are insufficiently investigated.

In this work, the microstructure and surface morphology of glass ceramics based on $(\text{Ba}_{0.75}, \text{Sr}_{0.25})\text{TiO}_3$ doped by Mn with composition $25.95\text{BaO}-8.65\text{SrO}-(29.4-x)\text{TiO}_2-22\text{SiO}_2-12\text{Al}_2\text{O}_3-2\text{BaF}_2-x\text{MnO}_2$ ($x = 0-0.5$ mol.%), prepared from melted and quenched mixed powders. The as-quenched glass was annealed and subjected to controlled crystallization in air for 2 h in temperature range from 850 to 950 °C.

Microstructure study of the polished surface BST-Mn samples using scanning electron microscopy revealed dendritic clusters of crystalline phase with sizes from 3 to 6 μm in ceramic annealed at 850 °C with width of individual branch below 100 nm. The crystalline phase has a dense branching morphology formed by isotropic growth and tip splitting.

Value of fractal dimension obtained by box counting $D = 1.96$ sufficiently high than for DLA cluster ($D = 1.70$) [4]. In studied samples BST-Mn-850 °C with different amount of Mn were obtained close values of the fractal dimension.

The research was made possible by Russian Foundation for Basic Research (Grant 18-52-53032-NNSF-a). The equipment of the Ural Center for Shared Use “Modern Nanotechnology” Ural Federal University was used.

1. Q. Tan, P. Irwin, Y. Cao. *IEE Japan Transactions on Fundamentals and Materials* **126**, 1153 (2006).
2. Y. Zhang, J.J. Huang, T. Ma, X.R. Wang, C.S. Deng, X.M. Dai, *J. Am. Ceram. Soc.* **94**, 1805 (2011).
3. X. Wang, Y. Zhang, I. Baturin, T. Liang. *Mat. Res. Bull.* **48**, 3817 (2013).
4. E. Ben-Jacob, *Contemporary Physics* **34**, 247 (1993).

Investigation protein-based structures by SPM

S.G. Vasilev^{1,2}, D.S. Vasileva², S.A.Md. Tofail^{3,4}, V.Ya. Shur², A.L. Kholkin^{2,5}, E. O'Reilly¹

¹*Department of Chemical science, Bernal Institute, University of Limerick, Limerick, V94 T9PX, Ireland
semen.vasilev@ul.ie*

²*School of Natural Sciences and Mathematics, Ural Federal University, 620000 Ekaterinburg, Russia*

³*Department of Physics, University of Limerick, Limerick, V94 T9PX, Ireland*

⁴*Bernal Institute, University of Limerick, Limerick, V94 T9PX, Ireland*

⁵*Physics Department & CICECO – Aveiro Institute of Materials, University of Aveiro, 3810-193, Aveiro, Portugal*

Lectins are carbohydrate binding proteins capable of recognizing and binding glycan/sugar moieties present on a range of biomolecules including cells, viruses and proteins. Lectin functionalized biosensor (LFB) platforms present exciting opportunities as enhanced diagnostic tools enabling simple, rapid real time and label free detection, analysis and quantification of biological analytes with high sensitivity in small sample volumes. Use of high throughput LFB platforms could facilitate applications in biopharmaceutical product development or act as Process Analytical Technology (PAT) tools to enhance the fidelity and efficiency of production processes.

Diphenylalanine Phe-Phe is a model compound for investigating the self-assembly of organic molecules and formation of micro- and nanotubes and thin films [1]. Moreover, Phe-Phe microtubes have attracted significant research interest due to the excellent piezoelectric properties that these material exhibit [2] leading to their proposal for biocompatible piezoelectric elements for medical devices [3].

This work aims to produce biosensors by ink-jet printing of specific LFBs and Phe-Phe in a highly structured arrays to facilitate their use as a point of care diagnostic devices and screening arrays for biopharmaceutical production. Early results will present on the dielectric and piezoelectric properties of protein-based structures and surface morphology, protein orientation obtained post printing. Also, the sensitivity to the carbohydrate was tested.

The research was carried out using equipment of Ural Center for Shared Use “Modern Nanotechnologies” Ural Federal University with the financial support support by Career-FIT that has received funding from the European Union’s Horizon2020 research and innovation programme under the Marie Skłodowska-Curie grant agreement No. 713654

1. E. Gazit, *The Royal Society of Chemistry* **36**, 1263 (2007).
2. A. Kholkin et al., *ACS Nano* **4**, 610 (2010).
3. I. Coondoo et al., *Electrically Active Materials for Medical Devices* (Imperial College Press), 297-316 (2016)

Semi-contact AFM for surface characterisation in case of holographic PDADMAC films and functionalised paper

S. Vasilev^{1,2}, D. Vasileva², O. Luneva³, A. Vodyakshin³, D. Chezganov², V. Yuzhakov², V.Ya. Shur², E. Skorb³, A. Vinogradov³

¹Department of Chemical science, Bernal Institute, University of Limerick, Limerick, V94 T9PX, Ireland
semen.vasilev@ul.ie

²School of Natural Sciences and Mathematics, Ural Federal University, 620000 Ekaterinburg, Russia

³ITMO University, 191002 St. Petersburg, Russia

Atomic-Force Microscopy (AFM) is very popular method for investigation and surface characterisation of soft materials. This non-damaging method allows to investigate the sample surface in nanoscale with high resolution.

In this work, we investigated surface of holographic polyelectrolyte films and functionalised paper using atomic force microscope MFP 3D (Asylum, USA).

Free standing polyelectrolyte films exhibit reversible shape transitions, such as bending or stretching. They are very promising for such applications as artificial muscles, cantilevers, sensors and actuators. A freestanding film is not supported with substrate like silicon wafer or glass slide. In addition, polyelectrolyte films tend to be semiconductors. Nowadays, the development prospects and benefits of organic semiconductors from inorganic ones are noticeable. In this work the results of surface characterization in nanoscale of poly(sodium 4-styrenesulfonate)/poly(diallyldimethylammonium chloride) (PSS/PDADMAC) films will be presented (Fig. 1a).

We also studied the surface of the paper functionalised by the most promising methods that allow creating weak adhesion paper sheets. The surface of four sheets of paper with different coating was investigated. The coating agents were polystyrene, polyethylene vinyl acetate, polyvinyl alcohol and carboxymethyl cellulose. The smallest adhesion was found on the paper functionalised by polyethylene-vinyl acetate. It can be explained by peculiar morphology organized with nanoscale roughness (Fig. 1b).

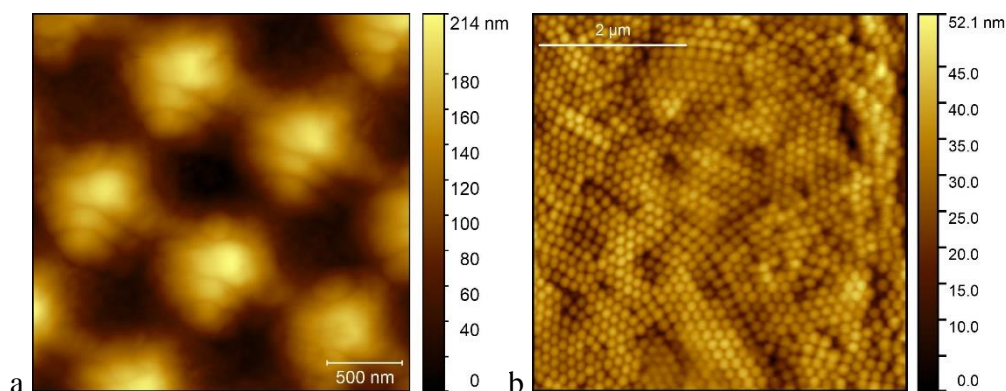


Figure 1. Semi-contact AFM topography images of: (a) holographic PDADMAC film, (b) paper functionalised by polyethylene-vinyl acetate.

The research was carried out using equipment of the Ural Center for Shared Use "Modern Nanotechnologies" Ural Federal University. A. Vinogradov acknowledges the scholarship of the President of the Russian Federation (SP-1158.2019.1): S. Vasilev acknowledges the mobility programs of the Institute of Natural Sciences and Mathematics for the Young scientists in the 2018 year.

Peculiarities of charged domain walls and local polarization reversal in β -glycine single crystals

D.S. Vasileva¹, S.G. Vasilev^{1,2}, T.D. Gubarev¹, A.L. Kholkin^{1,3}, V.Ya. Shur¹

¹*School of Natural Sciences and Mathematics, Ural Federal University, 620000 Ekaterinburg, Russia*

²*Department of Chemical science, Bernal Institute, University of Limerick, Limerick, V94 T9PX, Ireland
semen.vasilev@ul.ie*

³*Physics Department & CICECO – Aveiro Institute of Materials, University of Aveiro, 3810-193, Aveiro, Portugal*

Currently, inorganic ferroelectrics are widely used as efficient piezoelectrics, pyroelectrics, memory cells, and electrooptic modulators [1], but they are not biologically compatible and require encapsulation for contact with biological environment. In this context, piezoelectric or pyroelectric materials made from the building blocks used by nature may be used. Recent studies revealed that the softness of hydrogen bonds in some classes of biomolecular polar materials may be the origin of strong piezoelectric and pyroelectric properties at room temperature [2]. It was recently shown that the peculiar molecular packing in amino acids may give rise to the strong piezoelectric response, as exemplified by glycine [3]. Glycine is the simplest amino acid and is polymorphic in nature being ferroelectric in its polar β -phase [4]. Its strong piezoelectricity and ability to switch polarization under the action of electric field adds new functionality that can be further used in biomedical applications.

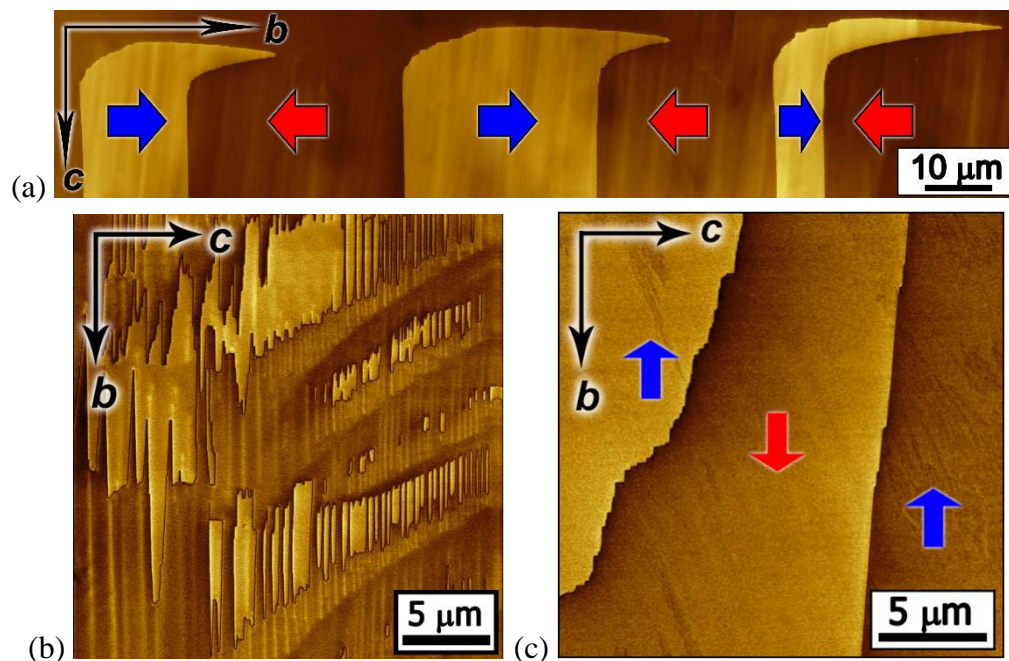


Figure 1. PFM images of the as-grown domain structure types: (a) striped domains with flat charged domain walls, (b) quasiperiodic ensembles of submicron width needle domains, (c) large area domains with irregular shaped domain walls.

The detail experimental study of the neutral and charged domain walls in β -glycine crystals was performed by PFM in the faceted single crystals with in-plane polar axis grown from aqueous solution via drop drying on Pt/SiO/Si substrate in air with controlled relative humidity. Three types of as-grown domain structure were found: (1) striped domains with flat charged domain walls, (2) quasiperiodic ensembles of submicron width needle domains, (3) large area domains with irregular shaped domain walls (Fig. 1). The formation of as-grown domain structure with flat charged domain walls and a smooth change in orientation near the crystal edges can be attributed to growth layers located perpendicular to the polar axis and representing a periodic change in the composition or concentration of impurities [5]. The local direction of spontaneous polarization is determined by the sign of composition or concentration gradient, so the domain walls are localized at the places where the gradient sign changes. The formation of two other types of the as-grown domain structure can be attributed to switching the polarization in the striped domains under the

action of the pyroelectric field E_{pyr} , which appears when the temperature of the crystal changes [6].

The two types of charged domain walls written by the probe differ in morphology. The tail-to-tail walls are straight and smooth, while the head-to-head walls are jagged and zigzag-shaped (Fig. 2). The roughness R_a of tail-to-tail walls was about 15 nm, whereas of head-to-head walls – about 200 nm. This fact also confirms the assumption that the charged tail-to-tail walls are conductive, which accelerates the bulk screening of the depolarization fields created by the bound charges, and low conductivity of the head-to-head walls leads to change in shape to reduce the density of bound charges.

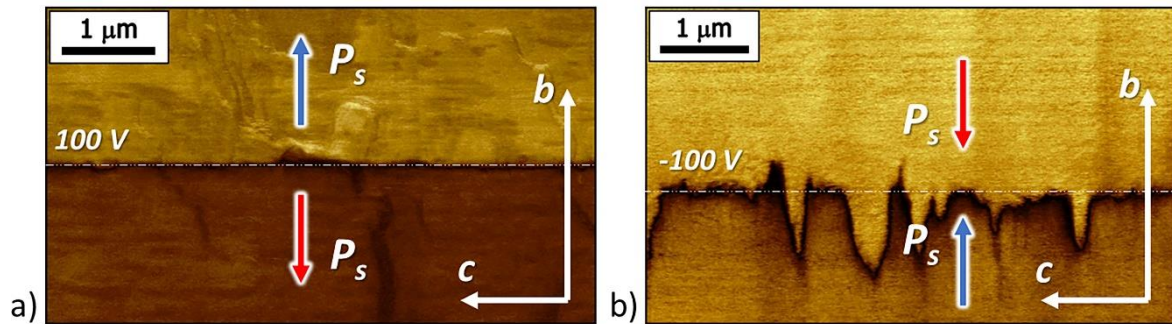


Figure 2. PFM images of the charged domain walls: (a) tail-to-tail and (b) head-to-head. Domain walls were written by local applying of (a) positive (100 V) and (b) negative (-100 V) voltage pulses with duration of 60 s at points located along the straight dotted line with period 1.5 μm .

PFM response at the charged domain walls is perpendicular to the polar axis thus indicating its complex structure. The shallow wells of 0.2-1 nm-depth and about 150 nm-width were revealed along the charged domain walls. The formation of these features was attributed to selective etching by water layer appeared at the crystal surface at the ambient conditions. In contrast the pits appeared at the neutral domain walls are due to deformation of the crystal lattice in the vicinity of the wall.

The research was carried out using equipment of Ural Center for Shared Use "Modern Nanotechnologies" Ural Federal University with the financial support by RFBR according to the research project № 18-32-00390.

1. M.E. Lines, A.M. Glass, *Principles and Applications of Ferroelectrics and Related Materials*, 1st ed., (Oxford: Clarendon Press), 559–604 (1977).
2. A.L. Kholkin, N. Amdursky, I. Bdikin, E. Gazit, G. Rosenman, *ACS Nano* **4**, 610 (2010).
3. S. Guerin, A. Stapleton, D. Chovan, R. Mouras, M. Gleeson, C. McKeown, M. Noor, C. Silien, F. Rhen, A. Kholkin, N. Liu, T. Soulimane, S. Tofail, D. Thompson, *Nat. Mater.* **17**, 180 (2018).
4. A. Heredia, V. Meunier, I.K. Bdikin, J. Gracio, N. Balke, S. Jesse, A. Tselev, P. Agarwal, B.G. Sumpter, S.V. Kalinin, A.L. Kholkin, *Adv. Funct. Mater.* **22**, 2996 (2012).
5. V.Ya. Shur, E.L. Rumyantsev, A.L. Subbotin, *Ferroelectrics* **140**, 305 (1993).
6. V.Ya. Shur, E.L. Rumyantsev, *J. Korean Phys. Soc.* **32**, 727 (1998).

Domain structure formation by electron beam irradiation in lithium niobate and lithium tantalate crystals at elevated temperatures

E.O. Vlasov, D.S. Chezganov, E.A. Pashnina, M.A. Chuvakova, A.A. Esin,
E.D. Greshnyakov, V.Ya. Shur

School of Natural Sciences and Mathematics, Ural Federal University, 62000, Ekaterinburg, Russia
evgeny.vlasov@urfu.ru

We experimentally studied the features of the domain formation by focused electron beam (e-beam) irradiation at the room and elevated temperatures in congruent lithium niobate (CLN) [1,2] and lithium tantalate (CLT) crystals covered by an artificial dielectric layer.

The studied samples represented the 0.5-mm-thick z -cut CLN and CLT plates. The domain structures have been produced by e-beam irradiation of z - polar surface covered by 2.5- μm -thick photoresist layer using scanning electron microscopes Auriga Crossbeam and Merlin (Carl Zeiss). The irradiation parameters and beam positioning were controlled by e-beam lithography system Elphy Multibeam (Raith). The irradiation at the temperatures up to 250 °C was carried out using thermal stage C1003 (Gatan Inc.). The static domain structures were visualized by scanning electron microscopy after selective chemical etching.

The dose and temperature dependencies of the geometrical parameters of the created domain structures were measured. It was shown that the domain area linearly increases with dose. The obtained linear behavior has been attributed to the external screening of the depolarization field by injected charges acting as current in the external circuit during the conventional switching. The domain size increase with temperature was attributed to a significant decrease of the threshold field.

The features of the isolated domain morphology at the room temperature were revealed. A distortion of the domain shape as a result of spontaneous backswitching caused by fast charge relaxation and bulk screening retardation after isolated dot irradiation was found. The effect was not observed for domains created by dot irradiation in arrays due to the additional contribution of the field of injected charges of the whole array to the local switching field. The formation of the domains as a result of linear and stripe irradiation was studied. It was shown that linear and stripe irradiation are similar in the studied width range due to electron scattering in the resist layer. The consideration of the irradiation with various doses as switching by field pulses of various amplitudes and durations allows distinguishing the consequent stages of domain formation. It was shown that the domains grew through the whole crystal wafer and appeared at the opposite polar surface as the quasi-regular chains of isolated domains. The dose increase led to the merging of chains into a continuous stripe domain. The domain shape at the $z+$ polar surface was explained by the effective screening conditions created by the electrode grounded during irradiation.

The revealed qualitative change in the domain morphology with temperature was explained by the highly non-equilibrium switching conditions due to the existence of the artificial dielectric layer and domination of the stochastic nucleation. It was shown that the effect of spontaneous backswitching decreased and then completely disappeared with temperature due to the acceleration of the bulk screening processes. The advantages of the domain formation by electron beam irradiation at elevated temperatures were demonstrated. The obtained results allow creation of the through periodically poled structures with periods from 10 to 40 μm in CLN [2].

The equipment of the Ural Center for Shared Use “Modern nanotechnology” Ural Federal University was used. The research was made possible by the Russian Science Foundation (Grant № 17-72-10152).

1. E.O. Vlasov, D.S. Chezganov, et al., *Scanning*, **2018**, 7809826 (2018).
2. D.S. Chezganov, E.O. Vlasov, et al., *Appl. Phys. Lett.* (in print).

Fabrication of a superhydrophobic and superoleophilic teflon surfaces using infrared laser irradiation

K.V. Volchetskaya, D.K. Kuznetsov, V.Ya. Shur

*School of Natural Sciences and Mathematics, Ural Federal University, 620000, Ekaterinburg, Russia
ks.volchetskaya@gmail.com*

Separating the mixture of water and oil by the superhydrophobic/superoleophilic materials has attracted increasing research and practical interests [1]. Various technologies have been developed to fabricate such materials. The femtosecond laser microfabrication becomes one of the wide used techniques because of its negligible heat-affected zone, precise ablation threshold and high spatial resolution [2].

In this work, the surface microstructuring of teflon (polytetrafluoroethylene, PTFE) substrates was done by IR laser ablation. The 2-mm-thick plates of PTFE were treated by means of CO₂ gas laser based on VLS-300/40 pulsed laser system, Universal Laser Systems, US. The obtained surface microstructures were imaged by means of scanning electron microscope Merlin, Carl Zeiss, Germany.

The treated surfaces showed both strong superhydrophobicity (low water adhesion) and ultrahigh superoleophobicity (high oil adhesion). Contact angles for water droplet on the surface before treatment was 101 degrees and on surface just after treatment with optimal parameters it increased up to 140 degrees. Analysis of the treated surfaces allowed to reveal the complicated surface structures containing several spatial scales.

The microstructured PTFE substrates were perforated by reach-through micro-holes with diameters ranged from 0.2 to 1 mm made by IR laser drilling. The produced perforated and treated plates demonstrated highly efficient oil/water separation due to their superhydrophobicity and superoleophilicity. The proposed technique exhibits the strong potential for practical application.

The equipment of the Ural Center for Shared Use “Modern nanotechnology” UrFU was used. The work was supported by Government of the Russian Federation (Act 211, Agreement 02.A03.21.0006), by financial support within the State Task from the Ministry of Science and Higher Education of the Russian Federation (contracts 3.7046.2017/7.8 and 3.4993.2017/6.7).

1. J. Yong et al., *Phys. Chem. Chem. Phys.*, **20**, 25140 (2018).
2. J. Yong et al., *Adv. Mater. Interfaces*, **5**, 1701370 (2018).

Cubic to cubic phase transition in $(\text{NH}_4)_3\text{SnF}_7$ ferroelastic crystal – Raman scattering study

A.N. Vtyurin^{1,2}, Y.V. Gerasimova^{1,2}, A.S. Krylov¹, N.M. Laptash³, S.N. Krylova¹

¹*Kirensky Institute of Physics, Federal Research Center KSC SB RAS, 660036, Krasnoyarsk, Russia*

²*Institute of Engineering Physics and Radio Electronics, Siberian Federal University, 660079, Krasnoyarsk, Russia*

³*Institute of Chemistry, Far Eastern Branch of RAS, 690022, Vladivostok, Russia
jul@iph.krasn.ru*

Binary salt of $(\text{NH}_4)_2\text{SnF}_6 \cdot \text{NH}_4\text{F}$ has been synthesized and crystallized by a special procedure of solvent crystallization providing high quality single crystal samples used for optical vibrational spectroscopy.

Detailed Raman scattering and infrared absorption in a wide temperature range confirmed phase transition in $(\text{NH}_4)_2\text{SnF}_6 \cdot \text{NH}_4\text{F}$ at 360 K. Earlier this phase transition was found to be between two cubic phases ($Pa-3 \leftrightarrow Pm-3m$) [1].

Wide band was found in the Raman spectra at 600 cm^{-1} , that corresponds to the full symmetry stretching mode $\nu_1(\text{A}_{1g})$ of octahedric SnF_6 groups. Under cooling it splits into a doublet at 586 cm^{-1} of the $(\text{Sn}2)\text{F}_6$ group and at 580 cm^{-1} – of the $(\text{Sn}1)\text{F}_6$ one. Internal bending vibrations $\nu_2(\text{E}_g)$ of SnF_6 groups were found at 470 cm^{-1} . Strong peak near 246 cm^{-1} is formed by two coinciding bending $\nu_5(\text{F}_{2g})$ modes of $(\text{Sn}2)\text{F}_6$ и $(\text{Sn}1)\text{F}_6$ octahedrons. Rotating modes of SnF_6 groups are found at 67 cm^{-1} and 87 cm^{-1} . Cooling down to 8 K results in slight displacements of these lines and activates several new ones. In particular new lines appear at 160 cm^{-1} and 25 cm^{-1} below 200 K but their temperature dependences do not look like of a soft mode but rather like being induced some relaxations typical for ordering processes.

All Raman active internal bending modes $\nu_2(\text{E})$ and $\nu_4(\text{F}_2)$ of NH_4 ions are observed in the $Pa-3$ phase though being rather wide, and cooling down to 8 K activates up to 10 peaks at least. Spectral band of NH_4 internal stretching at $3000-3350 \text{ cm}^{-1}$ is rather asymmetrical and may be deconvolved into four lines at least; under cooling down to 8 K it splits into six separated peaks.

All observed transformations of the Raman spectra are quite typical for ordering processes both SnF_6 and NH_4 groups below transition from the $Pm-3m$ phase to the $Pa-3$ one.

Besides these spectral transformations formation of some thin films was observed at the sample surface that did not produce traceable Raman signal and did not look like destruction of the binary salt in the bulk.

This work was supported by Russian Foundation for Basic Research (Grant N 17-02-00920).

1. I.N. Flerov, M.S. Molokeev, N.M. Laptash, A.A. Udovenko, E.I. Pogoreltsev, S.V. Mel'nikova, S.V. Misyul, *J. Fluor. Chem.* **178**, 86 (2015).

Light polarization and intensity behavior in aperture cantilevers with carbon tip created by focused ion beam

T.V. Mikhailova¹, Yu.E. Vysokikh^{2,3}, S.Yu. Krasnoborodko^{2,3}, A.S. Kolomiitsev⁴,
A.A. Fedotov⁴

¹V.I. Vernadsky Crimean Federal University, Simferopol, 295007, Russia
taciamic@yandex.ru

²Scientific and Technological Center of Unique Instrumentation of the RAS, Moscow, 117342, Russia
visokih@yandex.ru

³MTEON Ltd, Moscow, Zelenograd, 124617, Russia

⁴Southern Federal University, Rostov-on-Don, 344006, Russia
askolomiysev@sfn.ru

Nowadays atomic force microscopy (AFM) allows to investigate not only morphology and physical properties of the samples but also optical dates could be collected by the combination of AFM and near-field scanning optical microscopy (NSOM) methods. This combination allows one to research optical properties of the sample and morphology of same area simultaneously. One of modern technique of such combination is polarization near-field optical microscopy which allows to perform polarization depended measurements with high spatial resolution [1].

There are a number of probes which was created for NSOM. Historically optical fiber probes were used for this propose but it has the limitations of spatial resolution, light throughput and reproducibility [2]. Silicon cantilevers is one of modern type of the probes for NSOM methods. Authors propose to use focused ion beam technology to get carbon hollow pyramid tip on silicon cantilever for creation high reproducible aperture cantilevers with high light throughput and high spatial resolution [3]. In this paper authors shows light polarization and intensity behavior in aperture cantilevers with carbon tip created by focused ion beam.

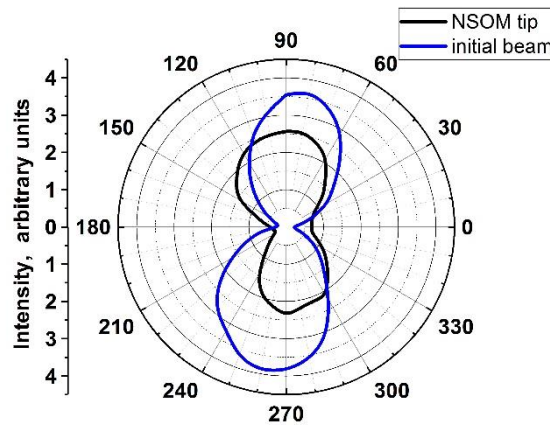


Figure 1. Intensity light dependence on aperture size with different angles of polarizer position.

Aperture cantilevers with different geometry and aperture size were created by FIB. Light polarization and intensity were measured as a function of aperture size and geometry.

1. Y.E. Vysokikh, A.V. Shelaev, A.R. Prokopov, V.I. Shevyakov, S.Y. Krasnoborodko, *J. Phys.: Conf. Series* **741**, 12190 (2016).
2. J.A. Veerman, A.M. Otter, L. Kuipers, N.F. Van Hulst, *Appl. Phys. Lett.* **72**, 3115, (1998).
3. A.S. Kolomiitsev, N.A. Shandyba, I.V. Panchenko, S.A. Lisitsyn, *IOP Conf. Series: Mat. Sci. Eng.* **443**, 012015, (2018).

The effect of a strong electric field on the dielectric properties of LiNbO_3

A.V. Yatsenko¹, S. M. Kostritskii²

¹Crimean Federal University, Simferopol, Russia
yatsenkoav@cfuv.ru

²RPC Optolink Ltd, Zelenograd, Moscow, Russia

Lithium niobate (LN) LiNbO_3 crystals are one of the most popular ferroelectric materials. During the operation of devices based on LN, the stability of their parameters under the influence of external factors is important. Due to the strong pyroelectric properties of LN crystals, its temperature change is accompanied by the appearance of an additional electric field both inside and outside the crystal, which significantly affects the performance properties of the product [1, 2]. Consequently, the question of the possible influence of a strong electric field on the material parameters of LN that are important for the operation of these devices [3] is very fundamental. However, there is no information about direct experiments of studying the effect of a strong electric field on the static dielectric properties of LN crystals, so the state of the problem can only be judged from indirect data that are quite contradictory [4-7]. Therefore, our main goal was to study the influence of a strong quasistatic electric field on the dielectric properties of nominally pure LN.

For experiments, a chip for an optical modulator manufacturing was used. It is a thin (1.00 mm) plate of a non-polar x -cut of LN (congruent composition) on the surface of which 5 main electrodes are formed. The width of the chip is 3.45 mm, and the distance from the electrodes to the edges of the chip is 0.80 mm. gaps between the electrodes are 14 μm . Additional electrodes from an indium-gallium eutectic were deposited on the polar faces of the chip. They are designed to control the state of the crystal in the process of making measurements. The investigated chip is shielded and located inside the heating chamber, which allows changing its temperature. The block diagram of the experimental setup is shown in Figure 1.

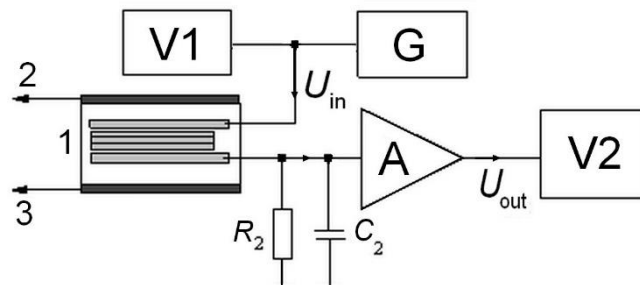


Figure 1. Block diagram of the experimental setup. (1) – chip under investigation; (2) and (3) – additional electrodes on polar surfaces; V1 and V2 – digital ac voltmeters; G – low frequency generator; A – digitally gain programmable ac amplifier.

The chip under investigation can be presented as connected in parallel interelectrode capacitance C_1 and active resistance R_1 . Because in our case $R_1 \gg R_2$, the magnitude of the transmission coefficient of the circuit, containing the investigated chip and the measuring amplifier with K_0 gain at angular frequency ω has the following form:

$$|K(\omega)| = \frac{U_{out}}{U_{in}} = \frac{K_0}{\sqrt{1 + R_2^2 C_1^2 \omega^2}}$$

where R_2 , C_2 and K_0 are known parameters. Measuring of $|K(\omega)|$ allows to calculate C_1 .

Direct experiments to study the effect of the electric field on the dielectric properties of LN were performed as follows. Additional electrodes were connected to a device that forms a slowly varying bipolar voltage, so that the maximum value of the potential difference between the chip polar faces was 4 kV. This is equivalent to electric field of $E_z = 11.6 \text{ kV/cm}$ along the polar axis of the crystal inside a chip of the same size, but without electrodes on a non-polar surface. A further

increasing of voltage could lead to electrical breakdown between additional and measuring electrodes despite the fact that the surface of the chip was degreased and dehydrated and a silica gel was present in a chamber. The measurements were carried out at frequencies of 0.1, 1.0 and 10 kHz at a temperature $T \cong 297$ K. Any changes in the capacitance C_1 in the process of increasing the potential difference between the additional electrodes within the accuracy of the experiment was not observed. Changing of polarity of the applied voltage also did not affect the results.

Besides, the detailed study of the dielectric properties dependence on temperature was carried out for the modulator chip. Figure 2 shows the experimental $C_1(T)$ dependences, which were obtained with and without a short circuit of additional electrodes under the same heating algorithm (maximum heating rate 1.8 K/min). Note, that no marked influence of pyroelectric field E_p on C_1 was observed, while the maximum value of E_p is estimated to be $(15 \div 22)$ kV/cm.

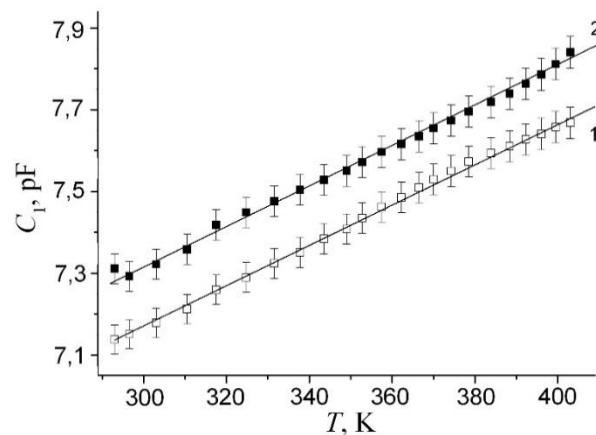


Figure 2. Temperature dependence of the interelectrode capacitance C_1 obtained at a frequency $f = 10$ kHz for: (1) polar faces of the chip are not mutually connected; (2) polar faces of the chip are short circuit.

It can be seen that both dependences do not have obvious anomalies and, within the limits of error, are well approximated by a first-degree polynomial. A slight shift in the dependences relative to each other is caused by the partial restructuring of an alternating electric field in the near-electrode region when additional electrodes are connected to each other. The same experiments were performed at frequencies of 0.1, 1.0, and 100 kHz, and no anomalies were observed similar to experiments at $f = 10$ kHz (Fig. 2). Thus, these results represent the first data on the temperature dependence of capacitance (dielectric permittivity) in the complex waveguide-device structure of LiNbO_3 modulator chip. Note, that the modulator chip studied is fundamentally different from the bulk-optics LiNbO_3 devices. There is inhomogeneity caused by the presence of waveguide within a certain part of the inter-electrode gap. In our chip, the ratio of the width of the gap and channel is 2.4. This inhomogeneity appears when narrow channel waveguides are formed through proton exchange reaction, as the capacitance and resistance within the proton-exchanged areas are different from ones in a rest crystal.

In conclusion, our results indicate that the quasi-static electric fields up to 15 kV/cm directed along or antiparallel to polar axis of LN crystal does not affect its dielectric properties in the low-frequency region within the measurement error.

1. P.F. Bordui, D.H. Jundt, E.M. Standifer et al, *J. Appl. Phys.* **85**, 3766 (1999).
2. E.J. Wooten, K.M. Kissa, A. Yi-Yan, et al. *IEEE J. Sel. Top. Quantum Electron.* **6**, 69 (2000).
3. J. Kushibiki, I. Takanaga, M. Arakawa, T. Sannomiya, *IEEE Trans. Ultrason. Ferroelectr. Freq. Control* **46**, 1315 (1999).
4. I. Fujimoto, *Acta Cryst. A* **38**, 337 (1982).
5. P.M. An, N.H. Thuong, A.I. Burkhanov, S.V. Mednikov, *Bull. RAS Physics.* **77**, 1056 (2013).
6. W. Yue, J. Yi-Jian, *Opt. Mater.* **23**, 403 (2003).
7. G.A. Samara, *Ferroelectrics.* **73**, 145 (1987).

Elastic and piezoelectric properties of diphenylalanine microtubes with different filling of nanochannels

V. Yuzhakov¹, A. Nuraeva¹, P. Zelenovskiy^{1,2}, D. Chezganov¹, A. Kholkin^{1,2}, V. Shur¹

¹*School of Natural Sciences and Mathematics, Ural Federal University, 620000, Ekaterinburg, Russia*
vladimir.yuzhakoff@mail.ru

²*Department of Physics & CICECO – Aveiro Institute of Materials, University of Aveiro, 3810-193, Aveiro, Portugal*

Self-assembled micro- and nanotubes of diphenylalanine (C₁₈H₂₀N₂O₃, FF) represent advanced functional biomaterial for developing new medical equipment [1], such as laboratory-on-chip, due to its outstanding piezoelectric [2] and mechanical [3] properties. After the self-assembly in aqueous solution water molecules remain inside the nanochannels and stabilize its structure [4]. However, the possibility of water substitution in nanochannels by other molecules and its effect on physical properties of FF microtubes still was not studied.

In this work we investigated the effect of nanochannels filling on piezoelectric and elastic properties of FF microtubes. The studied microtubes were grown from a solution of FF-monomer (Bachem AG, Switzerland) in mixture of 1,1,1,3,3,3-hexafluoro-2-propanol with water and then were dried at 80 °C for different times in a muffle furnace to empty the nanochannels. The consequent filling of nanochannels by water or ethanol molecules was carried out by keeping the empty microtubes in water or ethanol vapor for two weeks. Average concentration of water molecules in the microtubes was detected by confocal Raman microscope Alpha 300AR (WITEC GmbH, Germany) according to the earlier described procedure [5]. Young's modulus and micro-hardness were measured locally using NanoScan-4D scanning nano-hardness tester (FSBI TISNCM, Russia). The piezoelectric coefficient was measured using a scanning probe microscope MFP-3D (Asylum, USA).

As-grown FF microtubes demonstrate a bimodal distribution of the Young modulus values with characteristic values of 10 and 25 GPa and piezoelectric response of about 35 pm/V. Analysis of Raman spectra showed that the Young's modulus of 10 GPa corresponds to microtubes with 12 water molecules in the structural unit. Drying of microtubes leads to decrease of Young's modulus and piezoelectric response. Restoring the microtubes in water or ethanol vapor leads to increasing of Young's modulus values back to bimodal distribution with characteristic values that are close to values of initial (as-grown) tubes. Thus, water or ethanol molecules can enter the nanochannels in FF microtubes and allow recovering their elastic properties. However piezoelectric coefficient d_{15} of the refilled microtubes does not restored. The origin of this contradiction is not clear yet.

The research was carried out using the equipment of Ural Center for Shared Use "Modern Nanotechnologies", Ural Federal University, under financial support by Russian Science Foundation (grant № 18-72-00052).

1. A. Kholkin, N. Amdursky et al., *ACS Nano*, **4**, 610 (2010).
2. S. Vasilev et al., *J. Phys. Chem. Solids*, **93**, 68 (2016).
3. I. Azuri, L. Adler-Abramovich et al., *J. Am. Chem. Soc.*, **136**, 963 (2014).
4. T. Andrade-Filho, T. Martins et al., *Theor. Chem. Acc.*, **135**, 185 (2016).
5. P. Zelenovskiy et al., *J. Raman Spectrosc.*, **48**, 1401 (2017).

Confocal Raman study of electric fields in lithium niobate single crystals

P. Zelenovskiy, D. Alikin, V. Ya. Shur

*School of Natural Sciences and Mathematics, Ural Federal University, 620000, Ekaterinburg, Russia
zelenovskiy@urfu.ru*

The influence of homogeneous electric fields of different orientations on the Raman spectrum of lithium niobate single crystal is studied. Obtained results were applied to determine the values of residual electric fields in the vicinity of neutral and charged domain walls.

External homogeneous electric field was applied to metal electrodes deposited at different cross-sections of lithium niobate single crystals. The applied voltage ranged from -7 to +7 kV. Raman spectra were measured using confocal Raman microscope Alpha300AR (WITec GmbH, Germany) equipped by solid-state laser with wavelength 488 nm. Spectral grating with 1800 gr/mm provided spectral resolution about 1.2 cm^{-1} . Raman spectra were studied in different polarization geometries.

Field dependence of parameters of spectral lines $E(\text{TO}_1)$, $E(\text{TO}_8)$, and $A_1(\text{LO}_4)$ was analyzed. It was found that the position of studied spectral lines was linearly dependent on the applied field and the corresponding coupling coefficients were determined. For Z-cut lithium niobate the coupling coefficients were close to those published by G. Stone et al. [1].

It was demonstrated earlier that the position of $E(\text{TO}_1)$ and $E(\text{TO}_8)$ spectral lines changed in the vicinity of the neutral and charged domain walls [2]. This effect was attributed to the action of residual electric fields existed near the walls [2, 3]. The coupling coefficients obtained in this work allowed us to quantitatively determine the values of residual electric fields.

The bulk conductivity increase with the sample temperature leads to effective electric field screening. This, in turn, leads to disappearance of the spectral lines shift.

The research was made possible by Russian Science Foundation (Grant 19-72-10076). The equipment of the Ural Center for Shared Use “Modern nanotechnology” UrFU was used.

1. Stone G., Knorr B., Gopalan V., Dierolf V., *Phys. Rev. B*, **84**, 134303 (2011).
2. Zelenovskiy P., Shur V. Ya., Kuznetsov D., et al., *Ferroelectrics*, **398**, 34 (2010).
3. Zelenovskiy P.S., Fontana M.D., Shur V. Ya., et al., *Appl. Phys. A*, **99**, 741 (2010).

Cation ordering and phase structural transition of Eu³⁺-doped BMN ceramics

J. Shen, L.N. Hu, J. Zhou, W. Chen*

State Key Laboratory of Advanced Technology for Materials Synthesis and Processing, School of Materials Science and Engineering, Wuhan University of Technology, Wuhan 430070, P. R. China

*chenw@whut.edu.cn

Ba-based Ba(B'_{1/3}B''_{2/3})O₃-type complex perovskites ceramics have got widespread attention owing to their excellent dielectric properties in microwave communication systems. As is known, the sequencing of B-site and octahedral distortion play an important role in dielectric properties like Ba(Mg_{1/3}Nb_{2/3})O₃(BMN) and Ba(Mg_{1/3}Ta_{2/3})O₃(BMT) based ceramics [1]. Hence, it is meaningful to explore how structure changes in these materials. The photoluminescence properties of rare-earth (RE) ions is strongly dependent on the crystal symmetry of the sites occupied [2], which promises an alternative way to explore the structure characters in dielectric materials, such as cation ordering and octahedral distortion, by introducing a small of quantity of rare-earth (RE) ions and characterizing their luminescence properties. This work aims to investigate how the structure changes in Ba(Mg_{1/3}Nb_{2/3})O₃(BMN) with different sintering temperature by utilizing Eu³⁺ ions as a probe.

The Ba_{0.97}(Mg_{1/3}Nb_{2/3})O₃:3%Eu³⁺(BMN:3%Eu³⁺) ceramic powders were prepared by conventional solid-state reactions with different temperature. In this work, the phase structure, cation ordering and photoluminescence properties of Ba_{0.97}(Mg_{1/3}Nb_{2/3})O₃:3%Eu³⁺(BMN:3%Eu³⁺) ceramics were characterized. The XRD Rietveld refinement, Raman spectra and photoluminescence of Eu³⁺ ions demonstrated that the prepared ceramic phosphors undergo a cubic-hexagonal phase transformation with the sintering temperature increasing(1350 ~ 1500 °C), leading to cation ordering change of B sites and NbO₆ octahedral distortion in BMN. Photoluminescence properties of Eu³⁺ ions were studied based on Judd-Ofelt and crystal symmetry theories. There are two major emission peak at 598nm and 615nm due to transition magnetic dipole transition of ⁵D₀-⁷F₁ and electric dipole transition of ⁵D₀-⁷F₂, respectively. By calculating the asymmetry ratio (*R*) that is intensity ratio of transitions ⁵D₀-⁷F₂ to ⁵D₀-⁷F₁, $R=I_2(^5D_0-^7F_2)/I_1(^5D_0-^7F_1)$, the symmetry of the crystal field environment around Eu³⁺ ion can be detected. These results illustrated that relationship between luminescence performance and structure, providing theoretical support for a small quantity of Eu³⁺ ions can be served as a structural probe for these dielectric material.

1. D.K. Patel, B. Vishwanadh, V. Sudarsan, et al., *J. Am. Ceram. Soc.* **96** (2013).
2. X.M. Chen, T.L. Sun, et al., *AIP Advances.* **5**, 017106 (2015).

Bioinspired elastic piezoelectric composites for high-performance mechanical energy harvesting

Q.Y. Zhu, H. Sun, Y. Zhang

School of Materials Science and Engineering, Wuhan University of Technology, 430070, Wuhan, China
cglamri@whut.edu.cn

We report the sea sponge-inspired design and preparation of piezoelectric composite generators (PCGs) based on a three-dimensional electroceramic skeleton. Figure 1 shows the detailed fabrication process and the microstructure of obtained three-dimensional electroceramic skeleton. The remarkable improvements in the piezopotential of the bioinspired structure have been theoretically analyzed using numerical simulations based on a phase-field simulation, as illustrated by Figure 2. The open-circuit voltage, short-circuit current density and instantaneous power density of the bioinspired PCG reach up to ~ 25 V, ~ 550 nA/cm² and ~ 2.6 mW/cm², respectively, corresponding to about 16 times higher power than that of conventional particle based piezoelectric polymer composites. Moreover, the bioinspired PCG displays 30 times higher strain–voltage efficiency under stretching than the state-of-the-art performance of the flexible piezoelectric energy harvesters reported so far.

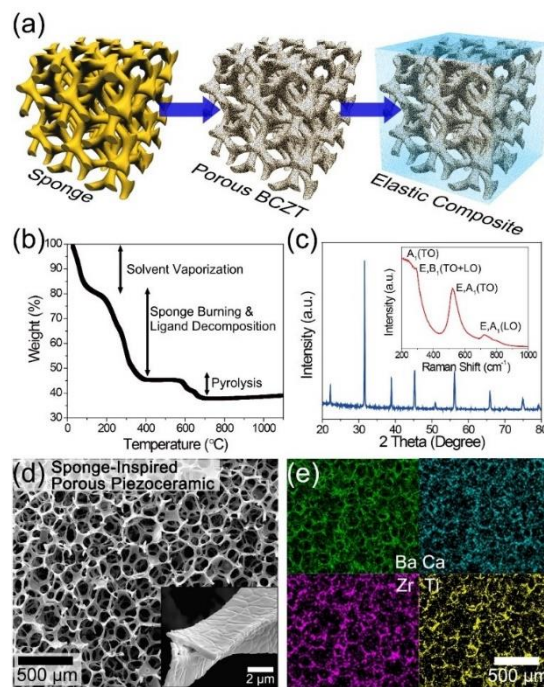


Figure 1. (a) Schematic of the fabrication process of the sea sponge-inspired 3D piezoelectric composite. (b) TGA curve during the thermal annealing and calcination. (c) XRD pattern and Raman spectrum (inset) of the bioinspired BCZT porous structure. (d) SEM image of BCZT porous structure. Inset: a magnified SEM image presenting the cross section of porous BCZT branch. (e) EDS mapping of BCZT porous structure.

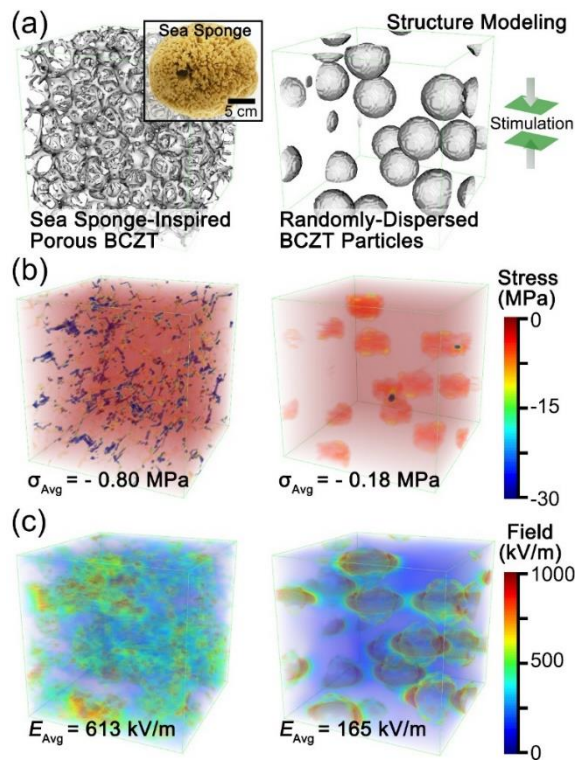


Figure 2. (a) Structure modelling of a sea sponge-inspired BCZT composite and a randomly-dispersed BCZT particle-based composite by using the phase-field simulation with the Fourier spectral iterative perturbation method. (b) Computation results of the formed stress within the composites when a compressive strain of 12% is applied. (c) Computation results of the piezopotential-based electrical field generated within the composites when 12% strain is applied.

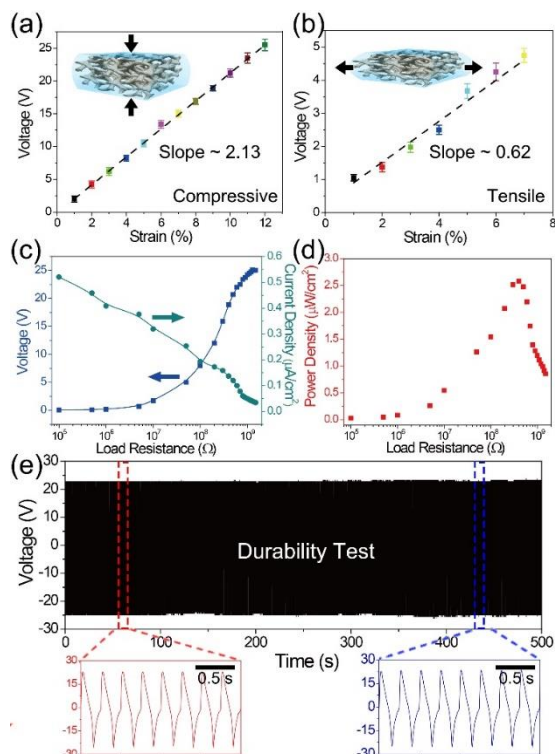


Figure 3. Strain-generated voltage of the elastic PCG according to (a) compressive and (b) tensile strain. (c) Output voltage, current density, and (d) instantaneous power density produced by the PCG according to circuitual load resistors. (e) The voltage signals generated from the PCG in the cyclic test.

High-aspect ratio probes with selected geometry for advanced MFM measurements

M.V. Zhukov¹, K.I. Belousov², A.O. Golubok¹

¹Institute for Analytical Instrumentation RAS, 198095, St. Petersburg, Russia
cloudjyk@yandex.ru

²St. Petersburg Academic University, 194021, St. Petersburg, Russia

In present-day recording technologies, magnetic force microscopy (MFM) is of particular interest, since it can be used to perform high-precision magnetic mapping and diagnostics of nanoelectronic elements [1], in particular, reading and writing of magnetic information with single domains accuracy [2,3]. It should be noted the importance of probes features in MFM technique, since geometric parameters and composition of the probe could influence on the sensitivity, resolution and contrast of the resulting MFM images.

The main aim of the work was to identify the optimal parameters of high-aspect ratio magnetic probes based on nanowhisker structures to improve the quality of the MFM measurements.

We considered two types of probes: standard pyramidal probe and high-aspect ratio nanowhisker (NW) probe covered by magnetic film. The simulation of the high-aspect probes was carried out in COMSOL Multiphysics by the finite element method. The Gauss law was used to the magnetic field to determine the distribution of the magnetic field. The equation (1) was used for the magnetized areas:

$$\mathbf{B} = \mu_0 (\mathbf{H} + \mathbf{M}), \quad (1)$$

where μ_0 – magnetic constant, H – vector of the magnetic field, M – vector of the material magnetization. The magnetic domain size was simulated as 30 nm, magnetic coating thickness of the probes 20-50 nm, NW width 25-75 nm, NW height 250-750 nm, radius of tip curvature 10 nm.

Simulation showed that NW probe has about twice larger force gradient values compared to the standard probe with the same thicknesses of magnetic material. Standard probe parameters were coincided with NSG01 tips (NT-MDT, Russia); NW tip parameters were: height – 500 nm, diameter without magnetic coating – 50 nm, magnetic material – Co, material of NW – Pt/C, magnetic coating for tips varied 20-50 nm.

The experimental results coincide with simulations. A hard drive disk with magnetic pits was measured by standard probes and NW probes, fabricated by focused electron beam technique at the top of standard probes with presence of gas-precursor.

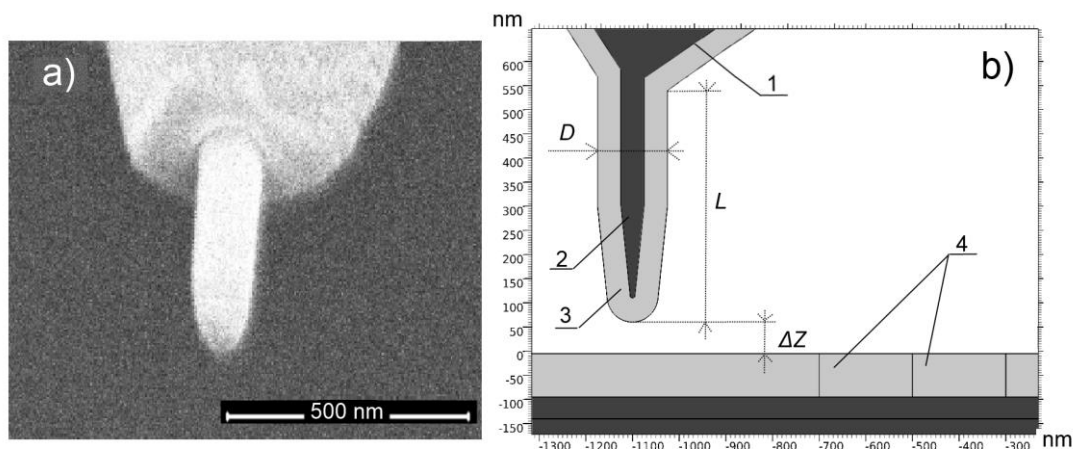


Figure 1. SEM image of the NW probe (a) and its model (b): 1 – the top of the Si pyramid, 2 – NW, 3 – the magnetic coating, 4 – magnetic domains, D – NW diameter (150 ± 30 nm), L – NW height (500 ± 50 nm), ΔZ – distance from the probe to the substrate (10 ± 0.1 nm).

In addition, simulation of the alteration of magnetic coating thickness, magnetic material and geometry of the NW probe was carried out. It was found that NW thickness (magnetic coating –

constant) increase and NW length decrease leads to force gradient reduction. As expected, increasing the thickness of the magnetic coating leads to force gradient increase. The lowest gradient values were obtained using Ni coating (5.8 $\mu\text{N/m}$ for NW), the best results were found for Co (31.4 $\mu\text{N/m}$) and especially for CoFe coating (239 $\mu\text{N/m}$). A gradual gradient increase was observed by increasing the angle of inclination of the NW relative to the surface normal.

Thus, the optimal parameters of high-aspect magnetic probes were found to improve the quality of the MFM measurements. It was found that NW probe has a larger magnetic force gradient compared to the standard probe with the same thicknesses of magnetic material, which should lead to an improvement of the MFM image quality in the phase contrast mode.

The authors appreciate financial support by Ministry of Education and Science of the Russian Federation, Russia, State Project № 075-00780-19-00, Subject № 0074-2019-0007.

1. E. Pinilla-Cienfuegos, S. Kumar, S. Mañas-Valero, et al. *Part. Part. Syst. Charact.* **32**, 693 (2015).
2. I. Lee, J. Kim, Y. Obukhov, et al, *Appl. Phys. Lett.* **99**, 162514 (2011).
3. N. Amos, A. Lavrenov, R. Fernandez, et al, *J. Appl. Phys.* **105**, 07D526 (2009).

Photocatalytic water purification: role of crystallinity, defects, surface area and hydroxyl ion concentration

M. Khanuja

*Centre for Nanoscience and Nanotechnology, Jamia Millia Islamia, New Delhi- 110025, India
manikakhanuja@gmail.com*

The presence of large number of industrial contaminants such as heavy metal ions Cr(VI), dyes and organic chemicals in water causing lung cancer, intestine cancer, kidney damage, asthma etc. [1-3]. Photocatalysis has been proved to be a capable method to remove water contaminants due to low cost, low energy consumption and regenerable solution [4-7]. Transition metal dichalcogenides (MoS₂, MoSe₂, WS₂, WSe₂) have enticed great attention due to special layered stable structure, high carrier mobility, direct bandgap, large surface area and controllable interfaces [8-10]. There are various methods to synthesize 2D nanostructures such as solvothermal, molecular beam epitaxy, electrochemical deposition, chemical vapour deposition etc. [13-16]. These methods are complicated or require high temperatures to operate. Hydrothermal is a simple, environment friendly and effective method to synthesize TMD's nanostructures and provides controlled growth rate, nucleation uniformity and it is suitable for large scale production. Photocatalytic degradation takes place at the interface between photocatalyst surface and pollutant, therefore it is expected that the photocatalytic activity is correlated with crystalline planes and surface structures. In this study, nanosheets and nanourchins of MoSe₂ were hydrothermally synthesized by varying the pH and comparative photocatalytic study on organic dyes (MB, MO) and heavy metal Cr(VI) were performed. Enhanced photocatalytic efficiency of nanosheets over nanourchins is correlated with crystallinity, enhanced surface area and hydroxyl ion concentration. Adsorption studies, role of reactive species, HPLC and regenerable properties of catalysts were also studied.

Study of structure of a surface of a break of ceramics on the basis of SiC-AlN

G.D. Kardashova, Sh.Sh. Shabanov, G.K. Safaraliev

*Dagestan State University, Makhachkala, 367000 Dagestan Rep., Russia
gulya-ka11@yandex.ru*

The article is devoted to the establishment of technological aspects of the formation of composite ceramics based on silicon carbide and aluminum nitride by the method of hot pressing and to a research of structure of samples by methods AFM and by scanning electron microscopy (SEM).

Problems of new functional and constructional materials formation on the basis of silicon carbide and aluminum nitride with predictable behavior make important the properties investigation. SiC-aluminum nitride (AlN) compositions are of great interest as perspective material for high-temperature devices.

Using of highly dispersed and active powders obtained by plasmochemical synthesis is especially is good for obtaining of fracture strength materials by hot-pressing. Dense fine-grained matrices are formatted with elongated grains of aluminum nitride and refractory grain boundary by use of such powders during hot-pressing.

The study shows structural features of SiC-AlN ceramic and its structurization and phase formation. The paper presents the results of the study of the microstructure of ceramics based on silicon carbide, obtained by hot pressing at temperatures up to 2170 K and pressures up to 35 MPa, of various compositions (0.9SiC - 0.1AlN; 0.7SiC - 0.3AlN; 0.5SiC - 0.5AlN; 0.3SiC - 0.7AlN; 0.1SiC - 0.9AlN), the average density of which is 3.21 g/cm^3 [1].

The structure of a surface of ceramics was investigated after preliminary grinding by diamond pastes and polishings. Scanning of a surface was carried out on an atomic force microscope (AFM). The semi-contact method was used, scanning was carried out by the probe sensor for semi-contact techniques.

Results of scanning showed that the grain size in ceramics on to silicon carbide basis with additive of 10% weight. AlN makes 10-20mkm. With increase in maintenance of AlN the size of grains decreases (Fig. 1) that is caused by the fact that nitride of aluminum interferes silicon carbide recrystallizations.

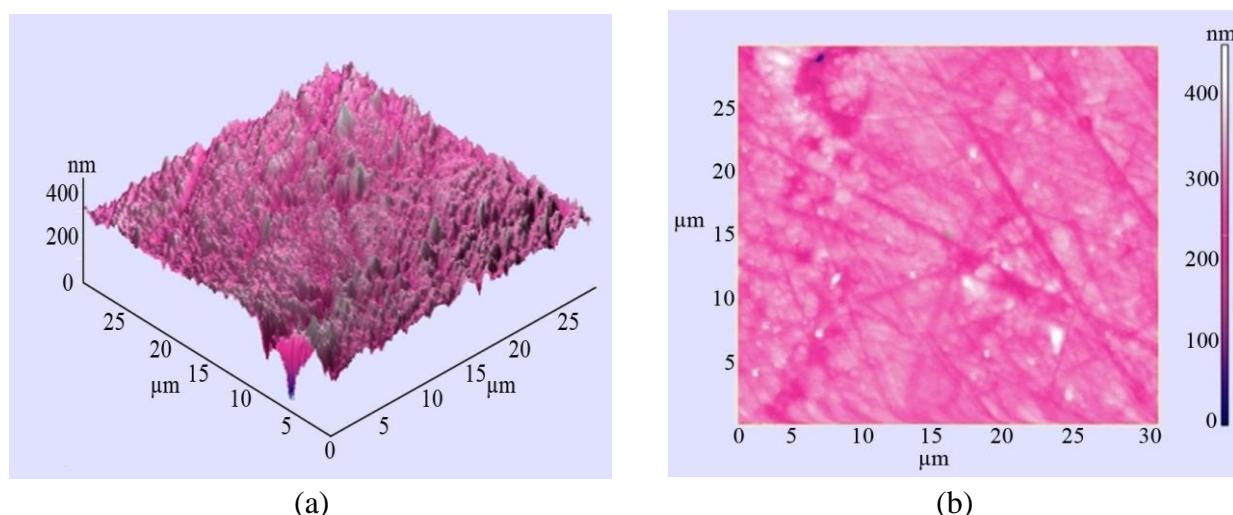


Figure 1. Photos of a surface of a break of a sample of ceramics on the basis of SiC-AlN (30% SiC – 70% AlN): (a) surface relief in volume (b) surface relief on the plane.

Qualitative chemical analysis of SiC-AlN for Si, Al, N, C element was made by scanning electron microscopy (SEM) at detection resolution 127 eV. Experiment carried out by the most bright $K\alpha$ spectra. This method require the prior etching of section and therefore the sample was etched in KOH at 750 K for 20 minutes with periodical mixing in order to remove faulted seam. It allowed getting whole etching of faulted surface material and obtaining nearly unruffled surface, which is preferable for local micro X-ray spectrum analysis.

Of special interest is phase formation in hot-pressed silicon carbide. The structure and composition of SiC ceramics is affected by various media and sintering temperatures, as well as the proportion of the content of mineralizers and modifiers.

The results of phase analysis of the SiC-AlN ceramic sample (70% weight of SiC) are given below. Using the SEM compositional contrast ratio method, it is possible to identify phases, grain rims and to determine the nature of the distribution of elements over the grain section, the chemical composition of various inclusions. The observed grain contrast ratio is used to detect various dispersed phases. As a result of the studies, photographs of the morphology of the sample with the distribution of phases throughout the sample were obtained.

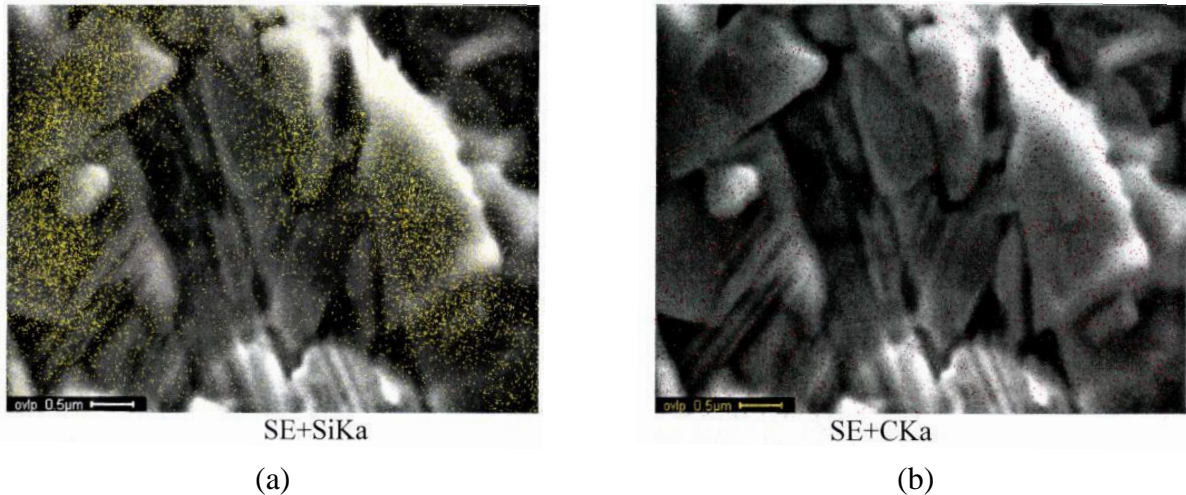


Figure 2. Results of the phase analysis of ceramics SiC-AlN (30% weight AlN): (a) distribution of a phase Si; (b) distribution of a phase C.

Obtained results allow to establish the features of synthesis of composite ceramic on the basis of silicon carbide and aluminum nitride and to optimize this formation technology.

1. Kardashova G.D. *Sintering processes and electrophysical properties of ceramics based on silicon carbide with activating additives* (Makhachkala: PhD dissertation) (2004).

Heat capacity and dielectric properties of multiferroic SmFeO_3

S.N. Kallaev¹, N.M.R. Alikhanov^{1,2}, M. Omarov¹, S.A. Sadykov²,
M.A. Sirota³, K.G. Abdulvahidov^{3,4}

¹*Institute of Physics, DagSC of RAS, Makhachkala, Russia*
kallaev-s@mail.ru

²*Dagestan State University, Makhachkala, Russia*

³*Southern Federal University, Rostov-on-Don, Russia*

⁴*Federal Research Center South Scientific Center RAS, Rostov-on-Don, Russia*

Samarium ferrite SmFeO_3 (SFO) belongs to the family of rare-earth orthoferrites with a perovskite-like crystal structure (Pnma / Pbnm, D^{16}_{2h}). SFO has a high magnetostriction coefficient, high temperatures of magnetic ordering $T_{NC} \sim 670$ K and spin reorientation $T_{SN} \approx 480$ K, which make it a potential candidate for magnetoelectric applications. Recently, the increased interest of researchers to this material is associated with the discovery in it of improper ferroelectric polarization at $T_C = 670$ K [1]. The coincidence of the Curie and Neel points ($T_C = T_N$) gives grounds to attribute this compound to second-order multiferroics, in which the ferroelectric (FE) phase is induced by the magnetoelectric (ME) interaction [2].

In this work, we studied the heat capacity and dielectric properties of SmFeO_3 microcrystalline and nanostructured ceramics obtained by the solid phase method, which was preceded by sintering treatment of the synthesized mixture at Bridgman anvils at room temperature in a wide range of temperatures between 300-800 K, including phase transitions. On the temperature dependences of the heat capacity C_p (Fig. 1.) and the dielectric constant ϵ , anomalous behavior is observed characteristic of the phase transition at temperatures $T_{NC} \approx 675$ K, $T^* \approx 558$ K, $T_{SN} \approx 465$ K.

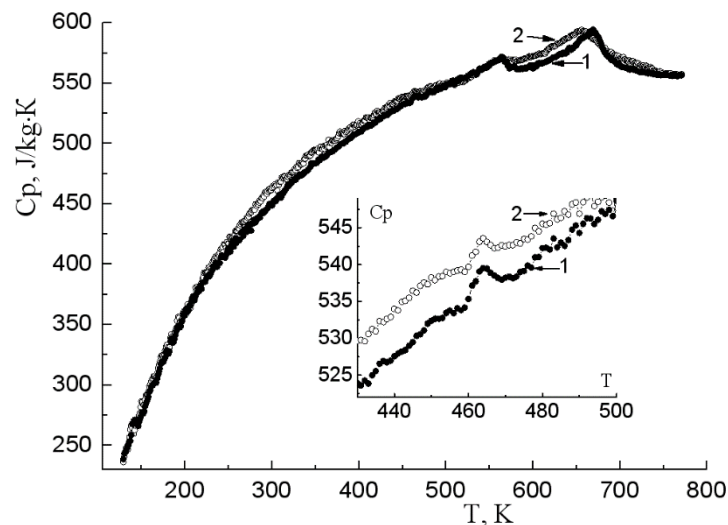


Figure 1. Temperature dependence of the heat capacity of microcrystalline (1) and nanostructured SmFeO_3 (2).

It has been established that the mechanical activation leads to a substantial smearing of the antiferromagnetic-ferroelectric transition and a shift of the phase transition temperature to the region of low temperatures. It is noted that the shift of the phase transition of the mechanically activated sample to the low temperature region may be due to a decrease in the crystallite size (size effect). It is shown that the defect structure can play a dominant role in the formation of the physical properties of ceramics. A phase transition was found at $T^* = 558$ K, which has a frequency-dependent character typical of ferro-relaxors.

1. J.-H. Lee, Y.K. Jeong, J.H. Park, et al., *Phys. Rev. Lett.* **107**, 117201 (2011).
2. A.P. Pyatakov, A.K. Zvezdin *Phys. Usp.* **55**, 557 (2012).

Dielectric properties and ac conductivities of $\text{Bi}_{1-x}\text{Sm}_x\text{FeO}_3$ ceramics

S.A. Sadykov¹, S.N. Kallaev^{1,2}, N.M.-R. Alikhanov^{1,2}

¹Dagestan State University, 367000 Makhachkala, Russia
ssadyk@yandex.ru

²Dagestan Institute of Physics after Amirkhanov, Dagestan SC RAS, 367000 Makhachkala, Russia

Multiferroics attract much attention of researchers due to simultaneous coexistence of ferroelectric and magnetic properties in one phase. One of the most promising multiferroics is BiFeO_3 . A great interest in this material is due to the high temperatures of the antiferromagnetic ($T_N = 370\text{ °C}$) and ferroelectric ordering $T_C = 830\text{ °C}$ [1,2]. The unique properties of BFO and materials based on it open wide prospects for use in various magnetoelectric devices, spintronics, sensor technology, magnetic memory. However, the functionality of BFO is limited by the presence of impurity phases and various kinds of structure defects that arise when it is produced and generate dielectric losses and high leakage currents. Low resistivity as well as high leakage current worsens its ferroelectric properties. Most authors attribute a deterioration in the electrical properties of BFO to non-stoichiometric oxygen deficiency [3,4], as well as the presence of concomitant phases [5].

In this work, we studied the structure, frequency and temperature dependences dielectric properties and ac conductivities of $\text{Bi}_{1-x}\text{Sm}_x\text{FeO}_3$ ($x = 0, 0.5, 0.1, 0.15, 0.20$) ceramics. BSFO ceramics were obtained by cold pressing of nanopowders thermally treated at 600 °C . Analysis shown that BSFO-5 as well as BFO crystallizes in rhombohedral structure with $R3c$ space group. XRD analysis of the composition BSFO-10 indicates the presence of a new orthorhombic (space group: $Pbam$) phase. With a 15% bismuth's substitution, the crystal structure is completely transformed from rhombohedral to orthorhombic phase.

The measurements dielectric constant (ε) and ac conductivity (σ_{ac}) were carried out in the frequency range $1\text{ kHz} - 10\text{ MHz}$ in the temperature range $25-600\text{ °C}$. Both components of ε undergo strong frequency dispersion. The intense temperature growth of the real part ε' begins above 200 °C , reaches its a local maximum at $\sim 230\text{ °C}$, and has a frequency-dependent character inherent to relaxors. Its maximum value $\varepsilon'(T)$ reaches at $\sim 300\text{ °C}$ (Fig. 1). We note that the dependences of $\varepsilon'(T)$ for all the samples studied are on the whole identical. However, there are some differences. Thus, the anomaly in the region $\sim 240\text{ °C}$ is clearly evident in compositions with a higher samarium concentration (BSFO15, BSFO20). Moreover, the maximum of the values of $\varepsilon'(T)$ for these compounds differs by almost an order of magnitude from the initial composition of the BFO. At room temperature and at a frequency of 1 kHz , ε' increases from 80 ($x = 0$) to 150 ($x = 0.2$).

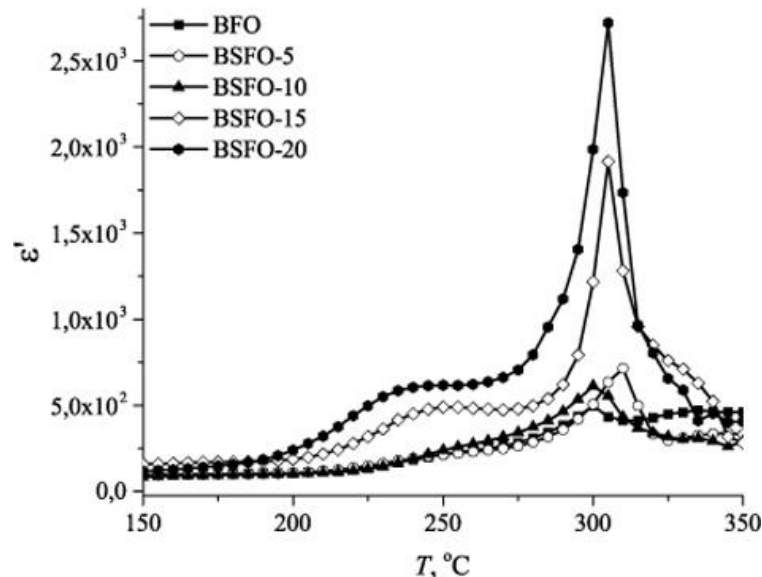


Figure 1. Thermal dependence $\varepsilon'(T)$ at 1 kHz for $\text{Bi}_{1-x}\text{Sm}_x\text{FeO}_3$

Figure 2 shows the different conductivity character in different temperature and frequency ranges. At low frequencies and temperatures above 300 °C the conductivity of all BSFO compositions gradually increases up to 600 °C. Conductivity is higher for samples with a high samarium concentration. As can be seen from Fig. 2 (insert), the dependence $\sigma_{ac}(T)$ for 10 MHz reaches to saturation and passes through a maximum. Moreover, the maximum conduction temperature is shifted to lower temperatures area with an increase in both the frequency and the percentage content of samarium.

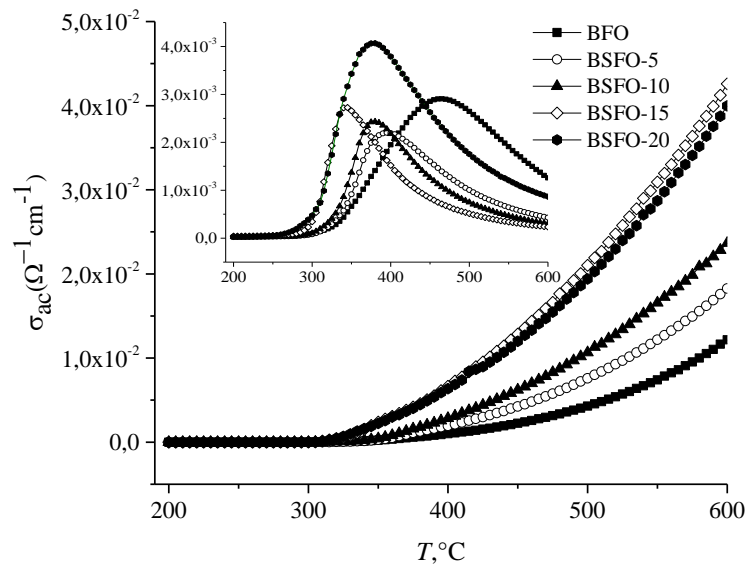


Figure 2. Thermal dependence $\sigma_{ac}(T)$ at 1kHz and 10 MHz (insert) for $\text{Bi}_{1-x}\text{Sm}_x\text{FeO}_3$

The low-frequency conductivity is identified with the dc conductivity (σ_{dc}). At frequencies > 100 kHz conductivity behavior can be interpreted in frame of the model of correlated barrier hopping (CBH) of charge carriers [6].

1. W. Eerenstein, N.D. Mathur, J.F. Scott, *Nature* **442**, 759 (2006).
2. G. Catalan, J.F. Scott, *Adv. Mater.* **21**, 2463 (2009).
3. T.D. Rao, S. Asthana, *J. Appl. Phys.* **116**, 164102 (2014).
4. E. Palaimiene, J. Macutkevicius, D.V. Karpinsky, A.L. Kholkin, J. Banys, *Appl. Phys. Lett.* **106**, 012906 (2015).
5. A. Lahmar, K. Zhao, S. Habouti, M. Dietze, C.-H. Solterbeck, M. Es-Souni, *Solid State Ionics* **202**, 1 (2011).
6. S.R. Elliott, *Adv. Physics* **36**, 135 (1987).